SUPERHYDROPHOBIC POLYMER COATINGS

FUNDAMENTALS, DESIGN, FABRICATION, AND APPLICATIONS

EDITED BY

SUSHANTA K. SAMAL, SMITA MOHANTY, AND SANJAY KUMAR NAYAK

ELSEVIER

SUPERHYDROPHOBIC POLYMER COATINGS

SUPERHYDROPHOBIC POLYMER COATINGS

Fundamentals, Design, Fabrication, and Applications

Edited by

SUSHANTA K. SAMAL

SMITA MOHANTY

SANJAY KUMAR NAYAK

ELSEVIER

Notices
Knowledge and best practice in this field are constantly changing. As new research and experience broaden our understanding, changes in research methods, professional practices, or medical treatment may become necessary.

Practitioners and researchers must always rely on their own experience and knowledge in evaluating and using any information, methods, compounds, or experiments described herein. In using such information or methods they should be mindful of their own safety and the safety of others, including parties for whom they have a professional responsibility.

To the fullest extent of the law, neither the Publisher nor the authors, contributors, or editors, assume any liability for any injury and/or damage to persons or property as a matter of products liability, negligence or otherwise, or from any use or operation of any methods, products, instructions, or ideas contained in the material herein.

Contributors

N. Abhinayaa
Dept. of Polymer and Surface Engineering, Institute of Chemical Technology, Mumbai, India

Tanvir Arfin
Environmental Materials Division, CSIR–National Environmental Engineering Research Institute (CSIR–NEERI), Nagpur, India

Sabarish Balakrishnan
Department of Metallurgical & Materials Engineering, Defence Institute of Advanced Technology (DU), Ministry of Defence, Pune, India

A.K. Bhosale
Self-cleaning Research Laboratory, Department of Physics, Raje Ramrao College (affiliated to Shivaji University, Kolhapur), Jath, India

J. Bruce Ralphin Rose
Aeronautical Engineering, Anna University Regional Campus, Tirunelveli, India

Sonalee Das
SARP–Laboratory for Advanced Research in Polymeric Materials CIPET, Bhubaneswar, India

Eno Ebenso
Department of Chemistry, School of Chemical and Physical Sciences; Material Science Innovation & Modelling (MaSIM) Research Focus Area, Faculty of Natural and Agricultural Sciences, North–West University, Mmabatho, South Africa

Ubong Eduok
Department of Mechanical Engineering, College of Engineering, University of Saskatchewan, Saskatoon, SK, Canada

Sherif A. El-Safty
National Institute for Materials Science (NIMS), Tsukubashi, Japan; Faculty of Engineering and Advanced Manufacturing, University of Sunderland, Sunderland, United Kingdom

Prakash M. Gore
Department of Metallurgical & Materials Engineering, Defence Institute of Advanced Technology (DU), Ministry of Defence, Pune, India

D. Jayadev
Department of Chemistry, School of Arts and Sciences, Amrita Vishwa Vidyapeetham, Kollam, India

Jitha S. Jayan
Department of Chemistry, School of Arts and Sciences, Amrita Vishwa Vidyapeetham, Kollam, India

Kuruvilla Joseph
Department of Chemistry, Indian Institute of Space Science and Technology, Thiruvananthapuram, India

Balasubramanian Kandasubramanian
Department of Metallurgical & Materials Engineering, Defence Institute of Advanced Technology (DU), Ministry of Defence, Pune, India

Ayesha Kausar
National University of Sciences and Technology, Islamabad, Pakistan

Aditya Kumar
Department of Chemical Engineering, Indian Institute of Technology (Indian School of Mines), Dhanbad, India

Sanjay S. Latthe
Henan Key Laboratory of Polyoxometalate Chemistry, Henan Joint International Research Laboratory of Environmental Pollution Control Materials, College of Chemistry and Chemical Engineering, Henan University, Kaifeng, People's Republic of China; Self-cleaning Research Laboratory, Department of Physics, Raje Ramrao College (affiliated to Shivaji University, Kolhapur), Jath, India

Shanhu Liu
Henan Key Laboratory of Polyoxometalate Chemistry, Henan Joint International Research Laboratory of Environmental Pollution Control Materials, College of Chemistry and Chemical Engineering, Henan University, Kaifeng, People's Republic of China

Hesam Makki
Department of Polymer Engineering and Color Technology, Amirkabir University of Technology, Tehran, Iran

Gaurav Manik
Department of Polymer and Process Engineering, Indian Institute of Technology Roorkee, Saharanpur, India

Mohsen Mohseni
Department of Polymer Engineering and Color Technology, Amirkabir University of Technology, Tehran, Iran

Debasis Nanda
Department of Chemical Engineering, National Institute of Technology, Rourkela, India

Zeena S. Pillai
Department of Chemistry, School of Arts and Sciences, Amrita Vishwa Vidyapeetham, Kollam, India

Sukanya Pradhan
SARP-Laboratory for Advanced Research in Polymeric Materials CIPET, Bhubaneswar, India

Anagha Sabnis
Dept. of Polymer and Surface Engineering, Institute of Chemical Technology, Mumbai, India

Kishor Kumar Sadasivuni
Center for Advanced Materials, Qatar University, Doha, Qatar

Sushanta K. Sahoo
Material Sciences and Technology Division, CSIR–National Institute for Interdisciplinary Science and Technology, Thiruvananthapuram, India

Swarnalata Sahoo
SARP-Laboratory for Advanced Research in Polymeric Materials CIPET, Bhubaneswar, India

Appukuttan Saritha
Department of Chemistry, School of Arts and Sciences, Amrita Vishwa Vidyapeetham, Kollam, India

Mohamed S. Selim
National Institute for Materials Science (NIMS), Tsukubashi, Japan; Petroleum Application Department, Egyptian Petroleum Research Institute (EPRI), Nasr City, Egypt

Sushanta K. Sethi
Department of Polymer and Process Engineering, Indian Institute of Technology Roorkee, Saharanpur, India

Mohamed A. Shenashen
National Institute for Materials Science (NIMS), Tsukubashi, Japan; Petroleum Application Department, Egyptian Petroleum Research Institute (EPRI), Nasr City, Egypt

Vikramaditya Shirsat
Dept. of Polymer and Surface Engineering, Institute of Chemical Technology, Mumbai, India

Bhawana Singh
Environmental Materials Division, CSIR–National Environmental Engineering Research Institute (CSIR-NEERI), Nagpur, India

Rajaram S. Sutar
Self-cleaning Research Laboratory, Department of Physics, Raje Ramrao College (affiliated to Shivaji University, Kolhapur), Jath, India

Jerzy Szpunar
Department of Mechanical Engineering, College of Engineering, University of Saskatchewan, Saskatoon, SK, Canada

Neelima Varshney
Environmental Materials Division, CSIR–National Environmental Engineering Research
Institute (CSIR–NEERI), Nagpur, India

Hossein Yahyaei
Department of Polymer Engineering and Color Technology, Amirkabir University of
Technology, Tehran, Iran

Fundamental, design and fabrication of superhydrophobic polymer coatings

CHAPTER 1

Fundamentals of superhydrophobic surfaces

Sushanta K. Sethi[a], Gaurav Manik[a], Sushanta K. Sahoo[b]
[a]Department of Polymer and Process Engineering, Indian Institute of Technology Roorkee, Saharanpur, India
[b]Material Sciences and Technology Division, CSIR-National Institute for Interdisciplinary Science and Technology, Thiruvananthapuram, India

1. Introduction

Nature is the inspiration for humankind to learn the mechanism of developing novel superhydrophobic surfaces for day-to-day use. Two thousand years ago, it was observed that many plant leaves have perpetual self-cleaning phenomena to survive in dirty habitats. Many natural species in nature such as lotus leaves, rice leaves, rose petals, cicada surface, water strider legs, mosquito eyes, etc. are well documented for exhibiting superhydrophobic property. They all show higher water contact angle (CA) and simultaneously exhibit very low sliding angles, and thus, exhibit self-cleaning nature. These surfaces provide valuable information regarding the fundamental mechanism behind superhydrophobic nature and self-cleaning behavior.

Controlling the wettability of a surface is vital for both fundamental and practical point of view. However, the reduced wettability as a macroscopic effect basically may be obtained by the combination of low surface energy alongside surface texture. Different microstructures (such as trichomes, cuticular folds, and cuticular wax) provide the rough surface, which induce hydrophobic nature as well as water repellency [1–3]. The dust particles present on the surfaces adhere strongly to water droplets rather than the surface itself because of its low surface energy and are carried away easily along with droplet due to superhydrophobic nature of the substrate. Many researchers fabricated artificial self-cleaning surfaces/coatings considering the nature-inspired approach. Nature exhibits over 200 species, which show the combination of surface chemistry with morphology to stay clean. Several researchers used template methods to mimic the surface topography using low surface energy polymers to produce biomimetic applications.

CA is a direct expression to quantify the hydrophobicity of a surface. Specifically, the surfaces showing CA's of >90 degrees and 150 degrees usually called as hydrophobic and superhydrophobic surfaces respectively. The materials possessing very low surface energy are hydrophobic (not superhydrophobic) in nature, which further can be modified by dual scale (micro and nano) surface texture in order to achieve superhydrophobicity.

Such surfaces do not allow water to spread thoroughly over the surface, thereby, making the water to form a droplet shape.

This chapter discusses the natural surfaces which exhibit superhydrophobic nature and the underlying mechanisms behind such superhydrophobicity. Additionally, the design and development of such artificial superhydrophobic surfaces by replicating the leaves and nano–fabrication techniques have been explained.

2. Basic concepts of superhydrophobicity

Wettability of a surface has been studied for a very long time which can be assessed by the static and dynamic performance of a liquid droplet on a surface. In 1805, Young [4] proposed the first fundamental equation that quantified the hydrophobicity/hydrophilicity of a surface by providing a static CA. As depicted in Fig. 1, the droplet gives three-phase interfacial tensions between solid-liquid (γ_{SL}), solid-vapor (γ_{SV}), and vapor-liquid (γ_{VL}). Balancing these interfacial tension lines in their tangential direction yields an equilibrium relation (Young's equation).

$$\gamma_{SL} + \gamma_{LV} \cos \theta_Y = \gamma_{SV} \tag{1}$$

$$\cos \theta_Y = \frac{\gamma_{SV} - \gamma_{SL}}{\gamma_{LV}} \tag{2}$$

Based on the CA value, the surfaces are classified as wetting (if CA < 90 degrees) and nonwetting (if CA ≥ 90 degrees). If the testing fluid used is water, based on the CA the surfaces are called hydrophilic and hydrophobic. This wetting behavior is primarily dependent and directly proportional to surface free energy. Wettable surfaces display a high surface energy value which varies between 500 and 5000 mN m^{-1} whereas nonwettable surfaces exhibit a low surface energy value which may vary between 10 and 50 mN m^{-1}.

Apart from the surface energy, the topographic design of the surface plays a key role in converting a hydrophobic surface to a superhydrophobic surface (CA ≥ 150 degrees). As depicted in Fig. 2, the surface texture of a dual scale (micro and nano) roughness gives a

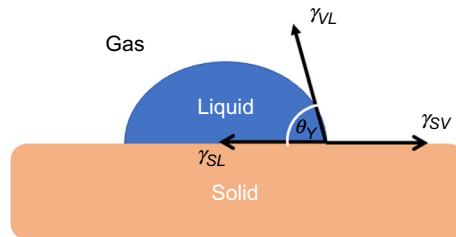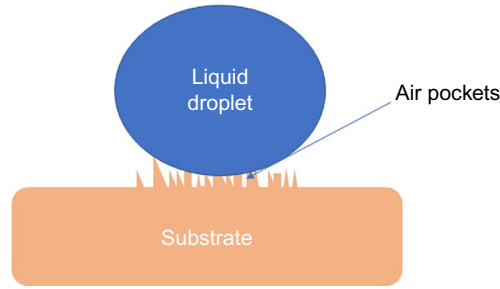**Fig. 1** Equilibrium contact angle of the liquid on a flat surface.

Fig. 2 Demonstration of water droplet relying on rough surface signifying the importance of air-pockets.

pathway to create air pockets. These air pockets additionally with the dual scale hydrophobic pillars hold the water to form a droplet shape, and thereby, resist it from spreading over the surface.

The combination of low surface energy and dual scale roughened texture provides a desirable high CA value of $\geq$90 degrees, and additionally, a low contact angle hysteresis (CAH) of $\leq$5 degrees. There are two types of superhydrophobic surfaces, one is adhesive, where CAH$\geq$5 degrees, where the water droplet gets adhered onto the surface and the other one is nonadhesive, where CAH$\leq$5 degrees wherein the water droplet rolls off. On both types of superhydrophobic surfaces, the water forms a droplet shape but the only difference is that in the former the droplet does not roll off easily while it does effortlessly on the later. It is notable that micro to nanoscale roughness of hierarchical structure of a surface yields nominal contact between the liquid and the solid surface. Water dispensed on such surfaces acquires almost spherical shape and remains suspended on the top of the micro/nanostructural pillars and easily rolls off at minimal inclinations [5].

3. Superhydrophobic surfaces in nature

Over 200 species including plant and animals present in nature are full of mysteries since they exhibit superhydrophobic surfaces and which are providing human beings motivation, inspiration, and learning to study their useful physical texture and chemical nature in order to develop artificial advanced materials. Different plant and animal surfaces exhibit a diversity of surface topography that has been investigated by scanning electron microscope (SEM) and well documented in the last two decades. The term "Biomimetic" is undeniably an exciting research subject attracting the attention of both academics and industries. In the last two decades, an adequate amount of data dealing with numerous plants and animals surfaces have been published.

3.1 Superhydrophobic plant surfaces

3.1.1 *Lotus leaf*

The most renowned superhydrophobic natural isotropic plant surface is lotus leaf, which is also famous as a symbol of purity for many years [6]. The extreme water-repellent ability of such a bio-surface is the combined result of dual scale hierarchical structures those are composed of papillose epidermal cells (of size ranging from 3 to 10 μm) and epicuticular wax (of size approximately 70–100 nm) [7, 8] as shown in Fig. 3. These hydrophobic wax crystals minimize the contact area between the water droplet and the lotus surface, and thereby, provide a higher CA of 161 ± 2 degrees and a very low CAH of less than 2 degrees [8]. Feng et al. [7] observed that by reducing the surface roughness that is, of outer diameters of the protruding structures, the CA shows a decreasing tendency, and thereby, signifies the importance of microstructures in providing superhydrophobicity. Such high CA and very low CAH of the lotus leaf surface along with nonadhesive nature categorizes the leaf as superhydrophobic surface and acknowledged as the lotus leaf effect by several researchers.
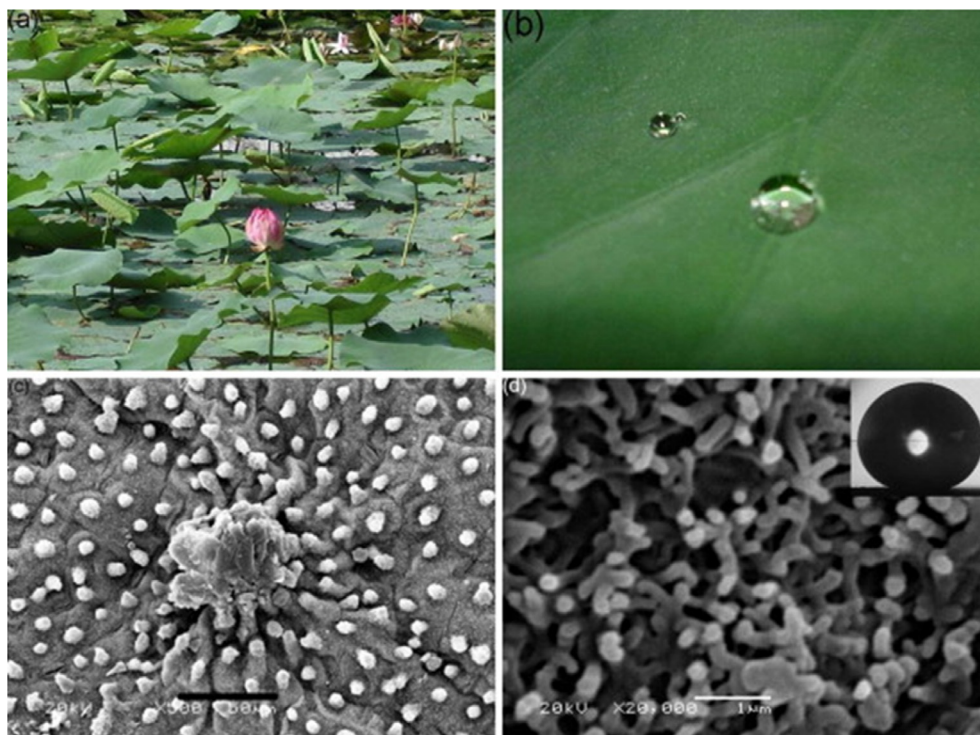

Fig. 3 (A) Image of lotus leaves on a pond, (B) floating of water droplets on lotus leaf, and (C, D) SEM images of lotus leaves at 50 and 1 μm magnifications. *(Reproduced with permission from Z. Guo, W. Liu, Biomimic from the superhydrophobic plant leaves in nature: binary structure and unitary structure, Plant Sci. 172 (6) (2007) 1103–1112.)*
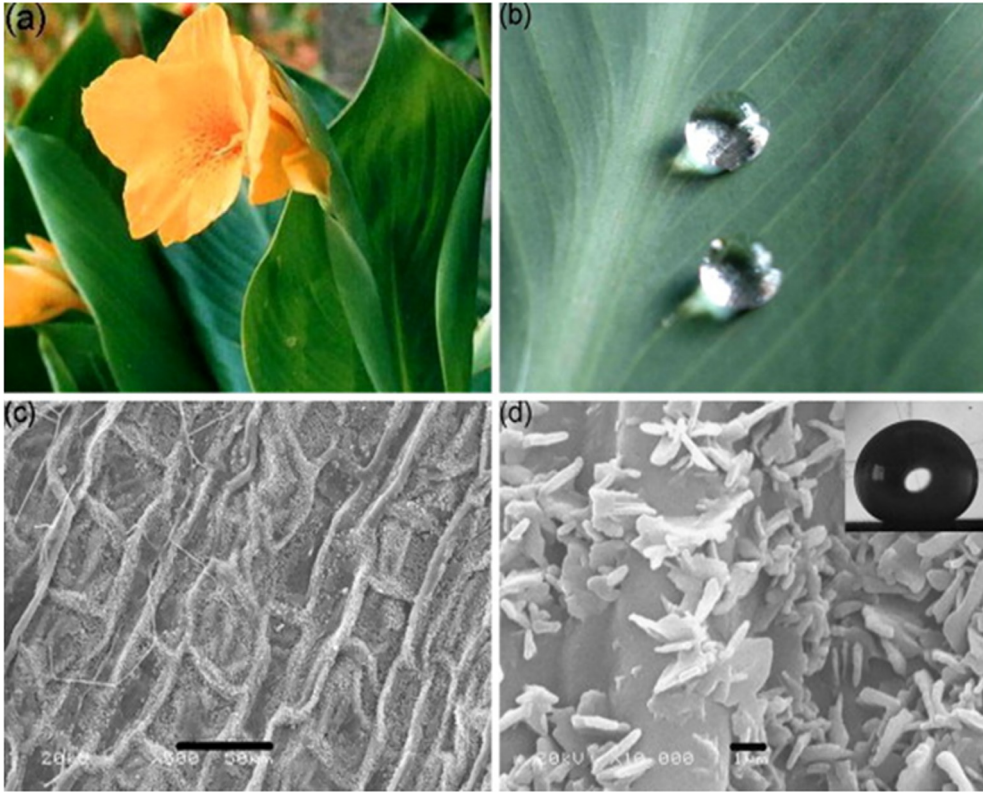
Fig. 4 Images of (A) Indian canna leaf, (B) water droplets forming spherical shape and floating on the surface, and (C, D) SEM image of canna leaf at different magnifications of 50 and 1 μm, respectively. *(Reproduced with permission from Z. Guo, W. Liu, Biomimic from the superhydrophobic plant leaves in nature: binary structure and unitary structure, Plant Sci. 172 (6) (2007) 1103–1112.)*

3.1.2 Canna leaf

Indian canna leaves have been found to have surface properties similar to that of lotus leaves. The canna flowers are cultivated mainly in tropical and subtropical regions of the world. The surfaces of canna leaves (Fig. 4A and B) are covered by randomly distrib-uted rod-like structures of wax platelets as observed from the SEM images depicted in Fig. 4C and D. The rough texture obtained by wax crystals enhances the amount of air that can be easily trapped inside the surface, and thereby, exhibits a higher CA of 165±2 degrees [8]. The hydrophobic pillars prevent water molecules from entering into the grooves where the air is previously trapped, which might not be possible if such pillars were hydrophilic in nature.

3.1.3 Rose petals

The petals of a red rose have a great biological and technological importance because of its superhydrophobic and simultaneously adhesive nature. The petals of the rose consist of
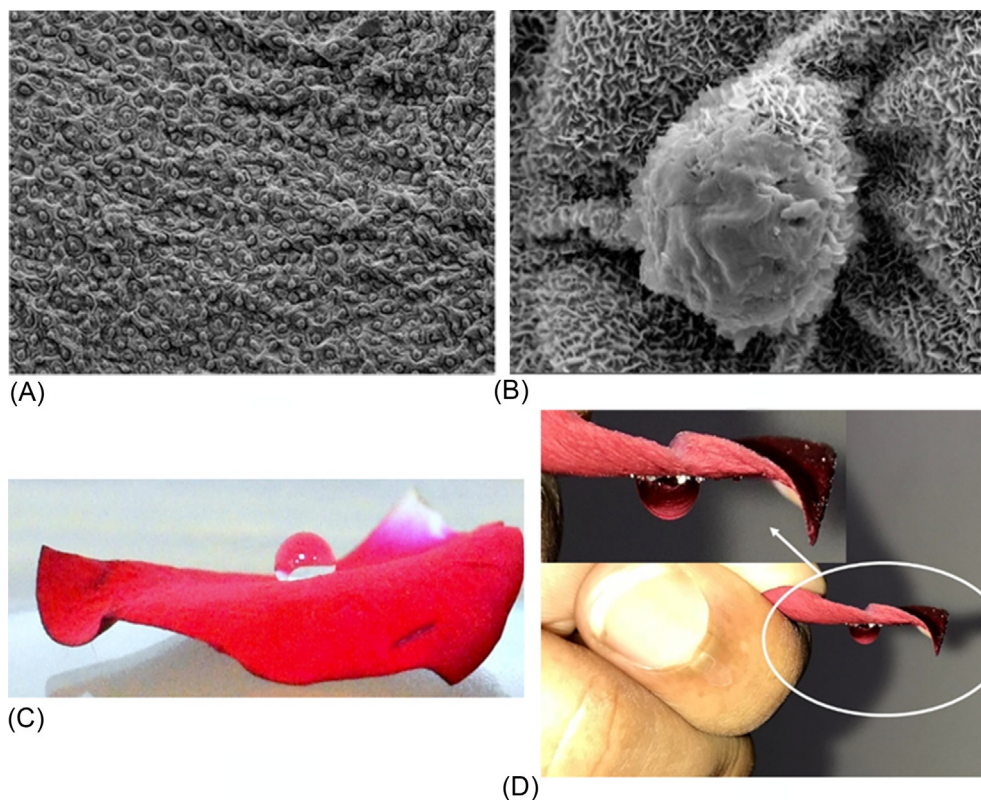
Fig. 5 (A, B) SEM images of red rose petal surface at different magnifications of 100 and 5 μm respectively; (C) water droplet forming spherical shape indicating super hydrophobic nature of surfaces; and (D) adhesion of water droplet with the petal surface when the surface turned upside down.

an array of micro-papillae of approx. diameter of 16 μm and a height of 7 μm with nanoscaled cuticular folds of around 730 nm width on their tops [9]. Such micro/nanostructure provides sufficient roughness on the surface which helps in achieving a CA of 152.4 degrees, but concurrently, it provides higher adhesive force with water as shown in Fig. 5. The superhydrophobic rose petal holds the water droplet in spherical shape even in upside down position. Compared to a lotus leaf, rose petals have larger separations among the microstructures, and additionally, displays adhesive nature with water droplets. Due to superhydrophobicity and simultaneous adhesive nature of rose petals, such surfaces are categorized as superhydrophobic–adhesive surfaces and such effect is well known as the petal effect.

3.1.4 Taro leaf

Apart from the aforementioned leaves, taro leaf also shows superhydrophobic nature. It is mainly harvested in subtropical and tropical regions of the world due to its edible nature
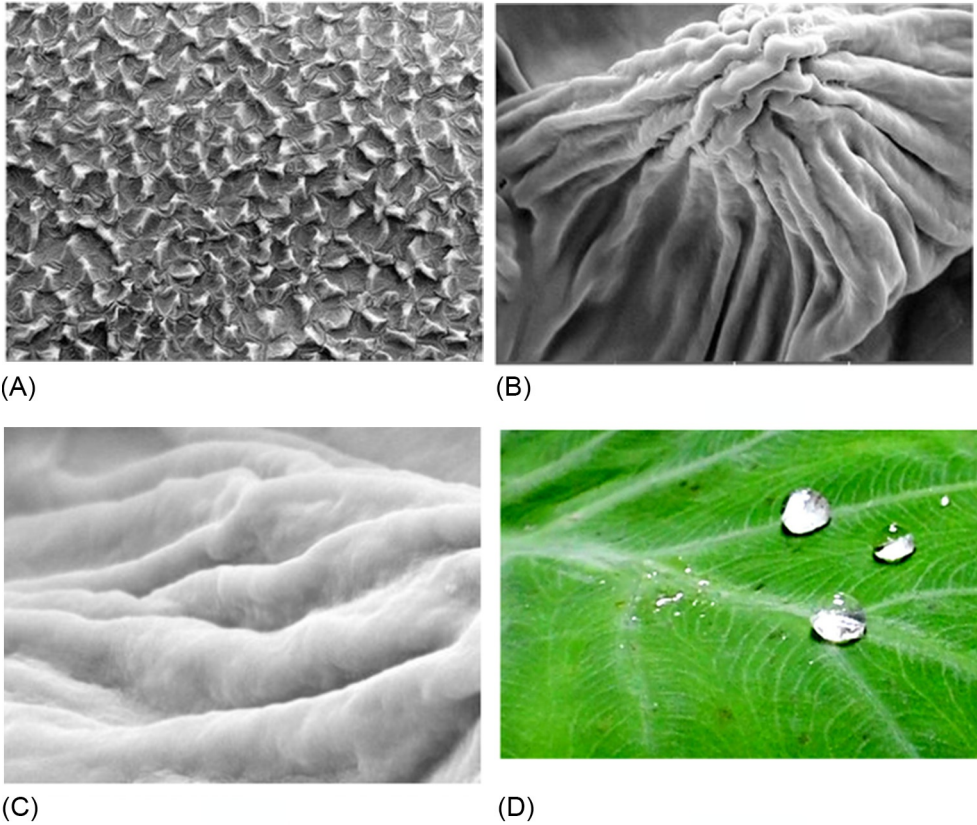
Fig. 6 (A–C) SEM images of a taro leaf surface at different magnifications scales of 100, 5, and 1 μm, respectively, and (D) water droplets floating on the taro leaf revealing super hydrophobicity.

as a staple food [10]. It is adopted in a moist atmosphere and is grown under rainfed or irrigated upland and flooded conditions. It is noticeable that taro leaves have elliptic microstructured protrusions with an average diameter of 10 μm, and additionally, these microstructures have nanoscaled hierarchical pins which are similar to lotus leaf [8] as shown in Fig. 6. This arrangement of surface structures greatly influences wettability by showing higher CA of 159 degrees and a lower CAH of 4 degrees.

3.1.5 Rice leaf (anisotropic)

Indian rice leaves have also been reported to be superhydrophobic and possess binary (micro and nano) rough structured surfaces [8] which possess low drag, water repellency, and self-clean nature. The leaves are covered with hierarchical structured micro papillae
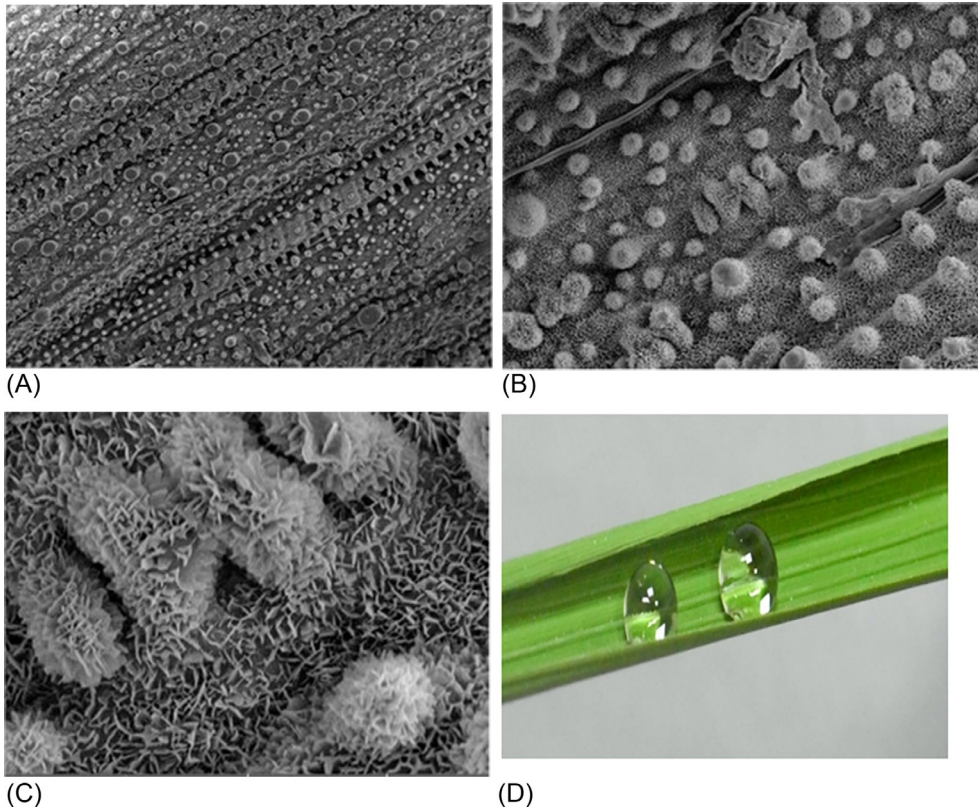
Fig. 7 (A–C) SEM images of a rice leaf surface at different magnifications of 100, 20, and 5 µm, respectively, and (D) water droplets floating on the rice leaf displaying super hydrophobicity.

with epicuticular wax and longitudinal grooves as shown in Fig. 7. These binary aniso-tropic structures vary from the range of few nanometers to few micrometers and provide positive prominence to frame the wax crystal which directs the water flow out of the surface, thereby displays a high CA of 157 degrees and a low CAH of 4 degrees.

3.2 Superhydrophobic surfaces of animals

3.2.1 Water strider

The insect water strider lives on ponds or other quiet water surfaces. It is evident from Fig. 8 that it can stand effortlessly on water, primarily due to its nonwetting superhydro-phobic coated legs [11]. One single leg of the water strider can support a force of up to
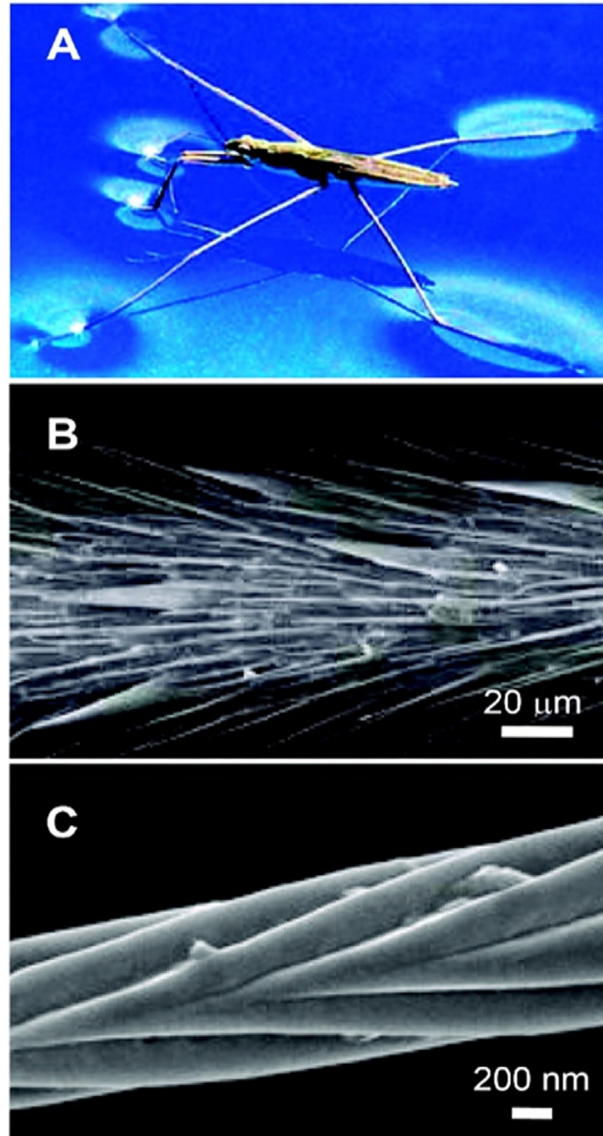
Fig. 8 (A) A water strider walking on the water surface, (B) SEM image of water strider leg numerous oriented needle-shaped microsetae, and (C) the nanoscale groove structure of a single seta. *(Reproduced with permission from Xi-Qiao Feng, Xuefeng Gao, Ziniu Wu, et al., Superior water repellency of water strider legs with hierarchical structures: experiments and analysis, Langmuir 23 (9) (2007) 4892–4896.)*

152 dyn, which is 15 times that of the weight of the water strider. Additionally, the legs are composed of several microscale needle-shaped setae, each of which has nanoscale grooves in it. When it crawls on the surface of the water, the buoyancy force offers sufficient upward force to prevent the penetration of its legs inside the water.

Such combination of the nanoscale grooves with its hydrophobic nature makes the water strider legs superhydrophobic due to which it merely floats on the water surface [12]. It helps in introducing a thin layer of air around the surface which decreases the fluidic drag, and subsequently, supports in floating on the water surface.

3.2.2 Butterfly wings

Butterfly wings exhibit astounding multifunctional properties such as structural color, chemical sensing capability, and fluorescence emission function [13]. Apart from such interesting properties, it also exhibits superhydrophobic self-clean properties. Fang et al. [14] studied the hydrophobic mechanism of butterfly wings and found the wings to be composed of micro–class scale and submicro–class vertical gibbosities. For micro-class scale, the length, width, and distance between the scales are 65–150 μm, 35–70 μm, and 48–91 μm respectively as shown in Fig. 9. Similarly, for submicro-class scale the length, width, and distance between the scales are 200–900 nm, 200–840 nm, and 1.06–2.74 μm, respectively. The combined micro–class and submicro class structures help in obtaining a CA of 136–156 degrees. Additionally, the butterfly wings provide the directional adhesive property [15].

Bixler and Bhushan [16] investigated the combination of anisotropic grooves with superhydrophobic nature providing low fluid drag property. Butterfly wings display directional adhesion ability along and against radial outward (RO) direction and away from the body's central axis as shown in Fig. 10 (left). The water droplet flows out of the butterfly wings surface at a very low CAH of ∼9 degrees. On the contrary, when nitrogen air blows, the droplet gets pinned to the surface and tilts upward.
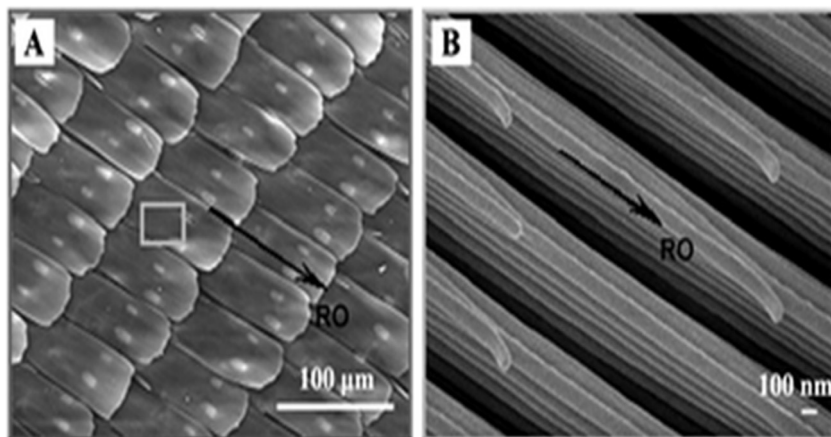

Fig. 9 (A) Image of butterfly wings showing micro-patterned scale structures like overlapping of tiles and (B) flat cross-section of vertically arranged gibbosities on the scale. *(Reproduced with permission from Kesong Liu, Xi Yao, Lei Jiang, Recent developments in bio-inspired special wettability, Chem. Soc. Rev. 39 (8) (2010) 3240–3255.)*
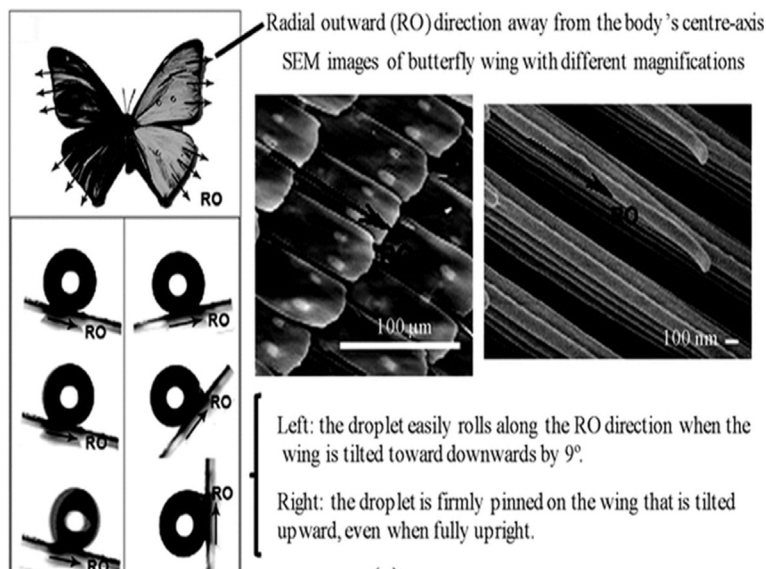
Fig. 10 Images of butterfly wings and its SEM images at different magnifications of 100 μm and 100 nm. (Reproduced with permission from S. Nishimoto, B. Bhushan, K. Koch, P. Walzel, T. Ochiai, T. Murakami, A. Fujishima, K. Nakata, H. Sakai, T. Murakami, M. Abe, T. Komine, A. Fujishima, Bioinspired self-cleaning surfaces with superhydrophobicity, superoleophobicity, and superhydrophilicity, RSC Adv. 3 (3) (2013) 671–690.)

Additionally, the droplet easily rolls off the surface when air blows along the RO direction, and the water droplet is restrained on the wings when the air blows against the RO direction. Such ability helps a butterfly to keep its wings clean during flying.

3.2.3 Cicadae wings

Researchers [17, 18] examined the superhydrophobic nature of different species of cicadae wings and found that the wings of cicadae are composed of a series of longitudinal and cross veins. The chemical compositions of the wings are basically protein, chitin, and cuticular waxes. The ventral and dorsal sides of both the fore- and hind-wings of cicadae are covered with hexagonal arrays of spherically capped, conical, nanoscale pillars in the range of 200 nm in height and 10–60 nm in diameter at base and top and spaced 170 nm apart as observed from SEM images depicted in Fig. 11. This nanoscale structured surface with the chemical composition of cuticular waxes together provide a CA of varying from 81.3 degrees to 143.8 degrees for different species, thereby exhibits superhydrophobicity.

3.2.4 Snail shell

The snails mainly appear in rainy seasons but still, their surfaces remain ever clean even while being underwater. The main chemical components of a snail shell are aragonite and protein.
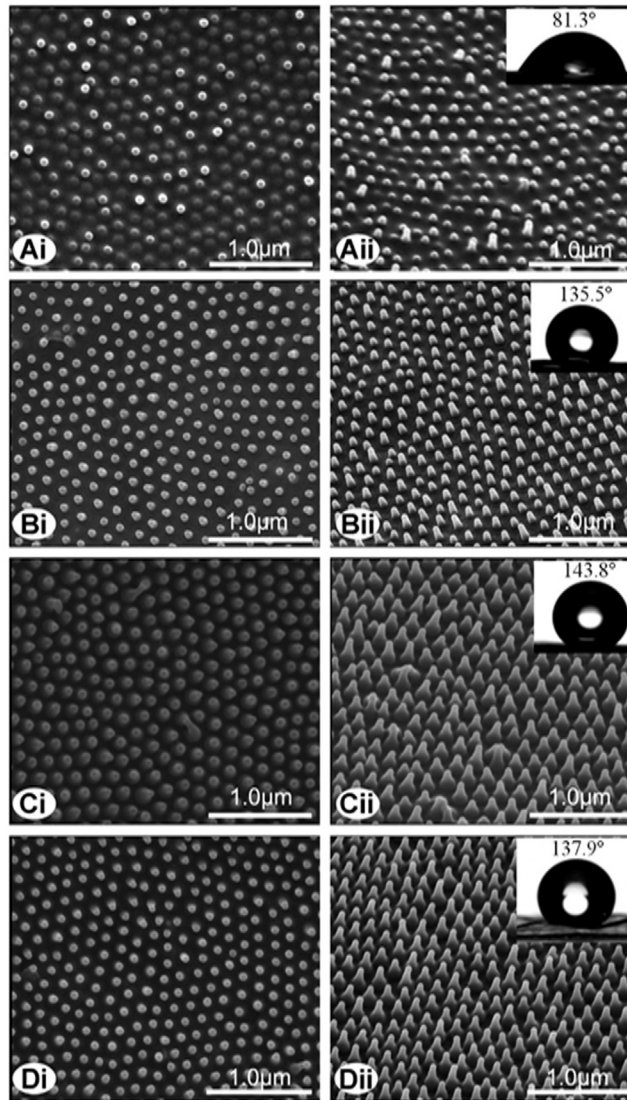
Fig. 11 SEM images cicada wing surfaces showing (i) top view and (ii) a 30 degrees inclined view of four species. (A) *Leptopsalta bifuscata*; (B) *Aola bindusara*; (C) Meimuna opalifer; and (D) *Cryptotympana atrata*. The CA of water droplets are shown in the insets. *(From M. Sun, A. Liang, G.S. Watson, J.A. Watson, Y. Zheng, J. Ju, et al., Influence of cuticle nanostructuring on the wetting behaviour/states on cicada wings, PLoS One 7 (4) (2012) e35056. No permission required for open access article as mentioned in journal web.)*
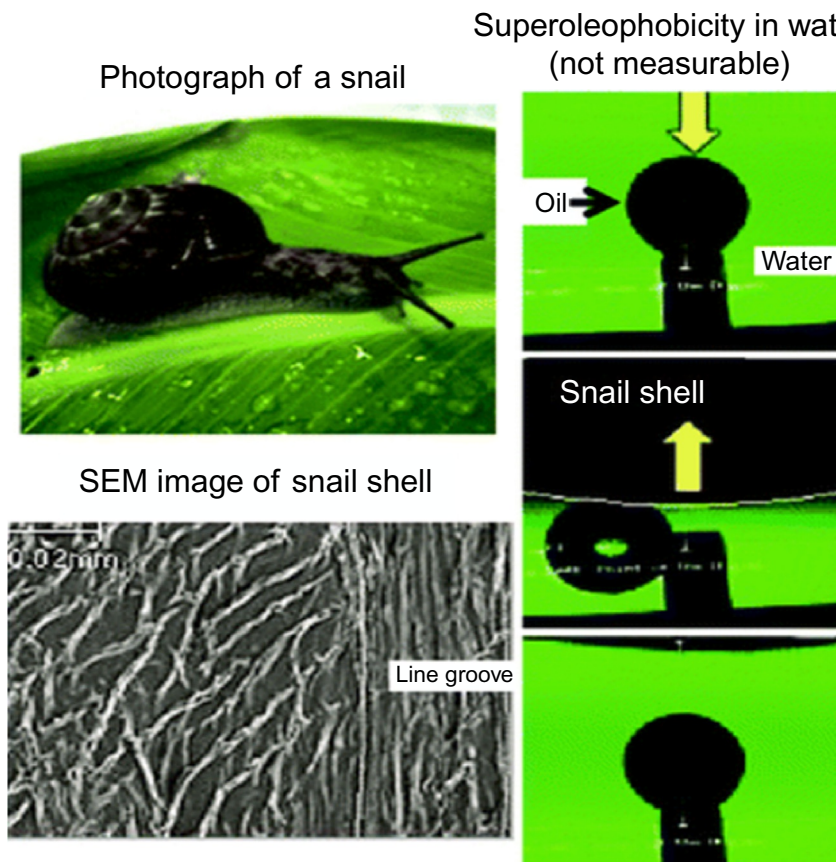
Fig. 12 Photographs of a snail shell and oil droplet sitting on the surface of snail shell in water. *(Reproduced with permission from S. Nishimoto, B. Bhushan, K. Koch, P. Walzel, T. Ochiai, T. Murakami, A. Fujishima, K. Nakata, H. Sakai, T. Murakami, M. Abe, T. Komine, A. Fujishima, Bioinspired self-cleaning surfaces with superhydrophobicity, superoleophobicity, and superhydrophilicity, RSC Adv. 3 (3) (2013) 671–690.)*

The surface of the snail's shell is comprised of several lines and 0.5 mm pitch grooves and 10 μm pitch microgrooves as depicted in Fig. 12. Such dual scale surface texture provides a water CA of 80 degrees [2, 19] and oil CA of 10 degrees [19]. But the same surface exhibits oleophobicity and antifouling nature under water, owing to its trapping of water layers in the submicron grooves on the surface [20]. The key of the snail shell to remain self-clean is due to its superoleophobicity rather than superhydrophobicity.

3.2.5 Fish scale

An astounding self-cleaning property can be observed on a fish scale even in polluted sea water. It has been investigated that the fish scales remain clean owing to its super oleophobic nature like snail shells. The fish scale exhibits super oleophilicity in the air
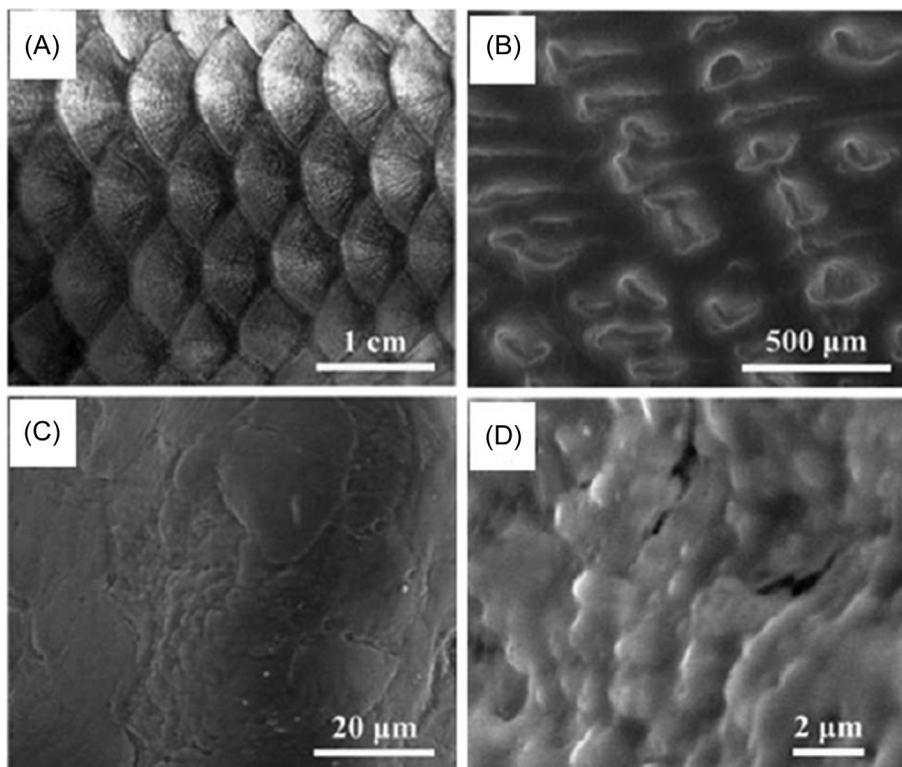
Fig. 13 (A) Optical image of fish scale showing the sectorial scales of diameter 4–5 mm arranged in array; (B) SEM images of fish scale showing oriented papillae of length 100–300 μm and 30–40 μm width on the surface of fish scale arranged in radial direction; (C) higher magnification SEM image showing the rough papillae surface; and (D) SEM image of papillae. *(Reproduced with permission from S. Nishimoto, B. Bhushan, K. Koch, P. Walzel, T. Ochiai, T. Murakami, A. Fujishima, K. Nakata, H. Sakai, T. Murakami, M. Abe, T. Komine, A. Fujishima, Bioinspired self-cleaning surfaces with superhydrophobicity, superoleophobicity, and superhydrophilicity, RSC Adv. 3 (3) (2013) 671–690.)*

but displays superoleophobicity inside water by displaying oil CA of 156.4 ± 3 degrees [19]. Liu et al. [21] studied the fish scale and observed that sectorial scales with a diameter of 4–5 mm and oriented papillae (of length and width of 100–300 μm and 30–40 μm, respectively) exist on the fish scale in the radial direction as shown in Fig. 13. The thin layers of mucus and the rough hierarchical structure basically attribute the surface in displaying properties of super oleophilicity in the air and super oleophobicity in water.

3.2.6 Mosquito eyes
It has been observed that the mosquito eyes possess superhydrophobic nature and additionally bears an effective protective mechanism to provide a clear vision even in humid

Fig. 14 (A) A photograph of antifogging mosquito eyes. Even though they are exposed to moisture, the surface of the eyes remains dry and clear w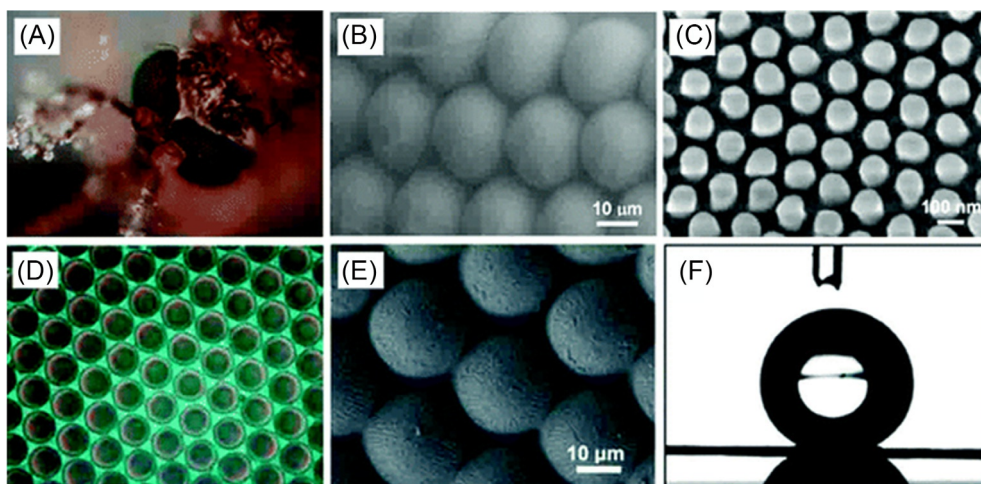hile the surrounding hairs nucleate many drops; (B) an SEM image of the hcp microhemisphere (ommatidia); (C) hexagonally ncp nanonipples covering an ommatidial surface; (D) an optical microscope image of artificial compound-eye analogues; (E) an SEM image of hcp PDMS microhemispheres mimicking the microstructures of mosquito compound eyes; and (F) a spherical water droplet on the artificial compound-eye surface. *(Reproduced with permission from Kesong Liu, Xi Yao, Lei Jiang, Recent developments in bio-inspired special wettability, Chem. Soc. Rev. 39 (8) (2010) 3240–3255.)*

habitat. The eyes of the mosquito are consisting of hexagonally nonclose-stuffed nipples and close-packed hemispheres at the nano and microscale level, respectively [22], as shown in Fig. 14. Such micro-nanoscaled nipples and hemispheres not only provide superhydrophobicity, but additionally, help in obtaining antifogging property by preventing the moisture to form spherical drops on its eye surface, and thereby, provide a clear vision to the mosquito. Such surfaces inspire mankind in developing novel antifogging coatings for automobile mirrors and swimming goggles applications.

3.2.7 Gecko feet
Geckos are well known for their extraordinary sticking and climbing ability. Hansen and Autumn [23] examined the gecko feet and found how the geckos keep their toes clean during climbing. The self-clean ability is due to its hierarchical structures present in its feet as shown in Fig. 15. Each toe of gecko consists of rows of lamellae, which are individually composed of millions of well-aligned microscale setae having length and diameter of 110 and 5 mm, respectively. The setae are present in uniform arrays on overlapping lamellar pads with a density of 14,400 per mm^2 and each seta splits into a nanoscale diameter of 200–500 nm spatula.
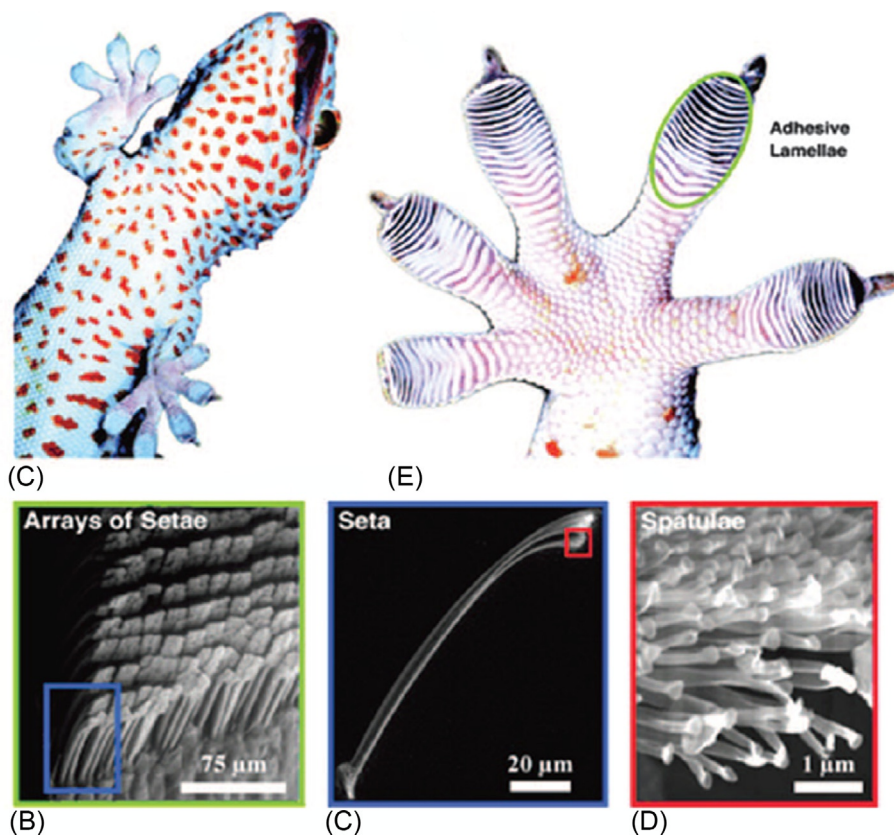
Fig. 15 Images of (A) a gecko climbing a vertical glass; (B) a gecko feet; (C) proximal portion of a single lamella, with array structure of individual setae; and (D, E) single seta with the branched structure at upper right, terminating in hundreds of spatular tips. *(Reproduced with permission from W.R. Hansen, K. Autumn, Evidence for self-cleaning in gecko setae, Proc. Natl. Acad. Sci. U. S. A. 102 (2) (2005) 385–389.)*

3.3 Other natural hierarchical structures

The superhydrophobic nature and dual scale (micro–nano) structures can also be found on several other petals of flowers. As a typical example, Chinese Kafir lily exhibits a periodic array of hexagonal close-packed of an average 75-µm side length and a 780-nm strip width in each hexagon [9] as shown in Fig. 16A. Apart from this, sunflower petals also carry a periodic array of parallel lines with a 15 µm of average diameter and a helix width of 2.5 µm of each line as depicted in Fig. 16B [9]. Several authors used different strategies for duplication of the microstructure pattern present in the surface texture of such leaves using PDMS and PS and developed artificial superhydrophobic surfaces.
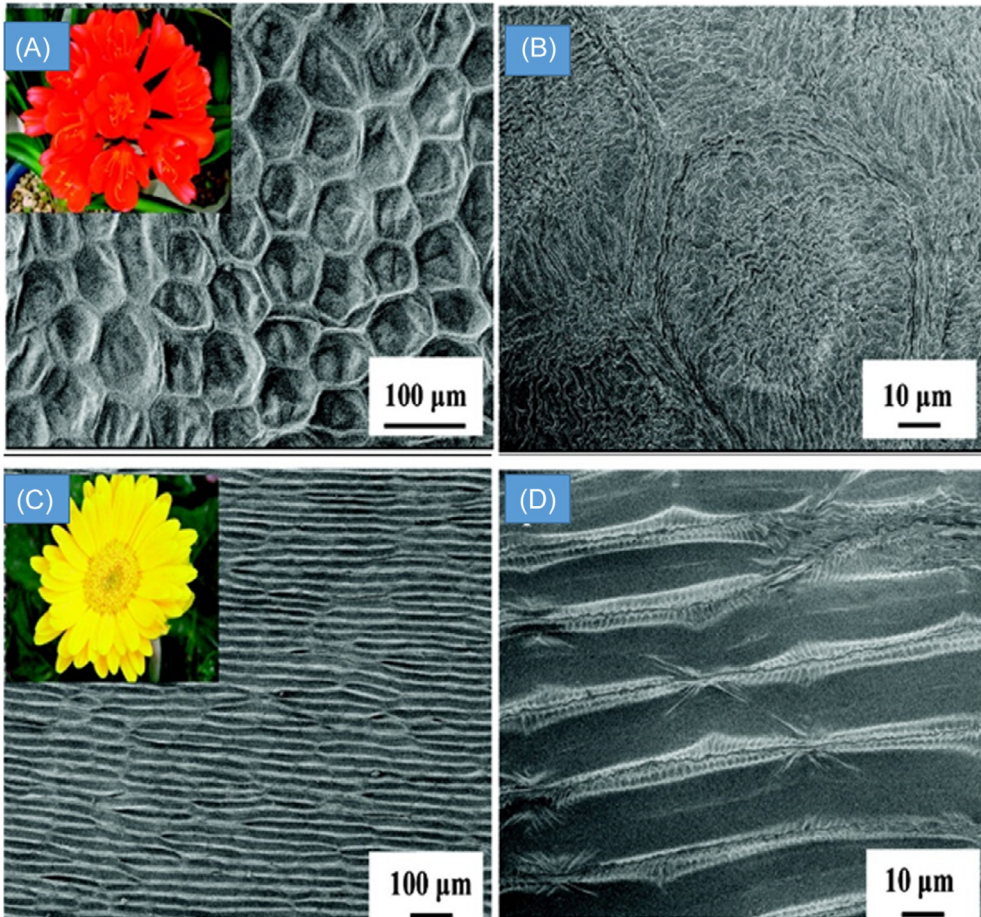
Fig. 16 SEM images of the surface of (A, B) Chinese Kafir lily petal and (C, D) sunflower petal. *(Reproduced with permission from L. Feng, Y. Zhang, J. Xi, Y. Zhu, N. Wang, F. Xia, L. Jiang, Lin Feng, Yanan Zhang, Jinming Xi, Ying Zhu, Nü Wang, Fan Xia, Lei Jiang, Petal effect: a superhydrophobic state with high adhesive force, Langmuir 24 (8) (2008) 4114–4119.)*

4. Superhydrophobicity with case study

4.1 The need of superhydrophobicity

The area of superhydrophobic surfaces is emerging and gaining rapid potential importance since the mid-1930s due to its wide industrial applications ranging from a self-clean coating to microfluidic devices [1]. When this superhydrophobicity is imparted to automobiles, it becomes weather resistant, displaying antifogging capability on glass by becoming resistant to water condensation, on an exhaust fan, propellers, textiles, or garments they become self-cleanable. The property of self-cleaning is potentially desirable not only in outdoor but also in indoor industrial applications as well. This keeps the

product self-clean, and thereby, increases the durability of the product, and in addition, also shows benefits in economics, aesthetic, and environmental point of view. Apart from this, superhydrophobic surfaces with enhanced capability of super oleophilic nature are widely used by oil industries in separating oil and water. Hence, focuses on fabrication, theoretical modeling and problems or obstacles related to its applicability of superhydrophobic surfaces are of great interest for researchers as well as industrialists.

4.2 Surface properties and surface energies of polymers

Different polymeric materials are widely used to coat high surface energy metals such as Ti ($1.98\,J/m^2$), Fe ($2.41\,J/m^2$), and Cu ($1.78\,J/m^2$) [24]. This is because the surface energy drives the surface wettability and it is also a key factor in tailoring the properties of functional materials. Higher will be the surface free energy, higher will be the adhesion ability. Hence, such metals show high adhesion toward the water, thereby, show either hydrophilicity or superhydrophilicity. To make such surfaces antistain, antifouling, anticorrosion, or antireflective several researchers have attempted numerous techniques to make the surfaces water repellent. The addition of superhydrophobic nature keeps the metals away from water, and additionally, provides self-clean property by simultaneously keeping the surface away from dust.

In general, low surface energy polymers such as poly (tetrafluoroethylene), poly (dimethylsiloxane) and perfluorooctane are of particular interest in fabricating superhydrophobic self-clean coating/surfaces. Such low surface energy polymers provide negligible interaction against water, oil, or a combination of both. Additionally, roughening such surfaces by several techniques such as lithography, plasma enhanced chemical vapor deposition, etching or sputtering [1] enhances the hydrophobic nature from a CA of ∼90–100 degrees to ∼120–140 degrees. Likewise, adding several nano-fillers to such surfaces like CNT [25], zinc oxide nanorods [26], or hydrophobic silica particles [27] in certain ways enhances its nature to provide superhydrophobic property by enhancing CA from ∼120–140 degrees to ∼150–170 degrees. The improvement in CA, reducing surface free energy, and facile sliding of water droplets turn such nonwettable surfaces into superhydrophobic surfaces.

4.3 Fabrication of biomimicked superhydrophobic polymeric surfaces

The plant leaves surfaces have been biomimicked utilizing various polymers such as resorcinol-formaldehyde (RF) gel, polydimethylsiloxane (PDMS), and polystyrene (PS) with the help of the replica molding process. Especially, RF gel is reported to be an interesting polymeric precursor for glassy carbon. The microstructures of leaves can be replicated on polymer surfaces to generate superhydrophobicity. Sharma et al. [3] reported the simplest methods of developing superhydrophobic surfaces by

biomimicking directly the patterns originated on natural hydrophobic plant leaves employing micro-molding technique and nanoimprint lithography (NIL). CA > 150 degrees was realized in biomimicked RF gel surfaces resulting in superhydrophobicity after subjecting to pyrolysis. In aqueous as well as organic media, RF gels can be utilized to obtain optimized superhydrophobic surface texture by micro-molding. Moreover, a direct replicate of the leaf patterns on various polymeric surfaces like RF gel, poly(methyl methacrylate), and poly(ethylene terephthalate) can be produced employing NIL technique. Fig. 17 depicts the demonstration of the process adopted to make a negative replica of the natural leaf surface in the polymer (PDMS).

The cross-linked PDMS block with implanted leaf was submerged in chloroform for some time to swell. After the desired swelling, the leaf gets completely removed from block sending off a negative replica. The same negative replica can be used to imitate the leaf patterns on PS and RF gel surfaces. RF sol can be taken in both aqueous and different organic media to generate the positive replica of the leaf in RF gel. The fabrication of superhydrophobic polymers from the negative replica has been shown in Fig. 18. Pattern transfer RF gel in organic media exhibited better performance than in aqueous media on account of the enhanced wetting ability of the PDMS. RF gel was made to undergo pyrolysis to generate superhydrophobic carbon surface of a larger area. CA was reported to be 152.3 degrees and 154.7 degrees, and the CAH was
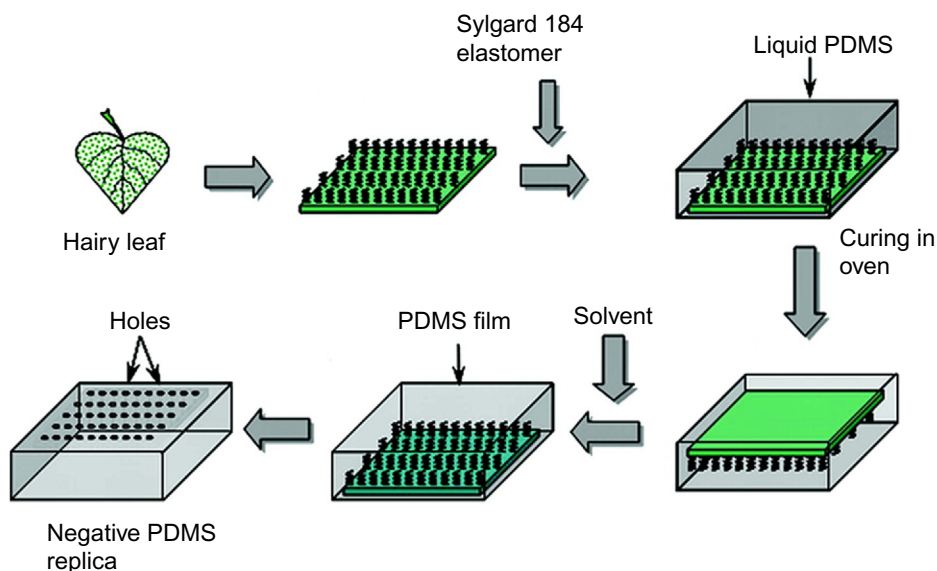

Fig. 17 Scheme for demonstration of the development of a negative PDMS replica from the plant leaf. *(Reproduced with permission from C.S. Sharma, K. Abhishek, H. Katepalli, A. Sharma, Biomimicked superhydrophobic polymeric and carbon surfaces, Ind. Eng. Chem. Res. 50 (2011) 13012–13020. Copyright 2011 American Chemical Society.)*
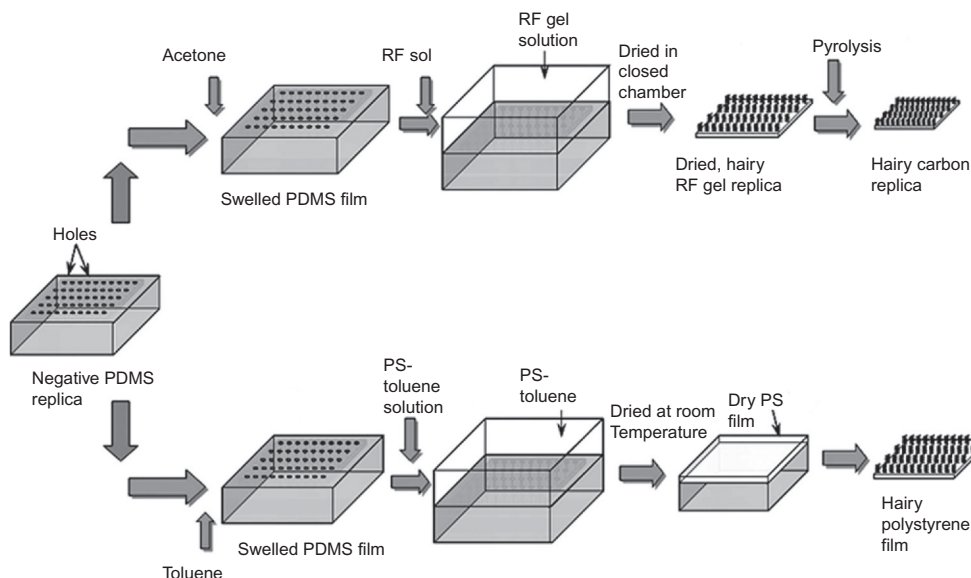
Fig. 18 Development of superhydrophobic polymer and carbon surfaces from the negative replica made in PDMS. *(Reproduced with permission from C.S. Sharma, K. Abhishek, H. Katepalli, A. Sharma, Biomimicked superhydrophobic polymeric and carbon surfaces, Ind. Eng. Chem. Res. 50 (2011) 13012–13020. Copyright 2011 American Chemical Society.)*

observed to be 14.7 degrees and 12.1 degrees for hairy RF gel and PS based surfaces, respectively. Similarly, the original plant leaves can be used as NIL molds in which leaf patterns were imprinted on polymers beyond glass transition temperature by applying a pressure of 10–30 bars. Further, these negative replicas can be used as template patterns to form positive replica by molding process as explained earlier These unique surfaces could find prospective applications in sensors and energy storage devices and also may significantly enable the water removal in devices like fuel cells.

4.4 Design and development of superhydrophobic polymer nanocomposite

Employing advances in nanofabrication technology, superhydrophobic polymer nano-composites have established themselves in various engineering fields like self-cleaning, anti-fouling, anticorrosion, antifogging, and oil–water separation [28]. Usually, construction of superhydrophobic surface involves the creation of hierarchical morphology, rough texture, and afterward coating with low energy molecules. Apart from lithography, etching, bio-mimetic, and stamping processes, fabrication of such surfaces is also made in a simplistic method by diffusing nanoparticles uniformly in a hydrophobic polymer matrix and then

coating the polymer nanocomposite dispersion on any substrate. The superb properties of the nanoparticles can be considered to generate rough morphology and develop multiple functionalities on the superhydrophobic surface. However, selection of hydrophobic polymer is precarious as some of the fluoropolymers release perfluorooctanoic acids (PFOAs) upon degradation, which are toxic for human beings and the environment. Further, carbon-based conductive superhydrophobic surfaces exhibit tremendous performance which is offered by carbon nanotubes (CNTs) or graphene with higher electrical and thermal conductivity, carbon black (CB) with high porosity, impermeability of graphene, etc.

Recently, Asthana et al. [29] reported a candid approach to develop polymer nanocomposite coatings with superhydrophobic characteristics, which is made up of an environmental friendly fluoropolymer matrix reinforced with nanofillers such as CNTs), CB, graphene nanoplatelets (GNP), and their mixture. They emphasized on developing multifunctional active surfaces along with the acceptable CA and least possible CAH. Fig. 19 depicts the surface synthesis process adopted to form various superhydrophobic polymer coatings.

Varying the composition of carbon nanoparticles (CB, CNT, GNP)/fluoropolymer (perfluoroalkylethyl acrylate/n-alkyl acrylate copolymer) ratio, the coating samples were cast on a glass substrate. The acrylic group takes part in surface bonding and helps in film formation while perfluoro group offers less surface energy as required to achieve superhydrophobic nature.
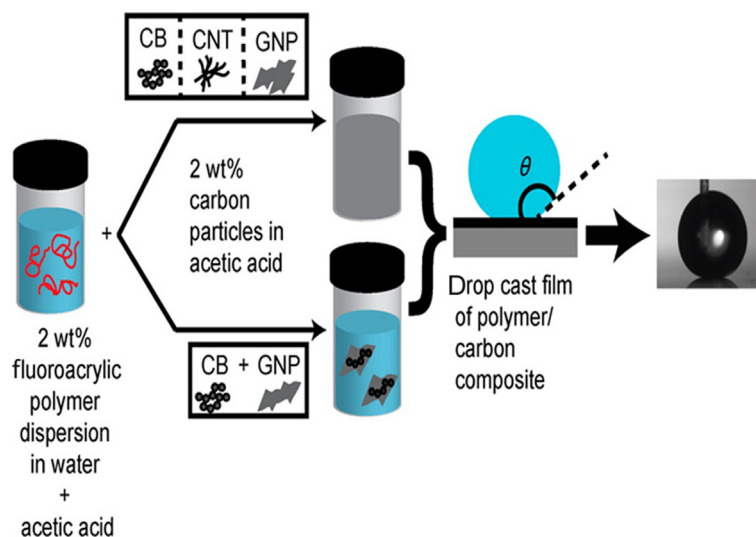

Fig. 19 Synthesis scheme of superhydrophobic nanocomposite using nanofillers. *(Reproduced with permission from A. Asthana, T. Maitra, R. Büchel, M.K. Tiwari, D. Poulikakos, Multifunctional superhydrophobic polymer/carbon nanocomposites: graphene, carbon nanotubes, or carbon black?, ACS Appl. Mater. Interfaces 6 (2014) 8859–8867, Copyright 2017 American Chemical Society.)*
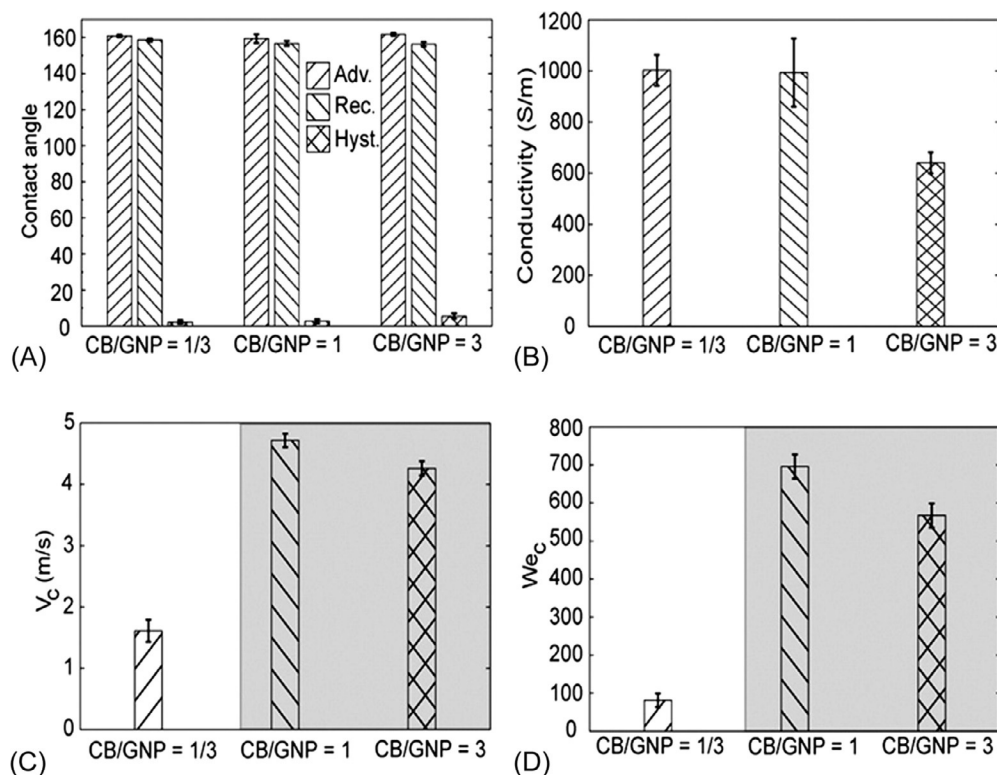
Fig. 20 (A) Contact angle, (B) electrical conductivity, (C) critical impalement velocity, and (D) critical Weber number for coatings with varying CB and GNP ratio. *(Reproduced with permission from A. Asthana, T. Maitra, R. Büchel, M.K. Tiwari, D. Poulikakos, Multifunctional superhydrophobic polymer/ carbon nanocomposites: graphene, carbon nanotubes, or carbon black?, ACS Appl. Mater. Interfaces 6 (2014) 8859–8867. Copyright 2017 American Chemical Society.)*

The CB-based coatings possessed a high critical value of Weber number revealing the best composition against impalement resistance. CNT-based surfaces demonstrated poor surface tension, while GNP-based coatings showed the highest conductivity of 1000 Siemens/m with lower impalement resistive nature. The superhydrophobic coatings based on both CB and CNT displayed greater resistance to wetting confirming the synergistic effect of both the fillers. Further, the combination of both the fillers CB and GNP in polymer coating yields outstanding properties such as dynamic impalement resistance and higher electrical conductivity (Fig. 20). Similarly, mineral oil can be separated from a water-based mixture by coating the CB and the CB/GNP nanocomposite solutions on the surface of filter papers employing the oleophilic property of the solutions. Considering the properties of these superhydrophobic coatings, it can be predicted for easy scale up and various potential applications, like in drag reduction, oil filtration, EMI shielding, etc.

In recent years, the durability of superhydrophobic coatings remained a topic of interest even compromising with antiwettability to some extent. With the help of essential chemistry on top of the hierarchical features, few designs can be presented to realize the surfaces that are capable of restoring the characteristics/behavior with time. This can be done by inducing either repairing or self-healing processes. The bioinspired superhydrophobicity developed is mainly owing to the co-occurrence of both the crucial surface chemistry and the proper hierarchical topography. However, the hierarchical topography is mostly generated by soft polymers or polymeric components which are prone to any damage when subjected to external pressures. Thus, it is challenging and also highly desirable to develop self-healable superhydrophobic materials for widespread applications in practical fields. Recently, Lv et al. [28] reported superhydrophobic shape memory polymer with self-healing ability in both damaged surface chemical composition and crushed hierarchical structures. This self-healing approach through the involvement of external stimuli is supposed to enforce a potential complexity in restoring the properties due to the difficulty in the maintenance of appropriate stimuli.

In this context, Das et al. [30] recently developed robust and self-healable superhydrophobic polymer coating with antifouling property restoring ability without the help of any external intervention. They designed structure of durable polymeric coatings, employing 1,4-conjugate addition reaction without any catalyst taking the combination of branched poly(ethylenimine) (BPEI), dipentaerythritol penta-acrylate (5Acl), and amino graphene oxide (AGO) nanocomplexes (depicted in Fig. 21). Michael addition reaction or covalent immobilization were adopted to form coating onto a modified fibrous substrate. The polymeric coating was subjected to the pressure of about 188 kPa to investigate the healing ability of physical integrity and the response of the material. On removal of pressure, both the characteristics and the deformation were found to be self-healed in the polymeric coating and ultimately developed superhydrophobic self-helable interfaces. The instantaneous rolling of a beaded water droplet with small tilting on the nonadhesive superhydrophobic surface dynamically helped in accumulating or detaching the dust and dirt ensuring a self-cleaning and waterproof surface.

The synthesized superhydrophobic polymeric coating exhibited reversible switching characteristics of two bioinspired wettabilities from nonadhesive (lotus leaf) to adhesive (rose petal) nature. Furthermore, this scalable, facile, and unique synthetic approach could be suitable for generating a superhydrophobic coating with unimpeachable resistance to physical or chemical invectives in broad areas and numerous potential applications.

Several authors have investigated the hydrophobic property using molecular dynamics simulation. Sbragaglia et al. [31] investigated the conspiring effects hydrophobicity and surface roughness and described the wetting and dewetting transitions of fluids in the presence of nanoscale grooves. In the same line, several authors have also investigated the blend compatibility [32] and self-clean [33, 34] properties for superhydrophobic coating applications.
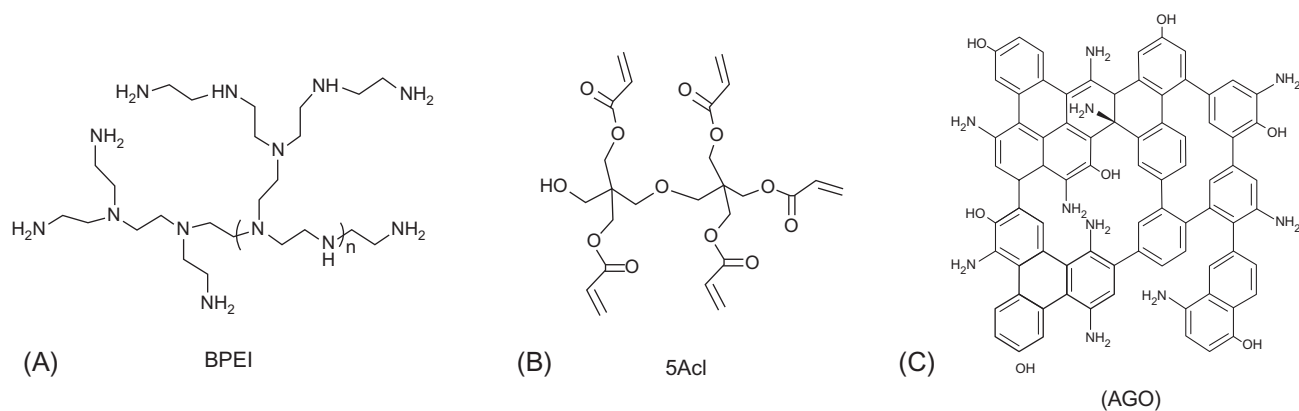
1,4-Conjugate addition reaction

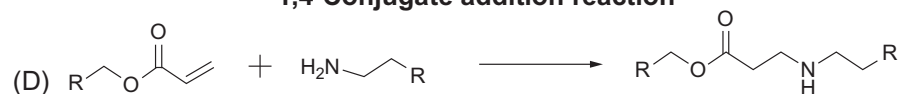**Fig. 21** Chemical structure of (A) poly(ethylenimine) (BPEI); (B) dipentaerythritol Penta-acrylate (5Acl); (C) amino-graphene oxide (AGO); and (D) 1,4-conjugate reaction. *(Reproduced with permission from A. Das, J. Deka, K. Raidongia, U. Manna, Robust and self-healable bulk-superhydrophobic polymeric coating, Chem. Mater. 29 (20) (2017) 8720–8728. Copyright 2017 American Chemical Society.)*

5. Conclusion

In this chapter, the naturally occurring superhydrophobic surfaces and the structural mechanism behind the hydrophobic phenomena are detailed. The biomimetic approach has been explained in fabricating different superhydrophobic polymers using micro-molding technique. Efficient and forceful methods have been demonstrated to develop superhydrophobic polymeric surfaces by biomimicking the naturally occurring hydrophobic leaf patterns with the help of repeated micro-molding. Based on recent findings, it is concluded that the combination of nanofillers (CB, CNT, and graphene platelets) enhance the superhydrophobicity of the polymer coatings and other desired properties. Considering the properties of these superhydrophobic coatings, it can be predicted for its easy scale up and various potential applications, like underwater drag reduction, oil filtration, and EMI shielding. The unique design of making durable and completely self-healable multifunctional surfaces could find an opportunity for smart applications, such as catalysis, delivery of hydrophilic small molecules, self-assembly, and reusable chemical sensing. Understanding the structure of the leaf surface and its biomimicking fabrication techniques in making a negative and positive replica of superhydrophobic polymers would enable researchers to realize the mechanism and inspire to develop industrial scale products. Though many noteworthy research attempts have been reported in last two decades in the field of superhydrophobic polymer surfaces, fabricating such smart products at industrial scale still remains a challenge and need to be addressed proactively with greater interest and attention.

References

[1] S.K. Sethi, G. Manik, Recent progress in super hydrophobic/hydrophilic self-cleaning surfaces for various industrial applications: a review, Polym. Plast. Technol. Eng. (2018) 1–21, https://doi.org/10.1080/03602559.2018.1447128.

[2] S. Nishimoto, B. Bhushan, K. Koch, P. Walzel, T. Ochiai, T. Murakami, A. Fujishima, K. Nakata, H. Sakai, T. Murakami, M. Abe, T. Komine, A. Fujishima, Bioinspired self-cleaning surfaces with superhydrophobicity, superoleophobicity, and superhydrophilicity, RSC Adv. 3 (2013) 671–690, https://doi.org/10.1039/C2RA21260A.

[3] C.S. Sharma, K. Abhishek, H. Katepalli, A. Sharma, Biomimicked superhydrophobic polymeric and carbon surfaces, Ind. Eng. Chem. Res. 50 (2011) 13012–13020, https://doi.org/10.1021/ie200369r.

[4] T. Young, An essay on the cohesion of fluids, Philos. Trans. R. Soc. Lond. 95 (1805) 65–87, https://doi.org/10.1098/rstl.1805.0005.

[5] A.C. Lima, J.F. Mano, Micro-/nano-structured superhydrophobic surfaces in the biomedical field: part I: basic concepts and biomimetic approaches, Nanomedicine 10 (2015) 103–119, https://doi.org/10.2217/nnm.14.174.

[6] C. Neinhuis, W. Barthlott, Characterization and distribution of water-repellent, self-cleaning plant surfaces, Ann. Bot. 79 (1997) 667–677, https://doi.org/10.1006/anbo.1997.0400.

[7] L. Feng, S. Li, Y. Li, H. Li, L. Zhang, J. Zhai, Y. Song, B. Liu, L. Jiang, D. Zhu, Super-hydrophobic surfaces: from natural to artificial, Adv. Mater. 14 (2002) 1857–1860, https://doi.org/10.1002/adma.200290020.

[8] Z. Guo, W. Liu, Biomimic from the superhydrophobic plant leaves in nature: binary structure and unitary structure, Plant Sci. 172 (2007) 1103–1112, https://doi.org/10.1016/J.PLANTSCI.2007.03.005.

[9] L. Feng, Y. Zhang, J. Xi, Y. Zhu, N. Wang, F. Xia, L. Jiang, L. Feng, Y. Zhang, J. Xi, Y. Zhu, N. Wang, F. Xia, L. Jiang, Petal effect: a superhydrophobic state with high adhesive force, Langmuir 24 (2008) 4114–4119, https://doi.org/10.1021/la703821h.

[10] S. Miyasaka, J. Hollyer, L.S. Kodani, Mulch and compost effects on yield and corm rots of taro, Field Crop Res. (2001) Elsevier, https://wwwsciencedirect.com/science/article/pii/S037842900100154X. (Accessed 13 September 2018).

[11] F. Shi, J. Niu, J. Liu, F. Liu, Z. Wang, X.-Q. Feng, X. Zhang, Towards understanding why a super-hydrophobic coating is needed by water striders, Adv. Mater. 19 (2007) 2257–2261, https://doi.org/10.1002/adma.200700752.

[12] X.J. Feng, L. Jiang, Design and creation of superwetting/antiwetting surfaces, Adv. Mater. 18 (2006) 3063–3078, https://doi.org/10.1002/adma.200501961.

[13] P. Vukusic, I. Hooper, Directionally controlled fluorescence emission in butterflies, Science 310 (2005) 1151, https://doi.org/10.1126/science.1116612.

[14] Y. Fang, G. Sun, T. Wang, Q. Cong, L. Ren, Hydrophobicity mechanism of non-smooth pattern on surface of butterfly wing, Chin. Sci. Bull. 52 (2007) 711–716, https://doi.org/10.1007/s11434-007-0120-5.

[15] J. Huang, X. Wang, Z.L. Wang, Controlled replication of butterfly wings for achieving tunable photonic properties, Nano Lett. (2006), https://doi.org/10.1021/NL061851T.

[16] G.D. Bixler, B. Bhushan, G.D. Bixler, B. Bhushan, Bioinspired rice leaf and butterfly wing surface structures combining shark skin and lotus effects, Soft Matter 8 (2012), http://pubs.rsc.org/en/content/articlehtml/2012/sm/c2sm26655e. (Accessed 18 September 2017).

[17] E.P. Ivanova, J. Hasan, H.K. Webb, V.K. Truong, G.S. Watson, J.A. Watson, V.A. Baulin, S. Pogodin, J.Y. Wang, M.J. Tobin, C. Löbbe, R.J. Crawford, Natural bactericidal surfaces: mechanical rupture of *Pseudomonas aeruginosa* cells by cicada wings, Small 8 (2012) 2489–2494, https://doi.org/10.1002/smll.201200528.

[18] M. Sun, A. Liang, G.S. Watson, J.A. Watson, Y. Zheng, J. Ju, L. Jiang, Influence of cuticle nanostructuring on the wetting behaviour/states on cicada wings, PLoS One 7 (2012) e35056, https://doi.org/10.1371/journal.pone.0035056.

[19] T. Li, T. Ren, J. He, The inspiration of nature: natural counterparts with self-cleaning functions, RSC Smart Mater. (2017) 1–24, https://doi.org/10.1039/9781782623991-00001.

[20] T. Shinohara, Y. Higaki, S. Nojima, H. Masunaga, H. Ogawa, Y. Okamoto, T. Aoki, A. Takahara, Molecular aggregation states and wetting behavior of a poly{2-(perfluorooctyl)ethyl acrylate} brush-immobilized nano-imprinted surface, Polymer (Guildf) 69 (2015) 10–16, https://doi.org/10.1016/J.POLYMER.2015.05.042.

[21] M. Liu, S. Wang, Z. Wei, Y. Song, L. Jiang, Bioinspired design of a superoleophobic and low adhesive water/solid interface, Adv. Mater. 21 (2009) 665–669, https://doi.org/10.1002/adma.200801782.

[22] X. Gao, X. Yan, X.X. Yao, L. Xu, K. Zhang, J. Zhang, B. Yang, L. Jiang, The dry-style antifogging properties of mosquito compound eyes and artificial analogues prepared by soft lithography, Adv. Mater. 19 (2007) 2213–2217, https://doi.org/10.1002/adma.200601946.

[23] W.R. Hansen, K. Autumn, Evidence for self-cleaning in gecko setae, Proc. Natl. Acad. Sci. U. S. A. 102 (2005) 385–389, https://doi.org/10.1073/pnas.0408304102.

[24] W.R. Tyson, W.A. Miller, Surface free energies of solid metals: estimation from liquid surface tension measurements, Surf. Sci. 62 (1977) 267–276, https://doi.org/10.1016/0039-6028(77)90442-3.

[25] K.K.S. Lau, J. Bico, K.B.K. Teo, M. Chhowalla, G.A.J. Amaratunga, W.I. Milne, G.H. McKinley, K.K. Gleason, Superhydrophobic carbon nanotube forests, Nano 3 (2003) 1701–1705, https://doi.org/10.1021/nl034704t.

[26] M.T.Z. Myint, G.L. Hornyak, J. Dutta, One pot synthesis of opposing 'rose petal' and 'lotus leaf' super-hydrophobic materials with zinc oxide nanorods, J. Colloid Interface Sci. 415 (2014) 32–38, https://doi.org/10.1016/J.JCIS.2013.10.015.

[27] H. Ogihara, J. Xie, J. Okagaki, T. Saji, Simple method for preparing superhydrophobic paper: spray-deposited hydrophobic silica nanoparticle coatings exhibit high water-repellency and transparency, Langmuir 28 (2012) 4605–4608, https://doi.org/10.1021/la204492q.

[28] T. Lv, Z. Cheng, E. Zhang, H. Kang, Y. Liu, L. Jiang, Self-restoration of superhydrophobicity on shape memory polymer arrays with both crushed microstructure and damaged surface chemistry, Small 13 (2017) 1503402, https://doi.org/10.1002/smll.201503402.

[29] A. Asthana, T. Maitra, R. Büchel, M.K. Tiwari, D. Poulikakos, Multifunctional superhydrophobic polymer/carbon nanocomposites: graphene, carbon nanotubes, or carbon black? ACS Appl. Mater. Interfaces 6 (2014) 8859–8867, https://doi.org/10.1021/am501649w.

[30] A. Das, J. Deka, K. Raidongia, U. Manna, Robust and self-healable bulk-superhydrophobic polymeric coating, Chem. Mater. 29 (2017) 8720–8728, https://doi.org/10.1021/acs.chemmater.7b02880.

[31] M. Sbragaglia, R. Benzi, L. Biferale, S. Succi, F. Toschi, Surface roughness-hydrophobicity coupling in microchannel and nanochannel flows, Nat. Mater. 2 (2003) 237, https://doi.org/10.1103/PhysRevLett.97.204503.

[32] S.K. Sethi, L. Soni, G. Manik, Component compatibility study of poly(dimethyl siloxane) with poly(vinyl acetate) of varying hydrolysis content: an atomistic and mesoscale simulation approach, J. Mol. Liq. (2018), https://doi.org/10.1016/J.MOLLIQ.2018.09.048.

[33] N. Kumar, G. Manik, Molecular dynamics simulations of polyvinyl acetate-perfluorooctane based anti-stain coatings, Polymer (Guildf) 100 (2016) 194–205, https://doi.org/10.1016/j.polymer.2016.08.019.

[34] V.H. Dalvi, P.J. Rossky, Molecular origins of fluorocarbon hydrophobicity, Proc. Natl. Acad. Sci. U. S. A. 107 (2010) 13603–13607, https://doi.org/10.1073/pnas.0915169107.

CHAPTER 2

Superhydrophobic polymer coating: A design perspective

Vikramaditya Shirsat, N. Abhinayaa, Anagha Sabnis
Dept. of Polymer and Surface Engineering, Institute of Chemical Technology, Mumbai, India

1. Introduction

Superhydrophobic surfaces have gained a huge attention due to their water–repellent nature and self–cleaning properties which are also commonly identified as the "lotus-effect." A roughness on both a micro and nanoscale and a low surface energy material are necessary conditions in order to mimic the properties of the lotus leaf found in nature. Superhydrophobic surfaces are generally characterized by a water contact angle (WCA) above 150 degrees, a low contact angle (CA) hysteresis (<10 degrees), and a low roll–off angle (<10 degrees) at which a water droplet rolls off a tilted surface [1]. Detailed reviews about the concept of superhydrophobicity have been explored by many of the researchers. In general, the wetting behavior can be classified into four different regimes based on WCA. WCA in the range of 0 degrees $< \theta <$ 10 degrees, 10 degrees $< \theta <$ 90 degrees, 90 degrees $< \theta <$ 150 degrees, and 150 degrees $< \theta <$ 180 degrees are termed as superhydrophilic, hydrophilic, hydrophobic, and superhydrophobic, respectively [2].

Hydrophobicity of a surface (wettability) is characterized by the static CA between the surface and water droplet. The CA depends on numerous factors including roughness, energy, preparation, and cleanliness of the surface [3]. Marmur points out that two factors define superhydrophobicity: a very high WCA and a very low roll–off angle, defined as the inclination angle at which a water drop rolls off the surface. High quality superhydrophobic surfaces exhibit a roll–off angle of less than 1 degree [4]. The enhancement of superhydrophobicity, through a hierarchical surface roughness where a nano-scale topology is superimposed on surface microscale roughness, has now been widely studied. In many cases, this has been related to fractal behavior [5].

The concept of wettability of rough surfaces has been investigated since the 1930s. However, the topic has received significant attention in the past few years due to the development of nanotechnology applications. The wetting of a solid by a liquid is characterized by the CA, which is the angle between the solid-air and the liquid-air interfaces. The more hydrophobic the material, the greater is the CA. The value of the CA is usually greater when the liquid is added (the so-called advancing CA) than when it is removed (the receding CA). The difference between the advancing and receding CA s constitutes

CA hysteresis. CA hysteresis is related to energy barriers, which a liquid droplet should overcome during its flow along a solid surface, and thus characterizes the resistance to flow [6].

McHale points out that during evaporation the wetting state changes from the Cassie-Baxter state to the Wenzel state when the droplet becomes smaller than a critical value on patterned surfaces [7]. Wetting on rough surfaces may assume either of two regimes: homogeneous wetting [8], where the liquid completely penetrates the roughness grooves, or heterogeneous wetting [9], where air (or another fluid) is trapped underneath the liquid inside the roughness grooves. The apparent CA on a rough surface in the homogeneous regime, W, is given by the Wenzel equation.

$$\cos \theta_W = r \cos \theta_Y$$

where θ_Y is the ideal Young CA and r is the roughness ratio, defined as the ratio of the true area of the solid surface to its projection area. It is clearly seen that if a surface is hydrophobic ($\theta_Y > 90$ degrees); roughness ($r > 1$) makes θ_W higher than θ_Y [8].

The apparent CA in the heterogeneous regime, θ_{CB}, is given by the Cassie-Baxter (CB) equation.

$$\cos \theta_{CB} = r_f \cos \theta_Y + f - 1$$

where f is the fraction of the projected area that is wet and r_f is the roughness ratio of the wet area. A high quality superhydrophobic surface will have a uniform layer of trapped or pinned air that produces a very high CA (approaching 180 degrees), a very low roll-off angle (approaching 0 degrees), small CA hysteresis (approaching 0 degrees), and will produce an optical mirror effect when the surface is submerged in water due to total internal reflections of light reflecting off the pinned air layer [9].

The relation between the water droplet size and surface geometric parameters governs the transition from composite solid-air-liquid interface to a homogeneous solid-liquid interface on superhydrophobic surfaces. The study presents the effect of varying droplet size on the wetting properties of patterned Si surfaces [3].

Two strategies are employed generally in the application of superhydrophobic coatings. The surface is first coated with a low surface energy material which has a WCA typically ranging between 90 degrees and 120 degrees on a flat substrate. Most of the materials used for this purpose contain hydrocarbons and fluorinated compounds. The other technique is to generate a sufficient level of roughness on the surface. An ideal surface should have a hierarchical topography that has features spanning multiple length scales that extend from micrometers to nanometers [10].

Rixens et al. point out that fluorinated polymers are most commonly used for superhydrophobic coatings due to their extremely low surface energies [11]. Ipekci et al. recently reported a self-healing superhydrophobic and superoleophobic coating that was made of fluorinated-decyl polyhedral oligomeric silsesquioxane and hydrolyzed

fluorinated alkyl silane (FAS). The coating not only restored its superrepellent feature after being damaged chemically but also showed excellent durability against both washing and abrasion treatments [10]. Zhou et al. developed superhydrophobic coatings mainly for the textile fibers. These highly durable superhydrophobic coatings were obtained by deposition of fluorinated and siloxane-containing compounds on fabrics benefiting from the presence of inherent microscale roughness in these materials [12].

In recent years, there has been an increasing interest in developing superhydrophobic surfaces of microscale to nanoscale architecture. Superhydrophobic nano-coatings have emerged to be important techniques in generating surface superhydrophobicity with remarkable change in surface and interfacial fields. In this chapter, the design perspective of superhydrophobic polymeric coatings has been discussed in detail.

2. Chemical modification

In past superhydrophobic surfaces were fabricated by using materials with low surface energy. Polytetrafluoroethylene (PTFE) is one of the most widely used polymers containing fluorine which can give superhydrophobicity. The hydrophobicity of materials can be improved by introducing organic groups like $-CF_3$, $-CH_3$, and $-CH_2-$, etc. The superhydrophobic materials can also be achieved by using polyethylene, polystyrene, polyvinyl chloride, polydimethylsiloxane (PDMS), and certain types of polyesters and polyurethanes (PUs) [13].

2.1 Fluorine-based coatings

A superhydrophobic paint was synthesized by using perfluorooctyltriethoxysilane (PFOTES), TiO_2 nanoparticles (NPs), and ethanol. The dipping, painting, and spraying methods were used for applying superhydrophobic paints to various substrates like an aquatic application even with high loading. In first step PFOTES was mixed with pure ethanol and the mixture was stirred for 5 min. SiO_2 NPs were added to the system under constant stirring. Depending on the viscosity of the superhydrophobic paint obtained it was applied by either dip or spray technique regardless the size and structure of aquatic vehicle along with the incorporation of adhesive [14].

The high molecular mass polystyrene or poly (vinyl acetate) as polymer binders were used along with 3-(heptafluoroisopropoxy) propyltrimethoxysilane (HFIP-TMS)-treated diatomaceous earth (DE) particles for preparing superhydrophobic coatings. DE is a highly hydrophilic material and it turns into superhydrophobic diatomaceous earth (HFIP-DE) after treating it with HFIP-TMS. Initially, 2 g of DE along with 20 mL of toluene was taken in a flask and 1% of *para*-toluenesulfonic acid was added to the mixture. HFIP-TMS was then added to the mixture in various quantities (0.01–1.0 mL). The mixtures were heated to 50°C for 4 h. Then after centrifugation of sample with 20 mL of hexane for the removal of excess unreacted fluorosilane the

supernatant was discarded. For removal of solvent and water, the samples were heated to 140°C for 4 h. The superhydrophobic polymer coatings were prepared by using different amounts of HFIP-DE (0%–70%) with polystyrene or poly (vinyl acetate). The mixtures were dispersed in 3.5-mL tetrahydrofuran solvent. The HFIP-TMS-treated DE particles with grafted silane amount of 1.2% or more found to be suitable for preparing superhydrophobic coatings. Superhydrophobicity of the polymer coatings depended on the fraction of surface being covered with treated DE particles. DE particles after reacting with fluorinated silane coupling agent can only appear on the surface regardless of their micro or nanosize. The highly superhydrophobic coatings could be achieved by increasing the mass fraction of treated DE and the micro-nano-hierarchical roughness [15].

Zhao et al. prepared the superhydrophobic coating by two-step process. The silica NP precursors (Si NPs) with different sizes were prepared as the central particles while the packet particles were synthesized on the central particle precursors simply through self-assembling of functional fluoride-silica NPs (F-Si NPs) by addition of tetraethoxysilane (TEOS) and perfluorodecyl triethoxysilane (HDFTES). The Stober process was used for synthesizing core silica NP precursors (Si NPs) of variable sizes followed by the addition of variable amounts of TEOS to the mixture over a period of 6 h at room temperature. The initial contents of TEOS were responsible for controlling the diameters of the prepared Si NPs. The packet particles were synthesized directly on the core particle precursors. The F-Si NPs were synthesized by addition of a small volume of TEOS and HDFTES mixture with different molecular ratios to the suspension. The F-Si–Si raspberry-like NPs suspension was obtained after the reaction. The raspberry-like NPs were superhydrophobic and showing good abrasion resistance and extremely water impact resistance due to surface roughness and low surface energy coating. The raspberry-like NPs have an effect on the surface macro-morphology, due to which it was applicable to various substrates like glass, plastic, metal, and paper [16].

The copolymers of fluoroalkyl methacrylates (FMAs) containing three to seven fluorine atoms in their monomer unit and glycidyl methacrylate (GMA) on the textured aluminum surface gives superhydrophobic properties to the polymer coatings. The modification of nontextured aluminum surfaces with polymers was based on FMAs which results in highly hydrophobic coatings with a CA of up to 120 degrees. To achieve superhydrophobic surfaces on aluminum substrates is a little difficult. This can be overcome by reliable chemical attachment of low surface energy polymers to the substrate. A mineral acid etching method was proposed for chemical attachment. The reduction of free surface energy was achieved via the modification of textured supports with copolymers that are based on FMAs and GMA. FMAs ensure water-repelling properties, and GMA acts as an attachment due to the presence of epoxide groups that can react with hydroxyl groups of the substrate.

The hydrochloric acid solutions with concentrations ranging from 2 to 5 M were used for etching of the aluminum surface. A GMA:FMA mole ratio of 0.6:1 was taken for the

synthesis of copolymers in MEK for 24 h at 70°C. The overall concentration of mono-mers was 1 mol/L. AIBN was used as an initiating agent. The copolymer was precipitated in cold hexane and then was dried under reduced pressure for 24 h. Three weight percent solutions of GMA- and FMA-based copolymers were prepared in MEK. It is possible to achieve a superhydrophobic state with CAs up to 169 degrees. The initial wetting mode is practically independent of fluorine content in the monomer unit. When the samples are in a water environment, the superhydrophobic state stability was increased with the increase in fluorine content from three to seven atoms in fluoroalkyl methacrylate [17]. Fluoro compounds get bioaccumulated and pose a serious threat to humans at various levels that encompass fluorosis and other neurological disorders [18].

2.2 Polyurethane coatings

The hydrophobically modified silica nanoparticles with finely tuned sizes and reactive silanol groups were introduced into bicomponent acrylic PU resin. A superhydrophobic coating with both nonwetting property and excellent mechanical properties was obtained based on the micro- and nanometer scale roughness structures constructed by hydrophobic silica NPs and their interaction with the resin matrix which can be applied by spraying method.

The superhydrophobic coatings were synthesized by dissolving hydroxyl acrylic resin into butyl acetate to make a homogeneous dilute resin solution along with F-silica NPs. Then hexamethylene diisocyanate was added based on the molar ratio of isocyanate groups to that of hydroxyl groups in part A of 1.1:1. After mixing both parts the coating can be applied by spraying or dropwise to the glass substrate. Superhydrophobic coating with good chemical resistance was synthesized based on bicomponent acrylic resin and fluoroalkyl silane modified silica NPs. The reaction between surface hydroxyl groups on F-silica NPs and isocyanate groups combined film forming property of acrylic resin and low surface energy, micro and nanoscale roughness of F-silica NPs. The resulting super-hydrophobic acrylate PU coating displayed a WCA higher than 162 degrees and a slip angle lower than 10 degrees [19].

2.3 Additive-type superhydrophobic coatings

To impart superhydrophobicity to a surface, additive particles may be employed in considerable amounts to a coating system. Recently, NPs have been used to achieve super-hydrophobicity via surface roughening. One method is to deposit the NPs on microroughened substrates to induce submicron-scale surface roughness on substrates are then treated chemically or covered with low surface energy coatings to enhance the hydrophobic nature of the produced surfaces. Another method is to mix the NPs with polymer solutions and then deposit on smooth surfaces such as glass and silicon.

2.4 Silicates and carbonates

Anitha et al. have applied the principles of Salvinia effect in superhydrophobic substrates. The metal silicates in silicone resin along with nanosilica, nanotitania, and aluminum stearate were used for synthesizing fluorine-free superhydrophobic coatings. The epoxy resin with no pigments and additives showed hydrophobic behavior with WCA of 93.5 degrees and tilting angle (TA) of 60 degrees. The incorporation of metal silicates resulted in increasing WCA to 156.8 degrees and TA to 28 degrees.

The obtained silica from rice husk was dissolved in 2.5 N sodium hydroxide and then neutralized with the 2.5 N solution of cobalt, copper, iron (III), and nickel chloride individually. The excess metal ions, chlorides and other impurities from the obtained gel were removed by water. The coatings formulation was formulated with fixed 36% volume solids and fixed 15% pigment volume concentration. In addition to the prepared silicates, other pigments like nanotitania, nanosilica, and aluminum stearate were used. The silicates prepared from rice husk were used for preparing salvinia inspired superhydrophobic coatings. The silicone resin was modified by various silicates like cobalt silicate, copper silicate, iron silicate, and nickel silicate. The prepared silicate pigments were hydrophilic in nature and imparted pinning effect, that is, Salvinia effect in the coating. The utilized nanosilica, nanotitania, aluminum stearate imparted multiscale roughness along with the pinning effect. The prepared superhydrophobic coatings have hydrophilic pigments to create with air retention property. This novel underwater air retaining superhydrophobic coatings has applications in the field of pipeline construction and shipbuilding [20].

The superhydrophobic composite films were prepared by adding SiO_2 NPs of various sizes into trimethoxyhexadecylsilane (THS) solutions. The formed composite films, with different NP concentrations and sizes, exhibit hierarchical structures in micro and nanoscale that are positively important for superhydrophobicity. THS was dissolved in white spirit to form the silane solutions of 6 wt%. Also, PDMS was also dissolved in white spirit to prepare PDMS solutions of 6 wt%. Silica (SiO_2) particles with average sizes of 7 and 14 nm were used for making THS–SiO_2 and PDMS–SiO_2 solutions in various concentrations. The THS–SiO_2 solutions were applied through the airbrush system while PDMS–SiO_2 solutions were dip coated onto test substrates due to the relatively high viscosity of PDMS.

The hierarchical structure of composite films with high roughness leads to the formation of superhydrophobic properties. The SiO_2 particles with 14 nm have a stronger potential to promote high CAs and stable CA hysteresis than 7-nm SiO_2 particles. The NP concentration with 2.0% w/v shows optimum behavior in terms of superhydrophobicity [21].

The layer-by-layer (LbL) deposition of poly(diallyldimethylammonium chloride) (PDDA)/sodium silicate multilayer films on a silica-sphere-coated substrate followed

with a fluorination treatment was used for preparing superhydrophobic surface. Initially, silica spheres of 600 and 220 nm were prepared on silica sphere coated surface and cross-linked with SiCl$_4$. Then a micro- and the nanostructured hierarchical surface was prepared by alternately assembling PDDA with sodium silicate. A superhydrophobic surface was successfully fabricated after chemical vapor deposition of fluoroalkylsilane. This superhydrophobic coating can be used as self-cleaning surfaces, antiadhesive coatings [22].

The superhydrophobic antireflective (AR) coatings in near-infrared region (NIR) were fabricated on silicon or quartz substrates by an LbL assembly technique. Initially, LbL deposition of PDDA and 200 nm SiO$_2$ NPs were used for synthesizing a porous PDDA/SiO$_2$ NP multilayer coating with AR. A two-level hierarchical surface on the PDDA/SiO$_2$ NP coating was prepared by alternately assembling PDDA with sodium silicate. Superhydrophobic AR coating was obtained after chemical vapor deposition of fluoroalkylsilane on the hierarchical surface with a WCA of 154 degrees. Quartz substrate with superhydrophobic AR coating can transmit a maximum above 98% of incident light in the NIR region, which is 5% more as compared with bare quartz substrate.

The adhesion of the subsequently deposited PDDA/SiO$_2$ NP films was promoted by the deposition of the precursor layer. A layer of SiO$_2$ NPs was deposited on top of PDDA layer. By repeating the deposition process of PDDA and SiO$_2$ NPs layers were arranged in a cyclic fashion. The AR coating with the introduction of superhydrophobicity has the potential of water repellency which results in the application of AR coatings in humid environments [23].

The superhydrophobic coatings were synthesized by using dimethyldiethoxy silane, TEOS, and hexamethyldisilazane as precursors. The source of nanoclay was obtained from organically modified montmorillonite clay. The concentration of hybrid silica sol was varied in superhydrophobic coatings and they can be applied by dip coating technique on soda lime glass substrates. The optimized compositions and heat treatment conditions of sol and nanoclay fillers were required for the generation of WCAs as high as 170 ± 2 degrees. A superhydrophobic behavior can take place due to the steric hindrance caused owing to the number of methyl groups on the surface, which may obstruct the silylation to take place. A high clay concentration and optimized process parameters like coating parameters, solvents, and curing temperatures can results in superhydrophobicity with WCAs up to 170 degrees and very low sliding angles [24].

Also, many researchers studied the fabrication of fluorine-free superhydrophobic coating which involves silicone binder, pigments like nanosilica, nanotitania, and magnesium silicate and aluminum stearate as additives. To prepare the superhydrophobic coatings, a simple one-step spraying process was applied using silicone polymer and micro/nano pigments. This method involved micro/nano pigments that self-organize by agglomeration to form micro/nano roughness required for superhydrophobic coatings. The pristine resin with no pigments and additives show hydrophobic behavior with WCA of 93.5 degrees and TA of 60 degrees. With the incorporation of pigments and

additives, the WCA raised to 152.5 degrees and TA to 20 degrees. The roughness increased and achieved an appropriate value to attain superhydrophobicity with increased concentration of nanosilica [25].

Yousefi et al. synthesized a noble robust superhydrophobic and highly oleophobic PU—SiO$_2$ NP coating using the sol–gel process. This new coating exhibits good pensile hardness as high as 6H with adhesive force grade of 5B. The concentration of the SiO$_2$ NPs and (heptadecafluoro-1,1,2,2-tetrahydrodecyl) trimethoxysilane FAS additive were varied in the coating solutions and oil/water contact and tilt angles were measured to ensure the optimal amphiphobicity. As a result, the PU-SiO$_2$ coating showed a water/oil CAs of 159 degrees/140 degrees and a SAs of 3 degrees/10 degrees, which can retain CAs of 150 degrees/130 degrees after 7 days immersion in water, respectively [26].

Zhao studied the superhydrophobic surfaces with excellent abrasion resistance using benzoxazine/mesoporous SiO$_2$. A variable amount of mesoporous SiO$_2$ (SBA-15) (weight ratio was varied from 5% to 30%) and (Bisphenol A-aniline benzoxazine monomer) BA-a mixture was spraying to a glass slide. Then the coated glass slide was put into an oven at 120°C for 2 h and 220°C for 2 h. The surfaces showed microstructures and nanostructures, with the roughness rising (Rq: >3 μm) with increasing content of SBA-15 from 15% to 30%. All surfaces became superhydrophobic with WCAs exceeding 150 degrees. For the superhydrophobic surface formation, randomly stacked SBA-15 generated microstructures and nanostructures, which in combination with BA-a (low-surface-energy material), rendered the surface in the Cassie state, leading to superhydrophobicity [27].

Hardman et al. described a facile route for the in situ modification of the surface properties of fibers produced by electrospinning polystyrene containing small quantities of compatible polymer additives, end-functionalized with 1–3 fluoroalkyl groups. During the electrospinning process, such additives undergo spontaneous surface segregation resulting in fibers with low surface energy, fluorine-rich, superhydrophobic surfaces. Additives with 1, 2, and 3 C$_8$F$_{17}$ groups were investigated, and an increase in surface hydrophobicity was achieved by increasing the number of fluoroalkyl groups [28].

Xie et al. described in their work, micro-nanostructure polydimethylsiloxane/silicon dioxide (PDMS/SiO$_2$) composite coatings were fabricated on the surface of magnesium alloys with two different sizes of SiO$_2$ NPs by a simple painting method. SiO$_2$ particles with two different sizes (40 nm and 50–250 nm) modified by fluorine and PDMS were used to form micro-nano rough structure. They studied the influence of the proportion of different-sized particles on the wettability, wear, and corrosion performance of the composites. When the concentration of SiO$_2$ particles (40 nm) is more than 40 wt%, the coatings are hydrophobic, and the samples with 0.2 g SiO$_2$ (40 nm)/0.7 g, SiO$_2$ (50–250 nm) and 0.3 g SiO$_2$ (40 nm)/0.7 g, SiO$_2$ (50–250 nm) are superhydrophobic [29].

Wu et al. discovered a simple and facile methodology to prepare superhydrophobic poly(vinylidene fluoride) (PVDF) membrane via nonsolvent-induced phase inversion process. The addition of hydrophobically modified SiO_2 nanoparticles (HMSNs) in ethanol bath resulted in PVDF precipitation dominantly by solid-liquid demixing, and the obtained membrane was uniformly skinless and composed of spherical microparticles. He pointed out that, ethanol containing well-dispersed commercial hydrophobic modified SiO_2 nanoparticles (HMSNs) were used as a coagulation bath. The WCA of the obtained membranes gradually enhanced with the increase in HMSNs concentration. Increase in the HMSNs concentration benefited the antiwettability improvement. Higher HMSNs concentration in bath introduced more HMSNs on the membrane surface and formed superhydrophobic surface with WCA greater than 160 degrees [30].

The demand for effective self-cleaning, water repellant coatings has been developing over the past few years. Achieving superhydrophobic coatings with good mechanical durability has always been a key challenge. Kumar et al. created a superhydrophobic surface by the introduction of silica NPs in a polyvinylidene fluoride matrix (PVDF). In order to improve the adhesion of the coating to the substrate and to lower the surface energy, aminopropyltriethoxysilane (APTES) and FAS were used as surface-functionalizing agents respectively. The combination of a fluorinated polymer matrix and inorganic particulate fillers (SiO_2) and surface functionalizing agent APTES produced coatings with improved mechanical properties and good adhesion with the substrate. The static CA of the composite coating with PVDF:$SiO_2 = 1$:1 by weight was found to be 154 degrees with a sliding angle of <2 degrees [31].

Nano-silica particles were deposited on acid-etched hydrophilic aluminum (Al) substrates by immersion in well-dispersed nano-silica aqueous suspension and tetramethylammonium hydroxide, followed by heat treatment. The surface was then further treated by a reaction with fluorosilane. The use of nano-silica (with 0.025%, 0.05%, 0.1%, 0.2% suspensions) suspension significantly enhanced the hydrophobicity of the coated Al. The acid-etched Al substrates first treated with nano-silica suspension then with fluorosilane all showed a WCA in the range of 155–158 degrees, that is, superhydrophobicity. There was a slight increase in WCA as the concentration of nano-silica particles in the suspension increased from 0.025% to 0.1%, but further increase to 0.2% in particle concentration did not show any benefit in enhancing the WCA. The Al substrates treated with 0.1% and 0.05% nanosilica suspension featured the highest micro roughness and nano roughness, respectively [32].

The superhydrophobic coatings were synthesized by using nano-sized calcium carbonate ($CaCO_3$) particles modified with heptadecafluorodecyl trimethoxysilane under acidic water conditions. The hydrophobic coatings were manufactured with polyacrylate binder prepared via radical copolymerization of methyl methacrylate, butyl acrylate, acrylic acid, and b-hydroxyethyl methacrylate and modified $CaCO_3$. The modified $CaCO_3$ and the polyacrylate in a weight ratio of 8/2 were required for obtaining a

superhydrophobic coating with WCA of 155 degrees. The superhydrophobic property of coatings can be attributed to both the surface microstructure and the surface enrichment of fluoroalkyl chains [33].

2.5 Zinc oxide

The low surface energy additives or modifiers were used for preparing superhydrophobic hierarchical ZnO nanostructures by a convenient, inexpensive, and a reproducible method. WCA as high as 163.8 ± 1.5 degrees and lower CA hysteresis CAH$=1.2$ degrees were obtained by the prepared sample, indicating excellent superhydrophobic properties. A layer of the prepared ZnO particles was placed on a steel mesh as the support. The gravity force was used for the separation process of a mixture of chloroform/water (50%, v/v). The WCA and CAH values of superhydrophobic coatings were about 163.8 ± 1.5 degrees and 1.2 degrees, respectively. The separation of chloroform from water was successfully done by superhydrophobic ZnO particles with a satisfying separation efficiency, high flux, and good reusability. These coatings can be used for coating the metal meshes and cotton fabrics for oil–water separation process [34].

A simple and economical method was used to fabricate a superhydrophobic Zn coating with ZnO nanosheets on steel substrates. The superhydrophobicity was achieved by low-energy modification with pentadecafluorooctanoic acid and the Zn coating with ZnO nanosheets on steel substrate, with WCA of 158 degrees and the sliding angle of about 6 degrees. The prepared superhydrophobic Zn coating with ZnO nanosheets exhibited good stability and excellent self-cleaning property [35].

Arukalam et al. prepared a series of hydrophobic and superhydrophobic coatings by sol–gel process based on perfluorodecyltrichlorosilane (FDTS), nano–ZnO particles of varying diameters and poly(dimethylsiloxane) (PDMS) in ratio of 2:1, 1:1, and 1:2:: PDMS:nano–ZnO particles in each case. Nano–ZnO particles were selected to impart surface roughness and antimicrobial properties to the coatings and fluorinated decyltrichlorosilane (FDTS) for surface modification. He pointed out that the addition of FDTS and variation in diameter of nano–ZnO fillers and PDMS: nano–ZnO ratios influenced the liquid repellency, surface features, thermal stability, and tensile properties of the coatings considerably. The ZnO particles with the smallest diameter in series at a ratio of 1:1 with PDMS resulted in the highest barrier and anticorrosion properties [36].

2. Conclusion

The environmental conditions have played a prominent role in inspiring the researchers for the development of artificial superhydrophobic coatings. The concept of superhydrophobicity has been gaining tremendous attention these days with increasing demand in various applications such as metal refining, oil–water separation, self-cleaning, etc. Earlier, fluorinated compounds were used most commonly due to their ease of availability

and low surface energies but currently considering the environmental impacts and toxicity the halogenated compounds are not widely used. Nano-SiO_2, –ZnO, and –TiO_2 have attracted the researchers to a great extent in superhydrophobic coatings. Though there has been remarkable progress in the development of superhydrophobic coatings, there are still lot more opportunities to explore in the development of optimized coating.

References

[1] L. Ovaskainen, S. Chigome, N.A. Birkin, S.M. Howdle, N. Torto, L. Wågberg, C. Turner, Superhydrophobic polymeric coatings produced by rapid expansion of supercritical solutions combined with electrostatic deposition, J. Supercrit. Fluids 95 (2014) 610–617.

[2] A. Marmur, Terminology of wettability classification, Soft Matter 8 (2012) 6867–6870.

[3] Y.C. Jung, B. Bhushan, Wetting transition of water droplets on superhydrophobic patterned surfaces, Scr. Mater. 57 (2007) 1057–1060.

[4] A. Marmur, The lotus effect: superhydrophobicity and metastability, Langmuir 20 (2004) 3517–3519.

[5] F. Bottiglione, G. Carbone, Role of statistical properties of randomly rough surfaces in controlling superhydrophobicity, Langmuir 29 (2013) 599–609.

[6] M. Nosonovsky, Multiscale roughness and stability of superhydrophobic biomimetic interfaces, Langmuir 23 (2007) 3157–3161.

[7] G. McHale, S. Aqil, N.J. Shirtcliffe, M.I. Newton, H.Y. Erbil, Analysis of droplet evaporation on a superhydrophobic surface, Langmuir 21 (2005) 11053–11060.

[8] R.N. Wenzel, Resistance of solid surfaces to wetting by water, Ind. Eng. Chem. 28 (1936) 988–994.

[9] B.Y.A.B.D. Cassie, S. Baxter, Wettability of porous surfaces, Physics (College Park, Md) 40 (1944) 546–551.

[10] H.H. Ipekci, H.H. Arkaz, M.S. Onses, M. Hancer, Superhydrophobic coatings with improved mechanical robustness based on polymer brushes, Surf. Coat. Technol. 299 (2016) 162–168.

[11] B. Rixens, R. Severac, B. Boutevin, P. Lacroix-Desmazes, Y. Hervaud, Migration of additives in polymer coatings: phosphonated additives and poly(vinylidene chloride)-based matrix, Macromol. Chem. Phys. 206 (2005) 1389–1398.

[12] H. Zhou, H. Wang, H. Niu, A. Gestos, X. Wang, T. Lin, Fluoroalkyl silane modified silicone rubber/nanoparticle composite: a super durable, robust superhydrophobic fabric coating, Adv. Mater. 24 (2012) 2409–2412.

[13] K. Bazaka, O. Bazaka, Superhydrophobic polymers, in: Superhydrophobic Surfaces, Elsevier, 2015, pp. 67–85.

[14] G.B. Hwang, A. Patir, K. Page, Y. Lu, E. Allan, I.P. Parkin, Buoyancy increase and drag–reduction through a simple superhydrophobic coating, Nanoscale 9 (2017) 7588–7594.

[15] B.R. Sedai, B.K. Khatiwada, H. Mortazavian, F.D. Blum, Development of superhydrophobicity in fluorosilane-treated diatomaceous earth polymer coatings, Appl. Surf. Sci. 386 (2016) 178–186.

[16] Z.B. Zhao, D.M. Zhang, Y.F. Meng, L. Tai, Y. Jiang, One-pot fabrication of fluoride-silica@silica raspberry-like nanoparticles for superhydrophobic coating, Ceram. Int. 42 (2016) 14601–14608.

[17] E.V. Bryuzgin, V.V. Klimov, S.A. Repin, A.V. Navrotskiy, I.A. Novakov, Aluminum surface modification with fluoroalkyl methacrylate-based copolymers to attain superhydrophobic properties, Appl. Surf. Sci. 419 (2017) 454–459.

[18] N. Oruc, Occurrence and problems of high fluoride waters in Turkey: an overview, Environ. Geochem. Health 30 (2008) 315–323.

[19] F. Xue, D. Jia, Y. Li, X. Jing, Facile preparation of a mechanically robust superhydrophobic acrylic polyurethane coating, J. Mater. Chem. A 3 (2015) 13856–13863.

[20] C. Anitha, S. Syed Azim, S. Mayavan, Salvinia inspired fluorine free superhydrophobic coatings, Appl. Surf. Sci. 449 (2018) 250–260.

[21] N. Gao, Y.Y. Yan, X.Y. Chen, X.F. Zheng, Superhydrophobic composite films based on THS and nanoparticles, J. Bionic Eng. 7 (2010) S59–S66.

[22] L. Zhang, H. Chen, J. Sun, J. Shen, R.V. October, V. Re, M. Recei, V. December, Layer-by-layer deposition of poly (diallyldimethylammonium chloride) and sodium silicate multilayers on silica-sphere-coated substrate; facile method to prepare a superhydrophobic surface, Chem. Mater. 19 (2007) 948–953.

[23] L. Zhang, Y. Li, J. Sun, J. Shen, Layer-by-layer fabrication of broad-band superhydrophobic antire-flection coatings in near-infrared region, J. Colloid Interface Sci. 319 (2008) 302–308.

[24] R. Subasri, H. Hima, Investigations on the use of nanoclay for generation of superhydrophobic coatings, Surf. Coat. Technol. 264 (2015) 121–126.

[25] C. Anitha, S.S. Azim, S. Arunkumar, S. Mayavan, Progress in organic coatings one pot fabrication of superhydrophobic anticorrosive coating without fluoro compounds and inhibitive pigments, Prog. Org. Coat. 125 (2018) 137–145.

[26] E. Yousefi, M.R. Ghadimi, S. Amirpoor, A. Dolati, Preparation of new superhydrophobic and highly oleophobic polyurethane coating with enhanced mechanical durability, Appl. Surf. Sci. 454 (2018) 201–209.

[27] G. Zhao, Superhydrophobic surfaces with excellent abrasion resistance based on benzoxazine/meso-porous SiO_2, Mater. Lett. 186 (2016) 274–278.

[28] S.J. Hardman, N. Muhamad-Sarih, H.J. Riggs, R.L. Thompson, J. Rigby, W.N.A. Bergius, L.R. Hutchings, Electrospinning superhydrophobic fibers using surface segregating end-functionalized polymer additives, Macromolecules 44 (2011) 6461–6470.

[29] J. Xie, J. Hu, X. Lin, L. Fang, F. Wu, X. Liao, H. Luo, L. Shi, Robust and anti-corrosive PDMS/SiO_2 superhydrophobic coatings fabricated on magnesium alloys with different-sized SiO_2 nanoparticles, Appl. Surf. Sci. 457 (2018) 870–880.

[30] X. Wu, B. Zhao, L. Wang, Z. Zhang, J. Li, X. He, H. Zhang, X. Zhao, H. Wang, Superhydrophobic PVDF membrane induced by hydrophobic SiO_2 nanoparticles and its use for CO_2 absorption, Sep. Purif. Technol. 190 (2017) 108–116.

[31] D. Kumar, L. Li, Z. Chen, Progress in organic coatings mechanically robust polyvinylidene fluoride (PVDF) based superhydrophobic coatings for self-cleaning applications, Prog. Org. Coat. 101 (2016) 385–390.

[32] X. Shi, T. Anh, Z. Suo, J. Wu, J. Gong, R. Avci, Electrochemical and mechanical properties of super-hydrophobic aluminum substrates modified with nano-silica and fluorosilane, Surf. Coat. Technol. 206 (2012) 3700–3713.

[33] H. Wang, L. Tang, X. Wu, W. Dai, Y. Qiu, Fabrication and anti-frosting performance of super hydro-phobic coating based on modified nano-sized calcium carbonate and ordinary polyacrylate, Appl. Surf. Sci. 253 (2007) 8818–8824.

[34] E. Velayi, R. Norouzbeigi, Synthesis of hierarchical superhydrophobic zinc oxide nano-structures for oil/water separation, Ceram. Int. 44 (2018) 14202–14208.

[35] H. Li, S. Yu, J. Hu, E. Liu, A robust superhydrophobic Zn coating with ZnO nanosheets on steel sub-strate and its self-cleaning property, Thin Solid Films 666 (2018) 100–107.

[36] I.O. Arukalam, E.E. Oguzie, Y. Li, Nanostructured superhydrophobic polysiloxane coating for high barrier and anticorrosion applications in marine environment, J. Colloid Interface Sci. 512 (2017) 674–685.

CHAPTER 3

Methods and fabrication techniques of superhydrophobic surfaces

Aditya Kumar[a], Debasis Nanda[b]
[a]Department of Chemical Engineering, Indian Institute of Technology (Indian School of Mines), Dhanbad, India
[b]Department of Chemical Engineering, National Institute of Technology, Rourkela, India

1. Introduction

Surfaces with high water contact angle (>150 degrees), low sliding angle, antisticking, anticontamination, and self-cleaning effect are called superhydrophobic. These properties are attractive for many industrial and biological applications such as antibiofouling paints for boats, antisticking of snow for antennas and windows, self-cleaning windshields for automobiles, microfluidics, lab-on-a-chip devices, metal refining, stain-resistant textiles, antisoiling architectural coatings, and dust-free coatings on building glasses [1–6]. In nature, many kinds of special surfaces such as lotus leaves, rice leaves, butterfly wings, mosquito eyes, moth eyes, cicada wings, red rose petals, gecko feet, desert beetle, spider silks, and fish scales exhibit excellent hydrophobicity and/or superhydrophobicity [7–12]. These natural structures suggest new idea for designing the artificial superhydrophobic structures.

There are mainly two approaches of producing superhydrophobicity: creating hierarchical structures (micro- and nanostructures) on hydrophobic substrates or chemically modifying a hierarchical structured surface with a low surface energy material [13–20]. The various methods synthesis of superhydrophobic/oleophobic surfaces have been reported in literature such as electrochemical deposition [21], phase separation [22], emulsion [23], plasma method [24], template method [25,26], electrospinning [27], solution immersion [28], chemical vapor deposition (CVD) [29], wet chemical reaction [30], crystallization control [31], sol–gel processing [32–35], lithography [36], and others [37–39]. Some of these are simple and inexpensive; however, some of these involve multistep procedures and harsh conditions or require specialized reagents and equipment, which leads to increase the cost of coating.

Isotropic, high roughness, transparent superhydrophobic surfaces can be created using plasma etching; however, it requires costly precursor leading to increasing cost of coating. Chemical etching process creates hierarchical structures. Although it is cheap, simple, and facile method, but there are complication of mask selection and anisotropic etching. X-ray or atomic force microscopy (AFM) lithography creates regular patterns, but it

requires very costly equipment. Photolithography is also costly as well as slow process for producing high roughness and large area of periodic micro/nano patterns. Electron beam lithography can create accurate and excellent nanostructured superhydrophobic coatings, but it is having issues of charging, shot noise, and interaction between parallel electrons. Nanoimprinting process creates hierarchical structure superhydrophobic surfaces and is cheap and efficient process; however, this is having issue of overlay, bubble defects, template patterning, and template wear. Self-assembly is a facile, cheap, and time–saving method, but it requires a suitable precursor and defects due to weak intermolecular interaction. Electrochemical method is efficient, fast, facile, and low cost, but it is not environmental friendly. Among all synthesis techniques, dip coating, spray, spin, and sol–gel methods are cheap, fast, and easy to produce accurate and homogeneous superhydrophobic surfaces.

Since several years, the endless efforts have been carried out to develop the synthesis techniques to prepare superhydrophobic/oleophobic surfaces for industrial scale which are economical, easy to produce, environmental safe, high efficient, well adhesive, compatible, and high durability; but most of them are restricted to only fundamental research in laboratory and there is still much work required to be done for superhydrophobic/oleophobic surfaces preparation on commercial scale.

2. Theoretical background

Wetting of the surface takes place when water droplets spread on the surface and spreading is generally due to the presence of high-energy molecules on the surface which has a high affinity toward water. Static contact angle of the water droplet for these surfaces is found to be low. On the other hand, to repel water droplets from the nonwetting surfaces, static contact angle of water droplets need to be high. Increase in the contact angle of water makes the droplet spherical in shape which makes the minimum contact of droplet on the surface.

Static contact angle of water on a surface is determined by Young's equation (Eq. 1) on the rested droplet on the surface as shown in Fig. 1.

$$\gamma(sv) - \gamma(sl) - \gamma(lv) \cos \theta = 0 \qquad (1)$$

where θ is the contact angle, $\gamma(sv)$ the solid–vapor interfacial energy, $\gamma(sl)$ the solid–liquid interfacial energy, and $\gamma(lv)$ the liquid–vapor interfacial energy.

Based on the contact angle, wettability of the surface is also divided into four types, that is, superhydrophilic ($\theta \sim 0$ degrees, complete wetting of the surface), hydrophilic ($\theta < 90$ degrees, partial wetting of the surface), hydrophobic ($\theta > 90$ degrees but < 150 degrees, partial nonwetting of the surface), and superhydrophobic ($\theta > 150$ degrees, complete nonwetting of the surface).
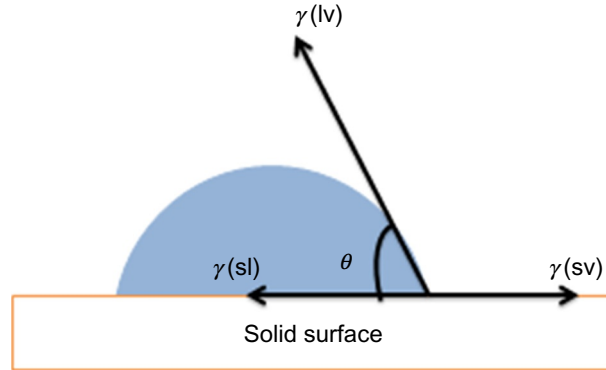
Fig. 1 Schematic diagram of contact angle measurement by Young's Experiment.

Another factor for surface to be self-cleaned is sliding angle or contact angle hysteresis which is shown in Fig. 2. It is measured by the difference between the advancing contact angle (θ_a) and the receding contact angle (θ_r) formed when the sample is tilted and liquid droplet starts to roll down due to the gravitational force. For self-cleaning application of superhydrophobic surface, the sliding angle of the sample must be <10 degrees.

Roughness plays an important role in generating superhydrophobic surfaces. Water droplet behavior changes according to the roughness. There are mainly two proposed models based on the roughness for superhydrophobic surface and these are:

2.1 Wenzel state

Wenzel state was proposed by Robert N. Wenzel [40]. It defines that the superwetting surface with roughness is a homogenous surface with no air pockets between the grooves as shown in Fig. 3.

When a droplet is placed on the surface, part of it penetrates into the grooves and subsequently it reduces the static contact angle and increases the sliding angle.
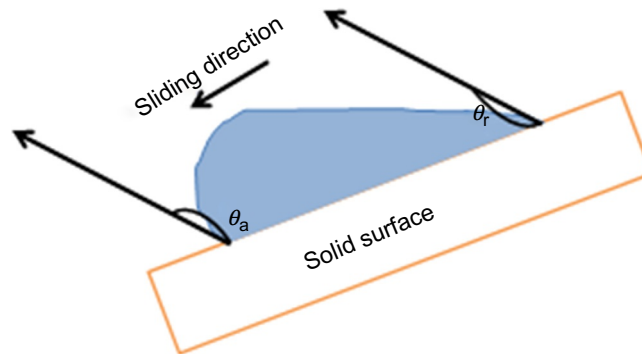

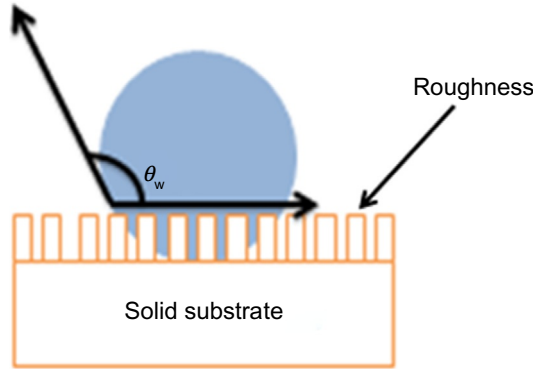**Fig. 2** Schematic diagram of contact angle hysteresis.

Fig. 3 Schematic diagram of Wenzel state on superwetting surface.

Increase in the sliding angle is due to the locking of droplet in between the grooves which is called as pinning. Wenzel proposed an equation which is given by

$$\cos \theta_{w} = r \cos \theta \qquad (2)$$

where θ_{w} is apparent contact angle which corresponds to the stable equilibrium state, r is roughness factor, and θ is Young's contact angle. Roughness factor is defined as ratio of true area and apparent area of the solid surface. Value of roughness factor is 1 and >1 for smooth and rough surface, respectively. According to the Wenzel theory, with increase in roughness wettability increases for hydrophilic surface. Whereas the adverse condition of wettability takes place for hydrophobic surface.

2.2 Cassie-Baxter state

This model was proposed by Cassie and Baxter [41]. It defines that rough surface is heterogeneous in nature with air pockets present in between the grooves of the roughness. Droplet remains on the surface and does not penetrate through it as shown in Fig. 4.
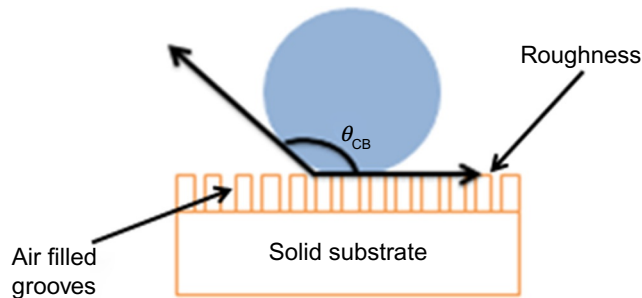

Fig. 4 Schematic diagram of Cassie Baxter state on superwetting surface.

In this model, the sliding angle or contact angle hysteresis is low compared to the Wenzel model. The Cassie-Baxter equation is given by

$$\cos \theta_{CB} = f_1 \cos \theta_1 + f_2 \cos \theta_2 \tag{3}$$

where θ_{CB} is the Cassie-Baxter contact angle, f_1 and f_2 are the surface fraction of phase 1 and phase 2, and θ_1 and θ_2 are the contact angle on phase 1 and phase 2. For the air-liquid surface, Eq. (3) can be further reduced to

$$\cos \theta_{CB} = f \cos \theta + f - 1 \tag{4}$$

where f is the solid fraction, that is, fraction of solid surface is wetted by the liquid.

Transition of the state from Cassie–Baxter state to Wenzel state can take place by applying pressure on droplet [42], varying the droplet size [43], and impact of droplet or by vibration [44,45].

3. Synthesis techniques

There are two main approaches for creating superhydrophobic surfaces: creating micro/nano-hierarchical structures on hydrophobic substrates and chemically modifying a hierarchical structured surface with a low surface energy material such as fatty acid, polymers, hydrocarbons, and fluorocarbons. The various methods of synthesis of these surfaces have been reported in literature such as electrochemical deposition, phase separation, emulsion, electrospinning, immersion, CVD, wet chemical reaction, lithography, and others. This chapter provides the overview of the recent progress in the synthesis and difficulties arise during the implementation of superhydrophobic surfaces.

3.1 Dip coating technique

Dip coating technique is a well-suitable process for the production of nanometric thick coatings. It is a continuous process in which the substrate is immersed into a solution of the material to be deposited at a constant immersion rate. After immersing of substrate in solution for a period, it starts to be pulled up. The film is deposited on the substrate while is pulled up. The withdrawal or pulling speed controls the thickness of the film. High speed produces a thin film. The excess of solution is drained from the surface while withdrawing. The solvent present in solution is evaporated, resulting a coating on the surface. It has several advantages such as simultaneous coating of top and bottom part of substrate, no wastage of material, suitable for all kind of materials, high output, uniform, highly durable, compact, stable coatings, and easily repairable. However, in this process, all components used in coating have to be submersible.

Using the dip coating technique, several works on superhydrophobicity have been published. For example, Zhang et al. [46] carried out a simple dipping process for the preparation of superhydrophobic coatings based on titanium dioxide nanowires dispersed

in tetrahydrofuran (THF) followed by the addition of polydimethylsiloxane (PDMS). Coating showed the water contact angle of 158 ± 2 degrees. After UV irradiation water contact angle reduced to 25 degrees. Coating had self-cleaning property.

Cui et al. [47] constructed a three-step procedure for fabrication of superhydrophobic epoxy paints through sandblasting and anchoring of SiO_2 nanoparticles. To enhance hydrophobicity, it was dip coated with modified epoxy adhesive. The apparent contact angles were found as high up to 167.8 ± 1.6 degrees. These superhydrophobic surfaces showed high durability and stability against scouring tests, neutral and basic aqueous solutions, organic solvents such as toluene and ethanol.

Klien et al. [48] fabricated a superhydrophobic surface on a polycrystalline alumina substrate by dip coating technique with a dilute suspension which was formed by dispersing nano-silica spheres. After a low-temperature heat treatment, the particles adhered to the surface. The surface was made hydrophobic by a reaction with a solution containing fluoroalkyltrichlorosilane which resulted in hydrophobicity increase due to decreasing area fraction of spheres.

Cengiz et al. [49] produced superhydrophobic and oleophobic rough copolymer surfaces by phase separation method using styrene-perfluoromethacrylate random copolymers which were dip coated on glass slides with THF and methyl ethyl ketone mixture containing methanol as nonsolvent. An increment of 146–160 degrees for water contact angle and 65–90 degrees for hexadecane contact angle was obtained.

Mahadik et al. [50] developed a simple and inexpensive method to fabricate superhydrophobic surfaces by preparing superhydrophobic silica coatings using organic-inorganic silica precursor methyltrimethoxysilane (MTMS) on quartz substrate by dip coating method. The water contact angle was achieved as 168 ± 2 degrees and water sliding angle as 3 ± 1 degrees. This coating surface showed properties of water repellency and superoleophilic nature along with the durability, thermal stability, and optical transparent nature.

Ramezani et al. [51] fabricated transparent superhydrophobic silica films by dip coating process on a glass substrate. These films have properties like high optical transmission and thermal stability. The water repellency of the silica films was controlled by a surface-modifying agent isooctyltrimethoxysilane (iso-OTMS). The maximum contact angle was achieved as 160 degrees. By using dip coating technique, Gao and He [52] developed broadband antireflective superhydrophobic coatings based on three types of sol: (1) silica sol obtained by hydrolysis of tetraethyl orthosilicate (TEOS) under acidic condition, (2) silica nanoparticle suspension prepared by Stober method, and (3) mesoporous silica nanoparticle suspension followed by CVD of 1H,1H,2H,2H-perfluoro octyltriethoxysilane. The maximum transmittance of coating achieved was 95.3% at a wavelength of 630 nm with a water contact angle of 153 degrees and sliding angle of <5 degrees. These antireflective superhydrophobic coatings have promising applications in solar cells optical detection, sensors, etc.

Liu et al. [53] fabricated a compact TiO_2 coatings on anodized aluminum surface by vacuum dip coating technique. This coating prevents aluminum corrosion in seawater.

Rao et al. [54] used dip coating technique to coat water–repellent porous silica films on glass substrate. A maximum static contact angle of 164 degrees and minimum sliding angle of 4 degrees was achieved. These films have self–cleaning and anticorrosive applications.

Nanda et al. [55] dip coated aluminum surface to make the surface superliquiphobic (both superhydrophobic and superoleophobic) in nature with self-cleaning and antifogging properties. The coated sample was stable to thermal, mechanical, and chemical test. Super-liquiphobic surface was able to repel water, ethylene glycol, glycerol, and hexadecane from its surface and showed contact angle of 168.0 ± 2.7 degrees, 165.0 ± 4.0 degrees, 166.0 ± 3.5 degrees, and 155.0 ± 4.1 degrees with sliding angle of $<3.0 \pm 0.5$ degrees, $<4.0 \pm 0.5$ degrees, $<4.2 \pm 0.5$ degrees, and 6.2 ± 0.5 degrees, respectively.

Sun et al. [56] fabricated superhydrophobic surfaces on zinc substrate by electrochemical processing using a mixed electrolyte composed of $NaNO_3$ and $NaCl$ followed by dip coating process with fluoroalkylsilane ethanol solution. The maximum water contact angle achieved was 165.3 degrees and tilting angle of 2 degrees.

3.2 Spin coating technique

Spin coating technique is used for making a thin coating on relatively flat substrates. The solution of material to be coated is deposited onto the substrate which is spun off at a high velocity in a range of 1000–8000 rpm and leaving a uniform layer. The angular speed, the solution viscosity, and the spinning time determine the ultimate thickness of the deposited film [57]. Thickness of film can be changed by changing spin speed or switching to a different photoresist. It is an excellent technique on laboratory scale. Despite of all advantage, it has demerit of incapable for large substrate, lack of material efficiency, and cost of disposal.

By employing spin coating technique, several works on superhydrophobicity have been published. For example, Soz et al. [58] carried out multistep spin coating of dispersed hydrophobic fumed silica on polymer-coated glass surface. Prior to coating, two different surfaces were developed on the glass surface by spin coating polymer films [hydrophobic segmented silicone urea copolymer and hydrophilic poly(methyl methacrylate) (PMMA), respectively]. The prepared sample exhibited contact angle >150 degrees with an average roughness of 125–150 nm.

Zhang et al. [59] prepared a MgAl-layered double hydroxide (LDH) film by spin coating a nanodispersed MgAl–LDH sol on an AZ31 magnesium alloy substrate. The corrosion resistance offered by the LDH films increases with the thickness of the film. These LDH films were also environment friendly corrosion-resistant coatings.

Eskandari et al. [60] used copper (II) acetate as a starting material for the preparation of cuprous oxide thin films and treating them in N_2 atmosphere at low temperature through

two-step sol–gel spin coating method. The contact angle achieved here is 45 degrees which results in hydrophilic surface and the surface can be used in photoelectrochemical application such as water splitting.

Zhang et al. [61] fabricated photoresponsive superhydrophobic surfaces by immobilizing fluorinated azobenzene derivatives onto silica surfaces which was prepared by spin coating silica particles on silicon wafers followed by modification with polydopamine. The water contact angle achieved was more than 150 degrees and the contact angle hysteresis was <10 degrees.

Xu et al. [62] fabricated transparent and robust superhydrophobic surfaces by spin coating of fluorosilane-modified silica nanoparticles on surfaces such as Si wafers, glass substrate, PMMA, and polyester fabric. In this method, pre- and posttreatment of the substrate was not required. The advancing water contact angle achieved was more than 150 degrees and water droplet roll-off angle was <5 degrees.

He and Wang [63] fabricated superhydrophobic ZnO nanorods on zinc foil substrate by electrochemical deposition. After being spin coated by perfluoroalkyl methacrylic copolymer (Zonyl 8607) over the ZnO surface, the maximum contact angle achieved was 167 degrees. It finds application as anticontamination, antifouling, and self-cleaning films.

3.3 Spray coating technique

In this technique, solution of materials to be coated is sprayed on the substrate by means of spray gun. The coating precursor is generally heated-melted by electrical or chemical means. This process is having several advantages such as simple, high availability, possibility of automation, quick, cost effective, repairable, and nontoxic. This technique can also be applied on substrates like plastics, metals, and fabrics. This coating method also finds applications in self-cleaning wind shields in automobiles and anticorrosive applications. Besides all the merits, it has also some limitations such as wastage of the material compared to other processes, high consumption of material, over spray, difficult to produce thick coatings, low degree of adhesion on small substrate, and extremely difficult for the substrate with small curvature.

Using this technique, several works have been published. For examples, Kim and Cho [64] used airbrush of 400 μm diameter nozzle for spray coating a sol–gel of polystyrene (PS) and multiwalled carbon nanotubes (MWCNTs) on cover glass. The prepared sample showed mechanically and aging stable superhydrophobic property with water contact angle of 163.8±2.5 degrees and water sliding angle 5.0±0.9 degrees.

Zhang et al. [65] synthesized superhydrophobic aluminum by single-step spray coating with sol–gel of methylsilicate functionalized hydrophobic SiO_2 nanoparticles and glass resin on chemically etched aluminum surface. The developed sample was

mechanically stable with regenerable property and has a static water contact angle of 155 degrees and a roll of angle of 4 degrees.

Cui et al. [66] prepared a micelle solution of PS and comb-structured fluorinated main chain with narrowly dispersed grafted chain. This micelle solution was then spray coated on aluminum oxide particles sandblasted glass surface to change its wettability to superhydrophobic. The sample exhibited maximum contact angle of 160 degrees and the sliding angle <6 degrees.

Ma et al. [67] created easily restorable superhydrophobic coating on cellulose substrates like leather, cotton fabrics, and filter papers. First, the polyacrylate emulsion was spray coated on the surface followed by spray coating hydrophobic silica nanoparticles. Superhydrophobicity was achieved with static contact angle of 170.3 degrees and sliding angle of 2 degrees after having eight layers of HN-SiO$_2$ spray coated on it.

Latthe and Rao [68] used single-step spray coating method to achieve superhydrophobic coating on glass surface by spraying sol–gel of MTMS and derived SiO$_2$ microparticles. The coating increased the contact angle of water to 162 ± 2 degrees and roll-off angle of 6 ± 1 degrees.

Tarwal et al. [69] created superhydrophobic surface on glass surface using spray pyrolysis technique (SPT). Seed-assisted growth of polycrystalline thin-film ZnO was prepared on glass surface which showed a maximum contact angle of 165 degrees which assured its applications in different fields like smart windows, biochips, environmental cleanups, microfluid devices, etc.

Ovaskainen et al. [70] used spray coating of rapid expansion of a supercritical solution (RESS) technique to make the surface of silica wafers superhydrophobic. Solution of poly (ε-caprolactone) (PCL) and a statistical copolymer of vinyl acetate and vinyl pivalate [P(VAc-VPi)] was coated in the presence of acetone as cosolvent which increased the static contact angle ranging from 120 to 155 degrees.

Xu et al. [71] fabricated chemically inert and anticorrosive superhydrophobic coating on copper mesh using single-step spray coating technique. The sample was prepared by the reaction of metals and alkanethiols which was formed by solution of silver nitrate in ethanol solution and *n*-octadecanethiol. The sample showed a static contact angle of above 158 degrees for different pore size mesh.

3.4 Electrochemical deposition technique

The principle of electrochemical deposition is inducing chemical reactions in an aqueous electrolyte solution with the help of applied voltage. Getting material into arbitrary three-dimensional (3D) geometry is a great strength of this process. It is also a low-energy process and therefore, uniquely suited for dealing with modification of soft matters. It also offers unique spatial selectivity and is flexible and cheap process [72]. It is well suited of

nano-, bio-, and microtechnologies. It can be used to grow functional material through complex 3D masks. It can be performed near room temperature from water-based electrolytes. It can be scaled down to the deposition of few atoms or up to large dimensions. This method is time saving, environment friendly. The main limitation of electrochemical deposition is in size and strength. It is only suitable for selected size and poor strength of structures. Moreover, it is required high temperature during deposition and has less control in growth.

This technique has potential to contribute for fabrication of superhydrophobic metal coatings industrially. For example, Liu et al. [73] synthesized controlled adhesion superhydrophobic coating on copper surface by one-step electrodeposition method. The adhesion force was controlled based on the reaction time. The copper surface was immersed in an electrolyte solution of cerium chloride and myristic acid in ethanol which increased the water contact angle to maximum of 161.7 degrees after 30 min of electrodeposition with low adhesion. It is observed that superhydrophobic property was achieved after 10 min of reaction time with high adhesion. Further increase in time the adhesion force reduces and had a low adhesion at 30 min of reaction time. The prepared sample was stable to different pH and also showed anticorrosive property.

Cao et al. [74] prepared superhydrophobic Bi/Bi_2O_3 surface by two facile single-step methods, that is, displacement reaction and electrodeposition. A layer of Bi_2O_3 was developed by the deposited Bi by surface passivation that changed the surface morphology to hierarchical porous dendritic structures that increased the water contact angle to 164 degrees.

Zhao et al. [75] changed the wettability of stainless steel surface to superhydrophobic by electrochemical deposition. First, microstructures were created by polishing with abrasive paper and then the roughed surface was electrodeposited by $Cu(CH_3(CH_2)_{12}COO)_2$ for 3 h that increased the water contact angle to 154.5 degrees.

Zhang et al. [76] changed the layer-by-layer (LBL) coated polyelectrolyte surface of indium tin oxide (ITO) to superhydrophobic by electrodeposition method with gold clusters. The prepared sample had a water contact angle of 156 degrees after 1000 s of electrodeposition followed by immersing overnight with n-dodecanethiol. The contact angle further increased to 173 degrees after 40 min exposure to ambient temperature.

Li et al. [77] developed a thin film of conductive hydrophobic zinc oxide layer on ITO glass substrate. The zinc oxide layer was deposited by cathodic electrochemical deposition. The wettability was then further decreased by modifying the surface with hydrolyzed (heptadecafluorodecyl)trimethoxysilane that increased the contact angle of water to 152 ± 2 degrees. The prepared superhydrophobic conductive thin films have an application in developing microfluidic devices.

Gnedenkov et al. [78] synthesized anticorrosive titanium, low-carbon steel, and magnesium alloy by deposition of silica nanoparticles dispersions on pretreated plasma electrolytic oxidation (PEO) metal surfaces. The roughed surface was further treated with

N,N,N-trimethyl–1–{3–[(2,2,3,3,4,4,5,5,6,6,7,7,8,8,8–pentadecafluorooctyl)–oxy]–propyl}–silane that increased the contact angle of water higher than 160 degrees.

Wang et al. [79] prepared biomimetric hierarchy structure on aluminum surface by three different steps. First, anodized porous alumina (APA) fabrication technique was used to form a template. These templates were electrodeposited by nickel and copper to form nanometer pillars between the pores of the aminopropyltriethoxysilane (APS) developed alumina surface. The roughed surface was then treated with fluoroalkylsilane that increased the contact angle of water to 152 degrees, tilt angle of 6 and 157 degrees, and tilt angle of 3 degrees for nickel and copper deposited nanopillars, respectively.

Mahajan et al. [80] developed superhydrophobic coating with static contact angle of 177 degrees on the surface of copper foil. Porous copper were deposited on the surface by electrodeposited galvanostatically via a hydrogen bubble templating method in the presence of CuTCNQ and CuTCNQF$_4$.

He and Wang [63] reduced the wettability of the zinc surface as the contact angle increased to 167 degrees by electrochemical deposition method. ZnO nanorods were grown on the surface of ZnO film by electrodeposition followed by spin coating with perfluoroalkyl methacrylic copolymer to achieve superhydrophobicity. The prepared samples have a promising application in the field of anticontamination, antifouling, and self–cleaning films.

Sun et al. [56] changed the surface of zinc surface to superhydrophobic by electrochemical processing in the presence of mixture of NaNO$_3$ and NaCl as electrolyte. The roughed surface was then dip coated in fluoroalkylsilane ethanol solution that increased the contact angle of water to 165.3 degrees and sliding angle of 2 degrees.

Huang et al. [81] electrodeposited copper on the surface of aluminum to create the desired roughness. The roughed surface was again electrochemically modified by stearic acid to increase the contact angle to 157 degrees.

Han et al. [82] developed superhydrophobic magnesium surface by electrodepositing of nickel on the surface followed by reducing the surface energy by stearic acid to achieve a contact angle 144.5 degrees.

3.5 Chemical etching process

Chemical etching is a process in which the surface elements are made to react by wet method, that is, by using highly acidic or basic solutions. It is required simple equipment with no capital investment. It provides high etching rate and high selectivity; therefore, it is fast process. The technique used is ecofriendly and also corrosion resistant. Along with many advantages, it has some demerits. It leads the contamination of the substrates. It requires high amount of etchant chemicals as they have to be consistently replaced in order to keep the same initial etching rate. It has poor process control.

Many studies have been reported in synthesis of superhydrophobic surfaces on different substrates using chemical etching method. For instance, Qian and Shen [83] chemically etched the surface of aluminum, copper, and zinc with Beck's dislocation etchant, Livingston's dislocation etchant and HCl solution, respectively. The etched surfaces were then immersed in the solution tridecafluoroctyltriethoxysilane to change the surfaces top superhydrophobic. Static water contact angle of 156, 153, and 155 degrees were achieved for aluminum, copper, and zinc after 15 s, 24 h, and 90 s of etching, respectively followed by fluoroalkyl treatment.

Quan et al. [84] synthesized antiicing coating on the surface of copper and aluminum surfaces. The surfaces were roughened by chemical etching with HCl solution followed by mixture of NaOH and $(NH_4)_2S_2O_8$ for copper surface. Similarly, aluminum surface was chemically etched by solution of equi–volume of oxalic acid and hydrochloric acid. The etched surfaces were treated with stearic acid to achieve a contact angle of 158.3 degrees and 158.6 degrees for copper and aluminum, respectively.

Qi et al. [85] prepared self–cleaning, antireflective coating on silicon wafer by chemically etching the surface with KOH and silver catalytic etching. The etching produced a hierarchical structures of pyramidal type which when treated with heptadecafluoro-1,1,2,2-tetrahydrodecyl triethoxysilane to increase the contact angle to 169 degrees and sliding angle <3 degrees.

Shi–heng et al. [86] developed superhydrophobic aluminum surface with contact angle of 151.3 degrees by chemically etching the surface by NaOH in ultrasonic bath followed by modifying the surface with 1H,1H,2H,2H-perfluorodecyltriethoxysilane.

Xie and Li [87] also fabricated superhydrophobic coating on surface of aluminum plate by chemically etching the surface with boiling aqueous solution of NaOH and then modifying the etched surface with lauric acid. The superhydrophobic aluminum surface exhibited a contact angle of >150 degrees.

Hao et al. [88] changed the surface of zinc into superhydrophobic and oleophobic where the water contact angle and peanut oil contact angle were measured to be 151.85 degrees and 145.62 degrees, respectively. The dual property on zinc surface was achieved by chemical etching with HCl followed by hydrothermal treatment with ammonium hydroxide. The etched surface was then modified by perfluorooctanoic acid to make the surface repel both water and oil.

Liao et al. [89] created roughness of micro/nano binary structures by chemically etching the aluminum surface first by $CuCl_2$ to achieve microstructures then by HCl to form nanostructures. These roughed surfaces were then treated with hexadecyltrimethoxy silane to achieve a contact angle of 161.9 ± 0.5 degrees. The prepared samples showed antiicing property and were stable to high temperature, exposure to sea water and sand abrasion test.

Liu et al. [90] created the roughness on aluminum surface by chemically etching the surface with hydrochloric acid. The etched surface was coated with polypropylene and

PS and polypropylene grafting maleic anhydride to make the surface superhydrophobic with contact angle of 157 degrees and 159 degrees, respectively.

Shen et al. [91] developed superhydrophobic coating on Ti_6Al_4V alloy surface. Surface was first sandblasted to create micro-roughness on which nanostructures were created. Different nanostructures such as nanowire by hydrothermal method, nanotube by anodic oxidation and nanomesh by two-step chemical reaction were developed. These surfaces were then modified with FAS-17 that increased the contact angle to 161 degrees and tilting angle of 6 degrees.

Xu et al. [92] achieved a contact angle of 151 degrees on the surface of copper foil by wet chemical etching method. The surface of copper foil was chemically etched with sodium hydroxide and sodium persulfate. Further, a thin film of Au was sputtered on this etched surface followed by surface modification by *n*-dodecanethiol solution to make the surface superhydrophobic.

Li et al. [93] achieved superhydrophobic property with low friction coefficient and anticorrosive property on copper surface. The superhydrophobic coating on copper surface was carried out by two-step immersion method. The surface roughness were created by acid etching in solution of $(NH_4)_2S_2O_8$ and HCl and then immersion in silver nitrate solution (replacement reaction). The roughed surface was then modified with stearic acid to increase the water contact angle to 160.5 degrees.

Lee et al. [94] developed superhydrophobic silicon surface with contact angle ~180 degrees. The silicon wafer was first immersed in Cu plating solution followed by immersion in solution of HF and H_2O_2 to form micro-nanostructure roughness. The roughed surface was then treated with Teflon by spin coating to achieve a highly superhydrophobic surface which can be used for microfluid transportation and self-cleaning applications.

Nimittrakoolchai and Supothina [72] chemically etched the polyelectrolyte layer coated glass surface by HCl solution to develop microporous roughness. SiO_2 nanoparticles were then deposited followed by surface modification with trichloro (1*H*,1*H*,2*H*,2*H*-perfluorooctyl) silane to increase the contact angle of water to 152 ± 4 degrees. The prepared sample had a good antiadhesive property and high optical transparency property.

Varshney et al. [95] developed mechanically, chemically, UV, and thermally stable superhydrophobic coating on aluminum surface by chemically etching the surface with HCl followed by surface modification with lauric acid. The static water contact angle was measured to be 172 ± 5 degrees and sliding angle of 4 ± 0.5 degrees. The prepared sample exhibited good self-cleaning and antifogging property.

Kumar and Gogoi [96] etched the surface of aluminum with mixture of HCl and HNO_3 to form microstructure roughness. The roughed surface was further modified with hexadecyltrimethoxysilane (HDTMS) to make the surface superhydrophobic with water contact angle 162.0 ± 4.2 degrees and tilting angle of 4 ± 0.5 degrees with self-

cleaning property. Besides this, the prepared sample was thermally, mechanically, and chemically stable.

Varshney et al. [97] prepared superhydrophobic steel mesh for oil–water separation. The sample was first chemically etched in a solution of hydrochloric acid and nitric acid followed by surface modification with lauric acid. The sample was mechanically, chemically, and thermally stable with static contact angle of 171 ± 4.5 degrees and a sliding angle of 4 ± 0.5 degrees.

Lomga et al. [98] synthesized self–cleaned, antifogged, and regenerable superhydrophobic aluminum surface by chemical etching with NaOH followed by surface modification with lauric acid. The prepared aluminum surface exhibited water contact angle of 170 degrees and sliding angle of 5 degrees. The prepared sample was mechanically and thermally stable. The sample was able to regenerate its property by immersing the sample in lauric solution.

Varshney et al. [99] developed superhydrophobic coating on aluminum surface by chemical etching with acid mixture of hydrochloric and nitric acids. The etched surface was then immersed in lauric acid solution to make the surface superhydrophobic with static contact angle of 170 ± 3.9 degrees and sliding angle of 4 ± 0.5 degrees. The prepared sample showed good self-cleaning and antifogging properties. Besides this, the samples were stable to mechanical disturbances.

Varshney et al. [100] fabricated superhydrophobic surface with static contact angle of 153 degrees and tilting angle of 5 degrees. The aluminum surface was chemically etched with KOH solution and was then modified by immersing in lauric acid. The prepared superhydrophobic aluminum surface showed self-cleaning and anticorrosive property. Besides this, the sample showed good mechanical, thermal, and UV stability.

3.6 Plasma-etching technique

It involves a high stream speed of glow discharge of an appropriate gas mixture being shot at a sample. The plasma generates volatile etch products and they etch the sample. Plasma treatment of surfaces can create micro/nanostructures. This technique has several advantages such as capability of automation, low material consumption, anisotropic, cheap, clean technique, chemical specific, and little damage to photoresist. It has several disadvantages such high capital investment, large number of process parameters to control (surface geometry, types of gases, flow rates, system conductance, radio frequency power to drive chemical reactions, water load, and patterning), resulting difficult to duplicate in other reactors, radiation from plasma causes surface damage, and poor pattern transfer and gases are quite toxic.

By employing plasma–etching technique, several studies have carried out for creating superhydrophobic surfaces. For example, Gao et al. [101] carried out two-step method in developing superhydrophobic zinc surface with water contact angle of 158 degrees and

sliding angle <5 degrees. The surface was treated with glow discharge electrolysis plasma (GDEP) for etching and surface functionalization by stearic acid. The prepared sample exhibited good stability to different pH and long-term environmental exposure.

Barshilia and Gupta [102] prepared superhydrophobic (PTFE) surfaces plasma etching of the surface by argon and oxygen. The etched surface exhibited a water contact angle of 158 degrees after 4 h of treatment. These surfaces can be implemented in different applications in field of biomedical, biotechnological, and electrical insulation.

Youngblood and McCarthy [103] synthesized superhydrophobic surface on polypropylene surface with water contact angle of carried out 172 degrees. Polypropylene surface was simultaneously etched and was coated by PFTE using inductively coupled radio frequency argon plasma.

Balu et al. [104] achieved superhydrophobicity on different type of papers surfaces by plasma-enhanced etching and film deposition of pentafluoroethane that increased the contact angle to 159.4 degrees.

Teshima et al. [105] synthesized superhydrophobic coating on poly(ethylene terephthalate) substrates by two dry step method. The surface was first etched by selective oxygen plasma etching to develop nano texture surface roughness followed by surface modification by plasma–enhanced CVD of heptadecafluoro-1,1,2,2-tetrahydrodecyl-1-trimethoxysilane. The superhydrophobic surface has a contact angle of more than 150 degrees with good transparency property.

Psarski et al. [106] developed nanostructured epoxy/γ-Al_2O_3 nanoparticle composite by replicating the microstructures developed on aluminum surface by laser. The derived nanocomposite was then treated with air plasma for creating nanoroughness by etching. The etched surface was then modified by dip coating in 1H,1H,2H,2H-perfluorotetradecyltriethoxysilane to achieve a contact angle 160 degrees and sliding angle is 8 degrees.

3.7 Hydrothermal synthesis

Hydrothermal method is another technique used for synthesis of superhydrophobic and superliquiphobic coating. This technique is to produce crystalline substances from hot aqueous solution at high vapor pressure. This method is mostly used for creating roughness on the surface of substrate by using high temperature and high pressure. In this process, crystals are grown in an autoclave where materials along with water are supplied. Temperature gradient is created in between the opposite ends of autoclave chamber. Materials dissolve at hotter end and they are deposited on the seed crystals at cooler end, thus desired crystals grow. It can create crystalline phases which are not stable at the melting point. Materials those have high vapor pressure at or near their melting points can be grown by this method. It has ability to synthesize large crystals of high quality. This process has potential to contribute industrially due to its simple approach. However,

it has inability to monitor crystals in the process of growth. The cost of equipment is also high.

By employing hydrothermal synthesis techniques, several works have been reported in literature. For example, Hao et al. [88] created the roughness on the surface of zinc by chemical etching with HCl followed by hydrothermal treatment with ammonium hydroxide. The roughed surface was further modified by perfluorooctanoic acid that showed both superhydrophobic and oleophobic property with contact angle of 151.85 degrees and 145.62 degrees for water and peanut oil, respectively.

Shen et al. [91] created different nanostructures by using different techniques on microstructured Ti_6Al_4V alloy surface. Nanostructures with nanowires were created by hydrothermal method, nanotubes by anodic oxidation, and nanomesh by two–step chemical reaction. The micro–nanostructured surface was then modified FAS-17 after which the contact angle of water increased to 161 degrees with tilting angle of 6 degrees.

Hu et al. [107] developed superhydrophobic glass surface with high adhesive force using two–step method. The surface was first coated with composite of carbon/silica. Carbon nanoparticles were developed on glass by hydrothermal method followed by depositing of SiO_2 prepared by hydrolysis. The surface was then modified by 1H,1H,2H,2H–perfluordecyltrimethoxysilane to increase the contact angle of water >150 degrees.

Xiao et al. [108] used hydrothermal method to fabricated superhydrophobic ZnO micro/nanocrystals assisted by PEG1000. The crystals developed were thermally and chemically stable with contact angle of water of 167 degrees.

Shi et al. [109] changed the surface of glass to superhydrophobic with water contact angle of 154 degrees and sliding angle lower than 3 degrees. The surface of glass was hydrothermally treated with solution of $Al(NO_3)_3 \cdot 9H_2O$, NaOH, and colloidal silica to develop rose like microstructures which were further modified by octyltrimethoxy-silane to achieve superhydrophobicity.

3.8 Self-assembly technique

By this process, a disordered system of preexisting components assembles in an organized way or a sequence. This pattern is due to local noncovalent molecular interactions among the components themselves and without external direction. It is also known as molecular self-assembly when the constitutive components are molecules. It forms complex struc-tures with minimal intervention. It grows the layer at low temperature without expensive equipment and tedious process. It has important implications with regards to the forma-tion of thin-film technology. This type of surface modification method can be widely used on engineering metals. But this process is time consuming and mechanism is complex.

Several works have done for creating superhydrophobic surface. Yin et al. [110] etched the surface of copper by immersing the surface in a solution of sodium hydroxide and potassium persulfate solution to produce flower-like structure and nanoneedles of $Cu(OH)_2$. The roughed surface was then immersed in dodecanoic acid which forms self-assembled layer on the surface which increased the water contact angle to 153 degrees.

Pan et al. [111] synthesized UV resistant and laundering-resistant superhydrophobic cotton surface with contact angle of 146.27 degrees. The sample was first coated with nano-Al sol and which was further modified sodium stearate and stearic acid which formed self-assembly on the surfaces to make the surface superhydrophobic.

Li et al. [112] similarly prepared superhydrophobic coating of cotton surface. The sample was immersed in silica hydrosol followed by immersion in HDTMS. The HDTMS forms self-assembled monolayers (SAMs) on the roughed surface that increased the water contact angle to 151 degrees.

Song et al. [113] created superhydrophobic silicon surface by self-assembly method with contact angle of 153 degrees. Oxide layer was first prepared on the surface by chemical etching. The surface modification of etched surface was carried out by CVD of aminopropyltrimethoxysilane (APTMS) which forms SAM on the surface by reacting with —OH ions on the surface.

Yin et al. [114] created self-assembled gold nanoparticles and fullerene pyridyl derivatives thin gold films at water/toluene interface. The film exhibited superhydrophobic property with contact angle of 157 degrees having its applications in the fields of optical, electronic, biosensor, and catalytic materials due to its self-cleaning and self-repairing property.

Huaiyuan et al. [115] synthesized PTFE/polyetheretherketone (PEEK) composites with self-assembled octadecyltrichlorosilane (OTS) molecules modified potassium titanate whiskers (PTW). The sample showed water contact angle of 141 degrees and excellent mechanical, friction, and wear resistance.

Badre et al. [116] modified the surface of zinc layered with zinc oxide using different fatty acids like stearic acid, oleic acid, and elaidic acid. The prepared samples were stable to UV radiation and long-term environmental exposure with maximum contact angle of 167 degrees.

Nanda et al. [117] synthesized superhydrophobic/superoleophilic coating on steel mesh by etching the surface with mixture of $FeCl_3$ and HCl. The etched surface was then immersed in HDTMS which increased the static contact angle of water to 167 ± 3 degrees with sliding angle of 6 ± 1 degrees. The prepared sample exhibited good thermal, mechanical, and chemical stability with an excellent oil–water separation application.

Chauhan et al. [118] immersed the cotton substrate on the solution of HDTMS to increase the water contact angle to 157 ± 5 degrees with tilt angle of 7 degrees. The

coating on cotton surface is due to the formation of SAM of HDTMS. The prepared sample was mechanically, chemically, thermally, and UV stable and was used for oil-water separation.

Panda et al. [119] developed superhydrophobic/superoleophobic coating on cotton surface by immersing the sample in a mixture of trichloro(octadecyl)silane and (penta-fluorophenyl)triethoxy silane. These silanes reacts to the surface and forms a layer of low surface energy material which increased the contact angle to 172.9 ± 3 degrees, 169 ± 3 degrees, and 167 ± 3 degrees for water, ethylene glycol, and glycerol, respectively. The superhydrophobic coating also exhibited good thermal, chemical, mechanical, and UV stability and was used for self-cleaning and oil-water application.

Nanda et al. [120] synthesized superhydrophobic coating on glass surface by dip coating on the solution of OTS-modified SiO_2 microparticles. The surface energy of the glass was reduced to the monolayers of OTS on the surface. The prepared sample was chemically, thermally, and mechanically stable with static contact angle of 165.5 ± 5.7 degrees and hysteresis of 2.0 ± 0.5 degrees. The aforesaid superhydrophobic glass surface was used for self-cleaning application.

3.9 LBL deposition technique

The LBL deposition technique is a simple and cheap method to construct thin-film coatings by depositing alternating layers. It uses electrostatic interaction and covalent bonds to form multilayer grafts. This process can be used to produce a wide variety of materials including polymers, metals, ceramics, nanoparticles, and biological molecules.

By using this technique, several studies have carried out for creating superhydrophobic surfaces. For example, Lu et al. [121] synthesized superhydrophobic cotton fabric with UV-resistant and antibacterial property. The surface was coated by layer by layers of ZnBDC followed by immersing aqueous solution of sodium stearate to increase the water contact angle to 151.4 degrees.

Zhang et al. [76] synthesized superhydrophobic coating on ITO surface. The surface was first deposited by layer by layer of polyelectrolyte followed by electrodeposition of gold clusters. The roughed surface was then immersed in n-dodecanethiol solution for overnight to achieve superhydrophobic property with water contact angle maximum of 173 degrees.

Bravo et al. [122] developed superhydrophobic glass surface or silicon wafers with high transparency and antireflective property by LBL deposition method. A layer of adhesion layer followed by layers of SiO_2 nanoparticles of different size were coated on the surface that provided the desire roughness. The roughed surface was further modified by trichloro($1H,1H,2H,2H$-perfluorooctyl) silane to reach a water contact angle of 160 degrees with sliding angle <10 degrees.

Amigoni et al. [123] deposited layer by layer of amino–functionalized silica nanoparticles and epoxy–functionalized smaller silica nanoparticles on glass surface. The prepared sample showed hierarchy structure and was further modified by (3-aminopropyl) trimethoxysilane to increase the water contact angle to 153 degrees and hysteresis of 12 degrees.

3.10 Lithography technique

This technique employs simple chemical processes to create an image. It produces two components: water repelling positive part and water retaining negative part. By this method different pattern including circular pillars, squared pillars, star-shaped pots, indented square pots of with different diameters, height, and spacing can be produced [124]. It is an expensive process. There are many ways in which lithography can be done. They are the following.

3.10.1 Photolithography

This process uses a mask of carrying the requisite pattern information and mask pattern that is to be transferred on the substrate by using some optical technique. It is widely used in integrated circuit manufacturing. It has three techniques: contact, proximity, and projection printing.

This process is not complex, simple, and fast. Small structures can be created with relatively inexpensive equipment. But this technique is limited due to mask wear, defect generation, and contamination. Mask required must be of same size that of substrate which increases the cost. It is also a slow process as it requires longer time to expose entire wafer. Moreover, it requires an environmental chamber for reducing noise, vibrations, controlling temperature, humidity, and this leads in increasing the cost of the process.

There are several published work on producing superhydrophobic coating using photolithography technique. For example, Oner and McCarthy [125] developed superhydrophobic coating on silicon wafers surface. Different lithographic pattern were created on silicon surface by photolithography followed by surface modification by dimethyldichlorosilane (DMDCS), n-octyldimethylchlorosilane (ODMCS), and heptadecafluoro-1,1,2,2-tetrahydrodecyldimethylchlorosilane (FDDCS) using vapor phase reaction. The contact angle of water was found to be 145 degrees, 143 degrees, and 150 degrees for DMDCS, ODMCS, and FDDCS, respectively.

3.10.2 Electron beam lithography

In this technique, surface roughness can be created by electron beam bombardment on the surface. The electron beam changes the solubility of resist, enabling selective removal of either the exposed/nonexposed regions of the resist by immersing it in solvent. It is a direct process to produce superhydrophobic surface where no mask is needed unlike photolithography, thus eliminating costs and time delay associated with mask production.

It is generally used to develop specialized and prototype devices. Besides, it is not an efficient process for industrial processing as it is complex, slow, and costly.

There is several published work on producing superhydrophobic coating using electron beam lithography technique. For example,

Feng et al. [126] created desired roughness of macroscopic hierarchical structure using electron beam lithography on wafer surfaces. The wafer surface changes to superhydrophobic with contact angle of 160 degrees after silanization with low surface energy.

Joki–Korpela et al. [127] developed antireflective polyurethane acrylate by solvent-free UV molding and fluoroalkylsilane modification which changed the wettability to hydrophobic and oleophobic in nature. The prepared acrylated was then replicated on the surface of PMMA by pair of nickel molds which was prepared by electron beam lithography and reaction ion etching.

3.10.3 X-Ray lithography

It is a process which uses X-rays to transfer a geometric pattern from a mask to a light-sensitive chemical photoresist on the substrate. A series of chemical treatments then engraves the produced patterns into the material under the photoresist. It has few advantages such as no diffraction effect, simple to use, no lens required, faster than electron beam lithography, uniform etching, and high resolution, applicable for large area. This technique can produce features at very small resolutions (lower than 10 nm). However, it has several disadvantages such as thin lens required, distortion in absorber, cannot be focused through lens, expensive mask, requires synchrotron facility, deformation and vibrations during the process, and time consuming.

Furstner et al. [34] studied the wetting and self-cleaning properties of three different specimen. First, a silicon wafer surface where spikes of regular pattern were obtained by X-ray lithography with surface modification by hexadecanthiol, second, replicate of water repelling leaves, and last metal foils which were hydrophobized by fluorinated agent. The silicon wafer with high spikes had a low sliding angle for which it can be applied in making self-cleaning surface from fog contamination.

3.10.4 Nano-imprint lithography

Nano–imprint lithography technique combines the speed of optical lithography with the resolution of electron beam lithography to make nanostructures on the surface. It creates coating by pressing and heating a thin film between a patterned template and surface. Due to heating, the patterned film adheres to the substrate. This technique can produce features at very small resolutions (lower than 10 nm) that cover a large area with a high throughput. It is relatively low-cost process and has commercial viability. This process is used in photodetectors, silicon quantum dots, quantum wires, and ring transistors. This process has been attracting attention from industries because it is used to mass–produce

nanostructure product at low cost and high throughput. Although it is a flexible process but main barrier for the production of small resolutions is the development of mold.

Wu et al. [128] studied the most suitable conditions to deposit SAMs with antiadhesive capability for nanoimprint lithography. They developed nanostructures of concentric square recess molds on silicon wafers using e-beam writer. Two different samples of prepared silicon wafer were then produced by surface modification with liquid phase OTS and vapor phase perfluorodecyltrichlorosilane (FDTS) where it was observed that FDTS was preferred at high-temperature nanoimprinting than OTS due to its high thermal stability.

Zhang et al. [129] created the imprinting on the surface of silicon wafer coated with PS and PMMA films using a FDTS-treated molds. These surfaces form hierarchy structures with contact angle increasing to 128 degrees and 104 degrees for PS and PMMA film, respectively, thus making its application in different engineering materials.

Huang et al. [130] created nanostructures on plastic film by nanoimprinting using a template of anodized aluminum oxide (AAO). The developed nanoprinted plastic thin film reaches the contact angle of 130 degrees.

Pozzato et al. [131] carried out nanoimprint lithography and wet chemical etching on silicon surface with micron-scale dimensions. Resistance to etching by HF was done by positive photoresist and residual removal of resist layer in nanoimprint by UV-ozoner treatment. The surface was further modified by OTS which increased the water contact angle to 167 degrees.

3.10.5 Interference lithography

Interference lithography, also known as holographic lithography, is a technique for creating arrays of fine features on the substrate without the use of complex optical systems or photomasks. In this method, two or more coherent light waves with interference pattern between them are set up and are recorded in photoresist. These interference patterns have both intensity of maxima and minima in a periodic series. After exposing of surface to photolithographic processing, a pattern of periodic intensity emergences on the surface based on the photoresist.

Advantages of interference lithography are that it can produce dense features over a wide area at short period of time without loss of focus for which it is mainly used as testing photoresist processes for different new wavelengths used in lithography techniques. But there also lies some disadvantages of interference lithography such as it cannot be used for drawing patterns of arbitrary shapes because of its patterning feature. Besides this, non-optical effect, secondary electron in case of ionizing radiation and diffusion cannot be avoided.

Berendsen et al. [132] synthesized superhydrophobic thermoplastic polymer surface (PS and PMMA) by thermal imprint method followed by plasma polymerization of hexafluoropropene layer. Thermal imprinting was carried out by nickel stamp which was

developed by customized laser interference lithography technique. The static water contact angle increased to 167 degrees with hysteresis below 5 degrees.

3.11 Template-assisted self-assembly

In this synthesis technique, a predefined structure (template) is introduced to self-assembly. In this method, colloidal are aggregated with controlled shape, size, and structures on the surface by removal of solvents from aqueous building blocks implemented on the patterned surface of two-dimensional (2D) arrays of templates. Colloidal particles get assembled according to the surface confinement provided by liquid droplets or by microfabricated to spherical objects by the building blocks. Colloidal crystals can also been grown on solid substrates by relieves in a patterned arrays.

Advantage of this process is that this method uses the combination of both lithography and self-assembly with their desirable aspects, that is, it controls the lithography as well as carried out self-assembly technique for which it has an upper hand as compared to both the techniques individually. It can produce different shape building blocks such as spheroid, cube, right bipyramid, and triangular with corner-to-corner junction. Template-assisted self-assembly (TASA) also provides flexibility in organizing the building blocks at nanoscale level because of its use of the capillary force.

Sun et al. [133] developed superhydrophobic glass surface by two simple techniques. The surface of glass was coated with micro and nanospheres silica by electrostatic absorbing technique and template directed self-assembly method. The surface was then modified with layer of fluoroalkylsilane that increased the water contact angle >160 degrees. The prepared coating can have its application in self-cleaning coating, microfluidic device, and thermal transfer apparatus.

Huaiyuan et al. [115] synthesized mechanical, friction, and wear-resistance coating with water contact angle of 141 degrees on PTW by PTFE/PEEK composites with self-assembled OTS.

3.12 Anodization

Anodization is a synthesis technique where a protective oxide layer of thickness 5–25 μm is developed on the surface of metal by electrolytic oxidation of metal surface in the presence of an acid. Besides, making the surface rough, the presence of oxide layer on anodized surfaces have high abrasion resistance and long-term stability as they do not get peel off from the surface even if at regular use. But the disadvantage of anodization technique is that it reduces the thermal conductivity of materials lower than the parent material. Also, colored anodized surface layer by organic dyes loses its color under sunlight after certain time of exposure.

Several works have been reported on superhydrophobicity using this technique. Liang et al. [134] developed chemically stable superhydrophilic/superhydrophobic

coating on titanium surface. The Ti surface was anodized in acid solution containing HF and HNO_3 and water which changed the surface wettability to superhydrophilic. The anodized surface was then immersed in fluoroalkylsilane to make the surface superhydrophobic with water static contact angle of 160 degrees and sliding angle of 1.7 degrees.

Gao et al. [135] created complex micropore structure on the surface of Ti-6Al-4V alloy by anodization in the mixture of NaOH and H_2O_2 acid mixture. The etched surface wettability was made superhydrophobic by treating the surface with tridecafluoroctyl-triethoxysilane which increased the water contact angle 158.5 ± 1.9 degrees and rolling angle of 5.3 ± 1.1 degrees. The prepared superhydrophobic surface was stable to air exposure, 3.5% NaCl solution and sand abrasion test.

Wang et al. [79] synthesized hierarchical structure by electrochemical deposition of nickel and copper on a template which was developed by APA. The deposit formed nanometer pillars in the pore of APA. The surface was then modified by FAS to obtain water contact angle of 152 degrees and sliding angle of 6 degrees for nickel and 157 degrees and a sliding angle of 3 degrees for copper.

Lee et al. [136] studied the water-droplet adhesiveness on aluminum surface. The AAO layers were fabricated by two-step anodization. The AAO was acid etched to change the roughness structure form nanopore to nanopillar arrays. The nanopillar roughed surface was further modified heptadecafluoro-1,1,2,2-tetrahydrodecyl-trichlorosilane to increase the water contact angle to 166.6 ± 1.2 degrees.

Yin et al. [137] synthesized anticorrosive, superhydrophobic aluminum surface by anodization in the presence of sulfuric acid. The anodized surface wettability was changed to superhydrophobic after modification with myristic acid with seawater contact angle of 154 degrees.

Vanithakumari et al. [138] achieved superhydrophobicity on titanium surface with contact angle of water of 150 degrees. The surface was first anodized in the presence of H_2SO_4 followed by surface modification by 1*H*,1*H*,2*H*,2*H*-perfluorooctyltriethoxy-silane. The prepared sample was stable to sea water and mild nitric acid solution.

3.13 Sol-gel process

Sol–gel technique is the most common method to synthesis superhydrophobic coating on different substrate surface. It is a method where colloidal particles with different sizes ranging from 1 to 100 nm are dispersed in gels that have an interconnected rigid network with pores size of submicrometer and polymeric chains of average length of $>1 \, \mu m$. Here conversion of monomer takes place to colloidal solution (sol) that acts an initiator for integrated network (gel) for polymers or particles. The scale of the structure on surface ranging to nanoscale can be controlled at early stage of synthesis. This method is mainly used for bioinspired and bio-templating fabrications. The benefit of using this technique is it can be applied to any type of surfaces with homogenous coating as compared to

traditional ceramic method. But the drawback of the coating technique is the large volume shrinkage, formation of crack while drying, increase in carbon content while using organic reagents during preparative step, densification during sintering and regular monitoring of process is essential.

Several studies have been carried out in synthesis of superhydrophobic coating on different surfaces using sol–gel method. For instance, Laksmi et al. [139] spray coated the sol–gel composite of fumed silica and perfluoroalkylmethacrylic copolymer in a hybrid sol–gel matrix on glass and aluminum surface. The prepared samples showed superhydrophobic and oleophobic property with contact angle of 158 degrees, 146 degrees, and 113 degrees for water, ethylene glycol, and lubricating oil, respectively. The repellency of oil was due to the presence of small amount of fluorine.

Fan et al. [140] developed superhydrophobic copper wafer with water contact angle 155.4 degrees. The surface of copper was first etched in acid solution followed by coating with sol–gel of vinyl trimethoxylsilane, ethanol, water, and ammonia water. The prepared sample remained stable in 3.5% NaCl solution making its application for self-cleaning and anticorrosive.

Lakshmi and Basu [141] synthesized superhydrophobic composite film with long stability on environmental exposure and tape peeling test. The sample was prepared by incorporating stearic acid modified colloidal zinc chloride fabricated in a sol–gel matrix. The prepared sample was then sprayed on glass surface which increased the water contact angle to 165 degrees and sliding angle <2 degrees.

Wang et al. [142] developed superhydrophobic wood surface with water contact angle of 164 degrees and tilting angle below 3 degrees. The surface was first immersed in a sol–gel TEOS, water, and NH_4OH, where the SiO_2 nanoparticles were deposited on wood surface. The deposited surface was then modified by 1H,2H,2H-perfluoroalkyltriethoxysilanes (POTS) using CVD to achieve superhydrophobicity. The prepared sample also exhibited good stability to ambient atmosphere.

Wang et al. [143] prepared a superhydrophobic sol–gel of trimethyl-modified silica particles. The sol–gel was then coated on canvas surface by LBL process of PTFE and superhydrophobic sol–gel. The water contact angle was measured be 153.3 ± 3.1 degrees and 152.3 ± 2.1 degrees after two and three bilayers. The prepared samples also exhibited self-cleaning property with excellent water impact test, tensile test, and accelerated weathering test.

Huang and Lin [144] developed superhydrophobic, transparent glass surface by coating the surface in a sol–gel of silicic acid and silica nanoparticles followed by coating with 1H,1H,2H,2H-perfluorooctyltrichlorosilane. The coated glass surface had a water contact angle >160 degrees and also showed good chemical and mechanical stability.

Su et al. [145] prepared a sol–gel of by-product of APS KH550 and polymethyl hydrosiloxane (PMHS) made from hydrolysis and condensation of the product. The prepared

sol–gel was then coated on the surface of glass which showed water contact angle of 157 degrees and hysteresis angle is <1 degrees.

Wen et al. [146] fabricated superhydrophobic glass with water contact angle of 156 degrees and sliding angle of 5 degrees by coating sol-gel of methyltriethoxysilane (MTEOS)/TEOS/tri(isopropoxy)vinylsilane (TIPVS) in organic siloxane-modified polyacrylate emulsion (OSPA emulsion). The organic-inorganic derived sol–gel was produced by alkaline-catalyzed co–hydrolysis and copolycondensation reactions between tetraethoxysilane (TEOS), MTEOS, and TIPVS.

Lakshmi et al. [147] spray coated a sol-gel of silica nanoparticles embedded in hybrid sol-gel of MTEOS and colloidal silica produced due to partial condensation on glass surface. The prepared superhydrophobic glass surface exhibited a contact angle of 162.5 degrees with improved hardness.

Satapathy et al. [148] developed superhydrophobic glass surface by dip coating sol-gel of SiO_2 nanoparticles embedded in linear low-density polyethylene (LLDPE) polymer matrix. Different samples of porous (using ethanol as nonsolvent) and nonporous matrix were developed. The porous SiO_2 nanoparticles embedded in LLDPE showed a water contact angle of 170 degrees and tilting angle of 3.8 degrees. Besides this, the sample also exhibited good thermal, mechanical, and chemical stability with an excellent self-cleaning property.

Nanda et al. [149] synthesized self–cleaning superamphiphobic (both superhydrophobic and superoleophobic) coating on steel surface by casting the sol-gel solution of PFOTS-modified SiO_2 nanoparticle. The coated sample showed a contact angle of 167.0 ± 3.1 degrees, 165.0 ± 3.7 degrees, 164.0 ± 4.0 degrees, and 157.1 ± 2.1 degrees with sliding angles of 2.5 ± 0.5 degrees, 4.0 ± 0.5 degrees, 3.2 ± 0.5 degrees, and 5.6 ± 1 degrees for water, glycerol, ethylene glycol, and hexadecane, respectively. Superamphiphobic surface retained its property up to 350°C and also exhibited excellent chemical and mechanical stability.

Satapathy et al. [150] casted sol–gel of SiO_2 nanoparticles and LLDPE solution on filter paper to achieve superhydrophobicity with water contact angle of 167.8 ± 1.4 degrees and sliding angle of 3.8 ± 0.5 degrees for oil–water separation. The prepared sample also showed stability to mechanical, thermal, and chemical test.

3.14 Chemical vapor deposition

CVD technique has its wide application in materials-processing technology. In this method, the precursor is heated into gas form at high temperature and it then deposited on the surface of the substrate due to reaction with the hot surface and thus forms a thin-film layer on the surface. This technology is widely used in producing bulk materials and powders with high purity, deposition of materials on surface, and development of

composite material via infiltration techniques. CVD technique is also used in fields of semiconductor and producing synthetic diamonds.

Advantage of using this process is it produces highly dense pure materials, uniform coating with good adhesion for complex-shaped components, surface morphology, crystal structure, and orientation can be controlled by controlling CVD parameters and use of wide range of chemicals deposition over a large spectrum of materials. Besides this, CVD techniques do have also some disadvantages such as use of toxic, corrosive, flammable, and explosive precursor gases can cause chemical and safety hazards and multicomponent component with proper stoichiometry is difficult to be coated because of their different vaporization rates [151].

Several works have been done on superhydrophobicity using CVD technique. For example, Rezaei et al. [152] synthesized superhydrophobic coating on glass, aluminum, and silicon slides using CVD technique. The surface were coated with TEOS, vinyltri-methoxysilane (VTMS), ammonia, and water which increased the contact angle of water above 160 degrees with hysteresis <5 degrees.

Wang et al. [153] coated the surface of PDMS film that showed water contact angle of 155.4 ± 2 degrees and sliding angle of 3.1 ± 0.3 degrees. ZnO nanocrystals were developed by CVD technique which was further modified by APS. The modified ZnO nanocrystals were then dispersed in PDMS to achieve superhydrophobic film.

Huang et al. [38] created aligned carbon nanotubes (CNT) on Fe-N coated Si substrate using CVD technique. The sample surface was then modified by ZnO thin film using filtered cathodic vacuum arc technique to achieve superhydrophobicity with water contact angle of 159 degrees.

4. Conclusions

Superhydrophobic coating has intense applications in the field of self-cleaning, antifogging, antibacteria, and environmental remediation because of its nonwetting behavior as water contact angle on these surfaces are >150 degrees. These surfaces are biomimic from the nature like lotus leaf, butterfly wings, skin of shark, etc. In this chapter, idea regarding the superhydrophobic surfaces has been discussed. It also provides the idea about the different models, that is, Wenzel model and Cassie-Baxter model governing on superhydrophobic surfaces. Different techniques for synthesis of artificial superhydrophobic coatings with their advantages and disadvantages are also discussed.

References

[1] M. Nosonovsky, B. Bhushan, Superhydrophobic surfaces and emerging applications: non-adhesion, energy, green engineering, Curr. Opin. Colloid Interface Sci. 14 (2009) 270–280.
[2] P.A. Levkin, F. Svec, J.J.M. Frechet, Porous polymer coatings: a versatile approach to superhydrophobic surfaces, Adv. Funct. Mater. 19 (2009) 1993–1998.

[3] B. Bhushan, Y.C. Jung, K. Koch, Self-cleaning efficiency of artificial superhydrophobic surfaces, Langmuir 25 (2009) 3240–3248.

[4] X. Zhang, F. Shi, J. Niu, Y.G. Jiang, Z.Q. Wang, Superhydrophobic surfaces: from structural control to functional application, J. Mater. Chem. 18 (2008) 621–633.

[5] J.R. Dorvee, A.M. Derfus, S.N. Bhatia, M.J. Sailor, Manipulation of liquid droplets using amphiphilic, magnetic one-dimensional photonic crystal chaperones, Nat. Mater. 3 (2004) 896–899.

[6] K.Y. Suh, M.C. Park, P. Kim, Capillary force lithography: a versatile tool for structured biomaterials interface towards cell and tissue engineering, Adv. Funct. Mater. 19 (2009) 2699–2712.

[7] B. Bhushan, Y.C. Jung, Natural and biomimetic artificial surfaces for superhydrophobicity self-cleaning, low adhesion, and drag reduction, Prog. Mater. Sci. 56 (2011) 1–108.

[8] T. Wagner, C. Neinhuis, W. Barthlott, Wettability and contaminability of insect wings as a function of their surface sculptures, *Acta Zool.* 77 (1996) 213–225.

[9] A.R. Parker, C.R. Lawrence, Water capture from desert fogs by a Namibian beetle, Nature 414 (2001) 33–34.

[10] X. Gao, L. Jiang, Biophysics: water-repellent legs of water striders, Nature 432 (2004) 36.

[11] D. Byun, J. Hong, J.H.K. Saputra, Y.J. Lee, H.C. Park, B.K. Byun, J.R. Lukes, Wetting characteristics of insect wing surfaces, J. Bionic Eng. 6 (2009) 63–70.

[12] K. Koch, B. Bhushan, W. Barthlott, Diversity of structure, morphology and wetting of plant surfaces, Soft Matter 4 (2008) 1943–1963.

[13] A. Nakajima, K. Hasimoto, T. Watanabe, Recent studies on super-hydrophobic films, *Monatsh. Chem.* 132 (2001) 31–41.

[14] H.Y. Erbil, A.L. Demirel, Y. Avci, O. Mert, Transformation of a simple plastic into a superhydrophobic surface, Science 299 (2003) 1377–1380.

[15] H. Li, X. Wang, Y. Song, Y. Liu, Q. Li, L. Jiang, D. Zhu, Super–amphipholic aligned carbon nanotube films, Angew. Chem. Int. 40 (2001) 1743–1746.

[16] T. Sun, G. Wang, H. Liu, L. Feng, L. Jiang, D. Zhu, Control over the wettability of an aligned carbon nanotube film, *J. Am. Chem. Soc.* 125 (2003) 14996–14997.

[17] Y. Wu, H. Sugimura, Y. Inoue, O. Takai, Thin films with nanotextures for transparent and ultra water-repellent coatings produced from trimethylmethoxysilane by microwave plasma CVD, Chem. Vap. Depos. 8 (2002) 47–50.

[18] N.J. Shirtcliffe, G. McHale, M.I. Newton, C.C. Perry, Intrinsically super hydrophobic organo–silica sol–gel foams, Langmuir 19 (2003) 5626–5631.

[19] C. Guo, L. Feng, J. Zhai, G. Wang, Y. Song, L. Jiang, D. Zhu, Large area fabrication of a nanostructure induced hydrophobic surface from a hydrophilic polymer, Chem. Phys. Chem. 5 (2004) 750–753.

[20] W. Lee, M.K. Jin, W.C. Yoo, J.K. Lee, Nanostructuring of a polymeric substrate with well-defined nanometer-scale topography and tailored surface wettability, Langmuir 20 (2004) 7665–7669.

[21] J.T. Han, X.R. Xu, K.W. Cho, Diverse access to artificial superhydrophobic surfaces using block co-polymers, Langmuir 21 (2005) 6662–6665.

[22] N.J. Shirtcliffe, G. McHale, M.I. Newton, G. Chabrol, C.C. Perry, Dual-scale roughness produces unusually water-repellent surfaces, Adv. Mater. 16 (2004) 1929–1932.

[23] H.S. Hwang, S.B. Lee, I. Park, Fabrication of raspberry-like superhydrophobic hollow silica particles, *Mater. Lett.* 64 (2010) 2159–2162.

[24] Y.H. Huang, J.T. Wu, S.Y. Yang, Direct fabricating patterns using stamping transfer process with PDMS mold of hydrophobic nanostructures on surface of micro-cavity, Microelectron. Eng. 88 (2011) 849–854.

[25] T. Yang, H. Tian, Y. Chen, Preparation of superhydrophobic silica films with honeycomb-like structure by emulsion method, J. Sol-Gel Sci. Technol. 49 (2009) 243–246.

[26] H. Kinoshita, A. Ogasahara, Y. Fukuda, N. Ohmae, Superhydrophobic/superhydrophilic micropatterning on a carbon nanotube film using a laser plasma-type hyperthermal atom beam facility, Carbon 48 (2010) 4403–4408.

[27] Z.G. Guo, J. Fang, J.C. Hao, Y.M. Liang, W.M. Liu, A novel approach to stable superhydrophobic surfaces, *Chem. Phys. Chem.* 7 (2006) 1674–1677.

[28] K.K. Lau, J. Bico, K.B.K. Teo, M. Chhowalla, G.A.J. Amaratung, W.I. Milne, G.H. McKinley, K.K. Gleason, Superhydrophobic carbon nanotube forests, Nano Lett. 3 (2003) 1701–1705.

[29] F. Mumm, A.T.J. van Helvoort, P. Sikoski, An easy route to superhydrophobic copper based droplet microfluidic systems, ACS Nano 3 (2009) 2647–2652.

[30] S.S. Latthe, H. Imai, V. Ganesan, A.V. Rao, Superhydrophobic silica films by sol-gel co-precursor method, Appl. Surf. Sci. 256 (2009) 217–222.

[31] V.V. Ganbavle, U.K.H. Bangi, S.S. Latthe, S.A. Mahadik, A.V. Rao, Self-cleaning silica coatings on glass by single step sol-gel route, Surf. Coat. Technol. 205 (2011) 5338–5344.

[32] S.S. Latthe, H. Hirashima, A.V. Rao, TEOS based water repellent silica films obtained by a co-precursor sol-gel method, Smart Mater. Struct. 18 (2009) 1–6.

[33] A.V. Rao, S.S. Latthe, C. Kappenstein, V. Ganesan, M.C. Rath, S.N. Sawant, Wetting behavior of high energy electron irradiated porous superhydrophobic silica films, *Appl. Surf. Sci.* 257 (2011) 3027–3032.

[34] R. Furstner, W. Barthlott, C. Neinhuis, P. Walzel, Wetting and self-cleaning properties of artificial superhydrophobic surfaces, Langmuir 21 (2005) 956–961.

[35] M. Ma, Y. Mao, M. Gupta, K.K. Gleason, G.C. Rutledge, Superhydrophobic fabrics produced by electrospinning and chemical vapor deposition, Macromolecules 38 (2005) 9742–9748.

[36] X. Zhang, Y. Guo, P. Zhang, Z. Wu, Z. Zhang, Superhydrophobic CuO–Cu2S nanoplate vertical arrays on copper surfaces, *Mater. Lett.* 64 (2010) 1200–1203.

[37] H. Liu, L. Feng, J. Zhai, L. Jiang, D.B. Zhu, Reversible wettability of a chemical vapor deposition prepared ZnO film between superhydrophobicity and superhydrophilicity, Langmuir 20 (2004) 5659–5661.

[38] L. Huang, S.P. Lau, H.Y. Yang, E.S.P. Leong, S.F. Yu, S. Prawer, Stable superhydrophobic surface via carbon nanotubes coated with a ZnO thin film, J. Phys. Chem. B 109 (2005) 7746–7748.

[39] L.B. Zhu, Y.H. Xiu, J.W. Xu, P.A. Tamirisa, D.W. Hess, C.P. Wong, Superhydrophobicity on two-tier rough surfaces fabricated by controlled growth of aligned carbon nanotube arrays coated with fluoro-carbon, Langmuir 21 (2005) 11208–11212.

[40] R.N. Wenzel, Resistance of solid surfaces to wetting by water, Ind. Eng. Chem. 28 (1936) 988–994.

[41] A.B.D. Cassie, S. Baxter, Wettability of porous surface, Trans. Faraday Soc. 40 (1944) 546–551.

[42] A. Lafuma, D. Quere, Superhydrophobic states, Nat. Mater. 2 (2003) 457–460.

[43] M. Reyssat, J.M. Yeomans, D. Quere, Impalement of fakir drop, Europhys. Lett. 81 (2008) 1–5.

[44] M. Reyssat, A. Pepin, F. Marty, Y. Chen, D. Quere, Bouncing transitions on microtextured materials, Europhys. Lett. 74 (2006) 306–312.

[45] D. Bartolo, F. Bouamrirene, E. Verneuil, A. Buguin, P. Silberzan, S. Moulinet, Bouncing or sticking droplets: impalement transitions on superhydrophobic micropatterned surfaces, Europhys. Lett. 74 (2006) 299–305.

[46] X. Zhang, Y. Guo, Z. Zhang, P. Zhang, Self-cleaning superhydrophobic surface based on titanium dioxide nanowires combined with polydimethylsiloxane, Appl. Surf. Sci. 284 (2013) 319–323.

[47] Z. Cui, L. Yin, Q. Wang, J. Ding, Q. Chen, A facile dip-coating process for preparing highly durable superhydrophobic surface with multi-scale structures on paint films, J. Colloid Interface Sci. 337 (2009) 531–537.

[48] R.J. Klien, P.M. Bieshuevel, B.C. Yu, C.D. Meinhart, F.F. Lange, Producing superhydrophobic surfaces with nanosilica spheres, Z. Metallkd. 94 (2003) 377–380.

[49] U. Cengiz, H.Y. Erbil, Superhydrophobic perfluoropolymer surfaces having heterogeneousroughness created by dip-coating from solutions containing a non-solvent, Appl. Surf. Sci. 292 (2014) 591–597.

[50] S.A. Mahadik, V. Parale, R.S. Vhatkara, D.B. Mahadik, M.S. Kavale, P.B. Wagh, S. Gupta, J. Gurav, Superhydrophobic silica coating by dip coating method, Appl. Surf. Sci. 277 (2013) 67–72.

[51] M. Ramezani, M.R. Vaezi, A. Kazemzadeh, Preparation of silane-functionalized silica films via two-step dip coating sol–gel and evaluation of their superhydrophobic properties, Appl. Surf. Sci. 317 (2014) 147–153.

[52] L. Gao, J. He, A facile dip-coating approach based on three silica sols to fabrication of broadband anti-reflective superhydrophobic coatings, J. Colloid Interface Sci. 400 (2013) 24–30.

[53] T. Liu, F. Zhang, C. Xue, L. Li, Y. Yin, Structure stability and corrosion resistance of nano-TiO_2 coatings on aluminum in seawater by a vacuum dip-coating method, Surf. Coat. Technol. 205 (2010) 2335–2339.

[54] A.V. Rao, A.B. Gurav, S.S. Latthe, R.S. Vhatkar, H. Imai, C. Kappenstein, P.B. Wagh, S. C. Gupta, Water repellent porous silica films by sol–gel dip coating method, J. Colloid Interface Sci. 352 (2010) 30–35.
[55] D. Nanda, P. Varshney, M. Satapathy, S.S. Mohapatra, B. Bhushan, A. Kumar, Single step method to fabricate durable superliquiphobic coating on aluminum surface with self-cleaning and anti-fogging properties, *J. Colloid. Interfacial Sci*. 507 (2017) 397–409.
[56] J. Sun, F. Zhang, J. Song, L. Wang, Q. Qu, Y. Lu, I. Parkin, Electrochemical fabrication of superhydrophobic Zn surfaces, *Appl. Surf. Sci*. 315 (2014) 346–352.
[57] V. Senez, V. Thomy, R. Dufour, Nanotechnologies for Synthetic Super Non-wetting Surfaces, John Wiley and Sons, Inc, 2014.
[58] C.K. Soz, E. Yilgor, I. Yilgor, Influence of the average surface roughness on the formation of super-hydrophobic polymer surfaces through spin-coating with hydrophobic fumed silica, Polymer 62 (2015) 118–128.
[59] F. Zhang, M. Sun, S. Xu, L. Zhao, B. Zhang, Fabrication of oriented layered double hydroxide films by spin coating and their use in corrosion protection, Chem. Eng. J. 141 (2008) 362–367.
[60] A. Eskandari, P. Sangpour, M.R. Vaezi, Hydrophilic Cu_2O nanostructured thin films prepared by facile spin coating method: investigation of surface energy and roughness, Mater. Chem. Phys. 147 (2014) 1204–1209.
[61] J. Zhang, W. Zhang, N. Zhou, Y. Wenga, Z. Hu, Photoresponsive superhydrophobic surfaces from one-pot solution spin coating mediated by polydopamine, *RSC Adv*. 4 (2014) 24973–24977.
[62] L. Xu, R.G. Karunakaran, J. Guo, S. Yang, Transparent, superhydrophobic surfaces from one-step spin coating of hydrophobic nanoparticles, ACS Appl. Mater. Interfaces 4 (2012) 1118–1125.
[63] G. He, K. Wang, The super hydrophobicity of ZnO nanorods fabricated by electrochemical deposition method, Appl. Surf. Sci. 257 (2011) 6590–6594.
[64] H.K. Kim, Y.S. Cho, Fabrication of a superhydrophobic surface via spraying with polystyrene and multi-walled carbon nanotubes, Colloids Surf. A Physicochem. Eng. Asp. 465 (2015) 77–86.
[65] Y. Zhang, D. Ge, S. Yang, Spray-coating of superhydrophobic aluminum alloys with enhanced mechanical robustness, J. Colloid Interface Sci. 423 (2014) 101–107.
[66] Z. Cui, J. Ding, L. Scoles, Q. Wang, Q. Chen, Superhydrophobic surfaces fabricated by spray-coating micelle solutions of comb copolymers, *Colloid Polym. Sci*. 291 (2013) 1409–1418.
[67] J. Ma, X. Zhang, Y. Bao, J. Liu, A facile spraying method for fabricating superhydrophobic leather coating, Colloids Surf. A Physicochem. Eng. Asp. 472 (2015) 21–25.
[68] S.S. Latthe, A.V. Rao, Superhydrophobic SiO_2 micro-particle coatings by spray method, Surf. Coat. Technol. 207 (2012) 489–492.
[69] N.L. Tarwal, V.M. Khot, N.S. Harale, S.A. Pawar, S.B. Pawar, V.B. Patil, P.S. Patil, Spray deposited superhydrophobic ZnO coatings via seed assisted growth, Surf. Coat. Technol. 206 (2011) 1336–1341.
[70] L. Ovaskainen, I.R. Meizoso, N.A. Birkin, S.M. Howdle, U. Gedde, L. Wågberg, C. Turner, Towards superhydrophobic coatings made by non-fluorinated polymers sprayed from a supercritical solution, J. Supercrit. Fluids 77 (2013) 134–141.
[71] X.H. Xu, Z.Z. Zhang, J. Yanga, X.T. Zhu, Study of the corrosion resistance and loading capacity of superhydrophobic meshes fabricated by spraying method, Colloids Surf. A Physicochem. Eng. Asp. 377 (2011) 70–75.
[72] O.U. Nimittrakoolchai, S. Supothina, Deposition of organic-based superhydrophobic films for anti-adhesion and self-cleaning applications, J. Eur. Ceram. Soc. 28 (2008) 947–952.
[73] Y. Liu, S. Li, J. Zhang, Y. Wang, Z. Han, L. Ren, Fabrication of biomimetic superhydrophobic surface with controlled adhesion by electrodeposition, Chem. Eng. J. 248 (2014) 440–447.
[74] L. Cao, X. Lu, F. Pu, X. Yin, Y. Xia, W. Huang, Z. Li, Facile fabrication of superhydrophobic Bi/ Bi_2O_3 surfaceswith hierarchical micro-nanostructures by electroless deposition or electrodeposition, Appl. Surf. Sci. 288 (2014) 558–563.
[75] Z. Zhao, H. Zhang, M. Zhao, W. Chen, X. Liu, Electrochemical Deposition and Superhydrophobic Behavior of $Cu(CH_3(CH_2)_{12}COO)_2$ on Stainless Steel, IEEE, 2011, pp. 283–286.
[76] X. Zhang, F. Shi, X. Yu, H. Liu, Y. Fu, Z. Wang, L. Jiang, X. Li, Polyelectrolyte multilayer as matrix for electrochemical deposition of gold clusters: toward super-hydrophobic surface, J. Am. Chem. Soc. 126 (2004) 3064–3065.

[77] M. Li, J. Zhai, H. Liu, Y. Song, L. Jiang, D. Zhu, Electrochemical deposition of conductive superhy-drophobic zinc oxide thin films, J. Phys. Chem. B 107 (2003) 9954–9957.

[78] S.V. Gnedenkov, S.L. Sinebryukhov, V.S. Egorkin, D.V. Mashtalyar, A.M. Emelyanenko, L. B. Boinovich, Electrochemical properties of the superhydrophobic coatings on metals and alloys, J. Taiwan Inst. Chem. Eng. 45 (2014) 3075–3080.

[79] J. Wang, A. Li, H. Chen, D. Chen, Synthesis of biomimetic superhydrophobic surface through elec-trochemical deposition on porous alumina, J. Bionic Eng. 8 (2011) 122–128.

[80] M. Mahajan, S.K. Bhargava, A.P. O'Mullane, Electrochemical formation of porous copper 7,7,8,8-tetracyanoquinodimethane and copper 2, 3,5,6-tetrafluoro-7,7,8,8 tetracyanoquinodimethane honey-comb surfaces with superhydrophobic properties, Electrochim. Acta 101 (2013) 186–195.

[81] Y. Huang, D.K. Sarkar, X.G. Chen, Fabrication of superhydrophobic surfaces on aluminum alloy via electrodeposition of copper followed by electrochemical modification, Nano-Micro Lett. 3 (2011) 160–165.

[82] M. Han, Y. Park, J. Hyun, Y. Ahn, Facile method for fabricating superhydrophobic surface on mag-nesium, Bull. Kor. Chem. Soc. 31 (2010) 1067–1069.

[83] B. Qian, Z. Shen, Fabrication of superhydrophobic surfaces by dislocation-selective chemical etching on aluminum, copper, and zinc substrates, Langmuir 21 (2005) 9007–9009.

[84] Y.Y. Quan, P.G. Jiang, L.Z. Zhang, Development of fractal ultra-hydrophobic coating films to prevent water vapor dewing and to delay frosting, Fractals 22 (2014) 1440002 (1–12).

[85] D. Qi, N. Lu, H. Xu, B. Yang, C. Huang, M. Xu, L. Gao, Z. Wang, L. Chi, Simple approach to wafer-scale self-cleaning antireflective silicon surfaces, Langmuir 25 (2009) 7769–7772.

[86] Y. Shi-heng, Z. Bin, L. Yun-chun, Y. Ji, K. Tong-chun, Fabrication of superhydrophobic aluminum plate by surface etching and fluorosilane modification, Chem. Res. Chin. Univ. 28 (2012) 903–906.

[87] D. Xie, W. Li, A novel simple approach to preparation of superhydrophobic surfaces of aluminum alloys, Appl. Surf. Sci. 258 (2011) 1004–1007.

[88] L. Hao, Y. Sirong, H. Xiangxiang, L. Enyang, Z. Yan, Fabrication of superhydrophobic and oleopho-bic surface on zinc substrate by a simple method, Colloids Surf. A Physicochem. Eng. Asp. 469 (2015) 271–278.

[89] R. Liao, Z. Zuo, C. Guo, Y. Yuan, A. Zhuang, Fabrication of superhydrophobic surface on aluminum by continuous chemical etching and its anti-icing property, Appl. Surf. Sci. 317 (2014) 701–709.

[90] W. Liu, L. Sun, Y. Luo, R. Wub, H. Jiang, Y. Chena, G. Zeng, Y. Liu, Facile transition from hydro-philicity to superhydrophilicity and superhydrophobicity on aluminum alloy surface by simple acid etching and polymer coating, Appl. Surf. Sci. 280 (2013) 193–200.

[91] Y. Shen, H. Tao, S. Chen, Y. Xie, T. Zhou, T. Wang, J. Tao, Water repellency of hierarchical super-hydrophobic Ti6Al4V surfaces improved by secondary nanostructures, Appl. Surf. Sci. 321 (2014) 469–474.

[92] X. Xu, Z.Z. Zhang, W.M. Liu, Stable biomimetic super-hydrophobic copper surface fabricated by a simple wet-chemical method, J. Dispers. Sci. Technol. 31 (2010) 488–491.

[93] P. Li, X. Chen, G. Yang, L. Yu, P. Zhang, Fabrication of a superhydrophobic etched copper–silver/stearic acid composite coating evaluation of its friction-reducing and anticorrosion abilities, Mater. Express 4 (2014) 309–316.

[94] J.P. Lee, S. Choi, S. Park, Extremely superhydrophobic surfaces with micro- and nanostructures fab-ricated by copper catalytic etching, Langmuir 27 (2011) 809–814.

[95] P. Varshney, J. Lomga, P.K. Gupta, S.S. Mohapatra, A. Kumar, Durable and regenerable superhydro-phobic coatings for aluminium surfaces with excellent water-repellent self-cleaning and anti-fogging properties, Tribol. Int. 119 (2018) 38–44.

[96] A. Kumar, B. Gogoi, Development of durable self-cleaning superhydrophobic coatings for aluminium surfaces via chemical etching method, Tribol. Int. 118 (2018) 114–118.

[97] P. Varshney, D. Nanda, S.S. Mohapatra, A. Kumar, A facile modification of steel mesh for selective separation of oil-water mixtures, New J. Chem. 41 (2017) 7463–7471.

[98] J. Lomga, P. Varshney, D. Nanda, M. Satapathy, S.S. Mohapatra, A. Kumar, Fabrication of durable and regenerable superhydrophobic coatings with excellent self-cleaning and anti-fogging properties for alu-minium surfaces, J. Alloys Compd. 712 (2017) 161–170.

[99]   P. Varshney, S.S. Mohapatra, A. Kumar, Fabrication of mechanically stable superhydrophobic aluminium surface with excellent self-cleaning and anti-fogging properties, Biomimetics 2 (2017) 1–12.
[100] P. Varshney, S.S. Mohapatra, A. Kumar, Superhydrophobic coatings for aluminium surfaces synthesized by chemical etching process, Int. J. Smart Nano Mater. 7 (2016) 248–264.
[101] J. Gao, Y. Li, Y. Li, H. Liu, W. Yang, Fabrication of superhydrophobic surface of stearic acid grafted
       zinc by using an aqueous plasma etching technique, Cent. Eur. J. Chem. 10 (2012) 1766–1772.
[102] H.C. Barshilia, N. Gupta, Superhydrophobic polytetrafluoroethylene surfaces with leaf-like microprotrusions through Ar + O_2 plasma etching process, Vacuum 99 (2014) 42–48.
[103] J.P. Youngblood, T.J. McCarthy, Ultrahydrophobic polymer surfaces prepared by simultaneous ablation of polypropylene and sputtering of poly(tetrafluoroethylene) using radio frequency plasma,
       Macromolecules 32 (1999) 6800–6806.
[104] B. Balu, J.S. Kim, V. Breedveld, D.W. Hess, Design of superhydrophobic paper/cellulose surfaces
       via plasma enhanced etching and deposition, in: Contact Angle, Wettability and Adhesion, vol. 6,
       Taylor & Francis Group, 2009, pp. 235–249.
[105] K. Teshima, H. Sugimura, Y. Inoue, O. Takai, A. Takano, Transparent ultra-water-repellent
       poly(ethylene terephthalate) substrates fabricated by oxygen plasma treatment and subsequent hydrophobic coating, *Appl. Surf. Sci.* 244 (2005) 619–622.
[106] M. Psarski, J. Marczak, J.B. Grobelny, G. Celichowski, Superhydrophobic surface by replication of
       laser micromachined pattern in epoxy/alumina nanoparticle composite, J. Nanomater. 2014 (2014)
       1–11. Article ID 547895.
[107] R. Hu, G. Jiang, X. Wang, X. Xi, R. Wang, Facile preparation of superhydrophobic surface with high
       adhesive forces based carbon/silica composite films, Bull. Mater. Sci. 36 (2013) 1091–1095.
[108] C. Xiao, J. Yang, T. Li, Fabrication and superhydrophobic property of ZnO micro/nanocrystals via a
       hydrothermal route, *J. Nanomater.* 2014 (2014) 1–6. Article ID 680592.
[109] F. Shi, X. Chen, L. Wang, J. Niu, J. Yu, Z. Wang, X. Zhang, Roselike microstructures formed by
       direct in situ hydrothermal synthesis: from superhydrophilicity to superhydrophobicity, *Chem. Mater.*
       17 (2005) 6177–6180.
[110] S. Yin, D. Wu, J. Yang, S. Lei, T. Kuang, B. Zhu, Fabrication and surface characterization of biomimic superhydrophobic copper surface by solution-immersion and self-assembly, Appl. Surf. Sci.
       257 (2011) 8481–8485.
[111] C. Pan, L. Shen, S. Shang, Y. Xing, Preparation of superhydrophobic and UV blocking cotton fabric
       via sol–gel method and self-assembly, Appl. Surf. Sci. 259 (2012) 110–117.
[112] Z.X. Li, Y.J. Xing, J.J. Dai, Superhydrophobic surfaces prepared from water glass and non-fluorinated
       alkylsilane on cotton substrates, Appl. Surf. Sci. 254 (2008) 2131–2135.
[113] X. Song, J. Zhai, Y. Wang, L. Jiang, Self-assembly of amino-functionalized monolayers on silicon
       surfaces and preparation of superhydrophobic surfaces based on alkanoic acid dual layers and surface
       roughening, *J. Colloid Interface Sci.* 298 (2006) 267–273.
[114] G. Yin, W. Xue, F. Chen, X. Fan, Self-repairing and superhydrophobic film of gold nanoparticles and
       fullerene pyridyl derivative based on the self-assembly approach, Colloids Surf. A Physicochem. Eng.
       Asp. 340 (2009) 121–125.
[115] W. Huaiyuana, Z. Yanjia, F. Xin, L. Xiaohua, The effect of self-assembly modified potassium titanate
       whiskers on the friction and wear behaviors of PEEK composites, Wear 269 (2010) 139–144.
[116] C. Badre, P. Dubot, D. Lincot, T. Pauporte, M. Turmine, Effects of nanorod structure and conformation of fatty acid self-assembled layers on superhydrophobicity of zinc oxide surface, *J. Colloid Interface Sci.* 316 (2007) 233–237.
[117] D. Nanda, A. Sahoo, A. Kumar, B. Bhushan, Facile approach to develop durable and reusable superhydrophobic/superoleophilic coatings for steel mesh surfaces, J. Colloid Interface Sci. 535 (2019)
       50–57.
[118] P. Chuahan, A. Kumar, B. Bhushan, Self-cleaning, stain-resistant and anti-bacterial superhydrophobic
       cotton fabric prepared by simple immersion technique, J. Colloid Interface Sci. 535 (2019) 66–74.
[119] A. Panda, P. Varshney, S.S. Mohapatra, A. Kumar, Development of liquid repellent coating on cotton
       fabric by simple binary silanization with excellent self-cleaning and oil–water separation properties,
       Carbohydr. Polym. 181 (2018) 1052–1060.

[120] D. Nanda, P. Varshney, M. Satapathy, S.S. Mohapatra, A. Kumar, Self-assembled monolayer of functionalized silica microparticles for self-cleaning applications, Colloids Surf. A Physicochem. Eng. Asp. 529 (2017) 231–238.

[121] L. Lu, C. Hu, Y. Zhu, H. Zhang, R. Li, Y. Xing, Multi-functional finishing of cotton fabrics by water-based layer-by-layer assembly of metal–organic framework, Cellulose 25 (2018) 4223–4238.

[122] J. Bravo, L. Zhai, Z. Wu, R.E. Cohen, M.F. Rubner, Transparent superhydrophobic films based on silica nanoparticles, Langmuir 23 (2007) 7293–7298.

[123] S. Amigoni, E.T. Givenchy, M. Dufay, F. Guittard, Covalent layer-by-layer assembled superhydrophobic organic-inorganic hybrid films, Langmuir 25 (2009) 11073–11077.

[124] E. Celia, T. Darmanin, E.T. Givenchy, S. Amigoni, F. Guittard, Recent advances in designing superhydrophobic surfaces, J. Colloid Interface Sci. 402 (2013) 1–18.

[125] D. Oner, T.J. McCarthy, Ultrahydrophobic surfaces. effects of topography length scales on wettability, Langmuir 16 (2000) 7777–7782.

[126] J.S. Feng, M.T. Tuominen, J.P. Rothstein, Hierarchical superhydrophobic surfaces fabricated by dual-scale electron-beam-lithography with well-ordered secondary nanostructures, *Adv. Funct. Matter.* 21 (2011) 3715–3722.

[127] F.J. Korpela, J. Karvinen, B. Päivänranta, A. Partanen, M. Suvanto, M. Kuittinen, T. T. Pakkanen, Hydrophobic and oleophobic anti-reflective polyacrylate coatings, Microelectron. Eng. 114 (2014) 38–46.

[128] C.W. Wu, Y.K. Shen, S.Y. Chuang, C.S. Wei, Anti-adhesive effects of diverse self-assembled monolayers in nanoimprint lithography, Sens. Actuators A Phys. 139 (2007) 145–151.

[129] F. Zhang, J. Chan, H.Y. Low, Biomimetic, hierarchical structures on polymer surfaces by sequential imprinting, Appl. Surf. Sci. 254 (2008) 2975–2979.

[130] C.F. Huang, Y. Lin, Y.K. Shen, Y.M. Fan, Optimal processing for hydrophobic nanopillar polymer surfaces using nanoporous alumina template, Appl. Surf. Sci. 305 (2014) 419–426.

[131] A. Pozzato, S.D. Zilio, G. Fois, D. Vendramin, G. Mistura, M. Belotti, Y. Chen, M. Natali, Superhydrophobic surfaces fabricated by nanoimprint lithography, Microelectron. Eng. 83 (2006) 884–888.

[132] C.W.J. Berendsen, M. Skeren, D. Najdek, F. Cerny, Superhydrophobic surface structures in thermoplastic polymers by interference lithography and thermal imprinting, Appl. Surf. Sci. 255 (2009) 9305–9310.

[133] C. Sun, L.Q. Ge, Z.Z. Gu, Fabrication of super-hydrophobic film with dual-size roughness by silica sphere assembly, Thin Solid Films 515 (2007) 4686–4690.

[134] J. Liang, K. Liu, D. Wang, H. Li, P. Li, S. Li, S. Su, Y. Luo, Facile fabrication of superhydrophilic/superhydrophobic surface on titanium substrate by single-step anodization and fluorination, Appl. Surf. Sci. 338 (2015) 126–136.

[135] Y. Gao, Y. Sun, D. Guo, Facile fabrication of superhydrophobic surfaces with low roughness on Ti–6Al–4V substrates via anodization, Appl. Surf. Sci. 314 (2014) 754–759.

[136] W. Lee, B.G. Park, D.H. Kim, D.J. Ahn, Y. Park, S.H. Lee, K.B. Lee, Nanostructure-dependent water-droplet adhesiveness change in superhydrophobic anodic aluminum oxide surfaces: from highly adhesive to self-cleanable, Langmuir 26 (2010) 1412–1415.

[137] Y. Yin, T. Liu, S. Chen, T. Liu, S. Cheng, Structure stability and corrosion inhibition of superhydrophobic film on aluminum in seawater, Appl. Surf. Sci. 255 (2008) 2978–2984.

[138] S.C. Vanithakumari, R.P. George, U.K. Mudali, Influence of silanes on the wettability of anodized titanium, Appl. Surf. Sci. 292 (2014) 650–657.

[139] R.V. Lakshmi, T. Bharathidasan, P. Bera, B.J. Basu, Fabrication of superhydrophobic and oleophobic sol–gel nanocomposite coating, Surf. Coat. Technol. 206 (2012) 3888–3894.

[140] Y. Fan, C. Li, Z. Chen, H. Chen, Study on fabrication of the superhydrophobic sol–gel films based on copper wafer and its anti-corrosive properties, Appl. Surf. Sci. 258 (2012) 6531–6536.

[141] R.V. Lakshmi, B.J. Basu, Fabrication of superhydrophobic sol–gel composite films using hydrophobically modified colloidal zinc hydroxide, J. Colloid Interface Sci. 339 (2009) 454–460.

[142] S. Wang, C. Liu, G. Liu, M. Zhang, J. Li, C. Wang, Fabrication of superhydrophobic wood surface by a sol–gel process, Appl. Surf. Sci. 258 (2011) 806–810.

[143] S.D. Wang, B.J. Lin, C.C. Hsieh, C.C. Lin, Application of superhydrophobic sol gel on canvas, Appl. Surf. Sci. 307 (2014) 101–108.

[144] W.H. Huang, C.S. Lin, Robust superhydrophobic transparent coatings fabricated by a low-temperature sol–gel process, Appl. Surf. Sci. 305 (2014) 702–709.

[145] D. Su, C. Huang, Y. Hu, Q. Jiang, L. Zhang, Y. Zhu, Preparation of superhydrophobic surface with a novel sol–gel system, Appl. Surf. Sci. 258 (2011) 928–934.

[146] X.F. Wen, K. Wang, P.H. Pi, J.X. Yang, Z.Q. Cai, L. Zhang, Y. Qian, Z.R. Yang, D. Zheng, J. Cheng, Organic–inorganic hybrid superhydrophobic surfaces using methyltriethoxysilane and tetraethoxysilane sol–gel derived materials in emulsion, Appl. Surf. Sci. 258 (2011) 991–998.

[147] R.V. Lakshmi, T. Bharathidasan, B.J. Basu, Superhydrophobic sol–gel nanocomposite coatings with enhanced hardness, Appl. Surf. Sci. 257 (2011) 10421–10426.

[148] M. Satapathy, P. Varshney, D. Nanda, S.S. Mohapatra, A. Behera, A. Kumar, Fabrication of durable porous and non-porous superhydrophobic LLDPE/SiO$_2$ nanoparticles coatings with excellent self-cleaning property, Surf. Coat. Technol. 341 (2018) 31–39.

[149] D. Nanda, T. Swetha, P. Varshney, P.K. Gupta, S.S. Mohapatra, A. Kumar, Temperature dependent switchable superamphiphobic coating on steel surface, J. Alloys Compd. 727 (2017) 1293–1301.

[150] M. Satapathy, P. Varshney, D. Nanda, A. Panda, S.S. Mohapatra, A. Kumar, Fabrication of superhydrophobic and superoleophilic polymer composite coatings on cellulosic filter paper for oil-water separation, Cellulose 24 (2017) 4405–4418.

[151] K.L. Choy, Chemical vapour deposition of coatings, Prog. Mater. Sci. 48 (2003) 57–170.

[152] S. Rezaei, I. Manoucheri, R. Moradian, B. Pourabbas, One-step chemical vapor deposition and modification of silica nanoparticles at the lowest possible temperature and superhydrophobic surface fabrication, Chem. Eng. J. 252 (2014) 11–16.

[153] B.B. Wang, J.T. Feng, Y.P. Zhao, T.X. Yu, Fabrication of novel superhydrophobic surfaces and water droplet bouncing behavior — Part 1: stable ZnO–PDMS superhydrophobic surface with low hysteresis constructed using ZnO nanoparticles, J. Adhes. Sci. Technol. 24 (2010) 2693–2705.

CHAPTER 4

Nanomaterials for design and fabrication of superhydrophobic polymer coating

Ayesha Kausar
National University of Sciences and Technology, Islamabad, Pakistan

1. Introduction

Superhydrophobic materials are highly hydrophobic and it is extremely difficult to wet such surfaces [1]. The water contact angle of superhydrophobic materials may exceed 150 degrees. Superhydrophobic surfaces have been used for numerous engineering applications such as self-cleaning, antibiofouling, anticorrosion, biomedical, and textiles [2]. Significantly protecting properties of the coatings have been achieved using superhydrophobic materials. Successful fabrication of superhydrophobic surfaces demands controlled generation of hierarchical rough morphology [3]. The choice of hydrophobic polymers such as fluoropolymers, perfluorooctanoic acids, etc. is also important to form superhydrophobic surfaces [4, 5]. Superhydrophobic polymer morphology and roughness can also be altered using nanoparticles, lithography, etching, biomimetic, and stamping processes [6]. The superhydrophobic surfaces may have additional features such as magnetic, mechanical, wear, thermal, conducting, etc. [7–10]. The hydrophobic polymers have been reinforced with various nanoparticles (carbon nanotube (CNT), graphene, carbon nanofiber, carbon black (CB), zinc oxide, silica, etc.) to form superhydrophobic materials [11–13]. Nanocarbon-based superhydrophobic surfaces are low cost having high electrical and thermal conductivity and strength. The multifunctional polymer/nanocarbon superhydrophobic surfaces have been employed in electronics, electromagnetic interference (EMI) shielding devices, strength and wear demanding materials, and biomedical. In this chapter, progress in the field of polymer/nanocarbon, polymer/inorganic nanoparticle, and polymer/hybrid organic-inorganic nanoparticle for superhydrophobic coatings is comprehended. Initially, basics of superhydrophobic coatings and nanocomposite coatings have been outlined. Finally, future opportunities and challenges in the emerging technological field of superhydrophobic coatings have been discussed.

Fig. 1 Superhydrophobic coating. *(Reproduced with permission from Ovaskainen, L., et al., Superhydrophobic polymeric coatings produced by rapid expansion of supercritical solutions combined with electrostatic deposition (RESS-ED), J. Supercrit. Fluids 95 (2014) 610–617, Elsevier.)*

2. Superhydrophobic polymer coating

Superhydrophobic surfaces have gained interest owing to excellent water repulsion and self–cleaning properties (Fig. 1) [14]. This effect is commonly known as "lotus effect." The properties of lotus leaf have been mimicked using micro– and nanoscale materials [15, 16]. Good superhydrophobic surfaces must have water contact angle >150 degrees. On the other hand, contact angle hysteresis and roll–off angle must be low <10 degrees. Several polymers have been used to form superhydrophobic surfaces such as polystyrene (PS), poly(vinyl fluoride), poly(methyl methacrylate), epoxy, and several other vinyl and acrylic polymers. Spin coating, electrospraying, electrodeposition, electrospinning, etc. have been used to form superhydrophobic surfaces [17]. The superhydrophobic coating of PS was prepared using electrospinning process and dimethylformamide (DMF) solvent. The water contact angle of >150 degrees was obtained [18]. Superhydrophobic surface of poly(hydroxybutyratecohydroxyvalerate) (PHBV) and chloroform has been prepared using electrospinning [19]. The PHBV surface had water contact angle of 76 degrees. The surface roughness and water contact angle were increased up to 158 degrees. The dispersion of polytetrafluoroethylene nanoparticles in poly[tetrafluoroethylene-*co*(vinylidenefluoride)-*co*-propylene] was prepared using electrospinning and water contact angle of >150 degrees was attained [20]. Ovaskainen et al. [21] produced superhydrophobic polymeric coatings using rapid expansion of supercritical solution (RESS) and electrostatic deposition (ED). Poly(vinyl acetate)poly(vinyl pivalate) was dissolved in supercritical carbon dioxide and acetone. The mixture was sprayed through a nozzle with an applied voltage of 8 kV. Fig. 2 shows setup for spraying technique used for ED, that is, RESS–ED. Processing parameters were well controlled using RESS–ED technique and the superhydrophobic surface produced with spraying was excellent water repellent. Moreover, RESS–ED process may yield large, fine, and thin coatings.
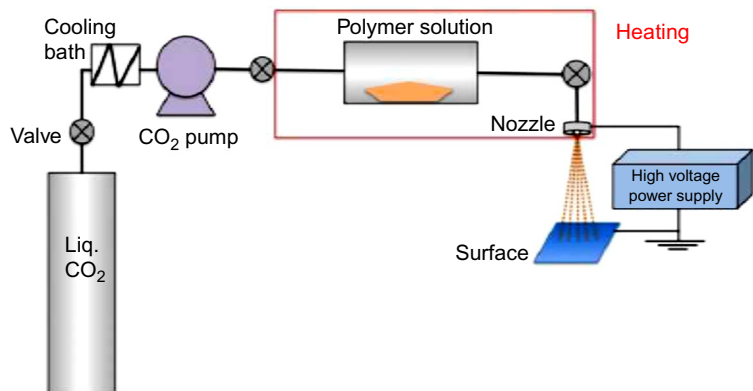
Fig. 2 Schematic diagram of RESS-ED setup used in spraying experiments. *(Reproduced with permission from Ovaskainen, L., et al., Superhydrophobic polymeric coatings produced by rapid expansion of supercritical solutions combined with electrostatic deposition (RESS-ED), J. Supercrit. Fluids 95 (2014) 610–617, Elsevier.)*

3. Superhydrophobic polymer nanocomposite coating

Carbon nanomaterials have been focused for superhydrophobic coatings on metals, polymers, wood, or textile [22, 23]. Nanocarbon such as CB, graphene, and CNT is water repellent agents [24]. These nanocarbon allotropes can be structured at micro/nanoscale to gain superhydrophobic properties. Vertically aligned CNT arrays or CNT forests have been used to imitate water repellent properties of lotus leaves [25]. Carbon nanomaterials (graphene (Gr) and CNT) have been deposited on rough wood surface to create superhydrophobicity. Simple drop casting and dip coating methods have been used to form carbon nanomaterials [24]. The contact angle measurements of wood coated material were >130 degrees. The Gr and CNT were physically bonded to the wood surface. Fig. 3 shows a proposed model for carbon nanomaterial deposition on wood. The surface is partly wetted by water. The superhydrophobic effect was observed due to micro–
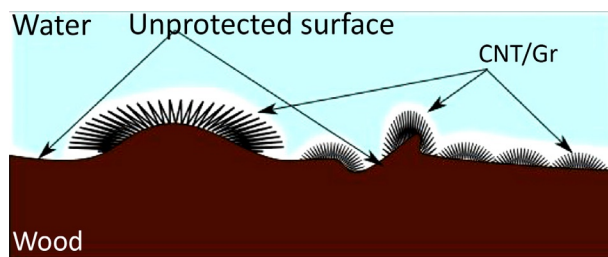
Fig. 3 Cassie's impregnating state model for wood covered with carbon nanomaterial. *(Reproduced with permission from Łukawski, D., et al., Towards the development of superhydrophobic carbon nanomaterial coatings on wood, Prog. Org. Coat. 125 (2018) 23–31, Elsevier.)*

roughness of the wood surface. The CNT/H$_2$O/BW and Gr/H$_2$O/BW (CNT=carbon nanotube; Gr=graphene; and BW=balsa wood) became superhydrophobic (contact angle > 130 degrees) after surfactant removal (Fig. 4A). The contact angle was stable after 10 min for CNT/H$_2$O/BW, that is, 134 degrees (Fig. 4B). Moreover, the deposited droplets were steadfastly attached to the surface (Fig. 4C). On the other hand, the presence of surfactant render the coatings hydrophilic (Fig. 4D). Using polymeric nanocomposite hydrophilic wood surface has been successfully transformed into the superhydrophobic materials. The superhydrophobic nanocomposite coatings of polyethylene terephthalate/multiwalled carbon nanotube (MWCNT)/silica nanoparticles were fabricated using spray method [26]. The nanocomposite coating with 0.2 wt% MWCNT had excellent hydrophobicity with contact angle of 156.7 degrees. There was 95.7% transparency and sheet resistance of $3.2 \times 10^4 \Omega$ sq.$^{-1}$. Superhydrophobic self-cleaning nanocomposite coating of polytetrafluoroethylene/TiO$_2$ has been reported [27]. The superhydrophobic polymer/tungsten oxide (WO$_3$) nanocomposite coatings were developed on glass substrates [28, 29]. Thus, various designs and compositions of polymer nanocomposite coatings have shown unique chemical structure, enhanced superhydrophobicity, and highly rough surface to be employed in relevant applications.
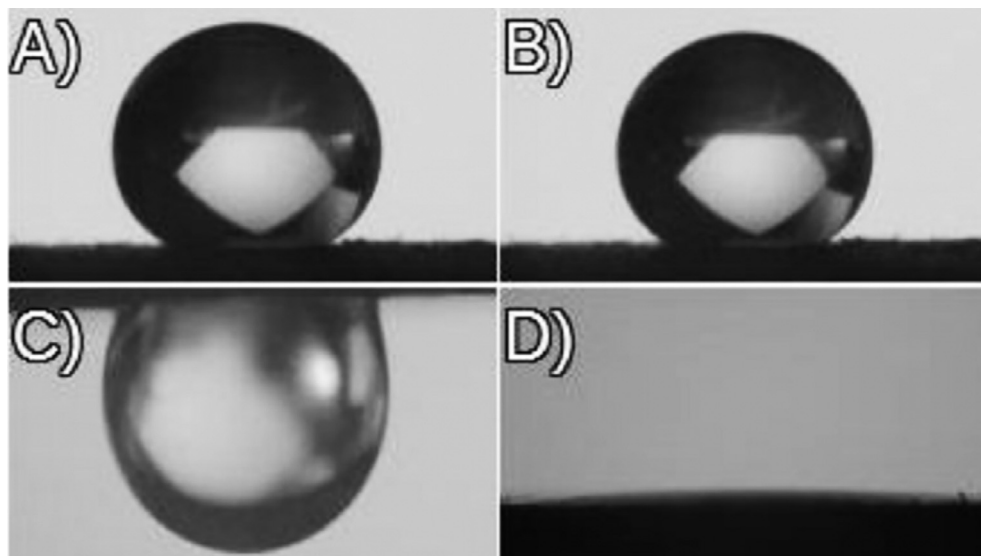
Fig. 4 A droplet of water at CNT/H$_2$O/BW (A) immediately after dropping; (B) 10 min after dropping; (C) with surface turned upside-down; and (D) without surfactant rinsing. *(Reproduced with permission from Łukawski, D., et al., Towards the development of superhydrophobic carbon nanomaterial coatings on wood, Prog. Org. Coat. 125 (2018) 23–31, Elsevier.)*

4. Polymer/nanocarbon nanocomposite coating

4.1 Polymer/nanodiamond-based superhydrophobic coating

Nanodiamond (ND) is a unique nanocarbon having exclusive surface properties, electronic and optical features, hardness, and biocompatibility useful for polishing technology, coatings, catalysis, drug carriers, cosmetics, etc. [30, 31]. Polymer and ND core-shell particles have been prepared with superior surface roughness, efficient light scattering, thermal conductivity, and superhydrophobicity [32, 33]. Physical or chemical adsorption of polymers on ND using intermolecular interaction such as ionic interaction/hydrogen bonding may form stable superhydrophobic structures. ND is a promising nanocarbon material used in various applications demanding superhydrophobicity. Takafuji et al. [34] demonstrated superhydrophobic thin ND layer by mixing polymer particles. Cao et al. [35] prepared superhydrophobic coating of hydroxylated ND, polydopamine (PDA), and $1H,1H,2H,2H$-perfluorodecanethiol (PFDT). The PDA modified ND nanoparticles were anchored on commercial polyurethane (PU) sponge. The sponge was used for the selective removal of oil from water. Fig. 5 shows the absorption capacity of superhydrophobic ND coated PU sponge. The foam was tested for diesel, pump oil, and gasoline over 10 consecutive cycles. The sponge was found highly stable with a variation of 10 cycles. Future research on polymer/ND films or sponges may lead to very
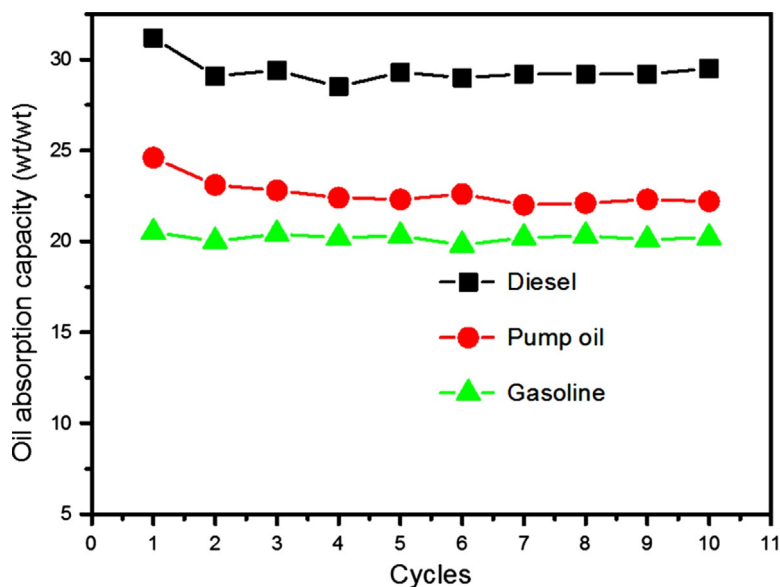
Fig. 5 The oil absorption capacity of superhydrophobic nanodiamond coated polyurethane sponge after 10 cycles of oil removal process. *(Reproduced with permission from Cao, N., et al., Polyurethane sponge functionalized with superhydrophobic nanodiamond particles for efficient oil/water separation, Chem. Eng. J. 307 (2017) 319–325., Elsevier.)*

high organic adsorption capacity and superhydrophobicity. The materials possess low cost, feasible fabrication, and excellent performance toward superhydrophobic properties, oil/water separation, and other desirable practical applications.

4.2 Polymer/fullerene-based superhydrophobic coating

Fullerenes are nanocarbon spheroidal molecules having hollow cage structures of 60 or more atoms, which are often known as buckminsterfullerene [36]. Fullerenes are useful materials in optoelectronics, semiconductors, and energy storage devices [37]. Polymer/ fullerene nanomaterials had characteristic properties in electrochemistry, photoelectrochemistry, and hydrophobicity. The C_{60}-porphyrin cocrystals have been self-assembled to form hierarchical architectures [38]. Though, controllable fabrication of fullerene hierarchical structures is challenging [39]. Nakanishi et al. [40] developed superhydrophobic surfaces of polymer and fullerene. Due to π-π and vander Waals interactions between polymer aliphatic chains and fullerene moieties, hierarchical, supramolecular layers were prepared. The superhydrophobic surfaces have high durability. Zheng et al. [41] used drop drying process to form self-assembled superhydrophobic hierarchical fullerene microstructures. The polymer/C_{60} or polymer/C_{70}-based hierarchical structures with superhydrophobicity can be used in high photoluminescence and water–proof optoelectronics.

4.3 Polymer/graphene-based superhydrophobic coating

Research on novel superhydrophobic films having superior self-cleaning, antisticking coating, and oil–water separation has gained attention. Graphene is a single atom-thick nanosheet composed of sp^2-hybridized carbon atom having high hydrophobicity [42]. Fluorinated polymers have high superhydrophobicity and chemical and environmental stability [43]. Poly(vinylidene fluoride) (PVDF) form superhydrophobic surface with low surface roughness and decreased water contact angle. Polymer/graphene nanocomposites have gained increasing consideration owing to improved mechanical properties, electrical conductivity, thermal conductivity, and stimulation–responsive properties [44]. Surface wettability of these materials has been controlled using various graphene nanosheet content [12]. Graphene has been used to enhance the hydrophobicity and roughness to form high-performance superhydrophobic materials [45]. In this regard, PVDF/graphene composites possess superhydrophobicity [46]. Inclusion of small amount of graphene in PVDF led to morphology change as well as significantly enhanced surface roughness. Li et al. [38] developed superhydrophobic hierarchically wrinkled surfaces having high water contact angle of >160 degrees and water sliding <5 degrees. A 500 nm nanostructure was fabricated on PVDF through nanoimprint lithography. Zha et al. [47] formed superhydrophobic PVDF/graphene nanoporous materials. Graphene addition varied the surface properties of superhydrophobic PVDF coatings. Construction of multileveled polymer/graphene structure may reveal critical features of superhydrophobic surface for micro- and nanoscaled devices.

4.4 Polymer/CNT-based superhydrophobic coating

CNT is a nanoallotrope of carbon having cylindrical structure. Caron nanotubes are nanofibrils which may be assembled to form useful structures for technical applications such as electronics, optics, and other materials science relevance [48]. Superhydrophobic CNT materials have been prepared through noncovalent/covalent attachment of nano-filler to hydrophobic polymer molecules [49]. Superhydrophobic CNT layers have been assembled using various techniques such as spray coating, chemical vapor deposition, Langmuir–Blodgett deposition, vacuum filtering, drop casting, etc. [50]. Wang et al. [51] prepared stable superhydrophobic polymer/CNT coatings. The superhydrophobic materials had excellent environmental stability after bending/pressing. Li et al. [52] pre-pared homogeneous dispersion of an azide copolymer poly(4-azidophenylmethacryla-te-*co*-methyl acrylate) and MWCNT in various organic solvents. The π–π interactions were developed between the polymer and nanotube. Addition of MWCNT transformed the material to superhydrophobic with water contact angle of 154 degrees. Yang et al. [53] formed stable and transparent superhydrophobic PS/CNT nanocomposite films using spray casting process. The superhydrophobic films possess high water contact angle of 160 degrees and sliding angle of 38 degrees. The film had light transmittance of 78%. The superhydrophobic polymer/MWCNT films coated on glass, metals, or polymers are highly water repellent, self-cleaning, and having high water contact angles. The polymer/MWCNT-based superhydrophobic coatings may have potential applications in nonwetting surfaces, microfluidic devices, bioseparation, etc.

4.5 Polymer/CB-based superhydrophobic coating

Micro- and nanoscale hierarchically structured surfaces are found vital in producing superhydrophobic surface [54]. CB is a paracrystalline carbon with high surface area-to-volume ratio. Numerous methods have been used to form superhydrophobic surface of polymer and CB such as lithographic patterning, electrodeposition, plasma etching, layer-by-layer assembly, chemical vapor deposition, etc. The CB particles were modified by blending with antioxidant stabilizer to form superhydrophobic film [55]. The perfor-mance of polymer/CB composite surface has been enhanced using modified carbon black (MCB). The raspberry-like PS/CB particles have been prepared using heterocoa-gulaion process through π–π interactions between PS and MCB particles. The hetero-coagulation process offered colloid stability in various liquid media [56]. Bao et al. [57] developed raspberry-like PS/CB composite microsphere using heterocoagulation method. Scanning electron microscopy (SEM) was used to study the morphology of raspberry-like PS covered CB particles. The superhydrophobic surface was prepared using the colloidal suspension of PS/CB film. Fig. 6 shows the fabrication process for superhydrophobic particulate film. The MCB dispersion was dropped on PS micro-spheres under 1020 rpm. The dispersion was further centrifuged at 3000 rpm to remove
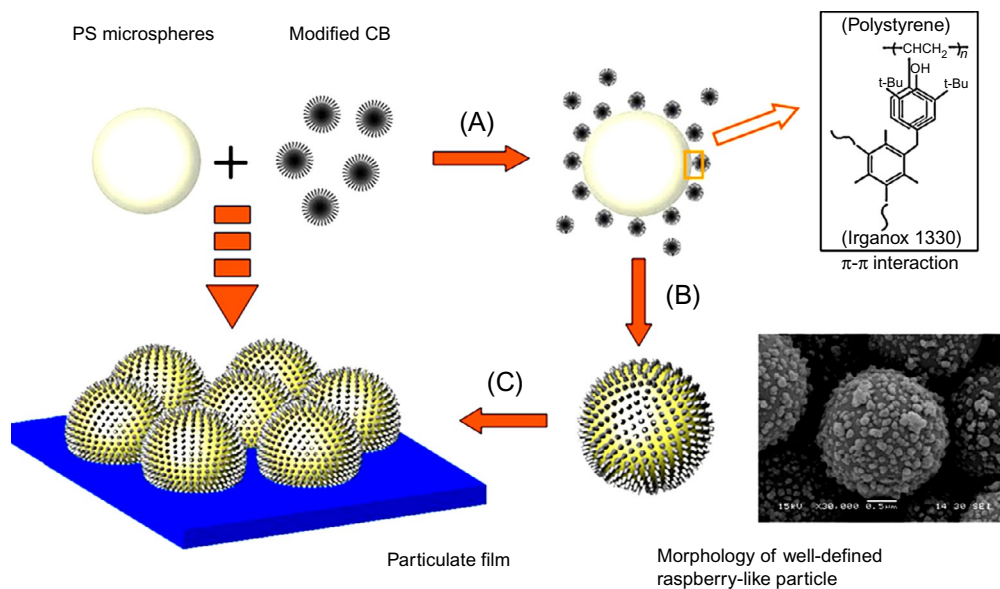
Fig. 6 Schematic illustration for the fabrication of superhydrophobic particulate film: (A) Modified carbon black dispersion on PS microspheres; (B) centrifugation; and (C) superhydrophobic film formation. Inset: SEM photograph of well-defined raspberry-like particles (MCB content 10 wt%). *(Reproduced with permission from Bao, Y., et al., Tailoring the morphology of raspberry-like carbon black/polystyrene composite microspheres for fabricating superhydrophobic surface, Mater. Res. Bull. 46 (5) (2011) 779–785, Elsevier.)*

free CB particles. Finally, superhydrophobic particulate film was deposited. Table 1 reveals the surface properties and root main square (rms) roughness of the particulate film. According to the results, 10 wt% MCB content was found suitable to fabricate the superhydrophobic surface with appropriate surface roughness. The CB-based superhydrophobic surfaces are low cost, scalable, and easy to prepare on commercial scale [58]. The self-cleaning ability of polymer/CB superhydrophobic layers may enable expedient

Table 1 WCA, sliding angle of surface, and rms roughness of relevant raspberry-like particles.

MCB content (wt%)	Water contact angle (WCA) (degrees)	Sliding angle (degrees)	Root main square (rms) roughness (nm)
5	120.3	63.2	16.8 ± 0.7
8	142.5	56.5	19.7 ± 0.6
10	155.2	29.5	28.9 ± 1.0
12	148.0	47.3	23.3 ± 0.8
15	141.4	55.2	17.9 ± 1.4

Reproduced with permission from Bao, Y., et al., Tailoring the morphology of raspberry-like carbon black/polystyrene composite microspheres for fabricating superhydrophobic surface, Mater. Res. Bull. 46 (5) (2011) 779–785, Elsevier.

recycling process toward various technical applications. The polymer/CB superhydrophobic substrate may have future potential related to solar evaporation.

4. Polymer/inorganic nanoparticle-based superhydrophobic nanocomposite coating

Incorporation of inorganic nanoparticles in polymers enhanced the superhydrophobic nature of coating materials [59, 60]. Superhydrophobic materials based on polymers and inorganic nanoparticles offered large-area, stable, and mechanically robust films on various substrates. The durability of material may be enhanced through cross-linking or covalent bonding between the coating and substrate. Bormashenko et al. [61] developed superhydrophobic surface of disordered triple-scaled arrays of PVDF and metal nanoparticles. The hydrophobicity of inherently wettable surfaces was studied. Liu et al. [62] prepared stable superhydrophobic films of $1H,1H,2H,2H$-perfluorooctyltrichlorosilane [$CF_3(CF_2)_5(CH_2)_2SiCl_3$] and zinc nanoparticles. The films had effective corrosion resistance when tested in 3%NaCl solution for 29 days. Ebert and Bhushan [63] developed superhydrophobic surfaces using polycarbonate and poly(methyl methacrylate) with surface functionalized SiO_2, ZnO, and indium tin oxide nanoparticles. The surfaces possess high water contact angle, low contact angle hysteresis, high transmission, and good wear resistance. However, fabrication of such surfaces often involves complex or expensive techniques which are not suitable for variety of materials and substrates. Low-abrasion durability is also one of the major issues for polymer/inorganic superhydrophobic coatings.

6. Polymer/hybrid organic-inorganic-based superhydrophobic coating

Organic-inorganic hybrids have been used for superhydrophobic surfaces with fine self-cleaning, antifogging, stability, and biocompatibility properties [64]. For example, incorporation of nanoparticle/microparticle in hybrid polymer matrix may lead to fine superhydrophobicity and other enhanced coating characteristics. Han et al. [65] developed novel organic-inorganic hybrid films of poly(allylamine hydrochloride) and ZrO_2 nanoparticles coated with poly(acrylic acid) using layer-by-layer deposition. Incorporation of hybrid coated ZrO_2 nanoparticles in matrix enhanced the superhydrophobicity and mechanical properties of the organic film. Bayer et al. [66] fabricated nanostructured self-cleaning superhydrophobic polymer/organoclay hybrids. Hybrids of organically modified montmorillonite and acrylic adhesives have been used as superhydrophobic coatings. Organically modified nanoclay in fluoro-methacrylic latex enhanced the abrasion resistant, contact angle, and decreased the hysteresis. Basu and Paranthaman [67] prepared hybrid superhydrophobic surfaces of PVDF/hydrophobically modified fumed silica. With the increase in silica content from 33.3% to 71.4% in PVDF, the water contact angle was

enhanced from 117 degrees to 168 degrees. According to SEM, irregular microcavities and nanofilaments on the surface were found responsible for superhydrophobicity and roughness of the hybrid coatings. The method was simple and cost effective for preparing self-cleaning superhydrophobic coatings. Kou and Gao [68] reported silica nanoparticle-coated graphene oxide (GO-SiO$_2$) nanohybrids. Simple drop-coating method was used. The GO-SiO$_2$ hybrid had high surface area and semitransparent nature. Adopting new coating methodologies and hybrid materials may pave way for making large surface area hybrid superhydrophobic surfaces. Moreover, the generation of fibrillary hybrid structures and phase separation of polymers may also enhance the surface roughness and superhydrophobicity.

7. Commercial and future prospects and summary

The carbon nanomaterials have natural tendency to transform hydrophilic materials to superhydrophobic. Inclusion of only small wt% of graphene and CNT is enough to acquire waterproofing layer. The coatings can be prepared using drop-casting, dip-coating, spin coating, solution coating, melt coating, blading, chemical vapor deposition, lithography, or other suitable technique to form nanomaterial dispersion. The carbon nanoallotropes, that is, graphene and CNT have enhanced the water contact angle to produce homogenous coatings with long-lasting superhydrophobic effect. According to an estimated value, market price of $1\,m^2$ coating may be equal 0.02 USD for CNT-based coating and 0.3 USD for CNT-based material. Thus, polymer/CNT nanocomposite may offer high-performance superhydrophobic coatings at very low cost compared with graphene or fullerene-based materials. The CB and CNT-based superhydrophobic surfaces have shown excellent mechanical durability without any additional surface functionalization treatment [69]. Thus, polymer/nanocarbon nanocomposite may offer fine mechanical properties and electrical conductivity in coatings [70, 71]. The carbon nanomaterials act as hydrophobic agents to be employed in polymer sponge, metal mesh, textile, and cellulose materials such as cotton. The microporous structure and low surface energy of carbon nanoallotropes are accountable for superhydrophobicity of coatings. Graphene and nanocarbon materials have been used to enhance the non-wettability of cellulose nanocomposites [72, 73]. Increase in the robustness of superhydrophobic surfaces may bring engineered applications. Nanocarbon-based coatings have high electrical conductivity $\sim 1000\,S/m$ [74]. The synergistic effect of two or more nanocarbon may demonstrate enhanced features for practical applications. The electrical conductivity of superhydrophobic coatings has been used in EMI shielding, enhanced condensation heat transfer, electronics, etc. [75–77]. An important application of superhydrophobic surfaces is oil–water separation [78, 79]. The oleophilic properties of superhydrophobic nanocomposite coatings based on CB, graphene, or CNT have been used to separate out oil from oil/water mixture. The superhydrophobic/oleophilic

coatings have been exploited as a filtration membrane for oil/water separator. This chapter presents state-of-the-art discussion regarding superhydrophobic nanocomposite coatings. Organic as well as inorganic nanofillers have been reinforced in polymers to form superhydrophobic surfaces having controlled surface properties, wettability, self-healing, self-cleaning, antifouling, and anticorrosion properties. Moreover, polymeric nanocomposite-based superhydrophobic coating must have improved physical features such as optical, conducting, magnetic, mechanical, and thermal characteristics. High-performance superhydrophobic nanocomposite coatings have been employed in electrical and electronic devices, EMI shielding materials, strengthened materials, and biomedical applications.

References

[1] Q. Wen, Z. Guo, Recent advances in the fabrication of superhydrophobic surfaces, Chem. Lett. 45 (10) (2016) 1134–1149.

[2] A. Asthana, et al., Multifunctional superhydrophobic polymer/carbon nanocomposites: graphene, carbon nanotubes, or carbon black? ACS Appl. Mater. Interfaces 6 (11) (2014) 8859–8867.

[3] C.-H. Xue, et al., Large-area fabrication of superhydrophobic surfaces for practical applications: an overview, Sci. Technol. Adv. Mater. 11 (3) (2010) 033002.

[4] I. Yilgor, et al., Facile preparation of superhydrophobic polymer surfaces, Polymer 53 (6) (2012) 1180–1188.

[5] R. Rioboo, et al., Drop impact on porous superhydrophobic polymer surfaces, Langmuir 24 (24) (2008) 14074–14077.

[6] C.-P. Hsu, et al., Facile fabrication of robust superhydrophobic epoxy film with polyamine dispersed carbon nanotubes, ACS Appl. Mater. Interfaces 5 (3) (2013) 538–545.

[7] Q.F. Xu, B. Mondal, A.M. Lyons, Fabricating superhydrophobic polymer surfaces with excellent abrasion resistance by a simple lamination templating method, ACS Appl. Mater. Interfaces 3 (9) (2011) 3508–3514.

[8] N.-R. Chiou, et al., Growth and alignment of polyaniline nanofibres with superhydrophobic, superhydrophilic and other properties, Nat. Nanotechnol. 2 (6) (2007) 354.

[9] J. Genzer, K. Efimenko, Creating long-lived superhydrophobic polymer surfaces through mechanically assembled monolayers, Science 290 (5499) (2000) 2130–2133.

[10] Y. Zhu, et al., Multifunctional carbon nanofibers with conductive, magnetic and superhydrophobic properties, ChemPhysChem 7 (2) (2006) 336–341.

[11] R. Lakshmi, et al., Fabrication of superhydrophobic and oleophobic sol–gel nanocomposite coating, Surf. Coat. Technol. 206 (19–20) (2012) 3888–3894.

[12] J. Rafiee, et al., Superhydrophobic to superhydrophilic wetting control in graphene films, Adv. Mater. 22 (19) (2010) 2151–2154.

[13] L. Shen, et al., Fabrication of Ketjen black–polybenzoxazine superhydrophobic conductive composite coatings, Appl. Surf. Sci. 268 (2013) 297–301.

[14] L. Feng, et al., Super-hydrophobic surfaces: from natural to artificial, Adv. Mater. 14 (24) (2002) 1857–1860.

[15] J.P. Rothstein, Slip on superhydrophobic surfaces, Annu. Rev. Fluid Mech. 42 (2010) 89–109.

[16] X. Zhang, et al., Superhydrophobic surfaces: from structural control to functional application, J. Mater. Chem. 18 (6) (2008) 621–633.

[17] G.-Y. Lee, et al., Resistive pressure sensor based on cylindrical micro structures in periodically ordered electrospun elastic fibers, Smart Mater. Struct. (2018).

[18] R. Jurdi, et al., Electrospun polymer blend with tunable structure for oil–water separation, J. Appl. Polym. Sci. (2018) 46890.

[19] S. Sirin, S. Cetiner, A.S. Sarac, Polymer nanofibers via electrospinning: factors affecting nanofiber quality, Kahramanmaras Sutcu Imam Univ. J. Eng. Sci. 16 (2) (2013) 1–12.

[20] R. Menini, M. Farzaneh, Production of superhydrophobic polymer fibers with embedded particles using the electrospinning technique, Polym. Int. 57 (1) (2008) 77–84.

[21] L. Ovaskainen, et al., Superhydrophobic polymeric coatings produced by rapid expansion of supercritical solutions combined with electrostatic deposition (RESS-ED), J. Supercrit. Fluids 95 (2014) 610–617.

[22] K.K. Lau, et al., Superhydrophobic carbon nanotube forests, Nano Lett. 3 (12) (2003) 1701–1705.

[23] C.H. Lee, et al., The performance of superhydrophobic and superoleophilic carbon nanotube meshes in water–oil filtration, Carbon 49 (2) (2011) 669–676.

[24] D. Łukawski, et al., Towards the development of superhydrophobic carbon nanomaterial coatings on wood, Prog. Org. Coat. 125 (2018) 23–31.

[25] K. Liu, X. Yao, L. Jiang, Recent developments in bio-inspired special wettability, Chem. Soc. Rev. 39 (8) (2010) 3240–3255.

[26] W. Yao, et al., Transparent, conductive, and superhydrophobic nanocomposite coatings on polymer substrate, J. Colloid Interface Sci. 506 (2017) 429–436.

[27] T. Kamegawa, K. Irikawa, H. Yamashita, Multifunctional surface designed by nanocomposite coating of polytetrafluoroethylene and TiO2 photocatalyst: self-cleaning and superhydrophobicity, Sci. Rep. 7 (1) (2017) 13628.

[28] S. Dixon, et al., Synthesis of superhydrophobic polymer/tungsten (VI) oxide nanocomposite thin films, Eur. J. Chem. 7 (2) (2016) 139–145.

[29] A. Zhuang, et al., Transforming a simple commercial glue into highly robust superhydrophobic surfaces via aerosol-assisted chemical vapor deposition, ACS Appl. Mater. Interfaces 9 (48) (2017) 42327–42335.

[30] V.N. Mochalin, et al., The properties and applications of nanodiamonds, Nat. Nanotechnol. 7 (1) (2012) 11.

[31] J.H. Lee, Y.S. Youn, D.H. Lee, Thermal oxidative purification of detonation nanodiamond in a gas-solid fluidized bed reactor, Korean Chem. Eng. Res. 56 (5) (2018) 738–751.

[32] Z. Qian, et al., A novel approach to raspberry-like particles for superhydrophobic materials, J. Mater. Chem. 19 (9) (2009) 1297–1304.

[33] H. Zhang, X. Wang, D. Wu, Silica encapsulation of n-octadecane via sol–gel process: a novel micro-encapsulated phase-change material with enhanced thermal conductivity and performance, J. Colloid Interface Sci. 343 (1) (2010) 246–255.

[34] M. Takafuji, et al., One-pot green process for surface layering with nanodiamonds on polymer microspheres, J. Supercrit. Fluids 127 (2017) 217–222.

[35] N. Cao, et al., Polyurethane sponge functionalized with superhydrophobic nanodiamond particles for efficient oil/water separation, Chem. Eng. J. 307 (2017) 319–325.

[36] R. Saran, M.N. Nordin, R.J. Curry, Facile fabrication of PbS nanocrystal: C60 fullerite broadband photodetectors with high detectivity, Adv. Funct. Mater. 23 (33) (2013) 4149–4155.

[37] S.S. Babu, H. Möhwald, T. Nakanishi, Recent progress in morphology control of supramolecular fullerene assemblies and its applications, Chem. Soc. Rev. 39 (11) (2010) 4021–4035.

[38] Y. Li, et al., Superhydrophobic surfaces from hierarchically structured wrinkled polymers, ACS Appl. Mater. Interfaces 5 (21) (2013) 11066–11073.

[39] H. Tsai, et al., Structural dynamics and charge transfer via complexation with fullerene in large area conjugated polymer honeycomb thin films, Chem. Mater. 23 (3) (2010) 759–761.

[40] T. Nakanishi, et al., Nanocarbon superhydrophobic surfaces created from fullerene-based hierarchical supramolecular assemblies, Adv. Mater. 20 (3) (2008) 443–446.

[41] S. Zheng, M. Xu, X. Lu, Facile method toward hierarchical fullerene architectures with enhanced hydrophobicity and photoluminescence, ACS Appl. Mater. Interfaces 7 (36) (2015) 20285–20291.

[42] O. Leenaerts, B. Partoens, F. Peeters, Water on graphene: hydrophobicity and dipole moment using density functional theory, Phys. Rev. B 79 (23) (2009) 235440.

[43] K. Wang, et al., Stable superhydrophobic composite coatings made from an aqueous dispersion of carbon nanotubes and a fluoropolymer, Carbon 49 (5) (2011) 1769–1774.

[44] G. Carotenuto, et al., Graphene-polymer composites, in: IOP Conference Series: Materials Science and Engineering, IOP Publishing, 2012.
[45] R. Asmatulu, M. Ceylan, N. Nuraje, Study of superhydrophobic electrospun nanocomposite fibers for energy systems, Langmuir 27 (2) (2010) 504–507.
[46] C. Peng, et al., Preparation and anti-icing of superhydrophobic PVDF coating on a wind turbine blade, Appl. Surf. Sci. 259 (2012) 764–768.
[47] D.-a. Zha, et al., Superhydrophobic polyvinylidene fluoride/graphene porous materials, Carbon 49 (15) (2011) 5166–5172.
[48] L. Hu, D.S. Hecht, G. Gruner, Carbon nanotube thin films: fabrication, properties, and applications, Chem. Rev. 110 (10) (2010) 5790–5844.
[49] Y. Ren, Z. Li, H.R. Allcock, Molecular engineering of polyphosphazenes and SWNT hybrids with potential applications as electronic materials, Macromolecules 51 (14) (2018) 5011–5018.
[50] P.D. Bradford, et al., A novel approach to fabricate high volume fraction nanocomposites with long aligned carbon nanotubes, Compos. Sci. Technol. 70 (13) (2010) 1980–1985.
[51] C.-F. Wang, et al., Pressure-proof superhydrophobic films from flexible carbon nanotube/polymer coatings, J. Phys. Chem. C 114 (37) (2010) 15607–15611.
[52] G. Li, et al., A facile approach for the fabrication of highly stable superhydrophobic cotton fabric with multi-walled carbon nanotubes−azide polymer composites, Langmuir 26 (10) (2010) 7529–7534.
[53] J. Yang, et al., Fabrication of stable, transparent and superhydrophobic nanocomposite films with polystyrene functionalized carbon nanotubes, Appl. Surf. Sci. 255 (22) (2009) 9244–9247.
[54] X.-M. Li, D. Reinhoudt, M. Crego-Calama, What do we need for a superhydrophobic surface? A review on the recent progress in the preparation of superhydrophobic surfaces, Chem. Soc. Rev. 36 (8) (2007) 1350–1368.
[55] Z. Jiang, et al., Effect of surface modification of carbon black (CB) on the morphology and crystallization of poly (ethylene terephthalate)/CB masterbatch, Colloids Surf. A Physicochem. Eng. Asp. 395 (2012) 105–115.
[56] R. Xu, Progress in nanoparticles characterization: sizing and zeta potential measurement, Particuology 6 (2) (2008) 112–115.
[57] Y. Bao, et al., Tailoring the morphology of raspberry-like carbon black/polystyrene composite microspheres for fabricating superhydrophobic surface, Mater. Res. Bull. 46 (5) (2011) 779–785.
[58] Y. Liu, et al., Floatable, self-cleaning, and carbon-black-based superhydrophobic gauze for the solar evaporation enhancement at the air–water interface, ACS Appl. Mater. Interfaces 7 (24) (2015) 13645–13652.
[59] T. Darmanin, F. Guittard, Recent advances in the potential applications of bioinspired superhydrophobic materials, J. Mater. Chem. A 2 (39) (2014) 16319–16359.
[60] H. Zhou, et al., Fluoroalkyl silane modified silicone rubber/nanoparticle composite: a super durable, robust superhydrophobic fabric coating, Adv. Mater. 24 (18) (2012) 2409–2412.
[61] E. Bormashenko, et al., Wetting properties of the multiscaled nanostructured polymer and metallic superhydrophobic surfaces, Langmuir 22 (24) (2006) 9982–9985.
[62] H. Liu, et al., Preparation of superhydrophobic coatings on zinc as effective corrosion barriers, ACS Appl. Mater. Interfaces 1 (6) (2009) 1150–1153.
[63] D. Ebert, B. Bhushan, Transparent, superhydrophobic, and wear-resistant coatings on glass and polymer substrates using SiO2, ZnO, and ITO nanoparticles, Langmuir 28 (31) (2012) 11391–11399.
[64] J. Wang, et al., Control over the wettability of colloidal crystal films by assembly temperature, Macromol. Rapid Commun. 27 (3) (2006) 188–192.
[65] J.T. Han, et al., Stable superhydrophobic organic−inorganic hybrid films by electrostatic self-assembly, J. Phys. Chem. B 109 (44) (2005) 20773–20778.
[66] I.S. Bayer, et al., Transforming anaerobic adhesives into highly durable and abrasion resistant superhydrophobic organoclay nanocomposite films: a new hybrid spray adhesive for tough superhydrophobicity, Appl. Phys. Express 2 (12) (2009) 125003.
[67] B.B.J. Basu, A.K. Paranthaman, A simple method for the preparation of superhydrophobic PVDF–HMFS hybrid composite coatings, Appl. Surf. Sci. 255 (8) (2009) 4479–4483.

[68] L. Kou, C. Gao, Making silica nanoparticle-covered graphene oxide nanohybrids as general building blocks for large-area superhydrophilic coatings, Nanoscale 3 (2) (2011) 519–528.

[69] S. Naha, S. Sen, I.K. Puri, Flame synthesis of superhydrophobic amorphous carbon surfaces, Carbon 45 (8) (2007) 1702–1706.

[70] Z. Spitalsky, et al., Carbon nanotube–polymer composites: chemistry, processing, mechanical and electrical properties, Prog. Polym. Sci. 35 (3) (2010) 357–401.

[71] M.H. Al-Saleh, U. Sundararaj, A review of vapor grown carbon nanofiber/polymer conductive composites, Carbon 47 (1) (2009) 2–22.

[72] W. Shao, et al., Preparation of bacterial cellulose/graphene nanosheets composite films with enhanced mechanical performances, Carbohydr. Polym. 138 (2016) 166–171.

[73] M. Sanchis, et al., Monitoring molecular dynamics of bacterial cellulose composites reinforced with graphene oxide by carboxymethyl cellulose addition, Carbohydr. Polym. 157 (2017) 353–360.

[74] A. Zaikovskii, S. Novopashin, Effects of the arc-discharge parameters on the morphology and the electrical conductivity of the synthesized carbon materials, Mater. Today Proc. 4 (11) (2017) 11406–11410.

[75] Z.P. Wu, et al., Electromagnetic interference shielding of carbon nanotube macrofilms, Scr. Mater. 64 (9) (2011) 809–812.

[76] W. Alshaer, et al., Numerical investigations of using carbon foam/PCM/Nano carbon tubes composites in thermal management of electronic equipment, Energy Convers. Manag. 89 (2015) 873–884.

[77] R. Lotfi, A.M. Rashidi, A. Amrollahi, Experimental study on the heat transfer enhancement of MWNT-water nanofluid in a shell and tube heat exchanger, Int. Commun. Heat Mass Transfer 39 (1) (2012) 108–111.

[78] Q. Ma, et al., Recent development of advanced materials with special wettability for selective oil/water separation, Small 12 (16) (2016) 2186–2202.

[79] N. Baig, F.I. Alghunaimi, T.A. Saleh, Hydrophobic and oleophilic carbon nanofiber impregnated styrofoam for oil and water separation: a green technology, Chem. Eng. J. 300 (2018) 1613–1622.

CHAPTER 5

Characterization of superhydrophobic polymer coating

D. Jayadev[a], Jitha S. Jayan[a], Zeena S. Pillai[a], Kuruvilla Joseph[b], Appukuttan Saritha[a]
[a]Department of Chemistry, School of Arts and Sciences, Amrita Vishwa Vidyapeetham, Kollam, India
[b]Department of Chemistry, Indian Institute of Space Science and Technology, Thiruvananthapuram, India

1. Introduction

Characterization and analysis of superhydrophobic surfaces are of pronounced relevance because of their importance in many applications. Surfaces with exciting wettability behavior such as superhydrophobic and superhydrophilic have been the focus of numerous studies in material science. Interest in superhydrophobic surfaces is increasing steadily due to their scientific significance as well as innumerable potential applications in self-cleaning, antifogging, blood compatible devices, and so on [1–5]. Two approaches are commonly practiced for the fabrication of these surfaces. The former lays stress on the roughening of a hydrophobic surface and the latter gives weightage to the modification of an already rough surface with materials possessing low surface energy. Superhydrophobic coatings are present in certain leaves like the lotus, colocasia, and wings of some insects. Hence, these materials can be considered as biomimetic. Nanocomposites based on polymers, which forms one of the hottest areas of research in almost all technical disciplines find application in the fabrication of superhydrophobic coatings also [6–12]. Superhydrophobic coating can be considered as a nanosurface layer with the capacity to repel water. Droplets encountering such surfaces rebound fully. Superhydrophobic coatings are employed in ultradry surface applications in industry. Nanoparticles can be utilized for altering the surface roughness since they can be synthesized with uniform size and hence nanocomposites with tunable wettability can be tailored through surface modification of nanoparticles [13].

For the creation of superhydrophobic surfaces, two factors should be taken into consideration. First, it must have appropriate roughness at micro and nanoscales and second, the surface must have a hydrophobic surface chemistry [6]. A noticeable model for superhydrophobicity present in nature is none other than the lotus leaf with 10-μm papillae along with hydrophobic wax crystals arranged in a nanostructure fashion. This arrangement paves way toward the realization of a surface with a very high water contact angle

(WCA) of 160 degrees, which enables the water drops to roll–off creating a tilt angle lesser than 5 degrees [14]. The frivolous crusade of the droplets depicts the fact that the contact angle (CA) hysteresis is less. CA hysteresis depicts the discrepancy between the advancing and receding CAs. Negligible CA hysteresis alone permits the characterization of the wetting properties of the surface by a static CA. This can be carried out by the introduction of a droplet onto the surface and determining the angle by means of optical measurements. Generally, advancing and receding CAs (dynamic CA) should be measured if the surface has considerable roughness. This is because in such a situation a static CA can assume any value in between the advancing and receding ones.

Taking inspiration from nature, material scientists around the world are in a constant effort to mimic the lotus leaf effect and create novel hydrophobic surfaces with the aid of new technological advancements. Even though quite a few applications of hydrophobic and even superhydrophobic surfaces have established its way into industry, research is still being carried out toward the fabrication of superhydrophobic surfaces using various novel methods [15–18]. Hydrophobicity is easily calculated by the observation of CA of clean water on a spotless solid surface. Once the CA tends to be greater than 150 degrees, the surface turns out to be superhydrophobic and hence, the measurement of CA is considered vital in the study of these surfaces. In the absence of the aforementioned study, a perfect scientific understanding of these engineered surfaces could not be ascertained. Surfaces containing trifluoromethyl carbon ligands as the terminal entity enjoy the highest affinity between electron and fluorine. Subsequently, the lowest surface energy will be possessed by these materials [19, 20]. It has been established from earlier studies that the CA shows direct relationship with roughness of a hydrophobic surface, whereas it shows inverse relationship with the roughness of a hydrophilic surface. This connection established by Wenzel is referred to as Wenzel's law [21, 22]. Due to their extremely low surface energies, fluorinated polymers are considered as important candidates in the production of superhydrophobic surfaces [16, 23–35]. Polytetrafluoroethylene (PTFE) takes the first position among the fluorinated polymers and they are generally utilized as antiadhesion agents and chemical insulators. In addition to surface energy, there is another important parameter called roughness of the solid which is also taken into consideration to determine the variation of the CA. The surface energy of a solid depends to a great extent on the chemistry of its surface, which in turn is dependent on the chemical constitution as well as the arrangement of atoms at the vicinity of the surface. Various phenomena like relaxation, rearrangement of the surface, and variation in the surface composition can result in the reduction of surface energy. Hence, a thorough knowledge of the morphology, topography as well as surface features and composition is highly inevitable for the study of superhydrophobic surfaces. Here comes the relevance of various characterization techniques which enable us to disclose the features of the surface.

2. Characterization techniques for superhydrophobic polymer coatings

Various characterization methods have been used in the studies of superhydrophobic surfaces. These methods help us to identify the nature of the surface and compare its superhydrophobicity with the already available materials. The major techniques used in common studies are discussed below.

2.1 CA measurement

CA is the angle created by a liquid with a solid surface when these materials are in contact. This angle is dependent on the properties of both the materials as well as the attractive and repulsive interaction between them. When the liquid is spread on the surface, it forms a small CA while the CAs will be higher when the area of contact between the solid and liquid is less [36]. There are two types of CAs—static CA and dynamic CA.

Static CAs are determined by placing the drop in a standing position on the surface and thereby keeping the three-phase boundary static. **Dynamic CA**, as the term indicates is measured when the three-phase boundary is in motion. This movement is denoted as advancing and receding angles and the difference between them is denoted as *CA hysteresis*. This phenomenon arises due to various reasons like the heterogeneous chemical and topographical nature of the surface, impurities remaining on the surface or entrapment, or rearrangement of solvent molecules on the surface.

The CA of a liquid on an entirely smooth and homogeneous solid surface is calculated using the well-known Young's equation [37].

$$\cos\theta = \frac{\left(\gamma_{sv} - \gamma_{sl}\right)}{\gamma_{lv}} \tag{1}$$

where γ_{sv} represents the interfacial tension of the solid–vapor, γ_{sl} is the solid–liquid, and γ_{lv} is the liquid–vapor interface. Later Wenzel [38] established a model in which the liquid has the possibility of migrating into the grooves. Under such circumstances, the CA on such a rough surface is determined using the equation

$$\cos\theta_w = \frac{r\left(\gamma_{sv} - \gamma_{sl}\right)}{\gamma_{lv}} = r\cos\theta \tag{2}$$

θ_w represents the angle of contact on a rough surface and θ is the Young's CA on a smooth surface. The surface roughness factor is represented by r. According to this equation, roughness enhances wetting process, when θ is <90 degrees and vice versa. Nevertheless, when $\theta > 90$ degrees, air bubbles will occupy the rough grooves. Under such conditions, the liquid droplet is considered to be located on the surface of a composite. The subsequent performance and the wetting characteristics can be described

by Cassie and Baxter model [39]. The CA in such a condition is given by a relation connecting surface fractions f_1 and f_2 CAs on phase $1(\theta_1)$ and phase $2(\theta_2)$ with apparent CA θ_c

$$\cos\theta_c = f_1 \cos\theta_1 + f_2 \cos\theta_2 \tag{3}$$

In the case of air–liquid interface, f signifies the fraction of the solid surface which is getting wetted by the liquid. The resulting CA can be calculated using $\theta = 180$ degrees for air as shown below

$$\cos\theta_c = f \cos\theta + (1-f)\cos 180° = f\cos\theta + f - 1 \tag{4}$$

The parameter f can take values between 1 and 0 depending on whether the liquid droplet touches the surface or not. The wetting behavior of liquid droplet on a rough surface is shown in Fig. 1.

2.1.1 The sessile drop method
One of the commonly employed methods in sessile drop method is the goniometer-based telescope method of measurement of CAs. In order to have a better view of the angle, the commercial goniometers have an objective lens in the telescope. The different types of sessile drop methods available for the determination of CAs are:

The static sessile drop method—in this method, the CA is measured by observing it through a goniometer after depositing it on a surface by a syringe which is located on the top of the sample surface. The instrument has an inbuilt high–resolution camera which captures the image of the sample either from the top or side. The image can then be subjected to analysis using an image analysis software. Since the size of the droplet remains static throughout the measurement, it is called static drop method (Fig. 2).
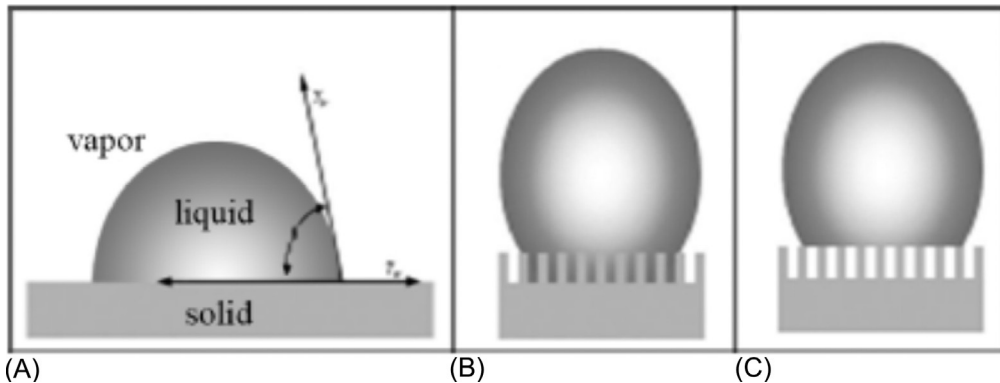
Fig. 1 The wetting behavior of a liquid droplet on rough solid surface (A) Young's mode, (B) Wenzel's mode, and (C) Cassie's mode [40].
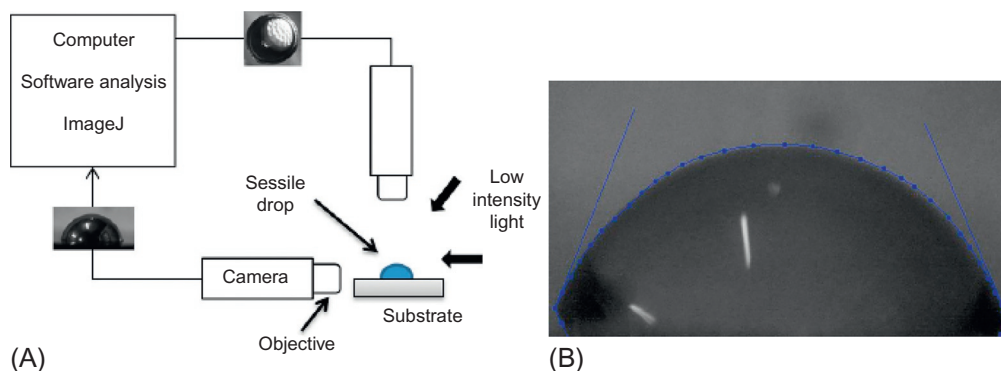
Fig. 2 (A) Schematic representation of the goniometer, planar and side view of sessile drops and (B) photograph of a drop during measurement of the contact angle in the software image. *(Reproduced with permission from Jonathan Schuster, Carlos Schvezov, Mario Rosenberger, Influence of experimental variables on the measure of contact angle in metals using the sessile drop method, Procedia Mater. Sci. 8 (2015) 742–751. https://doi.org/10.1016/j.mspro.2015.04.131, Elsevier.)*

The dynamic sessile drop method—this is analogous to the static method with the only change that the drop is modified after the deposition. After being deposited by means of a syringe, its volume is altered. This alteration in volume is done without changing the interfacial area between the solid and the liquid and the maximum angle measured in this case is called the advancing angle. Similarly, the volume is lowered and the smallest possible angle which is called the receding angle is measured. *CA hysteresis* is the term used to depict the difference between the two angles measured.

Fig. 3 depicts a typical sequence of images used for this evaluation. Fig. 3A and B denotes the advancing and receding angles, respectively [41].

Liu et al. [42] considered a simple technique which involved the in situ polymerization of butyl methacrylate and ethylene dimethacrylate in the presence of 1,4–butanediol (BDO) and N-methyl-2-pyrrolidone (NMP) to produce superhydrophobic polymeric surfaces which are porous. They evaluated the relationship between the composition of the polymerization mixture and hydrophobicity by changing the ratios of the co–porogens and the monomers. Fig. 4 shows the outcome of the mass ratio of the monomers on the CA measurements in the study. When the ratio between the monomers is 40:60, the system exhibits a maximum CA. When the ratio of the monomers to co–porogens is 45:55, the surface exhibits a CA of 159.5 degrees. The angle shows a gradual decrease with the increase in the ratio. This observation clarifies that the amount of co–porogens employed is directly proportional to the pores developed on the surface. In this study since the amount of porogen is less, the polymer surface contains a few pores and hence results in a weak degree of phase separation (Fig. 5).

Erbil et al. [43] converted simple plastic to a surface with a water CA of 160 degrees using a novel preparation method. Xu et al. [44] devised a new method to attain a surface
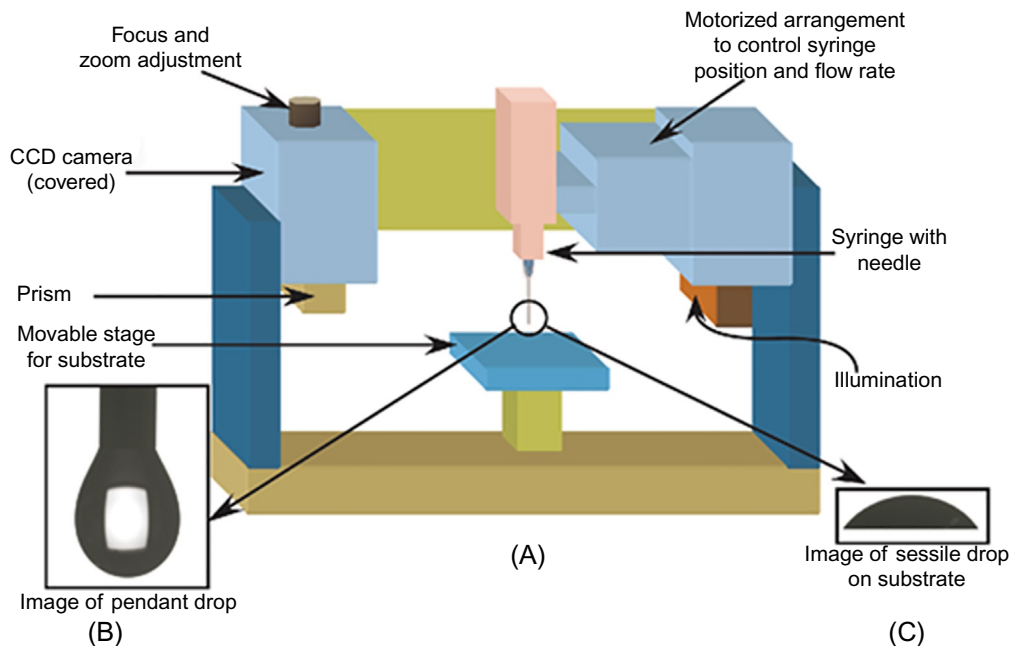
Fig. 3 (A) Schematic drawing of the experimental setup used for dynamic contact angle and surface tension measurements, (B) image of pendant drop, and (C) image of sessile drops captured from the CCD camera. *(Reproduced with permission from Prashant Waghmare, Sushanta K. Mitra, Contact angle hysteresis of microbead suspensions, Langmuir 26 (2010) 17082–17089, American Chemical Society.)*

with superhydrophobicity by electron less galvanic deposition of nano silver film. This was followed by the self-assembly of *n*-octadecanethiol on the metal surface. This surface displayed an extreme nonwetting property. Even after the exposure of the sample for 1 week at −20°C, the samples exhibited superhydrophobicity with high CAs. The surface exhibited a CA of 169 degrees ± 2 degrees when the deposition of silver was carried out for 30 s. Water drops exhibited difficulty in sticking to the surface which is evident from the sliding angle (SA) of around 0 degrees ± 2 degrees on the surface.

Wimalasiri et al. [45] developed silica-based nonfluorinated superhydrophobic coatings for natural rubber surfaces. The coating was synthesized using nanosilica dispersion and a polychloroprene-type binder as a compatibilizer. This nano-coating of silica was applied on to the surface of finished natural rubber gloves, by spray coating or dipped coating methods. The nano-coating demonstrates a water CA of greater than 150 degrees and SA of 7 degrees. The morphological features of the coatings were studied using scanning electron microscopy (SEM) and atomic force microscopy (AFM). CA of coated and uncoated rubber films was measured by goniometer. The initial water CA was 151 degrees and 149 degrees for spray-coated and dip-coated gloves, respectively, while the uncoated gloves demonstrated a CA of 35 degrees.
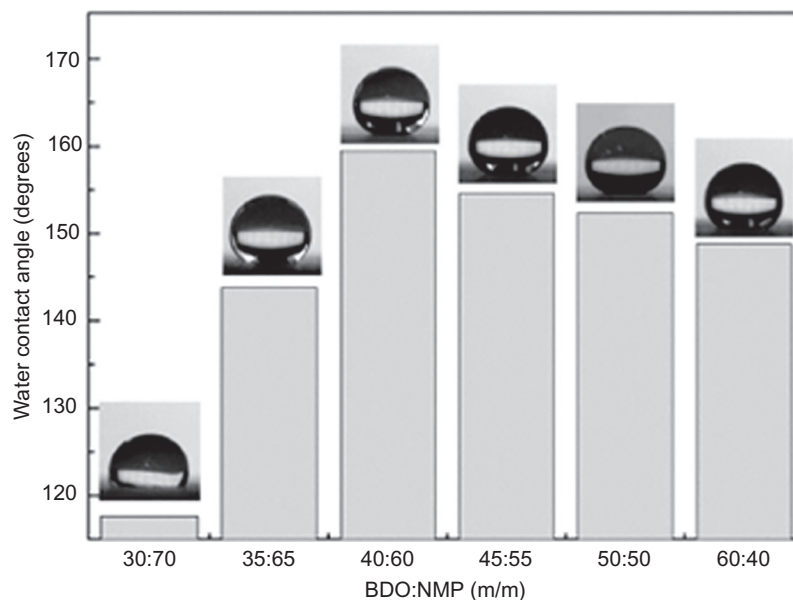
Fig. 4 The effect of the mass ratio of monomers (BDO:NMP) on the hydrophobicity (contact angle measurement). *(Reproduced with permission from Jianfeng Liu, Xinyan Xiao, Yinlong Shi, Caixia Wan, Fabrication of a superhydrophobic surface from porous polymer using phase separation, Appl. Surf. Sci. 297 (2014) 33–39, ISSN 0169-4332, https://doi.org/10.1016/j.apsusc.2014.01.053, Elsevier.)*

Brassard et al. [46] synthesized mono–dispersive silica nanoparticles of ∼120 nm diameter and functionalized it using fluoroalkyl silane molecules and coated on different substrates such as silicon, aluminum alloy, and glass. To evaluate the superhydrophobicity of functionalized silane on these substrates, both the static and dynamic CAs were measured. It was observed that, the increase in the number of layers of the coating increases the water CA up to a critical number, after which CA values remained same. Low surface energy of the fluorinated species as well as roughness of the surface contributes to the increase in the water CA.

Flexible superhydrophobic carbon/polymer composite film of polyvinylidene fluoride (PVDF) incorporated with mesoporous submicron carbon capsules (MCC) was fabricated by Mittal et al. [47]. This material displayed a hierarchical roughness that leads to the rendering of superhydrophobicity. Flexible film was found to be stable in a humid and corrosive environment over a wide pH range. Water CA changed from 110 degrees to 160 degrees upon the incorporation.

Sriramulu et al. [48] in order to understand the influence of molecular arrangement on hydrophobicity of the silica particles, functionalized it with perylene derivatives and octadecyl groups. Macroscale CAs were measured by sophisticated fully automated CA dosing system. The surface with a nonfunctionalized nanoparticle exhibited a CA of zero degree, whereas perylene functionalized ones showed hydrophobicity with CA greater than 130 degrees.
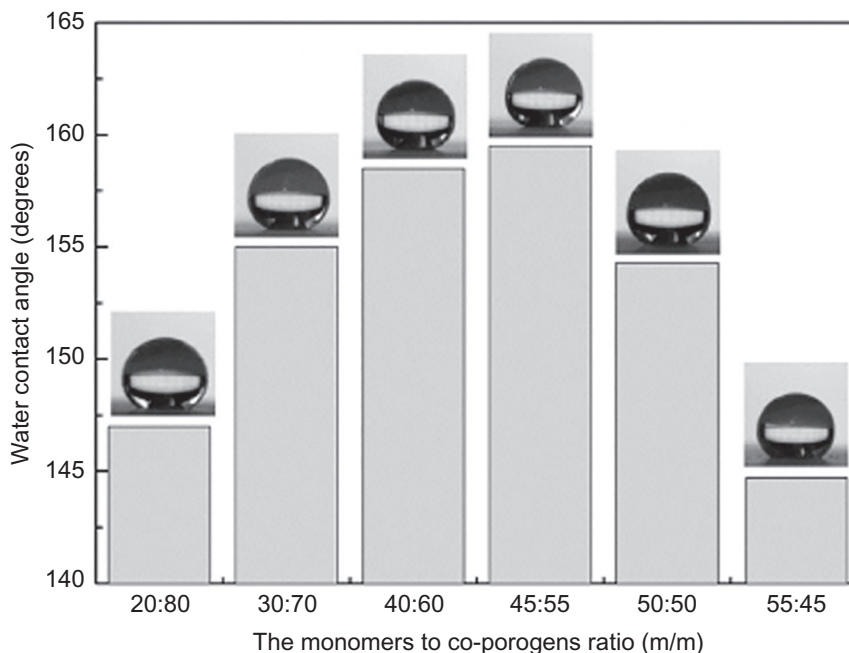
Fig. 5 The effect of the ratio of monomers to co-porogens on the hydrophobicity. *(Reproduced with permission from Jianfeng Liu, Xinyan Xiao, Yinlong Shi, Caixia Wan, Fabrication of a superhydrophobic surface from porous polymer using phase separation, Appl. Surf. Sci. 297 (2014) 33–39, ISSN 0169-4332, https://doi.org/10.1016/j.apsusc.2014.01.053, Elsevier.)*

A vapor–induced method to fabricate superhydrophobic surfaces using fluorine free material was developed by Guan et al. [49]. The inorganic and organic components were mixed in ethyl acetate to get a homogeneous suspension and were dip coated on to the substrate. The entire process was fine tuned to control the surface roughness. The roughness of the surface was found to increase with increase of polyethylene wax content from 15 to 20 wt%.

Liquid repellency from the textured surfaces has been an area of interest during the last two decades and an increased attention was grabbed by the repellency. The liquid repellency of currently developed engineered surface textures is so complicated that the liquid droplets do not adhere at all to these substrates. For the characterization of such highly sophisticated surfaces, the sessile drop technique is considered inadequate. Due to the low adhesion, the droplet finds it difficult to get detached from the syringe tip. Even if it gets detached, the droplets will have a tendency to roll-off the surface thereby making the measurement of the CAs difficult or erroneous. It is highly indispensable that a thorough understanding of the repellency properties of a textured surface is needed upon immersion in a liquid [50–53]. The air pockets at the Cassie-Baxter origin are stable on a robust surface. The complete replacement of the air pockets leads to a transition from the

Cassie–Baxter wetting system to a Wenzel system, whereas fractional replacement leads to a mixed wetting regime. Such transitions occur with time, changing the surface tension of the liquid and the pressure of the flow [54–57]. Thus, there arises a requirement of innovative approaches for the simulation of pressure and confinement conditions accompanying the immersed state [58–67].

A novel technique used to estimate the wetting properties of superhydrophobic surfaces lately is the Wilhelmy plate tensiometer method. Originally based on a microbalance method, this technique provides reliable information of the triple-line anchoring force. The corresponding capillary force enables the calculation of the CA. It also differs from the sessile drop technique in the fact that the latter provides indirect information about the retention force. The various experimental parameters can be changed and the experiment can be carried out by immersing the sample. The discrepancy in the dynamic CAs measured with the sessile drop and Wilhelmy plate tensiometer technique is still under debate [68–70].

2.2 Roll-off angle measurement

The roll-off angle is used to characterize ultra-hydrophobic surfaces with very high CAs. Lateral adhesion can also be measured using this technique. It decreases with decrease in roll-off angle which in turn leads to an increase in liquid repellency.

A typical representation of roll-off angle measurement method is shown in Fig. 6. The volume of the drop needs to be specified while determining the roll-off angle. Javad et al. [71] experimented on superhydrophobic nanocomposite coatings with improved mechanical and thermal resistance. Water CAs determined shows that coating thermoplastic polyurethane with nano silica increased the CAs thus exhibiting a synergistic effect.

Shang et al. studied the surface morphologies as well as the CAs of silica-based coatings [72]. The different surface structures include the one with dip-coated sol-gel films, uniformly sized spherical nanoparticles, nanofibers, etc. as shown in Fig. 7.
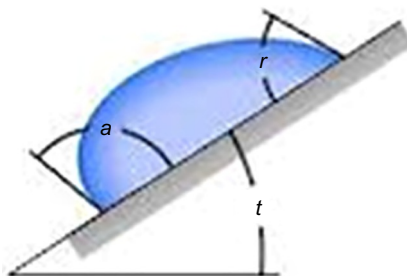
Fig. 6 The advancing and receding contact angles capture by tilting base method. (*Figure taken from online file by Rame-Hart Instrument Company.*)
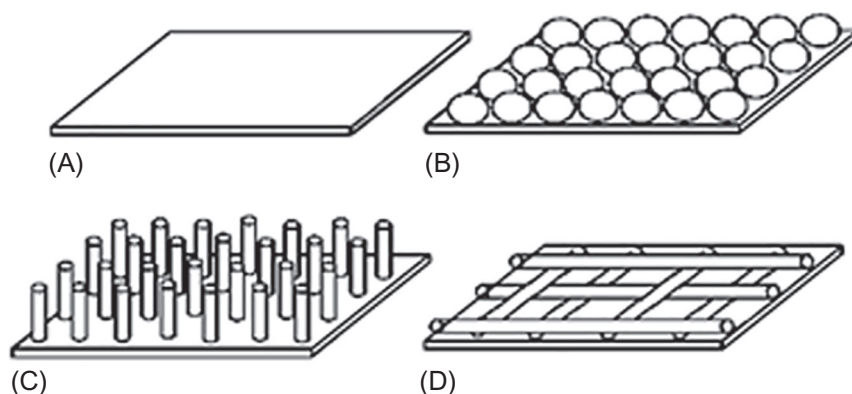
Fig. 7 The four types of surface morphologies (A) a smooth surface, (B) is assembly of uniformly sized nanoparticles, (C) is uniformly sized nanorod array unidirectionally aligned perpendicular to surface, and (D) is open mesh of nanofibers lying parallel on substrate. *(Reproduced with permission from H.M. Shang, Y. Wang, K. Takahashi, G.Z. Cao, D. Li, Y.N. Xia, J. Mater. Sci. 40 (2005) 3587–3591., Springer.)*

The varying CA is attributed to the varying roughness of the surfaces. Karapanagiot et al. [73] studied the effect of coating silica nanoparticles on to the surface of natural paper using silane/siloxane solution. Four types of paper like blank paper, printed paper, old paper, and Japanese tissue paper were used for this experiment. Table 1 shows the effect of silane coating on CA of the papers with respect to different volume fraction.

From the studies, it was concluded that the surface of the deposited film exhibited super–hydrophobic ($\theta_S > 160$ degrees), water repellent ($\theta_i < 3$ degrees), and self-cleaning properties.

2.3 Scanning electron microscopy

In SEM, a focused beam of high-energy electrons generates signals at the surface of the substrate. Information regarding the texture, chemical composition, crystalline structure,

Table 1 Static (θ_S) and tilt (θ_t) contact angles

Contact angle (degrees)	Particle concentration (w/v) (%)	Paper substrate			
		Blank paper	Printed paper	Old paper	Japanese paper
θ_S	0	126.4 ± 0.3	121.0 ± 0.9	126.0 ± 0.6	122.2 ± 0.5
	2	161.3 ± 0.8	164.7 ± 0.7	163.2 ± 1.1	162.0 ± 1.2
θ_i	0	10.8 ± 0.1	11.0 ± 0.3	10.9 ± 0.7	10.8 ± 0.6
	2	2.4 ± 0.3	1.8 ± 0.3	2.1 ± 0.2	2.3 ± 0.4

and orientation of materials can be drawn from this method. The lotus leaf turns out to be the most common self-cleaning surface observed in nature as shown in Fig. 8. The surface is covered by low surface energy wax as well as complicated micro and nanoscopic framework. The surface roughness as well as low surface energy are the two essential properties that reduces the adhesion of water [74, 75].

Hexamethyldisilazane was coated on to alumina substrate by Nevin et al. [76]. The CA measurements showed that the surface roughness can be properly tuned to obtain a superhydrophobic surface. The SEM image (Fig. 9) showed nano pores of diameter 250 nm with pyramidal-shaped protrusions which impart roughness and thereby hydrophobicity to the substrate.

Cobalt chloride ($CoCl_2$) was coated on to a glass substrate using chemical bath deposition process by Mohsin et al. [77]. WCA values increases due to the increase in the formation of pin-like structures. As the time of deposition increases, the pin formation increases leading to the formation of flower-like structures (Figs. 10 and 11). Adhesion is also found to improve with increase in coating time.
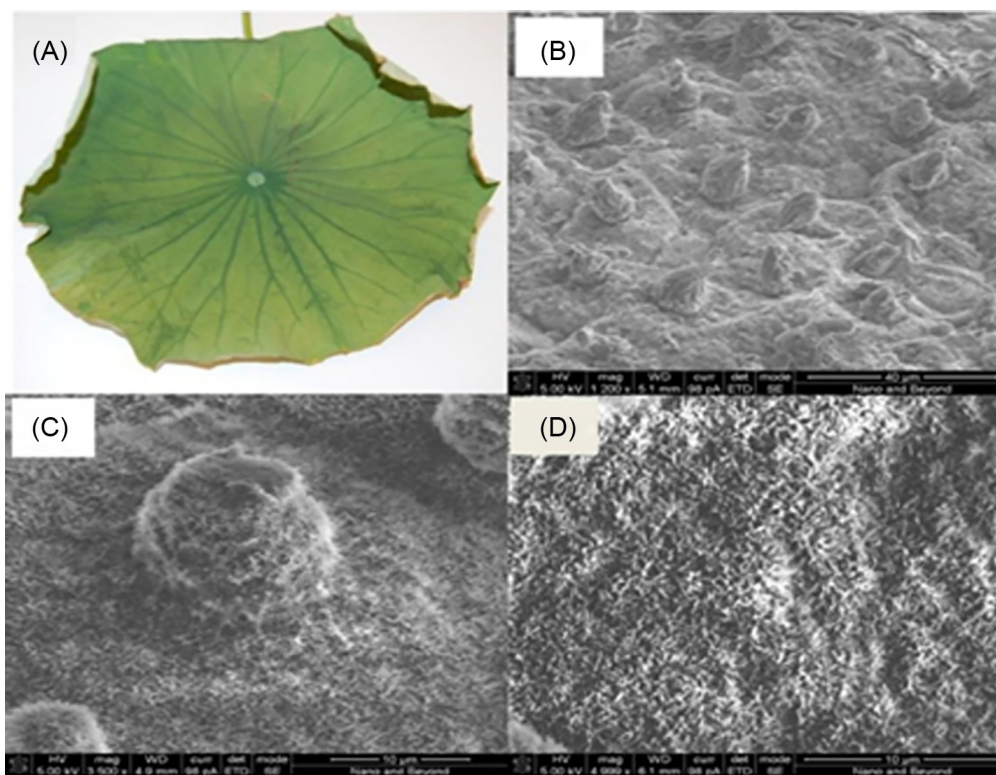
Fig. 8 (A) Natural lotus leaf and (B–D) SEM images of lotus leaf [75].
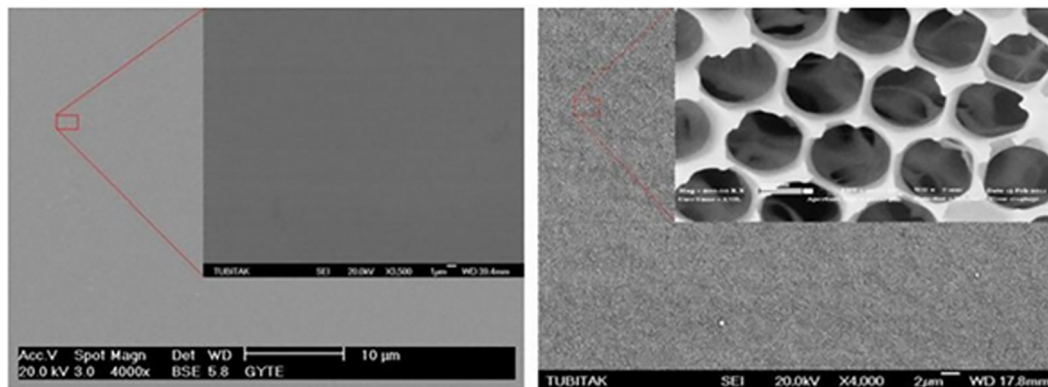
Fig. 9 SEM images of alumina surfaces prepared by anodic oxidation of Al (A) thin film alumina surface and (B) nanoporous alumina surface [76].
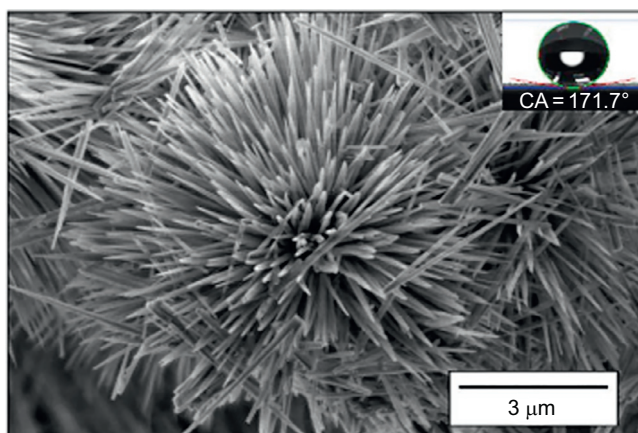
Fig. 10 SEM image of Co-based superhydrophobic coating using 0.1 M CoCl$_2$ at 22 h [77].

Superhydrophobic coatings using bisphenol were made by Zhao et al. [78]. Fig. 12 shows the surface with flower-like particles randomly stacked together. This resembles the surface of lotus leaf with excellent superhydrophobic nature. Wei and coworkers [79] synthesized 2,2,3,4,4,4-hexafluorobutyl methacrylate copolymers. In this case, surface roughness was controlled by phase separation using ethanol.

Liu et al. studied fabrication of a superhydrophobic surface from porous polymer using phase separation [80]. Hydrophobic polymer surfaces were prepared by in situ polymerization on glass substrate. The polymerization mixture consists of butyl methacrylate, ethylene dimethacrylate, BDO, NMP, and 2,2′-azobisisobutyronitrille. SEM
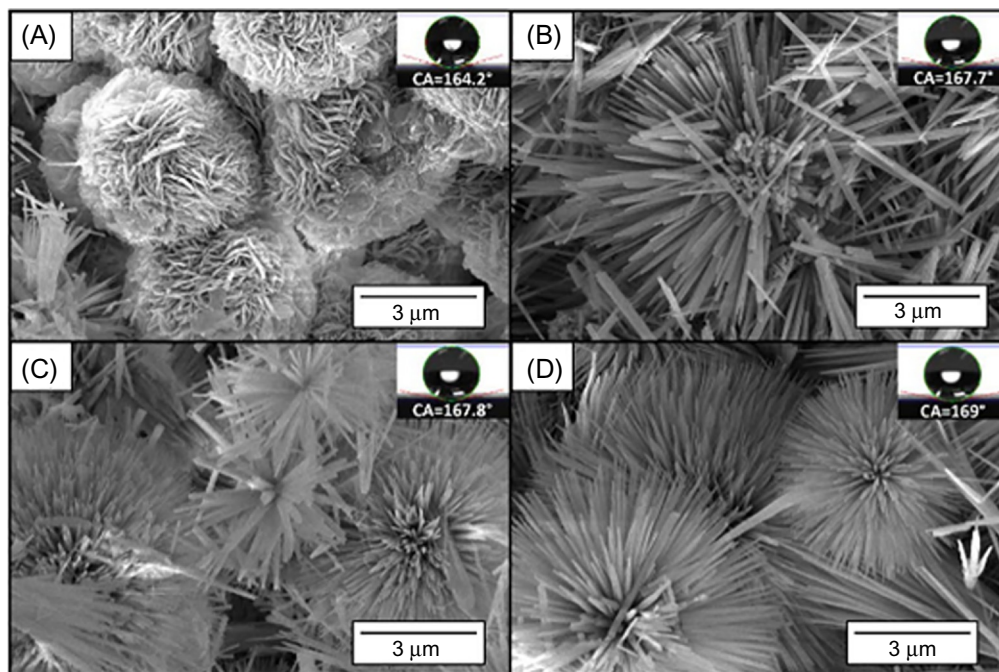
Fig. 11 SEM image of evolution of superhydrophobic coating morphology with deposition time (A) 6 h, (B) 8 h, (C) 10 h, and (D) 12 h [77].

images of the surfaces with varying compositions of BDO and NMP are shown in Fig. 13. Increasing ratio of BDO to NMP improves the superhydrophobicity.

Li et al. [81] developed a bionic surface with hierarchical structure by the incorporation of carbon nanotubes (CNTs) in polystyrene (PS) matrix. The technique employed for the fabrication was chemical self-assembly. Interestingly CNT assembled in a net-like fashion on the surface of hexagonally close packed PS microspheres. This hierarchical arrangement of CNT on the surface of PS gives rise to excellent electrochemical properties which enable the material to function as gas sensors with good selectivity and sensitivity.

The interaction of superhydrophobic nano-textured silica with molten powder-coat resins produces "resin marbles." This technique employs an electrostatic process involving polymer resins in the dry form. It is observed that the blended powder coat resins can create surfaces with microporosity and interconnections which extend throughout the sample surface.

Liu et al. [82] synthesized fluoropolymer composite containing silica particles using sol–gel method. The composites exhibited micro/nanoscale binary structures which exhibited excellent nonwettability and high water CA. Kim and coworkers [83] fabricated surfaces exhibiting very low CA hysteresis (<5 degrees) by making use of a
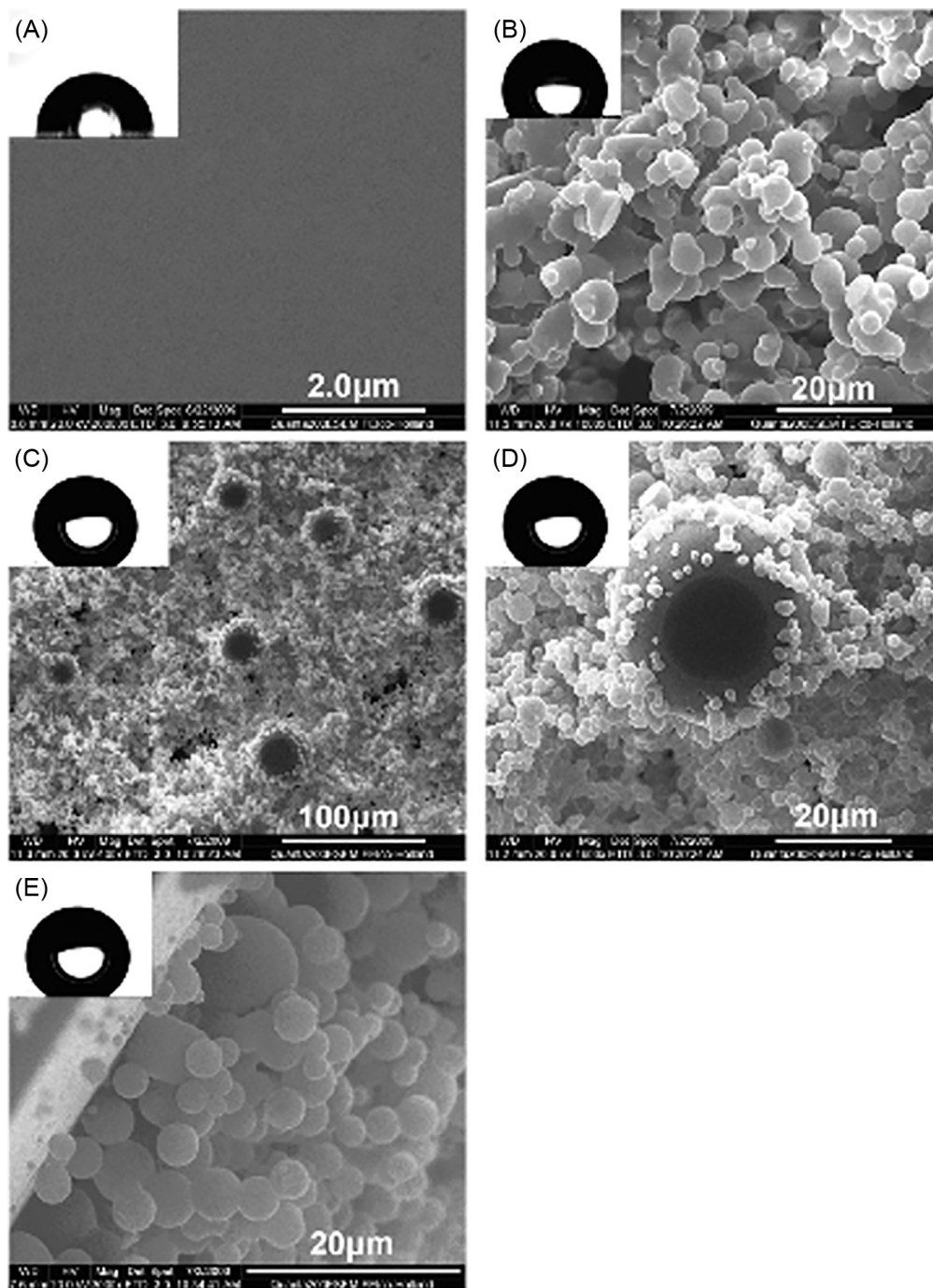
Fig. 12 SEM images of copolymer films obtained with different ethanol content in copolymer solution: (A) 0%; (B) 30%; (C) 50%; (D) is the higher magnification ESEM image of (C); and (E) is the section image of (C). Insets are the water contact angles on the copolymer films. *(Images reprinted from Z.J. Wei, W.L. Liu, D. Tian, C.L. Xiao, X.Q. Wang, Preparation of lotus-like superhydrophobic fluoropolymer films, Appl. Surf. Sci. 256 (12) (2010) 3972–3976, https://doi.org/10.1016/j.apsusc.2010.01.059. Reproduced with permission from Elsevier.)*
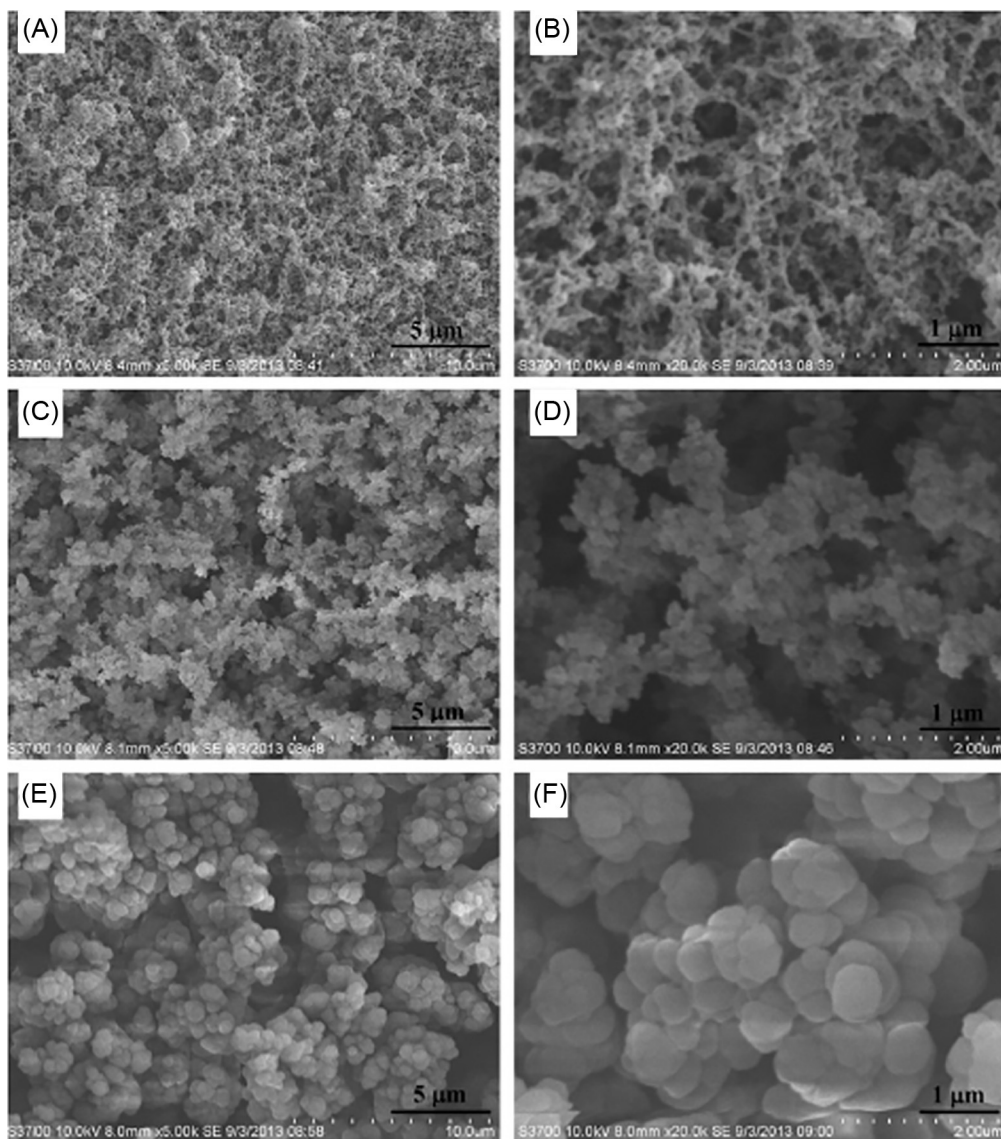
Fig. 13 SEM image of surfaces with different mass ratio of BDO to NMP. (A and B) 30:70, (C and D) 40:60, and (E and F) 50:50. *(Reproduced with permission from Jianfeng Liu, Xinyan Xiao, Yinlong Shi, Caixia Wan, Fabrication of a superhydrophobic surface from porous polymer using phase separation, Appl. Surf. Sci. 297 (2014) 33–39, ISSN 0169-4332, https://doi.org/10.1016/j.apsusc.2014.01.053, Elsevier.)*

hydrophobic coating and created an interesting nanoscale roughening feature in it. In 2004, researchers at the ORNL used fiber-drawing techniques to fabricate cone spike arrays (see Fig. 14) with 7 μm periodicity and 12 μm height [84]. This array of glass cones exhibited an interesting chemistry with which the surface turned out to be hydrophobic upon treatment with fluorinated silane. This peculiar glass cone array is perhaps one of the most water-repellent surfaces in the world.
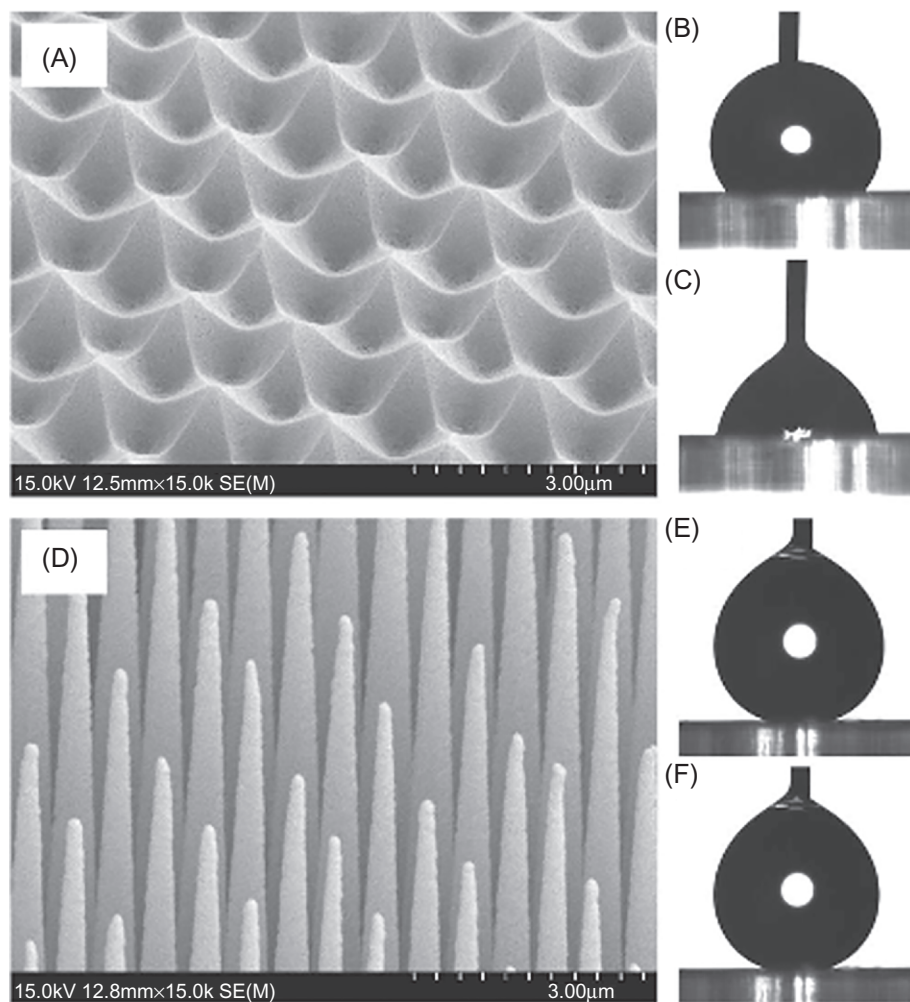
Fig. 14 SEM images of nanocone arrays and optical images of water drops on nanocone arrays. (A) Lowest aspect ratio nanocones tested with (B) advancing drop and (C) receding drop. (D) Highest aspect ratio nanocones tested with (E) advancing drop and (F) receding drop. *(Reproduced with permission from B. D'Urso, J.T. Simpson, Emergence of superhydrophobic behavior on vertically aligned nanocone arrays, Appl. Phys. Lett. 90 (2007) 044102, IOPScience.)*

Liu et al. have carried out studies on superhydrophobic surfaces from nanocomposite materials based on silica nanoparticles and self-assembled monolayers of perfluorooctyl-triethoxysilane using spin coating [80]. SEM image in Fig. 15 shows distinguishable porous structures which allow the trapping of small-scale air pockets. The morphology remains more or less similar before and after the treatment.

Cha et al. [85] used a nanostructured Si wafer coated with modified and unmodified diamond-like carbon. The surfaces maintained hydrophobic nature to a temperature up to 350°C. On further heating, thermal degradation occurs leading to a superhydrophilic
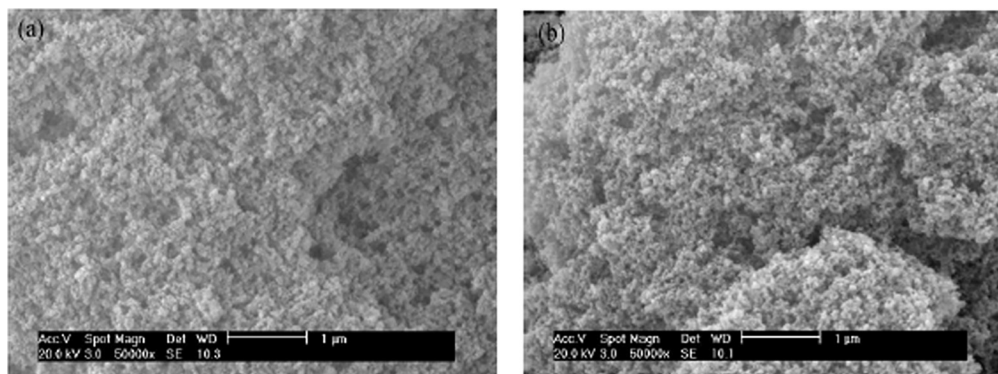
Fig. 15 SEM images of silica nanoparticles coating (A) before and (B) after surface treatment [80].

nature. Based on the studies carried out so far, plasma treatment using dry etching technique turns out to be the efficient method to fabricate nano pillar structures as well as superhydrophobic coating.

Brassard et al. [46] synthesized mono-dispersive silica nanoparticles of ∼120 nm diameter which was further functionalized using fluoroalkylsilane. The synthesized fluorinated silica nanoparticles have been spin coated on flat aluminum alloy, silicon, and glass substrates. SEM images show the randomly stacked layers of spherical fluorinated silica nanoparticles in various depths.

Abbas et al. [86] studied the durability of superhydrophobic functionalized silica nanoparticles and PS using dodecyltrimethoxysilane on carbon steel. This is a cost-effective method which might have industrial applications like reducing fouling and corrosion. From SEM examination, it is understood that the shape of silica particles imparts surface roughness to the samples.

Wimalasiri et al. [45] developed silica-based nonfluorinated superhydrophobic coatings for natural rubber surfaces. The coating was synthesized using nano silica dispersion and a polychloroprene-type binder as a compatibilizer. This nano-coating of silica was applied on to the surface of finished natural rubber gloves, by spray coating or dip coating methods. The morphological properties of the coating have been studied using SEM and AFM. Both spray-coated and dip-coated natural rubber films demonstrated a rough surface with a porous microstructure. The surface of the spray-coated gloves appears to be rougher than the dipped coated surface due to the presence of nano-sized particles embedded within the matrix. The particle size plays a major role in imparting superhydrophobicity to the coating, reducing the interfacial area between water droplets and the surface.

Becker et al. [87] reported the attainment of superhydrophobicity on poly(ethylene terephthalate) (PET) surface using magnetron sputtering assisted laser technique carried out on fluoropolymers. The sophisticated technique produced surfaces with enhanced wettability performance and the morphological features of the surface was studied using SEM.

Mo et al. [88] blended fluorinated silicone oil with titania nanoparticles and coated it on to a steel substrate by a sol–gel technique. The surface properties were studied using SEM and electrochemical measurements. The results indicated that it had a good anticorrosion property.

Hwang et al. [89] synthesized silica/polymer composites which were utilized as superhydrophobic surfaces. The surfaces were prepared by spray deposition of silica/ polymer composites in organic solvent and the morphology was analyzed by SEM.

SiO_2 particles were synthesized using the Stöber procedure. Silica/poly(Zonyl-*co*-MMA) composite was synthesized by free radical polymerization. Coating process adopted was airbrush spray coating. The spray-coated composite has a rough structure consisting of silica particles assembled by poly(Zonyl-*co*-MMA) copolymer.

A SEM analysis by Feng et al. [90] reveals that the ZnO nano-films are superhydrophobic due to the rough surfaces. Artus et al. [91] conducted SEM analysis of silicon nano-filaments and observed the irregularly bent, hooked thin filaments and the entangled fibers. These make the surface protruded and thus superhydrophobic. SEM images of superhydrophobic ORMOSIL (organically modified silica) aero gel thin films indicate that all the films had highly porous networks [92]. Cui et al. [93] studied the effect of binary length scale on the contact line and hysteresis from the SEM analysis. Deng et al. used SEM to show the effect of particles, which are fixed to the first layer in determining the harshness of the surface. Surface harshness in turn increases microscale roughness and superhydrophobicity [94]. Liu et al. [42] revealed the porous and roughness of the surface using the advantage of SEM. Gao et al. [95] also took SEM images to understand the surface morphology of superhydrophobic SiO_2-coated ZnO nanorod arrays.

2.4 Atomic force microscopy

AFM technique helps to observe the surface in its own glory. This is a very useful surface analyzing technique in determining the properties of superhydrophobicity needed. AFM gives a detailed picture of the surface morphology even in the nanometer regime.

A typical AFM image (Fig. 16) of a superhydrophobic aluminum surface [96] is as given below.

AFM can also be used to compare the surface properties at different environmental conditions and to conclude the effect of the conditions on the superhydrophobicity.

Yao et al. [97] studied in detail the effect of destructive NaCl aqueous solution on highly corrosive resistive and durable superhydrophobic surface of copper with the aid of the technique of AFM. By utilizing the benefits of nanostructures and the altering the chemistry of surface, they effectively fabricated highly corrosive-resistant surface. They immersed the surface in the NaCl solution and studied the leading degradation of superhydrophobicity as well as the mechanical property with the aid of an AFM.
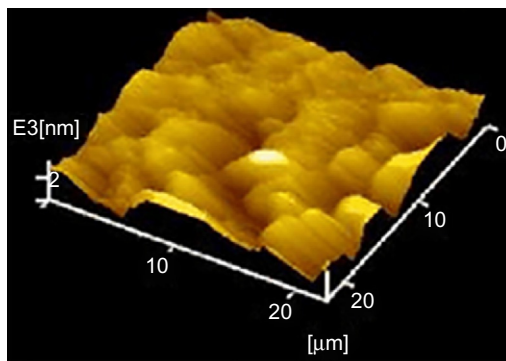
Fig. 16 A typical AFM image of a superhydrophobic aluminum surface [96].

Table 2 Roughness parameters and AFM images of superhydrophobic surface after corrosion test and solvent treatment

	Surface		
Property	Superhydrophobic copper surface	Superhydrophobic copper surface after corrosion test	Superhydrophobic copper surface after immersion in 3.5 wt% NaCl for 24 h
Three-dimensional image			
Roughness R_q (nm)	333.86 ± 5	322.54 ± 16	326.82 ± 5
Stiffness value (N/m)	4.25 ± 0.05	4.24 ± 0.26	4.23 ± 0.20

The details of the study are shown in Table 2. The three-dimensional (3D) images and the calculated roughness values are useful in analyzing the nanoscale structures.

Rezaei et al. [98] fabricated superhydrophobic surface using polypropylene-grafted SiO_2 nanoparticles by following the technique of dip coating. This was done to make the surface rough by aiming the reduction in wettability.

As can be seen in Fig. 17, AFM is used to measure roughness parameters and to study the chemistry. Higher membrane resistance is obtained over the bare membrane due to the pore structure of the graft. The roughness parameters for the bare and coated surfaces are tabulated in Table 3. The coating makes the surface rougher (126–160 nm) and thus superhydrophobic (139–154 degrees).

Ebert et al. [99] made transparent superhydrophobic surfaces by coating functionalized indium tin oxide (ITO), SiO_2, ZnO nanoparticles over poly(methyl methacrylate) (PMMA), polycarbonate, and glass by means of dip coating. AFM were used to study the
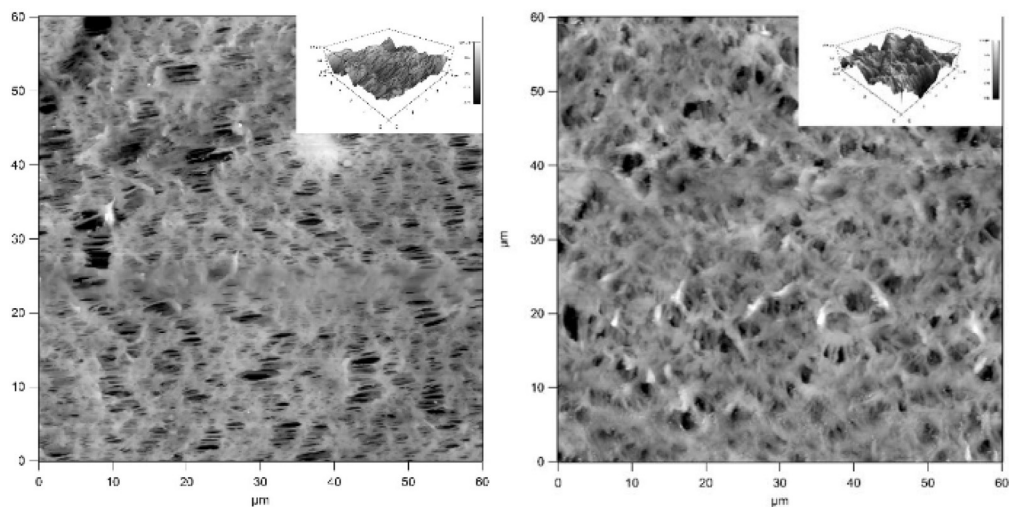
Fig. 17 AFM images of original and modified membranes, before treatment on left and after treatment on right [98].

Table 3 Roughness values measured through AFM before and after silica treatment

Membrane	Roughness parameters	
	R_a (nm)	R_q (nm)
PP original	87	108
PP SiO$_2$ modified	126	160

wear resistance by following the multiscale wear experiments. They modified the nano-particle surface using octadecylphosphonic acid (ODP). Fig. 18 shows the change in the surface height maps and sample surface after AFM wear test.

Joshi et al. [100] made nano-silica and nano-clay coated superhydrophobic cotton by following the methods of dip coating and layer-by-layer self-assembly. AFM study reveals the enhanced superhydrophobicity of the fabric.

Wimalasiri et al. [45] developed silica-based nonfluorinated superhydrophobic coatings for natural rubber surfaces. By AFM analysis, it was found that the 3D surface of the spray-coated rubber surface demonstrates sphere-like shapes in its topological image. Surface roughness of the spray coating has an average thickness of 100 nm and a root mean square (RMS) roughness of 81 nm. A continuous coating is obtained when it is spray coated onto rubber surface where the roughness along the surface is not uniform. This increased roughness at nanoscale facilitates superhydrophobicity on the surface coating.
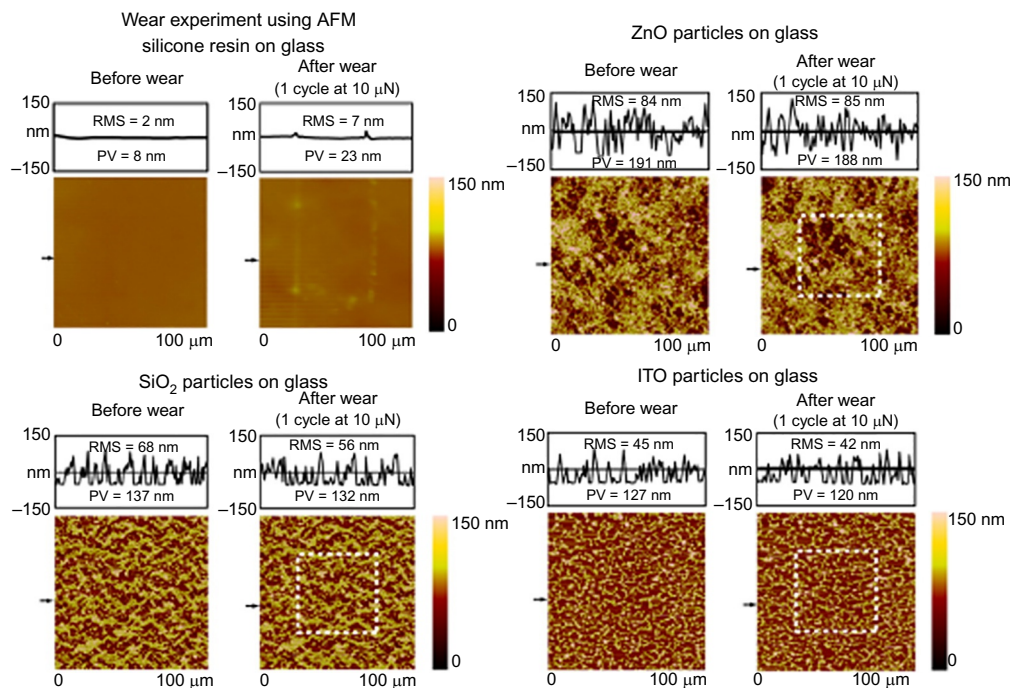
Fig. 18 Surface height maps and sample surface profiles (locations indicated by *arrows*) before and after AFM wear experiment using 15 μm radius borosilicate ball at load of 10 μN for glass samples with silicone resin alone, SiO₂ nanoparticles, ZnO nanoparticles, and ITO nanoparticles. *(Reproduced with permission from D. Ebert, B. Bhushan, Transparent, superhydrophobic, and wear-resistant coatings on glass and polymer substrates using SiO2, ZnO, and ITO nanoparticles, Langmuir 28 (2012) 11391–11399, American Chemical Society.)*

Miwa et al. [101] considered the consequence of roughness of superhydrophobic surfaces on SAs by means of AFM. Zhai et al. [102] analyzed the surface containing hydrophilic bilayers of poly(allylamine hydrochloride)/poly(acrylic acid) (PAH/PAA) using AFM. From the AFM images, it is clear that the superhydrophobicity is attributed by silica. Bhushan and Her [103] with the help of AFM analyzed that the surfaces with high and low adhesion exhibited rose effect. Li et al. [104] characterized the morphology and surface roughness of surfaces prepared from water glass and nonfluorinated alkylsilane on cotton substrate by SEM and AFM. The cooperation of self-assembling of hydrophobic hexadecyl groups and the rough surface by sol–gel coating converted the cotton surface from hydrophilic to superhydrophobic. Farhadi et al. [105] observed by means of surface characterization techniques like SEM and AFM, that the superhydrophobic materials with very hard or elastic rough structures have a better durability under icing and deicing conditions. From AFM, Kulinich and Farzaneh [106] got roughness at microscale and thus air entrapment is expected during wetting. Tavana et al. [107] analyzed the superhydrophobic surfaces of *n*-hexatriacontane using AFM technique. They calculated the height of the clusters and the roughness from AFM measurements. From the detailed AFM analysis, Song et al. [108] concluded that by

controlling the deposition time it is able to adjust the morphology of the self-assembled films. Hence, by adjusting the morphology, the nature of surface can be converted to hydrophobic from hydrophilic. If the deposition time is less, silane coverage is less, hence philic in nature. As the time of deposition increases, the coverage area will be broad which can be clearly understood from AFM. Hence, surface becomes hydrophobic.

2.5 White light interferometry

White light interferometry (WLI) alternatively known as coherence scanning interferometry is a type of noncontact optical technique for the surface analysis; which helps in obtaining 3D image of surface with calculation of surface parameters. This technique relies on the visible-wavelength light (white light) hence the name WLI [109]. This technique is based on the wave superposition; hence, the resulting pattern is determined by the phase difference between the two waves. Measurement is carried out by following the principle of the Michelson interferometer, which consist of a light source having coherence length in the micron range [110]. This technique is widely used for the surface characterization of superhydrophobic surfaces.

Waugh and Lawrence sought the help of white light interferometer for investigating the modification carried out on PMMA surface using CO_2 laser. This is done to vary the surface wettability and to study the effect of laser treatment on CA [111]. This property is improved by generating patterns of various topography over PMMA using laser and the properties of samples having four different topographies were characterized using WLI. It is observed that the sample roughness increased up to 3.1 μm leading to superhydrophobicity, which is shown in Fig. 19.

Robust interpenetrating polymer network (IPN) coating was made using PU and PMMA by Wong et al. [112]. The superhydrophobic nature was found to enhance by the integration of flouro–functionalized silica nanoparticle onto the curing IPN. Surface roughness of the obtained material was quantified by RMS and WLI techniques. The surface exhibited a significantly higher roughness than the individual components PMMA and PU. Fig. 20 shows high magnification WLI color-map analysis on PU-PMMA IPNs before and after F–SiO$_2$ impregnation. This sprayable acrylic IPN colloid exhibits outstanding abrasion resistance and turns out to be a low-cost and highly scalable platform for fabricating superhydrophobic coatings.

Using the same technique, Söz et al. [113] observed the random distribution of silica particles of varying heights on a superhydrophobic surface. Average surface roughness values were also determined from WLI measurements on uncoated and silica-coated segmented thermoplastic polydimethylsiloxane-urea copolymer (TPSC) samples. Dong et al. [114] fabricated superhydrophobic Cu surfaces by chemical etching and laser treatment. The topography and the microstructures were studied using WLI. Forsberg et al. [115] studied Cassie-Wenzel and Wenzel-Cassie transitions on immersed superhydrophobic surfaces under hydrostatic pressure using WLI. 3D topography of aluminum
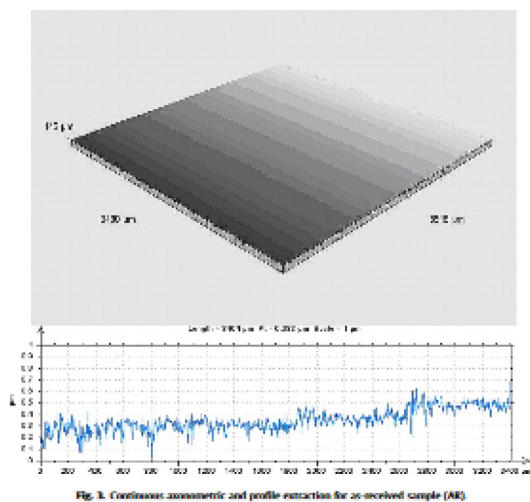
(A)
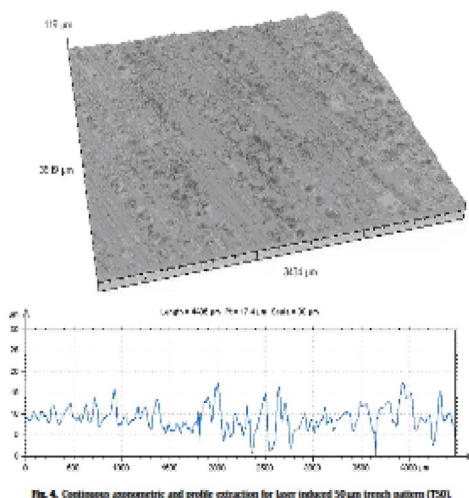
(B)
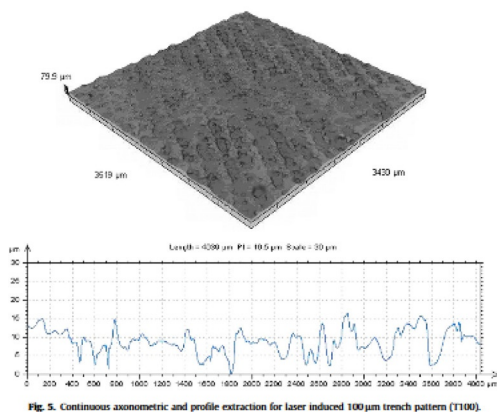
(C)
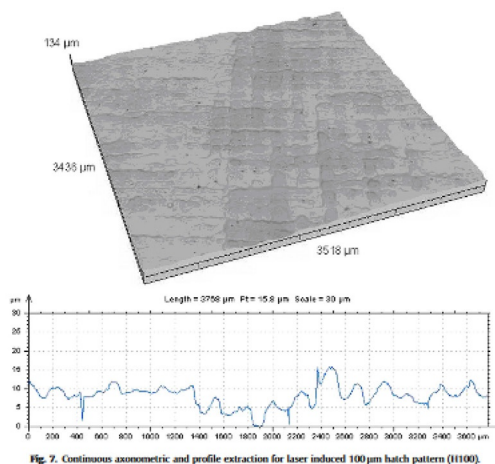
(D)

Fig. 19 (A) As received sample (A1), (B) laser-induced 50 µm trench pattern (A3), (C) laser-induced 100-µm trench pattern (B1), and (D) laser-induced 50-µm hatch pattern (B2) [111].

surface was studied by Song et al. [116]. Wong et al. [117] made flexible transparent hier-archical nanomesh exhibiting rose effect. In the case of heavily beaded films, the struc-tural properties were in par with the good wetting behavior resembling lotus leaf.

2.6 Other characterization techniques

Lately, a few techniques like optical profilometer were employed to measure the thickness of the superhydrophobic coatings. The peculiarity of this instrument is that it makes use of a sensor which is based on confocal microscopy. Ovaskainen et al. [118] utilized this technique
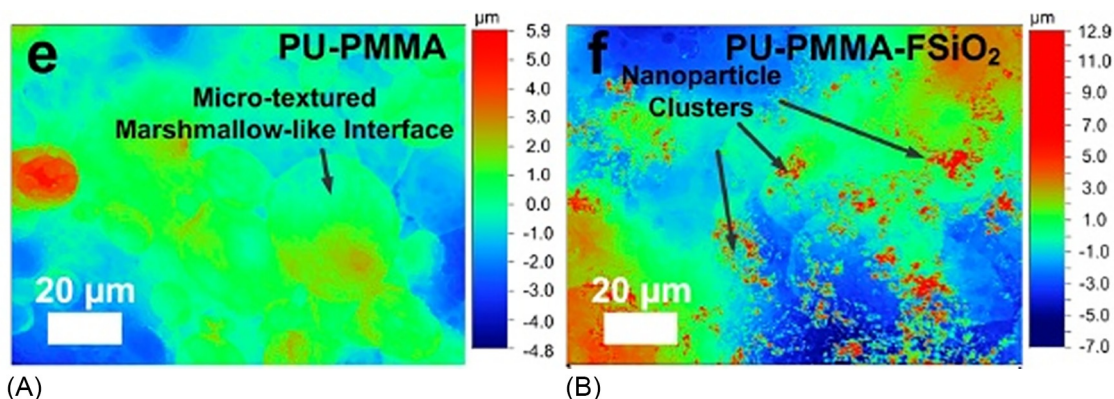
Fig. 20 High magnification (500×) WLI color-map analysis on PU-PMMA IPNs before (A) and after F-SiO$_2$ impregnation (B). *(Reproduced with permission from William Wong, Zbigniew Stachurski, David Nisbet, Antonio Tricoli, Ultra-durable and transparent self-cleaning surfaces by large-scale self-assembly of hierarchical interpenetrated polymer networks, ACS Appl. Mater. Interfaces 8 (2016), https://doi.org/10.1021/acsami.6b03414, American Chemical Society.)*
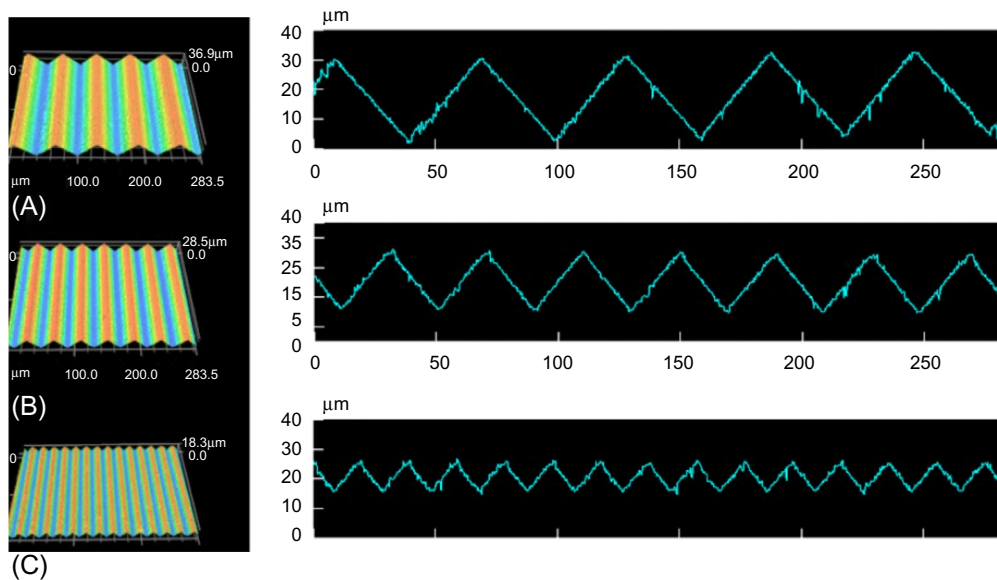
Fig. 21 Confocal microscopy images of the fabricated pattern on the mold with (A) 10 μm, (B) 20 μm, and (C) 30 μm depths [120].

for the determination of thickness of superhydrophobic surfaces prepared from a PVA-based copolymer. Yilgor et al. [119] employed X-ray photoelectron spectroscopy for the characterization of superhydrophobic surfaces from PS and cured epoxy resin. In another interesting study, Lee et al. [120] fabricated anisotropic coatings having superior water repellence by dip coating and compression molding and the morphology of the polymer surface was monitored using confocal microscopy. Fig. 21 clearly shows the grooves on the surface of the polymer which gives the characteristic wettability to the polymer.

3. Conclusions and future scope

Owing to the escalating demand for superhydrophobic coatings, the preparation and property evaluation of these materials will be beyond doubt one of the most demanding and fascinating areas of research in materials science for the next two decades. Fulfilling the adequate requirements of the surface micro/nanostructures, maintaining the low surface energy turns out to be a major challenge. Lately, there were attempts to mimic the lotus leaf–like surface morphology which is considered to be an ideal superhydrophobic surface. Several lab-scale studies have been carried out in this area. In order to scale up the process, various properties like mechanical robustness, resistance to scratch, optical transparency, etc. are needed for applications like self-cleaning. The nature of the adherent coating material is crucial in determining the anticorrosive coating on the metals. It is

obvious that gradually the inorganic superhydrophobic coatings will be replaced with polymeric superhydrophobic coatings because of their high mechanical stability and optical transparency and hence, the future of superhydrophobic research is very much dependent on the development of polymer nanocomposites. In view of the fact that the characterization methods are inevitable in almost all the steps of fabrication of these coatings, the entire novel methods used for the characterization of polymer/inorganic surfaces can be employed for superhydrophobic coatings as well. The traditional techniques used for the characterization of these coatings coupled with the present sophisticated methods will definitely pave way toward the enhanced performance of the new generation superhydrophobic coatings.

References

[1] R. Furstner, W. Barthlott, Wetting and self-cleaning properties of artificial superhydrophobic surfaces, Langmuir 21 (2005) 956–961.

[2] N.J. Shirtcliffe, G. McHale, S. Atherton, M.I. Newton, An introduction to super-hydrophobicity, Adv. Colloid Interf. Sci. 161 (2010) 124–138.

[3] I. Hejazi, B. Hajalizadeh, J. Seyfi, G.M.M. Sadeghi, S.H. Jafari, H.A. Khonakdar, Role of nanoparticles in phase separation and final morphology of superhydrophobic polypropylene/zinc oxide nanocomposite surfaces, Appl. Surf. Sci. 293 (2014) 116–123.

[4] J. Seyfi, I. Hejazi, S.H. Jafari, H.A. Khonakdar, G.M.M. Sadeghi, A. Calvimontes, F. Simon, On the combined use of nanoparticles and a proper solvent/non-solvent system in preparation of superhydrophobic polymer coatings, Polymer 56 (2015) 358–367.

[5] Y. Qing, C. Yang, C. Hu, Y. Zheng, C. Liu, A facile method to prepare superhydrophobic fluorinated polysiloxane/ZnO nanocomposite coatings with corrosion resistance, Appl. Surf. Sci. 326 (2015) 48–54.

[6] W. Barthlott, C. Neinhuis, Purity of the sacred lotus, or escape from contamination in biological surfaces, Planta 202 (1997) 1–8, https://doi.org/10.1007/s004250050096.

[7] D.R. Paul, L.M. Robeson, Polymer nanotechnology: nanocomposites, Polymer 49 (2008) 3187–3204.

[8] M. Barmouz, J. Seyfi, M.K. BesharatiGivi, I. Hejazi, S.M. Davachi, A novel approach for producing polymer nanocomposites by in-situ dispersion of clay particles via friction stir processing, Mater. Sci. Eng. A 528 (2011) 3003–3006.

[9] I. Hejazi, J. Seyfi, G.M.M. Sadeghi, S.M. Davachi, Assessment of rheological and mechanical properties of nanostructured materials based on thermoplastic olefin blend and organoclay, Mater. Des. 32 (2011) 649–655.

[10] J. Seyfi, S.H. Jafari, H.A. Khonakdar, Opposing effects of nanoclay on viscoelastic response of reactive phenoxy/poly (trimethylene terephthalate) blends: clay-induced transreactions versus percolated network formation, Polym. Compos. 32 (2011) 114–124.

[11] K. Jeddi, N. Taheri Qazvini, S.H. Jafari, H.A. Khonakdar, J. Seyfi, U. Reuter, Investigating the effect of nanolayered silicates on blend segmental dynamics and minor component relaxation behavior in poly(ethylene oxide)/poly(methyl methacrylate) miscible blends, J. Polym. Sci. B Polym. Phys. 49 (2011) 318–326.

[12] J. Seyfi, S.H. Jafari, H.A. Khonakdar, P. Saha, V. Goodarzi, Investigating the role of transreactions on degradation behavior of phenoxy/poly(trimethylene terephthalate)/clay nanocomposites using thermal analysis techniques, Thermochim. Acta 511 (2010) 59–66.

[13] X. Du, X. Li, J. He, Facile fabrication of hierarchically structured silica coatings from hierarchically mesoporous silica nanoparticles and their excellent super-hydrophilicity and superhydrophobicity, ACS Appl. Mater. Interfaces 2 (2010) 2365–2372.

[14] H. Mertaniemi, et al., Superhydrophobic tracks for low-friction, guided transport of water droplets, Adv. Mater. 23 (2011) 2911–2914, https://doi.org/10.1002/adma.201100461.

[15] Z. Yuan, H. Chen, J. Zhang, D. Zhao, Y. Liu, X. Zhou, S. Li, P. Shi, J. Tang, X. Chen, Preparation and characterization of self-cleaning stable superhydrophobic linear low-density polyethylene, Sci. Technol. Adv. Mater. 9 (4) (2008) 045007.

[16] C. Su, J. Li, H. Geng, Q. Wang, Q. Chen, Fabrication of an optically transparent super-hydrophobic surface via embedding nano-silica, Appl. Surf. Sci. 253 (5) (2006) 2633–2636.

[17] H. Wang, J. Fang, T. Cheng, J. Ding, L. Qu, L. Dai, X. Wang, T. Lin, One-step coating of fluoro-containing silica nanoparticles for universal generation of surface superhydrophobicity, Chem. Commun. (7) (2008) 877–879.

[18] T. Onda, S. Shibuichi, N. Satoh, K. Tsujii, Super-water-repellent fractal surfaces, Langmuir 12 (9) (1996) 2125–2127.

[19] T. Nishino, M. Meguro, K. Nakamae, M. Matsushita, Y. Ueda, The lowest surface free energy based on $-CF_3$ alignment, Langmuir 15 (1999) 4321.

[20] S.H. W U, Polymer Interface and Adhesion, Marcel Dekker, New York, 1982.

[21] R.N. Wenzel, Resistance of solid surfaces to wetting by water, Ind. Eng. Chem. 28 (1936) 988.

[22] A.W. Adamson, A.P. Gast, Physical Chemistry of Surface, sixth ed., Wiley, New York, 1997.

[23] M. Peng, H. Li, L. Wu, Q. Zheng, Y. Chen, W. Gu, Porous poly(vinylidene fluoride)membrane with highly hydrophobic surface, J. Appl. Polym. Sci. 98 (3) (2005) 1358–1363.

[24] J.L. Zhang, J.A. Li, Y. Fan, Y.C. Han, Fabricating superhydrophobic lotus-leaf-like surfaces through soft-lithographic imprinting, Macromol. Rapid Commun. 25 (2004) 1105–1108.

[25] H.-J. Song, Z.-Z. Zhang, X.-H. Men, Superhydrophobic PEEK/PTFE composite coating, Appl. Phys. A 91 (1) (2008) 73–76.

[26] E. Burkarter, C.K. Saul, F. Thomazi, N.C. Cruz, L.S. Roman, W.H. Schreiner, Superhydrophobic electro sprayed PTFE, Surf. Coat. Technol. 202 (1) (2007) 194–198.

[27] K.K.S. Lau, J. Bico, K.B.K. Teo, et al., Superhydrophobic carbon nanotube forests, Nano Lett. 3 (12) (2003) 1701–1705.

[28] S. Minko, M. Müller, M. Motornov, M. Nitschke, K. Grundke, M. Stamm, Two-level structured self-adaptive surfaces with reversibly tunable properties, J. Am. Chem. Soc. 125 (13) (2003) 3896–3900.

[29] S.H. Kim, J.H. Kim, B.K. Kang, H.S. Uhm, Superhydrophobic CFx coating via in-line atmospheric RF plasma of He—CF4—H2, Langmuir 21 (26) (2005) 12213–12217.

[30] D.K. Sarkar, M. Farzaneh, R.W. Paynter, Superhydrophobic properties of ultrathin rf-sputtered Teflon films coated etched aluminum surfaces, Mater. Lett. 62 (8–9) (2008) 1226–1229.

[31] P. Favia, G. Cicala, A. Milella, F. Palumbo, P. Rossini, R. d'Agostino, Deposition of super-hydrophobic fluorocarbon coatings in modulated RF glow discharges, Surf. Coat. Technol. 169–170 (2003) 609–612.

[32] V. Stelmashuk, H. Biederman, D. Slavínská, J. Zemek, M. Trchová, Plasma polymer films rf sputtered from PTFE under various argon pressures, Vacuum 77 (2) (2005) 131–137.

[33] M. Hikita, K. Tanaka, T. Nakamura, T. Kajiyama, A. Takahara, Super-liquid-repellent surfaces prepared by colloidal silica nanoparticles covered with fluoroalkyl groups, Langmuir 21 (16) (2005) 7299–7302.

[34] L. Yan, K. Wang, L. Ye, Super hydrophobic property of PVDF/CaCO3 nanocomposite coatings, J. Mater. Sci. Lett. 22 (23) (2003) 1713–1717.

[35] B.J. Basu, A.K. Paranthaman, A simple method for the preparation of superhydrophobic PVDF-HMFS hybrid composite coatings, Appl. Surf. Sci. 255 (8) (2009) 4479–4483.

[36] Y. Yuan, T.R. Lee, Contact angle and wetting properties, in: G. Bracco, B. Holst (Eds.), Surface Science Techniques, Springer Series in Surface Sciences, vol. 51, Springer, Berlin, Heidelberg, 2013.

[37] T. Young, An essay on the cohesion of fluids, Philos. Trans. R. Soc. B 95 (1805) 65–87, https://doi.org/10.1098/rstl.1805.0005.

[38] R.N. Wenzel, Resistance of solid surfaces to wetting by water, Ind. Eng. Chem. 28 (8) (1936) 988–994, https://doi.org/10.1021/ie50320a024.

[39] A.B.D. Cassie, S. Baxter, Wettability of porous surfaces, Trans. Faraday Soc. 40 (1944) 546–551, https://doi.org/10.1039/tf9444000546.

[40] J. Schuster, C. Schvezov, M. Rosenberger, Influence of experimental variables on the measure of contact angle in metals using the sessile drop method, Procedia Mater. Sci. 8 (2015) 742–751, https://doi.org/10.1016/j.mspro.2015.04.131.

[41] P. Waghmare, S.K. Mitra, Contact angle hysteresis of microbead suspensions, Langmuir 26 (2010) 17082–17089.

[42] J. Liu, X. Xiao, Y. Shi, C. Wan, Fabrication of a superhydrophobic surface from porous polymer using phase separation, Appl. Surf. Sci. 0169-4332297 (2014) 33–39, https://doi.org/10.1016/j.apsusc.2014.01.053.

[43] H. Yıldırım Erbil, A. Levent Demirel, Y. Avcı, O. Mert, Transformation of a simple plastic into a superhydrophobic surface, Science 299 (5611) (28 Feb 2003) 1377–1380, https://doi.org/10.1126/science.1078365.

[44] X. Xu, Z. Zhang, J. Yang, Fabrication of biomimetic superhydrophobic surface on engineering materials by a simple electroless galvanic deposition method, Langmuir 26 (5) (2009) 3654–3658.

[45] V.K. Wimalasiri, H.U. Weerathunga, N. Kottegoda, V. Karunaratne, Silica based superhydrophobic nanocoatings for natural rubber surfaces, Research Article, J. Nanomater. 2017 (2017), 2102467. https://doi.org/10.1155/2017/2102467.

[46] J.-D. Brassard, D.K. Sarkar, J. Perron, Synthesis of monodisperse fluorinated silica nanoparticles and their superhydrophobic thin films, ACS Appl. Mater. Interfaces 3 (9) (2011) 3583–3588, https://doi.org/10.1021/am2007917.

[47] N. Mittal, D. Deva, R. Kumar, A. Sharma, Exceptionally robust and conductive super hydrophobic free-standing films of mesoporous carbon nanocapsule/polymer composite for multifunctional applications, Carbon 93 (2015) 492–501. Elsevier Science Direct.

[48] D. Sriramulu, E.L. Reed, M. Annamalai, T.V. Venkatesan, S. Valiyaveettil, Synthesis and characterization of superhydrophobic, self-cleaning NIR-reflective silica nanoparticles, Sci. Rep. 6 (35993) (2016), https://doi.org/10.1038/srep35993.

[49] Y. Guan, C. Yu, J. Zhu, R. Yang, D. Wei, X. Xu, Design and fabrication of vapor-induced superhydrophobic surfaces obtained from polyethylene wax and silica nanoparticles in hierarchical structures, RSC Adv. 8 (2018) 25150–25158, https://doi.org/10.1039/C8RA01666F.

[50] T. Liu, C.-J. Kim, Turning a surface superrepellent even to completely wetting liquids, Science 346 (6213) (2014) 1096–1100.

[51] J. Yang, Z. Zhang, X. Xu, X. Zhu, X. Men, X. Zhou, Superhydrophilic–superoleophobic coatings, J. Mater. Chem. 22 (7) (2012) 2834–2837.

[52] J. Yang, Z. Zhang, X. Xu, X. Men, X. Zhu, X. Zhou, Superoleophobic textured aluminum surfaces, New J. Chem. 35 (11) (2011) 2422–2426.

[53] A. Tuteja, W. Choi, M. Ma, J.M. Mabry, S.A. Mazzella, G.C. Rutledge, G.H. McKinley, R.E. Cohen, Designing superoleophobic surfaces, Science 318 (5856) (2007) 1618–1622.

[54] W. Barthlott, T. Schimmel, S. Wiersch, K. Koch, M. Brede, M. Barczewski, S. Walheim, A. Weis, A. Kaltenmaier, A. Leder, et al., The salvinia paradox: superhydrophobic surfaces with hydrophilic pins for air retention under water, Adv. Mater. 22 (21) (2010) 2325–2328.

[55] C. Chang-Hwan, U. Ulmanella, J. Kim, C.-M. Ho, C.-J. Kim, Effective slip and friction reduction in nanograted superhydrophobic microchannels, Phys. Fluids 18 (8) (2006) 087105.

[56] K.A. Stephani, D.B. Goldstein, An examination of trapped bubbles for viscous drag reduction on submerged surfaces, J. Fluids Eng. 132 (2010) 041303.

[57] D. Dilip, N.K. Jha, R.N. Govardhan, M.S. Bobji, Controlling air solubility to maintain "Cassie" state for sustained drag reduction, Colloids Surf. A Physicochem. Eng. Asp. 459 (2014) 217–224.

[58] H. Liu, S. Szunerits, W. Xu, R. Boukherroub, Preparation of superhydrophobic coatings on zinc as effective corrosion barriers, ACS Appl. Mater. Interfaces 1 (6) (2009) 1150–1153.

[59] Y. Yin, T. Liu, S. Chen, T. Liu, S. Cheng, Structure stability and corrosion inhibition of superhydrophobic film on aluminum in seawater, Appl. Surf. Sci. 255 (2008) 2978–2984.

[60] F. Zhang, L. Zhao, H. Chen, S. Xu, D.G. Evans, X. Duan, Corrosion resistance of superhydrophobic layered double hydroxide films on aluminum, Angew. Chem. Int. Ed. 47 (13) (2008) 2466–2469.

[61] J. Genzera, K. Efimenkoa, Recent developments in superhydrophobic surfaces and their relevance to marine fouling: a review, Biofouling 22 (5) (2006) 339–360.

[62] M.S. Bobji, S.V. Kumar, A. Asthana, R.N. Govardhan, Underwater sustainability of the "Cassie" state of wetting, Langmuir 25 (20) (2009) 12120–12126.

[63] M. Sakai, T. Yanagisawa, A. Nakajima, Y. Kameshima, K. Okada, Effect of surface structure on the sustainability of an air layer on superhydrophobic coatings in a water ethanol mixture, Langmuir 25 (1) (2009) 13–16.

[64] Q. Zheng, Y. Yu, Z. Zhao, Effects of hydraulic pressure on the stability and transition of wetting modes of superhydrophobic surfaces, Langmuir 21 (15) (2005) 12207–12212.

[65] M.A. Samaha, H.V. Tafreshi, M. Gad-el-hak, Influence of flow on longevity of superhydrophobic coatings, Langmuir 28 (2012) 9759–9766.

[66] L.M. Lander, L.M. Siewierski, W.J. Brittain, E.A. Vogler, A systematic comparison of contact angle methods, Langmuir 9 (8) (1993) 2237–2239.

[67] A. Krishnan, Y.-H. Liu, P. Cha, R. Woodward, D. Allara, E.A. Vogler, An evaluation of methods for contact angle measurement, Colloids Surf. B: Biointerfaces 43 (2) (2005) 95–98.

[68] R. Di Mundo, F. Palumbo, Comments regarding "an essay on contact angle measurements", Plasma Process. Polym. 8 (1) (2011) 14–18.

[69] K. Abe, H. Takiguchi, K. Tamada, Dynamic contact angle measurement of Au(111)—thiol self-assembled monolayers by the Wilhelmy plate method, Langmuir 16 (111) (2000) 2394–2397.

[70] I.L. Liakos, R.C. Newman, E. McAlpine, M.R. Alexander, Study of the resistance of SAMs on aluminium to acidic and basic solutions using dynamic contact angle measurement, Langmuir 23 (12) (2007) 995–999.

[71] J. Seyfi, S.H. Jafari, H.A. Khonakdar, G.M.M. Sadeghi, G. Zohuri, I. Hejazi, F. Simon, Fabrication of robust and thermally stable superhydrophobic nanocomposite coatings based on thermoplastic polyurethane and silica nanoparticles, Appl. Surf. Sci. 347 (2015) 224–230.

[72] H.M. Shang, Y. Wang, K. Takahashi, G.Z. Cao, D. Li, Y.N. Xia, Nanostructured superhydrophobic surfaces, J. Mater. Sci. 40 (2005) 3587–3591.

[73] I. Karapanagiotis, D. Grosu, D. Aslanidou, K.E. Aifantis, Research Article. Facile method to prepare superhydrophobic and water repellent cellulosic paper, Hindawi Publishing Corporation, J. Nanomater. (2015) 219013. 9 pages, https://doi.org/10.1155/2015/219013.

[74] B. Cortese, S. D'Amone, M. Manca, I. Viola, R. Cingolani, G. Gigli, Superhydrophobicity due to the hierarchical scale roughness of PDMS surfaces, Langmuir 24 (6) (2008) 2712–2718, https://doi.org/10.1021/la702764x.

[75] Y. Yoon, D. Kim, J.-B. Lee, Hierarchical micro/nano structures for super–hydrophobic surfaces and super–lyophobic surface against liquid metal, Micro Nano Syst. Lett. 2 (2014) 3. http://www.mnsl-journal.com/content/2/1/3.

[76] N. Tasaltin, D. Sanli, A. Jonáš, A. Kiraz, C. Erkey, Preparation and characterization of superhydrophobic surfaces based on hexamethyldisilazane-modified nanoporous alumina, Nanoscale Res. Lett. 6 (2011) 487. Springer.

[77] H. Mohsin, U. Sultan, Y.F. Joya, S. Ahmed, M.S. Awan, S.N. Arshad, Development and characterization of cobalt based nano-structured super hydrophobic coating, in: IOP Conf. Series: Materials Science and Engineering, vol. 146, 2016, p. 012038, https://doi.org/10.1088/1757-899X/146/1/012038.

[78] N. Zhao, J. Xu, Q. Xie, L. Weng, X. Guo, X. Zhang, L. Shi, Fabrication of biomimetic superhydrophobic coating with a micro-nano-binary structure, Macromol. Rapid Commun. 26 (2005) 1075–1080.

[79] Z.J. Wei, W.L. Liu, D. Tian, C.L. Xiao, X.Q. Wang, Preparation of lotus-like superhydrophobic fluoropolymer films, Appl. Surf. Sci. 256 (12) (2010) 3972–3976, https://doi.org/10.1016/j.apsusc.2010.01.059.

[80] J. Liu, Z.A. Janjua, M. Roe, F. Xu, B. Turnbull, K.-S. Choi, X. Hou, Super-hydrophobic/icephobic coatings based on silica nanoparticles modified by self-assembled monolayers, Nanomaterials 6 (2016) 232, https://doi.org/10.3390/nano6120232.

[81] Y. Li, X.J. Huang, S.H. Heo, C.C. Li, Y.K. Choi, W.P. Cai, S.O. Cho, Superhydrophobic bionic surfaces with hierarchical microsphere/SWCNT composite arrays, Langmuir 23 (2007) 2169–2174.

[82] Y. Liu, X. Chen, J. Xin, Super-hydrophobic surfaces from a simple coating method: a bionic nanoengineering approach, Nanotechnology 17 (2006) 3259.

[83] T.-Y. Kim, B. Ingmar, K. Bewilogua, K.H. Oh, K.-R. Lee, Wetting behaviours of a C:H:Si:O film coated nano-scale dual rough surface, Chem. Phys. Lett. 436 (2007) 199–203.

[84] B. D'Urso, J.T. Simpson, Emergence of superhydrophobic behavior on vertically aligned nanocone arrays, Appl. Phys. Lett. 90 (2007) 044102.

[85] S.-C. Cha, E.K. Her, T.-J. Ko, S.J. Kim, H. Roh, K.-R. Lee, O. Kyu Hwan, M.-W. Moon, Thermal stability of superhydrophobic, nanostructured surfaces, J. Colloid Interface Sci. 391 (2013) 152–157. Elsevier.

[86] R. Abbas, A. Hefnawy, W.I. El-Dessouky, A. El-Halag, W.A. Sadik, A.G.M. El-Demerdash, Effect of durable superhydrophobic FS/PS using DCTES on carbon steel, J. Mater. Sci. Eng. (2018), https://doi.org/10.4172/2169-0022.1000408.

[87] C. Becker, J. Petersen, G. Mertz, D. Ruch, A. Dinia, High superhydrophobicity achieved on poly(ethylene terephthalate) by innovative laser-assisted magnetron sputtering, J. Phys. Chem. C 115 (21) (2011) 10675–10681.

[88] C. Mo, Y. Zheng, F. Wang, Q. Mo, A simple process for fabricating organic/TiO2 super-hydrophobic and anti-corrosion coating, Int. J. Electrochem. Sci. 10 (2015) 7380–7391.

[89] H. S. Hwang, J. K. Shim, I. Park, Superhydrophobic surfaces from a spray coating process, in: 18th International Conference on Composite Materials, n.d.

[90] X.J. Feng, L. Feng, M.H. Jin, J. Zhai, L. Jiang, D.B. Zhu, Reversible superhydrophobicity to super-hydrophilicity transition of aligned ZnO nanorod films, J. Am. Chem. Soc. 126 (2004) 62–63. This was the first report of reversible switching between superhydrophobicity and superhydrophilicity made from inorganic materials.

[91] G.R.J. Artus, S. Jung, J. Zimmermann, H.-P. Gautschi, K. Marquardt, S. Seeger, Silicone nanofila-ments and their application as superhydrophobic coatings, Adv. Mater. 18 (2006) 2758–2762, https://doi.org/10.1002/adma.200502030.

[92] H. Budunoglu, A. Yildirim, M.O. Guler, M. Bayindir, Highly transparent, flexible, and thermally stable superhydrophobic ORMOSIL aerogel thin films, ACS Appl. Mater. Interfaces 3 (2011) 539–545, https://doi.org/10.1021/am101116b.

[93] Z. Cui, Q. Wang, Y. Xiao, C. Su, Q. Chen, The stability of superhydrophobic surfaces tested by high speed current scouring, Appl. Surf. Sci. 254 (2008) 2911–2916.

[94] X. Deng, L. Mammen, Y. Zhao, P. Lellig, K. Müllen, C. Li, H.-J. Butt, D. Vollmer, Transparent, thermally stable and mechanically robust superhydrophobic surfaces made from porous silica capsules, Adv. Mater. 23 (2011) 2962–2965.

[95] Y. Gao, I. Gereige, A. El Labban, D. Cha, T.T. Isimjan, P.M. Beaujuge, Highly transparent and UV-resistant superhydrophobic SiO2-coated ZnO nanorod arrays. ACS Appl. Mater. Interfaces 6 (2014) 2219–2223, https://doi.org/10.1021/am405513k.

[96] Z. Ahmad, A. Khan, R. Farooq, N. Mastoi, T. Saif, Hydrophobicity—A Green Technique for Enhancing Corrosion Resistance of Alloys. (2015), https://doi.org/10.5772/60815.

[97] C.-W. Yao, D. Sebastian, I. Lian, Ö. Günaydın-Şen, R. Clarke, K. Clayton, C.-Y. Chen, K. Kharel, Y. Chen, Q. Li, Corrosion resistance and durability of superhydrophobic copper surface in corrosive NaCl aqueous solution. Coatings 8 (2) (2018) 70, https://doi.org/10.3390/coatings8020070.

[98] R. Mohammad, W. Samhaber, Wetting behaviour of superhydrophobic membranes coated with nanoparticles in membrane distillation, Chem. Eng. Trans. 47 (2016) 373, https://doi.org/10.3303/CET1647063.

[99] D. Ebert, B. Bhushan, Transparent, superhydrophobic, and wear-resistant coatings on glass and poly-mer substrates using SiO2, ZnO, and ITO nanoparticles, Langmuir 28 (2012) 11391–11399.

[100] M. Joshi, A. Bhattacharyya, N. Agarwal, A. Parmar, Nanostructured coatings for super hydrophobic textiles, Bull. Mater. Sci. 35 (6) (2012) 933–938.

[101] M. Miwa, A. Nakajima, A. Fujishima, K. Hashimoto, T. Watanabe, Effects of the surface roughness on sliding angles of water droplets on superhydrophobic surfaces, Langmuir 16 (2000) 5754–5760.

[102] L. Zhai, M.C. Berg, F.Ç. Cebeci, Y. Kim, J.M. Milwid, M.F. Rubner, R.E. Cohen, Patterned super-hydrophobic surfaces: toward a synthetic mimic of the Namib Desert beetle, Nano Lett. 6 (6) (2006) 1213–1217.

[103] B. Bhushan, E.K. Her, Fabrication of superhydrophobic surfaces with high and low adhesion inspired from rose petal, Langmuir 26 (11) (2010) 8207–8217, https://doi.org/10.1021/la904585j.

[104] Z. Li, Y. Xing, J. Dai, Superhydrophobic surfaces prepared from water glass and non-fluorinated alkylsilane on cotton substrates, Appl. Surf. Sci. 254 (2008) 2131–2135.

[105] S. Farhadi, M. Farzaneh1, S.A. Kulinich, Anti–icing performance of superhydrophobic surfaces, Appl. Surf. Sci. 257 (2011) 6264–6269, https://doi.org/10.1016/j.apsusc.2011.02.057.

[106] S.A. Kulinich, M. Farzaneh, How wetting hysteresis influences ice adhesion strength on superhydro-phobic surfaces, Langmuir 25 (16) (2009) 8854–8856, https://doi.org/10.1021/la901439c.

[107] H. Tavana, A. Amirfazli, A.W. Neumann, Fabrication of superhydrophobic surfaces of n-hexatriacontane, Langmuir 22 (2006) 5556–5559.

[108] X. Song, J. Zhai, Y. Wang, L. Jiang, Fabrication of superhydrophobic surfaces by self-assembly and their water-adhesion properties, J. Phys. Chem. B 109 (2005) 4048–4052.

[109] J.C. Wyant, White light interferometry, in: Proc. SPIE 4737, Holography: A Tribute to Yuri Deni-syuk and Emmett Leith, 9 July 2002, https://doi.org/10.1117/12.474947.

[110] L. Yan, Y.M. Rong, F. Jiang, Z.X. Zhou, Three-dimension surface characterization of grinding wheel using white light interferometer, Int. J. Adv. Manuf. Technol. 55 (1–4) (July 2011) 133–141.

[111] D. Waugh, J. Lawrence, Wettability characteristics variation of PMMA by means of CO2 laser gen-erated surface patterns, in: ICALEO 2009—28th International Congress on Applications of Lasers and Electro-Optics, Congress Proceedings, 2009, p. 102.

[112] W. Wong, Z. Stachurski, D. Nisbet, A. Tricoli, Ultra-durable and transparent self-cleaning surfaces by large-scale self-assembly of hierarchical interpenetrated polymer networks, ACS Appl. Mater. Inter-faces 8 (2016), https://doi.org/10.1021/acsami.6b03414.

[113] C.K. Söz, E. Yilgör, I. Yilgör, Influence of the average surface roughness on the formation of super-hydrophobic polymer surfaces through spin-coating with hydrophobic fumed silica, Polymer 62 (7 April 2015) 118–128, https://doi.org/10.1016/j.polymer.2015.02.032.

[114] C. Dong, Y. Gu, M. Zhong, L. Li, K. Sezer, M. Ma, W. Liu, Fabrication of superhydrophobic Cu surfaces with tunable regular micro and random nano-scale structures by hybrid laser texture and chemical etching, J. Mater. Process. Technol. 211 (2011) 1234–1240, https://doi.org/10.1016/j.jmatprotec.2011.02.007.

[115] P. Forsberg, F. Nikolajeff, M. Karlsson, Cassie–Wenzel and Wenzel–Cassie transitions on immersed superhydrophobic surfaces under hydrostatic pressure, Soft Matter 7 (2011) 104–109, https://doi.org/10.1039/C0SM00595A.

[116] J.-l. Song, W.-j. Xu, X. Liu, Y. Lu, J. Sun, Electrochemical machining of super-hydrophobic Al sur-faces and effect of processing parameters on wettability, Appl. Phys. A 108 (3) (September 2012) 559–568.

[117] W.S.Y. Wong, N. Nasiri, G. Liu, N. Rumsey-Hill, V.S.J. Craig, D.R. Nisbet, A. Tricoli, Flexible transparent hierarchical nanomesh for rose petal-like droplet manipulation and lossless transfer, Adv. Mater. Interfaces (2015) 1500071, https://doi.org/10.1002/admi.201500071.

[118] L. Ovaskainen, S. Chigome, N.A. Birkin, S.M. Howdle, N. Torto, L. Wågberg, C. Turner, Superhydrophobic polymeric coatings produced by rapid expansion of supercritical solutions combined with electrostatic deposition (RESS-ED), J. Supercrit. Fluids 95 (2014) 610–617.

[119] I. Yilgor, S. Bilgin, M. Isik, E. Yilgor, Tunable wetting of polymer surfaces, Langmuir 28 (41) (2012) 14808–14814, https://doi.org/10.1021/la303180k.

[120] K.-M. Lee, C.-V. Ngo, J.-Y. Jeong, E.-c. Jeon, T.-J. Je, D.-M. Chun, Fabrication of an anisotropic superhydrophobic polymer surface using compression molding and dip coating, Coatings 7 (11) (2017) 194, https://doi.org/10.3390/coatings7110194.

CHAPTER 6

The stability of the superhydrophobic surfaces

Jitha S. Jayan[a], D. Jayadev[a], Zeena S. Pillai[a], Kuruvilla Joseph[b], Appukuttan Saritha[a]
[a]Department of Chemistry, School of Arts and Sciences, Amrita Vishwa Vidyapeetham, Kollam, India
[b]Department of Chemistry, Indian Institute of Space Science and Technology, Thiruvananthapuram, India

1. Introduction

Superhydrophobic and superhydrophilic surfaces with exciting wettability performance have fascinated material scientists not only due to their scientific significance but also due to their probability to be utilized in a vast array of applications [1–5]. Superhydrophobic coatings find applications in various fields [6, 7]. Modification of these surfaces thereby imparting corrosion resistance to these materials is a deep-rooted problem, currently faced by scientists. Owing to their versatility, surface properties, and ease of formation, polymer materials have gained recognition as good precursors for producing superhydrophobic surfaces regardless of being soft when compared to inorganic materials. Inorganic materials can be made with a better stiffness than polymers but most of them need to be subjected to surface modification in order to render them hydrophobic. Hence, polymers are regarded as the most suitable candidate for this purpose [8–23]. Interestingly polymers change their surface morphology when the temperature is above the glass transmission temperature, and then they start to melt. At higher temperatures, the polymer starts to degrade, and thus superhydrophobicity is lost. Hence, it is essential that the properties of polymers be thoroughly modified so that it can effectively utilized in the field of superhydrophobic coatings. Recent studies point out the fact that nanostructuring could certainly impart thermal stability to these materials. One of the main challenges faced by these materials is thermal damage. It is really mandatory for high-end applications that these nonwettable coatings should function well over a wide range of temperatures, especially extreme high temperatures. Such thermally durable coatings are frequently prepared by the inclusion of inorganic particles in the polymer matrix and or by using polymers having high melting or glass transition temperatures. Nevertheless, utilizing polymers for such applications still remains a challenge. This is due to the fact that the polar groups are found to disrupt the hydrophobic nature. This behavior becomes more pronounced at elevated temperatures. Hence, it is highly essential to ensure the stability of these surfaces in order to make them meet the requirements for high-end applications.

There has been considerable interest in the recent years in the development of super-hydrophobic coatings based on polymer nanocomposites. Furthermore, investigations of the mechanical and thermal stabilities of such nanocomposite coatings have been carried out by various research groups across the world. The thermal degradation of the coating is principally due to an alteration in the chemical composition of the surface rather than by a transformation in surface morphology and roughness. Hydrophobic functional groups are diminished either by oxidation reaction or the breaking of chemical bonds with which it is connected to the substrate matrix. As superhydrophobic films find application in harsh chemical environments, chemical stability is also a compulsory requirement. When superhydrophobicity and chemical stability are exhibited simultaneously by a material, it finds application as coatings in optoelectronics, micro electromechanical systems, etc. [24–27]. Another important area where superhydrophobic surfaces find application is the improvement of device reliability in microelectronics packaging [28]. Hence, for superior performance of a superhydrophobic film, it is mandatory to ensure stability in all the above-mentioned conditions.

2. Chemical stability

Two indispensable features for a superhydrophobic film are roughness and low surface energy. Hence, a film might lose its chemical stability due to the loss in surface roughness or due to the dissolution of the surface layer upon exposure to a corrosive environment. With an outlook to valid applications, environmental stability and robustness are still the crucial matters of research as it limits the applications of superhydrophobic surfaces. As these surfaces are widely used for making pipes especially in marine and space applications, it is necessary that it should be adaptable to harsh environmental conditions [29]. More over in the case of space and automotive applications, the chemical stability has an unavoidable role [30–33]. It is highly essential that the different classes of chemical stability of superhydrophobic surfaces such as solvent, thermal, humidity, pH, and UV, as shown in Fig. 1, should be monitored for its better applications.
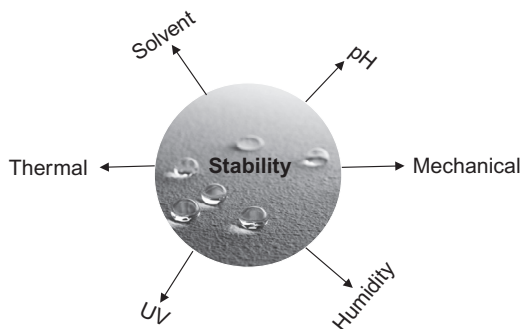
Fig. 1 The important chemical stabilities that have to be monitored for enhanced application of superhydrophobic surfaces.

2.1 Solvent stability

Solvent stability is an important aspect of chemical stability for ensuring the application in different fields [34–37]. There are many reports regarding the solvent stability of superhydrophobic surfaces and films. The surface of a material is always prone to attack by various solvents depending on its application [38–41]. Hence, the coating material should exhibit considerable stability toward solvents. The stability of this superhydrophobic surface has immense importance in determining the potential application. Various studies have been reported in which the effect of contact angle (CA) and sliding angle (SA) are measured in numerous organic and inorganic solvents [42–44].

Zeng et al. [45] reported an easy and efficient method to synthesize superhydrophobic surfaces showing good solvent-resistance property. They synthesized superhydrophobic cotton fabric with enhanced nonwettability by a one-pot method consisting of a fluorinated alkyl silane and silica nanoparticles. They studied the solvent uptake capacity as well as the solvent resistance of the fabric in different organic solvents. The water CA as well as the SA was measured as shown in Fig. 2. In addition, it was interesting to note that there was no change for both the CA and SA values after keeping the sample in contact with the various organic solvents. The exceptional stability exhibited by the fabric against the various solvents and acid/base was attributed to the chemical stability of the photoresist epoxy (cross-linked SU-8). When exposed to UV, the fluorinated alkyl silane forms an extremely cross-linked arrangement which has exceptional chemical stability. The effect of solvents on polymer coated polyester fabric was studied by Yoo et al. [46]. A solvent resistant fabric material was prepared by grafting a diblock copolymer on to a cotton fabric and a subsequent study was carried out by Zou et al. [47]. Sun et al. [48] integrated superwettability within covalent organic frameworks for functional coating which exhibited excellent chemical and mechanical properties. Satapathy et al. [49] fabricated stable porous and nonporous superhydrophobic linear low-density polyethylene (LLDPE) coatings with excellent self-cleaning property by incorporating silica nanoparticles in LLDPE matrix. The material exhibited excellent water repellency and better stability even after annealing. The fact that the surface possessed better chemical stability and capability to withstand abrasion test indicates its mechanical stability. Heinonen et al. [50] conducted study on antibacterial and chemical stability of superhydrophobic surfaces containing silver nanoparticles.

A solvent resistant study of superhydrophobic surface made using titania nanoparticles and perfluorodecyltriethoxysilane on a steel surface was conducted by Isimjan et al. [51]. Resistance of the superhydrophobic surface to water, chloroform, and decane was analyzed by immersing it in these solvents and measuring CA at specific intervals. There was no change in superhydrophobicity even after 8 days. From Fig. 3, it can be understood that chloroform affects the CA. Bayer et al. [52] made solvent resistant superhydrophobic films from carnauba wax alcohol emulsions, which exhibited self-emulsifying property.
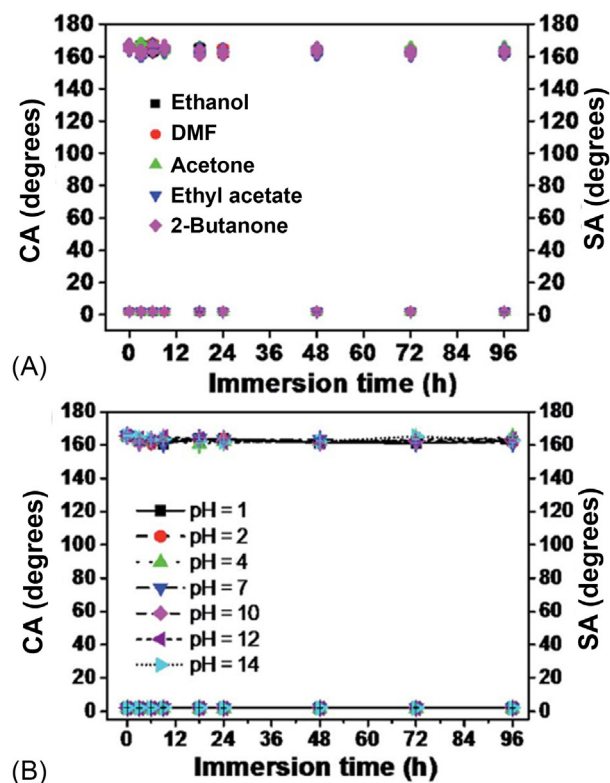
Fig. 2 Water contact angle (WCA) and sliding angle (SA) of the coated cotton fabric after immersion in (A) various organic solvents and (B) aqueous solutions with different pH values. *(Reproduced with permission from C. Zeng, H. Wang, H. Zhou, T. Lin, Self-cleaning, superhydrophobic cotton fabrics with excellent washing durability, solvent resistance and chemical stability prepared from an SU-8 derived surface coating, RSC Adv. 5 (75) (2015) 61044–61050, https://doi.org/10.1039/C5RA08040A (web archive link), Royal Society of Chemistry.)*

The films exhibited exceptional solvent stability. The various aggressive solvents used in the study were chloroform, toluene, acetone, and alcohols.

A self-standing, robust nanocomposite film prepared by the incorporation of carbon nanotube (CNT) followed by the subsequent curing of the epoxy resin was found to exhibit superhydrophobic characteristics, with water contact angle (WCA) > 152 degrees. The observance of superhydrophobicity can be attributed to the orderly alignment of CNTs on the surface of the nanocomposite film forming micrometer-size plateaus [53]. Asthana et al. [54] fabricated conductive polymer-based superhydrophobic coatings, containing different types of carbon nanoparticles. They were made by drop casting process. It was observed from this study that the coatings incorporating graphene nanoplatelets, carbon black, CNTs, etc. exhibited superhydrophobic and oleophilic behavior.
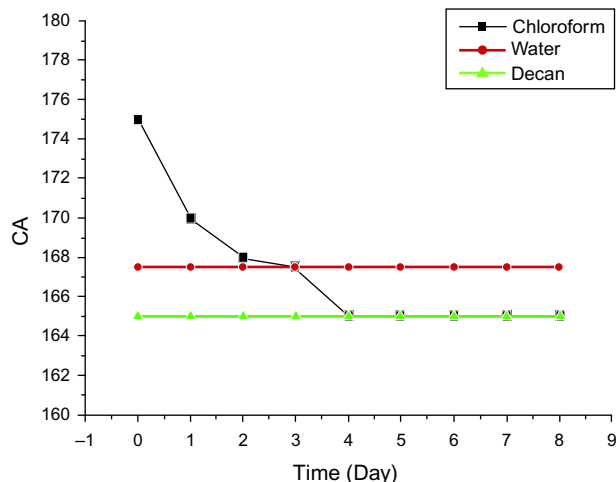
Fig. 3 Static contact angle of solvents treated samples on some period of time. *(Reproduced with permission from T.T. Isimjan, T. Wang, S. Rohani, A novel method to prepare superhydrophobic, UV resistance and anti-corrosion steel surface, Chem. Eng. J. 210 (2012) 182–187, Elsevier.)*

(A)

(B)
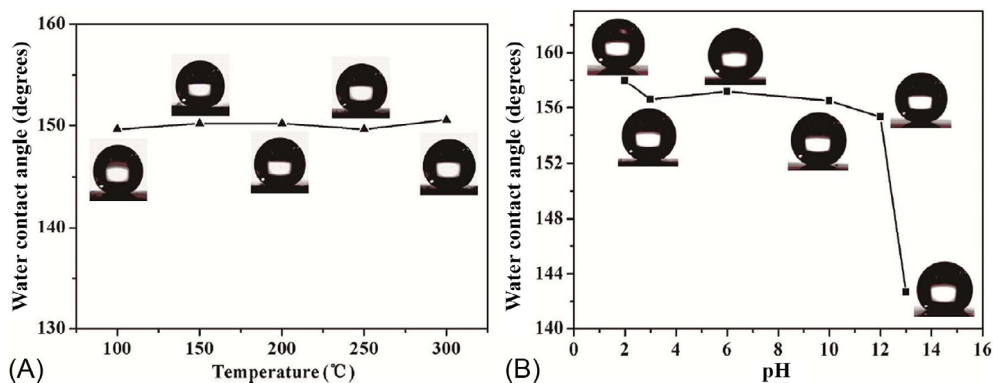
Fig. 4 (A) Water contact angle changes with different temperature treatment for 1 h, (B) water contact angles of coating surface with deposition of MTCS after immersing in different liquids of pH ranging from 1 to 13. *(Reproduced with permission from L. Xiao, W. Zeng, G. Liao, C. Yi, Z. Xu, Thermally and chemically stable candle soot superhydrophobic surface with excellent self-cleaning properties in air and oil, ACS Appl. Nano Mater. 1 (3) (2018) 1204–1211, https://doi.org/10.1021/acsanm.7b00363 (web archive link), American Chemical Society.)*

Xiao et al. [55] made thermally stable superhydrophobic surfaces based on candle soot on glass substrate. The surfaces exhibited CA of 150 degrees even after the treatment with corrosive sulfuric acid at high temperature. The obtained changes in CA can be observed in Fig. 4. Xie et al. [56] fabricated a bio-ionic superhydrophobic coating using polypropylene-*block*-(polymethyl methacrylate) block copolymer. The nanohierarchal surface of the material was analogous to that of a lotus leaf.
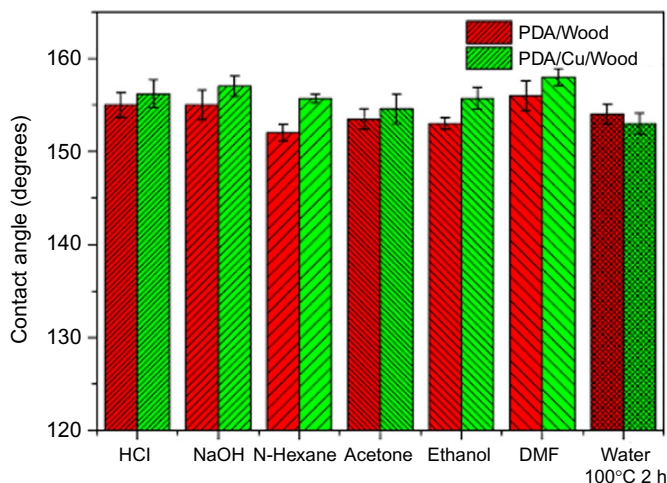
Fig. 5 CA of wood samples stored in different solvents for 24 h [57].

Wang et al. [57] made superhydrophobic wood by coating it with polydopamine and Cu. Superhydrophobic wood surfaces show enhanced stability in harsh conditions such as HCl, NaOH, *n*-hexane, acetone, ethanol, and DMF. Fig. 5 shows the change in CA upon treatment with these solvents. Nguyen et al. [58] made moisture-resistant and superhydrophobic metal–organic frameworks.

Ye et al. [59] made tough composite coatings using silica sol and silicone-acrylic copolymer (SAC). This study was fascinating in a sense that the composite was prepared from a nonfluorinated material system. They also analyzed the CA obtained while coating it with different substances and studied the morphology of the surface in detail. These observations are plotted in Fig. 6. The composite samples were dipped in organic solvents as well as acid and bases which are corrosive in nature. The subsequent behavior of the coating was estimated by analyzing the variation associated with the CA as well as SA as depicted in Fig. 7. The composite coatings showed an elevated WCA of about 157.7 degrees with a small SA of about 3 degrees on glass slide. The observation is attributed to methyl groups, which are low in energy as well as due to the surface roughness of silica particles. Owing to the secure cross-linked configuration among the silica particles and the resin, the composite coating displayed an elevated constancy chemically as well as mechanically.

Erbil et al. [60] converted a simple plastic surface into a superhydrophobic one through an effortless and inexpensive technique by employing polypropylene. The technique was made economical and hassle free and the surface roughness of the fabricated material was controlled through judicious selection of solvents and temperature. The resultant gel-like porous coating exhibited a WCA of 160 degrees. According to the authors, this robust technique can be extended to an assortment of surfaces for the fabrication of materials with superhydrophobicity.
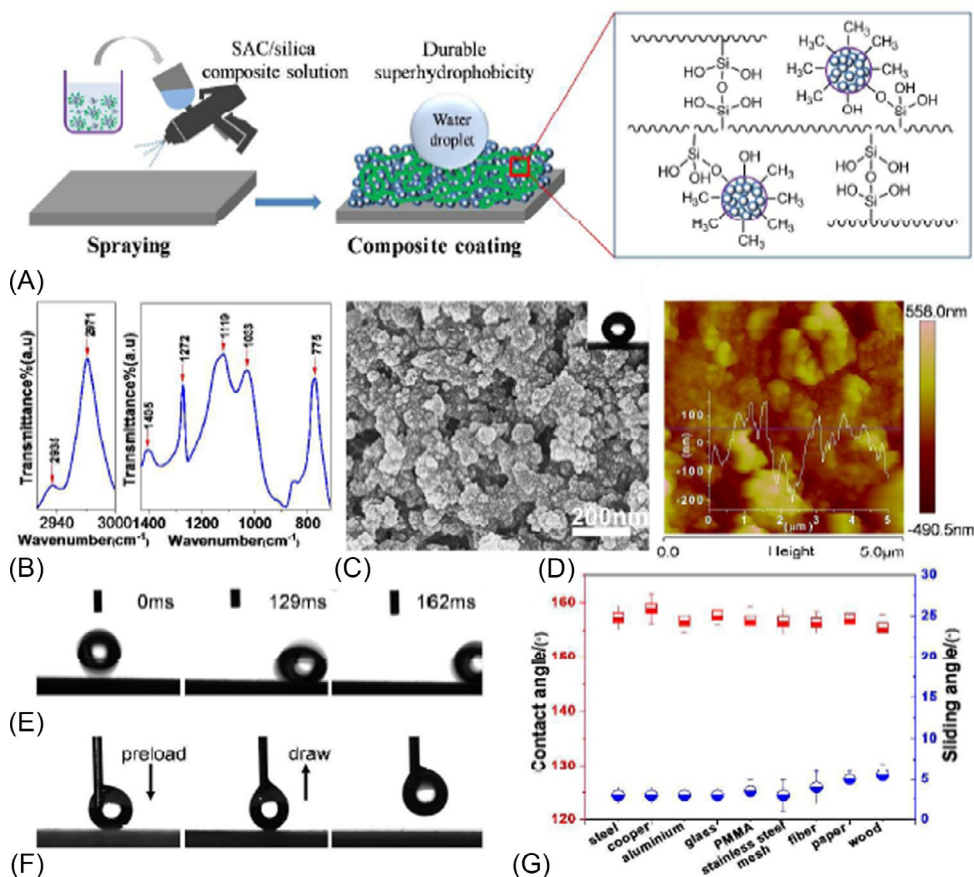
Fig. 6 Synthesis of composite superhydrophobic coatings: (A) Schematic illustration for the fabrication of super hydrophobic coating and the possible bonding structure in the composite coating, (B) Fourier transform infrared (FTIR) spectra of the composite coating, (C) scanning electron microscopic (SEM) image of the composite coating on glass slide, (D) atomic force microscopy (AFM) height image of the superhydrophobic surface, (E) time-resolved images of a 9.0-μL water droplet spreading quickly on the composite coating with 162 ms, (F) the contact deformation and departure processes of a water droplet on the composite coating, and (G) the water contact angle and sliding angle of the composite coatings on various substrates. *(Reproduced with permission from H. Ye, L. Zhu, W. Li, H. Liu, H. Chen, Simple spray deposition of a water-based superhydrophobic coating with high stability for flexible applications, J. Mater. Chem. A 5 (20) (2017) 9882–9890, Royal Society of Chemistry.)*

Iqbal et al. [61] synthesized a polydimethylsiloxane (PDMS)–derived candle soot coated superhydrophobic surface having excellent mechanical and chemical stability. Zhou et al. [62] prepared a fabric having superhydrophobicity coupled with high separation efficiency under intense environmental conditions.

Bär et al. [63] conducted a comparative study of effect of solvents on the method of fabrication of robust superhydrophobic surfaces. Various surfaces such as rough
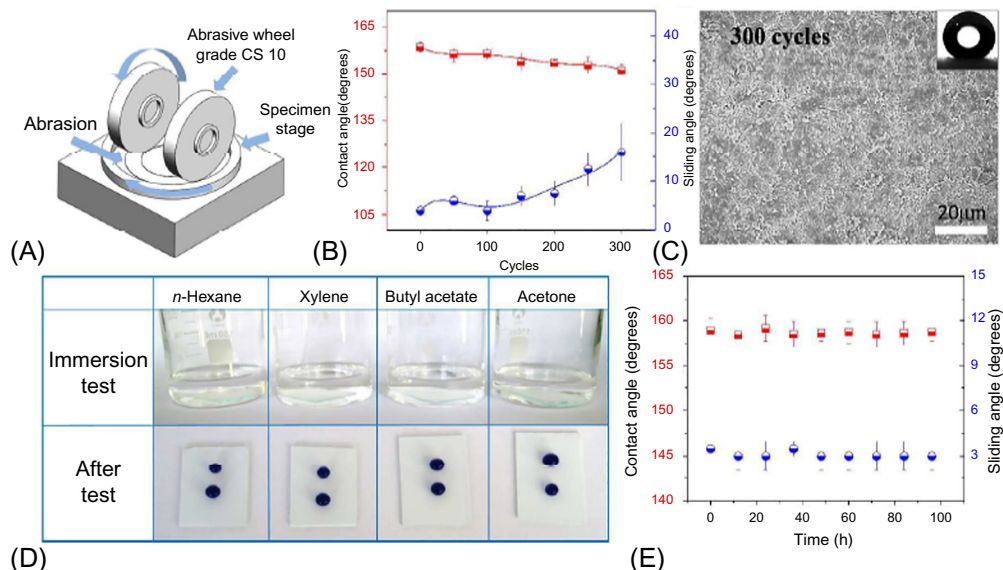
Fig. 7 Mechanical and chemical stability of the composite coating: (A) Abrasion damage analysis apparatus model, (B) the average contact angle and sliding angle of the composite coatings under different abrasion number, (C) SEM image of the coating after 300 abrasion cycles, (D) superhydrophobicity after immersing in different organic solvents for 20 days, and (E) the average contact angle and sliding angle of the composite coatings after photodegradation damage test. *(Reproduced with permission from H. Ye, L. Zhu, W. Li, H. Liu, H. Chen, Simple spray deposition of a water-based superhydrophobic coating with high stability for flexible applications, J. Mater. Chem. A 5 (20) (2017) 9882–9890, Royal Society of Chemistry.)*

polystyrene, nonporous poly(divinylbenzene) chalk, spray-deposited silica nanoparticles, poly(butyl methacrylate-*co*-ethylenedimethacrylate) modified poly(2-hydroxyethyl methacrylate-*co*-ethylene dimethacrylate, candle soot and commercial coating, etc. were prepared and solvent stability was compared. From the detailed study, they inferred that, in acetone the rough surface of polystyrene is completely dissolved. In the case of the PDVB chalk fabricated the combing dip coating and candle soot method, acetone significantly, reduced the SCA (θs) as depicted in Fig. 8. Hence, water droplets show pinning effect over the surface after treatment with acetone and ethanol, it was observed solvents like acetone and ethanol do not effect on the superhydrophobicity. Table 1 gives the further details of the investigation.

Lu et al. [64] made superhydrophobic coating over zinc substrates using homogeneous solution of high-density polyethylene (HDPE) in ethanol and xylene containing different weight percentage of graphene oxide (GO) at ambient temperature. They obtained static water CA higher than 150 degrees. Surface stability toward the harsh corrosive environment was confirmed by dipping it in sodium chloride solution for about 29 days. Interestingly, the CA increased to 160 degrees upon exposure to NaCl. Fig. 9
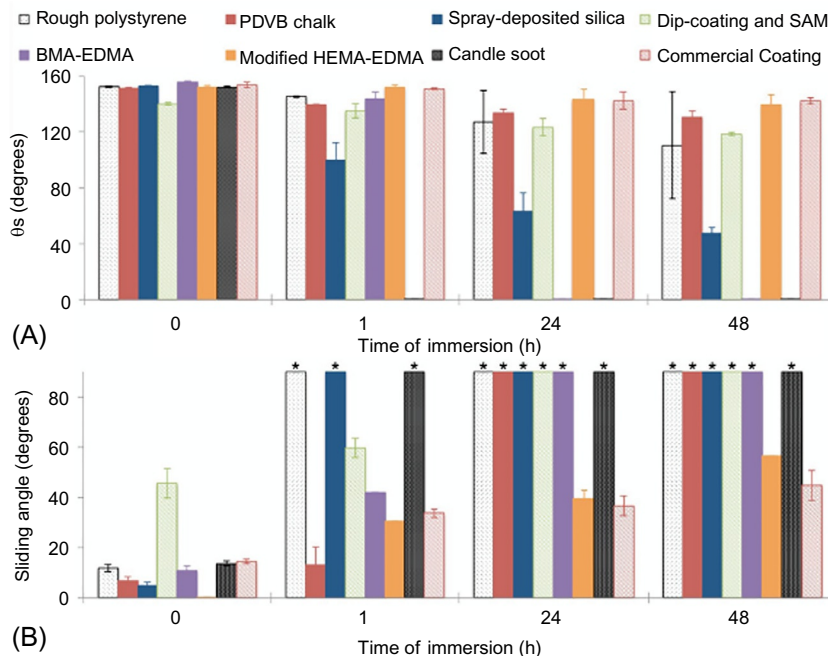
Fig. 8 Stability of the Cassie-Baxter state in buffer at different periods. Contact angle (A) and sliding angle (B) of the surfaces were measured on surfaces incubated in water for different time periods. *(Reproduced with permission from R.M. Bär, S. Widmaier, P.A. Levkin, Facile fabrication of robust superhydrophobic surfaces: comparative investigation, RSC Adv. 6 (100) (2016) 98257–98266, Royal Society of Chemistry.)*

depicts the change of CA observed in the study. After 8 months of air exposure, the water CA remained unchanged. It shows the long-term stability as well as enhanced durability of the superhydrophobic surface.

Scanning electron microscopy (SEM) images show the morphological changes before and after the immersion in 3% solution of NaCl, which further confirms the corrosion of zinc substrate surface as is shown in Fig. 10. It can be noted that the change of the Static water contact angle (SWCAs) is less in the case of 5% HDPE/GO (Fig. 10C and D).

2.2 pH stability

A constructive superhydrophobic surface should be able to resist the wetting process even after extended contact in water. The coating should be capable to endure change in pH, surface additives as well as organic or inorganic solvents. pH stability is of great importance as it focuses on environmental stability [24, 65–72]. It is monitored by measuring the change in CA. Zimmermann et al. [37] observed the persisting chemical stability of silicone nano-filaments containing superhydrophobic coating. By immersing the coated

Table 1 Result of the characterization of the different superhydrophobic coatings

Surface	Rough polystyrene	Nanoporous PDVB chalk	Spray-deposited silica nanoparticles	Dip-coating and SAM	BMA-EDMA	Modified HEMA-EDMA	Candle soot	Commercial coating
Transparency	<1%	max. 22% (6.10 nm)	max. 19% (612 nm)	100%	22–100%	<1% (300–500 nm), max. 100% (900 nm)	<2%	<1% (300–400 nm), max. 16% (900 nm)
θs, θnd, θre [*]	152.1±1.8, 164.7±0.5, 148.6±0.5	151.3±1.4, 159.9±0.5, 148.5±0.5	151.7±1, 1159.6±0.3, 147.6±1.7	137.7±4.5, 155.7±1.0, 126.9±2.6	160.2±0.6, 165.8±0.7, 150.7±3.2	152.0±3.6, 158.2±0.6, 142.9±2.4	151.6±1.7, 155.8±0.3, 140.3±2.4	154.7±1.4, 166.5±0.8, 152.4±1.2
Sliding angle (*)	13.9±3.8	7.4±1.5	5.8±2.4	55.5±5.2	5.71±1.1	6.3±1.6	113±2.1	14.8±13.4
Mechanical stability (θs) after 5 × tape test) [*]	77.1±1.8	86.4±4.0	108.4±1.8	90.83±2.8	101.4±2.0	157.3±0.9	43.9±9.4	122.1±1.0
Stability in water (immersion for 48 h) (θs [*], sliding angle [*])	140.8±2.1, 23.3±3.2	134.7±4.1, 4.9±1.1	58.1±10.1, *	128.2±1.1, *	0*, *	145.6±3.2, 26.2±3.7	42.8±2.2, *	143.4±1.3, 37.6±1.8
Stability in buffer (immersion for 48 h) (θs [*], sliding angle [*])	110.4±38.4, *	130.6±4.5, *	47.2±4.3, *	118.7±1.3, *	0*, *	139.4±7.2, 56.4±0.1	0*, *	142.2±2.2, 44.7±6.0
Stability in acetone (immersion for 1 h) (θs) [*], sliding angle [*])	Dissolved, dissolved	127.1±11.0, *	151.0±0.6, 20.6±6.2	117.4±10.7,*	157.8±0.2, 8.6±1.8	154.6±0.6, 12.3±1.9	48.0±2.6, *	152.7±0.5, 29.8±0.4
Stability in ethanol (immersion for 1 h) (θs [*], sliding angle [*])	152.6±03, 155±1.2	148.9±1.5, *	151.9±0.7, 17.5±2.8	128.1±4.2, *	156.9±0.5, 6.8±1.3	152.3±1.2, 14.3±1.5	114.0±20.4, *	150.8±0.6, 21.3±1.2

The properties including transparency (UV/Vis), WCAs, sliding angle, mechanical stability, and stability in water, PBS–Buffer, and organic solvents. Asterisks indicate that water droplet did not roll off the surface.
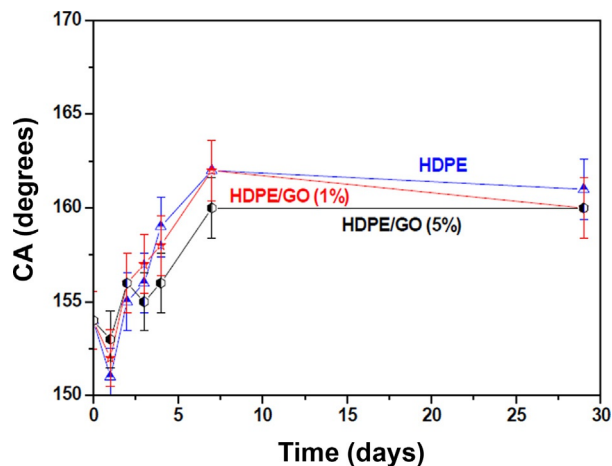
Fig. 9 Change of CA of HDPE/GO coated Zn samples dipped in 3% NaCl aqueous solution over time. *(Reproduced with permission from S. Lu, H. Gao, Q. Wang, W. Xu, S. Szunerits, R. Boukherroub, Fabrication of stable homogeneous superhydrophobic HDPE/graphene oxide surfaces on zinc substrates, RSC Adv. 6 (35) (2016) 29823–29829, Royal Society of Chemistry.)*
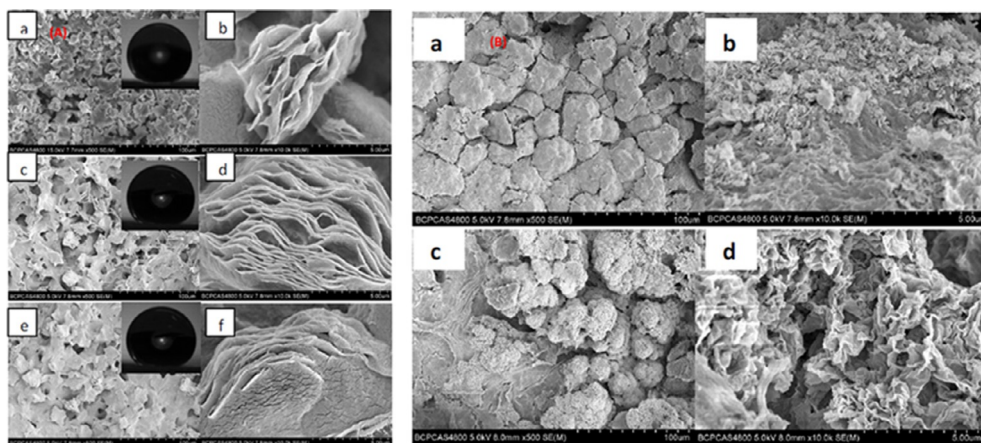
Fig. 10 (A) SEM images of HDPE/GO surfaces deposited on zinc substrate at room temperature. HDPE/GO (0%) (a and b); HDPE/GO (1%) (c and d); HDPE/GO (5%) (e and f) and corresponding contact angles in inset. (B) SEM images of different surfaces after immersion in 3% NaCl aqueous solution for 29 days: zinc substrate (a, b); HDPE/GO (5%) (c, d). *(Reproduced with permission from S. Lu, H. Gao, Q. Wang, W. Xu, S. Szunerits, R. Boukherroub, Fabrication of stable homogeneous superhydrophobic HDPE/graphene oxide surfaces on zinc substrates, RSC Adv. 6 (35) (2016) 29823–29829, Royal Society of Chemistry.)*
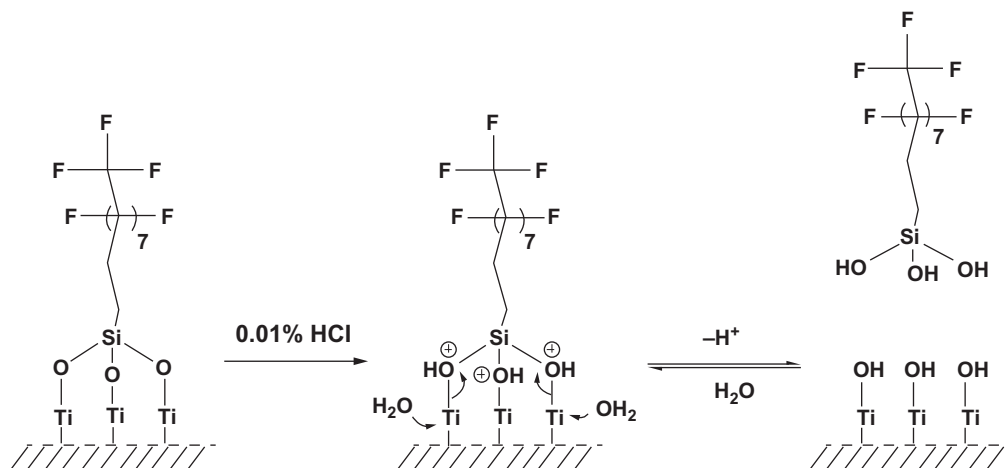
Fig. 11 The mechanism of losing superhydrophobicity of PTES-based surface after treating with 0.01% HCl solution. *(Reproduced with permission from T.T. Isimjan, T. Wang, S. Rohani, A novel method to prepare superhydrophobic, UV resistance and anti-corrosion steel surface, Chem. Eng. J. 210 (2012) 182–187, Elsevier.)*

surface in a variety of liquids for a phase of 6 months, they have analyzed the durability. These surfaces exhibit outstanding consistency in organic solvents, aqueous solutions of variable pH as well as mildly acidic detergent solutions. Zeng et al. [45] checked pH stability of superhydrophobic fabric by dipping it in aqueous solutions having different pH value ranging from 1 to 14. Fabric coated with TiO_2–SiO_2 was found to be stable in the pH range 2–12. Isimjan et al. [51] also studied the stability of superhydrophobic substances at lower pH. There is a reduction in water CA due to the reaction of surface with HCl as shown in Fig. 11. HCl makes the surface hydrophilic. No change in morphology was observed and the samples retained the anticorrosion property. Yong et al. [73] fabricated superhydrophobic surface which contains hierarchical mesh porous structure and exhibits high pH stability using femtosecond laser. These surfaces exhibit stability in the pH range 1–14. This stability is extremely hard to attain by any other artificial superhydrophobic surface. Jiang et al. [68] made pH-responsive surfaces using gold nanostructures.

Ishizaki et al. [74] made a film, which is superhydrophobic and by following the microwave plasma–enhanced chemical vapor deposition, they have effectively deposited it on a magnesium alloy. The film surface was superhydrophobic with a static WCA larger than 150 degrees. The most important property of the coated surface was the additional stability in the acidic, neutral, and alkaline solutions. Khanjani [75] fabricated pH stable cellulose-based superhydrophobic surfaces and studied the dynamics of coupled chemical system.

Guo et al. [76] fabricated copolymer-based surface which is stable in the range of pH from 1 to 14. There were no fluctuation of the CA values over a pH range 1–14 as shown
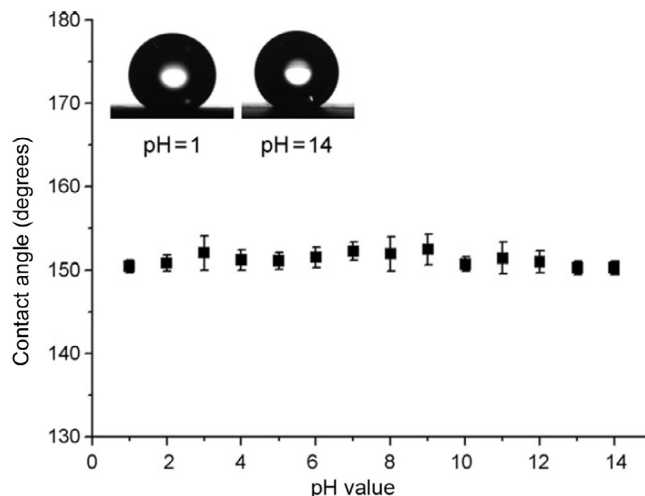
Fig. 12 The relationship between pH value and CA on the super hydrophobic surface of P(ETPDMS-co-BPA) film on rough substrate. *(Reproduced with permission from L. Guo, W. Yuan, J. Li, Z. Zhang, Z. Xie, Stable superhydrophobic surfaces over a wide pH range, Appl. Surf. Sci. 254 (7) (2008) 2158–2161, Elsevier.)*

in Fig. 12. All CA values range from about 150.28 degrees to 152.48 degrees, which points out that the pH values of the aqueous solution have negligible effect on CAs of surface. Films which are superhydrophobic with a WCA of 151 ± 2 degrees were fabricated by Liu et al. [77]. Zinc surface was dipped in a methanolic solution of perfluorooctyltrichlorosilane following annealing at 130°C. These films exhibited stability over a wide pH range.

Liu et al. [77] fabricated stable superhydrophobic surface from a low-density polyethylene (LDPE)/ethylene-propylene-diene terpolymer (EPDM), which is a thermoplastic vulcanizate. These surfaces were possessing outstanding environmental stability which was monitored by dipping them in aqueous solution of different pH from 1 to 14. It is seen that pH has a very little influence on water CA and it remained constant as 152 degrees, even after varying the pH. Even when tilted slightly, the water moved easily indicating the superhydrophobicity. Guo et al. [78] described an easy and economical technique to fabricate superhydrophobic surfaces on Al and its alloy. These surfaces showed higher WCAs in aqueous solutions of different pH.

Mittal et al. [79] made a new mesoporous carbon nanocapsule-based polymer composite. These composite films were capable of exhibiting superhydrophobic properties with a WCA of about 160 degrees and a SA of 5 degrees. The composite films were having a tremendous thermal stability up to 350°C in air and were good conductors of electricity. The surface was capable of retaining the superhydrophobicity in corrosive acidic as well as basic conditions, which was confirmed by immersing it in Conc. HNO₃ and
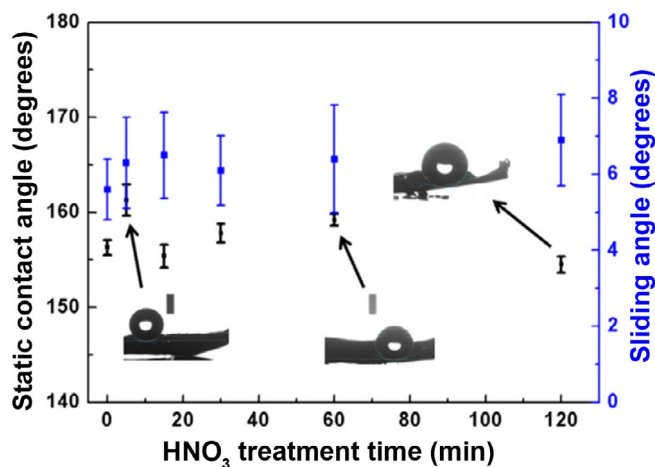
Fig. 13 Variation of CAs with HNO₃ acid treatment of MCC/PVDF-PFS-based superhydrophobic film. *(Reproduced with permission from N. Mittal, D. Deva, R. Kumar, A. Sharma, Exceptionally robust and conductive superhydrophobic free-standing films of mesoporous carbon nanocapsule/polymer composite for multifunctional applications, Carbon N Y 93 (2015) 492–501, Elsevier.)*

NaOH solutions of pH 1.29 and 13.54, respectively. These surfaces showed outstanding stability in a humidity range of 35%–83% as shown in Fig. 13.

Xu et al. [80] combined electroless galvanic deposition as well as self-assembly to fabricate superhydrophobic surface. These surfaces have WCA 160 degrees and SA 0 degrees. The change in CAs of water droplet as a function of pH is shown Fig. 14. The CA remains unchanged in the range 1–13 degrees.

Xu et al. [81] made nanoporous silica thin films by coating it with perfluorooctyltrichlorosilane. These films were very stable to aqueous HCl and aqueous NaOH having pH 1 and 14, respectively. The water CA (162 ± 2 degrees) changed to 153 ± 2 degrees after 5 min contact with strong acid and base. When PFTS hydrophobilizes the film, most of the mesoporous silica nanosheets get modified with fluorosilane. Small amounts of silica nanosheets will remain uncoated and remains hydrophilic due to the hydroxyl groups, which is more philic to base than acid and water. Hence, have lower CA to base than water and acid. Evidently, the thin films are durable to the attack of corrosive acids and bases. The change in CA by the treatment with acid and base and the surface morphologies of the thin films after scratching it with 3H pencil is depicted in Fig. 15.

Madidi et al. [82] developed superhydrophobic surface based on TiO₂ nanoparticles using an inexpensive spray coating technique. These coatings were capable of retaining their stability in various pH range and conductivities, even after prolonged treatment. These surfaces were also stable to harsh UV, heating, and mechanical conditions.
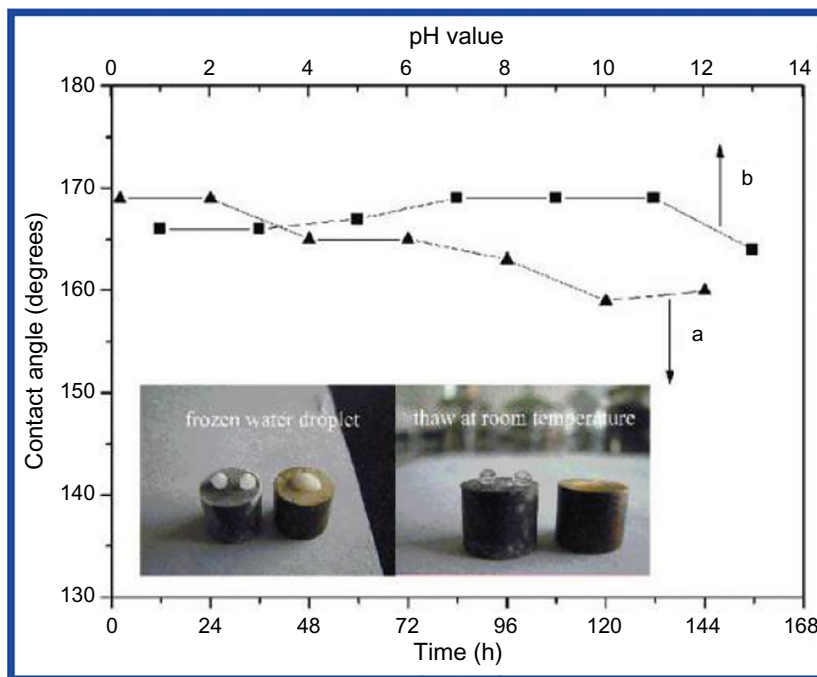
Fig. 14 Variation of the apparent contact angle of the as-prepared superhydrophobic surface with different freezing times at −20°C (A) and contact angles of water droplets with different pH values on the prepared superhydrophobic surface (B) inset picture shows the frozen water droplet on the surface. *(Reproduced with permission from X. Xu, Z. Zhang, J. Yang, Fabrication of biomimetic superhydrophobic surface on engineering materials by a simple electroless galvanic deposition method, Langmuir 26 (5) (2009) 3654–3658, American Chemical Society.)*

The surface fabricated in acidic condition shows better nonwettability than that prepared from alkaline condition. Feng et al. [83] fabricated a surface showing superhydrophobicity as well as good adhesive property toward water especially in the pH range from 1 to 11 even after being in contact with the air for a year. Taghizadeh et al. [84] made a nanoscopic superhydrophobic surface that showed great water repellent nature. The long-term stability of these surfaces was analyzed by keeping it for about continuous 6 months in open atmosphere. Even after long-term exposure to atmosphere, these surfaces were able to retrain its superhydrophobic nature. These coatings retained superhydrophobicity as well as CA (>140 degrees) in wide pH range 4–12.

2.3 Thermal stability

Thermal stability is an important property of superhydrophobic surfaces in determining its application [85, 86]. Deterioration of superhydrophobicity due to thermal effect and
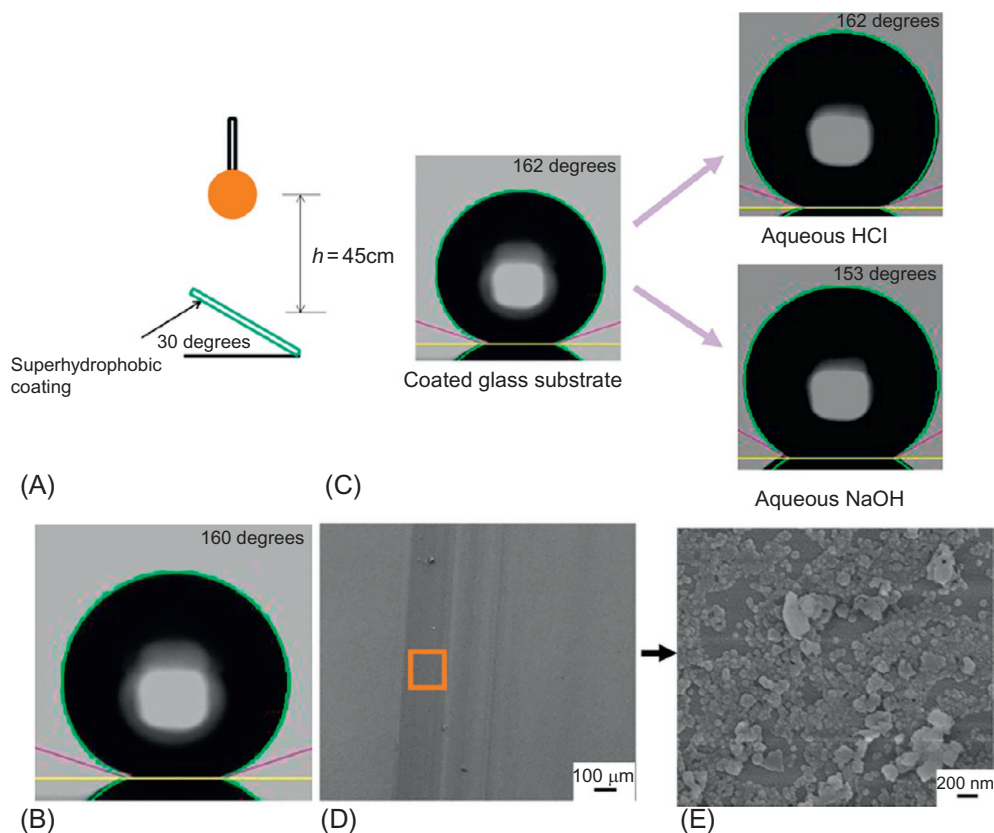
Fig. 15 (A) Sketch of the setup for testing the thin film long-term resistance against water droplet impacts. (B) Static water contact angle of the coated glass substrate after impacts of 5000 water droplets. (C) Water droplets on the coated glass substrate before and after contacting strong acid and base solutions. (D) SEM image of the thin film after scratching with 3H pencil. (E) Magnified SEM image of the scratched area. *(Reproduced with permission from L. Xu, Z. Geng, J. He, G. Zhou, Mechanically robust, thermally stable, broadband antireflective, and superhydrophobic thin films on glass substrates, ACS Appl. Mater. Interfaces 6 (12) (2014) 9029–9035, American Chemical Society.)*

thermal instability of materials makes them unsuitable for the application under elevated temperatures [87–90]. There are many reports which focus on the thermal stability of superhydrophobic surfaces, most of which determine the change in CA with annealing [91–94]. Thermal analysis like thermogravimetric analysis (TGA), and simple annealing followed by the measurement of CA and SA is the usual practice [95–97].

A microcapsule possessing a micro/nano-shell and a phase change material core has been reported by Wu et al. [98]. The most interesting aspect to be noted is that this one-pot method is economical. The surfaces thus prepared were able to withstand thermal treatment up to about 240°C; the CA and SA being 167.4 ± 0.3 degrees and 5 ± 0.5 degrees, respectively.

The thermal stability after the process of annealing was carried out by Cha et al. [99]. To check durability of the nanostructured surfaces, which are superhydrophobic in nature, plasma polymerization of the surface was followed by coating using hydrophobic diamond-like carbon (DLC). The WCA underwent a gradual decrease from 90 degrees to 60 degrees whereas the superhydrophobicity was maintained even at temperature larger than 150 degrees for annealing temperatures between 25°C and 300°C. Nano-structured surfaces having an aspect ratio >5.2 nm was found to retain superhydropho-bicity at annealing temperatures as high as 350°C; Hydrophobicity of nanostructured surfaces having low aspect ratio gradually degraded above this temperature. The graph in Fig. 16 clearly shows that regardless of the aspect ratio, all superhydrophobic surfaces get converted to superhydrophilic surfaces above temperature of 500°C.

Deng et al. [100] designed superamphiphobic coating, in which candle soot was coated with a 25 nm thick silica gel. Levkin et al. [101] studied thermal stabilities of porous super-hydrophobic polymer surfaces. Mahadik et al. [102] fabricated methyltriethoxysilane-based superhydrophobic coating on glass substrates. The surface thus obtained exhibited high optical transparency, improved thermal stability, and static water CA.

Thermogravimetric method was used by Pashinin et al. [103] in order to study the thermal stability of superhydrophobic coatings over quartz and KBr. Freschauf et al. [104] studied in detail regarding the superhydrophobicity of antibacterial surfaces in ther-mally stable consumer plastics. Tsougeni et al. [105] made superhydrophobic surfaces from poly(methyl methacrylate) and poly(ether ether ketone) surfaces by means of O_2
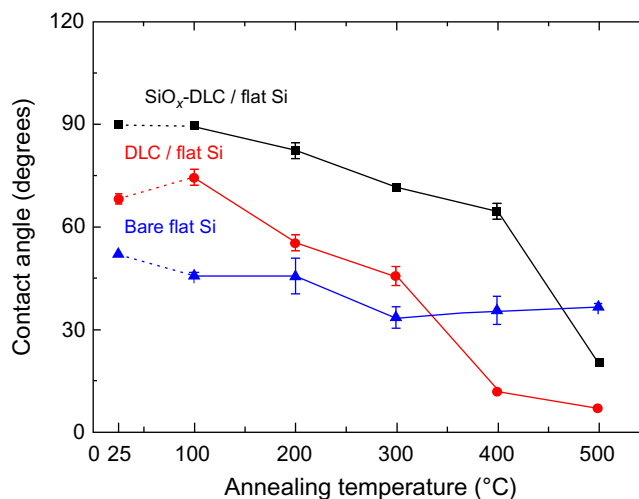
Fig. 16 Measured values of water CAs on various surfaces with annealing temperature. *(Reproduced with permission from S.-C. Cha, E.K. Her, T.-J. Ko, S.J. Kim, H. Roh, K.-R. Lee, et al., Thermal stability of superhydrophobic, nanostructured surfaces, J. Colloid Interface Sci. 391 (2013) 152–7, Elsevier.)*

plasma etching. Chen et al. [106] prepared silicone latex-based waterborne superhydrophobic coatings which exhibited stability in various thermal conditions.

Thermal stability of superhydrophobic surfaces made by Xiao et al. was confirmed by heating it from 100°C and 300°C at an interval of 50°C for 1 h. The water CA varied up and down at 150 degrees from 100°C to 300°C. The curve shown in Fig. 17 reveals the temperature stability of the surface up to 300°C.

Xu et al. [81] observed the thermal stability of the surfaces of nonporous silica thin films up to 300°C. At higher annealing temperatures, the superhydrophobicity reduces to hydrophobicity and leads to hydrophilicity. Fig. 18 clearly shows the changes in CA upon annealing. Cha et al. [99] studied thermal stability of superhydrophobic nanostructured Si surface up to 500°C. It was found that both SiO_x–DLC and pure DLC-coated flat surfaces underwent thermal degradation only at higher annealing temperature.
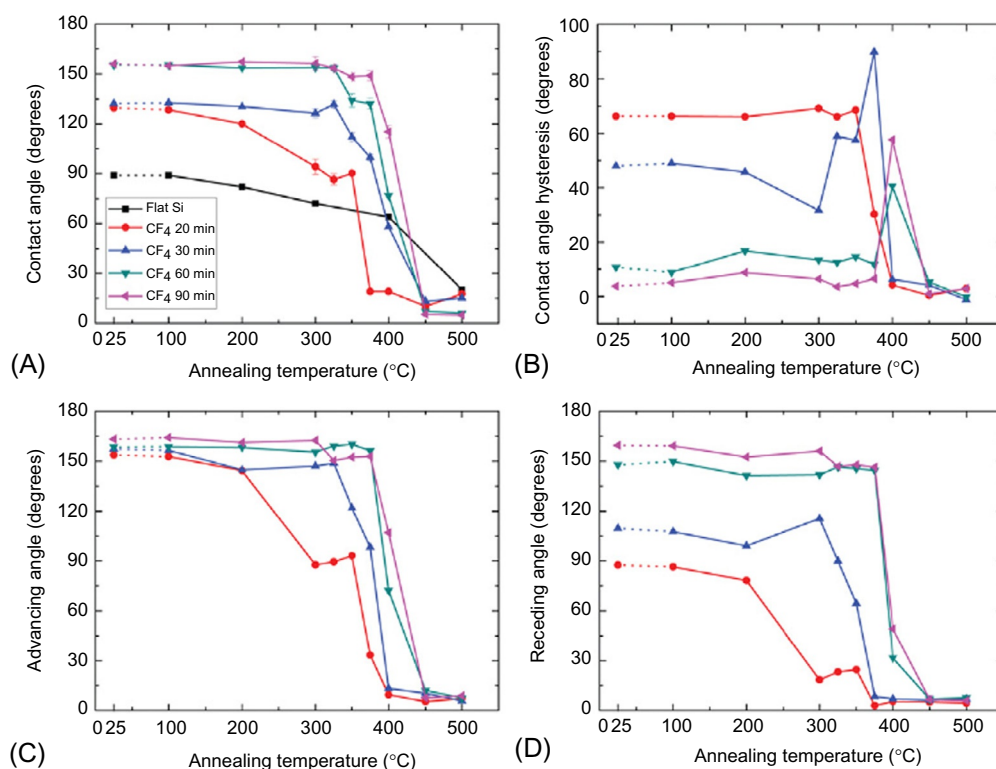
Fig. 17 (A) Water CA measurements in static water drop and (B) CAH measurements are estimated by the difference between the (C) advancing and (D) receding CAS on the nanostructured surfaces with various CF_4 plasma-treatment duration. *(Reproduced with permission from L. Xiao, W. Zeng, G. Liao, C. Yi, Z. Xu, Thermally and chemically stable candle soot superhydrophobic surface with excellent self-cleaning properties in air and oil, ACS Appl. Nano Mater. 1 (3) (2018) 1204–1211, https://doi.org/10.1021/acsanm.7b00363 (web archive link), American Chemical Society.)*
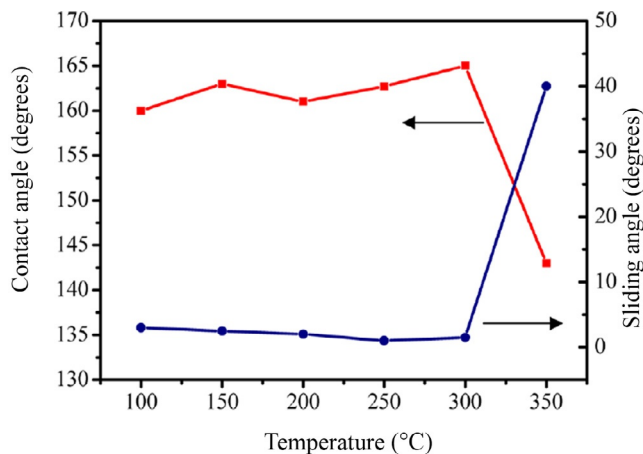
Fig. 18 Static water contact angle and sliding angle on the sample annealed for 2 h at varied temperatures. The surface lost its super hydrophobicity after annealing at 350°C. *(Reproduced with permission from L. Xu, Z. Geng, J. He, G. Zhou, Mechanically robust, thermally stable, broadband antireflective, and superhydrophobic thin films on glass substrates, ACS Appl. Mater. Interfaces 6 (12) (2014) 9029–9035, American Chemical Society.)*

This is attributed to the degradation of hydrogen–carbon bonds. On the other hand, for SiO_x-DLC coated nanostructured surfaces, the CA continued at 155 degrees even up to 350°C, indicating thermal stability of the surface, but CA rapidly declined below 10 degrees at temperatures of about 450°C or higher. Kumar [107] made excellent water repellent and thermally stable superhydrophobic coatings for ceramic and metallic surfaces. Lasprilla–Botero et al. [108] fabricated bilayer coating, which are superhydrophobic as well as thermally stable.

Ye et al. [59] studied the thermal stability of the surfaces by analyzing the water CA after thermal treatment. It retained the thermal stability for about 4 h at a temperature of 400°C. Even after 80 h treatment, the surface retained the CA at 151.8 degrees thus retaining superhydrophobicity. Thermal treatment for 200 h, cleaves O—CH_3 groups, thus making the surface hydrophilic. Moreover, silanol concentration increases after the heat treatment, which further confirms the hydrophilic nature above 200°C. Replacement of methyl group is further confirmed by the reduction in C content and increase in O content. Thermogravimetric studies (TG) studies exhibited a cleavage of bound methyl groups at 430°C. Only 12% reduction at 400°C was observed, which throws light on the thermal resistance of the composite coating.

Varshney and Mohapatra [109] fabricated corrosion–resistant superhydrophobic coatings with self-cleaning property by chemical etching process. A simple test was carried out to assess the thermal properties by placing the sample in a hot air oven at varying
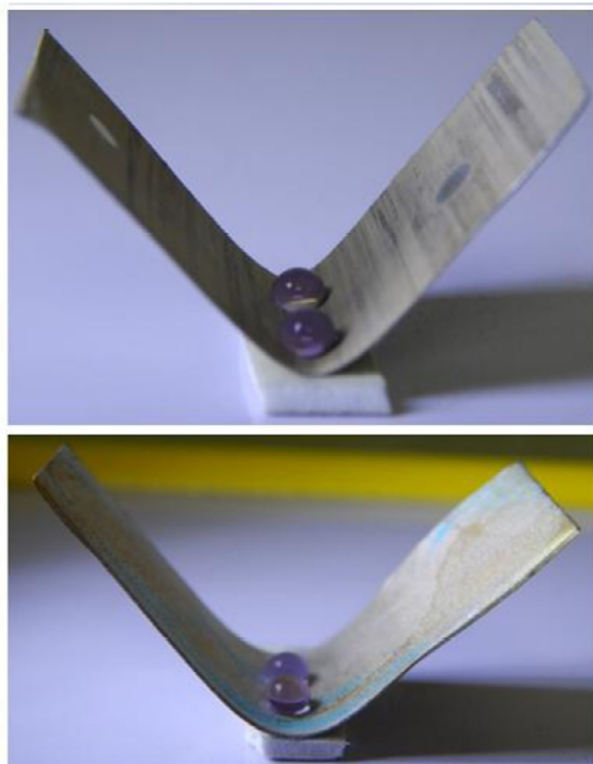
Fig. 19 Optical images of surface bending of superhydrophobic coating on aluminum and copper surfaces [109].

temperatures and subsequently the CAs were measured. The superhydrophobic metallic surfaces are shown in Fig. 19.

An inexpensive technique for the manufacture of superhydrophobic surface on a glass substrate was developed by Awais et al. [110]. Stearic acid functionalized SiO_2 particles made by sol-gel methods with an average size of about 200 ± 10 nm were also used to coat the glass substrate. After the coating process, the solvent was removed by drying. In the study, they changed the drying temperature and monitored the CA as is shown in Fig. 20. The surface exhibited superhydrophobicity until the decomposition temperature of the stearic acid showing that superhydrophobicity is due to the functionalization of silica.

The thermal resistance of the superhydrophobic surfaces made from porous silica capsules were analyzed by Deng et al. [86] by annealing it at temperature range from 20°C to 400°C for about 10 h. SA and CA remained steady till 350°C, this shows the outstanding thermal stability of the hydrophobized silica shells. The morphological properties were studied using transmission electron microscopy (TEM) and atomic force microscopy
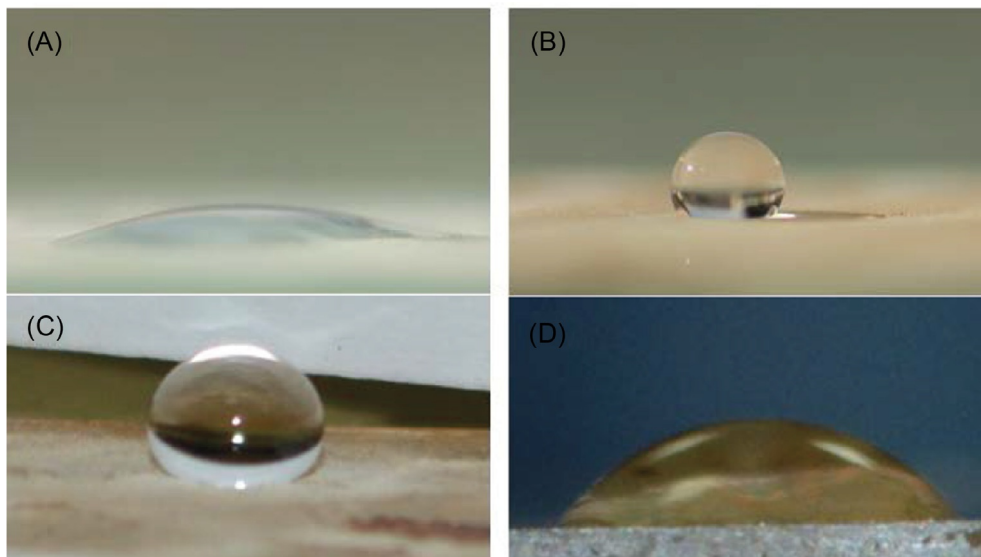
Fig. 20 The contact angle of water droplet with (A) uncoated glass substrate and dried at (B) 100°C, (C) 180°C, and (D) 260°C [110].

(AFM). Highly stable carbon nanoparticles were prepared from easily available paraffin candle by Qahtan et al. [111]. They were found to be thermally stable over up to 400°C with no change in SCA and SA.

Organically modified silica aerogel thin films which are thermally stable, flexible, and transparent were prepared by Budunoglu et al. [87]. They also analyzed the effect of calcination temperature on nonwettability. It was observed that the surface maintained its hydrophobicity up to 500°C. The surface turned hydrophilic after 35 min of continuous heating at 600°C. A transparent superhydrophobic surface on a glass substrate using various ratios and types of silica ormosil aerogels and their hybrid materials was fabricated by Nagappan et al. [112] a rough surface was obtained.

2.4 UV stability

It is highly desirable for a superhydrophobic coating to have UV stability and durability. UV protective coatings can be used in food packaging, paints, and textiles [113]. Wang et al. [57] studied the UV stability of superhydrophobic wood using long exposure to UV radiation. It was observed that the CA for polydopamine (PDA)/wood and PDA/Cu/wood surfaces remained unchanged (150 degrees) even after UV irradiation for about 160 h.

Superhydrophobic and superoleophobic surfaces from fluorinated–decyl polyhedral oligomeric silsesquioxane and hydrolyzed fluorinated alkyl silane were fabricated by
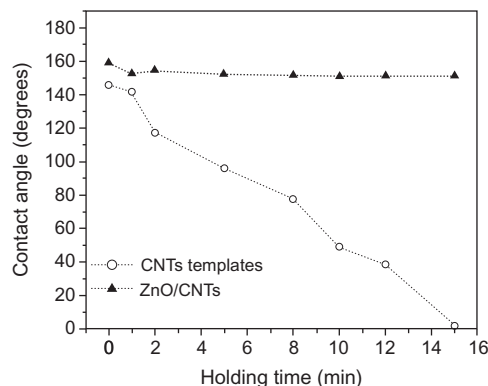
Fig. 21 UV exposure time dependence of water contact angles for ZnO film on the CNT template and Si wafer. *(Reproduced with permission from L. Huang, S.P. Lau, H.Y. Yang, E.S.P. Leong, S.F. Yu, S. Prawer, Stable superhydrophobic surface via carbon nanotubes coated with a ZnO thin film, J. Phys. Chem. B 109 (16) (2005) 7746–7748, American Chemical Society.)*

Wang et al. [114]. They analyzed the UV stability on a coated fabric with a middle-pressure Hg lamp (450 W). Even after 24 h of irradiation, the super liquid repellency remained unchanged. The uncoated fabric becomes hydrophilic after 1 h of irradiation.

Huang et al. [115] studied the alternate effect of UV radiation and dark storage on the superhydrophobicity of such films. They irradiated the surface with UV light for 5 h, and observed that CA changed to 46 degrees. The superhydrophobic surface was converted to a hydrophilic one. The sample was kept in the dark for 12 h and the CA was found to be 150 degrees. The superhydrophobic nature of the surface was thus recovered. The change in CA upon the exposure to UV is shown in Fig. 21.

Malavasi et al. [116] developed a durability protocol to test the robustness and durability of different superhydrophobic surfaces by evaluating damage after the irradiation of 16 h. Xiu et al. [117] studied the thermal and UV stability of polymeric superhydrophobic surface made by sol-gel process. The study reveals the adverse effect of UV radiation on superhydrophobicity. Isimjan et al. [51] tested UV stability of two kinds of steel surfaces. One of the surfaces was coated with TiO_2 P25 nanoparticle and other one was coated with SiO_2 layers. It was observed that SiO_2 nanoparticles adds on to the UV durability of superhydrophobic steel surfaces whereas a minimum UV resistance is exhibited by pure P25-coated surface. UV radiation generates OH free radicals, which oxidize the two CH_2 that are located between —Si and —CF_2, which is schematically represented in Fig. 22. Zhu et al. [118] fabricated cotton fabrics with multilayered superhydrophobic coating which possessed properties like UV shielding, capacity to separate oil and water, and ability to clean its own surface. The prepared superhydrophobic fabric was found to withstand abrasion without change in the water CA. Ren et al. [119] fabricated superhydrophobic fabric with enhanced mechanical stability, as well as UV shielding and
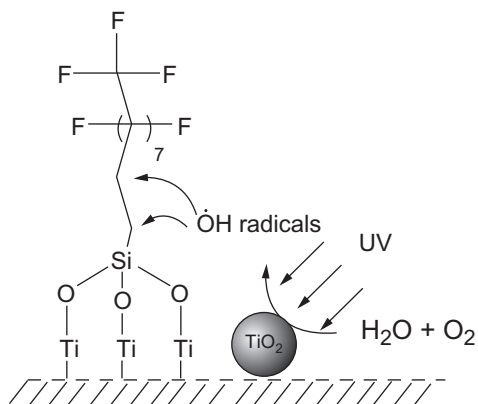
Fig. 22 Schematic representation of photodegradation process of PTES-based superhydrophobic surface. *(Reproduced with permission from T.T. Isimjan, T. Wang, S. Rohani, A novel method to prepare superhydrophobic, UV resistance and anti-corrosion steel surface, Chem. Eng. J. 210 (2012) 182–187, Elsevier.)*

durability. The force binding the fibers with the ZnO–PDMS coating is so strong that it allows the coated fabric to retain the superhydrophobic nature even after hand twisting, knife scratching, finger touching, and even 20 cycles of sandpaper abrasion. The UV resistant nature of PDMS retains the superhydrophobicity of ZnO–PDMS coated fabric even after long-term UV irradiation.

Nakata et al. [120] have prepared TiO_2–PDMS nanocomposite material that exhibits rewritable wettability transition stimulated by UV irradiation and thermal treatment. In another study, it can be observed that the incorporation of micro or nanoparticles of silica in a polyurethane matrix may lead to superhydrophobic character [121]. Wang [122] fabricated films from microstructured ZnO coatings, which form a superhydrophobic/ superoleophilic mesh. These films are devoid of any fluorinated compounds and are found to retain their superhydrophobic/leophilic nature even after UV irradiation. The CA before UV irradiation was found to be 156 degrees as shown in Fig. 23. The spherical water droplets rolled off very easily. The water CA of this mesh film diminished significantly on irradiation. It attained a superhydrophilic state within 2 h and the water droplets started penetrating the film on contact. Interestingly, in the case of films coated with the flower-like ZnO microstructures, the water CA remained unchanged after irradiation thus making them suitable candidates for outdoor applications.

Low-surface energy silica coatings were prepared using sol–gel processing technique by Xiu et al. [123] from tetraethoxysilane and trifluoropropyltrimethoxysilane precursors. Superhydrophobic surfaces made from organic polymers are prone to UV degradation. The UV-labile segments, impurities (i.e., catalyst) and UV-absorbing groups that may be present in polymers act as a site for UV degradation process thus making the surface hydrophilic. Therefore, it is very essential that the superhydrophobic surface be UV
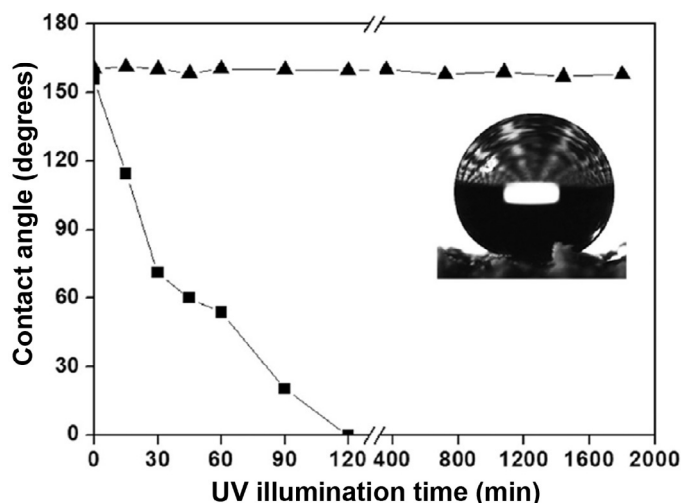
Fig. 23 Evolution of water contact angle on samples aligned ZnO nanorod arrays; *squares and flower like* ZnO microstructure; *triangles* under UV irradiation. *(Reproduced with permission from C.-F. Wang, F.-S.Tzeng, H.-G. Chen, C.-J. Chang, Ultraviolet-durable superhydrophobic zinc oxide-coated mesh films for surface and underwater–oil capture and transportation, Langmuir 28 (26) (2012) 10015–10019, American Chemical Society.)*

resistant unless otherwise its durability will be affected badly. It can be observed in Fig. 24 that this inorganic surface has better UV stability compared to other common organic polymer surfaces. The superhydrophobicity was retained even after UV exposure to about 1000 h. Such superhydrophobic surfaces are expected to withstand harsh environment and thus can be used for outdoor applications. In the case of hydrophobic silica material, ($—Si—(CH_2)_3CF_3$) groups which exist on the material surface, shows more stability than polymers. This is due to the strength of $Si—(CH_2)_3CF_3$ bond and the minor amount of UV-labile components present over the silica–coated surface. Due to the $Si—O$ bonds in silica, the surface shows better UV stability than organic polymers this is because of the higher bond strength. Huang et al. [124] made superhydrophobic cotton fabrics by coating TiO_2 for UV shielding properties with a CA of 160 degrees and SA of 10 degrees. Xue et al. [125] fabricated superhydrophobic TiO_2–coated fabric having better UV shielding properties. Lim et al. [126] fabricated a photoswitchable wetting surface, which involves introduction of photoresponsive groups on to the top-most layer using layer-by-layer assembly. UV-responsive microcapsules were successfully synthesized via emulsion polymerization by Chen et al. [127]. According to their studies, the surface was found to retain its superhydrophobic and self-cleaning ability under UV light even after it was mechanically damaged or contaminated with organics.

Gao et al. [128] made UV-resistant superhydrophobic arrays of ZnO nanorods, coated by SiO_2, which are transparent in nature. Hydrophobic surfaces were fabricated
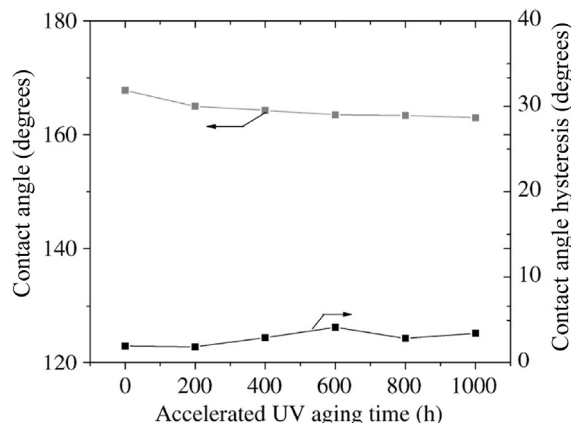
Fig. 24 UV stability test results for superhydrophobic silica films formed from a TFPS:TEOS ratio of 3:1. *(Reproduced with permission from Y. Xiu, D.W. Hess, C.P. Wong, UV-resistant and superhydrophobic self-cleaning surfaces using sol–gel processes, J. Adhes. Sci. Technol. 22 (15) (2008) 1907–1917, Taylor & Francis.)*

at low temperature ($<150°C$) on glass plate as well as polyethylene terephthalate (PET) sheets in a sequential manner. The UV–activated photooxidation and it leads to hydrophilicity. This can be avoided by protecting the surface with a barrier, which is UV resistant in nature. In order to protect the surface, they deposited SiO_2 over the surface to form a thin layer by means of chemical vapor deposition using tetraethoxysilane in the presence of ammonia. Thin SiO_2 layers of thickness 1 nm were found to be sufficient enough to protect the ZnO surface from the intense surge in hydrophilicity caused by UV-triggered photooxidation reactions. Change in water CA with the UV irradiation is shown in detail in Fig. 25.

Wang et al. [129] coated cotton fabrics with silica and titania hybrid sol. The sample was found to maintain superhydrophobicity under long time UV irradiation. If the cotton fabrics are coated only with TiO_2, alone was found to deteriorate under UV light irradiation (Fig. 26).

Superhydrophobic filter paper was prepared by Gao et al. [130] using amorphous titanium dioxide and epoxy resin (TiO_2/EP). Due to the high viscosity of the epoxy resin, it attaches to the surface of the filter paper strongly and imparted structural stability to the superhydrophobic surface. Eventually, the modification of the filter paper with octadecyltrichlorosilane (OTS) made it superhydrophobic. Wang et al. [114] prepared superhydrophobic cotton fabric from fluorinated-decyl polyhedral oligomeric silsesquioxane and hydrolyzed fluorinated alkyl silane. Even after 24 h of UV irradiation, there were no changes in the superhydrophobicity. But the uncoated fabric becomes completely hydrophilic with CA of 0 degrees, after irradiation for 1 h.
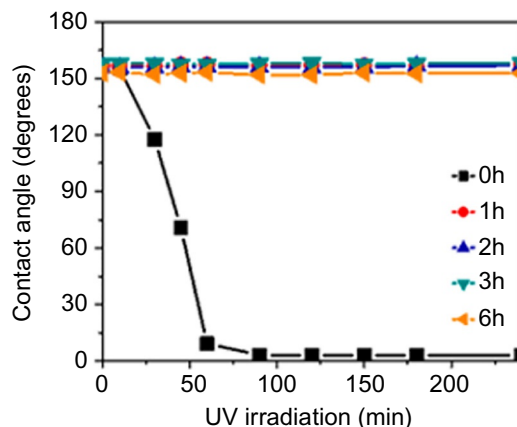
Fig. 25 Change in contact angle with UV irradiation. *(Reproduced with permission from Y. Gao, I. Gereige, A. El Labban, D. Cha, T.T. Isimjan, P.M. Beaujuge, Highly transparent and UV-resistant superhydrophobic SiO2-coated ZnO nanorod arrays, ACS Appl. Mater. Interfaces 6 (4) (2014) 2219–2223, American Chemical Society.)*
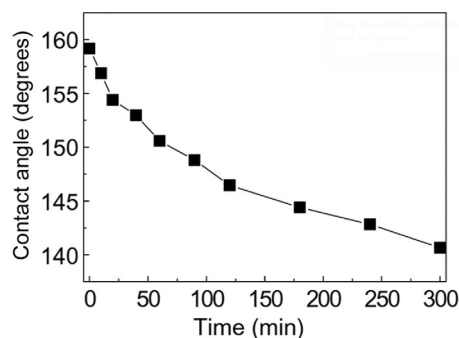
Fig. 26 The relation between water CAs on super hydrophobic cotton samples and UV light irradiation time [129].

3. Mechanical stability

Mechanical stability of the microscopic surface is essential for maintaining large CAs. The practical use of superhydrophobic surfaces is hampered by the weak mechanical stability. Maintenance of rough surface is a key to develop superhydrophobicity [131]. The mechanical stability of the topographic surface is very important in determining the dura–bility of superhydrophobic surface. Recent studies have revealed the importance of hier–archical roughness structures on the surface for enhancing the mechanical stability without affecting the CA [132, 133]. Waterfall and sand grain abrasion tests are common methods to check the mechanical stability of superhydrophobic surfaces. Scratch tests
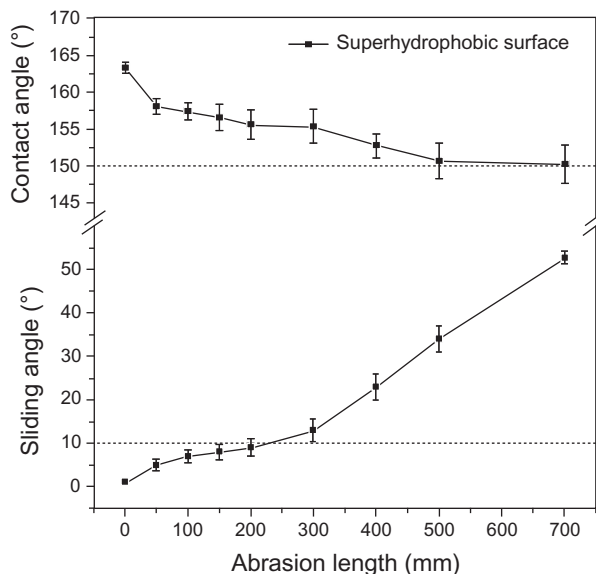
Fig. 27 The CA of the superhydrophobic surface as a function pressure. *(Reproduced with permission from Z. She, Q. Li, Z. Wang, L. Li, F. Chen, J. Zhou, Researching the fabrication of anticorrosion superhydrophobic surface on magnesium alloy and its mechanical stability and durability, Chem. Eng. J. 228 (2013) 415–424, American Chemical Society.)*

were also used to investigate the mechanical stability of the superhydrophobic surfaces. Ma et al. [134] fabricated Pd-based metallic glass surfaces with micro–nano–hierarchical structures to enhance the mechanical stability and confirmed by scratch test. She et al. [135] fabricated wear resistant coating over glass and polymer using nanoparticles. Fig. 27 shows that the silica nanoparticle–coated surface shows better resistance over silicon resin–coated one.

Deng et al. [86] made superhydrophobic surfaces from porous silica capsule, which are thermally and mechanically stable. It was observed that chemically bound silica bridges exhibit better mechanical stability and nonwettability. By following a method of coaxial electrospinning, Han and Steckl [136] fabricated superhydrophobic surface based on poly caprolactone having better mechanical stability. Li and Amirfazli [137] developed a set of criteria for superhydrophobic surfaces, which are accountable for both superhydrophobicity and mechanical durability. Further, they used the criterion to examine the relation between a designed hierarchical structure and superhydrophobicity. Artus et al. [138] made superhydrophobic surface from silicon nano–filaments having chemical stability, but lack mechanical stability. After mechanical rubbing test, there was decrease in CA. Mechanically stable superhydrophobic surfaces capable in withstanding tape-peeling and abrasion tests were fabricated by Wang et al. [139]. Ellinas et al. [140] recently reviewed durability of superhydrophobic and superamphiphobic polymeric surfaces

focusing on the mechanical stability. Dashairya et al. [141] fabricated superhydrophobic and superoleophilic surfaces using reduced graphene oxide-coated cotton (rGO@cotton) by a facile one-step hydrothermal method. Long et al. [142] fabricated superhydrophobic surfaces having excellent durability and thermal stability by spin coating method. Saengkaew et al. [143] made superhydrophobic coating from fluoroalkylsilane modified natural rubber encapsulated SiO_2 composites for self-driven oil/water separation. Zou et al. [144] fabricated superhydrophobic coatings using raspberry-like hollow silica nanoparticles, which has enhanced thermal and chemical stability along with outstanding mechanical flexibility and durability.

4. Surface chemistry and stability

The surface chemistry determines the superhydrophobicity as well as the stability of the surface. Chemistry between the surface and water determines the surface hydrophilic or phobic nature. The surface material exhibits superhydrophobic nature if CA is high. Hence, the surface molecules have immense importance in determining the superhydrophobic nature.

Chen et al. [145] studied the stability of plasma treated superhydrophobic surfaces using X-ray photoelectron spectroscopy (XPS) as shown in Fig. 28. After plasma treatment, the concentration of $—CF_2$ and $—CF_3$ decreased while those of C—O and C=O increased. Therefore, plasma induces transition from superhydrophobic to superhydrophilic nature due to the decrease in fluorine containing groups. Esmeryan et al. [146] made thermally stable superhydrophobic carbon soot coatings, the surface properties of which were studied using energy dispersive X-ray spectroscopy (EDS) and XPS.

Han et al. [147] fabricated artificial superhydrophobic surface, using the porous (PAH/PAA-coated ZrO_2) films. These were treated with 11 nm silica nanoparticles having hydroxyl groups, and then fluorinated by treating with perfluorodecyltrichlorosilane. This makes the surface similar to lotus leaf. The water CAs of the films are nearly zero, which means that the top surface of the film is covered with hydrophilic silica nanoparticles.

Ye et al. [59] used XPS technique to analyze chemistry of the composite in order to investigate the change in the surface chemical composition due to the heating process. The Si 2p spectrum obtained at 102.6, 103.4, and 104.5 eV confirms the presence of Si—O—C, Si—O—Si, and Si—OH, respectively, before heating the surface. However, after the heating process the peak corresponding to Si—O—C disappeared which indicates the decomposition of the hydrophobic O—CH_3 groups. There was a simultaneous increase in the concentration of hydrophilic Si—OH. These results show changes in superhydrophobic to hydrophilic nature.

Zhang et al. [148] used EDS and Fourier-transform infrared (FTIR) techniques to analyze the unmodified as well as modified surface. The surface was modified using
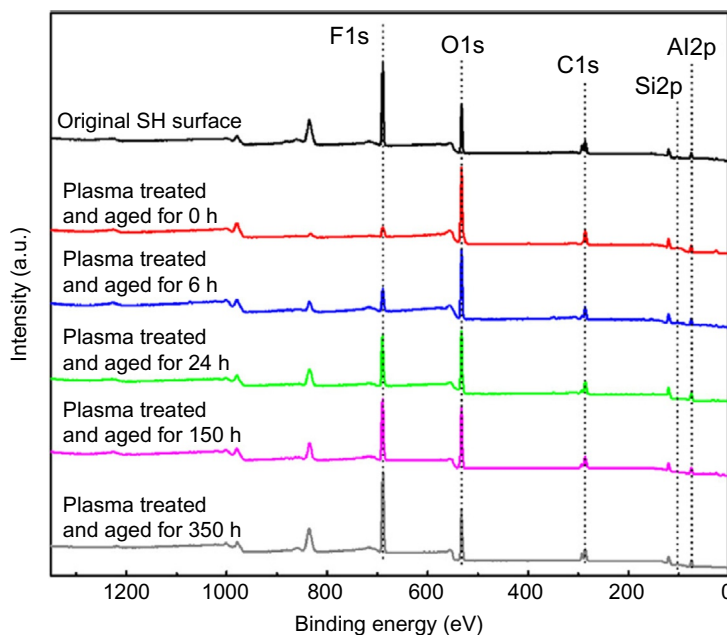
Fig. 28 XPS spectra of the original SH surface and plasma treated SH surface after aging for 0 h, 6 h, and 24 h. *(Reproduced with permission from F. Chen, J. Liu, Y. Cui, S. Huang, J. Song, J. Sun, et al., Stability of plasma treated superhydrophobic surfaces under different ambient conditions, J. Colloid Interface Sci. 470 (2016) 221–228, Elsevier.)*

dodecyltrimethoxysilane. From the EDS spectra shown in Fig. 29, one can understand the increase in the atomic ratio of Si from 10.09% to 11.58% after the modification using dodecyltrimethoxysilane (DTMS). This contributes the superhydrophobic nature of the surface. Zhao et al. [149] fabricated water-based coatings from silica nanoparticles modified using polyhedral oligomeric silsesquioxane (POSS). FTIR results indicate the grafting of MPTMS-POSS-PFDT on to silica (1H,1H,2H,2H-perfluorodecanethiol [PFDT]).

Wang et al. [139] studied the effect of hydrogen peroxide and acid in developing the superhydrophobic surface over steel. It shows a change from hydrophobic to a stage where there is large CA and high adhesion to water (known as rose effect) and finally to the lotus effect. Surface modification was achieved at the oxidized region of the steel surface. Zou et al. [144] described the chemistry behind the superhydrophobicity by fluorination of silica nanoparticle. The silica particles are found to be connected by the fluorine-containing chains. Lee et al. [150] observed that for the surfaces coated with different types of ZnO nanorods, those surfaces with sealed air pockets and narrow pore entrance enhances superhydrophobicity.
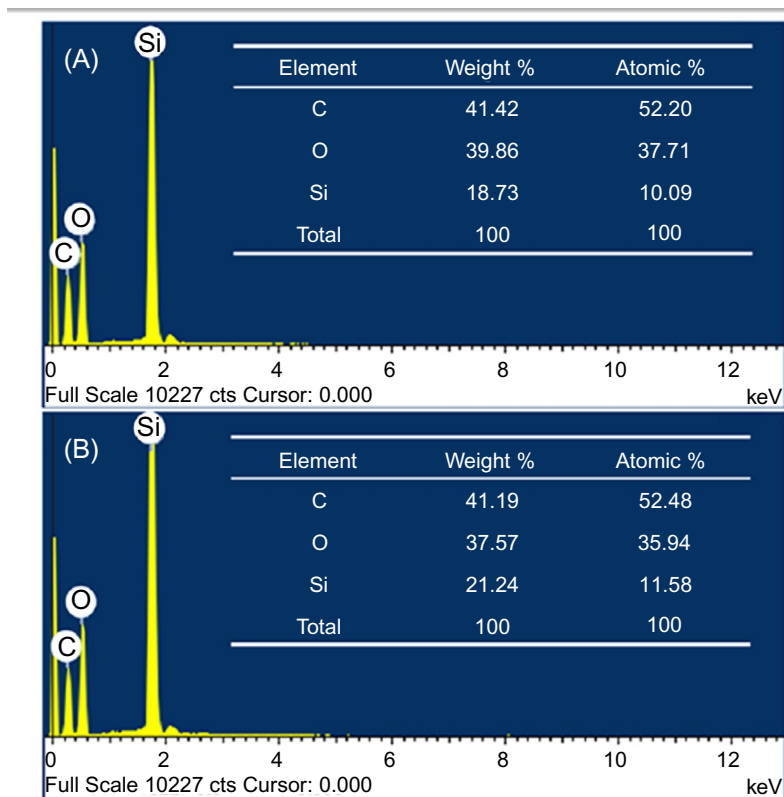
Fig. 29 Chemical compositions of the coatings. EDS spectra of the coatings before (A) and after (B) modification with DTMS, respectively [148].

5. Conclusion and future scope

From the detailed study, one can easily understand the importance of stability of super-hydrophobic surfaces with respect to a variety of parameters. As these surfaces are expected to be put into a variety of applications where they have to face harsh environmental conditions, it is essential to ensure thermal, solvent, pH, and UV stability. Nano-materials especially silica and fluorinated silica are capable of enhancing the superhydrophobicity. A detailed study on the surface chemistry throws light on the superhydrophobicity as well as its stability in various chemical conditions. Many researchers have developed superhydrophobic surfaces, which exhibits thermal, solvent, and pH stability. Even though quite a lot of good superhydrophobic surfaces have been fabricated, a thorough research on the UV stability is lacking due to the lack of surfaces, which are tough enough to resist UV irradiation. Fabrication of superhydrophobic surfaces stable enough to withstand the harsh environmental conditions continues to be a challenge to the researchers thus making this a potential research topic which demands immediate attention.

References

[1] R. Fürstner, W. Barthlott, C. Neinhuis, P. Walzel, Wetting and self-cleaning properties of artificial superhydrophobic surfaces, Langmuir 21 (3) (2005) 956–961, https://doi.org/10.1021/la0401011.

[2] N.J. Shirtcliffe, G. McHale, S. Atherton, M.I. Newton, An introduction to superhydrophobicity, Adv. Colloid Interf. Sci. 161 (1–2) (2010) 124–138.

[3] I. Hejazi, B. Hajalizadeh, J. Seyfi, G.M.M. Sadeghi, S.-H. Jafari, H.A. Khonakdar, Role of nanoparticles in phase separation and final morphology of superhydrophobic polypropylene/zinc oxide nanocomposite surfaces, Appl. Surf. Sci. 293 (2014) 116–123.

[4] J. Seyfi, I. Hejazi, S.-H. Jafari, H.A. Khonakdar, G.M.M. Sadeghi, A. Calvimontes, et al., On the combined use of nanoparticles and a proper solvent/non-solvent system in preparation of superhydrophobic polymer coatings, Polymer (Guildf) 56 (2015) 358–367.

[5] Y. Qing, C. Yang, C. Hu, Y. Zheng, C. Liu, A facile method to prepare superhydrophobic fluorinated polysiloxane/ZnO nanocomposite coatings with corrosion resistance, Appl. Surf. Sci. 326 (2015) 48–54.

[6] H. Bagheri, M. Aliofkhazraei, H.M. Forooshani, A.S. Rouhaghdam, Facile fabrication of uniform hierarchical structured (UHS) nanocomposite surface with high water repellency and self-cleaning properties, Appl. Surf. Sci. 436 (2018) 1134–1146.

[7] H.M. Forooshani, M. Aliofkhazraei, A.S. Rouhaghdam, Superhydrophobic aluminum surfaces by mechanical/chemical combined method and its corrosion behavior, J. Taiwan Inst. Chem. Eng. 72 (2017) 220–235.

[8] C. Extrand, P. Somasundaran, A.T. Hubbard, Encyclopedia of Surface and Colloid Science, Taylor & Francis Group, 2006, p. 5846.

[9] R.N. Wenzel, Resistance of solid surfaces to wetting by water, Ind. Eng. Chem. 28 (8) (1936) 988–994.

[10] J. Genzer, A. Marmur, Biological and synthetic self-cleaning surfaces, MRS Bull. 33 (8) (2008) 742–746.

[11] F. Xia, L. Jiang, Bio-inspired, smart, multiscale interfacial materials, Adv. Mater. 20 (15) (2008) 2842–2858.

[12] M. Ma, R.M. Hill, G.C. Rutledge, A review of recent results on superhydrophobic materials based on micro-and nanofibers, J. Adhes. Sci. Technol. 22 (15) (2008) 1799–1817.

[13] D. Quéré, Wetting and roughness, Annu. Rev. Mater. Res. 38 (2008) 71–99.

[14] X.-M. Li, D. Reinhoudt, M. Crego-Calama, What do we need for a superhydrophobic surface? A review on the recent progress in the preparation of superhydrophobic surfaces, Chem. Soc. Rev. 36 (8) (2007) 1350–1368.

[15] J. Genzer, K. Efimenko, Recent developments in superhydrophobic surfaces and their relevance to marine fouling: a review, Biofouling 22 (5) (2006) 339–360.

[16] A.B.D. Cassie, S. Baxter, Wettability of porous surfaces, Trans. Faraday Soc. 40 (1944) 546–551.

[17] M. Järn, F.J. Brieler, M. Kuemmel, D. Grosso, M. Lindén, Wetting of heterogeneous nanopatterned inorganic surfaces, Chem. Mater. 20 (4) (2008) 1476–1483.

[18] B. Bhushan, Y.C. Jung, Natural and biomimetic artificial surfaces for superhydrophobicity, self-cleaning, low adhesion, and drag reduction, Prog. Mater. Sci. 56 (1) (2011) 1–108.

[19] Z. Guo, W. Liu, B.-L. Su, Superhydrophobic surfaces: from natural to biomimetic to functional, J. Colloid Interface Sci. 353 (2) (2011) 335–355.

[20] X. Yao, Y. Song, L. Jiang, Applications of bio-inspired special wettable surfaces, Adv. Mater. 23 (6) (2011) 719–734.

[21] K. Liu, X. Yao, L. Jiang, Recent developments in bio-inspired special wettability, Chem. Soc. Rev. 39 (8) (2010) 3240–3255.

[22] C.-H. Xue, S.-T. Jia, J. Zhang, J.-Z. Ma, Large-area fabrication of superhydrophobic surfaces for practical applications: an overview, Sci. Technol. Adv. Mater. 11 (3) (2010) 33002.

[23] M. Nosonovsky, B. Bhushan, Superhydrophobic surfaces and emerging applications: non-adhesion, energy, green engineering, Curr. Opin. Colloid Interface Sci. 14 (4) (2009) 270–280.

[24] L. Feng, Z. Yang, J. Zhai, Y. Song, B. Liu, Y. Ma, et al., Superhydrophobicity of nanostructured carbon films in a wide range of pH values, Angew. Chem. 115 (35) (2003) 4349–4352.

[25] Y. Zhu, J. Zhang, Y. Zheng, Z. Huang, L. Feng, L. Jiang, Stable, superhydrophobic, and conductive polyaniline/polystyrene films for corrosive environments, Adv. Funct. Mater. 16 (4) (2006) 568–574.

[26] S. Pan, A.K. Kota, J.M. Mabry, A. Tuteja, Superomniphobic surfaces for effective chemical shielding, J. Am. Chem. Soc. 135 (2) (2012) 578–581.

[27] J. Zhang, S. Seeger, Superoleophobic coatings with ultralow sliding angles based on silicone nanofilaments, Angew. Chem. Int. Ed. 50 (29) (2011) 6652–6656.

[28] C.P. Wong, K.-S. Moon, Y. Li, Nano-Bio-Electronic, Photonic and MEMS Packaging, Springer, 2010.

[29] N. Cohen, A. Dotan, H. Dodiuk, S. Kenig, Superhydrophobic coatings and their durability, Mater. Manuf. Process. 31 (9) (2016) 1143–1155.

[30] T. Ishizaki, Y. Masuda, M. Sakamoto, Corrosion resistance and durability of superhydrophobic surface formed on magnesium alloy coated with nanostructured cerium oxide film and fluoroalkylsilane molecules in corrosive NaCl aqueous solution, Langmuir 27 (8) (2011) 4780–4788.

[31] B. Deng, R. Cai, Y. Yu, H. Jiang, C. Wang, J. Li, et al., Laundering durability of superhydrophobic cotton fabric, Adv. Mater. 22 (48) (2010) 5473–5477.

[32] C.-H. Xue, Y.-R. Li, P. Zhang, J.-Z. Ma, S.-T. Jia, Washable and wear-resistant superhydrophobic surfaces with self-cleaning property by chemical etching of fibers and hydrophobization, ACS Appl. Mater. Interfaces 6 (13) (2014) 10153–10161.

[33] J. Ou, W. Hu, M. Xue, F. Wang, W. Li, Superhydrophobic surfaces on light alloy substrates fabricated by a versatile process and their corrosion protection, ACS Appl. Mater. Interfaces 5 (8) (2013) 3101–3107.

[34] G. Wu, J. An, X. Tang, Y. Xiang, J. Yang, A versatile approach towards multifunctional robust microcapsules with tunable, restorable, and solvent-proof superhydrophobicity for self-healing and self-cleaning coatings, Adv. Funct. Mater. 24 (43) (2014) 6751–6761.

[35] Y. Yin, T. Liu, S. Chen, T. Liu, S. Cheng, Structure stability and corrosion inhibition of superhydrophobic film on aluminum in seawater, Appl. Surf. Sci. 255 (5) (2008) 2978–2984.

[36] Z.-Y. Deng, W. Wang, L.-H. Mao, C.-F. Wang, S. Chen, Versatile superhydrophobic and photocatalytic films generated from TiO2–SiO2@PDMS and their applications on fabrics, J. Mater. Chem. A 2 (12) (2014) 4178–4184.

[37] J. Zimmermann, G.R.J. Artus, S. Seeger, Long term studies on the chemical stability of a superhydrophobic silicone nanofilament coating, Appl. Surf. Sci. 253 (14) (2007) 5972–5979.

[38] H. Xiang, L. Zhang, Z. Wang, X. Yu, Y. Long, X. Zhang, et al., Multifunctional polymethylsilsesquioxane (PMSQ) surfaces prepared by electrospinning at the sol–gel transition: superhydrophobicity, excellent solvent resistance, thermal stability and enhanced sound absorption property, J. Colloid Interface Sci. 359 (1) (2011) 296–303.

[39] S. Zhu, Y. Li, J. Zhang, C. Lü, X. Dai, F. Jia, et al., Biomimetic polyimide nanotube arrays with slippery or sticky superhydrophobicity, J. Colloid Interface Sci. 344 (2) (2010) 541–546.

[40] Z. Cui, Q. Wang, Y. Xiao, C. Su, Q. Chen, The stability of superhydrophobic surfaces tested by high speed current scouring, Appl. Surf. Sci. 254 (10) (2008) 2911–2916.

[41] H. Zhu, D. Chen, W. An, N. Li, Q. Xu, H. Li, et al., A robust and cost-effective superhydrophobic graphene foam for efficient oil and organic solvent recovery, Small 11 (39) (2015) 5222–5229.

[42] J. Zou, H. Chen, A. Chunder, Y. Yu, Q. Huo, L. Zhai, Preparation of a superhydrophobic and conductive nanocomposite coating from a carbon-nanotube-conjugated block copolymer dispersion, Adv. Mater. 20 (17) (2008) 3337–3341.

[43] Q. Zhu, Y. Chu, Z. Wang, N. Chen, L. Lin, F. Liu, et al., Robust superhydrophobic polyurethane sponge as a highly reusable oil-absorption material, J. Mater. Chem. A 1 (17) (2013) 5386–5393.

[44] Y. Lee, K.-Y. Ju, J.-K. Lee, Stable biomimetic superhydrophobic surfaces fabricated by polymer replication method from hierarchically structured surfaces of Al templates, Langmuir 26 (17) (2010) 14103–14110.

[45] C. Zeng, H. Wang, H. Zhou, T. Lin, Self-cleaning, superhydrophobic cotton fabrics with excellent washing durability, solvent resistance and chemical stability prepared from an SU-8 derived surface coating, RSC Adv. 5 (75) (2015) 61044–61050, https://doi.org/10.1039/C5RA08040A.

[46] Y. Yoo, J.B. You, W. Choi, S.G. Im, A stacked polymer film for robust superhydrophobic fabrics, Polym. Chem. 4 (5) (2013) 1664–1671.

[47] H. Zou, S. Lin, Y. Tu, G. Liu, J. Hu, F. Li, et al., Simple approach towards fabrication of highly durable and robust superhydrophobic cotton fabric from functional diblock copolymer, J. Mater. Chem. A 1 (37) (2013) 11246–11260.

[48] Q. Sun, B. Aguila, J.A. Perman, T. Butts, F.-S. Xiao, S. Ma, Integrating superwettability within covalent organic frameworks for functional coating, Chem 4 (2018) 1726–1739.

[49] M. Satapathy, P. Varshney, D. Nanda, S.S. Mohapatra, A. Behera, A. Kumar, Fabrication of durable porous and non-porous superhydrophobic LLDPE/SiO2 nanoparticles coatings with excellent self-cleaning property, Surf. Coat. Technol. 341 (2018) 31–39.

[50] S. Heinonen, E. Huttunen-Saarivirta, J.-P. Nikkanen, M. Raulio, O. Priha, J. Laakso, et al., Anti-bacterial properties and chemical stability of superhydrophobic silver-containing surface produced by sol–gel route, Colloids Surf. A Physicochem. Eng. Asp. 453 (2014) 149–161.

[51] T.T. Isimjan, T. Wang, S. Rohani, A novel method to prepare superhydrophobic, UV resistance and anti-corrosion steel surface, Chem. Eng. J. 210 (2012) 182–187.

[52] I.S. Bayer, D. Fragouli, P.J. Martorana, L. Martiradonna, R. Cingolani, A. Athanassiou, Solvent resistant superhydrophobic films from self-emulsifying carnauba wax–alcohol emulsions, Soft Matter 7 (18) (2011) 7939–7943.

[53] C.-P. Hsu, L.-Y. Chang, C.-W. Chiu, P.T.C. Lee, J.-J. Lin, Facile fabrication of robust superhydrophobic epoxy film with polyamine dispersed carbon nanotubes, ACS Appl. Mater. Interfaces 5 (3) (2013) 538–545.

[54] A. Asthana, T. Maitra, R. Büchel, M.K. Tiwari, D. Poulikakos, Multifunctional superhydrophobic polymer/carbon nanocomposites: graphene, carbon nanotubes, or carbon black? ACS Appl. Mater. Interfaces 6 (11) (2014) 8859–8867.

[55] L. Xiao, W. Zeng, G. Liao, C. Yi, Z. Xu, Thermally and chemically stable candle soot superhydrophobic surface with excellent self-cleaning properties in air and oil, ACS Appl. Nano Mater. 1 (3) (2018) 1204–1211, https://doi.org/10.1021/acsanm.7b00363.

[56] Q. Xie, G. Fan, N. Zhao, X. Guo, J. Xu, J. Dong, et al., Facile creation of a bionic super–hydrophobic block copolymer surface, Adv. Mater. 16 (20) (2004) 1830–1833.

[57] K. Wang, Y. Dong, W. Zhang, S. Zhang, J. Li, Preparation of stable superhydrophobic coatings on wood substrate surfaces via mussel-inspired polydopamine and electroless deposition methods, Polymers (Basel) 9 (6) (2017) 218.

[58] J.G. Nguyen, S.M. Cohen, Moisture-resistant and superhydrophobic metal−organic frameworks obtained via postsynthetic modification, J. Am. Chem. Soc. 132 (13) (2010) 4560–4561.

[59] H. Ye, L. Zhu, W. Li, H. Liu, H. Chen, Simple spray deposition of a water–based superhydrophobic coating with high stability for flexible applications, J. Mater. Chem. A 5 (20) (2017) 9882–9890.

[60] H.Y. Erbil, A.L. Demirel, Y. Avcı, O. Mert, Transformation of a simple plastic into a superhydrophobic surface, Science (80-) 299 (5611) (2003) 1377–1380.

[61] R. Iqbal, B. Majhy, A.K. Sen, Facile fabrication and characterization of a PDMS-derived candle soot coated stable biocompatible superhydrophobic and superhemophobic surface, ACS Appl. Mater. Interfaces 9 (36) (2017) 31170–31180.

[62] H. Zhou, H. Wang, H. Niu, A. Gestos, X. Wang, T. Lin, Fluoroalkyl silane modified silicone rubber/nanoparticle composite: a super durable, robust superhydrophobic fabric coating, Adv. Mater. 24 (18) (2012) 2409–2412.

[63] R.M. Bär, S. Widmaier, P.A. Levkin, Facile fabrication of robust superhydrophobic surfaces: comparative investigation, RSC Adv. 6 (100) (2016) 98257–98266.

[64] S. Lu, H. Gao, Q. Wang, W. Xu, S. Szunerits, R. Boukherroub, Fabrication of stable homogeneous superhydrophobic HDPE/graphene oxide surfaces on zinc substrates, RSC Adv. 6 (35) (2016) 29823–29829.

[65] W. Hou, Q. Wang, Stable polytetrafluoroethylene superhydrophobic surface with lotus–leaf structure, J. Colloid Interface Sci. 333 (1) (2009) 400–403.

[66] T. Ishizaki, N. Saito, Rapid formation of a superhydrophobic surface on a magnesium alloy coated with a cerium oxide film by a simple immersion process at room temperature and its chemical stability, Langmuir 26 (12) (2010) 9749–9755.

[67] L. Zhai, F.C. Cebeci, R.E. Cohen, M.F. Rubner, Stable superhydrophobic coatings from polyelec-
trolyte multilayers, Nano Lett. 4 (7) (2004) 1349–1353.

[68] Y. Jiang, Z. Wang, X. Yu, F. Shi, H. Xu, X. Zhang, et al., Self-assembled monolayers of dendron
thiols for electrodeposition of gold nanostructures: toward fabrication of superhydrophobic/superhy-
drophilic surfaces and pH-responsive surfaces, Langmuir 21 (5) (2005) 1986–1990, https://doi.org/
10.1021/la047491b.

[69] D.-D. La, T.A. Nguyen, S. Lee, J.W. Kim, Y.S. Kim, A stable superhydrophobic and superoleophilic
Cu mesh based on copper hydroxide nanoneedle arrays, Appl. Surf. Sci. 257 (13) (2011) 5705–5710.

[70] J. Liang, D. Li, D. Wang, K. Liu, L. Chen, Preparation of stable superhydrophobic film on stainless
steel substrate by a combined approach using electrodeposition and fluorinated modification, Appl.
Surf. Sci. 293 (2014) 265–270.

[71] W. Song, V.S. Gaware, Ö.V. Rúnarsson, M. Másson, J.F. Mano, Functionalized superhydrophobic
biomimetic chitosan-based films, Carbohydr. Polym. 81 (1) (2010) 140–144.

[72] M. Qu, B. Zhang, S. Song, L. Chen, J. Zhang, X. Cao, Fabrication of superhydrophobic surfaces on
engineering materials by a solution-immersion process, Adv. Funct. Mater. 17 (4) (2007) 593–596.

[73] J. Yong, Q. Yang, F. Chen, D. Zhang, H. Bian, Y. Ou, et al., Stable superhydrophobic surface with
hierarchical mesh-porous structure fabricated by a femtosecond laser, Appl. Phys. A Mater. Sci. Pro-
cess. 111 (1) (2013) 243–249.

[74] T. Ishizaki, J. Hieda, N. Saito, N. Saito, O. Takai, Corrosion resistance and chemical stability of super-
hydrophobic film deposited on magnesium alloy AZ31 by microwave plasma-enhanced chemical
vapor deposition, Electrochim. Acta 55 (23) (2010) 7094–7101.

[75] P. Khanjani, Cellulose-Based Superhydrophobic Surfaces and Dynamics of Coupled Chemical Sys-
tems, 2015.

[76] L. Guo, W. Yuan, J. Li, Z. Zhang, Z. Xie, Stable superhydrophobic surfaces over a wide pH range,
Appl. Surf. Sci. 254 (7) (2008) 2158–2161.

[77] H. Liu, S. Szunerits, W. Xu, R. Boukherroub, Preparation of superhydrophobic coatings on zinc as
effective corrosion barriers, ACS Appl. Mater. Interfaces 1 (6) (2009) 1150–1153.

[78] Z. Guo, F. Zhou, J. Hao, W. Liu, Stable biomimetic super-hydrophobic engineering materials, J. Am.
Chem. Soc. 127 (45) (2005) 15670–15671.

[79] N. Mittal, D. Deva, R. Kumar, A. Sharma, Exceptionally robust and conductive superhydrophobic
free-standing films of mesoporous carbon nanocapsule/polymer composite for multifunctional appli-
cations, Carbon N Y 93 (2015) 492–501.

[80] X. Xu, Z. Zhang, J. Yang, Fabrication of biomimetic superhydrophobic surface on engineering mate-
rials by a simple electroless galvanic deposition method, Langmuir 26 (5) (2009) 3654–3658.

[81] L. Xu, Z. Geng, J. He, G. Zhou, Mechanically robust, thermally stable, broadband antireflective, and
superhydrophobic thin films on glass substrates, ACS Appl. Mater. Interfaces 6 (12) (2014) 9029–9035.

[82] Madidi, G. Momen, M. Farzaneh, Development of a stable TiO2 nanocomposite self-cleaning coat-
ing for outdoor applications, Adv. Mater. Sci. Eng. 2016 (2016)7958152. 8 pages, https://doi.org/
10.1155/2016/7958152.

[83] L. Feng, Y. Liu, H. Zhang, Y. Wang, X. Qiang, Superhydrophobic alumina surface with high adhe-
sive force and long-term stability, Colloids Surf. A Physicochem. Eng. Asp. 410 (2012) 66–71.

[84] M.J. Taghizadeh, S. Afghihi, H. Saidi, Superhydrophobic surface based silica nanoparticle modified
with diisocyanate and short and long normal chain alcohols, Asian J. Nanosci. Mater. 1 (2018) 71–77.

[85] G. Gong, J. Wu, J. Liu, N. Sun, Y. Zhao, L. Jiang, Bio-inspired adhesive superhydrophobic polyimide
mat with high thermal stability, J. Mater. Chem. 22 (17) (2012) 8257–8262.

[86] X. Deng, L. Mammen, Y. Zhao, P. Lellig, K. Müllen, C. Li, et al., Transparent, thermally stable and
mechanically robust superhydrophobic surfaces made from porous silica capsules, Adv. Mater. 23 (26)
(2011) 2962–2965.

[87] H. Budunoglu, A. Yildirim, M.O. Guler, M. Bayindir, Highly transparent, flexible, and thermally
stable superhydrophobic ORMOSIL aerogel thin films, ACS Appl. Mater. Interfaces 3 (2) (2011)
539–545.

[88] N. Wang, J. Xi, S. Wang, H. Liu, L. Feng, L. Jiang, Long-term and thermally stable superhydrophobic
surfaces of carbon nanofibers, J. Colloid Interface Sci. 320 (2) (2008) 365–368.

[89] J. Lin, H. Chen, T. Fei, C. Liu, J. Zhang, Highly transparent and thermally stable superhydrophobic coatings from the deposition of silica aerogels, Appl. Surf. Sci. 273 (2013) 776–786.

[90] J. Seyfi, S.H. Jafari, H.A. Khonakdar, G.M.M. Sadeghi, G. Zohuri, I. Hejazi, et al., Fabrication of robust and thermally stable superhydrophobic nanocomposite coatings based on thermoplastic polyurethane and silica nanoparticles, Appl. Surf. Sci. 347 (2015) 224–230.

[91] L. Xu, D. Zhu, X. Lu, Q. Lu, Transparent, thermally and mechanically stable superhydrophobic coating prepared by an electrochemical template strategy, J. Mater. Chem. A 3 (7) (2015) 3801–3807.

[92] K. Seo, M. Kim, Candle-based process for creating a stable superhydrophobic surface, Carbon N Y 68 (2014) 583–596.

[93] A.V. Rao, S.D. Bhagat, H. Hirashima, G.M. Pajonk, Synthesis of flexible silica aerogels using methyltrimethoxysilane (MTMS) precursor, J. Colloid Interface Sci. 300 (1) (2006) 279–285.

[94] R.P.S. Chakradhar, G. Prasad, P. Bera, C. Anandan, Stable superhydrophobic coatings using PVDF–MWCNT nanocomposite, Appl. Surf. Sci. 301 (2014) 208–215.

[95] S.A. Mahadik, D.B. Mahadik, V.G. Parale, P.B. Wagh, S. Gupta, A.V. Rao, Recoverable and thermally stable superhydrophobic silica coating, J. Sol-Gel Sci. Technol. 62 (3) (2012) 490–494.

[96] W. Ma, C. Yang, X. Gong, K. Lee, A.J. Heeger, Thermally stable, efficient polymer solar cells with nanoscale control of the interpenetrating network morphology, Adv. Funct. Mater. 15 (10) (2005) 1617–1622.

[97] N. Saleema, M. Farzaneh, Thermal effect on superhydrophobic performance of stearic acid modified ZnO nanotowers, Appl. Surf. Sci. 254 (9) (2008) 2690–2695.

[98] G. Wu, C. Hu, J. Cui, S.-C. Chen, Y.-Z. Wang, Concurrent superhydrophobicity and thermal energy storage of microcapsule with superior thermal stability and durability, ACS Sustain. Chem. Eng. 5 (9) (2017) 7759–7767.

[99] S.-C. Cha, E.K. Her, T.-J. Ko, S.J. Kim, H. Roh, K.-R. Lee, et al., Thermal stability of superhydrophobic, nanostructured surfaces, J. Colloid Interface Sci. 391 (2013) 152–157.

[100] X. Deng, L. Mammen, H.-J. Butt, D. Vollmer, Candle soot as a template for a transparent robust superamphiphobic coating, Science (80-) 335 (6064) (2012) 67–70.

[101] P.A. Levkin, F. Svec, J.M.J. Fréchet, Porous polymer coatings: a versatile approach to superhydrophobic surfaces, Adv. Funct. Mater. 19 (12) (2009) 1993–1998, https://doi.org/10.1002/adfm.200801916.

[102] S.A. Mahadik, D.B. Mahadik, M.S. Kavale, V.G. Parale, P.B. Wagh, H.C. Barshilia, et al., Thermally stable and transparent superhydrophobic sol–gel coatings by spray method, J. Sol-Gel Sci. Technol. 63 (3) (2012) 580–586.

[103] A.S. Pashinin, V.I. Zolotarevskii, M.R. Kiselev, A.M. Emel'yanenko, L.B. Boinovich, Thermal stability of superhydrophobic coatings, in: Doklady Physical Chemistry, Springer, 2011, pp. 19–22.

[104] L.R. Freschauf, J. McLane, H. Sharma, M. Khine, Shrink-induced superhydrophobic and antibacterial surfaces in consumer plastics, PLoS One 7 (8) (2012) e40987.

[105] K. Tsougeni, N. Vourdas, A. Tserepi, E. Gogolides, Mechanisms of oxygen plasma nanotexturing of organic polymer surfaces: from stable super hydrophilic to super hydrophobic surfaces, Langmuir 25 (19) (2009) 11748–11759, https://doi.org/10.1021/la901072z.

[106] K. Chen, K. Gu, S. Qiang, C. Wang, Environmental stimuli-responsive self-repairing waterbased superhydrophobic coatings. RSC Adv. 7 (2017) 543–550, https://doi.org/10.1039/c6ra25135h.

[107] A. Kumar, Development of excellent water-repellent coatings for metallic and ceramic surfaces, in: International Conference on Mechanical and Intelligent Manufacturing Technologies (ICMIMT), IEEE, 2017, pp. 11–15.

[108] J. Lasprilla-Botero, S. Torres-Giner, M. Pardo-Figuerez, M. Álvarez-Láinez, J. M Lagaron, Superhydrophobic bilayer coating based on annealed electrospun ultrathin poly (ε-caprolactone) fibers and electrosprayed nanostructured silica microparticles for easy emptying packaging applications, Coatings 8 (5) (2018) 173.

[109] P. Varshney, S.S. Mohapatra, Fabrication of durable and renegerable superhydrophobic coatings on metallic surfaces for potential industrial applications. in: 2017 8th International Conference on Mechanical and Intelligent Manufacturing Technologies (ICMIMT), 2017, https://doi.org/10.1109/ICMIMT.2017.7917427.

[110] M. Awais, M. Jalil, U. Zulfiqar, S.W. Husain, A facile approach towards fabrication of super hydrophobic surface from functionalized silica particles, in: IOP Conference Series: Materials Science and Engineering, IOP Publishing, 2016, p. 12022.

[111] T.F. Qahtan, M.A. Gondal, I.O. Alade, M.A. Dastageer, Fabrication of water jet resistant and thermally stable superhydrophobic surfaces by spray coating of candle soot dispersion, Sci. Rep. 7 (1) (2017) 7531.

[112] S. Nagappan, J.J. Park, S.S. Park, C.-S. Ha, Preparation of superhydrophobic and transparent micro-nano hybrid coatings from polymethylhydroxysiloxane and silica ormosil aerogels, Nano Converg. 1 (1) (2014) 30.

[113] T. Ogawa, B. Ding, Y. Sone, S. Shiratori, Super-hydrophobic surfaces of layer-by-layer structured film-coated electrospun nanofibrous membranes, Nanotechnology 18 (16) (2007) 165607.

[114] H. Wang, Y. Xue, J. Ding, L. Feng, X. Wang, T. Lin, Durable, self-healing superhydrophobic and superoleophobic surfaces from fluorinated-decyl polyhedral oligomeric silsesquioxane and hydrolyzed fluorinated alkyl silane, Angew. Chem. Int. Ed. 50 (48) (2011) 11433–11436.

[115] L. Huang, S.P. Lau, H.Y. Yang, E.S.P. Leong, S.F. Yu, S. Prawer, Stable superhydrophobic surface via carbon nanotubes coated with a ZnO thin film, J. Phys. Chem. B 109 (16) (2005) 7746–7748.

[116] I. Malavasi, I. Bernagozzi, C. Antonini, M. Marengo, Assessing durability of superhydrophobic surfaces, Surf. Innov. 3 (1) (2014) 49–60.

[117] Y. Xiu, D.W. Hess, C.P. Wong, UV and thermally stable superhydrophobic coatings from sol–gel processing, J. Colloid Interface Sci. 326 (2) (2008) 465–470, https://doi.org/10.1016/j.jcis.2008.06.042.

[118] T. Zhu, S. Li, J. Huang, M. Mihailiasa, Y. Lai, Rational design of multi-layered superhydrophobic coating on cotton fabrics for UV shielding, self-cleaning and oil–water separation, Mater. Des. 134 (2017) 342–351.

[119] G. Ren, Y. Song, X. Li, B. Wang, Y. Zhou, Y. Wang, et al., A simple way to an ultra-robust superhydrophobic fabric with mechanical stability, UV durability, and UV shielding property, J. Colloid Interface Sci. 522 (2018) 57–62.

[120] K. Nakata, H. Kimura, M. Sakai, T. Ochiai, H. Sakai, T. Murakami, et al., UV/thermally driven rewritable wettability patterns on TiO2−PDMS composite films, ACS Appl. Mater. Interfaces 2 (9) (2010) 2485–2488.

[121] C. Su, Facile fabrication of a lotus-effect composite coating via wrapping silica with polyurethane, Appl. Surf. Sci. 256 (7) (2010) 2122–2127.

[122] C.-F. Wang, F.-S. Tzeng, H.-G. Chen, C.-J. Chang, Ultraviolet-durable superhydrophobic zinc oxide-coated mesh films for surface and underwater–oil capture and transportation, Langmuir 28 (26) (2012) 10015–10019.

[123] Y. Xiu, D.W. Hess, C.P. Wong, UV-resistant and superhydrophobic self-cleaning surfaces using sol–gel processes, J. Adhes. Sci. Technol. 22 (15) (2008) 1907–1917.

[124] J.Y. Huang, S.H. Li, M.Z. Ge, L.N. Wang, T.L. Xing, G.Q. Chen, X.F. Liu, S.S. Al-Deyab, K.Q. Zhang, T. Chen, Y.K. Lai, Robust superhydrophobic TiO2@fabrics for UV shielding, self-cleaning and oil–water separation. J. Mater. Chem. A 3 (2015) 2825–2832, https://doi.org/10.1039/C4TA05332J.

[125] C.-H. Xue, S.-T. Jia, H.-Z. Chen, M. Wang, Superhydrophobic cotton fabrics prepared by sol–gel coating of TiO2 and surface hydrophobization, Sci. Technol. Adv. Mater. 9 (3) (2008) 35001.

[126] H.S. Lim, J.T. Han, D. Kwak, M. Jin, K. Cho, Photoreversibly switchable superhydrophobic surface with erasable and rewritable pattern, J. Am. Chem. Soc. 128 (45) (2006) 14458–14459.

[127] K. Chen, S. Zhou, S. Yang, L. Wu, Fabrication of all-water-based self-repairing superhydrophobic coatings based on UV-responsive microcapsules, Adv. Funct. Mater. 25 (7) (2015) 1035–1041.

[128] Y. Gao, I. Gereige, A. El Labban, D. Cha, T.T. Isimjan, P.M. Beaujuge, Highly transparent and UV-resistant superhydrophobic SiO2-coated ZnO nanorod arrays, ACS Appl. Mater. Interfaces 6 (4) (2014) 2219–2223.

[129] X.-W. Wang, C. Guo, Z.-H. Yuan, The stability of superhydrophobic cotton fabrics prepared by sol–gel coating of SiO2 and TiO2, Surf. Rev. Lett. 20 (06) (2013) 1350064.

[130] Z. Gao, X. Zhai, F. Liu, M. Zhang, D. Zang, C. Wang, Fabrication of TiO2/EP super-hydrophobic thin film on filter paper surface, Carbohydr. Polym. 128 (2015) 24–31.
[131] B.P. Dyett, A.H. Wu, R.N. Lamb, Mechanical stability of surface architecture—consequences for superhydrophobicity, ACS Appl. Mater. Interfaces 6 (21) (2014) 18380–18394.
[132] T. Verho, C. Bower, P. Andrew, S. Franssila, O. Ikkala, R.H.A. Ras, Mechanically durable superhydrophobic surfaces, Adv. Mater. 23 (5) (2011) 673–678.
[133] A.V. Rao, S.S. Latthe, S.A. Mahadik, C. Kappenstein, Mechanically stable and corrosion resistant superhydrophobic sol–gel coatings on copper substrate, Appl. Surf. Sci. 257 (13) (2011) 5772–5776.
[134] J. Ma, X.Y. Zhang, D.P. Wang, D.Q. Zhao, D.W. Ding, K. Liu, et al., Superhydrophobic metallic glass surface with superior mechanical stability and corrosion resistance, Appl. Phys. Lett. 104 (17) (2014) 173701.
[135] Z. She, Q. Li, Z. Wang, L. Li, F. Chen, J. Zhou, Researching the fabrication of anticorrosion superhydrophobic surface on magnesium alloy and its mechanical stability and durability, Chem. Eng. J. 228 (2013) 415–424.
[136] D. Han, A.J. Steckl, Superhydrophobic and oleophobic fibers by coaxial electrospinning, Langmuir 25 (16) (2009) 9454–9462, https://doi.org/10.1021/la900660v.
[137] W. Li, A. Amirfazli, Hierarchical structures for natural superhydrophobic surfaces, Soft Matter 4 (3) (2008) 462–466.
[138] G.R.J. Artus, S. Jung, J. Zimmermann, H. Gautschi, K. Marquardt, S. Seeger, Silicone nanofilaments and their application as superhydrophobic coatings, Adv. Mater. 18 (20) (2006) 2758–2762.
[139] N. Wang, D. Xiong, Y. Deng, Y. Shi, K. Wang, Mechanically robust superhydrophobic steel surface with anti-icing, UV-durability, and corrosion resistance properties, ACS Appl. Mater. Interfaces 7 (11) (2015) 6260–6272.
[140] K. Ellinas, A. Tserepi, E. Gogolides, Durable superhydrophobic and superamphiphobic polymeric surfaces and their applications: a review, Adv. Colloid Interf. Sci. 250 (2017) 132–157.
[141] L. Dashairya, M. Rout, P. Saha, Reduced graphene oxide-coated cotton as an efficient absorbent in oil–water separation, Adv. Compos. Hybrid Mater. 1 (1) (2018) 135–148.
[142] M. Long, S. Peng, W. Deng, X. Yang, K. Miao, N. Wen, et al., Robust and thermal-healing superhydrophobic surfaces by spin-coating of polydimethylsiloxane, J. Colloid Interface Sci. 508 (2017) 18–27.
[143] J. Saengkaew, D. Le, C. Samart, H. Sawada, M. Nishida, N. Chanlek, et al., Superhydrophobic coating from fluoroalkylsilane modified natural rubber encapsulated SiO2 composites for self-driven oil/water separation, Appl. Surf. Sci. 462 (2018) 164–174.
[144] X. Zou, C. Tao, K. Yang, F. Yang, H. Lv, L. Yan, et al., Rational design and fabrication of highly transparent, flexible, and thermally stable superhydrophobic coatings from raspberry-like hollow silica nanoparticles, Appl. Surf. Sci. 440 (2018) 700–711.
[145] F. Chen, J. Liu, Y. Cui, S. Huang, J. Song, J. Sun, et al., Stability of plasma treated superhydrophobic surfaces under different ambient conditions, J. Colloid Interface Sci. 470 (2016) 221–228.
[146] K.D. Esmeryan, C.E. Castano, A.H. Bressler, M. Abolghasemibizaki, R. Mohammadi, Rapid synthesis of inherently robust and stable superhydrophobic carbon soot coatings, Appl. Surf. Sci. 369 (2016) 341–347.
[147] J.T. Han, Y. Zheng, J.H. Cho, X. Xu, K. Cho, Stable superhydrophobic organic − inorganic hybrid films by electrostatic self-assembly, J. Phys. Chem. B 109 (44) (2005) 20773–20778.
[148] Z. Zhang, H. Wang, Y. Liang, X. Li, L. Ren, Z. Cui, et al., One-step fabrication of robust superhydrophobic and superoleophilic surfaces with self-cleaning and oil/water separation function, Sci. Rep. 8 (1) (2018) 3869.
[149] R. Zhao, Y. Chen, G. Liu, Y. Jiang, K. Chen, Fabrication of self-healing waterbased superhydrophobic coatings from POSS modified silica nanoparticles, Mater. Lett. 229 (2018) 281–285.
[150] M. Lee, C. Yim, S. Jeon, Characterization of underwater stability of superhydrophobic surfaces using quartz crystal microresonators, Langmuir 30 (27) (2014) 7931–7935, https://doi.org/10.1021/la5006665.

Biological adhesion behavior of superhydrophobic polymer coating

Tanvir Arfin, Bhawana Singh, Neelima Varshney
Environmental Materials Division, CSIR–National Environmental Engineering Research Institute (CSIR–NEERI), Nagpur, India

1. Introduction

Sustainable development is found to be the trendiest topic in the recent era of growth in society. This concept has gathered attention mainly in the influence and regeneration as such it maintains equity with the application of various resources interacting among the humans and the ecosystem [1–5]. In the recent research study, the innovation of new material in an advanced form will serve to be an important task [6–10]. Such material is used in the different subdivision of analytical chemistry to identify qualitatively and quantitatively the analytes within the fewer volume samples that are in the complicated form [11–15]. Such material is suitable for the research field in the techno–economic sector possessing various applications in a wide range [16–20]. The polymer is a type of macromolecule composed of the large number of repetitive unit monomers, which is derived from the Greek word "*monos.*" It is found either in natural form or can be human–made [21–25]. In the current scientific study, polymer and its derivatives are considered as a significant aspect for the survival of human being [26–30]. The surface, which has a more advancing contact angle of water and has less water contact angle hysteresis is known as superhydrophobic surfaces. Nowadays, this is a very hot topic, and it attracts attention due to its unique property like self–cleaning and water repellent. It has potential in a different practical application like in self–cleaning and also in biotechnology [31]. The process is described by Cassie-Baxter model [32]. According to this model, microgrooves of rough surface trapped air and the droplets of water consist of a "composite" surface comprised of air and the microprotrusion tops. Many plants and animals also behave as a natural water repellent and have superhydrophobic surface. For example, lotus leaves provide a superhydrophobic surface.

Recently in these years, there is an increment of superhydrophobic surfaces from microscale to the nanoscale. Literature report says that a superhydrophobic coating is present. There is various type of natural material like lotus leaves, animal species and their different specific part has different superhydrophobic properties [33]. In this technique, the essential ingredient is nanoscale, which helps in the coating at the nanoscale level [34].

If we compare lotus leaves and rose petal according to a hierarchical structure, then we can see differences in their chemical composition and microstructures because of small water contact angle hysteresis on lotus leaves and even waxy protrusions water cannot enter into the micrometrical structures. High hysteresis is observed when the drops adhere on the surface, and the micropapillae is sealed by the water in the petal [35].

2. Properties

In the current years, there has been improved attention for creating superhydrophobic surfaces between microscale to nanoscale design. As indicated by the recent reports, superhydrophobic coatings are available in the environment. Various properties are listed in Fig. 1.

Yang et al. [36] gave their observations relating to the contact between droplets and surfaces, which displaces fractal structure. It provides information about the dependence of the contact angle of surface roughness on average square root and independence of fractal dimension at nano–metric level.

Li et al. [37] gave information about energy barrier concept, which suppresses when starter guideline optimizes the future design of superrepellent compound. This theory was proved by the spontaneous and reversible process, given by Cassie and Wenzel. The Cassie state corresponds to the smaller texture and Wenzel to the larger one. Smaller rugosities do not allow trapping of water drops irreversibly nano-Cassie surface preserves the property of hydrophobicity and can induce penetration of drops by larger rugosities reversibly.
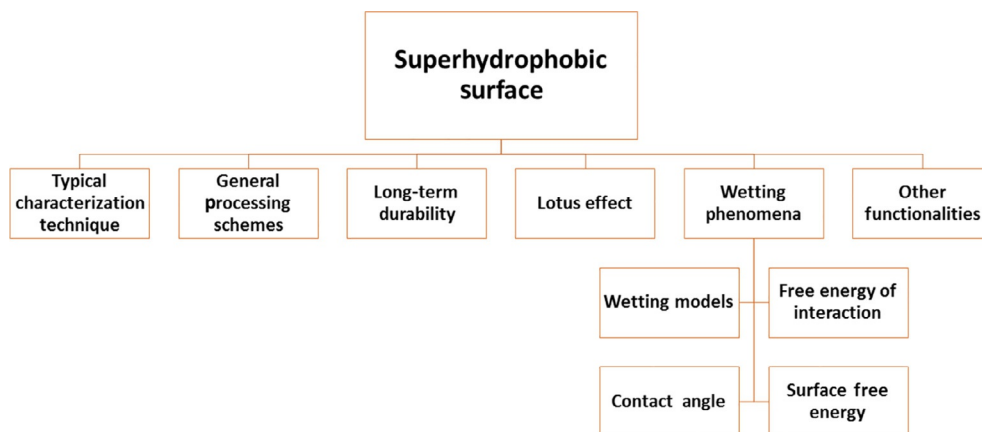
Fig. 1 Properties of superhydrophobic.

3. Superhydrophobic polymer's mechanical robustness

Polypropylene surfaces are superhydrophobic; their mechanical robustness can be improved. These possibilities to improve mechanical robustness were explored by Huovinen et al. [38], who suggested for the enhancement of the durability of hierarchical structures, which are superhydrophobic. This can be done by addition of micro-pillars, which acted as votive protection. The surfaces of structured polypropylene had static contact angles higher than roll-off angles. Even though huge micro-pillars took the place of some portions of fine-scale patterns, delicate nanostructures could be still protected by sacrificial surfaces without interfering the functional properties like self-cleaning and nonwetting of surfaces.

4. Long-term durability

In spite of the large extend study in term of superhydrophobic surfaces, it still faces difficulty in the applications. The superhydrophobic surfaces need micro/nanoroughness as well as the low energy on the surface. Owing to the delicate structure and rapid degradation of surface chemistry, they undergo through weak durability. With the lessening of the micro/nano-topographical structures, there will be a reduction in superhydrophobicity of the surface. The loss of superhydrophobicity may occur due to the degradation in surface energy along with the damaging of the surface structure. The area was resistance not required; the superhydrophobic surface is used to attain a better outcome. The superhydrophobic surface is employed in the walls and the ceiling of the hospitals for reducing the bacterial adhesion.

   Hence, it is mandatory to go through the durability target for imposing it in the manufacturing of enhances superhydrophobic structure [39].

5. Smooth surface wettability

The chemical composition, as well as surface packing of chemical modifier, affects the surface wettability. Usual self-assembled monolayers consist of some defects in structures which forbids the compact preparation on a large surface. This limitation can be overcome by depositing modifiers on a flexible substrate, which cause mechanical deformation of the substrate. Efimenko and Genzer [40] suggested that this structural defect can be removed by substratum stretching or deposition of reactive molecules like organosilanes resulting in stabilization of substratum strain.

6. Effect of physical roughness

The significant involvement of the governing length scale was considered for the study of physical roughness effect. In some cases, the authors reported various length scales of

roughness. After a detailed investigation of the lotus leaf, the results revealed the existence of multiple length scales on the leaf surface, varying from nano to micrometers. Cheng et al. [41] examined the attribute of various roughnesses on lotus leaf's hydrophobic property and stated that numerous scale lengths are prominent for the effectiveness of the lotus leaf. The essential capability of self-cleaning lotus leaf was significantly decreased by burning away the leaf's nano-sized hair.

7. Hierarchical structuring

Chemical heterogeneity was created on the surface as only structural elements tips were in contact with water in Cassie state. Living organisms augmented this phenomenon over 450 million years of evolution, which lead to the bewildering diversity of hierarchically structured surfaces. Approximately 180 degrees contact angels are observed in lotus leaves [42].

Hierarchical sculpturing levels of natural surfaces:

7.1 Structural level: First

According to the resolution scale of a scanning electron microscopy (SEM), flat surfaces are demarcated by their hydrophobic and hydrophilic properties. The flat is a similar property that can be determined by size. Structures that have a height less than 10 nm are defined as flat surfaces. Leaves of plants like rubber, figs, and some animals are seldom found to have flat surfaces.

7.2 Structural level: Second

Rodlets, tubules, and platelets are shapes that shows vast spectrum. These spectrums are made by crystals of epicuticular wax. Epicuticular wax formed on plants can build structures up to the height of 20–200 µm, sometimes they may even exceed 200 µm of height.

7.3 Structural level: Third

Different shapes of external cell wall lead to unicellular structures. These cell walls can be present in convex or papillose cells. In hair, it is either multicellular or unicellular; in trichomes, the dimensions vary from 2 µm to several centimeters.

7.4 Structural level: Fourth

Epidermal cell's group has different arrangement patterns, which lead to multicellular structures resulting in numerous possibilities for structuring in this group.

7.5 Structural level: Fifth

Organ surfaces with microscopically visible curvatures often have separate functional compartments on organism's surfaces. Combination of two levels, which is adequate to generate a superhydrophobic surface can be defined as hierarchical structuring. For achieving persistent superhydrophobicity like in lotus, three combinations of standards can be required.

8. Nontoxic bioadhesion control

Minimum one pattern polymer is required for enhancing bioadhesion or coating a surface for repelling. The base surface of this patterned polymer should possess coating layer of plurality features. Each features at least should have a microscale dimension ($<1\,mm$) and a neighboring function of considerably different geometry. Roughness factor (R) typically ranges from 4 to 50 units when coated with the layer in a given pattern. The bioadhesion can be enhanced or resisted relative to the base surface [43].

9. Transparent superhydrophobic coating

Superhydrophobic transparent coatings can provide the substrates with the lotus leaf effect, which can resist the change in optical properties ranging in the visible region. Superhydrophobic coating construction essentially requires a micro or nanoscale surface roughness [44]. However, superhydrophobic coatings can show low transparency due to rough surfaces. When light from surrounding comes in contact with the layer, a part of it gets reflected to surrounding leading to loss of light whereas remaining light is refracted through the surface. The light is negligibly absorbed by coating when the coating thickness is ¼ times less than the wavelength of surrounding light. The refracted light intensity is increased which leads to the enhancement of transparency of coatings [45]. The scattered and reflected light is reduced. For the design of superhydrophobic transparent coatings, the superhydrophobicity and transparency are considered as competitive properties. Construction of superhydrophobic transparent coating thus requires rationally designing of the surface microstructures.

Zhao et al. [46] found that transparency and superhydrophobicity of coatings are greatly influenced by multiwalled carbon nanotubes (MWCNT) concentrations and hydrolytic polycondensations of hexadecyltrimethoxysilane (HDTMS). These factors are also dependent on the coating's microstructure. Silica nanotubes@polydimethylsiloxane (SNTs@PDMS) coatings have excellent transparency durability and superhydrophobicity, which was superior to other superhydrophobic coatings available. Severe water jetting ($100\,kPa$ for $60\,min$) did not affect SNTs@PDMS coating's superhydrophobicity to much extent as it has a high cross-linked network and there was no detection of a change in coating's surface microstructure.

10. Polymeric superhydrophobic coating

Surface with interfacial field and generation of superhydrophobization with some charges in the surface can be possible by superhydrophobic nanocoating technique. Superhydrophobic coating material should have some unique properties like low cost, good processability, and flexibility. The polymer consists of a more significant number of molecular units with different functional and structural groups connected with covalent bonds and produces different types of configurations. They are used for low adhesion and friction [47]. Therefore, by the respective characteristics, the nano-functionalized superhydrophobic surface needs to be formulated to show its varied application is given in Fig. 2.

11. Antifouling surface

Antifouling surfaces show low protein adsorption playing a significant task for many areas like biomedical devices and boat, which are not cleaned frequently. Biofouling of some
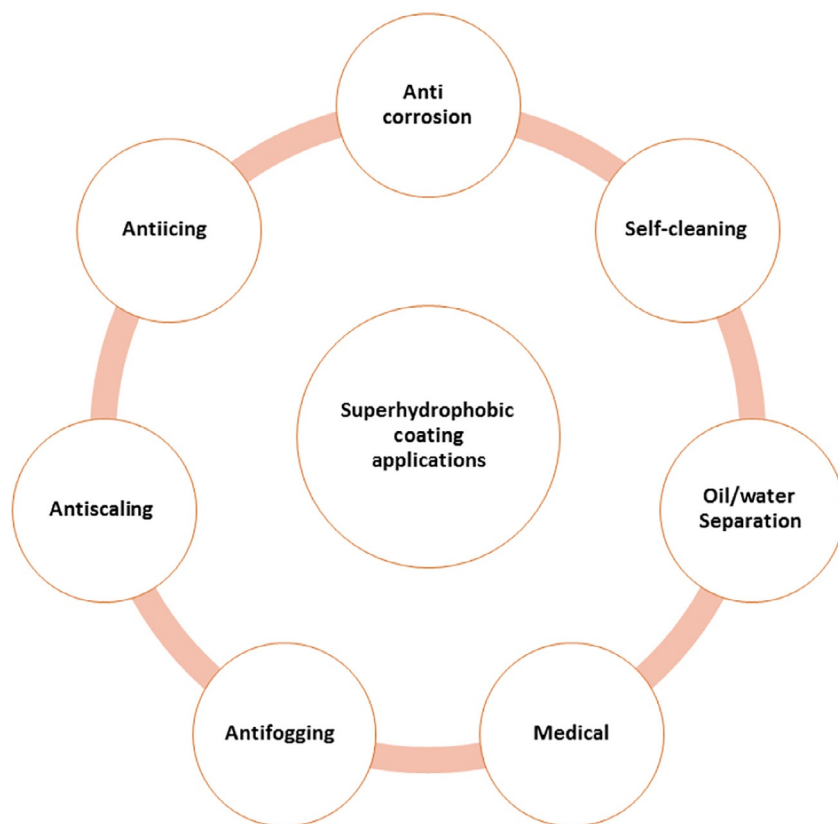
Fig. 2 Applications of superhydrophobic nanocoatings.

pipes and boat hulls increases consumption of energy in large amount. The first stage of biological contamination of surfaces is protein adsorption with the binding of a cell to a preadsorbed layer of protein before spreading and increasing. Cell growth reduces at the surfaces that obstruct or hinders this new adsorption process. The reaction, which is catalyzed in protein adsorption is another problematic area, where the rate of response reduces by the enzyme adsorption. Cross-diffusion and interfacial area maximize by flat channels [48], they have high-efficiency apparatus for the biological and chemical process under micro and nanodevices.

12. Protein adhesion

Protein adhesion has reduced through different ways such as surfaces coated by chemical, surfaces attached by proteolytic enzyme [49], surfaces sites filled with molecules [50]. Current publications highlighted the probabilities of coatings with superhydrophobic [51] but also shows the little work, which has been done in this area [52].

The protein, which binds to hydrophobic surfaces contain some qualities such as conformational changes [53], the binding ability of platelet, and lower cell. Due to a reduction in surfaces are of solid at the liquid interface [54], superhydrophobic surfaces can reduce the extra protein adsorption. By relaxation of protein structure [55], we can determine the time extension of protein adsorption. Protein adsorption is progressive on the pseudo-porous surface because of the nature of the surfactant [56].

Atomic force microscopy (AFM), surface plasmon resonance (SPR), circular dichroism (CD), optical waveguide light-mode spectroscopy (OWLS), and Fourier transform infrared/attenuated total reflectance (FTIR/ATR) are the techniques, which are used for the study of protein adsorption. The ability to adsorb molecules to alter their configuration when it interacts with the surface generates the complexity of protein adsorption process. The original structure of a protein is the conclusion of the delicate interaction among hydrophobic interaction, electrostatic, and van der Waals coupled with solvent effects. This balance can be destroyed by a sizeable interacting surface. It is established that the protein adsorption on hydrophobic layer tends to open [57].

The generation of hydrophilic less adhesive surfaces is comparatively easy and the water dissolving polymers immobilization upon the surface is one of the possibilities. Hence, these polymers could adsorb water strongly, and the presence of a large amount of water content upon the surfaces has been considered as the potential of the biomaterial concerning its similarity with the living matter and mainly for providing interface tension at a minimum, which in contact with blood reduces the adsorption of the protein [58].

Bovine serum albumin (BSA) is a protein model, which is used to adhere the surfaces. Further, it is essential in a different biological application like polymerase chain reaction, present in high content in serum and is generally used as an agent for surface blocking due

to binding property. The size of this protein is 15 nm and can be destroyed when adhering strongly [59].

Wei et al. [60] experimented with a study of adsorption by lysozyme, which interacts with a surface of polythene in a watery environment at large scale of simulations of atomistic molecular dynamics. When a protein absorbs the structural surface gets deformed, the protein mobility and dehydration process corresponds on to a hydrophobic surface. The method of adsorption can be classified into three stages: dehydration, surface transport and deformation after protein adsorption entirely on the surface. During the carriage to the surface, lysozyme enzyme preserves it's secondary and tertiary structure.

Adsorption detected with wetting quality upon plasma surfaces ranges from superhydrophilic to superhydrophobic serum protein. Protein adsorption on superhydrophilic siloxane coating reduction was observed when it was compared to hydrophobic surfaces and on superhydrophobic coatings was found at a more significant reduction. Bacterial attachment indicates minimum for both after and before adsorption trails on superhydrophobic and also confirmed protein adhesion resistance [61].

13. Bacterial adhesion

Industrial and healthcare sector face difficulties due to biofilm development on abiotic space by proliferation and adhesion of bacteria on it. Now, this increases the need for developing a material which resistor minimizes bacterial colonization on it [62]. First, leaching biocides were adopted as the oldest method for designing bacteria-free surface, which helps in killing nearby and adhered bacteria. Increased biocides usage leads to increased immunity of bacteria toward antibiotics [63]. So, biocides should be used wisely [64]. Metallic ions of metals such as Mo [65], Cu [66], and Ag [67] were used as an antibacterial agent to resist bacterial growth [68]. As the Ag gets dissolved totally, the antibacterial effects are wholly lost. Along with the outcome, the main concern is regarding its application in the field of health and the surrounding environments.

The antibacterial materials growth dependent on the superhydrophobicity is the novel trends that are flourishing in the society. The technique of superhydrophobicity came up for designing bacteria-free materials [69], which reduce the adhesion of bacteria on the surface instead of killing them by reducing adhesion force [70].

14. Material features on bacterial adhesion

Study of bacterial-material interaction is essential to analyze how material properties influence the bacterial adhesion. Although, only material properties do not affect bacterial-material interaction somewhat it also depends on the experimental conditions under which material is kept. The features are given in Fig. 3.
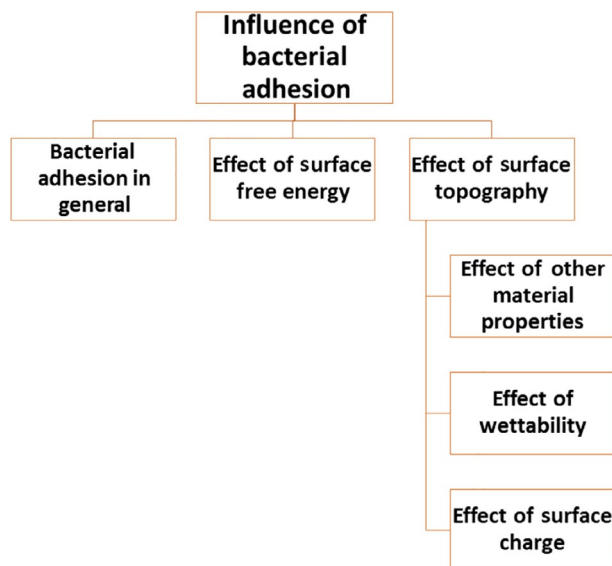
Fig. 3 Features of bacterial adhesion.

15. State-of-the-art improvement in superhydrophobic surface

15.1 To minimize bacterial adhesion

Study of bacterial adhesion has included a superhydrophobic surface, which is investigated by number of researchers [71].

Tang et al. [72] with different wettabilities have investigated *Staphylococcus aureus* adhesion on the material surface. The SEM images of *S. aureus* surface material are taken after 2 and 4h. On TiO_2 nanotube superhydrophobic surface with a water contact angle of 156 degrees in comparison to those on the hydrophilic surface with a water contact angle of 54 degrees and the hydrophobic surface with a water contact angle of 133 degrees. *S. aureus* remains scattered on the hydrophobic and superhydrophobic surface, while it remains intact on the hydrophilic surface so could be removed easily. Superhydrophobicity is emerging as a hot topic in reducing bacterial adhesion, and many phenomena and the concepts still need to be developed and investigated.

15.2 To minimize protein adsorption

In addition to superhydrophobic surface studies in reducing bacterial adhesion on the material surface, it is observed that lesser protein adsorption plays a vital role in resisting bacterial adhesion [73]. Different types of interaction handle bacterial adhesion by

specific or nonspecific interaction like through adsorbed protein film. Biofilm formation is promoted by the structure of the protein layer. Protein tends to adsorb more favorably onto the surfaces with contact angle 60–90 degrees and on hydrophobic surfaces. The surface designing is done for enhancing the hydrophobic interaction along with the large surface area [74]. Such study gives a brief understanding of the role of the roughness of the surface due to bacterial adhesion imposed with various surface energy. Rod *Escherichia coli* were taken as the best example for studying the features of the surface of the polymeric material for minimizing the bacterial adhesion. Various bacterial properties like shapes also affect adhesion, so these are also considered in analytical procedures studies [75]. Sabry and Al-mosawi [76] selected a facile method for fabrication of antibacterial superhydrophobic surfaces with high chemical stability and enhanced self-cleaning features by applying the phase separation technique and solvent/nonsolvent selected. The materials of low surface energy were environmentally friendly and inexpensive. AgNps stabilized on the petals or branches of the polycarbonate surface structure play a crucial role in bacterial inhibition and creation of a disease-resistant environment.

16. Biofouling

The marine industry faces biofouling problem. It leads to various drawbacks namely downtime for cleaning, releasing pressure in the pipe system, enlarged dragging on the ship hulls, etc. Fouling is the method where the marine microorganism binds itself toward the surface forming various marine animals such as algae and invertebrates, which then proliferate on that layer [77].

Recent research showed that alumina surfaces represent anode with nanoscale cylindrical pores of diameter less than 25 nm are capable of reducing bacterial attraction for several bacterial strains. An exact prediction of bacterial interaction with the surface is essential to optimize surface's topographical and physicochemical properties and thus prevent biofilm formation.

Hwang et al. [78] have represented that antiadhesion property of superhydrophobic surfaces is short lived and enhance bacterial colonization. This is important rather than reducing bacterial colonization; superhydrophobic surfaces may function in bacterial survival. This study corrects wrong information regarding antifouling immersion and offers appreciated data for expansion of antimicrobial surfaces.

17. Antibiofouling coating

Rahmawan et al. [79] investigated that biofouling can be prevented at cellular extend by coating the surface textures with the material posing low biocompatibility and surface energy. Polymer pillar at microscale was covered by a wrinkle of nanoscale making

hierarchical structures, which were fabricated by using a thin coating of carbon having diamond-like composition (DLC) and poly-(dimethylsiloxane) replica molding micropillars. Studies of adhesion on surfaces having a hydrophobicity of various degrees revealed that calf pulmonary artery endothelial (CPAE) cell proliferation was restricted to superhydrophobic surfaces to a great extent. These surfaces had smaller spacing than the cell diameter and restricted the entry of cells, which lead to aggregation of suspended cells and even restricted the growth. The cell growth and adhesion were reduced by DLC as it has less surface free energy.

18. Cell adhesion

Cell material surface interaction study is essential for tissue engineering and various other biomedical services. Within 20 years, the surface properties, like surface energy approximately affected the growth and cell adhesion on the surface of the material.

The substrate engineering involves various aspects for the development of extra-cellular microenvironment by maintaining in vivo conditions. Cells in vivo undergo difficult chemical and topographical properties differing only in extracellular matrix and basement membrane [80]. Due to this reason, there is increasing material for the regeneration of tissue by the combination of both micro and nanoscale properties to guide cell response attraction and migrate to differentiation and lastly for tissue formation [81].

Since superhydrophobic surface are used for the creation of cell patterns, the approach employed possess various defects in its application. Hence, it needs another apparent tool to modify such superhydrophobic surface. The method applied is generally transient where the hydrophilicity reduces with time, leading to the change in the original state [82]. However, to overcome with drawbacks, a traditional approach is required to modify the superhydrophobic surface. In the above context, the proficient and potent method has been developed by the polydopamine coating to alter the superhydrophobic surface [83].

Kang and Choi [84] suggested that polydopamine-coated surface provides a suitable background for the control of adhesion where the superhydrophobic surface was used in the form of cell-repellent platforms. They clarified that such method was quite sufficient to attain precise control mechanism on cell adhesion.

Mundo et al. [85] investigated and suggested about the process how the different topographic features on two-etched fluorinated surface, posing roughness, variated hydrophobic behaviors tend to change the morphology of cell of Saos2 cell lines. Further afterwards it reflects that the surface becomes less rough as such less adhesion is achieved in comparison to the flat reference. Such activity clarifies that efficient topography scale is observed by the cell, which balances the hostile wetting effects to some extent.

Zangi et al. [86] observed that superhydrophobic sample synthesized in the absence of nanocomposite shows high water-repellent activity in comparison to the superhydrophobic material. But yet it was noted that the cell adhesion mechanism was defeated in contrast to the other one. They showed nanoscale induces more roughness. Later on, another comparative study was made for the dry sample in the varied temperature range. By the results, it was reflected that surface topography was capable of playing a significant role for cell adhesion of polymeric surface in comparison to surface energy.

Kang and Choi [84] observed that this technique could be utilized as a capable device for accomplishing accuracy by managing above cell adhesion.

19. Restrictions of superhydrophobic surfaces

Since more than 10 years' research is carried in the account of the novel water-repellency capacity of the superhydrophobic surface as well as material. Still, success is yet to achieve in the current field. The list given in Fig. 4 clarifies about its failure.

20. Conclusion

In the new era, polymers have turned into an essential part of our lives with their different applications. The multifunctionality of polymers has been adventured in numerous commercial applications with protuberant outcomes [87–91]. The standard of complexity essential for recapitulated is the three-dimensional (3D) environmental is yet another topic of concern, requiring better innovation and correlation with the surface of the cell interface. The superhydrophobic surface possesses great superiority and is capable of reducing the bacterial adhesion and bacterial interaction cell as well. This surface turns out to be posing better and enhanced strategy in the designing of the antibacterial surface. The result of such outcome was mainly from minimized protein adsorption. It is capable of trapping the layer of air in between the surface and the cells of bacteria.
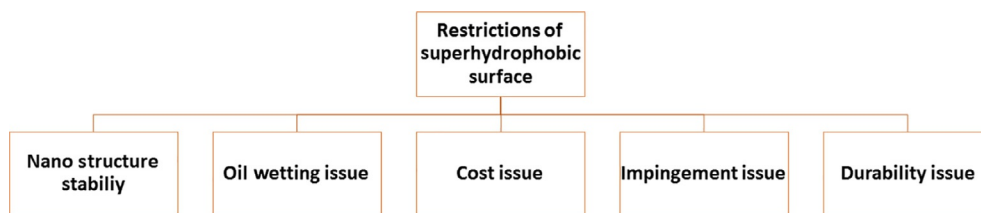
Fig. 4 Restrictions of superhydrophobic surface.

References

[1]   T. Arfin, Applications of bentonite and its role as a base of engineering chemistry, in: A.K. Mishra (Ed.), Bentonite: Characteristics, Uses and Implications for the Environment, Nova Science Publishers, New York, 2015, pp. 127–135 (Chapter 5).

[2]   T. Arfin, S. Athar, Graphene for advanced organic photovoltaics, in: S. Kanchi, S. Ahmed, M.I. Sabela, C.M. Hussain (Eds.), Nanomaterials: Biomedical, Environmental, and Engineering Applications, Scrivener Publishing LLC, Beverly, MA, 2018, pp. 93–104 (Chapter 3).

[3]   T. Arfin, A. Tarannum, Engineered nanomaterials for industrial application: an overview, in: C.M. Hussain (Ed.), Handbook of Nanomaterials for Industrial Applications, Elsevier, The Netherlands, 2018, pp. 127–134 (Chapter 6).

[4]   T. Arfin, Chitosan and its derivatives: overlook of commercial application in diverse field, in: S. Ahmed, S. Ikram (Eds.), Chitosan: Derivatives, Composites and Applications, Scrivener Publishing LLC, Beverly, MA, 2017, pp. 115–150 (Chapter 5).

[5]   T. Arfin, A. Tarannum, K. Sonawane, Green and sustainable advanced materials: an overview, in: S. Ahmed, C.M. Hussain (Eds.), Green and Sustainable Advanced Materials: Processing and Characterization, vol. I, Scrivener Publishing LLC, Beverly, MA, 2018, pp. 1–34 (Chapter 1).

[6]   T. Arfin, K. Sonawane, An excellence method on starch-based materials: a promising stage for environmental application, in: S. Ahmed, C.M. Hussain (Eds.), Green and Sustainable Advanced Materials: Applications, vol. II, Scrivener Publishing LLC, Beverly, MA, 2018, pp. 177–208 (Chapter 8).

[7]   T. Arfin, P.R. Mogarkar, Bio-based material protein and its novel applications, in: S. Ahmed, S. Ikram, S. Kanchi, K. Bisetty (Eds.), Biocomposites: Biomedical and Environmental Applications, Pan Stanford Publishing, USA, 2018, pp. 405–432 (Chapter 15).

[8]   A.C. Sophia, T. Arfin, E.C. Lima, Recent developments in adsorption of dyes using graphene-based nanomaterials, in: M. Naushad (Ed.), A New Generation Material Graphene: Applications in Water Technology, Springer International Publishing, Cham, 2019, pp. 439–471 (Chapter 18).

[9]   F. Mohammad, T. Arfin, N. Saba, M. Jawaid, H.A. Al-Lohedan, Electrical conductivity and biological efficacy of ethyl cellulose and polyaniline-based composites, in: A. Khan, M. Jawaid, A.A.P. Khan, A.M. Asiri (Eds.), Electrically Conductive Polymers and Polymer Composites: From Synthesis to Biomedical Applications, Wiley-VCH Verlag, Germany, 2018, pp. 181–197 (Chapter 9).

[10] A.U. Khan, N. Malik, T. Arfin, Nanofibrillated cellulose and copoly(amino acid) hydrogel matrices in biotechnology and biomedicine, in: M. Jawaid, F. Mohammad (Eds.), Nanocellulose and Nanohydrogel Matrices: Biotechnological and Biomedical Applications, Wiley-VCH Verlag, Germany, 2017, pp. 331–352 (Chapter 12).

[11] S. Athar, R. Bushra, T. Arfin, Cellulose nanocrystals and PEO/PET hydrogel material in biotechnology and biomedicine: current status and future prospects, in: M. Jawaid, F. Mohammad (Eds.), Nanocellulose and Nanohydrogel Matrices: Biotechnological and Biomedical Applications, Wiley-VCH Verlag, Germany, 2017, pp. 139–173 (Chapter 7).

[12] R. Borkar, S.S. Waghmare, T. Arfin, Bacterial cellulose and polyester hydrogel matrices in biotechnology and biomedicine: current status and future prospects, in: M. Jawaid, F. Mohammad (Eds.), Nanocellulose and Nanohydrogel Matrices: Biotechnological and Biomedical Applications, Wiley-VCH Verlag, Germany, 2017, pp. 21–46 (Chapter 2).

[13] S. Athar, T. Arfin, Commercial and prospective applications of gelatin, in: S. Ikram, S. Ahmed (Eds.), Natural Polymers: Derivatives, Blends and Composites, vol. II, Nova Science Publishers, New York, 2017, pp. 199–216 (Chapter 11).

[14] P.R. Mogarkar, T. Arfin, Chemical and structural importance of starch-based derivative and its applications, in: S. Ikram, S. Ahmed (Eds.), Natural Polymers: Derivatives, Blends and Composites, vol. II, Nova Science Publishers, New York, 2017, pp. 77–87 (Chapter 5).

[15] T. Arfin, N. Yadav, Impedance characteristics and electrical double-layer capacitance of composite polystyrene–cobalt–arsenate membrane, J. Ind. Eng. Chem. 19 (2012) 256–262.

[16] T. Arfin, A. Falch, R.J. Kriek, Evaluation of charge density and the theory for calculating membrane potential for a nano-composite nylon-6,6 nickel phosphate membrane, Phys. Chem. Chem. Phys. 14 (2012) 16760–16769.

[17] T. Arfin, Rafiuddin, An electrochemical and theoretical comparison of ionic transport through a polystyrene-based cobalt arsenate membrane, Electrochim. Acta 56 (2011) 7476–7483.

[18] D.C. Onwudiwe, T. Arfin, C.A. Strydom, R.J. Kriek, Synthesis, spectroscopic characterization and behaviour of AC impedance spectroscopy of Cd(II) bis (N-para-methylphenyl dithiocarbamate), Electrochim. Acta 104 (2013) 19–25.

[19] T. Arfin, R. Bushra, F. Mohammad, Electrochemical sensor for the sensitive detection of o-nitrophenol using graphene oxide-poly(ethyleneimine) dendrimer-modified glassy carbon electrode, Graphene Technol. 1 (2016) 1–15.

[20] T. Arfin, F. Jabeen, R.J. Kriek, An electrochemical and theoretical comparison of ionic transport through a polystyrene based titanium-vanadium (1:2) phosphate membrane, Desalination 274 (2011) 206–211.

[21] T. Arfin, Current innovative chitosan-based water treatment of heavy metals: a sustainable approach, in: S. Ahmed, S. Kanchi, G. Kumar (Eds.), Handbook of Biopolymers: Advances and Multifaceted Applications, Pan Stanford Publishing Pte. Ltd, Singapore, 2019, pp. 167–183 (Chapter 7).

[22] T. Arfin, S. Athar, S. Rangari, Proteins and their novel applications, in: S. Ahmed, S. Kanchi, G. Kumar (Eds.), Handbook of Biopolymers: Advances and Multifaceted Applications, Pan Stanford Publishing Pte. Ltd, Singapore, 2019, pp. 75–93 (Chapter 4).

[23] T. Arfin, K. Sonawane, Bio-based materials: past to future, in: S. Ahmed (Ed.), Bio-Based Materials for Food Packaging, Springer, Singapore, 2018, pp. 1–32 (Chapter 1).

[24] T. Arfin, A. Tarannum, Polymer materials: from the past to the future, in: S. Ahmed, Annu, S. Ikram (Eds.), Green Polymeric Materials, Nova Science Publishers, New York, 2017, pp. 35–52 (Chapter 2).

[25] T. Arfin, F. Mohammad, Chemistry and structural aspects of chitosan towards biomedical, in: S. Ikram, S. Ahmed (Eds.), Natural Polymers: Derivatives, Blends and Composite, vol. 1, Nova Science Publishers, New York, 2016, pp. 265–280 (Chapter 13).

[26] T. Arfin, F. Mohammad, Dendrimer and its role for the advancement of nanotechnology and bioengineering, in: M.C. Wythers (Ed.), Advances in Materials Science Research, vol. 21, Nova Science Publishers, New York, 2015, pp. 157–174 (Chapter 7).

[27] T. Arfin, F. Mohammad, N.A. Yusof, Applications of polystyrene and its role as a base in industrial chemistry, in: C. Lynwood (Ed.), Polystyrene: Synthesis, Characteristics and Applications, Nova Science Publishers, New York, 2015, pp. 269–280 (Chapter 10).

[28] T. Arfin, A. Tarannum, Rapid determination of lead ions using polyaniline-zirconium (IV) iodate-based ion selective electrode, J. Environ. Chem. Eng. 7 (2019) 102811.

[29] T. Arfin, S.N. Rangari, Graphene oxide-ZnO nanocomposite modified electrode for the detection of phenol, Anal. Methods 10 (2018) 347–358.

[30] F. Mohammad, T. Arfin, Cytotoxic effects of polystyrene-titanium-arsenate composite in cultured H9c2 cardiomyoblasts, Bull. Environ. Contam. Toxicol. 91 (2013) 689–696.

[31] M. Callies, D. Quere, On water repellency, Soft Matter 1 (2005) 55–61.

[32] D. Oner, T.J. McCarthy, Ultrahydrophobic surfaces: effects of topography length scales on wettability, Langmuir 16 (2000) 7777–7782.

[33] X. Gao, L. Jiang, Biophysics: water-repellent legs of water striders, Nature 432 (2004) 36.

[34] Y. Si, Z. Guo, Superhydrophobic nanocoatings: from materials to fabrications and to applications, Nanoscale 7 (2015) 5922–5946.

[35] L. Feng, Y. Zhang, J. Xi, Y. Zhu, N. Wang, F. Xia, L. Jiang, Petal effect: a superhydrophobic state with high adhesive force, Langmuir 24 (2008) 4114–4119.

[36] C. Yang, U. Tartaglino, B.N. Persson, Influence of surface roughness on superhydrophobicity, Phys. Rev. Lett. 97 (2006) 116103.

[37] Y. Li, D. Quere, C. Lv, Q. Zheng, Monostable superrepellent materials, Proc. Natl. Acad. Sci. U. S. A. 114 (2017) 3387–3392.

[38] E. Huovinen, L. Takkunen, T. Korpela, M. Suvanto, T.T. Pakkanen, T.A. Pakkanen, Mechanically robust superhydrophobic polymer surfaces based on protective micropillars, Langmuir 30 (2014) 1435–1443.

[39] X. Zhang, L. Wang, E. Levanen, Superhydrophobic surfaces for the reduction of bacterial adhesion, RSC Adv. 3 (2013) 12003–12020.

[40] J. Genzer, K. Efimenko, On designing and creating long-lived superhydrophobic surfaces through mechanically assembled monolayers (MAMs), Science 290 (2000) 2130–2133.

[41] Y.T. Cheng, D.E. Rodak, C.A. Wong, C.A. Hayden, Effects of micro-and nano-structures on the self-cleaning behaviour of lotus leaves, Nanotechnology 17 (2006) 1359–1362.

[42] W. Barthlott, M. Mail, C. Neinhuis, Superhydrophobic hierarchically structured surfaces in biology: evaluation, structural principles and biomimetic applications, Phil. Trans. R. Soc. A 374 (2016) 20160191.

[43] A.B. Brennan, R.H. Baney, M.L. Carman, T.G. Estes, A.W. Feinberg, L.H. Wilson, J.F. Schumacher, Surface Topography for Non-Toxic Bioadhesion Control, US 7,143,709 B2, Dec. 5, 2006.

[44] X. Yao, L. Xu, L. Jiang, Fabrication and characterization of superhydrophobic surfaces with dynamic stability, Adv. Funct. Mater. 20 (2010) 3343–3349.

[45] E.M. Benetti, X. Sui, S. Zapotoczny, G.J. Vancso, Surface-grated gel-brush/metal nanoparticle hybrids, Adv. Funct. Mater. 20 (2010) 939–944.

[46] X. Zhao, B. Yu, J. Zhang, Transparent and durable superhydrophobic coatings for anti-bioadhesion, J. Colloid Interface Sci. 501 (2017) 222–230.

[47] J. Li, Y. Zhao, J. Hu, L. Shu, X. Shi, Anti-icing performance of a superhydrophobic PDMS/modified nano-silica hybrid coating for insulators, J. Adhes. Sci. Technol. 26 (2012) 665–679.

[48] J. Bearinger, S. Terretaz, R. Michel, N. Tirelli, H. Vogel, M. Textor, J. Hubbell, Chemisorbed poly(propylene sulphide)-based copolymers resist biomolecular interactions, Nat. Mater. 2 (2003) 259–264.

[49] S. Taylor, S. Smith, B. Windle, A. Guiseppi-Elie, Impact of surface chemistry and blocking strategies on DNA microarrays, Nucleic Acids Res. 31 (2003) e87.

[50] P. Asuri, S. Karajanagi, R. Kane, J. Dordick, Polymer–nanotube–enzyme composites as active antifouling films, Small 3 (2007) 50–53.

[51] M. Callow, R. Fletcher, The influence of flow surface energy materials on bioadhesion: a review, Int. Biodeterior. Biodegradation 34 (1994) 333–348.

[52] J. Genzer, K. Efimenko, Recent developments in superhydrophobic surfaces and their relevance to marine fouling: a review, Biofouling 22 (2006) 339–360.

[53] Y. Wu, F.I. Simonovsky, B.D. Ratner, T.A. Horbett, The role of adsorbed fibrinogen in platelet adhesion to polyurethane surfaces: a comparison of surface hydrophobicity, protein adsorption, monoclonal antibody binding, and platelet adhesion, J. Biomed. Mater. Res. A 74A (2005) 722–738.

[54] T. Sun, H. Tan, D. Han, Q. Fu, L. Jiang, No platelet can adhere-largely improved blood compatibility on nanostructured superhydrophobic surfaces, Small 1 (2005) 959–963.

[55] G. Toes, K. van Muiswinkel, W. van Oeveren, A. Suurmeijer, W. Timens, I. Stokroos, J. van den Dungen, Superhydrophobic modification fails to improve the performance of small diameter expanded polytetrafluoroethylene vascular grafts, Biomaterials 23 (2002) 255–262.

[56] L. Vroman, Effect of adsorbed proteins on the wettability of hydrophilic and hydrophobic solids, Nature 196 (1962) 476–477.

[57] J. Buijis, W. Norde, J.W.T. Lichtenbelt, Changes in the secondary structure of adsorbed IgG and F(ab)2 studied by FTIR spectroscopy, Langmuir 12 (1996) 1605–1613.

[58] P.K. Chu, J.Y. Chen, L.P. Wang, N. Huang, Plasma-surface modification of biomaterials, Mater. Sci. Eng. 36 (2002) 143–206.

[59] P. Roach, D. Farrar, C. Perry, Surface tailoring for controlled protein adsorption: effect of topography at the nanometer scale and chemistry, J. Am. Chem. Soc. 128 (2006) 3939–3945.

[60] T. Wei, M.A. Carignano, I. Szleifer, Lysozyme adsorption on polyethylene surfaces: why are long simulations needed? Langmuir 27 (2011) 12074–12081.

[61] C.P. Stallard, K.A. McDonnell, O.D. Onayemi, J.P. O'Gara, D.P. Dowing, Evaluation of protein adsorption on atmospheric plasma deposited coatings exhibiting superhydrophilic to superhydrophobic properties, Biointerphases 7 (2012) 1–12.

[62] J.A. Lichter, K.J.V. Vliet, M. Rubner, Design of antibacterial surfaces and interfaces: polyelectrolyte multilayers as a multifunctional platform, Macromolecules 42 (2009) 8573–8586.

[63] K. Poole, Mechanisms of bacterial biocide and antibiotic resistance, J. Appl. Microbiol. 92 (2002) 55S–64S.

[64] A.D. Russell, Antibiotic and biocide resistance in bacteria: introduction, J. Appl. Microbiol. 92 (2002) S1–S3.

[65] M. Yasuyuki, K. Kunihiro, S. Kurissery, N. Kanavillil, Y. Sato, Y. Kikuchi, Antibacterial properties of nine pure metals: a laboratory study using *Staphylococcus aureus* and *Escherichia coli*, Biofouling 26 (2010) 851–858.

[66] M. Rai, A. Yadav, A. Gade, Silver nanoparticles as a new generation of antimicrobials, Biotechnol. Adv. 27 (2009) 76–83.

[67] M.T. Hsiao, S.F. Chen, D.B. Shieh, C.S. Yeh, One-pot synthesis of hollow Au3Cu1 spherical-like and biomineral botallackite Cu2(OH)3Cl flowerlike architectures exhibiting antimicrobial activity, J. Phys. Chem. B 110 (2006) 205–210.

[68] C.M. Jones, E.M.V. Hoek, A review of the antibacterial effects of silver nanomaterials and potential implications for human health and the environment, J. Nanopart. Res. 12 (2010) 1531–1551.

[69] B.J. Privett, J. Youn, S.A. Hong, J. Lee, J. Han, J.H. Shin, M.H. Schoenfisch, Antibacterial fluorinated silica colloid superhydrophobic surfaces, Langmuir 27 (2011) 9579–9601.

[70] C.R. Crick, S. Ismail, J. Pratten, I.P. Parkin, An investigation into bacterial attachment to an elastomeric superhydrophobic surface prepared via aerosol assisted deposition, Thin Solid Films 519 (2011) 3722–3727.

[71] J. Ma, Y. Sun, K. Gleichauf, J. Lou, Q. Li, Nanostructure on Taro leaves fouling by colloids and bacteria under submerged conditions, Langmuir 27 (2011) 10035–10040.

[72] P. Tang, W. Zhang, Y. Wang, B. Zhang, H. Wang, C. Lin, L. Zhang, Effect of superhydrophobic surface of titanium on *Staphylococcus aureus* adhesion, J. Nanomater. 2011 (2011) 178921.

[73] I. Banerjee, R.C. Pangule, R.S. Kane, Anti-fouling coatings: recent developments in the design of surfaces that prevent fouling by proteins, bacteria, and marine organisms, Adv. Mater. 23 (2011) 690–718.

[74] C.P. Stallard, K.A. McDonnell, O.D. Onayemi, J.P. O'Gara, D.P. Dowing, Evaluation of protein adsorption on atmosphere plasma deposited coatings exhibiting superhydrophilic to superhydrophobic properties, Biointerphases 7 (2012) 31.

[75] Y. Yuan, M.P. Hays, P.R. Harwidge, J. Kim, Surface characteristics influencing bacterial adhesion to polymeric substrates, RSC Adv. 7 (2017) 14254–14261.

[76] R.S. Sabry, M.A. Al-mosawi, Novel approach to fabricate polycarbonate antibacterial superhydrophobic surfaces, J. Adhes. Sci. Technol. 31 (2017) 2424–2434.

[77] G. Feng, Y. Cheng, S.-Y. Wang, D.A.B. Tasciuc, R.W. Worobo, C.A. Moraru, Bacterial attachment and biofilm formation on surfaces are reduced by small-diameter nanoscale pores: how small is small enough? NPJ Biofilms Microbiomes (2015), 15022.

[78] G.B. Hwang, K. Page, A. Patil, S.P. Nair, E. Allan, I.P. Parkin, The anti-biofouling properties of superhydrophobic surfaces are short-lived, ACS Nano 12 (2018) 6050–6058.

[79] Y. Rahmawan, K.-J. Jang, M.-W. Moon, K.-R. Lee, Anti-biofouling coating by wrinkled, dual-roughness structures of diamond-like carbon (DLC), BioChip J. 3 (2009) 143–150.

[80] K.A. Bush, B.R. Downing, S.E. Walsh, G.D. Pins, Conjugation of extracellular matrix proteins to basal lamina analogues enhances keratinocyte attachment, J. Biomed. Mater. Res. 80 A (2006) 444–452.

[81] J.J. Norman, T.A. Desai, Methods for fabrication of nanoscale topography for tissue engineering scaffolds, Ann. Biomed. Eng. 34 (2006) 89–101.

[82] M. Kitsara, J. Ducree, Integration of functional materials and surface modification for polymeric microfluidic systems, J. Micromech. Microeng. 23 (2013) 033001.

[83] H. Lee, S.M. Dellatore, W.M. Miller, P.B. Messersmith, Mussel-inspired surface chemistry for multifunctional coatings, Science 318 (2007) 426–430.

[84] S.M. Kang, I.S. Choi, Control of cell adhesion on a superhydrophobic surface by polydopamine coating, Bull. Kor. Chem. Soc. 34 (2013) 2525–2527.

[85] R.D. Mundo, M. Nardulli, A. Milella, P. Favia, R. Agostino, R. Gristina, Cell adhesion on nanotextured slippery superhydrophobic substrates, Langmuir 27 (2011) 4919–4921.

[86] S. Zangi, I. Hejazi, J. Seyfi, E. Hejazi, H.A. Khonakdar, S.M. Davachi, Tuning cell adhesion on polymeric and nanocomposite surfaces: role of topography versus superhydrophobicity, Mater. Sci. Eng. C 63 (2016) 609–615.

[87] F. Mohammad, T. Arfin, H.A. Al-Lohedan, Enhanced biological activity and biosorption performance of trimethyl chitosan-loaded cerium oxide particles, J. Ind. Eng. Chem. 45 (2015) 33–43.

[88] T. Arfin, F. Mohammad, DC electrical conductivity of nano-composite polystyrene-titanium-arsenate membrane, J. Ind. Eng. Chem. 19 (2013) 2046–2051.

[89] T. Arfin, Rafiuddin, Metal ion transport through a polystyrene-based cobalt arsenate membrane: application of irreversible thermodynamics and theory of absolute reaction rates, Desalination 284 (2012) 100–105.

[90] F. Mohammad, T. Arfin, H.A. Al-Lohedan, Sustained drug release and electrochemical performance of ethyl cellulose-magnesium hydrogen phosphate composite, Mater. Sci. Eng. C 71 (2017) 735–743.

[91] T. Arfin, Rafiuddin, Electrochemical properties of titanium arsenate membrane, Electrochim. Acta 54 (2009) 6928–6934.

CHAPTER 8

Superhydrophobic foul resistant and self-cleaning polymer coating

Mohamed S. Selim[a,b]**, Sherif A. El-Safty**[a,c]**, Mohamed A. Shenashen**[a,b]
[a]National Institute for Materials Science (NIMS), Tsukubashi, Japan
[b]Petroleum Application Department, Egyptian Petroleum Research Institute (EPRI), Nasr City, Egypt
[c]Faculty of Engineering and Advanced Manufacturing, University of Sunderland, Sunderland, United Kingdom

1. Introduction

Biofouling is caused by abiotic and biotic dissolved materials, animals, and plants in sea-water and negatively affects immersed man-made structures [1, 2]. It causes severe ecological and economic problems for the shipping industry with nearly US$150 billion annual cost in transportation. Fouling adhesion to the hull increases the ship's frictional resistance and hydrodynamic weight and reduces its velocity [2, 3]. This phenomenon results in elevated consumption of fuel and emissions of deleterious gases to the atmosphere [4]. Much emphasis is given on the fouling prevention of ship hulls [5]. The increased global embargo and restrictions associated with the application of biocide-containing antifouling coatings resulted in the development of ecofriendly alternatives [6]. Nonstick fouling release (FR) nanocoatings represent moving targets with conformationally mobile surfaces that prevent the adhesion of fouling species. FR coating technology, including silicone compounds and fluoropolymers, prevents fouling via a self-cleaning design [7]. Silicone polymers (especially polydimethylsiloxane (PDMS)) are more effective than fluoropolymers in FR coatings [8]. Fouling attachments are not facilely released because the stiff fluorine atoms cannot rotate about in the polymeric backbone linkages [9].

PDMS-based coatings provide nontoxic, hydrophobic, high molecular mobility, fouling repellence, and heat and oxidation resistance [8]. PDMS films exhibit high smoothness, hydrophobic character, structural mobility, reduced porosity, and free energy [10]. The FR attitude of PDMSs is improved by the distribution of inorganic nanoscale fillers [11]. This technique is cost efficient for marine durable coating applications [12]. Inorganic-organic surfaces can enhance the ability of self-cleaning and FR behavior of PDMS via designing superhydrophobic surfaces. These surfaces exhibit reduced surface free energy, increased contact angle (>150 degrees), homogenous roughness, and minimized contact angle hysteresis (<10 degrees), which afford FR terminology [13]. Self-cleaning surfaces can also introduce creative solutions for innovative

FR paints [14]. Such nanocoated surface depends on chemical functionality and micro/nano binary structure of the nanocomposite coatings [15].

High superhydrophobicity and self-cleaning features were induced using metal oxide nanostructures and graphene–based materials as nanofillers in the FR nanocomposite coatings [16]. These trends introduce ecofriendly and durable alternatives to the commercial antifouling paints [17].

In this chapter, the main achievements in superhydrophobic FR and self-cleaning nanosurfaces are outlined. Environment-friendly coating techniques for fouling hindrance in the shipping industry are also demonstrated. The effects of various nanostructured materials on the efficiency of FR coatings were elicited. A comprehensive scientific approach to develop authentic green and cost-saving superhydrophobic self-cleaning nanocomposite solutions for marine antifouling problems was executed.

2. Marine biofouling

Marine biofouling is caused by various marine organisms, which can be sectioned based on their sizes, into biofilm, microfouling, and macrofouling [18, 19]. The gathering of microbial progenies on the extracellular polymeric substance material excreted by microorganisms is known as the biofilm [20, 21]. The cells of bacteria attach to the surface, divide to daughter cells, and grow and divide again [22]. Biofilm formation protects the microbial progenies against natural stresses, including osmotic shock, pH and temperature variations, desiccation, and biocides [23]. Biofilm is a complicated structure of aggregates, cells, and microbial progenies [24]. Adsorption of inorganic and organic macromolecules, such as protein and polysaccharides is the primary cause for biofilms [25, 26]. Microfouling can be divided into the following two categories [27]:

- *Primary colonization:* primary colonizers, such as diatoms and bacteria, adsorb on the biofilm through physical adhesion forces. These strains can be facilely eliminated, and thus, this adsorption is reversible.
- *Secondary colonization:* these colonizers, including protozoa and spores of macroalgae, are part of the microfilm [28, 29]. The mass of the microfilm increases nonlinearly.

Macrofouling, which can be soft or hard fouling, is of great research interest because it greatly affects the ship's drag resistance and hydrodynamic weight. Macrofouling is caused by organisms, such as animals and plants [30].

3. Fouling-related costs

Biofouling is a very costly problem, especially for the shipping industry. Billions of dollars are wasted every year because of fouling and their negative effects. More than 90% of the world trade is carried out by shipping, which represents the major facilitator for the global commerce. Fouling causes the following serious problems in maritime navigation (Fig. 1):
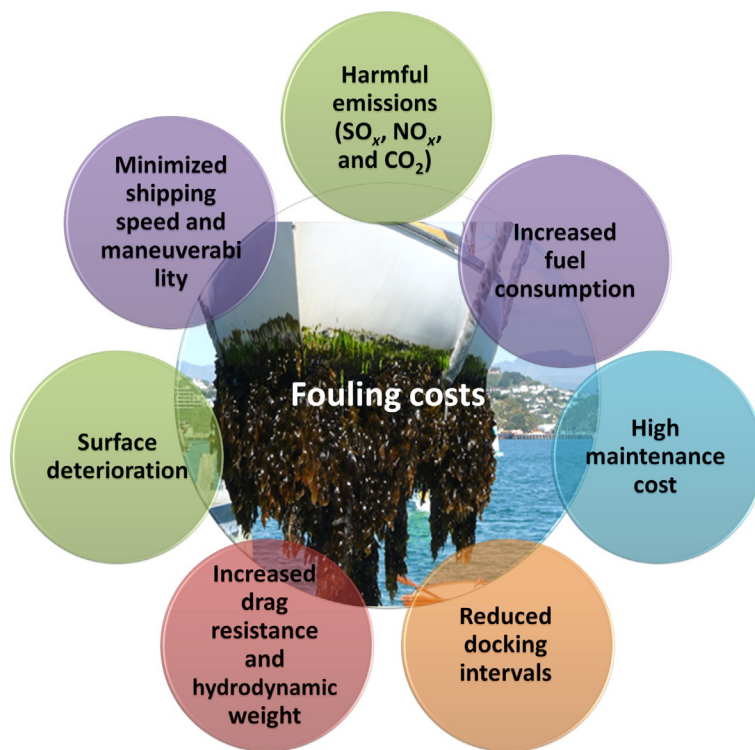
Fig. 1 Fouling costs after fouling attachments on the ship hull which cause serious problems.

- Drag resistance and hydrodynamic weight are increased by organisms' attachment to the vessels; thus, the vessel's velocity is decreased, the fuel consumption is increased, and the dry docking is shortened [31, 32].
- The corrosion of metallic surfaces is accelerated and the coating films undergo deterioration by fouling [33].
- Air pollution (CO_2, NO_x, and SO_x gases) is increased by fouling, which causes negative environmental hazards and wastes costing nearly €200 billion and kills 60,000 people annually [34].
- Conventionally, fouling settlements are prohibited through leaching biocides from the coated antifouling films; these biocides harm not only fouling organisms but also many nontarget species.
- The costs of antifouling paints amounted to about €3.5 billion in 2012 and are doubly increased in 2018 [35, 36].
- Assessing the total antifouling costs is extremely difficult because of the many parameters at play, such as physical material damage, mechanical problems, competition between biological species, and maintenance of the equipment [37].

- Using biocidal antifouling coatings yields wastewater contaminated with toxic additives. The treatment of the wastewater represents a cost parameter to remove these additives [38].

The severe environmental and cost-effective impacts induced by fouling and the defects in commercial antifouling biocides have pushed research toward ecofriendly technologies for the shipping industry [39]. Silicone FR coating technology is not a biocidal and economic solution. Thus, the surface will exhibit long-term durability resulting in a large return on investments.

4. Silicone FR coatings

In the past years, various fouling-prevention coatings were developed to address fouling growth on ship hulls. Pitch, tar, and wax were used as antifouling coatings to prevent macrofouling on marine vessels for over 2000 years [40]. In the 19th century, antifouling coatings composed of a biocide (especially tributyltin [TBT]) embedded in a polymer coating were also manufactured because of the advent of iron ships [41]. These self-polishing copolymer coatings dominate the polymer coating industry until the IMO (the International Maritime Organization of the United Nations that relates to the safety and security of shipping and the prevention of marine and air pollution by ships) banned the use of organotin compounds in 2003 considering their toxicant leaching and adverse environmental impact [42]. The ban on TBT-containing compounds prompted paint companies to develop alternative tin-free (TF) antifouling systems that can release synthetic algaecides, such as Cu^{2+}, as a replacement for TBT-containing compounds. However, the use of TF substances for fouling prevention faces critical obstacles because of environmental restrictions on copper release rates. Some algal groups are also tolerant of these compounds [43]. With the exacerbating environmental effects of biocides, environmentally friendly FR coatings were extensively investigated to inhibit fouling without toxicants [44].

FR self-cleaning coating technology is a superb alternative for fouling prohibition of the ship hulls. These FR coatings exhibit promising characteristics, including nonbiocidal properties, chemical durability, maximum speed, low fuel consumption, and prolonged fouling control, which reduces maintenance costs (Fig. 2) [45]. FR coatings were evolved in 1980 and was applied for full a fast ferry surface in 1996 to meet the needs of rapid transportation [46, 47]. The concept of developing FR surfaces was popular for over three decades. FR features are greatly demonstrated in the fluoro and silicone-based polymers [8, 47]. Fluoro-based polymeric surfaces exhibit nonporosity reduced free energy and nonstick features. However, they suffer from the limited structural mobility induced by the stiff fluorine atoms. The fluorine atoms are unable to rotate around the polymeric backbone linkages [48]. Thus, removing or release the attached organisms is not easy because of the increased modulus of elasticity and stiffness [49].

PDMS-based FR coating surfaces exhibit low free energy and modulus of elasticity, high hydrophobicity, and high resistance to the fouling cohesion physically via an
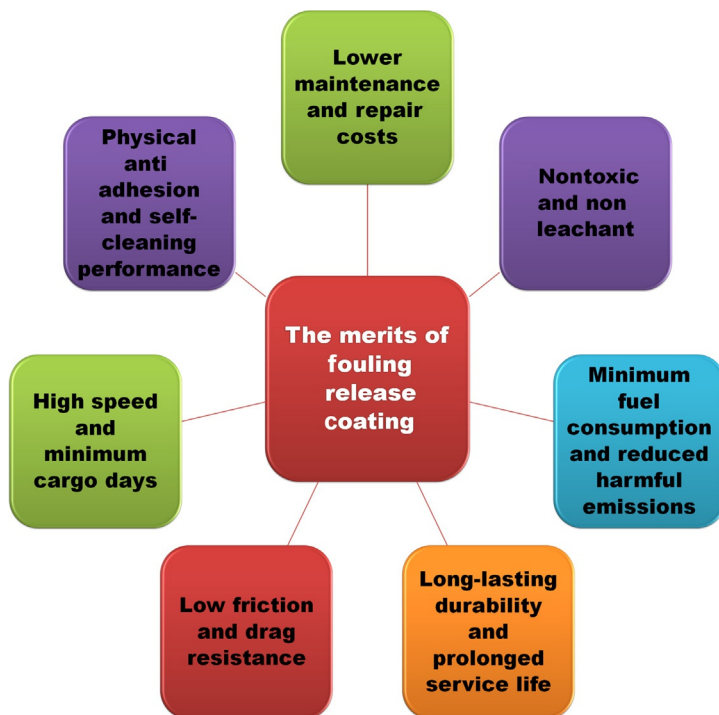
Fig. 2 The merits of FR coatings of ship hulls.

antiadhesion mechanism of the fouling organisms to the surface [50]. The siloxane back-bone bond (1.64 Å) in the PDMS structure is longer than that of the carbon—carbon bond (1.53 Å), which facilitates the rotation of the siloxane linkages. Moreover, the silox-ane angles are 143 degrees and 110 degrees (corresponding to Si—O—Si and O—Si—O, respectively) are greater than C—C—C and C—O—C angles [51]. These angles provide extreme flexibility and minimum rotational energy, low Tg (< -120 degrees) and free energy, and this condition allows the extremely mobile configuration [52, 53]. The methyl side chains have intense σ linkages, which protect the polar —Si—O— units [54]. Owing to their remarkable advantages, the silicone product market achieved 17.2 US\$2 billion in 2017 [9].

One of the main applications of silicone compounds in self-cleaning applications is based on contact angle, the surface free energy between surfaces and water droplets, and roughness measurements. However, the relationship between low surface energy and roughness remains unknown [10]. For example, Barthlott and plant surfaces stay clean because of superhydrophobicity, wherein water droplets do not cling to the surface, and droplets carry away dirt particles. The water repellency of the surface is caused by its smoothness and hydrophobic/hydrophilic properties [55].

5. Natural surfaces with superhydrophobicity

Superhydrophobic materials are used in different industrial fields, including antifouling, corrosion protection, antiicing coatings, separation of oil/water phases, and liquid–repellent textiles. Researchers and scientists developed advanced superhydrophobic surfaces by mimicking nature [56]. Many superhydrophobic surfaces are spotted in the natural world, especially the lotus leaf surface [57]. This surface is widely known as super-hydrophobic natural material, which allows drops of water to roll on the surface, thus removing dirt and debris [58]. Such superhydrophobic self-cleaning feature of lotus leaf (Fig. 3A and B) is due to the hierarchical micro/nano binary structure and the water-repellent epicuticular wax architecture formed with 20–40 μm protruding ganglion. Moreover, the leaves of taro exhibit surface micro/nanotexturing, where the microscale elliptic cusps and numerous nanoscale pins are disseminated on the surface as indicated by scanning electron microscopy (SEM) images (Fig. 3C and D). Numerous pins at the nanoscale are also disseminated on the surface, which possess a high contact angle (>159 degrees) and low sliding angle (<3 degrees) as indicated by the SEM images [59]. The rice leaf exhibits a reduced contact angle hysteresis (<10 degrees) and aniso-tropic texturing as indicated in Fig. 3E and F. Rice leaf has parallel microscale papillae
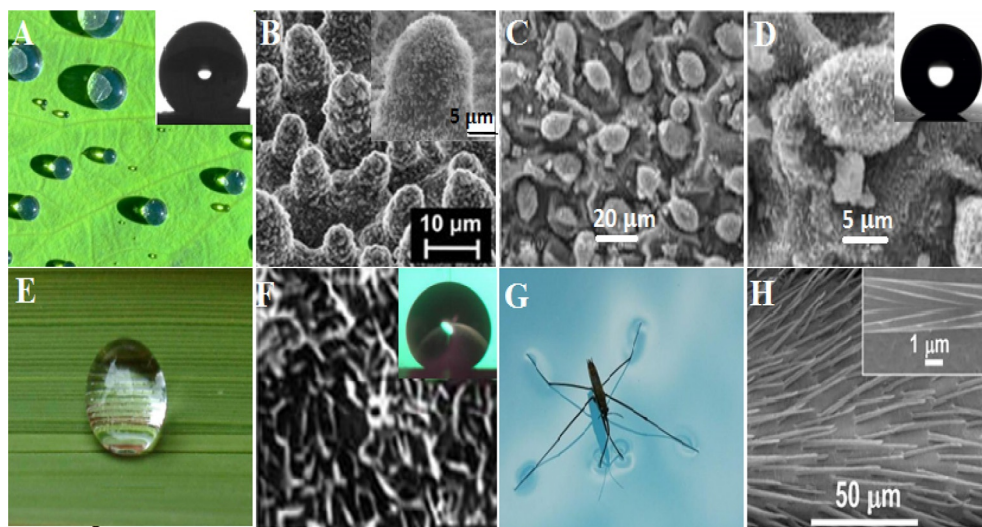
Fig. 3 (A) Superhydrophobic and self-cleaning lotus leaf (*Nelumbo nucifera*) surfaces; (B) SEM micrographs of some lotus leaf. (C) and (D) Taro leaf (Colocasia), while (E) and (F) rice leaf and its SEM image which contain longitudinal grooves with a transverse sinusoidal pattern, (G) water strider staying on the water surface, and (H) SEM image of oriented microsetae with needle shape and grooved nanostructure covering the water strider leg. *(Copyright 2007, reproduced with permission from B. Bhushan, Y.C. Jung, Natural and biomimetic artificial surfaces for superhydrophobicity, self-cleaning, low adhesion, and drag reduction, Prog. Mater. Sci. 56 (1) (2011) 1–108, Elsevier Ltd.)*

along the length of the leaf and many nanosized and numerous microscale surface pins [60]. The total water fern leaf surface is coated with wax crystals except for the terminals that have the eggbeater (capped) architecture established by the coherence of four hairs. This terminal cap exhibits slight hydrophilicity to improve air retention underwater [61, 62].

The superhydrophobic nature is also observed in many animals, such as the water striders legs, eyes of mosquito, and pigeon's feather [63, 64]. The legs of water striders have exceptional hierarchical rough structures and delicate nanogrooves. They are also responsible for their water resistance [65]. The legs' superhydrophobicity (contact angle = 167 degrees) is due to air trapping air in the surfaces' nanogrooves. This phenomenon permits the water striders to survive on the water surface (Fig. 3G and H) [66, 67]. These natural superhydrophobic surfaces are an excellent guide for researchers to design biomimetic surfaces. A superhydrophobic foam material, which mimics the respiration of plastron was developed by Shirtcliffe et al. [68]. Moreover, a bionic microrobot capable of walking on the surface of the water was introduced through mimicking the water strider by Zhang et al. [69]

6. Requirements for superhydrophobic self-cleaning coatings

6.1 Wettability of the surface

Studying the materials' surface wettability using liquids represents a key factor for applying the superhydrophobicity in different fields. When a droplet of water droplet is placed on a coating material, it gains spherical shape (antiwetting) or its surface becomes totally wet (superwetting) [70]. In this aspect, the contact angle is essential to determine the nanowettability through intersecting the liquid, solid, and gas–solid interface. Fig. 4 indicates the different shapes of the contact angle (hydrophilic, hydrophobic, and super-hydrophobicity) after dropping the liquid on a definite surface [71].
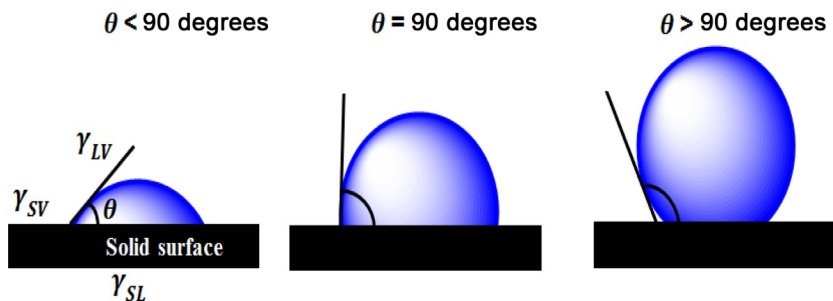
Fig. 4 Illustration of contact angles formed by sessile liquid drops on a smooth homogeneous solid surface [71].

6.2 Design of superhydrophobic surfaces

Recently, the micro/nanostructural designs of superhydrophobic surface coatings are regarded as essential. These surface materials can be applied to various industrial fields. In Germany, superhydrophobic surfaces were applied in speed cameras on highways [72]. Superhydrophobicity is controlled by surface roughness, free energy, and chemical homogeneity. Rough surfaces can entrap air in the grooves and stabilize superhydrophobicity through the Cassie–Baxter model. This air trapping will amplify surface hydrophobicity because air is a superhydrophobic material (contact angle of 180 degrees). By decreasing the free energy of a surface, the contact angle can be increased up to 120 degrees (for flat surfaces) and to 170 degrees (for rough surfaces) [73, 74].

6.2.1 Free energy of a surface

Reduction in the surface free energy is the main strategy for designing superhydrophobic surfaces. The free energy can be reduced by using a surfactant, such as the fluoroalkylsilanes, which are widely used to decrease the free energy of the surface [75, 76]. This phenomenon is caused by the presence of CF_3 and CF_2 units in the surfactant structures. However, these surfactants are expensive and have serious environmental hazards, and thus, other alternatives, such as stearic acid and polymeric materials are used [77, 78].

6.2.2 Rough structured surfaces

The fabrication of a rough surface is necessary for designing superhydrophobicity, where the air is trapped between water droplets and the roughed surface. Thus, the water drop is not in direct contact with all the points of a rough surface [76]. This air trapping will amplify surface hydrophobicity because air is a superhydrophobic material (contact angle is nearly 180 degrees). Water cannot sneak into the nanogrooves of the surfaces because of the decreased surface free energy, and water drops slip directly on the surface [78]. Top-down and bottom–up techniques were used to design uneven surfaces. The nanomaterials are used as the major ingredient in the former technique, whereas the latter uses different approaches, such as lithography and etching for surface construction [14, 79, 80]. Other techniques were developed to combine micro and nanostructures to yield superhydrophobic surfaces [81, 82].

6.2.3 Nonwetting approaches

It is necessary to discuss surface nonwettability approaches. Young's approach (1988) [83, 84] supposed that the surface is smooth topologically (not a rough). Reducing the energy variation between solid–air and solid–liquid interfaces can enhance the water contact angle values (Eq. 1).

$$Cos\ \theta = \left(\frac{\gamma_{SA} - \gamma_{SL}}{\gamma_{LA}}\right) \tag{1}$$

where the free energies (γ_{SA}, γ_{SL}, and γ_{LA}) represent those of a solid–air, solid–liquid as well as liquid–air interfaces. Young's equation supposed that the surface is smooth topologically (not a rough). From Eq. (1), the contact angle (θ) is directly proportional to the surface free energy. The Young's angle (Fig. 5A) is obtained via a thermodynamic equilibrium of the surface's free energy between liquid–solid–gas interfaces.

Different surfaces have various roughnesses which control the surface nonwettability, so most states of contact angles may not be explained by Young's approach. Wenzel approach (1936) [85] approved that the surface roughness and free energy affect its contact angle as illustrated in the following equation:

$$r(\gamma_{SA} - \gamma_{SL}) = \gamma_{LV}\ Cos\ \theta_w \tag{2}$$

where r represents the factor of nondimensional rough film and the contact angle of Wenzel is represented by θ_w, thus modified Wenzel's approach is as follow:

$$Cos\ \theta_w = rCos\ \theta \tag{3}$$

The grooves of a rough surface are filled with liquid, as discussed by this approach which is based on the homogeneity of the surface wetting (Fig. 5B). This approach cannot be applied to heterogeneous surfaces [86]. This approach is unable to discuss transforming hydrophilic (or oleophilic) surfaces to hydrophobic (or oleophobic) ones [87, 88].

For hydrophobic surfaces ($\theta > 90$ degrees), the roughness of the surface enhances the θ_w. On the other hand, for hydrophilic surfaces ($\theta < 90$ degrees), the θ_w is decreased by enhancing the surface's rough topology [89].

As a result, the Cassie–Baxter [90] model for heterogeneous surfaces (Fig. 5C) was developed and depends on two fractions:
- the first with a fractional surface area (f_1) and contact angle (θ_1) and
- the second with (f_2) and (θ_2).
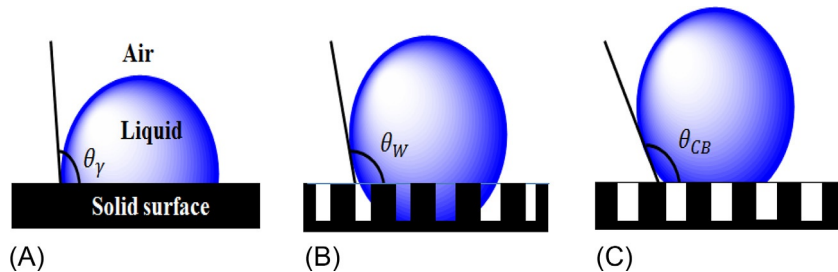
Fig. 5 Typical wetting behavior of a droplet on the solid substrates. (A) Young's model. (B) Wenzel's model. (C) Cassie-Baxter model.

The contact angle in this approach is presented in the following equation:

$$Cos\ \theta = f_1\ Cos\theta_1 + f_2\ Cos\theta_2 \tag{4}$$

where $(f_1 + f_2) = 1$.

This approach supposed that liquid contacts with the solid only at the tips of roughness which can trap air pockets and prevent water penetration to these pockets by the reduced free energy of the surface. Air is trapped between liquid and solid phases which increase the hydrophobicity of the surface. Since air is a superhydrophobic material (with a contact angle of 180 degrees), so the model assumed that θ_2 is 180 degrees and the following equation is produced.

$$Cos\ \theta_{CB} = f_s\ (Cos\theta_s + 1) - 1 \tag{5}$$

where the solid's contact angle and frictional area are expressed as θ_s and f_s. The Cassie model exhibits a higher advancing contact angle and considerably lower contact angle hysteresis than Wenzel model. Thus, the Cassie model is more general entire wetting regime than Wenzel model [89–91].

7. Superhydrophobic silicone nanocomposite coatings as FR surfaces

Surface roughness, free energy, and hydrophobicity are among the requirements to fabricate self-cleaning and superhydrophobic surfaces. PDMS nanocomposite with shark skin-like roughness showed high prohibition for various microorganisms [92]. Self-cleaning FR coating application is a fertile area to design micro/nanoscale roughness [93]. Silicone-based coatings are widely applied in the shipping industry as ecofriendly materials. Much research has concentrated on the fabrication of organic/inorganic hybrid nanocomposites. PDMS/inorganic nanofiller hybrid composites have various coating applications, especially in antifouling technology. Various nanoparticles, such as SiO_2, Al_2O_3, Fe_3O_4, titania, and graphene materials show high ability to improve the super-hydrophobicity and durability of PDMS-based coatings [94–96].

Controlling the shape, diameter, and amount of the inorganic nanomaterials can greatly influence the polymeric matrix features. Various nanomaterials (including natural sepiolite, metal oxide nanoparticles, and carbon-related materials) were used as fillers for silicone FR composite coatings [96]. Insertion of 0.1 wt% multiwall carbon nanotubes (MWCNTs) as inorganic fillers in PDMS improved FR efficiency without altering the bulk mechanical properties [97]. Incorporating natural sepiolite $Si_{12}O_{30}Mg_8(OH)_4(H_2O)_4 \cdot 8H_2O$ in a silicone matrix enhanced FR features by stabilizing the elastic modulus of the nanocomposite [94, 98]. The used sepiolite forms microchannels, which extend perpendicular to the direction of the fiber. The Si—O—Si linkages in the PDMS enable the covalent dispersion of the nanofillers. This nanocomposite prohibits the cohesion of various fouling organisms. The distribution of

low percentages of MWCNTs (0.05%) in the PDMS resin also improved the surface nonwettability and decreased the adhesion of adult barnacles on the coated surface by 50% [99]. The methyl side chains of PDMS exhibit strong CH-π interactions, and the MWCNTs possess a π-electron-rich surface, which provide the mobility of the polymer structure.

8. Hydrophobic/superhydrophobic FR nanocomposite coatings

FR coatings showed reduced fouling cohesion to the surface [98]. The recent advances in tailoring self-cleaning FR materials have concentrated on silicone nanostructured surfaces [99]. Superhydrophobic surfaces that exhibit water contact angle of >150 degrees, <10 degrees contact angle hysteresis, reduced free energy, and increased roughness are widely applied in self-cleaning and FR coating applications. Superhydrophobic PDMS coatings can be achieved by designing rough surfaces. These rough surfaces can be nanostructured, microstructured, or hierarchical micro/nanoscale structured with high contact angles and reduced free energies [100] (Fig. 6). The superhydrophobic PDMS/nanosilica hybrid composite coating may exhibit oleophobic features via modifying the nanocomposite's surface with fluoroalkylsilane surfactant. This process provides a rough surface with low free energy [101, 102]. The unparalleled morphologies and high surface area of one-dimensional (1D) nanostructured materials (including nanorods, nanowires, nanofibers, and nanotubes) enable their applications as nanofillers in FR and self-cleaning nanocomposite coatings [103]. Superhydrophobicity is produced via the functionalization of carbon nanotubes (CNTs) through poly(tetrafluoroethylene). Functionalization of the nanowires of SiC materials with perfluoroalkysilane exhibited an outstanding superhydrophobicity with surface renewability [104].

In 1990, the first artificial superhydrophobic surface was presented, and thus researchers developed numerous techniques to fabricate superhydrophobic surfaces [105]. Natural superhydrophobic surfaces do not only depend on the silicone methyl side
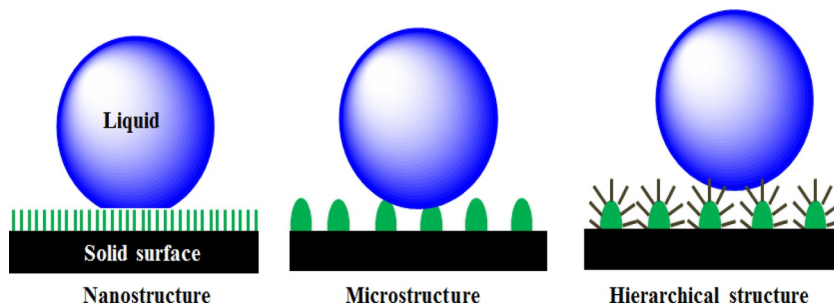
Fig. 6 Nanostructured, microstructured, and hierarchical structural surfaces of the prepared nanocomposites.

groups or the F atoms in the silicone and fluoropolymers [106]. Thus, recent developments based on the design of self–cleaning nanocomposites possess elevated nonwettability and roughness and reduced free energy [107, 108]. Advantages of controlled structures of nanomaterials help to create the rough morphology and generate additional functionalities for the superhydrophobic surfaces. Such materials are used for numerous coating applications, such as antifouling, easy-cleaning, antisticking, and anticorrosion coatings because of their desirable properties [109]. These superhydrophobic surfaces can be synthesized by electrochemical deposition, sol–gel, and plasma treatment techniques [110]. The distribution of water–repellent nanofillers in the polymeric matrix provides superhydrophobic surfaces. Several studies have introduced metal oxides and graphene-based nanomaterials in the polymer resin to develop antifouling coatings of the next generation. Synthesis functions and nanofiller percentages were introduced to control the structure-property relationship.

Different ZnO-based self–cleaning coatings were prepared through oxidizing Zn metal to form micro/nanoscale structures [111]. A nanocomposite of silicone polymer/nanomagnetite hybrid supported with aminopropyltriethoxysilane generates a superhydrophobic material (contact angle = 158.3 degrees) [112]. A micro/nanoscale composite of PDMS/$CaCO_3$ microparticles/silica nanoparticles hybrid exhibits superhydrophobic features [113]. A nanocomposite of organosilane/SiO_2 hybrid was also used as superhydrophobic coating material [114]. An in situ nanocomposite of PDMS/nanoalumina rod hybrid was fabricated to resist fouling adhesion on the ship hull (Fig. 7) [115]. Structure-property relationship was studied by dispersing different nanorod filler concentration, where the 0.5 wt% of γ-Al_2O_3 nanorods exhibited high superhydrophobicity, reduced surface free energy, and rough topology with outstanding antifouling features. An efficient FR technique was introduced by developing a nanocomposite PDMS/spherical magnetite nanoparticle (MNP) hybrid, which exhibits an elevated contact angle (153 degrees) and minimized surface free energy (13.91 mN/m) and microroughness [116] (Fig. 8).

An antifouling coating material of PDMS enriched with Ag@SiO_2 core-shell (0.5 wt%) nanocomposite was reported, and the coatings were tested in natural seawater for 90 days (Fig. 9) [117]. Solvothermal and Stöber techniques were used to control the core-shell material with an average diameter of 60 nm and {111} crystal plane, which enhanced the FR self–cleaning features with a contact angle of 156 degrees and a decreased surface energy of 11.15 mN/m. An in situ terminology was followed to prepare a fouling-resistant coating of silicone-enriched ZnO doped with SiO_2 core-shell nanocomposite (Fig. 10), which is an ecofriendly and inexpensive marine coating solution [118].

Nine et al. [119] introduced a graphene-based superhydrophobic coating material with high durability for self-cleaning applications. A self-cleaning PDMS/polystyrene/silica hybrid nanocomposite was developed through a blending technique [120].
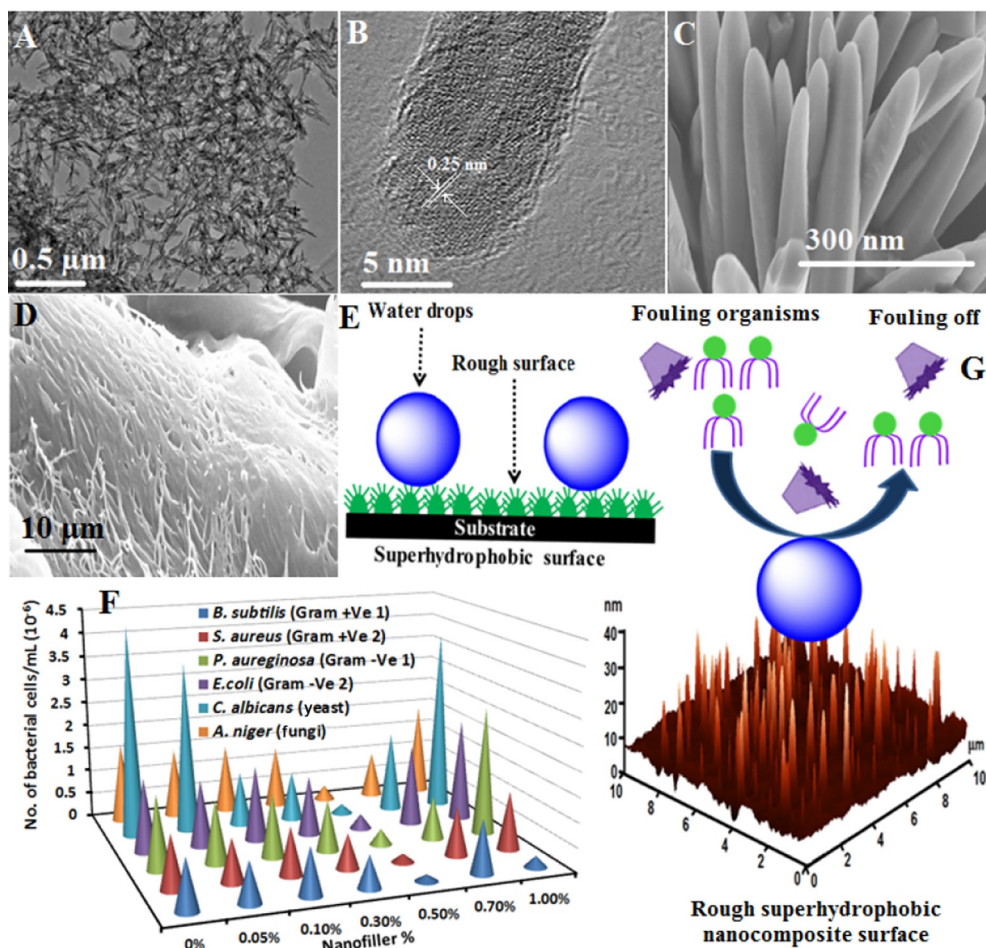
Fig. 7 (A) and (B) are the HRTEM captures of the as-synthesized γ-Al$_2$O$_3$ nanorods at different magnification powers; (C) is the FESEM images of the as-synthesized γ-Al$_2$O$_3$ nanorods; (D) is the FESEM image of PDMS/γ-Al$_2$O$_3$ nanorod composites indicates the surface roughness; (E) self-cleaning and FR coatings of the prepared silicone nanocomposite; and (F) represents the total means of bacterial counts (cells/mL) in biofilms of the nanorod composite coatings against different bacterial, yeast, and fungi strains after 28 days of incubation in broth media under light conditions. *(Copyright 2017, reproduced with permission from M.S. Selim, M.A. Shenashen, N.A. Fatthallah, A. Elmarakbi, S.A. El-Safty, In situ fabrication of one-dimensional-based lotus-like silicone/γ-Al$_2$O$_3$ nanocomposites for marine fouling release coatings. ChemistrySelect 2 (30) (2017) 9691–9700, WILEY-VCH.)*

Selim et al. [121] reported that the nanocomposite surface based on the enriched sil–icon with nanostructured ZnO nanorod was in situ manufactured for FR with unique features associated with nanometer–size textures, reduced free energy, and superhydro–phobic nature (Fig. 11). Results were verified by a tough field trial on the FR
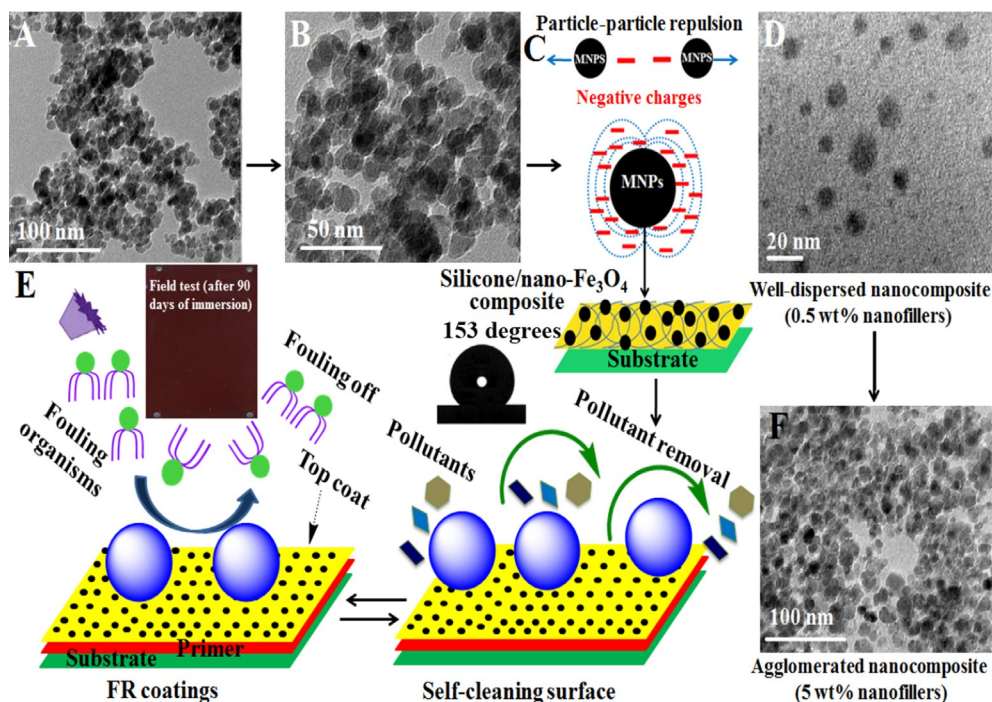
Fig. 8 (A) and (B) are the HRTEM captures of the as-synthesized magnetite nanospheres at different magnification powers; (C) nano-magnetite spheres stabilized with negatively charged citrate ions to form well-dispersed nanocomposites; (D) HRTEM of the well-dispersed PDMS/nano-magnetite (0.5 wt%); (E) FR and self-cleaning mechanism of the tailored nanocomposites; and (F) is the agglomerated nanocomposites which reduced the surface area and FR efficiency. *(Copyright 2018, reproduced with permission from M.S. Selim, A. Elmarakbi, A.M. Azzam, M.A. Shenashen, A.M. EL-Saeed, S.A. El-Safty, Eco-friendly design of superhydrophobic nano-magnetite/silicone composites for marine foul-release paints, Prog. Org. Coat. 116 (2018) 21–34, Elsevier.)*

nanocomposites for 6 months in marine water. The superhydrophobic surface was modeled by hybridizing PDMS matrix with nano–Fe_3O_4 materials [122]. Moreover, an ecofriendly and ecological solution for the negative impacts of marine fouling were addressed using a hybrid composite material using PDMS/graphene oxide–alumina as a superhydrophobic rough surface for FR coating of the ship hulls (Fig. 12) [123]. Three nanocomposites of polysiloxane/fumed nano–SiO_2 hybrids were applied as a superhydrophobic coating surface [124]. They differ in the surface rough topology, including microroughness, micro/nanoroughness, and nanoroughness. Applications based on superhydrophobic rough nanocomposites are thus promising and should be studied further because of their high diversity, characteristics, and FR coating advantages.
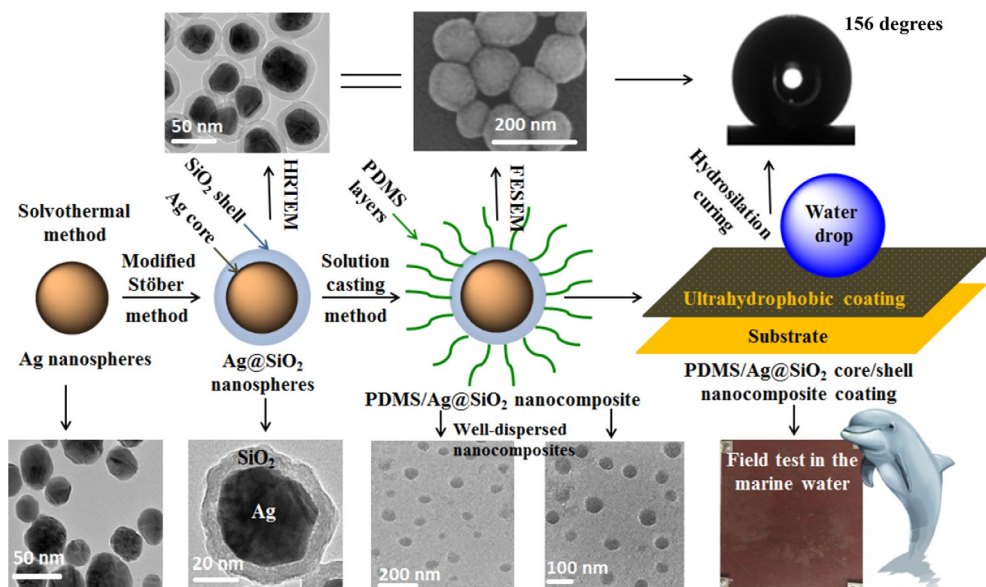
Fig. 9 Solution casting of PDMS/spherical Ag@SiO$_2$ core-shell nanocomposites and inside TEM and SEM images if Ag nanospheres, Ag@SiO$_2$ core-shell and well-dispersed PDMS/Ag@SiO$_2$ (0.5 wt%) nanocomposite film. *(Copyright 2018, reproduced with permission from M.S. Selim, H. Yang, F.Q. Wang, X. Li, Y. Huang, N.A. Fatthallah, Silicone/Ag@SiO$_2$ core–shell nanocomposite as a self-cleaning antifouling coating material, RSC Adv. 8 (2018) 9910–9921, Elsevier.)*
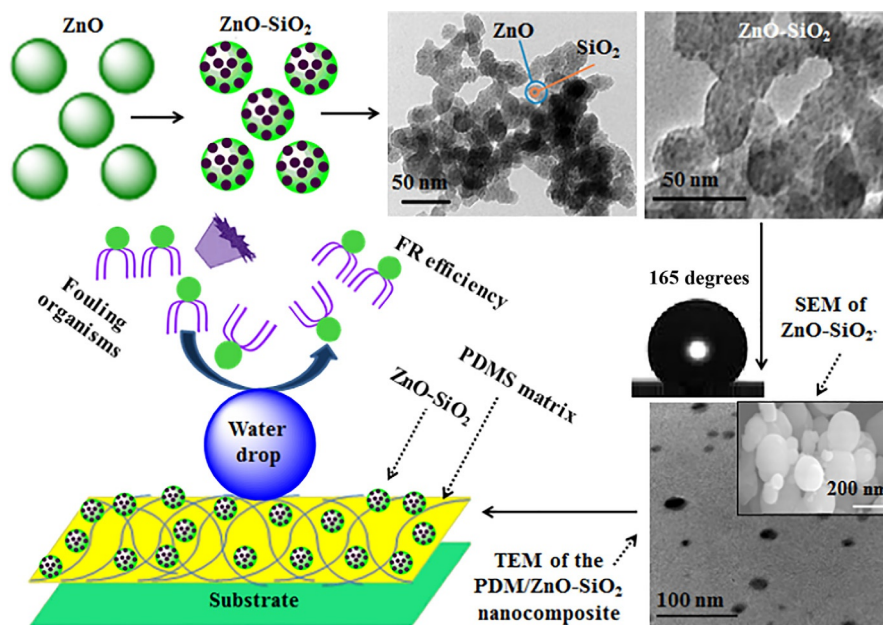
Fig. 10 In situ synthesis of PDMS/ZnO-SiO$_2$ nanocomposites and inside the TEM and SEM images of ZnO nanospheres, ZnO-SiO$_2$-doped nanoparticles and well-dispersed PDMS/ZnO-SiO$_2$ (0.5 wt%) nanocomposite film. *(Copyright 2017, reproduced with permission from M.S. Selim, M.A. Shenashen, S. Hasegawa, N.A. Fatthallah, A. Elmarakbi, S.A. El-Safty, Synthesis of ultrahydrophobic and thermally stable inorganic–organic nanocomposites for self-cleaning foul release coatings, Chem. Eng. J. 320 (2017) 653–666, Elsevier.)*
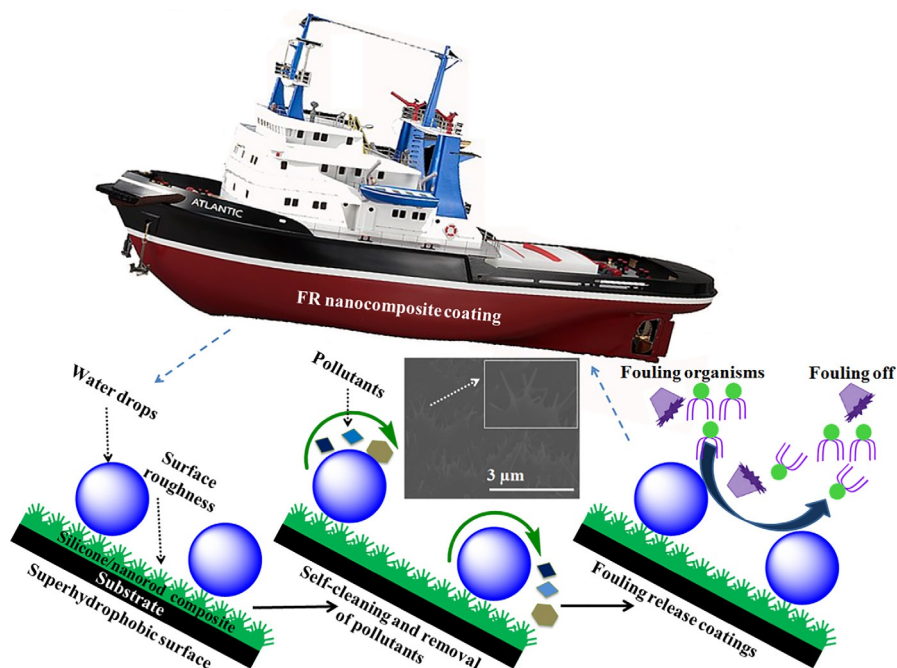
Fig. 11 The superhydrophobic, self-cleaning, and FR performance of silicone/nanorod composite surface. *(Copyright 2019, reproduced with permission from M.S. Selim, H. Yang, F.Q. Wang, N.A. Fatthallah, Y. Huang, S. Kuga, Silicone/ZnO nanorod composite coating as a marine antifouling surface, Appl. Surf. Sci. 466 (2019) 40–50, Elsevier.)*
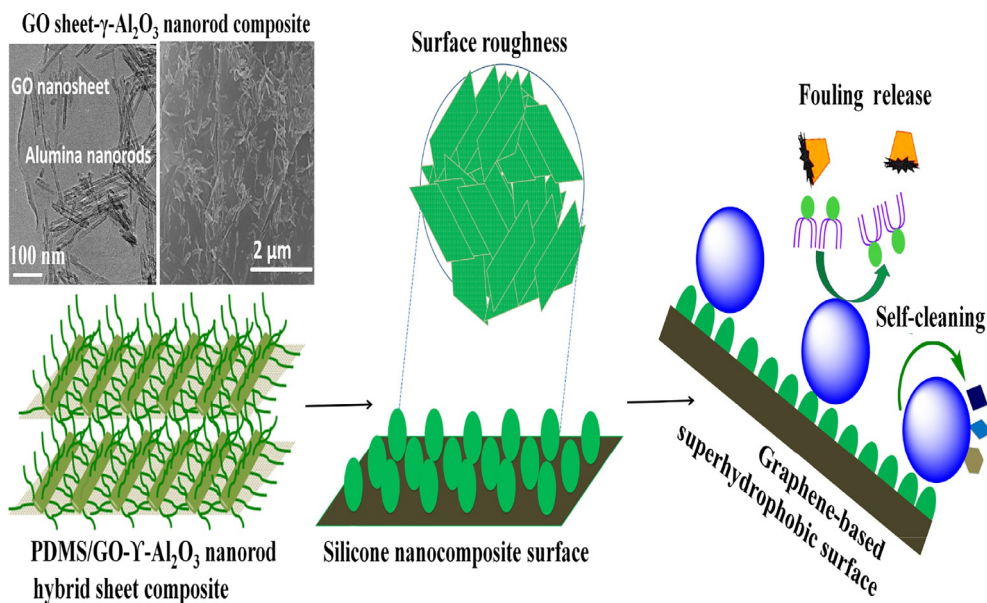
Fig. 12 Designing superhydrophobic PDMS/graphene oxide-Al₂O₃ nanorods hybrid sheet composites with self-cleaning and FR coating features. *(Copyright 2018, reproduced with permission from M.S. Selim, S.A. El-Safty, N.A. Fatthallah, M.A. Shenashen, Silicone/graphene oxide sheet-alumina nanorod ternary composite for superhydrophobic antifouling coating, Prog. Org. Coat. 121 (2018) 160–172, Elsevier.)*

9. Conclusion

Superhydrophobic nanostructured surfaces are an attractive solution for inhibiting the biofouling attachments in the shipping industry. This chapter highlights the critical aspects concerned with the applications of superhydrophobic coatings on the surface of marine ship hull to yield an ecofriendly alternative to the commercial biocidal antifouling paints. This approach has to face important aspects still representing open challenges. Superhydrophobicity produced via micro/nanoscale roughness increased fouling prevention and long-term durability. For the shipping industry, many superhydrophobic nanocomposites were fabricated and introduced to minimize the ship's drag resistance, fuel consumption, and fouling-adhesion capability. Natural superhydrophobic surfaces resulted in the development of novel self-cleaning and antifouling nanostructured materials because of their promising characteristics. Superhydrophobic FR technologies in maritime navigation offer many cost-effective and ecological merits. Superhydrophobic-based nanocomposites enjoy robust, fouling-resistance, self-cleaning, and anticorrosive properties with minimized costs. Further engineering of such nanosurfaces may provide long-term durability and improved mechanical and anticorrosive features.

Developed superhydrophobic graphene-based fouling-resistant nanocomposite materials are novel trends for antifouling application in maritime navigation. Synthesis functions and nanofiller percentages were introduced to control the structure-property relationship. The excellent distribution of nanofillers in the polymeric matrix will improve the FR and durability of the coating surface. Developed models can provide a spatial strategy for the shipping industry, where graphene-related materials yield durable FR coating with minimum maintenance cost. These trends are expected to reduce fuel consumption, maintenance cost, and docking intervals. This chapter helps in understanding the basics of designing ecofriendly fouling-resistance coatings with superhydrophobicity and self-cleaning characteristics.

References

[1] M. Lejars, A. Margaillan, C. Bressy, Fouling release coatings: a nontoxic alternative to biocidal antifouling coatings, Chem. Rev. 112 (8) (2012) 4347–4390.

[2] W.J. Yang, K.-G. Neoh, E.-T. Kang, S.L.-M. Teo, D. Rittschof, Polymer brush coatings for combating marine biofouling, Prog. Polym. Sci. 39 (2014) 1017–1042.

[3] S. Krishnan, C.J. Weinman, C.K. Ober, Advances in polymers for anti-biofouling surfaces, J. Mater. Chem. 18 (2008) 3405–3413.

[4] M.R. Detty, R. Ciriminna, F.V. Bright, M. Pagliaro, Environmentally benign sol-gel antifouling and foul-releasing coatings, Acc. Chem. Res. 47 (2) (2014) 678–687.

[5] R. Ciriminna, F.V. Bright, M. Pagliaro, Ecofriendly antifouling marine coatings, ACS Sustain. Chem. Eng. 3 (4) (2015) 559–565.

[6] (a)M.S. Selim, S.A. El-Safty, M.A. El-Sockary, A.I. Hashem, O.M. Abo Elenien, A.M. EL-Saeed, N.A. Fatthallah, Smart photo-induced silicone/TiO$_2$ nanocomposites with dominant [110]

exposed surfaces for self-cleaning foul-release coatings of ship hulls, Mater. Des. 101 (2016) 218–225. (b)M.S. Selim, S.A. El-Sockary, M.A. El-Sockary, A.I. Hashem, O.M. Abo Elenien, A.M. EL-Saeed, N.A. Fatthallah, Data on photo-nanofiller models for self-cleaning foul release coating of ship hulls, Data Brief 8 (2016) 1357–1364.

[7]   (a)C. Howell, T.L. Vu, J.J. Lin, S. Kolle, N. Juthani, E. Watson, J.C. Weaver, J. Alvarenga, J. Aizenberg, Self-replenishing vascularized fouling-release surfaces, ACS Appl. Mater. Interfaces 6 (15) (2014) 13299–13307. (b)K.V. Thomas, S. Brooks, The environmental fate and effects of anti-fouling paint biocides, Biofouling 26 (2010) 73–88.

[8]   F. Wan, X. Pei, B. Yu, Q. Ye, F. Zhou, Q. Xue, Grafting polymer brushes on biomimetic structural surfaces for anti-algae fouling and foul release, ACS Appl. Mater. Interfaces 4 (9) (2012) 4557–4565.

[9]   E. Johnston, S. Bullock, J. Uilk, P. Gatenholm, K.J. Wynne, Networks from alpha, omega-dihydroxypoly(dimethylsiloxane) and (tridecafluoro-1,1,2,2-tetrahydrooctyl) triethoxysilane: surface micro-structures and surface characterization, Macromolecules 32 (24) (1999) 8173–8182.

[10] A.F. Thünemann, R.H. Kublickas, Low surface energy polysiloxane complexes, J. Mater. Chem. 11 (2) (2001) 381–384.

[11] M.S. Selim, S.A. El-Safty, M.A. El-Sockary, A.I. Hashem, O.M. Abo Elenien, A.M. EL-Saeed, N.A. Fatthallah, Modeling of spherical silver nanoparticles in silicone-based nanocomposites for marine antifouling, RSC Adv. 5 (78) (2015) 63175–63185.

[12] A. Beigbeder, P. Degee, S.L. Conlan, R. Mutton, A.S. Clare, M.E. Pettitt, M.E. Callow, J.A. Callow, P. Dubois, Preparation and characterization of silicone-based coatings filled with carbon nanotubes and natural sepiolite and their application as marine fouling-release coatings, Biofuels 24 (4) (2008) 291–302.

[13] J. Chapman, F. Regan, Nanofunctionalized superhydrophobic antifouling coatings for environmental sensor applications—advancing deployment with answers from nature, Adv. Eng. Mater. 14 (4) (2012) B175–B184.

[14] L. Yao, J. He, Recent progress in antireflection and self-cleaning technology—from surface engineering to functional surfaces, Prog. Mater. Sci. 61 (2014) 94–143.

[15] E. Velayi, R. Norouzbeigi, Annealing temperature dependent reversible wettability switching of micro/nano structured ZnO superhydrophobic surfaces, Appl. Surf. Sci. 441 (2018) 156–164.

[16] T.M. Madkour, S. Fadl, M.M. Dardir, M.A. Mekewi, High performance nature of biodegradable polymeric nanocomposites for oil-well drilling fluids, Egypt. J. Pet. 25 (2016) 281–291.

[17] P. Buskens, M. Wouters, C. Rentrop, Z. Vroon, A brief review of environmentally benign antifouling and foul-release coatings for marine applications, J. Coat. Technol. Res. 10 (1) (2013) 29–36.

[18] C.M. Magin, S.P. Cooper, A.B. Brennan, Non-toxic antifouling strategies, Mater. Today 13 (2010) 36–44.

[19] R.F. Brady, I.S. Singer, Mechanical factors favoring release from fouling release coatings, Biofouling 15 (2000) 73–81.

[20] M.P. Schultz, J.A. Bendick, E.R. Holm, W.M. Hertel, Economic impact of biofouling on a naval surface ship, Biofouling 27 (1) (2010) 87–98.

[21] K.E. Cooksey, B. Wigglesworth-Cooksey, Adhesion of bacteria and diatoms to surfaces in the sea: a review, Aquat. Microb. Ecol. 9 (1995) 87–96.

[22] E.D. Van Hullebusch, M.H. Zandvoort, P.N.L. Lens, Metal immobilization by biofilms: mechanisms and analytical tools, Rev. Environ. Sci. Biotechnol. 2 (1) (2003) 9–33.

[23] J.-P. Maréchal, C. Hellio, Challenges for the development of new non-toxic antifouling solutions, Int. J. Mol. Sci. 10 (11) (2009) 4623–4637.

[24] S.O. Pehkonen, S. Yuan, Novel antibacterial coatings for biofouling and biocorrosion inhibition, in: S.O. Pehkonen, S. Yuan (Eds.), Interface Science and Technology, vol. 23, Elsevier, 2019, pp. 257–372 (Chapter 8).

[25] N. Bernbom, Y.Y. Ng, S. Kjelleberg, T. Harder, L. Gram, Marine bacteria from Danish coastal waters show antifouling activity against the marine fouling bacterium *Pseudoalteromonas* sp. strain S91 and zoospores of the green alga *Ulva australis* independent of bacteriocidal activity, Appl. Environ. Microbiol. 77 (24) (2011) 8557–8567.

[26] H.G. Silverman, F.F. Roberto, Understanding marine mussel adhesion, Mar. Biotechnol. 9 (2007) 661–681.

[27] S. Dash, C.L. Jin, O.O. Lee, Y. Xu, P.Y. Qian, Antibacterial and antilarval-settlement potential and metabolite profiles of novel sponge-associated marine bacteria, J. Ind. Microbiol. Biotechnol. 36 (2009) 1047–1056.

[28] V. Matranga, I. Corsi, Toxic effects of engineered nanoparticles in the marine environment: model organisms and molecular approaches, Mar. Environ. Res. 76 (2012) 32–40.

[29] C. Compere, M.N. Bellon-Fontaine, P. Bertrand, D. Costa, P. Marcus, C. Poleunis, Kinetics of conditioning layer formation on stainless steel immersed in seawater, Biofouling 17 (2001) 129–145.

[30] S. Cao, J.D. Wang, H.S. Chen, D.R. Chen, Progress of marine biofouling and antifouling technologies, Chin. Sci. Bull. 56 (2011) 598–612.

[31] S. Whalan, N.S. Webster, Sponge larval settlement cues: the role of microbial biofilms in a warming ocean, Sci. Rep. 4 (2014) 4072.

[32] D.M. Yebra, S. Kiil, K. Dam-Johansen, Antifouling technology—past, present and future steps towards efficient and environmentally friendly antifouling coatings, Prog. Org. Coat. 50 (2004) 75–104.

[33] E. Almeida, T.C. Diamantino, O. de Sousa, Marine paints: the particular case of antifouling paints, Prog. Org. Coat. 59 (2007) 2–20.

[34] L. Xue, X. Lu, H. Wei, P. Long, J. Xu, Y. Zheng, Bio-inspired self-cleaning PAAS hydrogel released coating for marine antifouling, J. Colloid Interface Sci. 421 (2014) 178–183.

[35] International Paint & Printing Ink Council, Global paint and coatings industry market analysis report (2007–2012), IPPIC, Washington, DC, 2009.

[36] W. Hintzsche, Challenges of Modern Antifoulings, Marine Coatings, Düsseldorf, Germany, 2014.

[37] T.Y. Suman, S.R. Radhika Rajasree, R. Kirubagaran, Evaluation of zinc oxide nanoparticles toxicity on marine algae Chlorella vulgaris through flow cytometric, cytotoxicity and oxidative stress analysis, Ecotoxicol. Environ. Saf. 113 (2015) 23–30.

[38] I. Cheyne, Regulation of marine antifouling in international and EC law, in: S. Dürr, J.C. Thomason (Eds.), Biofouling, Wiley-Blackwell, Chichester, 2010, , pp. 306–318.

[39] J.A. Callow, M.E. Callow, Trends in the development of environmentally friendly fouling-resistant marine coatings, Nat. Commun. 2 (2011) 244.

[40] G.G. Sankar, S. Sathya, P.S. Murthy, A. Das, R. Pandiyan, V.B. Venugopalan, M. Doble, Polydimethyl siloxane nanocomposites: their antifouling efficacy in vitro and in marine conditions, Int. Biodeterior. Biodegrad. 104 (2015) 307–314.

[41] E. Yilgor, I. Yilgor, Silicone containing copolymers: synthesis, properties and applications, Prog. Polym. Sci. 39 (2014) 1165–1195.

[42] IMO, International convention on the control of harmful antifouling systems on ships, International Maritime Organization, London, 2001/2008.

[43] S. Kiil, C.E. Weinell, M.S. Pedersen, K. Dam-Johansen, Analysis of self-polishing antifouling paints using rotary experiments and mathematical modeling, Ind. Eng. Chem. Res. 40 (18) (2001) 3906–3920.

[44] S. Kiil, C.E. Weinell, M.S. Pedersen, K. Dam-Johansen, Mathematical modelling of a self-polishing antifouling paint exposed to seawater: a parameter study, Chem. Eng. Res. Des. 80 (1) (2002) 45–52.

[45] C. Anderson, M. Atlar, M. Callow, M. Candries, A. Milne, R.L. Townsin, The development of fouling release coatings for seagoing vessels. Proceedings of the Institute of Marine Engineering, Science and Technology, 4. Part B, J. Mar. Des. Oper. B4 (2003) 11–23.

[46] J. Millett, C.D. Anderson, Fighting fast ferry fouling, in: Fast '97, Conference Papers, vol. 1, Baird Publications, Australia, 1997.

[47] R.L. Townsin, C.D. Anderson, Fouling control coatings using low surface energy, foul release technology, in: C. Hellio, D.M. Yebra (Eds.), Advances in Marine Antifouling Coatings and Technologies, Woodhead Publishing, Cambridge, 2009, , pp. 693–708.

[48] J.E. Gittens, T.J. Smith, R. Suleiman, R. Akid, Current and emerging environmentally-friendly systems for fouling control in the marine environment, Biotechnol. Adv. 31 (2013) 1738–1753.

[49] A. Tuteja, W. Choi, M. Ma, J.M. Mabbry, S.A. Mazzella, G.C. Rutledge, G.H. Mckinley, R.E. Cohen, Designing superoleophobic surfaces, Science 318 (2007) 1618–1622.

[50] J. Eliasson, Lloyd's List Event Conference: Prevention and Management of Marine Corrosion, Lloyds, London, 2003.

[51] L.D. Chambers, J.A. Wharton, R.J.K. Wood, F.C. Walsh, K.R. Stokes, Techniques for the measurement of natural product incorporation into an antifouling coating, Prog. Org. Coat. 77 (2) (2014) 473–484.

[52] R.F. Brady, Properties which influence marine fouling resistance in polymers containing silicon and fluorine, Prog. Org. Coat. 35 (1–4) (1999) 31–35.

[53] R.F. Brady, A fracture mechanical analysis of fouling release from nontoxic antifouling coatings, Prog. Org. Coat. 43 (1–3) (2001) 188–192.

[54] J.A. Mielczarski, E. Mielczarski, G. Galli, A. Morelli, E. Martinelli, E. Chiellini, The surface-segregated nanostructure of fluorinated copolymer-poly (dimethylsiloxane) blend films, Langmuir 26 (4) (2010) 2871–2876.

[55] (a)Y.-L. Zhang, H. Xia, E. Kim, H.-B. Sun, Recent developments in superhydrophobic surfaces with unique structural and functional properties, Soft Matter 8 (2012) 11217–11231. (b) H.J. Ensikat, P. Ditsche-Kuru, C. Neinhuis, W. Barthlott, Superhydrophobicity in perfection: the outstanding properties of the lotus leaf, Beilstein J. Nanotechnol. 2 (1) (2011) 152–161.

[56] P.P. Goodwyn, Y. Maezono, N. Hosoda, K. Fujisaki, Waterproof and translucent wings at the same time: problems and solutions in butterflies, Naturwissenschaften 96 (7) (2009) 781–787.

[57] X.F. Gao, L. Jiang, Biophysics: water-repellent legs of water striders, Nature 432 (2004) 36.

[58] M. Yeganeh, N. Mohammadi, Superhydrophobic surface of Mg alloys: a review, J. Magnes. Alloys 6 (1) (2018) 59–70.

[59] H. Zhang, X. Lu, Z. Xin, W. Zhang, C. Zhou, Preparation of superhydrophobic polybenzoxazine/ SiO$_2$ films with self-cleaning and ice delay properties, Prog. Org. Coat. 123 (2018) 254–260.

[60] B. Bhushan, Y.C. Jung, Natural and biomimetic artificial surfaces for superhydrophobicity, self-cleaning, low adhesion, and drag reduction, Prog. Mater. Sci. 56 (1) (2011) 1–108.

[61] H. Gundersen, H.P. Leinaas, C. Thaulow, Collembola cuticles and the three-phase line tension, Beilstein J. Nanotechnol. 8 (2017) 1714–1722.

[62] C. Liu, L. Zhu, W. Bu, Y. Liang, Superhydrophobic surfaces: from nature to biomimetic through VOF simulation, Micron 107 (2018) 94–100.

[63] (a)E. Vazirinasab, R. Jafari, G. Momen, Application of superhydrophobic coatings as a corrosion barrier: a review, Surf. Coat. Technol. 341 (2018) 40–56. (b)A.T. Abdulhussein, G.K. Kannarpady, A.B. Wright, A. Ghosh, A.S. Biris, Current trend in fabrication of complex morphologically tunable superhydrophobic nano scale surfaces, Appl. Surf. Sci. 384 (2016) 311–332.

[64] Z. Han, Z. Mu, W. Yin, W. Li, S. Niu, J. Zhang, L. Ren, Biomimetic multifunctional surfaces inspired from animals, Adv. Colloid Interf. Sci. 234 (2016) 27–50.

[65] E. Celia, T. Darmanin, D.T. de Givenchy, S. Amigoni, F. Guittard, Recent advances in designing superhydrophobic surfaces, J. Colloid Interface Sci. 402 (2013) 1–18.

[66] H. Cao, Q. Yu, R. Colby, D. Pandey, C.S. Park, J. Lian, D. Zemlyanov, I. Childres, V. Drachev, E.A. Stach, M. Hussain, H. Li, S.S. Pei, Y.P. Chen, Large-scale graphitic thin films synthesized on Ni and transferred to insulators: structural and electronic properties, J. Appl. Phys. 107 (2010) 044310–044317.

[67] D. Wang, A. Zhao, H. Sun, P. Chen, Q. He, Bio-inspired hierarchical hair arrays with tunable adhesive superhydrophobicity, Colloids Surf. A Physicochem. Eng. Asp. 538 (2018) 262–269.

[68] N.J. Shirtcliffe, G. McHale, M.I. Newton, C.C. Perry, F.B. Pyatt, Plastron properties of a superhydrophobic surface, Appl. Phys. Lett. 89 (2006) 104106.

[69] X. Zhang, J. Zhao, Q. Zhu, N. Chen, M. Zhang, Q. Pan, Bioinspired aquatic microrobot capable of walking on water surface like a water strider, ACS Appl. Mater. Interfaces 3 (2011) 2630–2636.

[70] N. Durand, D. Mariot, B. Améduri, B. Boutevin, F. Ganachaud, Tailored covalent grafting of hexafluoropropylene oxide oligomers onto silica nanoparticles: toward thermally stable, hydrophobic, and oleophobic nanocomposites, Langmuir 27 (7) (2011) 4057–4067.

[71] Y. Yuan, T.R. Lee, Contact angle and wetting properties, in: Surface Science Techniques, Springer, 2013, , pp. 3–34.

[72] M. Ma, R.M. Hill, Superhydrophobic surfaces, Curr. Opin. Colloid Interface Sci. 11 (4) (2006) 193–202.

[73] M.S. Kavale, D. Mahadik, V. Parale, P. Wagh, S.C. Gupta, A.V. Rao, H.C. Barshilia, Optically transparent, superhydrophobic methyltrimethoxysilane based silica coatings without silylating reagent, Appl. Surf. Sci. 258 (1) (2011) 158–162.

[74] R. Mohammadi, J. Wassink, A. Amirfazli, Effect of surfactants on wetting of super-hydrophobic surfaces, Langmuir 20 (22) (2004) 9657–9662.

[75] J. Genzer, K. Efimenko, Recent developments in superhydrophobic surfaces and their relevance to marine fouling: a review, Biofouling 22 (5) (2006) 339–360.

[76] T. Onda, S. Shibuichi, N. Satoh, K. Tsujii, Super-water-repellent fractal surfaces, Langmuir 12 (9) (1996) 2125–2127.

[77] S. Shibuichi, T. Onda, N. Satoh, K. Tsujii, Super water-repellent surfaces resulting from fractal structure, J. Phys. Chem. 100 (50) (1996) 19512–19517.

[78] G.B. Darband, M. Aliofkhazraei, S. Khorsand, S. Sokhanvar, A. Kaboli, Science and engineering of superhydrophobic surfaces: review of corrosion resistance, chemical and mechanical stability. Arab. J. Chem. (2018). https://doi.org/10.1016/j.arabjc.2018.01.013 (accepted manuscript).

[79] A. Rawal, S. Sharma, V. Kumar, H. Saraswat, Designing superhydrophobic disordered arrays of fibers with hierarchical roughness and low-surface-energy, Appl. Surf. Sci. 389 (2016) 469–476.

[80] A. Bake, N. Merah, A. Matin, M. Gondal, T. Qahtan, N. Abu-Dheir, Preparation of transparent and robust superhydrophobic surfaces for self-cleaning applications, Prog. Org. Coat. 122 (2018) 170–179.

[81] Y. Ouyang, J. Zhao, R. Qiu, S. Hu, Y. Zhang, P. Wang, Bioinspired superhydrophobic and oil-infused surface: which is the better choice to prevent marine biofouling, Colloids Surf. A Physicochem. Eng. Asp. 559 (2018) 297–304.

[82] R.J. Good, A thermodynamic derivation of Wenzel's modification of Young's equation for contact angles; together with a theory of hysteresis, J. Am. Chem. Soc. 74 (20) (1952) 5041–5042.

[83] T. Young, An essay on the cohesion of fluids, Philos. Trans. R. Soc. Lond. 95 (1805) 65–87.

[84] (a)N. Zhao, F. Shi, Z. Wang, X. Zhang, Combining layer-by-layer assembly with electrodeposition of silver aggregates for fabricating superhydrophobic surfaces, Langmuir 21 (10) (2005) 4713–4716. (b) N. Zhao, Q. Xie, L. Weng, S. Wang, X. Zhang, J. Xu, Superhydrophobic surface from vapor-induced phase separation of copolymer micellar solution, Macromolecules 38 (22) (2005) 8996–8999.

[85] R.N. Wenzel, Resistance of solid surfaces to wetting by water, Ind. Eng. Chem. 28 (8) (1936) 988–994.

[86] A. Marmur, Wetting on hydrophobic rough surfaces: to be heterogeneous or not to be? Langmuir 19 (20) (2003) 8343–8348.

[87] R. Blossey, Self-cleaning surfaces—virtual realities, Nat. Mater. 2 (5) (2003) 301–306.

[88] T. Darmanin, F. Guittard, Superhydrophobic and superoleophobic properties in nature, Mater. Today 18 (5) (2015) 237–285.

[89] J. Zhi, L.-Z. Zhang, Durable superhydrophobic surface with highly antireflective and self-cleaning properties for the glass covers of solar cells, Appl. Surf. Sci. 454 (2018) 239–248.

[90] A. Cassie, S. Baxter, Wettability of porous surfaces, Trans. Faraday Soc. 40 (1944) 546–551.

[91] H.Y. Erbil, C.E. Cansoy, Range of applicability of the Wenzel and Cassie–Baxter equations for super-hydrophobic surfaces, Langmuir 25 (24) (2009) 14135–14145.

[92] M. Wouters, C. Rentrop, P. Willemsen, Surface structuring and coating performance novel biocide free nanocomposite coatings with antifouling and fouling-release properties, Prog. Org. Coat. 68 (2010) 4–11.

[93] N. Roy, A.K. Bhowmick, Novel in situ polydimethylsiloxane-sepiolite nanocomposites: structure-property relationship, Polymer 51 (22) (2010) 5172–5185.

[94] (a) J. Santaren, E. Ruiz-Hitzky, Structural fluorine in sepiolite, Clay Clay Miner. 38 (1) (1990) 63–68. (b) M. Kotal, A.K. Bhowmick, Polymer nanocomposites from modified clays: recent advances and challenges, Prog. Polym. Sci. 51 (2015) 127–187.

[95] (a) E. Martinelli, M. Suffredini, G. Galli, A. Glisenti, M.E. Pettitt, M.E. Callow, J.A. Callow, D. Williams, G. Lyall, Amphiphilic block copolymer/poly (dimethylsiloxane) (PDMS) blends and

nanocomposites for improved fouling release, Biofouling 27 (5) (2011) 529–5413. (b) A. Aftab, A.R. Ismail, Z.H. Ibupoto, Enhancing the rheological properties and shale inhibition behavior of water-based mud using nanosilica, multi-walled carbon nanotube, and graphene nanoplatelet, Egypt. J. Pet. 26 (2017) 291–299.

[96] J. Rafiee, M.A. Rafiee, Z.Z. Yu, N. Koratkar, Superhydrophobic to superhydrophilic wetting control in graphene films, Adv. Mater. 22 (19) (2010) 2151–2154.

[97] C.J. Kavanagh, G.W. Swain, B.S. Kovach, J. Stein, C. Darkangelo-Wood, K. Truby, E. Holm, J. Montemarano, A. Meyer, D. Wiebe, The effects of silicone fluid additives and silicone elastomer matrices on barnacle adhesion strength, Biofouling 19 (6) (2003) 381–390.

[98] M.S. Selim, H. Yang, Y. Li, F.Q. Wang, X. Li, Y. Huang, Ceramic hyperbranched alkyd/γ-Al_2O_3 nanorods composite as a surface coating, Prog. Org. Coat. 120 (2018) 217–227.

[99] M.S. Selim, M.A. Shenashen, S.A. El-Safty, M. Sakai, S.A. Higazy, H. Isago, A. Elmarakbi, Recent progress in marine foul-release polymeric nanocomposite coatings, Prog. Mater. Sci. 87 (2017) 1–3.

[100] (a) P. Roach, N.J. Shirtcliffe, I. Michael, Progress in superhydrophobic surface development, Soft Matter 4 (2) (2008) 224–240. (b) R. Blossey, Self-cleaning surface-virtual realities, Nat. Mater. 2 (2003) 301–306. (c)M.S. Selim, S.A. El-Safty, M.A. El-Sockary, A.I. Hashem, O.M. Abo Elenien, A.M. EL-Saeed, N.A. Fatthallah, Tailored design of Cu_2O nanocube/silicone composites as efficient foul-release coatings, RSC Adv. 5 (26) (2015) 19933–19943. (d)M.S. Selim, M.A. Shenashen, A.I. Hashem, S.A. El-Safty, Linseed oil-based alkyd/Cu_2O nanocomposite coatings for surface applications, New J. Chem. 42 (2018) 10048–10058.

[101] B.J. Basu, T. Bharathidasan, C. Anandan, Superhydrophobic oleophobic PDMS-silica nanocomposite coating, Surf. Innov. 1 (1) (2013) 40–51.

[102] (a) G. Momen, M. Farzaneh, R. Jafari, Wettability behaviour of RTV silicone rubber coated on nanostructured aluminium surface, Appl. Surf. Sci. 257 (15) (2011) 6489–6493. (b) X. Huang, X. Fang, Z. Lu, S. Chen, Reinforcement of polysiloxane with superhydrophobic nano-silica, J. Mater. Sci. 44 (17) (2009) 4522–4530.

[103] J. Yuan, A.H.E. Müller, One-dimensional organic–inorganic hybrid nanomaterials, Polymer 51 (18) (2010) 4015–4036.

[104] X. Jiang, Y. Wang, T. Herricks, Y. Xia, Ethylene glycol-mediated synthesis of metal oxide nanowires, J. Mater. Chem. 14 (4) (2004) 695–703.

[105] (a) G. Wang, Z. Guo, W. Liu, Interfacial effects of superhydrophobic plant surfaces: a review, J. Bionic Eng. 11 (3) (2014) 325–345. (b) M.S. Selim, S.A. El-Safty, M.A. Shenashen, M.A. El-Sockary, O.M. Abo Elenien, A.M. EL-Saeed, Robust alkyd/exfoliated graphene oxide nanocomposite as a surface coating, Prog. Org. Coat. 126 (2019) 106–118.

[106] A. Nakajima, K. Hashimoto, T. Watanabe, Recent studies on super-hydrophobic films, Monatsh. Chem. 132 (1) (2001) 31–41.

[107] T.L. Sun, L. Feng, X.F. Gao, L. Jiang, Bioinspired surfaces with special wettability, Acc. Chem. Res. 38 (8) (2005) 644–652.

[108] D. Quere, Non-sticking drops, Rep. Prog. Phys. 68 (11) (2005) 2495–2532.

[109] M.S. Selim, F.Q. Wang, H. Yang, Y. Huang, S. Kuga, Hyperbranched alkyd/magnetite-silica nanocomposite as a coating material, Mater. Des. 135 (2017) 173–183.

[110] F. Mumm, A.T.J. van Helvoort, P. Sikoski, An easy route to superhydrophobic copper based droplet microfluidic systems, ACS Nano 3 (9) (2009) 2647–2652.

[111] J.L. Zhang, W.H. Huang, Y.C. Han, Wettability of zinc oxide surfaces with controllable structures, Langmuir 22 (7) (2006) 2946–2950.

[112] J.-Y. Shiu, C.-W. Kuo, P. Chen, C.-Y. Mou, Fabrication of tunable superhydrophobic surfaces by nanosphere lithography, Chem. Mater. 16 (4) (2004) 561–564.

[113] H. Yabu, M. Shimomura, Single-step fabrication of transparent superhydrophobic porous polymer films, Chem. Mater. 17 (21) (2005) 5231–5234.

[114] X.H. Li, Z. Cao, Z.J. Zhang, H.X. Dang, Surface modification in situ of nano-SiO_2 and its structure and tribological properties, Appl. Surf. Sci. 252 (2006) 7856–7861.

[115] M.S. Selim, M.A. Shenashen, N.A. Fatthallah, A. Elmarakbi, S.A. El-Safty, In situ fabrication of one-dimensional-based lotus-like silicone/γ-Al_2O_3 nanocomposites for marine fouling release coatings, ChemistrySelect 2 (30) (2017) 9691–9700.

[116] M.S. Selim, A. Elmarakbi, A.M. Azzam, M.A. Shenashen, A.M. EL-Saeed, S.A. El-Safty, Eco-friendly design of superhydrophobic nano-magnetite/silicone composites for marine foul-release paints, Prog. Org. Coat. 116 (2018) 21–34.

[117] M.S. Selim, H. Yang, F.Q. Wang, X. Li, Y. Huang, N.A. Fatthallah, Silicone/Ag@SiO$_2$ core–shell nanocomposite as a self-cleaning antifouling coating material, RSC Adv. 8 (2018) 9910–9921.

[118] M.S. Selim, M.A. Shenashen, S. Hasegawa, N.A. Fatthallah, A. Elmarakbi, S.A. El-Safty, Synthesis of ultrahydrophobic and thermally stable inorganic–organic nanocomposites for self-cleaning foul release coatings, Chem. Eng. J. 320 (2017) 653–666.

[119] M.J. Nine, M.A. Cole, L. Johnson, D.N.H. Tran, D. Losic, Robust superhydrophobic graphene-based composite coatings with self-cleaning and corrosion barrier properties, ACS Appl. Mater. Interfaces 7 (2015) 28482–28493.

[120] V.A. Ganesh, H.K. Raut, A.S. Nair, S. Ramakrishna, A review on self-cleaning coatings, J. Mater. Chem. 21 (2011) 16304–16322.

[121] M.S. Selim, H. Yang, F.Q. Wang, N.A. Fatthallah, Y. Huang, S. Kuga, Silicone/ZnO nanorod composite coating as a marine antifouling surface, Appl. Surf. Sci. 466 (2019) 40–50.

[122] (a) S. Munir, S.M. Shah, H. Hussain, R.A. Khan, Effect of carrier concentration on the optical band gap of TiO$_2$ nanoparticles, Mater. Des. 92 (2016) 64–72. (b) H.H. El-Maghrabi, E.A. Nada, F.S. Soliman, Y.M. Moustafa, A.E. Amin, One pot environmental friendly nanocomposite synthesis of novel TiO$_2$-nanotubes on graphene sheets as effective photocatalyst, Egypt. J. Pet. 25 (2016) 575–584.

[123] M.S. Selim, S.A. El-Safty, N.A. Fatthallah, M.A. Shenashen, Silicone/graphene oxide sheet-alumina nanorod ternary composite for superhydrophobic antifouling coating, Prog. Org. Coat. 121 (2018) 160–172.

[124] A.J. Scardino, H. Zhang, D.J. Cookson, R.N. Lamb, R. de Nys, The role of nano-roughness in anti-fouling, Biofouling 25 (8) (2009) 757–767.

CHAPTER 9

Superhydrophobic antiicing and ice-release polymer coatings

Hesam Makki, Hossein Yahyaei, Mohsen Mohseni
Department of Polymer Engineering and Color Technology, Amirkabir University of Technology, Tehran, Iran

1. Ice structure and ice formation

Understanding ice formation mechanisms on the molecular level is of great importance for designing icephobic surfaces. In other words, for designing such surfaces it is crucial to be able to delay the ice formation on the surface in the first place and remove the ice layer from the surface after having it formed. So, one needs to be aware of the morphology of the ice crystals and its relation to the chemistry and physics of the surface and then designs a surface with icephobic properties.

Among more than ten different solid forms of H_2O, only a few forms occur naturally on earth atmosphere and among them the sixfold symmetric one, that is, a hexagonal structure mostly exists [1]. Nevertheless, ice patterns, for example, snow crystals, can be categorized into more than 100 different shapes [2].

Icing usually occurs through two major paths: ice accretion from liquid water at or below the freezing point of water and frost formation from water vapor by desublimation process at supersaturated conditions [3]. In addition, ice could form on the surface as a result of precipitation of rain droplets or snowflakes by wind or it could be formed by in-cloud icing that is, freezing of small droplets of water at supercooled temperature while colliding with a very cold surface. Moreover, it is worth noting that the atmospheric condition could tremendously influence the ice formation such that the rime ice, white or opaque ice, often forms when air is trapped inside the ice as a result of precipitation mechanism by wind and a transparent glaze ice is usually made by in-cloud icing [4], see Fig. 1.

As a matter of fact, ice crystal patterns can be determined by different parameters which stem from macroscopic external forces and microscopic interfacial dynamics [5, 6]. When an external solid surface comes into play, more complications are introduced to the ice formation process. The presence of external solid surface exerts an asymmetrical external force at the interface with water molecules [7, 8], thus, ice crystal growth follows rather different patterns. Although an accurate correlation between the molecular structure of water at the interface with the solid surface and macroscopic ice patterns has not been yet fully established [6], the ice growth patterns on different solid surfaces with various surface chemistry have been studied quite extensively [6, 9, 10].

(A)   (B)
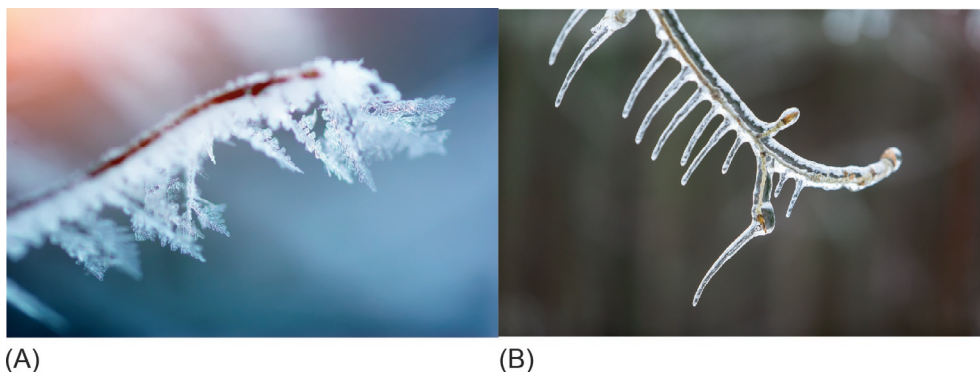
Fig. 1 (A) Rime ice and (B) glaze ice.

It has been shown that ice crystal grows off-surface on hydrophobic surfaces while the ice crystal grows along-surface on hydrophilic ones [6]. Thus, one expects that at normal condition, the ice/substrate interface area becomes larger in case of a hydrophilic substrate as compared to hydrophobic one, at least up to the point that ice crystals are isolated and the separated crystal has not overlapped. It is also showed that the roughness and temperature of the surface can significantly influence the morphology of the ice crystal. This emphasizes that although the affinity of the surface to water plays an important role in ice formation mechanisms, it is not the only determinant factor on the final morphology of the ice crystal. Moreover, after the formation of layers of ice crystal on the antiicing coatings, one might expect that it should be removed easily to obtain icephobic properties, see Section 3. It is worth emphasizing that although superhydrophobic surfaces (SHPs) have shown to be more successful in delaying formation of ice on the surface, sometimes they do not show a significant superiority over hydrophilic coatings in this respect, see Section 4.

Therefore, a better understanding of mechanisms of ice adhesion to the surface is another important issue for designing a successful antiicing coating.

2. Ice adhesion

Ice adheres to a broad range of surfaces with different natures, that is, roads, machinery components, telecommunication instruments, aircraft wings, etc. The ice-adhesion strength is a key point in icephobic systems. Therefore, in this section, first, we review some theoretical aspects of ice adhesion such as ice work of adhesion and adhesion strength and the effect of surface roughness and temperature on these properties. Then we introduce some experimental techniques to measure the adhesion between ice and different surfaces. Eventually, ice adhesion to hydrophilic and (super)hydrophobic surfaces will be reviewed.

2.1 Theoretical background

Ice adhesion, like adhesion of other materials, can be attributed to at least three main categories, that is, chemical, thermodynamic, and mechanical adhesion [11]. Other mechanisms have also been responsible for adhesion of different materials to each other; including diffusion, weak boundary layers, and electrostatic mechanisms. Adhesion of ice to metal substrates can be partially due to electrostatic interactions between ice and metals which contributes to chemical adhesion [12]. It is also shown that the van der Waals interaction between ice and substrates is not as significant as electrostatic one [13]. The mechanical adhesion is caused by much larger domains which are the micrometer porosities in which water diffuses and solidifies. The ice formed in these cavities causes adhesion by mechanically locking ice to the substrate. In addition, other mechanisms such as the formation of a quasiliquid layer can influence the ice adhesion as well [14]. This mechanism consists of the formation of a liquid–like layer at the interface that is believed to have a thickness of less than a nanometer.

In order to estimate the thermodynamic adhesion between ice and a surface, one could estimate the work of adhesion by thermodynamic relations. A drop of water on a solid surface forms an angle based on the surface tension of the solid surface. In thermodynamic equilibrium, the contact angle (CA) θ can be easily calculated based on Young's equation

$$\gamma_{\mathrm{sw}} + \gamma_{\mathrm{w}} \cos\theta = \gamma_{\mathrm{s}} \tag{1}$$

where γ_{sw} is interfacial tension between the solid surface and water, γ_{w} and γ_{s} are water and the solid surface tension, respectively. On the other hand, the thermodynamic work of adhesion reads

$$W_{\mathrm{ad}} = \gamma_{\mathrm{i}} + \gamma_{\mathrm{s}} - \gamma_{\mathrm{is}} \tag{2}$$

where γ_{i} and γ_{is} represent the surface tension of ice and interfacial tension between ice and solid. Assuming the surface tension of water and ice are more or less similar, by replacing Eq. (2) in Eq. (1), one obtains [15]

$$W_{\mathrm{ad}} = \gamma_{\mathrm{w}}(1 + \cos\theta). \tag{3}$$

Eq. (3) justifies a direct relation between the work of adhesion of ice and the substrate and the CA of water on the substrate. This implies that the work of adhesion for ice and superhydrophilic surfaces is much larger than the one for superhydrophobic ones. However, the work of adhesion only counts for the reversible component of mechanical work needed for removing ice from the surface. Moreover, the irreversible part of such work often has a much larger contribution than the reversible component such that in case of ice/steel interface, the experimental fracture energy has been measured as 1.1 N/m [16], while calculating work of adhesion from Eq. (3) gives 0.09 N/m, approximately [15]. The irreversible contribution of adhesion depends on the intermolecular

dissipative parameters. The irreversible contribution of work of adhesion becomes more influential in the case of ice adhesion due to the brittle/ductile transition of ice close to its melting point. Note that the irreversible contribution also depends on the mechanical properties of the solid surface; therefore, one can only speculate about the adhesion strength of the ice/substrate based on the affinity of the surface to water and jumping into conclusion about the strength of the adhesion based on the surface chemistry seems rather erroneous.

2.2 Influential parameters on the ice adhesion

2.2.1 Ice morphology

The adhesion of ice to a substrate can also be influenced by the morphology of the interface. In general, the true interface area between ice and substrate is not exactly the same as the apparent area due to several reasons, that is, defects at interface like micro air bubbles. If the true interface area is smaller than the apparent one, the actual adhesion strength will be less than the theoretical values. However, the opposite situation might also occur such that the true interface becomes larger than the apparent one due to the porosity or microscale roughness of the substrate. In this case, the actual adhesion becomes larger than the theoretical one. Considering the dual micro/nano roughness that most of SHPs has, the true surface area becomes significantly larger than the apparent surface area which possibly contributes to the much stronger ice adhesion as compared to the theoretical values calculated based on Eq. (3). Note that in real condition, water droplet collides to the surface with rather high speed and it penetrates to the porosities of surfaces due to its inertia and it turns to ice rapidly if the temperature is well below the freezing point of water. This also emphasizes on the fact that there could be considerably different ice-adhesion strengths to the same substrate based on the type of ice, for example, droplet accretion, and bulk-formed ice. On the other word, mechanical adhesion of ice to the substrate contributes to the adhesion strength while the mechanical locking of ice in the porosities of the surface is possible. This could explain the considerably different adhesion strengths between ice and Teflon [15] for different ice formation methods.

2.2.2 Temperature

Temperature is an important factor regarding ice-adhesion strength. It changes the mechanical properties of the ice and substrate as well as the ice/substrate interface properties. Ice shows a ductile behavior close to the freezing point and it becomes a brittle material far below this temperature. This could markedly affect the irreversible contribution of adhesion strength. Moreover, due to different thermal expansion coefficients of ice and substrate, altering temperature could dramatically change the shape of the interface between ice and the substrate. Apart from the change in material properties and interface effects of temperature, one should take it into account that changing temperature leads to change in the thickness of the liquid-like layer discussed above.

This could also explain why usually the adhesion of ice to the substrate, regardless of the substrate material, increases by decreasing temperature. To put it in a nutshell, considering so many different mechanisms that can be influenced by temperature, it is not straightforward to predict the exact change in adhesion strength as a function of temperature. However, one needs to take this effect into account while comparing the adhesion strengths of different systems. It is often suggested that ice–adhesion tests have to be taken at different temperature and the effect of temperature has to be addressed in these tests.

2.3 Experimental techniques

Based on the information given in the previous sections, ice-adhesion strength is a rather complex phenomenon such that, from the one hand, pure theoretical calculation fails to give a reliable value due to the lack of a theoretical background on this issue and on the other hand, considering the presence of so many affecting parameters, that is, material properties, temperature, type of ice formed on the surface, etc., it is difficult to keep control over all parameters at the same time to be able to obtain reliable and comparative results from normal adhesion experiments. Therefore, one has to take extra care of this complex set of parameters to tackle this problem such that controlled experiments are recommended in which all parameters but one are kept constant and effect of each affecting factors is studied one by one. It is also highly recommended not to compare the ice-adhesion strength from one type of experiment to other ones, quantitatively.

In general, there are two types of experimental techniques for ice-adhesion measurements: (1) normal stress measuring [17, 18] and (2) shear stress measuring techniques [19–21]. For the first category, a normal force to a prepared ice sample is applied and the value at break divided by the interface area between ice and the substrate will be reported as ice-adhesion strength, see Fig. 2A. For the second one, a shear force is exerted to the specimen and the force needed to slide the ice from the substrate is divided into the interface area, see Fig. 2B. It is worth noting that the centrifugal force field can also be used in order to exert shear stress to the sample, see Fig. 2C.

3. Icephobic, antiicing, and ice-release surface

Ice-confronting methods can be classified into two general categories, namely, active and passive methods [4]. Active methods consist of processes aiming for removing ice from untreated surfaces by mechanical and thermal methods or by employing chemicals such as glycol solvents. These methods have been found an inefficient and expensive process with environmentally considerable drawbacks. Therefore, passive methods have been developed in which the surface properties of the substrate are modified in such a way that it prevents, or delay, the ice formation on the substrate and/or after ice formation, it has limited adhesion to the ice by adding special features to the surface of the substrate. Therefore, generally, two major passive ice-confronting methods have been developed:
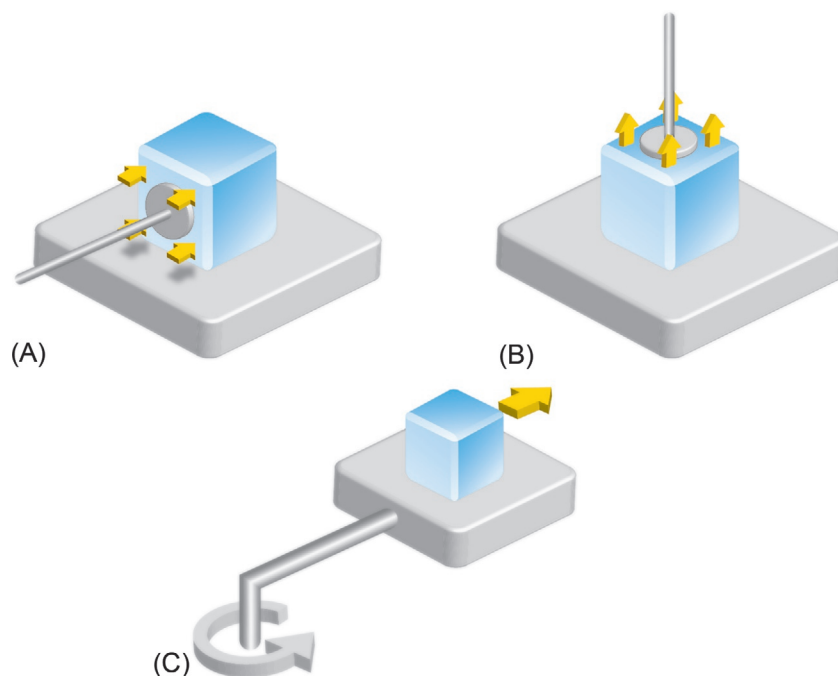
Fig. 2 A scheme of (A) normal stress (B) shear stress, and (C) centrifugal ice-adhesion strength tests.

(1) surfaces with the ability of (ideally) preventing ice formation or delaying such process and (2) surfaces with very low adhesion strength to ice [22]. The former method, which often called antiicing surface, can be classified into two approaches. The ones that prevent condensing water from coming to the surface and the ones prevent freezing of water droplets on the surface. For the second class, namely, ice-releasing or deicing coatings, despite considerable amount of research has been devoted to the field, a unique criterion for "low adhesion strength" has not been yet introduced, so that, the shear strength between 150 and 500 kPa are usually accepted [19, 23]; however, much lower values are also reported in the literature [24]. All in all, icephobic surface, in principle, can be assigned to a surface made by any passive method. However, Hejazi et al. suggest that an icephobic surface should be able to (ideally) prevent ice formation and if the ice layer is formed, the ice-adhesion strength should be weak so that the ice layer can be easily removed [22].

Based on the above classification, there should be appropriate strategies to provide icephobicity to the surface. In general, two major approaches are being employed for designing such surfaces, that is, using (super)hydrophobic or hydrophilic surfaces. As expected, SHPs are, in principle, good candidates for icephobic systems due to the water repellency feature they retain. However, there is an obvious contradictory in this regard in the literature. A group of scientists believes that SHPs can successfully delay the ice

formation better than other candidates do [25–28]. Nevertheless, another group of scientists does not consider such systems as successful antiicing ones [29, 30]. Moreover, the ice-release properties of (super)hydrophobic coatings are generally accepted among the scientist in the field [17, 18, 31–33]. Notwithstanding that, sometimes they do not show this ability efficiently in practical applications [34, 35]. All in all, rather contradictory statements found in the literature regarding the icephobicity of superhydrophobic coatings, yield to a logical demand for further elaboration on this issue. Therefore, before discussing the experimental and practical aspect of the topic, in the next section, we discuss this issue first.

4. Superhydrophobicity and icephobicity

It seems highly necessary to overview the reasons and logic of the scientists claiming either in favor or in opposition of icephobicity of superhydrophobic coatings. In other words, it is crucial to introduce what measures do different scientists use to specify if a system is icephobic or not and what conditions does each group take into consideration for their research. Anyway, it is worth emphasizing that according to the majority of research works published in the literature, the best icephobic systems are still superhydrophobic coatings even in the view of scientists who question the performance of these systems under certain conditions. However, it seems that more improvements are still needed for better performance and practical applications.

First of all, a superhydrophobic system is recognized by water CA of higher than 150 degrees and low CA hysteresis [36]. These systems mostly benefit from a nanometric surface roughness, which enhances the hydrophobic nature of them. As already mentioned in the above sections, the ability of these systems to repel water droplets made them a potential candidate for icephobic systems. However, it has been also mentioned that an acceptable icephobic surface is the one that not only delays ice formation but also if ice forms it can be easily removed from it. Therefore, apart from water/ice repellency, they need to have weak adhesion to ice.

SHPs tend to repel water. Thus, they often show very good antiicing properties such that the formation of ice on these surfaces is considerably delayed. On the other hand, Jung et al. showed that the antiicing properties do not always follow the wettability trend [29]. They showed that the scale of surface roughness, regardless of wettability, plays the major role since the molecular level rough surfaces delay the ice nucleation process for a longer time. Moreover, superhydrophobic coatings also show very low magnitudes of the reversible contribution of work of adhesion. This, as stated in the previous sections, does not guaranty weak ice-adhesion strength since the irreversible contribution of adhesion usually plays the dominant role. As a matter of fact, another dilemma arises from this contribution. The ice-release properties of superhydrophobic coatings showed to be dependent on the condition in which the ice layer formed on the surface. For instance,

the superhydrophobic coatings on which ice accretion occurred at higher relative humidity do not show weak adhesion strength to the ice [34, 35]. Moreover, it has been shown that icephobic behavior of SHPs deteriorates after several icing/deicing cycles [34]. Nosonovsky and Hejazi correspond the former observation to the size of micro cracks formed as a result of air bubbles during icing in the cavities of SHPs. As the relative humidity increases, the size of cavities becomes smaller due to the availability of water to be condensed in the cavities. So, smaller cavities lead to higher fracture energy at the ice/substrate interface.

All in all, although the SHPs are still the best candidates for passive icephobicity, there are some doubt arising about the range of application conditions in which such coatings can be used. In addition, the durability of these surfaces has not been considered very promising in such a way that after several icing/deicing cycles the icephobic performance considerably decays. It is worth noting that these drawbacks are usually related to the surface roughness of superhydrophobic systems. After all, having the theory and principals behind icephobic systems discussed, the most important case studies on this issue will be reviewed in the next section.

5. Case studies

The first case has been done by Farhadi and coworkers [34]. They prepared four different superhydrophobic samples such that sample A was containing CeO_2 with particle size less than 50 nm which was added into perfluoroalkyl methacrylic copolymer soluble in water and applied on Al alloy. For sample B, $1H,1H,2H,2H$-perfluorooctyltriethoxysilane was applied on etched aluminum. Sample C was a suspension of silver nanoparticle spin-coated on the surface followed by dip coating in a solution of perfluoroalkyl methacrylic copolymer in water and finally, sample D was a nanostructured superhydrophobic system which was prepared by adding of 3-wt% TiO_2 nanoparticles into room–temperature–vulcanized silicone rubber (RTV). They found that high surface roughness for all samples was in micro/nanoscale and due to this observation they expected that air entraps into such structures during wetting by water. They also expected that the Cassie wetting regime because of high surface roughness and low-energy top layers. Therefore, in the Cassie regime, a large amount of air entrapment in the surface irregularities on a rough hydrophobic surface leads to a very small area of the surface which is in contact with the water droplets. The water CA for samples A to D showed a range between 152 degrees and 155 degrees and hysteresis was about 5–7 degrees. However, they found a worth-noticing difference in wettability of sample in dry and wet condition. This caused shear stress of ice detachment of 150 kPa when the wet sample was iced whereas for dry sample it was 55 kPa. They concluded that using superhydrophobic coatings as icephobic system could be limited in a humid atmosphere because they lost their antiice efficiency and become, partially, icephallic.

Bharathidasan and coworkers [37] investigated icephobic properties of three types of hydrophilic, hydrophobic, and superhydrophobic coatings. Two hydrophilic coatings were polyurethane and polymethyl methacrylate coatings. Hydrophobic coatings were prepared by using 2-K silicone resin and room temperature vulcanized (RTV) silicone resin. Also, three superhydrophobic coatings were prepared as follows:

(a) Adding a hydrophilic nano-silica with particle size about 10–15 nm was added into 2-k silicone resin.

(b) Adding a hydrophilic nano-silica with particle size about 10–15 nm was added into RTV silicone resin.

(c) A hydrophobic nano-silica was added into PMMA.

The results showed that in spite of high water repellency of SHPs antiice property of hydrophobic coatings were better. The hydrophilic coatings showed the highest ice-adhesion strength. Also, ice-adhesion reduction factor (ARF) for hydrophobic coating was maximum in comparison with other hydrophilic and superhydrophobic coatings which revealed the good ice-phobic property of superhydrophobic systems. The authors have compared ice-phobic property of superhydrophobic coatings and observed that PMMA-nano-silica coating, due to higher surface energy, showed higher ice-adhesion strength. They also observed that hydrophobic and hydrophilic coatings were smooth whereas superhydrophobic coatings were rough with micro-bumps and nano-protrusions. They have concluded that a smooth surface with low surface energy is responsible for low ice-adhesion strength.

Zhang et al. [38] prepared a superhydrophobic coating by employing polybenzoxazine/SiO$_2$ which showed self-cleaning and ice delay properties. While the water CA of neat resin was 103 degrees, by incorporation of nano-silica up to 20 wt% it increased to 167 degrees and sliding angle about 5 degrees. In order to investigate ice delay properties of the coating, a water droplet (10 μL) was dropped on the surface of a sample containing 20 wt% nano-silica at −25°C to record the icing time. The same experiment was performed on the pristine glass substrate. The results showed that water droplet on the surface of the superhydrophobic coating required a longer time to form ice (386 and 247 s for superhydrophobic coating and gloss slide, respectively). The proposed mechanism for ice delay properties was that water droplet, due to the rough structure on the surface of the superhydrophobic coating, was suspended and could not completely penetrate into the surface. In this case, a three-phase interface system of solid–liquid–air was formed because of the presence of air pockets under the water droplet. The super-hydrophobicity stability of coating was checked and it was observed that the stability was sustained in the range of −25°C to 200°C for 1 h.

Wang and coworkers [39] prepared a flexible superhydrophobic (FS) coating by using poly(dimethylsiloxane) (PDMS) and zinc oxide (ZnO). They have tried to mimic the natural lotus-leaf surface and in SEM images the diameters of the papillars ranged from around 8–12 μm. In order to obtain low surface energy, FS was treated by

heptadecafluorodecyl tri–propoxy silane (FAS-17). They believed that the FS coating showed much better water repellency functions at low-temperature than natural lotus. In order to investigate the wettability of FS coating, it was put into a freezer and then some water droplets were dispensed on the surface. The temperature on the surface was controlled at $-20°C$ and humidity 90%. After 3 months, the center of the FS-surface was still dry, and the swollen ice was merely confined at the edge of the FS-surface. It was concluded that the elastic energy of the PDMS induced the rebounding of the droplet, and the ZnO nano-hairs induced a repulsive interaction between the surface and the air/water or air/ice interface.

Fu et al. [40] used Methyl triethoxysilane (MTEOS), 3-Glycidyloxypropyl tri-methoxysilane (GLYMO) and fluoroalkylsilane (FAS) to make icephobic sol-gel coatings on a glass substrate. Also, different amount of hydrophobic nano-silica was added to the coating to increase the roughness of coatings. It was observed that addition of nano-silica into the coatings increased surface roughness such that by adding 20 wt% of nano-silica, the surface roughness reached about 1.8 µm. Note that the value for the glass substrate was 0.001 µm initially. As expected, the water CA also increased as a result of elevated surface roughness (in consequence of increasing nano-silica loading). Note that the CA of the sample without FAS and 20 wt% of nano-silica was 164.4 degrees at room temperature, however, it decreased by lowering the temperature due to the condensation of water vapor on the surface. For a sample containing FAS, the CA was about 170 degrees and it also decreased slightly by decreasing temperature.

They also compared the ice adhesion of two groups of coatings containing and without FAS. It has been shown that about the similar roughness, the lower surface energy caused lower ice adhesion. It is worth emphasizing that for the sample without FAS, the ice adhesion increased by increasing roughness. However, for the sample containing FAS in which the nano-silica content has been kept constant and FAS loading increased, by increasing the amount of FAS, the surface roughness reached higher values, CA decreased, and ice adhesion also decreased. Finally, it was concluded that lower surface energy led to lower ice adhesion regardless of the roughness, while the roughness played a more complicated role. The wetting behavior of the droplet on the surface changed as temperature decreased and the antiicing performance was closely related to the antiwetting property of the surfaces at subzero temperatures.

Tang and coworkers [41], prepared superhydrophobic antiicing fluorinated sol-gel colloid coatings, used methyltriethoxysilane (MTES) and 3-[(Perfluorohexyl sulfonyl) amino]propyltriethoxysilane (HFTES) and nano-silica particle. The existing of fluori-nated groups on the surface and influence of surface roughness on the wettability and freezing delay time have been studied. Increasing of HFTES higher than 6 wt% caused excellent superhydrophobicity with CA of about 166 degrees at room temperature, but it was decreased gradually by reducing the temperature. Note that samples with high HFTES contents (above 30 wt%) exhibited special superhydrophobic and antiicing

properties under freeze temperature. It was also found that besides the surface roughness structure, the high fluoride enrichment on the surface could play a critical role in the superhydrophobicity and antiicing properties under overcooled conditions. The reason was rationalized as the more fluorinated groups covered the surface, the barrier for the transition of the surface wetting state from the Cassie-Baxter mode to the Wenzel mode was raised.

Ruan and coworkers [42] used aluminum isopropoxide and ethyl acetoacetate to fabricate rough micro–nano structures on various surfaces. Lauric acid (LA) dissolved was used as a modifier. The sample hydrophobicity and icephobicity properties were investigated by changing the rotation speed, rotation time, and coating thickness during spin-coating. The effect of the type and concentration of surface modifier used during surface hydrophobization was studied, too. The water CA was measured and the super-hydrophobic coating showed the angle about 157.6 degrees. To study icephobicity performance of the coating, water droplet was put on the surface and temperature reduced from 16.5°C to −10°C, at a cooling rate of 1.5°C/min and 1 m/s wind speed. It has been observed that the droplet on the uncoated substrate spread whereas being sphere-shaped on the coated substrate. After 14 min cooling and temperature about −4.1°C, icing began on the coated surface. However, the icing took place at a temperature of about −8.3°C and after 65 min. This has been attributed to a smaller water-solid contact area on the coated sample which was wetted in the Cassie-Baxter mode. Ice adhesion has been measured and it was reported for one droplet on the surface of the bare substrate about 0.2 and 0.1 N for superhydrophobic coating.

Wu and Chen [43] prepared a mechanically robust superhydrophobic transparent coating with self-cleaning and antiicing properties. Nano-silica, tetraethyl orthosilicate (TEOS), 3-glycidoxypropyltrimethoxysilane (GLYMO), and 1H,1H,2H,2H-perfluorooctyltriethoxysilane (PFOTES) were used in a sol–gel process and provided coatings with about 98% transparency. The time of stirring was used as the controlling parameter for dispersing of nano-silica and, in consequence, the surface roughness. The results showed that by stirring for 1 day, owing to the micro/nanostructures formed by the agglomeration of SiO_2 nanoparticles, superhydrophobic coating with water CA more than 160 degrees was obtained while increasing stirring rate reduced surface roughness and water CA. The ice-adhesion strength was as low as 58.2 kPa at −15°C and 69.5 kPa at −20°C. Despite, the ice-adhesion strength for samples without fluorine was more than 200 kPa. Also, a droplet of water on the bare glass slide started to freeze after 54.0 ± 2.6 s, whereas the superhydrophobic coated one began icing after 292 ± 4.1 s.

Zhu and coworkers [44] introducing phase-change microcapsules (PCMs). PMC was composed of melamine-formaldehyde as shell and n-dodecane and n-tetradecane with the ratio of 3:7 and 3 wt% n-hexatriacontane as the core. It was incorporated into two resin systems: RTV silicone resin containing hydrophobic nano-silica and fluoro–silicone

copolymer resin (FS). SEM images showed globular convex morphologies formed on the surface of composite coatings and the bulks become more densely distributed on the surface with an increase in the amount of PCM because of the incompatibility between PCM and RTV or FS. It has been observed that the surface roughness increased from 2.33 to 5.76 µm for RTV/PCM coatings and from 1.48 to 1.70 µm for FS/PCM coatings with the increasing content of PCM from 10% to 30%. Antiicing experiment demonstrated that the composite coating could delay icing of a water droplet on the coating surface due to the PCMs, which released a certain amount of latent heat during the temperature reduction. The ice shear strengths on RTV/PCM coating surfaces (102–132 kPa) were lower than those on FS/PCM coating surfaces (378–489 kPa), attributed to the RTV composition.

Li et al. [45] compared icephobicity of RTV silicone rubber coating and PDMS-modified nano-silica coatings. Water CA on the PDMS nanocomposite coating has been measured 161 degrees and 110 degrees for RTV. Time of ice formation was also measured on the surface of two coatings. After 10 min of exposure to cold fog, just water and few ice particles adhered to the PDMS/modified nano-silica coating, whereas ice layers and water films began to form on the RTV silicone rubber coated insulators and some small icicles appeared on their edges. After another 50 min of exposure, some discrete droplet-shaped and short strip-shaped ice started to form on the PDMS/modified nano-silica coating, whereas ice covered all the exposed surface of the RTV silicone rubber coating. It is worth noting that the ice layer on them was thicker and much more icicles formed and continued to grow on their edges. At 3 h of exposure to cold fog, ice appeared to have grown on both types of coatings. The icephobicity of PDMS/modified nano-silica coating has been attributed to the low surface energy of PDMS and multi-scale microstructure of nano-silica on the surface that cause superhydrophobicity and icephobicity.

Caldona et al. [46] used rubber modified polybenzoxazine (PBZ) and nano-silica to prepare superhydrophobic coatings with antiicing and anticorrosion properties. PBZ has been chosen due to its low surface free energy and low water absorptivity. It was observed that loading up to 35% of nano-silica could not cause enough water CA (132 degrees) to be considered as a superhydrophobic coating. However, water CA about 158 degrees was obtained by 50 wt% nano-silica. It has been attributed to the surface roughness brought about by the presence of the densely packed SiO_2 nanoparticles which has been confirmed by AFM images. The antiicing properties of coatings have been investigated by performing a series of experiments.

The first experiment involved exposure of both the bare and coated substrates in naturally occurring snow under a freezing weather temperature of $-3°C$. After 1.5 h, the bare substrate had some snow accretion, whereas the coated surface was observed to show no traces of snow accumulation. In the second experiment, a Milli-Q water droplet has been dispensed on the surface superhydrophobic coating and was placed just above

freezing liquid nitrogen until the water droplet froze. Air was blown afterward to the coating, and surprisingly after 2–3 s, the frozen droplet was carried away by air. This experiment shows that ice built up on the PRS50 surface had poor adhesion, thereby, can be easily removed by any means. This behavior has been attributed to partial Wenzel state in which water only penetrates into the microscale grooves of the rough surface but not into the nanoscale folds.

To a greater extent, they believed that these air pockets would remain trapped even under a condensing weather condition, so that, these trapped air pockets would considerably minimize the contact of ice/snow with the substrate surface and therefore significantly reducing the adhesion strength of the ice. In the third experiment, delay frost formation on the surface of superhydrophobic coating has been demonstrated. In this method, they immersed coated substrate into liquid nitrogen, took it out and dispensed droplet of water on the surface immediately. On the surface of the superhydrophobic coating, water droplets upon immediate contact with the cold surface flowed and slide off the surface before they could freeze. Whereas, on the surface of the coating with low water CA and bare substrate water immediately dropped on the inclined surfaces started freezing and sticking to the surface before they could slide. By this fact, it has been explained that because such uncoated substrates did not possess low surface energy property, water droplets would spread and maximized their contact area and adhesion with the surface. Electrochemical impedance spectroscopy has been used to study corrosion resistance of the coating. While the superhydrophobic coating showed a 1-day overall impedance value of $5 \times 10^5 \, \Omega \, cm^2$, other coatings and uncoated substrate showed much lower impedance values of about 7925 and $186 \, \Omega \, cm^2$, respectively. After a 7-day exposure time, the impedance values visibly decreased for the bare and hydrophobic coatings. Such a decrease corresponds to a reduction in resistance capability of the samples to corrosion attack. However, the superhydrophobic coating continued to display a very high impedance value, hence, demonstrating superior anticorrosion performance as well as icephobic properties.

Zuo et al. [47] tried to understand the effect of chemical composition on the antiicing properties of a nanostructured SHP. First, the surface of the glass substrate roughed by a radio frequency (RF) magnetron sputtering method. It was coated by HDTMS (a siloxane coupling agent), G502 (a partially fluorinated siloxane coupling agent), FAS-17 (a fully fluorinated siloxane coupling agent), and PDMS (polydimethylsiloxane). Four as-prepared SHP surfaces showed superhydrophobicity and water CA has been reported more than 160 degrees and sliding angle smaller than 10 degrees.

The as-prepared SHP surface which was modified with FAS-17 (SHP-FAS) demonstrated a superior antiicing/frosting performance. It was observed that approximately 56% of the entire SHP-FAS remained free of ice after spraying it for 60 min with glaze ice, and the average delay-frosting time (the time taken for the whole surface to become covered with frost) was more than 320 min at −5°C. Equivalent model analysis indicated

that ΔG, defined as the difference in free energy of the Cassie-Baxter and Wenzel states, of the SHP-FAS was much lower than the other three SHP surfaces, giving priority to Cassie state condensation and the self-transfer phenomenon helping to effectively inhibit the frosting process by delaying the ice-bridging process, which was beneficial for improving the antifrosting property.

Zhan and coworkers [48] used surface-initiated activators generated by electron transfer atom transfer radical polymerization (SI-AGET ATRP) to graft fluorinated polymer chains to silica nanoparticles. The removal of droplets efficiently was obtained based on high water CA (170.3 degrees) and small CA hysteresis less than 3 degrees. It was showed that the low-temperature water CA could postpone the freezing time from 196 to 10,054s which indicated the surface could prevent ice formation well. Also, differential scanning calorimetry (DSC) was used to measure the crystallization point of a water droplet on surfaces. It showed a good ability to lower the crystallization point and to delay the freezing time.

Yuan and coworkers [33] coated glass slides by low-density polyethylene (LDPE) in three methods. Smooth LDPE coating was applied by dissolving 1g LDPE in 100mL xylene at 120°C then applied on the substrate and solvent evaporation took place at 120°C for 2h. Superhydrophobic LDPE coating with high sliding angle was prepared by dropping the solution of LDPE in xylene on the substrate and solvent evaporated at 30°C for 10h. Superhydrophobic LDPE coating with a low sliding angle was prepared by adding NH_4HCO_3 into LDPE solution. It was applied on the substrate and solvent evaporated first for 0.5h in a dry atmosphere in the oven at 50°C and followed 2h at 30°C. The water CA of the smooth coating was only 103 degrees. It has been expressed that lower drying temperature for polymer solution increased the surface roughness of polymer coating and the corresponding water CA was increased. According to Wenzel equation, water CA increases with roughness. SEM images showed rougher surfaces and water CA has been reported at about 152 degrees. However, the water sliding angle was so high that the water droplet cannot slide off even though the LDPE coating was titled until vertical. To reduce sliding angle NH_4HCO_3 was used and lotus-leaf-like LDPE coating with water CA about 156 degrees and 1 degree sliding angle was obtained. The lotus-leaf-like behavior has been attributed to the Cassie-Baxter model and the air trapped in the pores and the LDPE.

On the surface of smooth LDPE, the coating was covered by separate water droplets at the first minute of spraying. After 5min, the ice film formed thoroughly. On the surface of superhydrophobic LDPE coating with high sliding angle, the water droplets were pinned on the surface and quickly transformed into ice and other water droplets preferred to accumulate around the original ice crystal, and the superhydrophobic LDPE coating with high sliding angle was completely covered by the ice after 7min of spraying. However, the sprayed water droplets rolled off the superhydrophobic LDPE coating with low sliding angle quickly, and no ice crystal or ice cake appeared on the superhydrophobic

LDPE coating with low sliding angle even after 60 min of spraying. Therefore, it was concluded that the ultralow water sliding angle is necessary for superhydrophobic antiicing coatings or materials.

Ding and coworkers [49] dispersed nanoparticles of TiO_2 ambient-cured fluorinated polysiloxane binder to prepare superhydrophobic self-cleaning coating with antiice properties. The excellent durability of coating in various environments was the main difference of this coating with others. While the coating without TiO_2 was smooth, as the TiO_2 content increases from 5 to 20 wt%, the surface roughness increases within the microscale range. The water CA increased by adding Tio_2 such that for 20–25 wt% content of nano-particles was higher than 160 degrees. Typical superhydrophobic coating with a WCA of as high as 168.7 degrees and a sliding angle of as low as 0.7 degrees could be achieved at 35 wt% of TiO_2. It was found that the amount of ice formed at the surface of the superhydrophobic coating containing 35 wt% TiO_2 was much lower than that at the surface of hydrophobic coating containing 10 wt% TiO_2. Furthermore, the adhesive force of ice on the superhydrophobic coatings was as low as 0.18 ± 0.07 MPa whereas on the hydrophobic coating was 0.66 ± 0.04 MPa.

Puretskiy and coworkers [50] used a polymer modified diatomite particle to fabricate antiice superhydrophobic coating. The hard inorganic DE particles form a core, which provides the shape required for superhydrophobic properties and the polymer shell provides the hydrophobicity. It was observed that the addition of polymer modified diatomite into polymers like PDMSMA increased water CA from 114 degrees to 151 degrees and created the superhydrophobic coating. The formation of liquid marbles on the surface was highly promising for the design of antiicing coatings.

Dotan et al. [51] attempted to found a relation between water wetting and ice adhesion. Polycarbonate, ultra-hydrophilic coating, hydrophobic coating based on epoxy silicone, hydrophobic coating based on fluorosilane and ultra-hydrophobic coating based on nano-morphology were prepared. It was concluded that the higher the CA the lower the ice adhesion. In the case of high CAs—hydrophobic surfaces—the adhesion of ice was weak. This unique surface was obtained using a combination of low surface energy and micro- and nano-roughness.

Dodiuk et al. [52] adopted a two-layered structure to mimic the lotus effect. Hydrophilic fumed silica was used in the inner layer to produce micrometric roughness. The outer layer of nano-metric roughness was produced using hydrophobic Fluorinated POSS. Another sample has been fabricated by mixing of these two. Ultra-hydrophobic surfaces with potential were obtained when silica and Fluorinated POSS were applied in a two-layer configuration using IPA as a solvent. In this sample, the water CA was higher than 165 degrees and sliding angle reached to 1 degree. They concluded that there is a relation between superhydrophobicity and icephobicity. Ice reduction factor has been calculated and showed that 4.4 for uncoated polycarbonate substrate and 18.3 for superhydrophobic coating.

6. Conclusion

In this chapter, after the mechanisms of ice formation and principles of icephobic systems were reviewed, the basics of ice adhesion to the substrates were established by which the mechanisms of antiicing and ice-release systems have been illustrated. It has been found that superhydrophobic systems are the most important potential candidates for icephobic systems due to the water repellency and low CA hysteresis they benefit from. In the case studies, it has been shown that these systems were mostly successful in delaying ice formation on the surface and lowering the ice-adhesion strength. So many successful examples have been reviewed as case studies; each follows different methods to make superhydrophobic coatings, for example, sol-gel systems, incorporation of inorganic nanoparticles, using hybrid nanoparticles, etc. However, some doubt has also been aroused such that superhydrophobic coatings do not show the significant icephobic abilities in all conditions and also they are not very durable to the icing/deicing cycles. As a matter of fact, the surface micro/nano roughness of such systems can be filled with water in some special conditions, such as very humid weather, and if the temperature is very low, ice forms in the cavities which is responsible for a significant magnitude of mechanical adhesion through locking ice to the porosities of such surfaces. All in all, superhydrophobic coatings are the leading candidates for passive icephobic applications so far and maintaining superhydrophobic nature of them and, at the same time, decreasing the surface roughness of such systems could significantly enhance the ability of them in practical ice-confronting applications.

References

[1] T. Konrad, S. Nie, Formation of hexagonal and cubic ice during low-temperature growth, Proc. Natl. Acad. Sci. 110 (29) (2013) 11757–11762.
[2] K. Katsuhiro, et al., A global classification of snow crystals, ice crystals, and solid precipitation based on observations from middle latitudes to polar regions, Atmos. Res. 132 (2013) 460–472.
[3] K.K. Varanasi, et al., Frost formation and ice adhesion on superhydrophobic surfaces, Appl. Phys. Lett. 97 (23) (2010) 234102.
[4] G. Heydari, Toward Anti-Icing and De-Icing Surfaces: Effects of Surface Topography and Temperature, (Doctoral thesis), KTH Royal Institute of Technology, 2016.
[5] E. Ben-Jacob, P. Garik, The formation of patterns in non-equilibrium growth, Nature 343 (6258) (1990) 523.
[6] J. Liu, et al., Distinct ice patterns on solid surfaces with various wettabilities, Proc. Natl. Acad. Sci. 114 (43) (2017) 11285–11290.
[7] O. Björneholm, et al., Water at interfaces, Chem. Rev. 116 (13) (2016) 7698–7726.
[8] A. Verdaguer, et al., Molecular structure of water at interfaces: wetting at the nanometer scale, Chem. Rev. 106 (4) (2006) 1478–1510.
[9] G. Algara-Siller, et al., Square ice in graphene nanocapillaries, Nature 519 (7544) (2015) 443.
[10] A. Michaelides, K.J.N.m. Morgenstern, Ice nanoclusters at hydrophobic metal surfaces, Nat. Mater. 6 (8) (2007) 597.
[11] Z. Ghalmi, et al., Theoretical studies and quantification of ice adhesion mechanisms, in: Proceeding of the 13th International Workshop on Atmospheric Icing of Structures, IWAIS, Andermatt, 2009.

[12] V.F. Petrenko, et al., Surface states of charge carriers and electrical properties of the surface layer of ice, J. Phys. Chem. B 101 (32) (1997) 6285–6289.
[13] L.A. Wilen, et al., Dispersion-force effects in interfacial premelting of ice, Phys. Rev. B 52 (16) (1995) 12426.
[14] N.H. Fletcher, Surface structure of water and ice, Philos. Mag. 7 (74) (1962) 255–269.
[15] L. Makkonen, Ice adhesion—theory, measurements and countermeasures, J. Adhes. Sci. Technol. 26 (4–5) (2012) 413–445.
[16] Y. Wei, et al., Ice/metal interfaces: fracture energy and fractography, J. Mater. Sci. 31 (4) (1996) 943–947.
[17] F. Wang, et al., Ice adhesion on different microstructure superhydrophobic aluminum surfaces, J. Adhes. Sci. Technol. 27 (1) (2013) 58–67.
[18] D.K. Sarkar, M. Farzaneh, Superhydrophobic coatings with reduced ice adhesion, J. Adhes. Sci. Technol. 23 (9) (2009) 1215–1237.
[19] A.J. Meuler, et al., Relationships between water wettability and ice adhesion, ACS Appl. Mater. Interfaces 2 (11) (2010) 3100–3110.
[20] C. Laforte, J.L. Laforte, Deicing strains and stresses of iced substrates, J. Adhes. Sci. Technol. 26 (4–5) (2012) 603–620.
[21] S.A. Kulinich, M. Farzaneh, On ice-releasing properties of rough hydrophobic coatings, Cold Reg. Sci. Technol. 65 (1) (2011) 60–64.
[22] A. Hejazi, et al., From superhydrophobicity to icephobicity: forces and interaction analysis, Sci. Rep. 3 (2013) 2194.
[23] R. Menini, M. Farzaneh, Elaboration of Al2O3/PTFE icephobic coatings for protecting aluminum surfaces, Surf. Coat. Technol. 203 (14) (2009) 1941–1946.
[24] K. Philseok, et al., Liquid-infused nanostructured surfaces with extreme anti-ice and anti-frost performance, ACS Nano 6 (8) (2012) 6569–6577.
[25] F. Arianpour, et al., Hydrophobic and ice-retarding properties of doped silicone rubber coatings, Appl. Surf. Sci. 265 (2013) 546–552.
[26] H. Wang, et al., Effects of nano-fluorocarbon coating on icing, Appl. Surf. Sci. 258 (18) (2012) 7219–7224.
[27] C. Liangliang, et al., Anti-icing superhydrophobic coatings, Langmuir 25 (21) (2009) 12444–12448.
[28] A. Alizadeh, et al., Dynamics of ice nucleation on water repellent surfaces, Langmuir 28 (6) (2012) 3180–3186.
[29] S. Jung, et al., Are superhydrophobic surfaces best for icephobicity? Langmuir 27 (6) (2011) 3059–3066.
[30] L. Yin, et al., In situ investigation of ice formation on surfaces with representative wettability, Appl. Surf. Sci. 256 (22) (2010) 6764–6769.
[31] L. Mishchenko, et al., Design of ice-free nanostructured surfaces based on repulsion of impacting water droplets, ACS Nano 4 (12) (2010) 7699–7707.
[32] S. Kulinich, M. Farzaneh, Ice adhesion on super-hydrophobic surfaces, Appl. Surf. Sci. 255 (18) (2009) 8153–8157.
[33] Z. Yuan, et al., Preparation and anti-icing property of a lotus-leaf-like superhydrophobic low–density polyethylene coating with low sliding angle, Polym. Eng. Sci. 52 (11) (2012) 2310–2315.
[34] S. Farhadi, et al., Anti-icing performance of superhydrophobic surfaces, Appl. Surf. Sci. 257 (14) (2011) 6264–6269.
[35] M. Nosonovsky, V. Hejazi, Why superhydrophobic surfaces are not always icephobic, ACS Nano 6 (10) (2012) 8488–8491.
[36] M. Minglin, R.M. Hill, Superhydrophobic surfaces, Curr. Opin. Colloid Interface Sci. 11 (4) (2006) 193–202.
[37] T. Bharathidasan, et al., Effect of wettability and surface roughness on ice-adhesion strength of hydrophilic, hydrophobic and superhydrophobic surfaces, Appl. Surf. Sci. 314 (2014) 241–250.
[38] H. Zhang, et al., Preparation of superhydrophobic polybenzoxazine/SiO2 films with self-cleaning and ice delay properties, Prog. Org. Coat. 123 (2018) 254–260.
[39] L. Wang, et al., Robust anti-icing performance of a flexible superhydrophobic surface, Adv. Mater. 28 (2016) 7729–7735.

[40] Q. Fu, et al., Development of sol-gel icephobic coatings: effect of surface roughness and surface energy, ACS Appl. Mater. Interfaces 6 (2014) 20685–20692.

[41] Y. Tang, et al., Superhydrophobic and anti-icing properties under overcooled temperature of fluorinated hybrid surface prepared via sol-gel process, Soft Matter 11 (2015) 4540–4550.

[42] M. Ruan, et al., Superhydrophobic and anti-icing properties of sol–gel prepared alumina coatings, Russ. J. Non-Ferrous Met. 57 (2016) 638–645.

[43] X. Wu, Z. Chen, A mechanically robust transparent coating for anti-icing and self-cleaning applications, J. Mater. Chem. A 6 (2018) 16043–16052.

[44] K. Zhu, et al., Improvement of anti-icing properties of low surface energy coatings by introducing phase-change microcapsules, Polym. Eng. Sci. 58 (2018) 973–979.

[45] J. Li, et al., Anti-icing performance of a superhydrophobic PDMS/modified nano-silica hybrid coating for insulators, J. Adhes. Sci. Technol. 26 (2012) 665–679.

[46] E.B. Caldona, et al., Superhydrophobic rubber-modified polybenzoxazine/SiO2 nanocomposite coating with anti-corrosion, anti-ice, and superoleophilicity properties, Ind. Eng. Chem. Res. 56 (2017) 1485–1497.

[47] Z. Zuo, et al., Improving the anti-icing/frosting property of a nanostructured superhydrophobic surface by the optimum selection of a surface modifier, RSC Adv. 8 (2018) 19906–19916.

[48] X. Zhan, et al., A novel superhydrophobic hybrid nanocomposite material prepared by surface-initiated AGET ATRP and its anti-icing properties, J. Mater. Chem. A 2 (2014) 9390–9399.

[49] X. Ding, et al., A facile and large-area fabrication method of superhydrophobic self-cleaning fluorinated polysiloxane/TiO$_2$ nanocomposite coatings with long-term durability, J. Mater. Chem. 21 (2011) 6161–6164.

[50] N. Puretskiy, et al., Anti-icing superhydrophobic surfaces based on core-shell fossil particles, Adv. Mater. Interfaces 2 (2015) 1500124–1500130.

[51] A. Dotan, et al., The relationship between water wetting and ice adhesion, J. Adhes. Sci. Technol. 23 (2009) 1907–1915.

[52] H. Dodiuk, et al., Do self-cleaning surfaces repel ice? J. Adhes. Sci. Technol. 26 (2012) 701–714.

CHAPTER 10

Superhydrophobic corrosion inhibition polymer coatings

Prakash M. Gore, Sabarish Balakrishnan, Balasubramanian Kandasubramanian
Department of Metallurgical & Materials Engineering, Defence Institute of Advanced Technology (DU), Ministry of Defence, Pune, India

1. Introduction

Surfaces exhibiting superhydrophobicity are widely observed in nature, for example, lotus leaf; insect legs, for example, water strider; and wings, for example, cicada [1]. These surfaces do not get wet by water, as they create high contact angle exceeding 150 degrees. Upon slight inclination, the water droplets roll–off instantly, and remove any dirt on their surfaces, that is, self-cleaning. The surfaces showing contact angle from 0 to 90 degrees exhibit hydrophilicity, from 90 to 150 degrees it exhibits hydrophobicity, and from 150 to 180 degrees it shows superhydrophobicity. Considering the antiwetting properties exhibited by hydrophobic and superhydrophobic surfaces, researchers have explored their applicability in various applications like anticorrosion, antiicing, drag reductions, for example, microfluidics, oil/water separation, etc. [1].

Wetting phenomena is described by boundary interactions of liquid, solid surface, and air (or gas). Wetting is mainly dependent on the interactions of cohesive forces of liquid, solid surface, and surround phases Fig. 1A [2]. Wetting is quantified by its contact angle (θ), where liquid and air (or gas) meet at interface meet at the surface as illustrated in Fig. 1B. The shape of the liquid droplet is influenced by three main acting forces, that is, interfacial tension at solid–liquid (γ_{sl}), liquid-gas (γ_{lg}), and solid–gas interfacial tensions (γ_{sg}), as shown in Fig. 1B [3, 4].

Wenzel [5] initially described the hydrophobic principles, where he stated that roughness is the prime factor which directly governs the hydrophobicity of the surface (Fig. 2A), which was given by the following equation [5]:

$$cos\theta = rcos\theta_\gamma \tag{1}$$

where θ is the static contact angle of flat surface, θ_γ the contact angle created by roughness and roughness factor, and r the surface ratio.

Surface ratio "r" is given by the following equation:

$$r = \frac{True\ surface\ area}{Horizontal\ projected\ area\ surface} \tag{2}$$

223
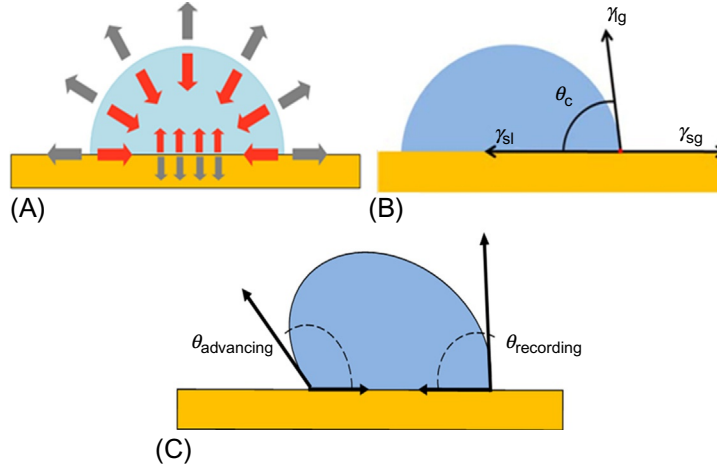
Fig. 1 (A) Forces acting on resting liquid droplet on surface, (B) contact lines of resting liquid drop, and (C) liquid drop during inclination, that is, receding and advancing positions.
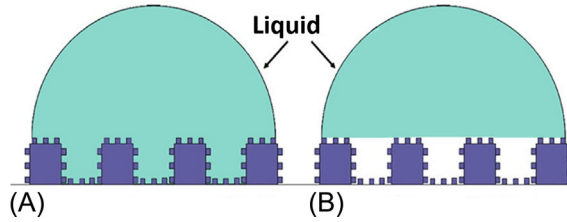
Fig. 2 (A) Wenzel state and (B) Cassie-Baxter state.

Wenzel's theory states that contact angle and its resulting hysteresis are directly proportional to the roughness factor. However, Wenzel's theory does not explain the decrease in hysteresis value after achieving a roughness factor value of 1.7 and the hydrophobicity on heterogeneous rough surfaces. Cassie and Baxter [6] reported that trapped air, that is, air bubbles, causes the water droplet to suspend over the rough surface (Fig. 2B). Cassie-Baxter's model is represented by the following equation [6]:

$$\cos\theta_c = f\cos\theta + f - 1 \qquad (3)$$

where θ_c is the apparent contact angle, f the solid fraction, and θ the Young's contact angle.

Cassie-Baxter's equation shows that the apparent contact angle is governed by solid fraction (f), and the contact with respective rough surface (θ_c).

Researchers [7] have reported the surfaces exhibiting hydrophobicity show receding and advancing angles, that is, minima and maxima, respectively, as represented in

Fig. 1C. The advancing angle is a state of liquid droplet when it creates maximum contact with the surface, whereas in receding angle, it creates minimum contact with the surface. The contact angle hysteresis, is the quantification of the heterogeneous nature of the surface based on receding and advancing angles, and it is given by the following equation [1, 4, 8]:

$$\theta_{hysteresis} = \theta_{advancing} - \theta_{receding} \tag{4}$$

A common misconception is that there are two main factors which govern the super-hydrophobicity, that is, low surface energy, and increased roughness of the surface. However, surface energy is the prime factor, and surface roughness helps in improving it. In simple terms, when the surface roughness increases, the surface area of the solid decreases, thereby decreasing the energy of surface [9, 10].

In various critical industrial and engineering applications, metals have been widely used due to their exceptional mechanical strength and stability [11]. During harsh service conditions, for example, underwater ship hull, gates of the dam, etc. these metals–based materials face severe corrosion problem due to reduction-oxidation reactions. It has been reported that the corrosion causes heavy loss of about 5000 billion US dollars to the global economy [12]. Corrosion is a widely observed industrial problem which causes degradation of metallic materials under the influence of aquatic medium, more technically, it is a local reduction and oxidation, that is, redox, electrochemical reaction, which occurs on a metallic surface [11]. In these reactions, electrons discharge as a result of the dissolution of a metallic substance, and get transported to other location on metal surface in oxidized water or to reduce hydrogen (H_2) ions, thereby causing gradual degradation of metal [13]. Fig. 3 depicts main chemical reactions which occur during the corrosion, that is, degradation, of the metals.

Corrosion can be classified into two important half electrochemical reactions, that is, metal oxidation (anodic reaction). All metallic substances show a tendency to dissolve and release positively charged metal ions under the influence of the corrosive environment, also they generate free electrons which roam through metal. The surplus generated electrons create a potential difference, which gets neutralized or absorbed via reduction of H_2

Oxidation reaction   **Reduction reaction**

$Fe \longrightarrow Fe^{2+} + 2e^-$ $2H^+ + 2e^- \longrightarrow H_2$

Reaction during neutral/basic conditions
(O_2 attack)

$$O_2 + 2H_2O + 4e^- \longrightarrow 4OH^-$$
$$Fe^{2+} + 2OH^- \longrightarrow Fe(OH)_{2\,(s)}$$
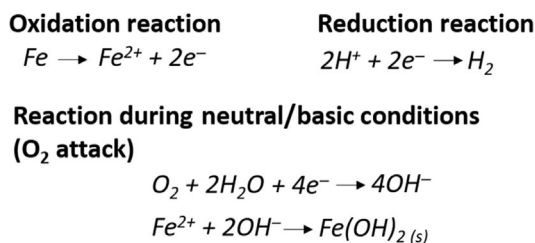
Fig. 3 Chemical reactions occurring during corrosion of metal surfaces.

ions on the cathode side [13, 14]. Apart from anodic and cathodic reactions, the presence of aquatic medium serves the purpose of ion transportations, which helps in free electrons to roam through the metallic substance. Furthermore, the basic and/or neutral conditions coupled with the presence of oxygen (O_2) can generate current via redox reactions (for producing oxidized water), thereby causing the formation of hydroxyl (OH) ions. Cathodic ions connect to anodic ions via electrolyte medium, that is, aquatic medium, where they react with iron ions, that is, Fe^{2+} ions, and form the insoluble iron hydroxides, that is, $Fe(OH)_2$, on metal surface [13–15].

Metal corrosion problem can be mitigated using hydrophobic-superhydrophobic functionalized polymeric coatings via techniques like sol-gel, spray coating, spin coating, chemical vapor deposition (CVD), dip coating [16], etc., by utilizing their antiwetting property [13, 15, 17, 18]. Chang et al. [19] have reported the fabrication of composite coating based on room temperature curable epoxy functionalized with graphene for effective corrosion inhibition of steel (cold-rolled) via solution mold casting. They reported that the incorporation of graphene-enhanced water contact of epoxy (pristine) coating from 82 to 127 degrees, that is, hydrophobic, for epoxy/graphene coating. They described that their epoxy/graphene composite revealed enhanced corrosion resistance with decreasing corrosion current density (I_{corr}), that is, from 6.49 to $0.09\,\mu A/cm^2$, and also the developed composite coating demonstrated protection efficiency of 99.33%. In one study, Valipour Motlagh et al. [20] have fabricated superhydrophobic anticorrosive coatings based on silane and fluoropolymer via spray-coating method. The developed fluoropolymer coating demonstrated water contact angle (WCA) of 166 degrees, with a corrosion protection efficiency of around 97.33%. Further, their electrochemical corrosion studies revealed a decrease in corrosion current density from 1.041×10^{-4} to $3.536\,mA/cm^2$. In another study, Zhou et al. [21] have reported hydrophobic benzoxazine–epoxy based polymeric coatings for preventing the corrosion of mild steel substrates via solution dip-coating method. They described the curing of the epoxy polymer via benzoxazine monomer with a two-stage curing at 80°C and 150°C. They evaluated the corrosion inhibition performance of these coatings under by dipping the coated substrates in NaCl solution (3.5 wt%), via electrochemical impedance spectroscopy (EIS), where they observed an improvement in corrosion resistance from 1.88 to $1.56\,k\Omega\,cm^2$ with corrosion protection efficacy up to 98.50% [21].

In this context, present chapter describes the utilization of hydrophobic polymeric coatings based on waste expanded polystyrene (WEP) and polyurethane (PU) functionalized with graphite particles. These coatings were fabricated using spray-coating, spin–coating, and bar–coating methods, and further, they demonstrated highly improved corrosion inhibition performance. The successive results show that these hydrophobic coatings can be effectively used for mitigating the corrosion problem of metal steel components for potential applications in a ship hull, automobiles, drag reduction in microfluidics, and piping industries.

2. Hydrophobic corrosion-resistant polymeric coatings based on WEP, PU, and graphite

The aim of the study was to investigate the applicability of WEP/graphite, and PU/graphite composite coatings as a hydrophobic corrosion–resistant coating for marine vessels, for example, underwater ship hull. The coating for the ship's hull consists of primer, two layers of anticorrosive coat, tie coat, and two layers of antifouling topcoat based on epoxy polymer. The replacement of a single layer of antifouling–coating costs Rs. 6.5 lakhs approximately for a ship about the length of 100 m. The study involved the development of cost-effective, eco-friendly hydrophobic coating as a top coat with a low-cost polymer system and cheapest additives.

2.1 Synthesis and fabrication of WEP/graphite coatings

During synthesis, 2 g of WEP was slowly dissolved in 10 mL toluene with varying concentration of graphite (1%–7% by weight) (Fig. 4). The viscosity of the prepared homogeneous solution was found to be 900 cP. Then the solution was ultrasonicated for 30 min at a temperature of 40°C. Two drops of the prepared solution were placed on cleansed glass-slide and spin coated by utilizing spin coater machine (Holmarc Model HO-TH-05) at 2000 rpm for 90 s. The procedure was repeated three times for preparing a thick layer of 20 μm (measured by thickness gauge). Prior to coating, glass slides were ultrasonicated at 20 kHz and 20 W in 20 mL ethanol for 15 min followed by ultrasonication in DI water twice for 5 min. For creating a hydrophobic surface, the first step is to create microstructure on the glass substrate, and hence it was roughened by using emery paper (Grade ∼80 number), and then coatings were applied by spin coater.
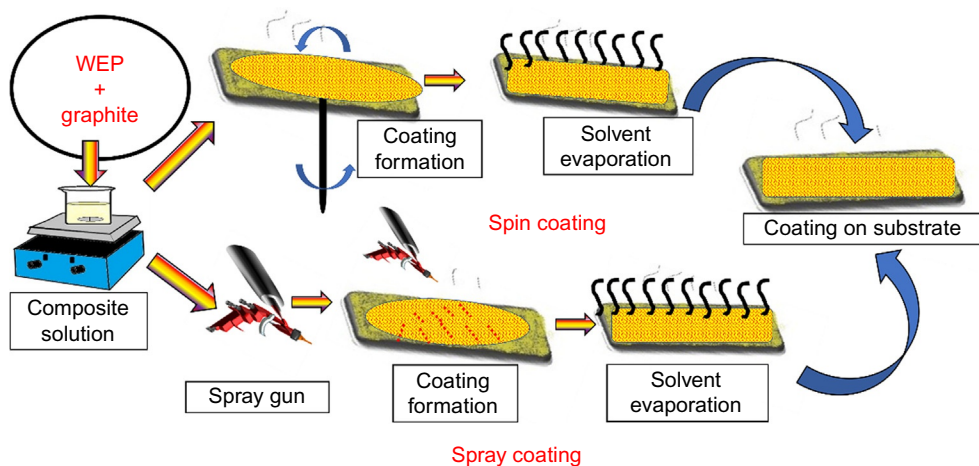
Fig. 4 Synthesis of polymeric coatings via spin coating and spray coating.

Further, same homogeneous solution of WEP/graphite was coated onto cleansed glass substrate via spray coating at a pressure of 20 psi.

2.2 Synthesis and fabrication of PU/graphite coatings

During the synthesis of PU/graphite coatings, 5 wt% of graphite was gradually added in polyester polyol base (OH value 500–600 mg/g) resin of 170 g. The mixture was ultrasonicated for 30 s at 20 kHz and 20 W power. Then the hardener of 35 g was added in polyol/graphite mixture, with a homogeneous stirring of using mechanical stirrer at 500 rpm for 10 min. Solvents of xylene, butyl acetate, and butyl cellulose acetate were then mixed in a ratio of 8:1:1 in a 100 mL homogenous solution. The synthesized solution was gradually added in the polyol/polyisocyanate mixture. Then, the PU/graphite blend solution was spray coated on mild steel panel and sheets at 20 psi air pressure. The thickness of 60 μm was maintained for all samples using a coating thickness gauge. Mild steel (MS) panels ($150 \times 100 \times 1.5$ mm) and mild steel sheets ($150 \times 50 \times 0.3$ mm) were degreased by xylene to remove oil, grease, and dirt particles. Then the substrates were grid blasted for coating applications as per ISO 8501-1:2007 Sa 21/2 standard. Before coating, steel substrates were preheated for removing the moisture present on the surface for maintaining the adhesion and uniformity of coating. Then, the cleaned MS panels and sheets were used for spray coating.

2.3 Results and analysis

Salt Spray Test. Salt spray method is used for evaluating the anticorrosion performance of coatings. The test was conducted as per ASTM B117-11 standard. This test utilizes a salty solution (5% NaCl) which is sprayed on coatings via an atomized nozzle [22]. Corrosive atmosphere supported with saline solution was maintained in the chamber for evaluating the performance of the coatings.

Sea Water Immersion Test. The mild steel specimen of coated samples of size $150 \times 100 \times 1.5$ mm were immersed in 5% NaCl bath or by artificial seawater bath for a specified period of time as per IS: 101 standards [23] (Table 1).

After the immersion tests, the samples were taken out from the bath, visually examined and photographed. Then the samples were investigated sign of corrosion and sign of deterioration, viz., blistering, detachment of film up to 500 h [24].

Table 1 Chemical composition of seawater

Analysis	Chloride	Sulfate	Sodium	Potassium	Magnesium	Nitrate
Concentration (mg/L)	314	80	60	48	50	70

2.4 Mechanical characterization

Adhesion Test. This test evaluates the pull–of bonding strength of coatings with its substrate, thereby indicating its durability. In the present study, adhesion strength was measured by the UTM (LLOYD, Model LR30K Plus) machine. The adhesion strength of the coating was calculated using the following equation [25]:

$$Adhesion\ strength = \frac{Load\ at\ break}{Initial\ crosssectional\ area} \tag{5}$$

Flexibility Test. This test was performed evaluating the flexibility cracking resistance of coated substrate during elongation as per IS: 101 standards. In this method, coatings are evaluated using "Pass or Fail" grading over a mandrel of a specific size [26]. The cracking-resistance value of a coated panel is the minimum diameter at which cracking does not appear. This testing procedure is applied as a "pass/fail" test by determining whether cracking is produced by bending over a specified mandrel diameter.

Tensile Test. This test evaluates the tensile performance of coatings prepared using film coater (Model No.335/1 Erickson) on glass–plates (via 300-μm dimension blade), which were precoated using methyl cellulose. After 1 week, the coatings were peeled–off from glass–plates, followed by cleaning with water and drying at room temperature.

Tensile strength and fracture strain of coatings were checked using UTM as per ASTM D-882-97 standard [27]. Coatings having a thickness of 200 μm were tested at a strain rate of 20 mm/min. For each series of 10 specimens, the average mean and standard deviation of each property for the specimens with the 5 highest tensile strengths were calculated.

Impact Test. This test evaluated the damage tolerance and energy dissipation of developed coatings. Coatings can face localized corrosion if the impact causes discontinuation and unsafe path to coated substrates.

In the present study, this test was performed as per ASTM D2794 standard, where a specific weight of 1 kg was dropped at a specific distance (with a gradual increase of 25 mm) on to coated steel substrate [28]. The cracks on coating were observed by applying $CuSO_4$ solution on a coated substrate, using pin–hole sensor (or tape–pull method) for quantifying the removed coating.

Scratch Hardness Test. This test was performed for evaluating the scratch penetration resistance of coating using a needle. This test evaluates the coating via GO and NO-GO grades, by increasing loads onto needle thereby checking its penetration resistance for the coated substrate. Scratch resistance of a protective coating was evaluated using Clemen scratch-resistance tester. It consists of a horizontal sliding test panel carrier mounted on a base frame. A scratching tool is fixed at the end and a sliding weight in the middle of a counterpoised lever that is supported by two pillars. Scratch hardness is measured by the force necessary to cut through the coating to the metal substrate. The scratch hardness test was performed as per IS:101 standard [29].

Abrasion Test. This test was performed as per ASTM D-4060-10 standard, using Taber Abraser. The resistance of the coating to marring is its ability to withstand and scuffing actions that tend to disfigure or change the appearance of its surface [30]. Mar abrasion consists of permanent deformations that have not ruptured the surface of a coating.

3. Spin-coated WEP coatings

Wettability Analysis. Fig. 5 shows wettability behavior of spin-coated WEP/graphite coatings, which shows a stepwise loss of hydrophilic property with an increasing weight percentage of graphite powder. It has been observed that WCA has enhanced from 89 to 98 degrees with an increase in graphite weight percent in WEP/graphite coating.

Further increase of graphite from 1 to 2 wt%, shows a marginal increase from 98 to 101 degrees. Similarly, WCA of 104 degrees was obtained for 3 wt% graphite in developed coating. But, the maximum WCA of 119 degrees was obtained with the addition of 5 wt% graphite powder in WEP coating. Further loading of graphite led to decrease of WCA from 115 and 110 degrees, that is, for 6- and 7-wt% graphite concentration, respectively. Increased WCA of WEP/graphite coating is attributed to its hierarchical surface roughness and morphology, which has been explained in FESEM and topographical, that is, AFM, analysis [10, 31–36].
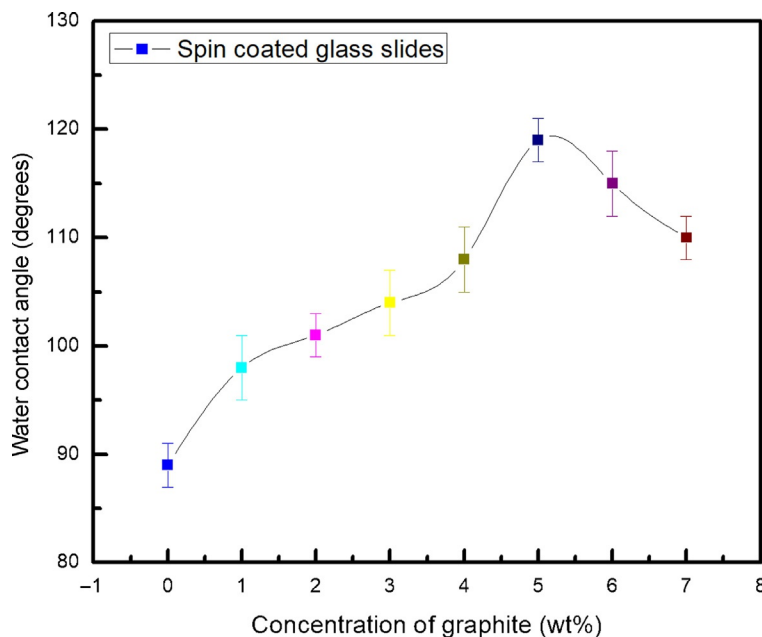
Fig. 5 Effect of concentration of graphite on water contact angle.

Stability Test. This test evaluates the stability of microparticles of developed coating in solution. It involves modification of the surface of particles by the introduction of polymer to generate effective steric repulsion forces from polymeric chains for enhancing the charge on the surface. When graphite particles are well dispersed, steric repulsion forces arising from polymeric chains of coating will be higher, which in turn increases hydrophobicity of WEP/graphite coating. The stability test was analyzed for WEP/graphite coating with 4- and 5-wt% graphite powder via surface analyzer [37]. The test was carried out for 30 min at ambient temperature. The graph (Fig. 6) shows that graphite particles are well-dispersed throughout the matrix and do not settle during the test duration.

Morphological Analysis. SEM analysis of the WEP/graphite coating revealed the evolution of different morphologies as shown in Fig. 7. SEM analysis reveals the presence of micro-sized graphite particles on the coated surface, whereas the aggregation of micro-sized particles was observed for 1 wt% graphite powder. Further increase in graphite loading from 1 to 2 wt% (Fig. 7A and B), the aggregates become continuous network to cover the surface of WEP coating [1, 2, 38, 39]. The multiscaled slippery surface is observed for increased graphite loading from 2 to 3 wt% as shown in Fig. 7B and C. Upon increasing the graphite loading to 4 wt% (Fig. 7D), increases aggregation and further gets converted to nano–flake–like morphology. Further, SEM analysis reveals hierarchical surface morphology with increasing graphite nanoparticle loading. These islands were composed of a forest of nano–flakes, and these nano–flakes are originated from the balance of spin rate and duration of the time period and result in enhancement of hydrophobicity as shown in
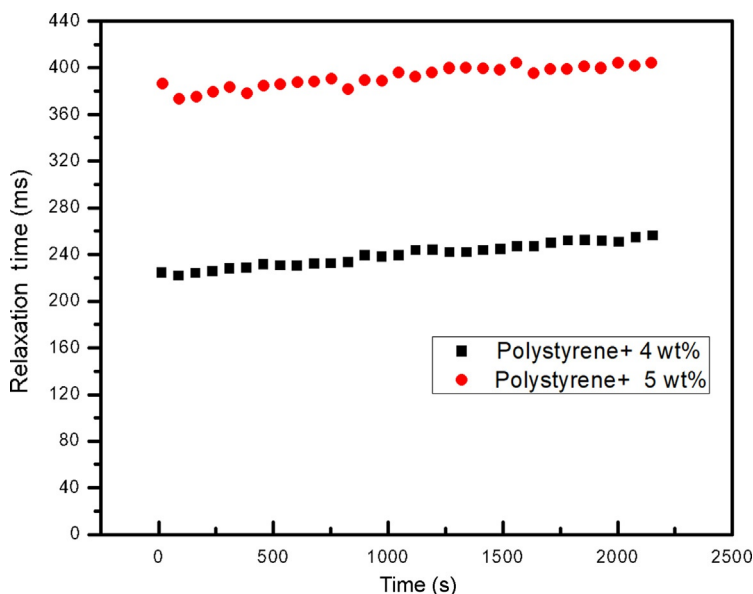
Fig. 6 Stability test of graphite powders of 4 and 5 wt% in polymer coating solution.
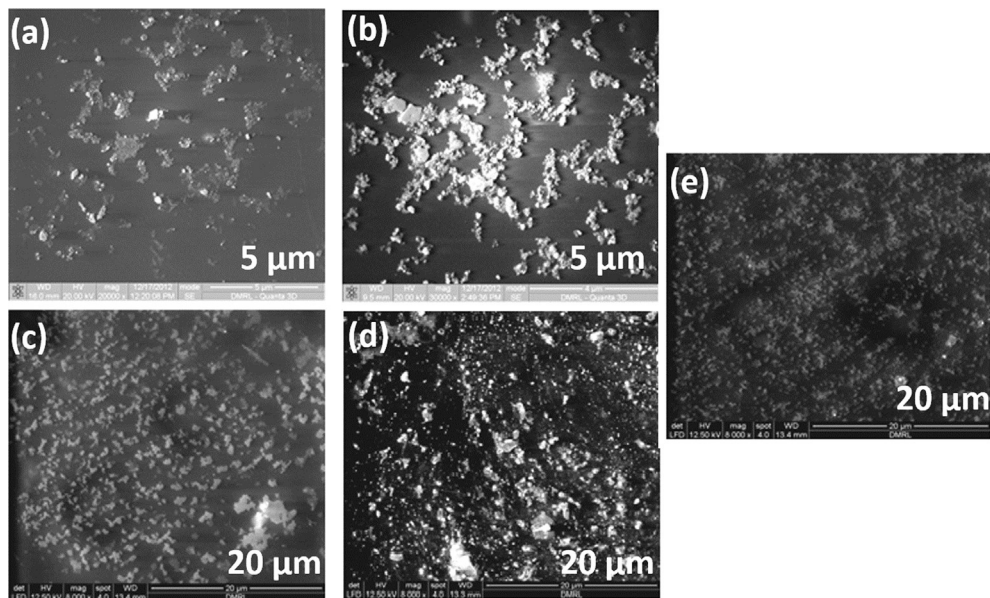
Fig. 7 SEM analysis of WEP/graphite coatings functionalized with (A) WEP/graphite (1 wt%) (B) WEP/graphite (2 wt%), (C) WEP/graphite (3 wt%), (D) WEP/graphite (4 wt%), and (E) WEP/graphite (5 wt%).

Fig. 7E. Further, the air-pockets get trapped between the nano–flakes following the Cassie-Baxter model, thereby enhancing the hydrophobicity via improved surface roughness. Thus, it can be concluded that the microscaled structure formation exhibiting nano–flake forest morphology provides more roughness enhances hydrophobicity [2, 10, 40, 41] which is also supported by the wettability analysis as discussed in the previous section.

Surface Topology Analysis. The influence of surface topology on wettability behavior was studied using AFM analysis as shown in Fig. 8.

Fig. 8 reveals micron or submicron scale aggregates of micro-sized particles with a forest of nano–flakes formed on the coated surface, resembling the rough surface with hierarchal morphology. The average roughness of coating, $S_a = 80.141$ nm was observed for WEP with 1 wt% graphite (Fig. 8A). Further increase in graphite loading up to 2 wt%, increases the average roughness up to 86.418 nm (Fig. 8A). Similarly, upon increasing the weight percentage of graphite powder from 2 to 3 wt%, a higher number of nano–flakes are observed which combine to form the forest as shown in Fig. 8C. Similar observations also establish an association between WCA, and roughness surface other samples, as discussed in wettability behavior of WEP/graphite coatings. The roughness of surface and WCA data collected from all the samples have been represented in Table 2. Maximum roughness of surface was found to be 109.078 nm for 5 wt% loading of graphite. It was also noticed that the maximum height of a single flake, that is, 160 nm, and separation
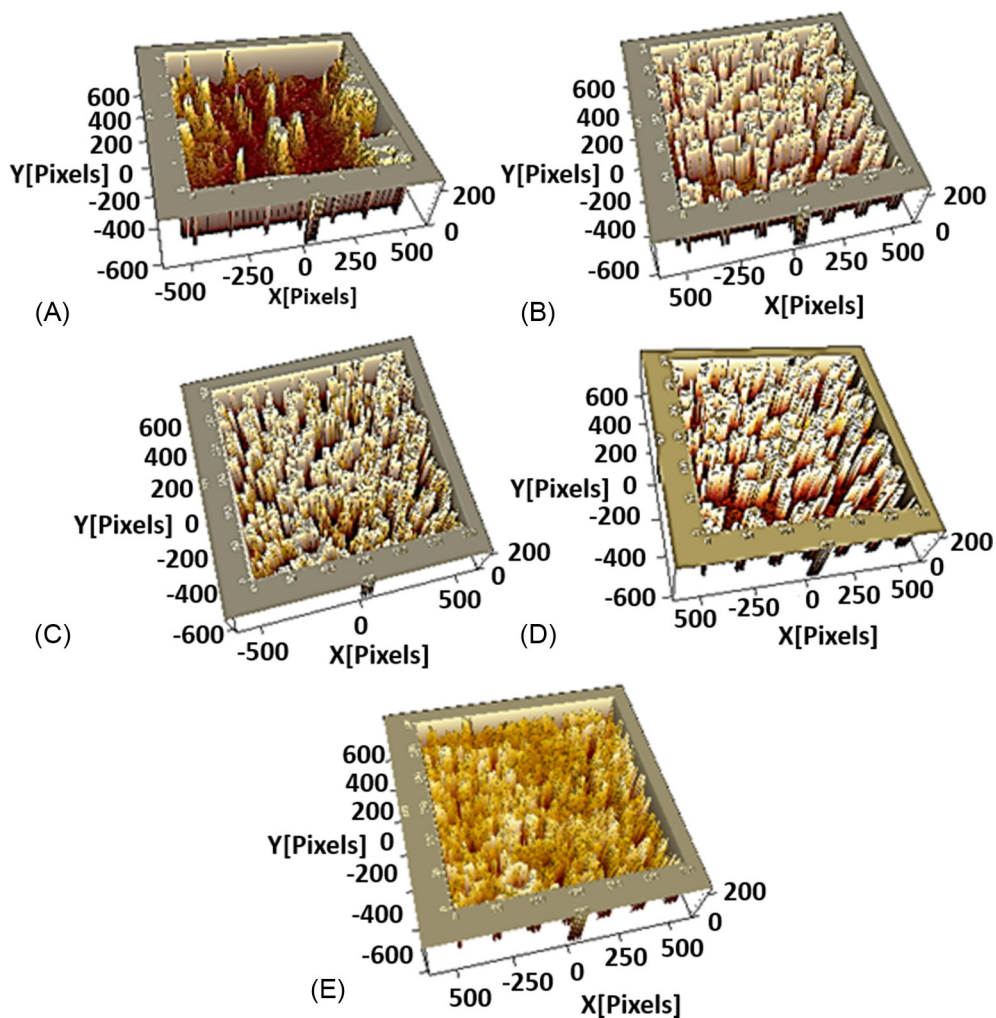
Fig. 8 AFM analysis of WEP/graphite coating with graphite loading of (A) 1 wt%; (B) 2 wt%; (C) 3 wt%; (D) 4 wt%; and (E) 5 wt%.

Table 2 Surface roughness and wetting trends

Graphite loading (wt%)	Average roughness (nm), S_a	Average height of peak (nm)	WCA (degrees)
0	20.009	14	89
1	80.141	30	98
2	86.418	40	101
3	88.064	65	104
4	93.567	79	108
5	109.078	110	119
6	104.560	102	115
7	95.120	80	110

between two flakes, that is, 0.2 nm, on the surface, which enables the anisotropic slippery surface [1, 2, 8, 40]. As the graphite loading was increased, the distance between the nano-flakes decreased gradually. The average height of peaks was found to be 110 nm for graphite loading of 5 wt% (Fig. 8E). It is seen that with 7-wt% graphite loading, the average height of peak reduced to 80 nm, thus decreasing the hydrophobicity. This observation supports the idea that surface topology plays a paramount role in influencing the wettability of surface than surface composition [1, 31].

4. Spray-coated WEP/graphite coatings

Wettability Behavior Study. Fig. 9 shows that the WCA of spray-coated WEP/graphite samples improved from 89 to 151 degrees with increasing graphite loading in WEP/graphite coatings. Maximum WCA obtained was 151 degrees, that is, superhydrophobicity, for 5-wt% graphite loading for spray-coated WEP/graphite samples.

Further loading of 6 wt% graphite decreased WCA to 125 degrees for WEP/graphite coating. The increase in hydrophobicity of coating is associated with the surface morphology for different concentrations of graphite in spray-coated WEP/graphite samples [32, 39].

FESEM Analysis. Fig. 10 shows FESEM analysis of spray-coated WEP/graphite coatings containing 3 and 5 wt% loading of graphite. As clearly shown in Fig. 10A, WEP without graphite does not give rough surface on the glass slide. It exhibits uniform coating with WCA of 89 degrees. But, with graphite at 3 wt%, the surface morphology
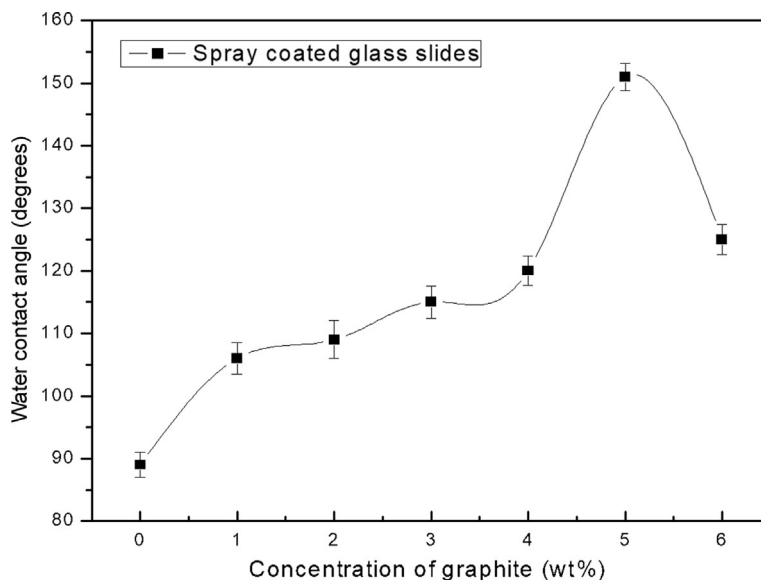
Fig. 9 Wettability analysis of spray-coated WEP/graphite.
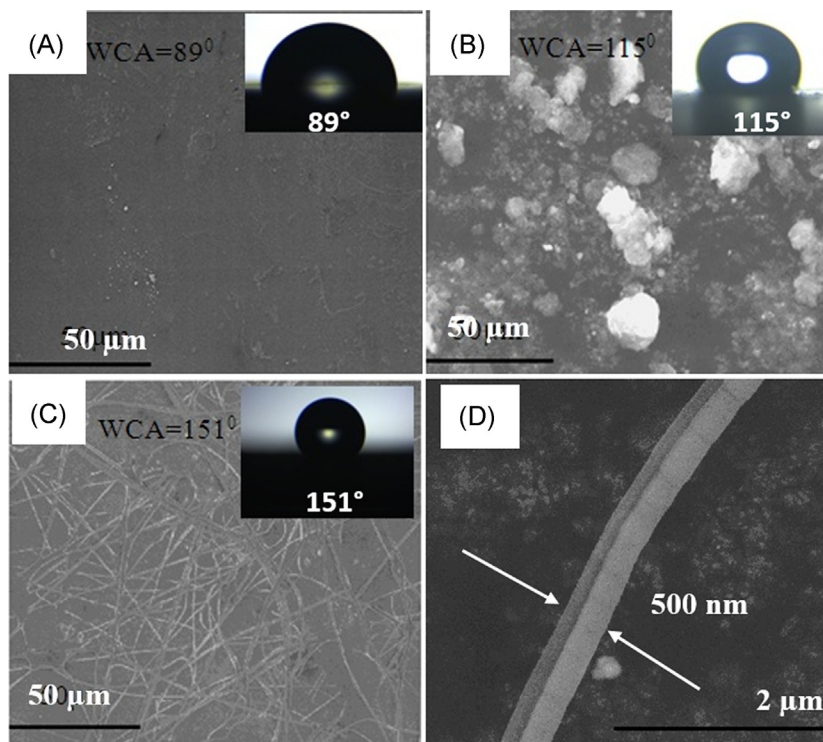
Fig. 10 FESEM images of WEP/graphite composite at different concentration of graphite: (A) Plain polystyrene, (B) WEP/graphite (3 wt%), (C) WEP/graphite (5 wt%), and (D) WEP/graphite (5 wt%) graphite.

reveals some roughness as shown in Fig. 10B. This surface roughness is attributed to the formation of rock–like nanostructures formed on the coated surface, which were also reported by Kulinich and Farzaneh [42], thus revealing the WCA of 115 degrees.

This result remarkably changed the wetting behavior of coating from being hydro–philic to superhydrophobic on the introduction of graphite additives. With introduction of higher concentration of graphite in the polymer solution sprayed onto glass surface reveals nanofiber-like structure which is shown in Fig. 10C, which is probably due to stretching of polymeric chains and rapid evaporation of solvent. The nanofibers-like morphology produced by spraying technique exhibits WCA of 151 degrees. Similar results were also reported and discussed by Liu et al. using electrospinning technique to fabricate PMMA fiber [43]. Similarly, Lee et al. have also fabricated electrospinning fiber using polystyrene with a small addition of additives which exhibits a WCA of greater than 150 degrees [44]. This surface roughness is considered as the key parameter for affecting the wettability of the surface [2, 6, 8]. High resolution of hierarchical nanofiber reveals a single fiber diameter of around 500 nm (Fig. 10D).

Similar results were reported by Lim et al., who fabricated ultra–hydrophobic nano–fibers with a WCA of 146 degrees using polyisobutylene–based thermoplastic material [45]. Fig. 10C shows hierarchical rough surface which causes the air bubbles to entrap between the hierarchical nanostructure of fibers and the water droplet, thus demonstrat–ing WCA of 151 degrees [6, 18, 40, 41, 46].

5. Spray-coated PU and PU/graphite coatings

Wetting and Surface Topology Analysis. Spray coating of PU on steel substrate revealed WCA of 92 degrees, whereas PU/graphite coating revealed WCA of 100 degrees. The result shows that the addition of 5 wt% of graphite in the PU system increases WCA by 8 degrees (Fig. 11).

AFM analysis was performed for evaluating the surface morphology PU/graphite coatings, as represented in Fig. 12A and B. AFM analysis revealed a homogeneous coating
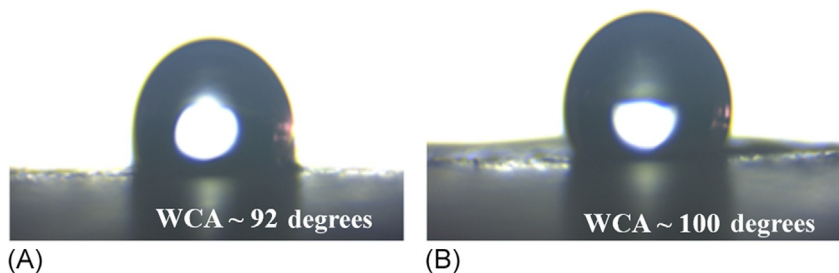
Fig. 11 (A) WCA of PU coating and (B) WCA of PU/graphite coating.
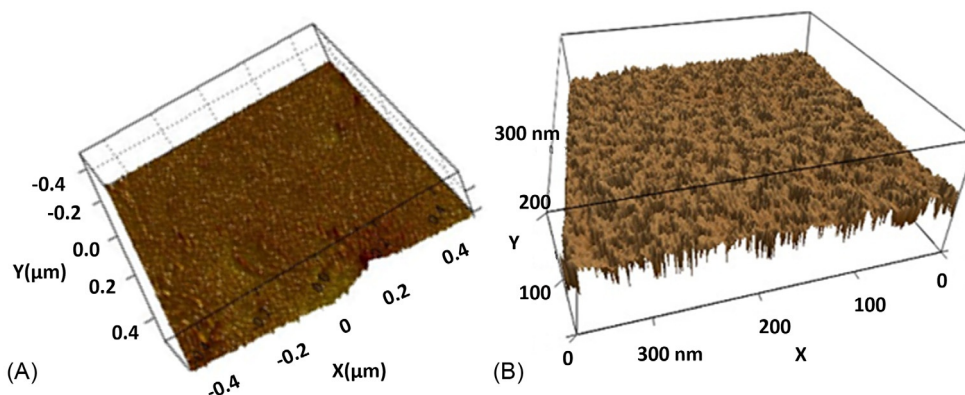
Fig. 12 (A) AFM image of plain PU-coated panel (B) AFM image of PU/graphite-coated panel.

with no agglomeration, and no traces of air-blisters and pin-holes for cured PU/graphite coatings [28, 47]. The roughness was found to be 1.363 and 20.45 nm for PU and PU/graphite coatings, respectively, and also confirmed the smooth and crack free surface of the coatings [23, 28].

FTIR Analysis. Pure PU and PU/graphite coatings were analyzed using FTIR (Perkin Elmer Spectrum 100) characterization. FTIR analysis was performed on both samples, that is, before and after curing, in order to determine the presence of NCO group PU coatings. The peak position between 2000 and 3000 cm^{-1} clearly shows the presence of NCO group in uncured PU/graphite coating (Fig. 13A), whereas this peak disappears when the curing reaction is completed [23, 48, 49] (Fig. 13B).

Adhesion Test. The adhesion strength of PU/graphite coatings was evaluated as per IS:101 (pull-off method) standard via UTM, with a uniform rate of 1 MPa/s. The adhesion strength of PU coating was found to be 5.8 MPa, whereas for the PU/graphite coating it was 6.5 MPa. A small increment in adhesion strength for PU/graphite coating indicates some degree of reinforcement due to the addition of graphite dispersion in PU system.

Tensile Test. This test was performed as per ASTM D338 standard. PU/graphite coatings (thickness ~200 μm) were strained at a rate of 20 mm/min. Tensile strength for PU coating was found to be 10.5 MPa at 135% elongation, whereas for PU/graphite coating, it was found to be 11 MPa at 130% elongation [23, 26].

Flexibility Test. PU and PU/graphite-coated mild steel sheets of size (150 × 100 × 0.3 mm) were subjected to cylindrical mandrel test as per IS: 101 test with mandrel size of 1/8 in (3.2 mm) diameter. Both the test specimens were passed without cracking and delamination of coating from the substrate after bend test (Fig. 14A).

Scratch Hardness Test. Scratch hardness was measured using Clemen Scratch Hardness tester on both PU and PU/graphite coatings. The test panels exhibited dimensions of
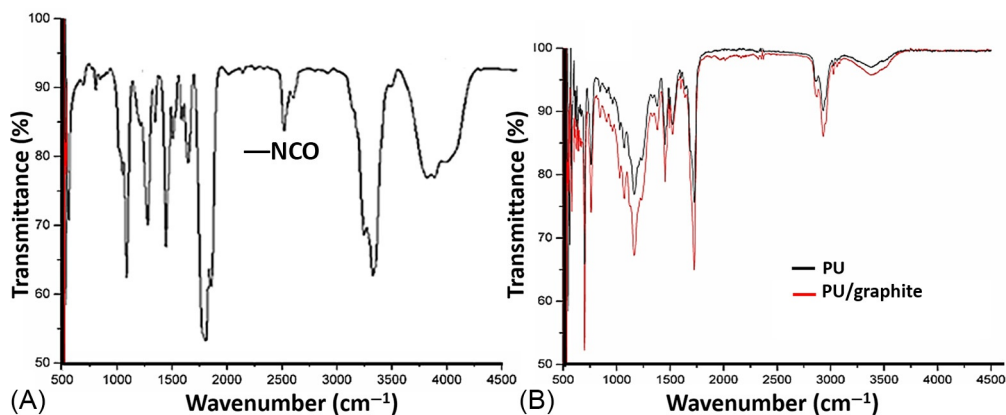
Fig. 13 FTIR spectra of (A) PU/graphite before curing, (B) PU/graphite after curing.
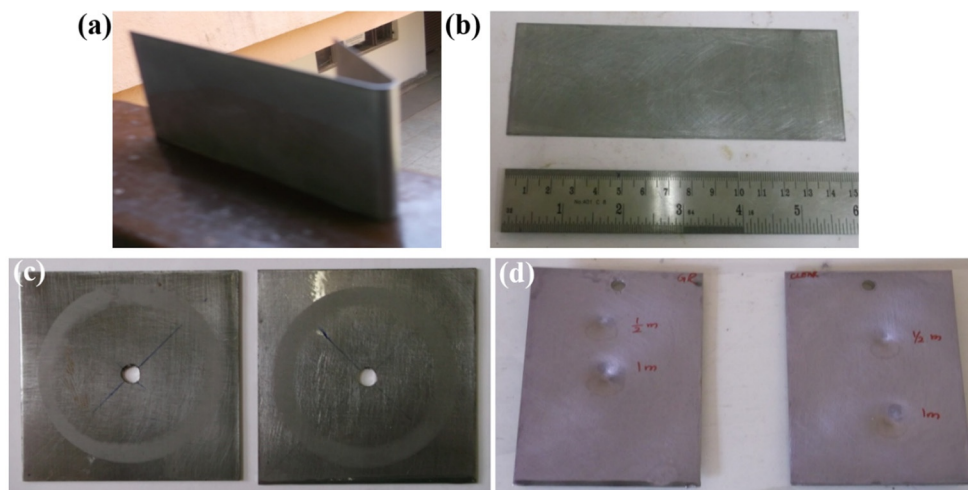
Fig. 14 (A) Bend tested sample (flexibility test), (B) scratch hardness tested sample, (C) abrasion tested samples, and (D) impact tested sample.

125×50 mm in size, whose scratch resistance was analyzed by successively increasing load of 0.5 kg, until failure of the coating (Fig. 14B). The scratch resistance of 2 and 2.5 kg was recorded on the PU and PU/graphite panels, respectively.

Abrasion Resistance. Abrasion resistance was measured by using Taber Abraser as per ASTM D4060 standard. The coated test panel of size 100×100 mm was prepared and mounted on the Abraser. The weight loss of 42.6 and 40 mg were observed after 500 cycles on PU and PU/graphite coating (Fig. 14C). Results of abrasion–resistance test clearly indicate that there was a small decrease in value of weight loss due to the addition of graphite on the PU system [50–52].

Impact Resistance. Impact resistance of PU and PU/graphite-coated panels were tested by falling weight apparatus as per ASTM D 2794 standard. Both coated samples passed the impact load of 2 kg from a height of 0.5 and 1 m. Impact tests clearly indicated that no visible cracks and deformation were observed on the addition of graphite particles in PU system [50, 53, 54] (Fig. 14D).

Corrosion-Resistance Properties. Corrosion resistance of coated substrates was investigated by salt spray (ASTM B117) and seawater immersion test using artificial seawater as per (IS: 101) for 160 h. PU and PU/graphite coatings did not show any sign of corrosion and deterioration, viz., blistering, detachment of film, and passed respective salt spray and seawater immersion tests [27, 55, 56] (Fig. 15) (Table 3).

The successive results demonstrated that the superhydrophobic PU and PU/graphite coatings on steel substrates can be effectively utilized as anticorrosive coatings for various industrial and engineering applications like underwater ship hull, automobiles, Naval vessels, aircrafts, pipelines, oil rigs, etc. [1, 2, 39, 56–61].
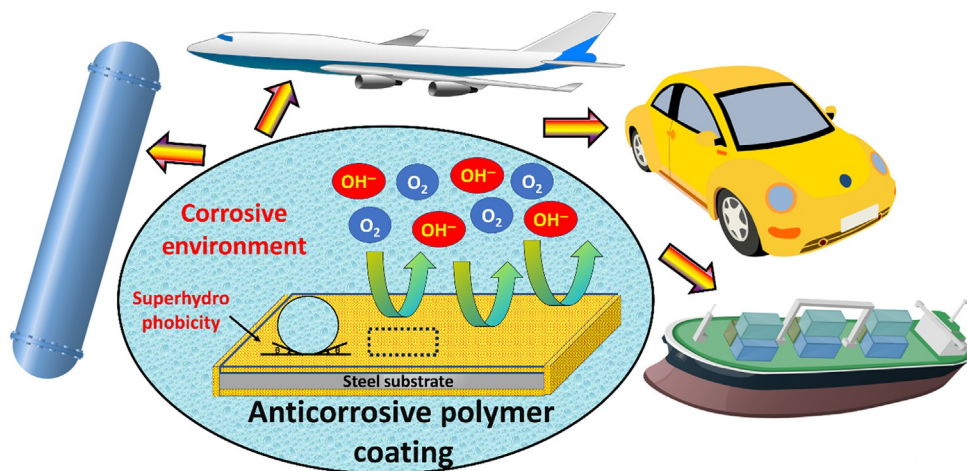
Fig. 15 Hydrophobic polymeric coatings for anticorrosive applications.

Table 3 Performance evaluation of PU and PU/graphite coatings

Sr. no.	Test method	PU coating	PU/graphite coating
1.	Pull off adhesion (in MPa) (IS:101)	5.8 MPa	6.5 MPa
2.	Tensile strength and elongation of film (ASTM-D338)	10.5 MPa at 135%	11 MPa at 130%
3.	Flexibility test (ASTM D 522)	Passed till 10 degrees with 1/8″ dia. mandrel	Passed up to 10 degrees with 1/8″ dia. mandrel
4.	Scratch resistance (tolerance weight in kg) (IS:101)	2	2.5
5.	Abrasion resistance (ASTM D 4060) (weight loss (mg/500 cycles)	42.6	42
6.	Impact resistance (ASTM D2794)	Passed till 1 m height	Passed till 1 m height
7.	Salt spray test (up to 160 h) (ASTM B117)	Passed (no blisters/rust)	Passed (no blisters/rust)
8.	Sea water immersion test (up to 160 h) (IS:101)	Passed (no rust–spot/blisters)	Passed (no rust–spot/blisters)

6. Conclusion

In summary, the study showed that WEP can be spin coated with graphite anticorrosive applications by its antiwetting properties where it shows WCA of 119 degrees with hierarchically structured morphology of surface, and further exhibits excellent dispersion of graphite particles in the hydrophobic coating. WEP/graphite coatings demonstrated

superhydrophobicity with WCA of 151 degrees when fabricated with spray coating at ambient temperature. SEM and AFM analysis confirmed hierarchically structured morphology with the presence of nanofibers on the entire surface, as a result of stretching of polymeric chains, and solvent evaporation. Brittle nature of WEP restricted further mechanical characterization; however, this process has demonstrated that hydrophobic/superhydrophobic coatings can be fabricated on large-scale for potential anticorrosive applications. PU coatings are well suitable as a top coat for marine applications due to their excellent durability, corrosion resistance, and good adhesion strength, and the addition of graphite further enhanced the hydrophobicity to 100 degrees (with an increase of 8 degrees). PU/graphite coating showed improved mechanical properties as compared to pristine PU coating. Thus, improved hydrophobicity without compromising mechanical and corrosion resistance were fabricated with reduced cost. The successive results demonstrated that the hydrophobic/superhydrophobic coatings-based WEP/graphite and PU/graphite can be effectively used for anticorrosive applications for marine underwater applications like ship hull.

References

[1] B.N. Sahoo, B. Kandasubramanian, Recent progress in fabrication and characterisation of hierarchical biomimetic superhydrophobic structures, RSC Adv. 4 (2014) 22053–22093, https://doi.org/10.1039/c4ra00506f.

[2] P.M. Gore, S. Zachariah, P. Gupta, K. Balasubramanian, Multifunctional nano-engineered and biomimicking smart superhydrophobic reticulated ABS/fumed silica composite thin films with heat-sinking applications, RSC Adv. 6 (2016) 105180–105191, https://doi.org/10.1039/c6ra16781k.

[3] B.N. Sahoo, B. Kandasubramanian, B. Sabarish, Controlled anisotropic wetting behaviour of multi-scale slippery surface structure of non fluoro polymer composite, Express Polym Lett 7 (2013) 900–909, https://doi.org/10.3144/expresspolymlett.2013.88.

[4] R. Tadmor, Line energy and the relation between advancing, receding, and young contact angles, Langmuir 20 (2004) 7659–7664, https://doi.org/10.1021/la049410h.

[5] R.N. Wenzel, Resistance of solid surfaces to wetting by water, Ind. Eng. Chem. 28 (1936) 988–994, https://doi.org/10.1021/ie50320a024.

[6] A.B.D. Cassie, S. Baxter, Wettability of porous surfaces, Trans. Faraday Soc. 40 (1944) 546–551, https://doi.org/10.1039/tf9444000546.

[7] A. Marmur, Contact angle hysteresis on heterogeneous smooth surfaces, J. Colloid Interface Sci. (1994), https://doi.org/10.1006/jcis.1994.1391.

[8] P. Gupta, B. Kandasubramanian, Directional fluid gating by Janus membranes with heterogeneous wetting properties for selective oil-water separation, ACS Appl. Mater. Interfaces 9 (2017) 19102–19113, https://doi.org/10.1021/acsami.7b03313.

[9] P.M. Gore, M. Dhanshetty, K. Balasubramanian, Bionic creation of nano-engineered Janus fabric for selective oil/organic solvent absorption, RSC Adv. 6 (2016) 111250–111260, https://doi.org/10.1039/C6RA24106A.

[10] P.M. Gore, B. Kandasubramanian, Heterogeneous wettable cotton based superhydrophobic Janus biofabric engineered with PLA/functionalized-organoclay microfibers for efficient oil-water separation, J. Mater. Chem. A 6 (2018) 7457–7479, https://doi.org/10.1039/c7ta11260b.

[11] W.D. Callister, Corrosion and degradation of materials, Mater. Sci. Eng. (2011), https://doi.org/10.1016/j.msec.2008.09.009.

[12] Jindal Ltd., The stainless post, J. Jindal Stainl. Ltd., 2014, pp. 1–19. 5.

[13] B.D.B. Tiu, R.C. Advincula, Polymeric corrosion inhibitors for the oil and gas industry: design principles and mechanism, React. Funct. Polym. (2015), https://doi.org/10.1016/j.reactfunctpolym.2015.08.006.

[14] D.E. Arthur, A. Jonathan, P.O. Ameh, C. Anya, A review on the assessment of polymeric materials used as corrosion inhibitor of metals and alloys, Int. J. Ind. Chem. (2013), https://doi.org/10.1186/2228-5547-4-2.

[15] A. Lutz, J.M.C. Mol, I. De Graeve, H. Terryn, Smart corrosion protection by multi-action self-healing polymeric coatings, in: Smart Composite Coatings and Membranes: Transport, Structural, Environmental and Energy Applications, 2015, https://doi.org/10.1016/B978-1-78242-283-9.00006-3.

[16] S. Gharde, B. Kandasubramanian, The importance of electroless metallic build-up on surface modified substrates for multifunctional engineering applications: a recent progress update, Trans. Indian Inst. Metals (2018), https://doi.org/10.1007/s12666-018-1397-6.

[17] V. Kumar, K. Balasubramanian, Progress update on failure mechanisms of advanced thermal barrier coatings: a review, Prog. Org. Coat. 90 (2016) 54–82, https://doi.org/10.1016/j.porgcoat.2015.09.019.

[18] S. Sahoo, M.E. Gruner, S.N. Khanna, P. Entel, First-principles studies on graphene-supported transition metal clusters, J. Chem. Phys. 141 (2014) 074707, https://doi.org/10.1063/1.4893328.

[19] K.-C. Chang, M.-H. Hsu, H.-I. Lu, M.-C. Lai, P.-J. Liu, C.-H. Hsu, W.-F. Ji, T.-L. Chuang, Y. Wei, J.-M. Yeh, W.-R. Liu, Room-temperature cured hydrophobic epoxy/graphene composites as corrosion inhibitor for cold-rolled steel, Carbon N. Y. 66 (2014) 144–153, https://doi.org/10.1016/j.carbon.2013.08.052.

[20] N. Valipour Motlagh, F.C. Birjandi, J. Sargolzaei, N. Shahtahmassebi, Durable, superhydrophobic, superoleophobic and corrosion resistant coating on the stainless steel surface using a scalable method, Appl. Surf. Sci. 283 (2013) 636–647, https://doi.org/10.1016/j.apsusc.2013.06.160.

[21] C. Zhou, X. Lu, Z. Xin, J. Liu, Y. Zhang, Hydrophobic benzoxazine-cured epoxy coatings for corrosion protection, Prog. Org. Coat. 76 (2013) 1178–1183, https://doi.org/10.1016/j.porgcoat.2013.03.013.

[22] P. Narute, A. Palanisamy, Study of the performance of polyurethane coatings derived from cottonseed oil polyol, J. Coat. Technol. Res. 13 (2016) 171–179, https://doi.org/10.1007/s11998-015-9741-9.

[23] K. Wazarkar, M. Kathalewar, A. Sabnis, Development of epoxy-urethane hybrid coatings via non-isocyanate route, Eur. Polym. J. 84 (2016) 812–827, https://doi.org/10.1016/j.eurpolymj.2016.10.021.

[24] A.B. Chaudhari, P.D. Tatiya, R.K. Hedaoo, R.D. Kulkarni, V.V. Gite, Polyurethane prepared from neem oil polyesteramides for self-healing anticorrosive coatings, Ind. Eng. Chem. Res. 52 (2013) 10189–10197, https://doi.org/10.1021/ie401237s.

[25] T. Arai, H. Fujita, M. Watanabe, Evaluation of adhesion strength of thin hard coatings, Thin Solid Films 154 (1987) 387–401, https://doi.org/10.1016/0040-6090(87)90381-6.

[26] S. Ahmad, S.M. Ashraf, A. Hasnat, S. Yadav, A. Jamal, Studies on urethane-modified alumina-filled polyesteramide anticorrosive coatings cured at ambient temperature, J. Appl. Polym. Sci. 82 (2001) 1855–1865, https://doi.org/10.1002/app.2029.

[27] R.B. Naik, D. Ratna, S.K. Singh, Synthesis and characterization of novel hyperbranched alkyd and isocyanate trimer based high solid polyurethane coatings, Prog. Org. Coat. 77 (2014) 369–379, https://doi.org/10.1016/j.porgcoat.2013.10.012.

[28] M. Kathalewar, A. Sabnis, D. D'Melo, Polyurethane coatings prepared from CNSL based polyols: synthesis, characterization and properties, Prog. Org. Coat. 77 (2014) 616–626, https://doi.org/10.1016/j.porgcoat.2013.11.028.

[29] L.K. Aggarwal, P.C. Thapliyal, S.R. Karade, Anticorrosive properties of the epoxy–cardanol resin based paints, Prog. Org. Coat. 59 (2007) 76–80, https://doi.org/10.1016/j.porgcoat.2007.01.010.

[30] R. Jain, R. Pitchumani, Fabrication and characterization of zinc-based superhydrophobic coatings, Surf. Coat. Technol. 337 (2018) 223–231, https://doi.org/10.1016/j.surfcoat.2018.01.014.

[31] S. Padhi, S. Gosavi, R. Yadav, B. Kandasubramanian, Quantitative evolution of wetting phenomena for super hydrophobic surfaces, Mater. Focus 7 (2018) 305–315, https://doi.org/10.1166/mat.2018.1509.

[32] B.N. Sahoo, B. Kandasubramanian, Photoluminescent carbon soot particles derived from controlled combustion of camphor for superhydrophobic applications, RSC Adv. 4 (2014) 11331–11342, https://doi.org/10.1039/c3ra46193a.

[33] B.N. Sahoo, B. Kandasubramanian, An experimental design for the investigation of water repellent property of candle soot particles, Mater. Chem. Phys. 148 (2014) 134–142, https://doi.org/10.1016/j.matchemphys.2014.07.022.

[34] S. Simon, B. Kandasubramanian, Facile immobilization of camphor soot on electrospun hydrophobic membrane for oil–water separation, Mater. Focus 7 (2018) 295–303, https://doi.org/10.1166/mat.2018.1511.

[35] S. Simon, A. Malik, B. Kandasubramanian, Hierarchical electrospun super-hydrophobic nanocomposites of fluoroelastomer, Mater. Focus 7 (2018) 194–206, https://doi.org/10.1166/mat.2018.1499.

[36] R. Yadav, S. Zachariah, K. Balasubramanian, Thermally stable transparent hydrophobic bio–mimetic dual scale spherulites coating by spray deposition, Adv. Sci. Eng. Med. 8 (2016) 181–187, https://doi.org/10.1166/asem.2016.1842.

[37] B.P. Singh, B.K. Jena, S. Bhattacharjee, L. Besra, Development of oxidation and corrosion resistance hydrophobic graphene oxide-polymer composite coating on copper, Surf. Coat. Technol. 232 (2013) 475–481, https://doi.org/10.1016/j.surfcoat.2013.06.004.

[38] B.N. Sahoo, K. Balasubramanian, Facile synthesis of nano cauliflower and nano broccoli like hierarchical superhydrophobic composite coating using PVDF/carbon soot particles via gelation technique, J. Colloid Interface Sci. 436 (2014) 111–121, https://doi.org/10.1016/j.jcis.2014.08.031.

[39] B.N. Sahoo, B. Sabarish, K. Balasubramanian, Controlled fabrication of non-fluoro polymer composite film with hierarchically nano structured fibers, Prog. Org. Coat. 77 (2014) 904–907, https://doi.org/10.1016/j.porgcoat.2013.12.015.

[40] R. Arora, K. Balasubramanian, Hierarchically porous PVDF/nano-SiC foam for distant oil-spill cleanups, RSC Adv. 4 (2014) 53761–53767, https://doi.org/10.1039/c4ra09245g.

[41] P. Mishra, K. Balasubramanian, Nanostructured microporous polymer composite imprinted with superhydrophobic camphor soot, for emphatic oil-water separation, RSC Adv. 4 (2014) 53291–53296, https://doi.org/10.1039/c4ra07410f.

[42] S.A. Kulinich, M. Farzaneh, How wetting hysteresis influences ice adhesion strength on superhydrophobic surfaces, Langmuir 25 (2009) 8854–8856, https://doi.org/10.1021/la901439c.

[43] H. Liu, J. Huang, Z. Chen, G. Chen, K.-Q. Zhang, S.S. Al-Deyab, Y. Lai, Robust translucent superhydrophobic PDMS/PMMA film by facile one-step spray for self-cleaning and efficient emulsion separation, Chem. Eng. J. 330 (2017) 26–35, https://doi.org/10.1016/j.cej.2017.07.114.

[44] M.W. Lee, S. An, S.S. Latthe, C. Lee, S. Hong, S.S. Yoon, Electrospun polystyrene nanofiber membrane with superhydrophobicity and superoleophilicity for selective separation of water and low viscous oil, ACS Appl. Mater. Interfaces 5 (2013) 10597–10604, https://doi.org/10.1021/am404156k.

[45] G.T. Lim, J.E. Puskas, D.H. Reneker, A. Jákli, W.E. Horton, Highly hydrophobic electrospun fiber mats from polyisobutylene–based thermoplastic elastomers, Biomacromolecules 12 (2011) 1795–1799, https://doi.org/10.1021/bm200157b.

[46] S. Das, S. Kumar, S.K. Samal, S. Mohanty, S.K. Nayak, A review on superhydrophobic polymer nanocoatings: recent development and applications, Ind. Eng. Chem. Res. 57 (2018) 2727–2745, https://doi.org/10.1021/acs.iecr.7b04887.

[47] R. Selvaraj, M. Selvaraj, S.V.K. Iyer, Studies on the evaluation of the performance of organic coatings used for the prevention of corrosion of steel rebars in concrete structures, Prog. Org. Coat. 64 (2009) 454–459, https://doi.org/10.1016/j.porgcoat.2008.08.005.

[48] G. Das, R.D. Kalita, H. Deka, A.K. Buragohain, N. Karak, Biodegradation, cytocompatability and performance studies of vegetable oil based hyperbranched polyurethane modified biocompatible sulfonated epoxy resin/clay nanocomposites, Prog. Org. Coat. 76 (2013) 1103–1111, https://doi.org/10.1016/j.porgcoat.2013.03.007.

[49] A.K. Mishra, R. Narayan, K.V.S.N. Raju, T.M. Aminabhavi, Hyperbranched polyurethane (HBPU)–urea and HBPU–imide coatings: effect of chain extender and NCO/OH ratio on their properties, Prog. Org. Coat. 74 (2012) 134–141, https://doi.org/10.1016/j.porgcoat.2011.11.027.

[50] R.B. Naik, S.B. Jagtap, D. Ratna, Effect of carbon nanofillers on anticorrosive and physico–mechanical properties of hyperbranched urethane alkyd coatings, Prog. Org. Coat. 87 (2015) 28–35, https://doi.org/10.1016/j.porgcoat.2015.05.001.

[51] H.-J. Song, Z.-Z. Zhang, X.-H. Men, Z.-Z. Luo, A study of the tribological behavior of nano-ZnO-filled polyurethane composite coatings, Wear 269 (2010) 79–85, https://doi.org/10.1016/j.wear.2010.03.011.

[52] C. Syamsundar, D. Chatterjee, M. Kamaraj, A.K. Maiti, Erosion characteristics of nanoparticle-reinforced polyurethane coatings on stainless steel substrate, J. Mater. Eng. Perform. 24 (2015) 1391–1405, https://doi.org/10.1007/s11665-015-1403-7.

[53] N. Ajalesh Balachandran, K. Philip, J. Rani, Effect of expanded graphite on thermal, mechanical and dielectric properties of ethylene–propylene–diene terpolymer/hexa fluoropropylene–vinylidinefluoride dipolymer rubber blends, Eur. Polym. J. 49 (2013) 247–260, https://doi.org/10.1016/j.eurpolymj.2012.08.014.

[54] S.D. Maurya, M. Purushothaman, P.S.G. Krishnan, S.K. Nayak, Effect of nano-calcium carbonate content on the properties of poly(urethane methacrylate) nanocomposites, J. Thermoplast. Compos. Mater. 27 (2014) 1711–1727, https://doi.org/10.1177/0892705712475011.

[55] N. Arianpouya, M. Shishesaz, M. Arianpouya, M. Nematollahi, Evaluation of synergistic effect of nanozinc/nanoclay additives on the corrosion performance of zinc-rich polyurethane nanocomposite coatings using electrochemical properties and salt spray testing, Surf. Coat. Technol. 216 (2013) 199–206, https://doi.org/10.1016/j.surfcoat.2012.11.036.

[56] S. Sommer, A. Ekin, D.C. Webster, S.J. Stafslien, J. Daniels, L.J. VanderWal, S.E.M. Thompson, M.E. Callow, J.A. Callow, A preliminary study on the properties and fouling–release performance of siloxane–polyurethane coatings prepared from poly(dimethylsiloxane) (PDMS) macromers, Biofouling 26 (2010) 961–972, https://doi.org/10.1080/08927014.2010.531272.

[57] J.M. Colwell, J.H. Khan, G. Will, K.E. Fairfull-Smith, S.E. Bottle, G.A. George, A. Trueman, Prognostic tools for lifetime prediction of aircraft coatings: paint degradation, Adv. Mater. Res. 138 (2010) 137–149, https://doi.org/10.4028/www.scientific.net/AMR.138.137.

[58] P. Gupta, K. Balasubramanian, Numerical investigation of heat loss in nano-fumed silica reinforced styrene acrylonitrile hydrophobic thermo-sheath for heat inhibition in hydronic boiler, Mater. Focus 5 (2016) 556–564, https://doi.org/10.1166/mat.2016.1362.

[59] C. Ma, L. Xu, W. Xu, G. Zhang, Degradable polyurethane for marine anti-biofouling, J. Mater. Chem. B 1 (2013) 3099, https://doi.org/10.1039/c3tb20454e.

[60] B.N. Sahoo, K. Balasubramanian, M.M. Sucheendran, Thermally triggered transition of superhydrophobic characteristics of micro and nano textured multiscale rough surfaces, J. Phys. Chem. C (2015), https://doi.org/10.1021/acs.jpcc.5b02917. 150610094322003.

[61] K.A. Zargiel, J.S. Coogan, G.W. Swain, Diatom community structure on commercially available ship hull coatings, Biofouling 27 (2011) 955–965, https://doi.org/10.1080/08927014.2011.618268.

CHAPTER 11

Superhydrophobic antibacterial polymer coatings

Ubong Eduok[a], Jerzy Szpunar[a], Eno Ebenso[b,c]
[a]Department of Mechanical Engineering, College of Engineering, University of Saskatchewan, Saskatoon, SK, Canada
[b]Department of Chemistry, School of Chemical and Physical Sciences, Faculty of Natural and Agricultural Sciences, North-West University, Mmabatho, South Africa
[c]Material Science Innovation & Modelling (MaSIM) Research Focus Area, Faculty of Natural and Agricultural Sciences, North-West University, Mmabatho, South Africa

1. Introduction: Background information

Modern health care has witnessed its own share of cost associated with the infections of medical devices. Inasmuch as these devices have recorded enormous successes in the quality of health care rendered, they are still plagued with infections. When assisted-care complications are associated with hospital acquired infections (HAIs), questions related to quality of practice, staff-training modules, and types of devices used are usually raised. With intensive education and improved surgical operations, these HAI complexities and treatment costs could significantly reduce. However, out of about 2,000,000 American (US) patients affected by HAI annually, about 100,000 result in death [1,2]. The prominent use of substandard and untreated biomedical implants also leads to bio-degradation, corrosion, and tissue infections. The high affinity of some alloys (e.g., magnesium) to corrosion in chloride-rich body fluids as well as hydrogen accumulation contributes to costly maintenance of implants. Increase in local pH (alkalinity) between tissues also leads to implant loosening [3,4]. The infection rate from these events will normally increase by 4% for some medical devices, with an extra cost of $50,000 rendered per patient if revision surgeries are required [5–8]. Venous catheters alone have led to an estimated 80,000 infection–health cases [9,10] while 80% of urinary tract infections per year have resulted from the use of urinary catheters in the United States [11,12].

HAIs from medical devices are caused by the settlement and growth of bacterial colonies on surfaces [13–17]. The attachment of bacterial cells on the surfaces of these devices subsequently results in biofilm formation and growth of larger colonies. Normally, the use of antibiotics reduces the bacterial growth patterns and maintains the integrity of these surfaces. However, with the development of resistance to antibiotics by some bacterial strains (e.g., benzyl penicillin–resistant strains of *Staphylococcus aureus* and *Neisseria gonorrhoeae*), more efficient antibacterial techniques are needed to combat device-related infections. This has led to the consensus by the European Union (EU) community

research committees (as well as the EU member states) that antimicrobial resistance is now a pressing international problem that needs urgent strategic solution (see *The Copenhagen Recommendations Report from the European Union Conference on 'The Microbial Threat,'* September 1998) [8]. To reduce bacterial adhesion on surfaces, recent developments in coating technology have led to the design and fabrication of antiinfective and superhydrophobic coatings. These coatings possess very low surface energies and unique architectures engineered to mimic the surfaces of lotus leaves [18]. Combined with their water-repelling properties, these superhydrophobic antibacterial polymer coatings significantly reduce bacterial adhesion by easing protein detachment and by discouraging attachment. The design of antiinfective coatings for medical devices, including implants, has become a major strategy in preventing device-related infections. The last decade has also witnessed improvement in a few areas, including aseptic techniques, control of environment sterility, and perioperative antibiotic prophylaxis [18]. Newer coating designs consider a wide spectrum of bacteria and their resistance to different infections when accounting for their efficacy toward successful wound healing. Most antibacterial biomaterials are designed to deliver selective medical substances to close-surface targets. These delivered substances may offer preventive functions against infections and even treatment to widen the scope of their applications [19]. A few polymeric gels have been deployed against sexually transmitted diseases (STDs). Some of them are injectable or even implantable for targeted delivery of antimicrobials (e.g., antibiotic-laden polymethyl methacrylate bead chains) [18]. Since most antibacterial polymer coatings are capable of killing bacterial cells, care is taken to address their cytotoxicity toward eukaryotic cells as well as the avoidance of unwanted tissue inflammation [18,20]. The objective of this review chapter is to present recent developments and challenges related to the superhydrophobic antibacterial polymer coating surfaces toward reduced bacterial adhesion. This chapter also covers biomedical applications toward minimizing medical device infections, marine biofouling and membrane fouling. The concept of antibacterial surfaces as it relates to superhydrophobic/low wetting surfaces is vividly explained. Summaries of research experiments using typical polymer coatings that limit bacterial adhesion on solid surfaces are enlisted with examples provided to show differences in coating-bacteria interactions.

1.1 Implant failures caused by infection

Before discussing the use of superhydrophobic antibacterial polymer coatings in antiinfective applications, let's review implant failures caused by bacterial infection. There is significant increase in the use of orthopedic implants for joint replacements, and more surgeries are expected within the next 15–20 years [21,22]. Currently, more than 300,000 hip and 700,000 knee replacement surgeries are conducted in the United States annually, and of this number, about 10% fail within 10–20 years, rendering significant

losses to patients [21]. With the increase in life expectancy, more people are outliving their implants leading to potential implant, failures in due course. Implant failures could originate from either aseptic loosening or infection, resulting in approximately 18% and 20% failures, respectively, from both cases. While causes of implant failures by aseptic loosening are beyond the scope of this chapter, we will dwell only on infections. When microbes (mostly bacteria) adhere on the surfaces of implants, the solid interfaces provide comfortable grounds for attachment, proliferation, and subsequent biofilm formation [21]. Upon multiplication, adhering bacterial cells produce extracellular polymeric substances (EPS). At this stage, these microbial colonies are considerably laborious to remove when compared to individual body-bound suspended planktonic bacteria. A combination of several antibiotics could be required for treatment if more one bacterial consortium is involved [21]. So many bacteria can cause device-related infections, but only small groups of these microbes (e.g., the *Staphylococcus* genus) constitute most observed pathogens in HAI. More than 70% implant infections are caused by a combination of *Staphylococcus epidermidis* and *S. aureus* alone while the next 8% could be attributed to *Pseudomonas aeruginosa* [21]. *Staphylococcus* also predominates the sources of infections as well as organisms isolated from cardiac implantable electronic devices (CIEDs); they account for about 60%–80% of all related cases (see Fig. 1A). Unlike the Gram-positive Bacilli (e.g., *Stenotrophomonas maltophilia*, *Acinetobacter xylosoxidans*,
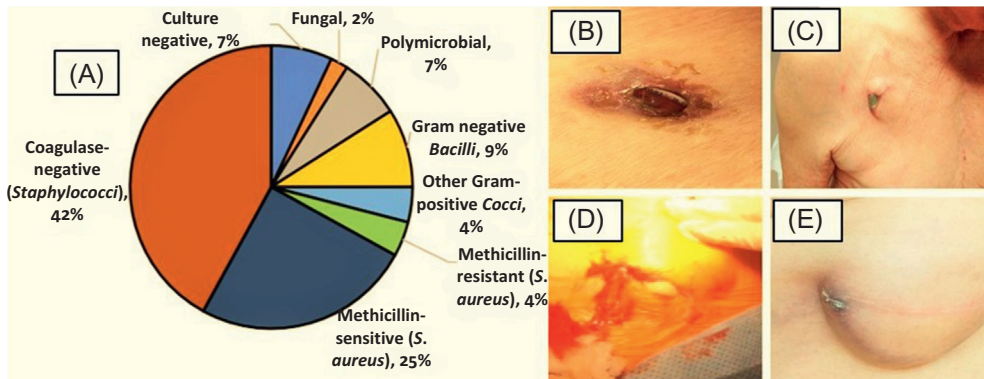
Fig. 1 (A) A microbiological survey of major infection-causing organisms isolated from permanent pacemaker and implantable cardioverter-defibrillator infections [16]. Bonding pattern between the device and skin with overt perforation of the device (B), and leads (C) representing pocket infection. The presence of pus at the incision site during CIED removal is conspicuous (D) while the bonding between the skin and the subcutaneous ICD generator shows some degree of perforation (E) [17]. *(Reproduced with permission from M.R. Sohail, D.Z. Uslan, A.H. Khan, P.A. Friedman, D.L. Hayes, W.R. Wilson, J.M. Steckelberg, S. Stoner, L.M. Baddour, Management and outcome of permanent pacemaker and implantable cardioverter-defibrillator infections, J. Am. Coll. Cardiol. 49 (2007) 1851–1859. K. Aljabri, A. Garlitski, J. Weinstock, C. Madias, Management of device infections, Card. Electrophysiol. Clin. 10 (2018) 153–162.)*

Propionibacterium spp., etc.), *S. aureus* (29%) and coagulase negative Staphylococci (CoNS, 42%) make up the most causative agents of CIED infections. This data survey covers reports collected from more than 189 cases involving permanent pacemaker and implantable cardioverter–defibrillator infections [16]. This kind of infection (on CIED) may differ to some degree depending on the type of bacteria. According to Aljabri et al. [17], signs of typical pocket infections may include local erythema, deep pain, subcutaneous swelling, etc.,; all these are all potential symptoms of infection from the device pocket. Fig. 1B–E presents some of the stages of symptoms suggestive to actual CIED infections. The presence of pus at the incision site during CIED removal is conspicuous (D) while the bonding between the skin and the subcutaneous ICD generator shows some degree of perforation (E). During corrective surgeries to replace orthopedic devices, infections may further complicate the pains and healing time. Plaquing most devices, infections of fracture and reconstructive implants have resulted from about 100,000 cases annually in the United States [23,24]. Around 0.2%–2.2% during total hip [25] and 2%–5% in spine replacement surgeries [26]. The frequent use of prophylactic systemic antibiotics has shown considerably reduction in most of these infections though site-specific delivery of antibiotics (including other antiinfective agents) could be more effective [27]. In modern diagnoses, factors related to aseptic failures and latent infections are considered when investigating the primary causes of orthopedic implant failures. More assertions have been brought forward in the recent times with some semblance of solutions as it relates to bacterial infections. Gristina et al. [28] have opined that in occasions where the cells of hosts proliferate the implant surfaces, stronger tissue integration and more resistance to microbial attachment and colonization will be attained. Modern implant designs principally consider the prevention of infection as well as implant/tissue compatibility over a prolonged period. Fig. 2 shows stages of bacterial infections that result in infection-led implant failures as well as some strategies that could address these challenges. Unlike the last two causes, initial infections could be significantly reduced if microbial adhesion

Fig. 2 Infection-related causes of implant failures and some strategies that address these challenges.

is delayed; this can be accomplished by deploying superhydrophobic antibacterial polymer coating surfaces. Their low surface energies induce water repellency, in turn discouraging reduce bacterial adhesion by easing protein detachment and attachment, with varying short and long-term effects, depending on the period of exposure.

2. The concept behind antibacterial surfaces

Antibacterial surfaces are known to resist the initial settlement and attachment of bacteria cells initiated by their inactivating effects upon interaction with bacterial cells. Most antibacterial surfaces are coated with polymer films enriched with bactericidal additives capable of reducing bacterial cellular growth by influencing in-cell osmotic stability and cytoplasmic pH. Upon direct interaction with these additives, the resultant actions lead to the leakage of cellular contents and subsequently, death [18,20,29]. According to Hasan et al. [29], antibacterial surfaces are classified as either *antibiofouling* or *bactericidal*. Inasmuch as this definition is not universal, its concept allows for a clearer explanation of associated surface phenomena. These authors opined that antibacterial surfaces are regarded as "antibiofouling" if their surface topographies or/and chemistries repel bacterial cellular attachment. Bactericidal surfaces normally will obstruct cellular contact, leading to death, but an antibacterial surface could also be both antibiofouling and bactericidal. Fig. 3 presents two distinct strategies for mitigating bacterial adhesion by superhydrophobic antibacterial coating surfaces; their surface repelling mechanism toward bacterial adhesion could be by exclusion steric or electrostatic repulsion or due to reduced surface energies while cytotoxicity is linked with the biocidal-release or contact-active mechanism.

3. Superhydrophobic antibacterial polymer coatings

The interactions of bacterial cells at surfaces are as complex as the quorum sensing mechanisms within their colonies. These processes lead to serious infections, biomedical implant failures as well as other diverse ill-health issues associated with medical devices. The use of antibiotics can alleviate these problems. However, the consistent use of traditional
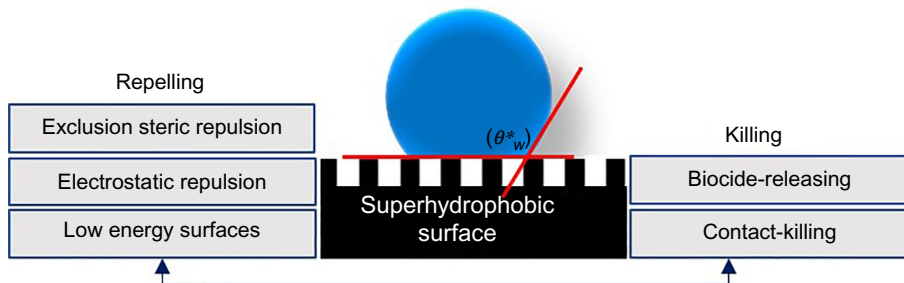
Fig. 3 Two distinct strategies for mitigating bacterial adhesion by superhydrophobic antibacterial coating surfaces.

antibiotics only makes these bacteria more resistant, and this is a significant problem in modern health care. Much older antibacterial surface designs involved the leaching out of biocidal antibiotics within surfaces capable of killing adhering bacterial cells, but their secondary environmental impacts call for more stringent approaches. To combat this scourge, the design of new materials with antibacterial properties has been the subject of intense discussions in the recent times [29]. Amphoteric metal oxides and some biopolymer derivatives (e.g., peptides and chitosan), as well as silver formulations have been reported to possess some interesting antibacterial properties. However, since the basis for selecting antibacterial agents for surface designs are based on some criteria as pointed out in Fig. 2, modern mitigation techniques adopt approaches that discourage the initial cellular adhesion using superhydrophobic surfaces (SHS). These surfaces alter the adhesion force at cellular/surface interfaces while also prompting the subsequent removal of settled bacteria cells before biofilms are formed. This approach has become a smarter strategy against bacterial infection. SHS are bioinspired with the high contact angle ($\theta_w^o > 150$ degrees) in lotus leaf surfaces. The lotus leaf surfaces were considered in the late 1990s to possess microscale topographies with coated convex microstructures on their epidermal cells. The presence of hierarchical nano and microstructures were revealed in the early 2000s and since then the superhydrophobic nature of these leaves has been equally linked with the presence of hydrophobic epicuticular wax and their microstructures. These surfaces are characterized by sufficiently high degree of water repellency that enables the rolling-off of dirt particles along with water droplets. This phenomenon is known as "lotus effect" [29]. Fig. 4 depicts typical fields of medical application that may use superhydrophobic antibacterial polymer coatings. Alongside the use of polymer coatings, other methods of fabricating SHS include: solution method [30–32], sol–gel [33,34], photolithography [35], plasma fluorination [36,37], in situ reduction [38], layer–by–layer (LBL) deposition [39], mussel–inspired strategy [40], phase separation/electrochemical deposition [41], chemical vapor deposition [42], crystallization control [43], assembly [44], solution-immersion methods [45], etc.
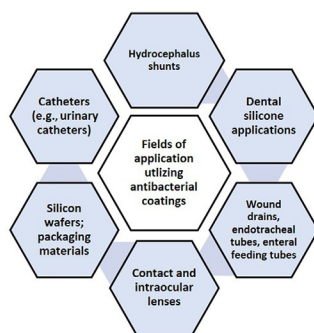
Fig. 4 Typical fields of medical applications that utilized superhydrophobic antibacterial polymer coatings.

3.1 Poly(lactic acid)-based coatings

In recent times, SHS induced by special polymer coatings have contributed to reduced bacterial adhesion due to weak surface attachment, low protein adsorption, and/or and easy protein detachment [46]. Since the hydrophobicity of most coating surfaces do not last, it has become imperative to incorporate low surface energy (LSE) additives [e.g., some bactericides, nanoparticles (NPs), surfactants, etc.] within these coatings for long-term performances. This has also led to significantly enhanced bioadhesion repelling effect within coatings [46]. It is worthy of note to mention that without effective antibacterial SHS, bacterial adhesion only increases with exposure of culture time. Fadeeva et al. [47] recorded 18 h period while studying bacterial retention time on superhydrophobic titanium surfaces prepared by laser ablation while 24 h was reported by Sousa et al. [48] from superhydrophobic poly(D-lactic acid) coating surface. In the latter study [48], authors were investigating the interaction between fabricated SHS and different bacteria (strains of *S. aureus* and *P. aeruginosa*). They discovered that even when both strains later colonized these substrates, significantly higher adhesion resistance toward *S. aureus* cells was observed on roughened SHS compared to the smooth hydrophobic surface. Scanning electron microscopy (SEM) evidence revealed the formation of EPS from *P. aeruginosa* on SHS surfaces due to the presence of bacterial biofilm consistent with this bacterium. A similar work was also investigated by Fadeeva et al. [47] using laser-treated biomimetic titanium (Ti) surface. Authors observed varying bacterial adhesion patterns from two pathogenic bacteria strains (*S. aureus* and *P. aeruginosa*). While more *S. aureus* cells colonized the SHS titanium substrate, no *P. aeruginosa* growth was revealed. Authors observed a hydrophobic Ti surface ($\theta_w^o = 166 \pm 4$ degrees). Results from these studies [47,48] were preliminary findings; additional studies should be conducted for more bacterial strains. The effect of more variables (e.g., surface characteristics) and experimental conditions (e.g., culture media, temperature, etc.) should also be investigated to address intraspecies variability. Poly(L-lactic acid) is a biodegradable polymer with biocompatible SHS potentials. It also has attracted lots of attention in biomedical application due to its prospects in cell growth substrata, tissue engineering, and drug delivery. This material was investigated by Song et al. [49] toward animal cell (mouse lung line L929) adhesion. Authors reported significantly reduced the presence of these animal cells on treated SHS surfaces relative to the smooth hydrophobic surfaces, even after Ar-plasma treatment. A similar trend was also observed by another group using bone marrow cells [50].

3.2 Polyethyleneimine-based coatings

Polyethyleneimine (PEI) is synthesized from cationic polymerization of aziridine; its quaternized forms are known for their proven antimicrobial activities. Like most cationic polymers with biocidal potentials, PEI permeates and ruptures bacterial cell membranes leading to cellular mortality. They are utilized as principal components for some antimicrobial coatings for medical devices and drug carriers in biomedical applications
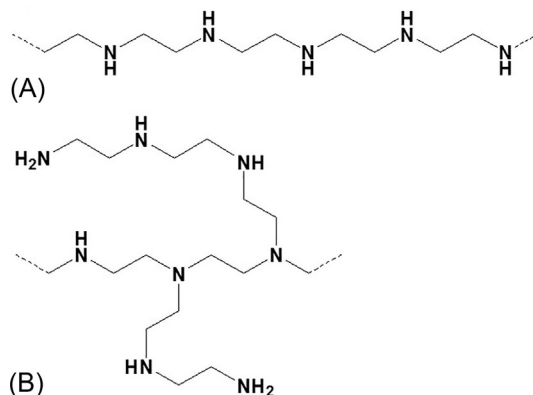
Fig. 5 (A) Linear and (B) branched PEIs are utilized as principal components of some antimicrobial coatings for medical devices and as drug carriers in biomedical applications.

[51]. Fig. 5 depicts typical linear and branched structures of PEIs with amino functionalities consistence with antimicrobial applications. Milovic et al. [52] have investigated a nonrelease model of antibacterial PEI coating on amino-glass against *Escherichia coli* and *S. aureus*. This coating demonstrated significant adhesion resistance against nearly 10^9-fold bacterial adhesion in live count due to the long hydrophobic polycationic chains on the PEI molecule. This work also recorded a 100% inactivation of these surface-adhering bacteria. In another work by Yudovin-Farber et al. [53], authors revealed that the extent of alkylation and N–methylation of quaternary ammonium PEI compounds could contribute to their antibacterial activities. They recorded a complete inhibition of *S. aureus* and *E. coli* growths at 80 and 320 µg/mL concentration, respectively. To address short-term stability of polyelectrolyte multilayer film (PMF) deployed under physiological conditions and its limits as an antibacterial coating for medical devices, He and Chan [54] proposed the use of PMF system comprising of PEI constructed by covalent LBL deposition. These PEI multilayers were very efficient against two distinct bacterial (*S. aureus* and *E. coli*) growths and more enhanced when modified with silver nanoparticles (AgNPs). This was attributed to the long–term release of AgNPs. Shen et al. [55] have investigated the extent of bacterial adhesion on poly(ethyleneimine)–Ag$^+$ complex assembled with poly(acrylic acid). This coating on a teflon substrate significantly limited bacterial adhesion in a self-cleaning mechanism due to its unique structured surface morphology. However, enhanced performance was observed in the presence of bactericidal Ag$^+$ ions due to selective delivery at desired sites. Ag-functionalized films were tested using Kirby-Bauer assay with 1000 *E. coli* cells. These NPs readily stabilize as they form within the PMFs via reduction of silver ions. PEI also demonstrated enhanced antibacterial potential since it could successful

bind with transition metal cations. Authors in these works [52–55] may not have measured significant low surface wetness, but the presence of immobilized long polymeric chains, alkylated, and cross-linked quaternary ammonium groups in most of these PEI coating systems suggests that their hydrophobicity could have been a contributing factor to their bactericidal activity.

3.3 Poly(vinylidene fluoride)-based coatings

Another superhydrophobic polymer reported within the literature is poly(vinylidene fluoride) (PVDF) due to the fluorine content within its chemical structure — $(CH_2CF_2)_n$—. PVDF has been used in soft tissue repairs, blood vessels prostheses, ligaments, vascular grafts as well as other biomedical applications, due to its biocompatibility [56,57]. It is also a nondegradable polymer used in long-term textile implants due to its thermoplastic properties toward durable engineering strength. Its surface tension prompts its usage for surface cleaning. PVDF is also chemical resistant with ferroelectric behaviors, very biocompatible and nontoxic. Its superior elasticity and strength (relative to high-density polyester and polypropylene) make it an excellent candidate for meshes for hernia repairs as well as modern synthetic and nonabsorbable medical sutures [56]. The four phases in PVDF, characterized by $—CH_2$ and $—CF_2$ conformations within its polymer chain, exhibit unique properties that contribute to its surface behaviors (including surface energy and roughness pattern) which is linked with its potential for biomedical applications [56,58]. Spasova et al. [57] have investigated the superhydrophobic nanofibrous materials of PVDF polymer and hexafluoropropylene copolymerized PVDF material synthesized from electrospinning technique. This material was functionalized with silanized ZnO NPs and with 5-chloro–8-hydroxyquinolinol (CHQ, a model drug). The incorporation of ZnO NPs within the PVDF nanofibers increased its gross contact angle $(\theta_w^o = 152$ degrees) and contributed to its antibacterial efficacy. The SEM micrographs of the normal PVDF-CHQ (A) and hexafluoropropylene-modified PVDF-CHQ (B) nanofibers are displayed in Fig. 6A and B. These fibers had average diameters of 118 ± 20 nm and 107 ± 30 nm for normal PVDF-CHQ and hexafluoropropylene-modified PVDF PVDFHFP/CHQ, respectively. These fibers were observed to possess limited adhesion toward E. coli and S. aureus revealing distinct inhibition zones against S. aureus (4.4 and 5.5 cm) and E. coli (3.5 and 4.9 cm) growths. This was hugely attributed to the presence of the hydroxyquinolinol drug and ZnO NPs within the polymeric fibers. Micrographs of inhibitory zones against growths of S. aureus and E. coli after 24 h interaction with different PVDF fibers are presented in Fig. 6C. Converse to the experimental results obtained in this study, Venault et al. [58] reported the preparation of a poly(ethylene glycol) (PEG)–based PVDF membrane; its hydrophilic nature was due to the presence of the PEG moiety within the membrane. The membrane was tested against the absorption of some proteins (bovine-serum-albumin, lysozyme, and
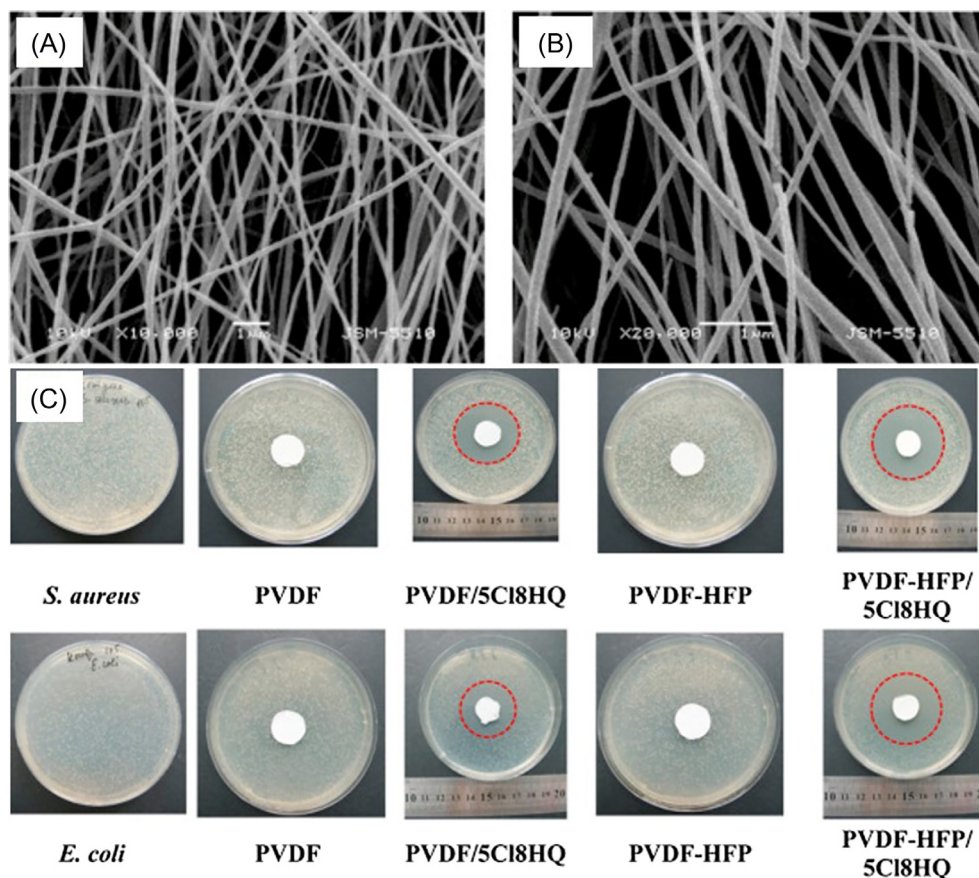
Fig. 6 The SEM micrographs of the normal PVDF-CHQ (A) and hexafluoropropylene-modified PVDF-CHQ (B) nanofibers. (C) Micrographs of inhibitory zones against growths of *S. aureus (upper row)* and *E. coli (lower row)* after 24h interaction with different PVDF fibers (alongside 5-chloro-8-hydroxyquinolinol drug). *(Reproduced with permission from M. Spasova, N. Manolova, N. Markov, I. Rashkov, Superhydrophobic PVDF and PVDF-HFP nanofibrous mats with antibacterial and anti-biofouling properties, Appl. Surf. Sci. 363 (2016) 363–371.)*

fibrinogen). Results revealed a nonspecific adsorption pattern associated with the chemistry and molecular weight of the proteins as well as the nature of the membrane. This PEGylated PVDF membranes were also efficient toward the resistance of bacterial (*S. epidermidis* and *E. coli*) attachment and their biofilm formation. The enhanced antibacterial activity of this modified PVDF membrane was linked with the presence of its PEGylated brushes, especially at a 3wt% PEG additive content. The preparation, modification, and applications of PVDF membranes have also been thoroughly reviewed by Kang and Cao [59].

3.4 Fluorinated silica coatings

Most coating surfaces could be enriched with chemical groups (e.g., fluorinated) capable of rending them superhydrophobic. Fluorinated silica coatings are known for their reduced surface energies and water-repellent properties due to the incorporation of fluorinated groups, achieved using special precursors (e.g., fluoroalkylsilane) [60]. Surface coatings synthesized from these precursors normally possess significantly high magnitudes of θ_w^o. Benjamin et al. [61] synthesized a xerogel silica coating using a LSE compound (heptadecafluoro-1,1,2,2-tetrahydrodecyl) trimethoxysilane (17FTMS). The resistance of its surface toward bacterial (*S. aureus* and *P. aeruginosa*) adhesion was attributed to its unique micro- and nanostructural features and LSE due to the presence of fluorinated groups on silica. Bacterial adhesion resistance was enhanced at higher 17FTMS concentrations toward the release of biocidal nitric oxide (NO) agents. The barrier performance of this coating was not only controlled by factors related to surface chemistries alone, but also by polymer composition and bacterial species [61]. Hammami et al. [62] have investigated the use of hydrophobic organosilica/poly(ether-imide) nanofibers as foul-resistant membrane for distillation. The coating showed increased flux up to 140% relative to commercial membranes due to organosilica particles (5%) doped within it. Its hydrophobicity was also linked with particulate contents as well as the presence of fluorinated groups incorporated using (pentafluorophenyl)triethoxysilane precursor. Fouling test was conducted using ampicillin-resistant *E. coli* strains after loading eugenol antimicrobial agent within the organosilica NPs. Ellinas et al. [63] also investigated the effect of coating hydrophobization using octafluorocyclobutane gas on a poly(methyl methacrylate) substrate. Bacterial adhesion test was conducted using unicellular cyanobacteria *Synechococcus* sp. PCC7942. Reduced cellular adhesion was observed and this was attributed to the material's micro-nanotextured pattern fabricated by high-density plasma reactor as well as the fluorinated surface groups. Fluorinated silica coatings have also recorded significant successes in surface treatments, especially with antibacterial superhydrophobic/oleophobic cotton [64] as well as wood fiber products [65]. Jin et al. [66] prepared LSE 1*H*,1*H*,2*H*,2*H*-perfluorooctyl trimethoxysilane self-assembled monolayers on the titania precoated cellulose surface against lysogenic *E. coli* cellular adhesion. Reduced bacterial adhesion was attributed to the coating's unique morphology as well as its LSE; the coating also possessed both superhydrophobic and oleophobic properties. Apart from these superhydrophobic siloxane derivatives, Kottmann et al. [67] have elaborately reviewed recent developments and antimicrobial applications of some polydimethylsiloxanes (PDMSs). Wang et al. [68] have investigated the performance of a mechanically enhanced hydrogel coating for a medical device. The structure of this coating was made of highly cross-linked poly(2-hydroxyethyl methacrylate) within alginate hydrogels with hierarchical surface "nested network (NN)." Fig. 7 shows (A) the SEM images of micropillar PDMS substrates without hydrogel coating and (B) with NN hydrogel-coated substrate. The pillars of the PDMS substrate were 350 μm between, with 150 μm diameter and 200 μm
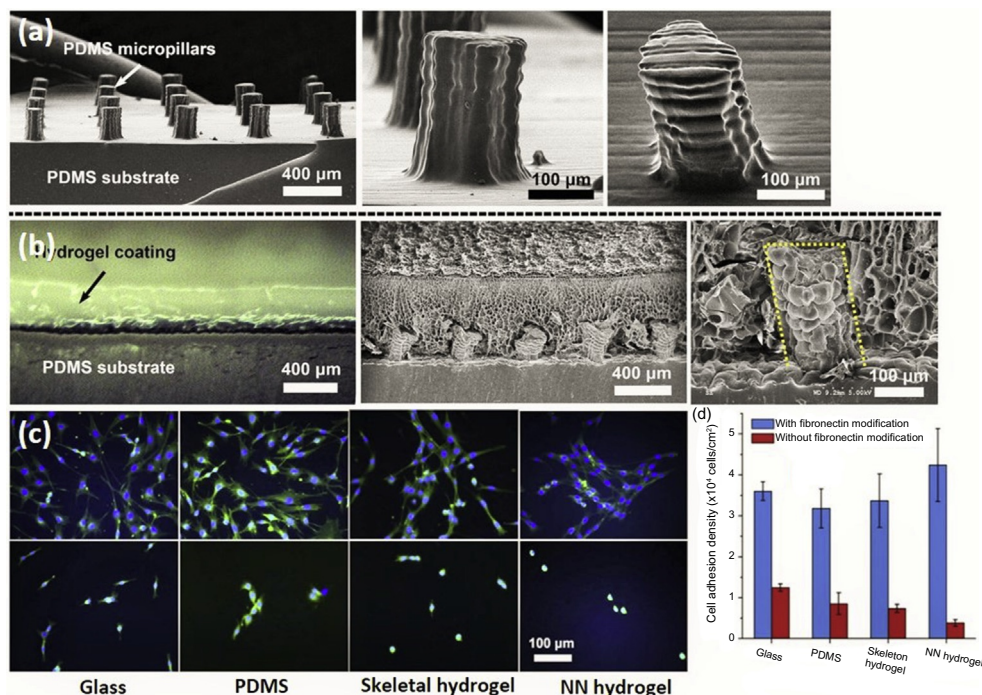
Fig. 7 Mechanically enhanced hydrogel coating: coating structure is made from highly cross-linked poly(2-hydroxyethyl methacrylate) within alginate hydrogels with hierarchical surface "nested network (NN)." (A) The SEM images of micropillar PDMS substrates without hydrogel coating and (B) with NN hydrogel coated substrate are represented in the first two rows. (C) Fluorescent images of NIH 3T3 fibroblasts stained with phalloidin-FITC and DAPI (4′,6-diamidino-2-phenylindole) on glass, PDMS, skeleton hydrogel, and NN hydrogel with and without fibronectin modification. This NN coating restricted the adhesion of stained NIH 3T3 fibroblasts on different substrates; the corresponding cell counts using nuclei staining is presented as mean values (D); lower values of cell adhesion on the coating are observed without fibronectin modification. *(Reproduced with permission from Z. Wang, H. Zhang, A.J. Chu, J. Jackson, K. Lin, C.J. Lim, D. Lange, M. Chiao, Mechanically enhanced nested-network hydrogels as a coating material for biomedical devices, Acta Biomater. 70 (2018) 98–109.)*

height. This coating restricted the adhesion of fibroblast cells as shown on the fluorescent micrographs of stained NIH 3T3 fibroblasts on different substrates. Reduced presence of the cells was observed on the hydrogel coating due to its LSE. The corresponding cell counts using nuclei staining are presented as mean values (D); lower values of cell adhesion on the coating were observed without fibronectin modification.

3.5 Superhydrophobic antimicrobial peptide coatings

Antimicrobial peptides (AMPs, or simply *host-defense peptides*) are a principal component of innate immune responses is all life forms. They are also a broad-spectrum antibiotic with demonstrated potentials for therapeutics. Their antibacterial mechanism is

based on two distinct features: (a) their highly rigid backbone and (b) side groups. AMPs may be anodic or cathodic or both, but these side groups are arranged in a way that one side has the hydrophobic group while the other has a cationic net charge [69]. They particularly distort bacterial cellular activities by opening the cell membranes with hydrophobic a backbone and side chains, in turn causing death after leakage of cellular contents. AMPs are effective toward the growth of a wide range of microbes including, Gram–negative and Gram–positive bacteria, fungi, and even some viruses. AMPs may not be hydrophobic, but in the recent times, several modifications steps have been taken to provide them with opportunities to combat demanding pathogens on superhydrophobic coating surfaces. Schmidtchen et al. [70] have reported the effect of hydrophobic modifications on several antibacterial peptides deployed against some multiresistant bacterial strains.

4. Particle-releasing coatings: Incorporating additives within polymer coatings

It has been established that the attainment of long-term hydrophobic surfaces is problematic. Since the hydrophobicity of most SHS do not last, the incorporation of secondary antibacterial additives (e.g., oxides, NPs, drugs, etc.) has become an effective alternative technique for creating antibacterial materials toward long-term performances. Copper and NOs as well as NPs of silver (AgNPs) are regularly deployed to prevent bacteria colonization on surfaces due to their efficient antibacterial activities [46]. These composite materials exhibit reducedGram–negative and Gram–positive bacterial cellular adhesion with significantly high inhibition toward their growth. However, their controlled-release mechanisms within protective coatings call for concern. Since most these additives cause cellular death by disrupting their walls/membranes, their effectiveness could be dependent on their active concentrations, penetration depth as well as the bacterial type. The cell walls of Gram–negative bacteria are made of two glycan–rich lipid membranes and also a murein layer while only one layer of lipid membrane (enveloped by a thick murein film) is present in that of the Gram–positive bacteria. Fig. 8 presents schematics of cell wall anatomies of both Gram–negative (A) and Gram–positive (B) bacteria [70]. The unique release mechanisms of these antibacterial agents contribute to reduced bacterial adhesion on surfaces and these phenomena depend on the degree of cellular interaction between each substance and the bacterial colony. When coated on the medical devices, these biocidal additives are either: (a) incorporated/impregnated within the polymer coatings, (b) adhered onto the coating surfaces by physical/chemical adsorption; or applied by (c) complexation or (d) conjugation. In any of these techniques, polymer coatings are deployed as carriers for these antibacterial agents while also enabling their controlled release at localized sites against microbial cells. In the presence of these additives, the initial bacterial settlement at surfaces are prevented, hence no subsequent biofilm formation is possible. The surfaces of most indwelling devices (e.g., urinary catheters,
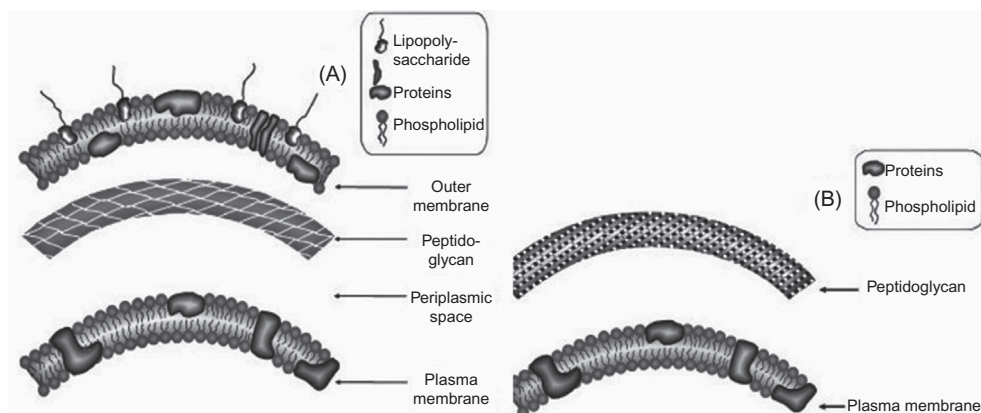
Fig. 8 Schematics of bacterial cell walls of Gram-negative (A) and Gram-positive (B) microbes: The cell walls of Gram-negative bacteria are made of two glycan-rich lipid membranes and a murein layer (negatively charged lipopolysaccharide) while only one layer of lipid membrane (enveloped by a thick a murein film) is present in that of the Gram-positive bacteria. *(Reproduced with permission from A. Schmidtchen, M. Pasupuleti, M. Malmsten, Effect of hydrophobic modifications in antimicrobial peptides, Adv. Colloid Interface Sci. 205 (2014) 265–274.)*

wound drains, endotracheal tubes, enteral feeding tubes, etc.) are precoated with antibiotic–enriched films that discourage bacterial adhesion [71,72]. The additives presented within this chapter were deployed as antibacterial agents but may not have contributed to the gross surface hydrophobicity of the coatings.

4.1 Silver nanoparticles

Apart from their antibacterial activities, AgNPs are known for their low cytotoxicity toward mammalian tissue cells. The encapsulation of these particles within coatings becomes an effective strategy toward the fabrication of antibacterial coatings. Ag is known beyond its aesthetic appeal as a precious metal and its antibacterial properties have been widely reported in the recent times [73]. The preference of Ag and its formulations above penicillin as antibacterial drugs for wound healing had been documented since the 1930 revolution [74]. Their applications in modern medicine were renewed yet again in the late 1970s. Today, successful trails have led to effective coatings for medical devices using Ag compounds due to their quick and unselective responses to both Gram–positive and Gram–negative bacteria with relatively less resistance [73]. It has been reported that mammalian cells do tolerate high Ag concentrations compared to bacteria, however, their cytotoxicity may significantly vary among different cells and the basis for comparison differs in most studies. While most studies investigate different Ag compounds, in the nanoscale, their properties may also differ due to

inherent surface functionalities and size–related factors. Unlike AgNPs, nanocrystalline Ag are known for causing aggravated tissue inflammation due to the occurrence of necrosis in immune cells [75]; experimental evidence has been recorded in cultured J774 macrophages [76]. Ag compounds and its formulation could be effective toward the death of bacterial cells, however, the potential implications toward human health and its environment are also a major concern.

4.2 Nitric oxide

This endogenous diatomic free radical has been widely utilized in neurotransmission and wound healing, including some physiological processes like immune response and vaso-dilation. NO's cytotoxic actions involve stress–induced nitrosative and oxidative processes via reactive byproducts (e.g., N_2O_3 and peroxynitrite), leading to cellular content modification (deoxyribonucleic acid cleavage, modification of membrane-based proteins, lipid peroxidation, etc.), disruption of cellular membrane, and subsequently, death [77]. This is accomplished at higher NO concentrations. NO also plays important roles in the mammalian immune response to pathogens [78]. Its auto-released and delivery mechanisms have contributed to several pharmacological applications using delivery agents like nitropress, L-proline, S-nitrosothiol, especially, polymeric coatings [77]. At reduced concentrations, NO normally signals growth activities of immune cells. The efficacy of NO increases acid and glutathione production by macrophages. Table 1 presents some NO release mechanisms at the surfaces of medical devices [79]. Lu et al. [78] have investigated the antibacterial properties of NO-releasing chitosan oligosaccharides against *P. aeruginosa*. No toxicity was observed for mouse fibroblast L929 cells. A similar test has also been investigated by Yang et al. [80] toward the antibacterial activity of NO-releasing hyperbranched polyamidoamines against common dental pathogens (*Aggregatibacter actinomycetemcomitans*, *Porphyromonas gingivalis*, *Actinomyces viscosus*, and *Streptococcus mutans*) and human gingival fibroblast cells.

4.3 Antibiotic and antiseptic-loaded coatings

The use of antibiotic–enriched coatings, though effective toward a few bacterial strains, has been reported for prosthetic Ti devices. Most of these antibiotics include cefalotin, geocillin, amoxycillin, mandol, tobramycin, vancocin, etc. [72]. However, the dynamics of substance release could be dependent on the rate of degradation of the based coatings in most cases. Vancocin might be effective against bone infections in the elderly during Ti–alloy hip implant, but the coating that "houses" this molecule might hinder this application. It has been reported that vancocin-loaded thin sol-gel coatings on Ti implants decreases its effectiveness in rats at higher concentrations against *S. aureus* cells [81,82]. Chlorhexidine is still utilized as an antiseptic agent against a wide spectrum of bacteria in modern medicine. It prevents bacterial (cellular) multiplication at lower

Table 1 NO release mechanisms in some medical devices

Types of devices	Release mechanism	Mode of NO release
Chemical release	Chitosan-NONOate $+ H_2O \rightarrow 2NO_{(g)}$	Chitosan-based diazenium diolates (NONOates) are synthesized by reacting NO with modified chitosan polymers and release NO in aq. media; the rate at which NO is released is dependent on amount of water, temperature, and pH
	$2RSNO \rightarrow 2NO_{(g)} + RSSR$	Interpolymer complexes with nitrosothiols derived from glutathione are decomposed in the presence of light, metal, or heat. The rate of NO release is dependent on the wound temperature
Free gas	$NO_{(p)} \rightarrow NO_{(g)}$	NO is stored under pressure and released over time at controlled levels
Adsorption/ release	Zeolite $xNO \rightarrow xNO_{(g)}$	Transition metal-exchanged zeolites adsorb and store NO (up to 1 mmol of NO/g of zeolite); stored NO is released on contact with an aq. environment; the release of the NO can be tuned by altering the chemical composition, amount of water, temperature, and pH
Cell and enzyme	Glucose $\rightarrow$ lactic acid (catalyzed by *Lactobacillus fermentum*)	Probiotic bacteria and enzymatic systems can be used to produce organic acids which will dismutate nitrite salts releasing NO overtime depending on temperature and pH

concentrations and it is also bactericidal when administrated in increased amount. The antibacterial activity of chlorhexidine-hydroxyapatite coatings has been reported by Campbell et al. [83] on stainless steel external fixation pins in the presence of *S. aureus* strains. Furanones are another set of additives that has been used for medical applications in the past few two decades; they are plant-based secondary metabolites. Furanones are a class of antibacterial heterocyclic compounds used in inhibiting bacterial colonization on surfaces by disrupting quorum sensing within biofilms. Francolini et al. [84] have investigated the effectiveness of benzofuranone against the initial attachment of *S. aureus* cells. Though this compound when loaded within polyurethane did not completely limit the bacterial growth, the development of most cells as well as their biofilm formation was distorted in the presence of usnic acid on the polymer surface. Most benzo-derivatives are expensive. However, sourcing 2-furanone for biomedical application is easy. It can now be synthesized by oxidation of furfural. This product also coexists in equilibrium with its tautomer (2-hydroxyfuran) (Fig. 9).
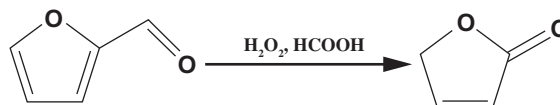
Fig. 9 Formation scheme for 2-furanone synthesis via oxidation of furfural.

4.4 Other organic and inorganic additives

Cysteine interacts negatively with microbial membranes of bacteria and fungi, thereby disrupting their physiology and metabolic processes toward cytotoxicity. New cysteine-based antibacterial coatings have been reported to reduce bacterial colonization on nasal silicone prongs [85]. The activities of defensins extracted from manila clam (*Ruditapes philippinarum*) have also been investigated [86]. By incorporating drugs within polymeric carriers, delivery at cell membranes is possible in most biomedical applications. A superhydrophobic PVDF nanofibrous polymer incorporated with ZnO NPs and 5–chloro–8–hydroxyquinolinol drug has been investigated by Spasova et al. [57] for its drug-delivery and barrier performance. The presence of ZnO NPs within the PVDF nanofibers increased the surface contact angle as well as the antibacterial properties to these nanofibers toward *E. coli* and *S. aureus* bacterial growth. Other organic [e.g., quaternary ammonium salts (QAS)], inorganic (Cu, Zn TiO_2 NPs, quantum dots, etc.), and natural (e.g., derivatives of chitosan, cellulose, carboxymethyl cellulose, alginate, etc.) antibacterial agents have been widely reported in the literature for numerous biomedical applications [87].

5. Superhydrophobic antifouling coatings

It is worthy of note to mention that fouling does not only occur on untreated medical devices; this phenomenon encompasses every human endeavor, from domestic to the industrial spheres. Fouling may be a general term that describes the accumulation of microbes (e.g., bacteria) on surfaces, but marine biological fouling defines the adhesion of every undesirable micro- and macroorganisms (flora and fauna) on submerged surfaces in seawater (e.g., ship hulls, aquaculture cages, pipelines, etc.).

5.1 Marine antibiofouling coatings

The adaption of fouling species to environmental changes within their niches renders biofouling control very challenging. Depending on the substrate and marine conditions, the initial biofouling stage normally involves the creation of conditioning films as polysaccharides and proteins accumulate on substrates [88]. This is immediately followed by the settlement of simple diatoms and bacteria as biofilms are formed. The colonialization of the next biological community (macrofouling) is controlled by these single–cellular species as well as the condition of microbial biofilms. When complex organisms (e.g., tubeworms, barnacles, arthropods, molluscs, etc.) take over the surfaces of submerged

substrates at the later stage after the minor foulers (e.g., algal spores, barnacle cyprids, and marine fungi), dire consequences do evolve. The control of marine biofouling is most effective if the initial settlement of marine bacteria and diatoms on submerged surfaces is prevented. Increase in surface roughness of ship hulls due to biofouling contributes to more hydrodynamic friction, in turn leading to more fuel consumption (by 40% increase) [88] as well as 20% increase in fish production cost due to routine hull cleaning procedures [89]. In line with effective biofouling control, researchers worldwide are now targeting the reduction and control of bacterial attachment in the early fouling stages, especially during the creation of conditioning films. Since most bacteria developed biofilm-based survival mechanisms against physical and chemical attacks, antifouling coating surfaces are designed to limit bacterial accumulation, disrupt cellular physiology, and discourage shear resistance of matrix-embedded multicellular bacterial communities [90]. There are numerous antibiofouling coatings in the market and so many are still being reported in the literature at various research stages. Fig. 10 represents some anti-fouling coating techniques corresponding to each fouling agents. Most of them are PDMS elastomer derived. PDMS coatings possess low adhesion against foulant adhesion because of their low surface energies and bulk moduli. PDMS can also be easily modified to incorporate more hydrophobic fluorinated chemical groups as well as bactericidal groups (e.g., QAS, etc.) against Gram–positive and Gram–negative bacteria, yeasts, and molds [88,90]. The high flexibility and hydrophobicity of pendant QAS-bearing PDMS coatings contribute to prolonged service life and resistance to a wide variety of bacteria. This surface modification also allows for changes in QAS alkyl chain length, concentration as well as the gross molecular weight in line with making coatings with the desired biocidal efficacy and mechanical strength against multiple foulers with limited surface interactions. The marine antibiofouling coatings enlisted in this chapter may not have been superhydrophobic, but they possessed efficient antifouling potentials against a wide spectrum of bacteria as well as other micro and macrofoulers due their low surface energies [91]. Tables 2 and 3 present a summary of superhydrophobic coatings with

Fig. 10 Antifouling coating techniques for selected fouling agents.

antibacterial potentials utilized or tested in marine antibiofouling and biomedical applications, respectively.

5.2 Mitigating membrane fouling

The inhibition of membrane fouling has also been a subject of many recent reviews [106–109], especially, in advanced wastewater treatment plants deploying reverse osmosis and nanofiltration. The challenges encountered during mitigation procedures depend on the foulant as well as changes in permeate flux, total dissolved solids, pressure drop, and filtration time. Some of the factors affecting the attachment of bacteria on membrane surfaces are presented in Fig. 11 [109]. The study reported by Spasova et al. [57] using superhydrophobic nanofibrous materials of PVDF polymer and hexafluoropropylene copolymerized PVDF material is a typical example. Authors observed significantly reduced bacterial (toward *E. coli* and *S. aureus*) adhesion. Venault et al. [58] have also investigated the resistance of PEGylated PVDF membranes toward *S epidermidis* and *E. coli* attachment. The antibacterial activity was attributed to the presence of its PEGylated brushes within the PVDF polymer matrix. A study by Hammami et al. [62] has also reported the barrier performance of a hydrophobic fluorinated organosilica/poly(etherimide) nanofibers as foul-resistant (ampicillin-resistant *E. coli*) membrane for distillation. The fouling resistance of this coating was also enhanced upon the introduction of eugenol antimicrobial agent within organosilica NPs. The reduction in Gram-negative bacterial (*Sphingomonas paucimobilis*) adhesion on polyamide reverse osmosis membranes via electrostatic interactions has been investigated using cationic phosphorylcholine polymer coating (p(MPC-*co*-AEMA)) [110]. Fig. 12 represents microscopic images with limited bacterial attachment on coated membranes after different test durations. Images were collected from confocal laser scanning microscopy (CLSM); Fig. 12C and F shows both living (green) and dead (red) bacteria [110].

6. Toxicological risks related with antimicrobial coating components in health care

The use of antimicrobial coatings has revolutionized modern health care in terms of inhibition of bacterial growths and infections, and this has been elaborately highlighted within this chapter. To improve this antibacterial strategy toward superior biocidal efficacy, most of these coatings are incorporated with (a) eluting agents (e.g., NPs of Ag, Cu, Zn, and even antibiotics, chloride and iodine); (b) active molecules that can be enabled upon contact with surfaces (e.g., peptides, chitosan, and polymers with quaternary ammonium groups); (c) photosensitive molecules that can be enabled upon interaction with light (e.g., TiO_2), etc. [111]. NPs of Ag, ZnO, and CuO have gained recognition over the years due to their antibacterial activities. They are active components of some hospital fabrics, bandages, wound dressings, catheters, etc. Utilizing antibacterial NP-modified coatings have replaced the traditional use of antibiotics since the latter

Table 2 Typical examples of superhydrophobic marine antibiofouling coatings deployed in protecting solid substrates

S/No.	Coating system	Substrate	Bacterial type	Other fouling organisms observed	Antifouling additives	The antibacterial activity of the coating was attributed to the following reason(s)	Ref.
1.	PDMS coating (modified with tethered quaternary ammonium salt)	Al panels	A marine bacterium *Cellulophaga lytica*	A marine alga, *Navicula incerta*	Quaternary ammonium salt [hexadecyldimethyl(3-trimethoxysilylpropyl) ammonium chloride]	The presence of quaternary ammonium salt improved the antifouling potential of the coating	[88]
2.	PDMS coating (modified with tethered quaternary ammonium salt)	Al panels	Two marine bacteria *Halomonas pacifica* and *Cellulophaga lytica*	Microalgae diatom *Navicul incerta*	Quaternary compound (1-iodooctane) and alkoxysilane–functional QAS	The presence of quaternary ammonium salt enhanced bacterial adhesion but led to surface delamination due to swelling	[89]
3.	Infused silicone (*i*PDMS) oil	Silicone catheter tubing	*Pseudomonas aeruginosa*, *Escherichia coli* and *Staphylococcus epidermidis*	None	Silicone oil	The antibacterial oil-infused PDMS film; the antibacterial property of the coating was linked with higher PDMS content; bacterial adhesion was reduced due to increased modulus and reduced surface energy	[90]
4.	Modified PDMS coating	Glass slides	*Vibrio fischeri*	A unicellular alga (*Dunaliella tertiolecta*), the crustacean (*Artemia salina*) and a fish (*Sparus aurata*) larvae	Dibutyltin diacetate; bismuth neodecanoate	The presence of dibutyltin diacetate was toxic toward *V. fischeri*; bacterial adhesion was reduced on the glass substrate	[91]
5.	PDMS/ polyurethane	Glass slides	Marine bacterium *Cellulophaga lytica*	Microalgae diatom *Navicula incerta* and adult barnacle (*Amphibalanus amphitrite*)	TiO$_2$, butyl acrylate, hydroxyethyl acrylate, dibutyltin diacetate, polyol	The presence of TiO$_2$ and dibutyltin diacetate pigments within the coating significantly reduced bacterial adhesion	[92]
6.	Multifunctional polyzwitterion/ enzyme/PDMS	Silicone catheter	*Staphylococcus aureus*	None	Zwitterionic and quaternary ammonium side groups, a contact biocidal derivative of that polymer with	The presence of the polycation-bearing zwitterionic groups was biocidal against *Staphylococcus aureus* settlement on silicone catheter	[93]

No.	Coating	Substrate	Antibacterial test organisms	Antifouling test organisms	Additive	Remarks	Ref.
					octyl groups, and the antibacterial hydrogen peroxide producing enzyme cellobiose dehydrogenase		
7.	PDMS hydrogel (Laser assisted)	Silicone hydrogel	*Escherichia coli* and *Staphylococcus aureus*	NIH/3T3 mouse fibroblast cells	ZnO NPs/ polyethylene glycol	The presence of ZnO-PEG nanocomposites on silicone hydrogels reduced bacterial adhesion but did not impose any toxic effect formouse fibroblast cells	[94]
8.	Perfluoropolyether/ PDMS	Glass slides	*Escherichia coli*	A microalgae diatom *Navicula incerta*	Acrylic polyols	The antibacterial properties of the coating were linked with its foul-release potential as well as its surface energy and elastic modulus	[95]
9.	Epoxy/PDMS	Sn and Al panels	*Staphylococcus aureus* and *Escherichia coli*	*Staphylococcus aureus* and *Escherichia coli*	Fluorosilane and amphiphilic quaternary ammonium salts	Incorporated fluorosilane and quaternary ammonium salt additives decreased the surface free energy of the coating as well as its antibacterial properties	[96]
10.	PDMS/ polyurethane coating	Glass fiber reinforced epoxy resin panels	*Micrococcus luteus*	A diatom *Navicula incerta* and barnacle cyprids	The coating was prepared from polyurethane with PDMS main chains and *N*-(2,4,6-trichlorophenyl) maleimide pendants	The antibacterial property of the coating was linked with higher PDMS content; bacterial adhesion was reduced due to increased modulus and reduced surface energy	[97]
11.	Quasiceramic silicone coating	Al panel	Sulfate-reducing bacteria (coated coupons were retrieved after a 90-day exposure period to soils containing SRB)	None	None	SiloXel improved the strength of the impervious barrier against fouling; the antibacterial property of the coating was linked with higher PDMS content; bacterial adhesion was reduced due to increased modulus and reduced surface energy	[98]
12.	PDMS	Al panel	*Gram-positive*: *Staphylococcus* sp. and *Bacillus* sp. *Gram-negative*: *Pseudomonas* sp., *Escherichia* sp. and *Candida* sp.	None	Single-crystal TiO$_2$ nanocomposites	TiO$_2$ nanoparticles enhanced the antifouling potential of the coating; the antibacterial property of the coating was linked with higher PDMS content; bacterial adhesion was reduced due to the surface morphology of the coating as well as its reduced surface energy	[99]

N/B: The marine antibiofouling coatings reported here may not have been superhydrophobic, but they possessed efficient antifouling potentials against a wide spectrum of bacteria as well as other micro and macrofoulers due their low surface energies.

Table 3 Summary of key findings from some superhydrophobic coatings with antibacterial potentials studied at different conditions

S/No.	Class of coating	Substrates	Bacteria	Highest recorded θ_w^o	With antibacterial properties?	Superhydrophobicity attributed to?	Functionality	Antibacterial activity was ascribed to the following reasons	Ref.
1.	Polyethylenimine	Amino-glass slide	*Escherichia coli* and *Staphylococcus aureus*	Not measured	Yes	This quantity was not measured	Hydrophobic[a] (this quantity was not measured)	The presence of antibacterial covalently derivatized with N-hexyl, methyl-PEI films	[52]
2.	Polyethylenimine	Glass slides	*Staphylococcus aureus* and *Escherichia coli*	Not measured	Yes	This quantity was not measured	Hydrophobic[a] (this quantity was not measured)	The extent of alkylation and N-methylation of quaternary ammonium PEI	[53]
3.	Polyethylenimine multilayer film	Glass slides	*Staphylococcus aureus* and *E. coli*	Not measured	Yes	This quantity was not measured	Hydrophobic[a] (this quantity was not measured)	The presence of antibacterial silver nanoparticles	[54]
4.	Superhydrophobic PVDF-based nanofibrous materials	PVDF material	*Escherichia coli* and *Staphylococcus aureus*	152 degrees	Yes	The presence of ZnO NPs within the PVDF nanofibers	Superhydrophobic	The presence of an antibacterial additives; ZnO NPs and 5-chloro-8-quinolinol	[57]
5.	PEGylated poly (vinylidene fluoride) (PVDF) membranes	Solutions of membrane precursors were casted with metallic casting knife on a glass plate	*Staphylococcus epidermidis* and *Escherichia coli*	132 degrees without PEG	No	Hydrophobic in the absence of PEG within membrane	Hydrophilic due to PEG content	The enhanced antibacterial activity of this modified PVDF membrane was linked with the presence of its PEGylated brushes, especially at a 3 wt% PEG additive content	[58]
6.	Xerogel silica coating	Glass substrates	*Staphylococcus aureus* and *Pseudomonas aeruginosa*	151 degrees	Yes	Low surface energy of the coating	Superhydrophobic	Low energy surface due to the presence of (heptadecafluoro-1,1,2,2-tetrahydrodecyl) trimethoxysilane	[61]
7.	Hydrophobic poly (ether imide) composite nanofiber membranes	Polyester nonwoven support	Ampicillin-resistant *Escherichia coli*	142 degrees	Yes	Nanostructured/independent of wetting properties	Hydrophobic	Low energy surface due to the presence of (pentafluorophenyl) triethoxysilane/organosilica nanoparticles	[62]

No.	Coating	Substrate	Bacteria	Contact angle		Comments	Wetting property	Reason	Ref.
8.	No base coating; plasma textured PMMA	Poly(methyl methacrylate) (PMMA) substrates	Cyanobacteria *Synechococcus* sp.	>155 degrees	Yes	The superhydrophobicity to the surface was attributed to presence of hierarchical nano and microstructures pattern fabricated on the substrate	Superhydrophobic	Low energy surface due to the presence of octafluorocyclobutane	[63]
9.	Cellulose–modified sol–gel type coating	Filter paper	Lysogenic *Escherichia coli*	158 degrees	Yes	Rough morphology of the etched filter paper and the low surface energy coating with 1*H*,1*H*,2*H*,2*H*-perfluorooctyl trimethoxysilane monolayers	Nanostructured/ independent of wetting properties	Antibacterial potential of cellulose	[66]
10.	Infused silicone (*i*PDMS) samples were prepared by immersing the cured PDMS in 5 cSt silicone oil	Silicone tubing	*Pseudomonas aeruginosa*, *Escherichia coli* and *Staphylococcus epidermidis*	112 degrees	Yes	The presence of low surface energy additive; silicone oil	Hydrophobic	Low energy surface due to the presence of silicone oil	[90]
11.	Sol–gel coatings (Epoxy/PDMS)	Sn/Al panels	*Staphylococcus aureus* and *Escherichia coli*	141 degrees	Yes	The presence of low surface energy additive; tridecafluoro-1,1,2,2-tetrahydrooctyl triethoxysilane	Hydrophobic	Low energy surface due to the presence of fluorosilane and quaternary ammonium salt	[96]
12.	Poly(L-lactic acid)	Glass slide	*Staphylococcus aureus* and *Pseudomonas aeruginosa*	154 degrees	Yes	The presence of low surface energy polymer matrix with poly(L-lactic acid) functionality	Superhydrophobic	Low energy surface due to the presence of poly(L-lactic acid) s and as well its antibacterial potential	[100]
13.	Sol–gel type coating	Al substrate	*Colibacillus*	158 degrees		Hierarchical micro- and nanostructures and fluorination treatment enhanced the superhydrophobicity of the material	Superhydrophobic	The presence of antibacterial silver nanoparticles	[101]
14.	Polyelectrolyte (PEI) multilayers	Glass substrate	*Staphylococcus epidermidis* and *Escherichia coli*	Not measured	Yes	This quantity was not measured	Hydrophobic[a] (this quantity was not measured)	The presence of antibacterial PEI films	[102]
15.	Silicon nanoparticles in alcohol	Silicon wafer substrate	*Staphylococcus aureus* and *Pseudomonas aeruginosa*	110 degrees	Yes	The presence of low surface energy additive; silicon nanoparticles	Hydrophobic	The presence of antibacterial silicon nanoparticles in alcohol	[103]

Table 3 Summary of key findings from some superhydrophobic coatings with antibacterial potentials studied at different conditions—cont'd

S/No.	Class of coating	Substrates	Bacteria	Highest recorded θ_w^o	With antibacterial properties?	Superhydrophobicity attributed to?	Functionality	Antibacterial activity was ascribed to the following reasons	Ref.
16.	Antibacterial cotton fabric prepared with modified carboxymethyl chitosan	Cotton fabric	*Staphylococcus aureus* and *Escherichia coli*	Not measured	Yes	This quantity was not measured	Hydrophobic[a] (this quantity was not measured)	The presence of antibacterial carboxymethyl chitosan/silver nanoparticles	[104]
17.	Octyltriethox -ysilane-led superhydrophobic antibacterial cotton textiles	Cotton textile	*Escherichia coli* and *Staphylococcus aureus*	151 degrees	Yes	The presence of low surface energy additive, octyltriethoxysilane	Superhydrophobic	The presence of antibacterial silver nanoparticles	[105]

[a]Authors ascribed the reason for surface hydrophobicity of coating to its low surface energies, though this quantity was not actually measured.
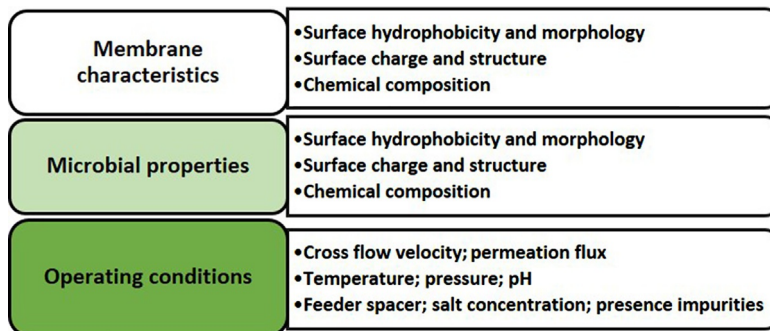
Fig. 11 Some factors affecting the attachment of bacteria cells and biofilms on membrane surfaces.
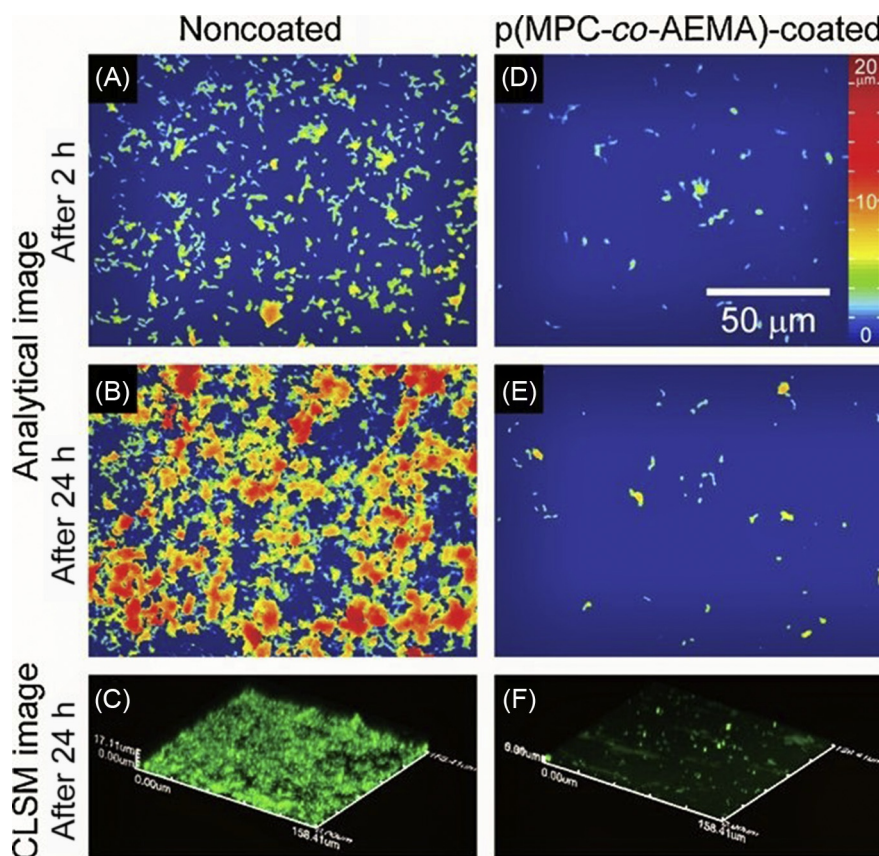
Fig. 12 Analytical (A, B, D, and E) and CLSM (C and F) micrographs showing reduced Gram-negative *Sphingomonas paucimobilis* adhesion on polyamide reverse osmosis membranes via electrostatic interactions (see *right column*). The base coating was a cationic phosphorylcholine polymer coating [p(MPC-*co*-AEMA)]. N/B: (C) and (F) presents both living *(green)* and dead *(red)* bacteria. *(Reproduced with permission from D. Saeki, T. Tanimoto, H. Matsuyama, Prevention of bacterial adhesion on polyamide reverse osmosis membranes via electrostatic interactions using a cationic phosphorylcholine polymer coating, Colloids Surf. A Physicochem. Eng. Asp. 443 (2014) 171–176.)*

technique promotes bacterial resistance and could lead to environmental pollution. However, there is also the issue of toxicological risks related with antimicrobial coatings in health care due to their designs and inherent components.

Recently, safe by–design (SbD) approaches have been adopted for coatings to eliminate potential health and safety risks during coating design phases. The objective of this design concept is aimed at making coating products that are health and safety compliant in line sustainable health regulations. Most cases prove challenging since there are no standard toxicity test protocols for these coating agents as well as reliable methods for measuring their mechanisms of action and penetration depths within body cells. There might not be sufficient data on their absorption patterns and bioaccumulation in most environments while conditions surrounding their metabolism and excretion in living systems might also be relatively unknown [112]. To further understand the fates of these nanomaterials within their environments, some EU programs (e.g., NanoFase, SafeNano, ProSafe, NaNoReg, and Euro-NanoTox) have been designed toward the assessment of their toxicity levels in a view to establishing standardized toxicological measurements for international standards. These programs aim at providing consolidated nanotoxicology information in different environments. The assessment of toxicological effects by in vitro and in vivo assays via multilevel European Center for Nanotoxicology (Euro-NanoTox) strategy has been reported by Adlhart et al. [112]; see Table 4. However, there are few setbacks. Table 5 presents the major challenges surrounding the design and fabrication of safe antimicrobial coatings, and the toxicity of additive materials appears to be a topmost concern. Apart from ZnO, Zr, Zn pyrithione ($C_{10}H_8N_2O_2S_2Zn$), TiO_2, and quaternary ammonium compounds, antimicrobial Ag-based agents dominate the current antibacterial coating market, also have posing toxicity concerns. Their environmental bio–persistence prompts extra interests in their usage within coatings while their potential health and environmental impacts also create a dilemma in the attempt to control device

Table 4 The assessment of toxicological effects via multilevel Euro-NanoTox strategy

Multi-level EURO-NANOTOX strategy

In vivo (acute immunotoxicology; mutogenicity; allergenicty)

In vitro *and* **ex vivo** (genotoxicology; xenobiotic clearance; nanoparticle degradation)

Cellular exposure (penetration/ permeation; cytotoxicology**)**

In vitro (physicochemical characterization; heamotoxicology; immunogenic potency)

Risk assessment (literature survey/formulation of testing strategy)

Table 5 Major challenges affecting the design and fabrication of safe antimicrobial coatings

Challenges affecting the design of safe coatings

- Toxicity of additive materials
- Factors related to bacterial resistance
- Durability of antimicrobial activity
- Lack of standardized methods for testing coating performance
- Potency of antimicrobial agents

infections and HAIs. NPs in antimicrobial coatings could be introduced to the human body from coated implants and other medical devices. Most of these NPs may have minute or zero impact on human health while some of their effects might also be unnoticed. These nanomaterials could also enter the body through the skin after surface degradation of the coatings carrying them; other feasible routes of exposure could also be the gastrointestinal tract and lungs. Their surface charge and crystallinity may impact on other properties, leading to diverse interaction patterns with body cells. The bioavailability of their ionic forms also fosters other chemical changes; however, their interactions with biological targets are affected by factors related to particulate size, surface area/charge, and shape. An ideal antimicrobial candidate for coatings with SHS should be selectively toxic to the targeted organisms (e.g., bacteria) at defined concentrations but not toxic to the hosts (i.e., humans). For a realistic evaluation of risk/benefit ratio, Marassi et al. [113] have highlighted the need for comparison between human toxicity and antimicrobial effect within selected exposure times. These authors designed a five-step approach for candidate screening of coating agents, using AgNPs as a case study for medical devices in modern health care. Castiglioni et al. [114] have also investigated the effects of AgNPs on bone cells (osteogenic cells) and bone marrow–mesenchymal stem cells utilized for orthopedic applications. Authors observed that these cells were resistant to AgNP–induced cytotoxic, with a half-maximal inhibitory concentration around $25\,\mu g/mL$ measured using MTT assay.

Depending of their concentrations and accumulation rates, the adsorption and traveling paths of NPs within the body could harm major internal organs. The mechanisms of action for less traceable and controllable NPs are barely understood; this has prompted toxicological risk assessments in order to address the risks associated with the exposure of living tissues to these substances [111,112]. In vivo toxicity of AgNPs is severe in animal models and could also have serious consequences on man, upon accumulation to defined concentrations. AgNPs have a half-maximal effective concentration (EC_{50})

around 10 mg/L in crustaceans and fish [115], and also demonstrate cytotoxicity against cell lines of rainbow trout (*Oncorhynchus mykiss*) [116]. However, the toxicity of AgNPs is size dependent as well as time and dose dependent. These NPs have no significant physiological function in humans so could be harmful. AgNPs have been reported to damage the liver when introduced intravenously [117] and could also interact with human primary peripheral blood mononuclear cells (PBMC), inducing oxidative stress in white cells [118]. Generally, the human health risks associated with Ag absorption through the dermal and gastrointestinal tract are relatively low; although argyria and skin (even corneas and conjunctiva) discoloration may set in upon long-term exposure. Severe pulmonary damage has been reported in mice after exposure to TiO_2 NPs, with increased susceptibility in rats when compared to hamsters [119]. Increased risk of lung cancer has also been highlighted as well as reduction in ventilatory capacity [120]. Humans can also be exposed to TiO_2 NPs from coated implants as well as through oral and dermal routes. TiO_2 NPs are normally incorporated within polymer films on titanium and stainless-steel implants, and are applied using beam-assisted techniques. The exposure limits to TiO_2 is 0.3 mg/m^3 up to 10 h per day during a 40-h working period, according to the National Institute for Occupational Safety and Health (NIOSH). There may be a correlation between cytotoxicity and the sizes and shapes of ZnO NPs. Although particulate size is associated with surface area, toxicity is induced by shape-related factors in line with cellular uptake. According to Lin et al. [121], concentration- and time-dependent cytotoxicity of ZnO could also lead to oxidative stress, lipid peroxidation, membrane damage, and oxidative DNA damage. Although toxicological prediction is not the main focus of this chapter, a few related issues have been highlighted. Ribeiro et al. [122] have also elaborately discussed the toxicity challenges involving engineered NPs deployed in health care and those exposed through other routes. These authors have vividly explained toxicology in relation with physicochemical properties of NPs (including TiO_2, Au, CuO, and ZnO) and their biological interactions.

7. Concluding remarks

Fouling is the colonization surfaces of substrates by microbes and may start from the adhesion of suspended planktonic bacterial cells, depending on the environment. Upon formation of EPS on medical devices, the attached bacterial colonies become substantially difficult to eradicate. In the presence of sufficient nutrients, these solid surfaces are dominated with bacterial growths as adhering cells proliferate the interfaces. Infection of medical devices by adhering bacterial cells has compounded significant burden on modern health care, in annual cost and life losses. Hospital-assisted infection has not been completely eradicated using traditional antibiotic therapies, and growing concerns over this issue has been declared an international threat by the EU member states. The use of efficient antibacterial superhydrophobic coating has become an efficient technique for

limiting the colonization of infection-causing pathogens on surfaces. With the recent developments in coating technology, these coatings are now designed to resist bacterial adhesion due to very low surface energies and unique morphological features. The encapsulation of antimicrobial additives within polymer coatings is regarded as one of the most effective approaches of creating antibacterial materials. The use of compatible polymer matrices also provides the medium for localized delivery of the antibacterial additives. These hybrid composite coating materials exhibit reduced Gram-negative and Gram-positive bacterial cellular adhesion with significantly high inhibition toward bacterial growth. However, the delivery mechanisms of these release-based antibacterial coatings call for concern. More than one encapsulation method should be adopted for these biocidal additives within the coating. Apart from physical/chemical adsorption or impregnation of these components within polymer coatings, complexation and conjugation should be adopted in incorporating additives within coatings. This chapter has featured recent developments and challenges in the design and application of superhydrophobic antibacterial polymer coatings toward reduced bacterial adhesion. We have also addressed typical infection cases in biomedical applications as well as in marine biofouling and membrane fouling. Summaries of typical polymer coatings that limit bacterial adhesion on solid surfaces are enlisted with examples provided to show differences in coating-bacteria interactions. Issues related to toxicity risks and biocompatibility of respective coatings with mammalian tissues and cells have also been briefly addressed with possible adverse innate immune inflammatory consequences.

References

[1] D.J. Anderson, D.G. Pyatt, D.J. Weber, W.A. Rutala, Statewide costs of health careassociated infections: estimates for acute care hospitals in North Carolina, Am. J. Infect. Control 41 (2013) 764–768.

[2] R.M. Klevens, J.R. Edwards, C.L. Richards Jr., T.C. Horan, R.P. Gaynes, D.A. Pollock, D.M. Cardo, Estimating health care-associated infections and deaths in U.S. hospitals, 2002, Public Health Rep. 122 (2007) 160–166.

[3] A. Ghanbari, A.B. Khiabani, A. Zamanian, B. Yarmand, M. Mozafari, The competitive mechanism of plasma electrolyte oxidation for the formation of magnesium oxide bioceramic coatings, Mater. Today Proc. 5 (2018) 15677–15685.

[4] T.S.N. Narayanan, I.I. Sankara, S. Park, M.H. Lee, Strategies to improve the corrosion resistance of microarc oxidation (MAO) coated magnesium alloys for degradable implants: Prospects and challenges, Prog. Mater. Sci. 60 (2014) 1–71.

[5] N. Graves, K. Halton, D. Paterson, M. Whitby, Economic rationale for infection control in Australian hospitals, Healthc. Infect. 14 (2009) 81–88.

[6] B. Gottenbos, H.J. Busscher, H.C. van der Mei, P. Nieuwenhuis, Pathogenesis and prevention of biomaterial centered infections, J. Mater. Sci. Mater. Med. 13 (2002) 717–722.

[7] K. Halton, N. Graves, Economic evaluation and catheter-related bloodstream infections, Emerg. Infect. Dis. 13 (2007) 815–823.

[8] A. Palantoken, M.S. Yilmaz, M.A. Yapaöz, E.Y. Tulunay, T. Eren, S. Piskin, Dual antimicrobial effects induced by hydrogel incorporated with UV-curable quaternary ammonium polyethyleneimine and $AgNO_3$, Mater. Sci. Eng. C 68 (2016) 494–504.

[9] P. Pronovost, D. Needham, S. Berenholtz, D. Sinopoli, H. Chu, S. Cosgrove, et al., An intervention to decrease catheter-related bloodstream infections in the ICU, N. Engl. J. Med. 355 (2006) 2725–2732.

[10] N.P. O'Grady, M. Alexander, L.A. Burns, E.P. Dellinger, J. Garland, S.O. Heard, et al., Guidelines for the prevention of intravascular catheter-related infections, Clin. Infect. Dis. 52 (2011) 162–193.

[11] S. Jacobsen, D. Stickler, H. Mobley, M. Shirtliff, Complicated catheter-associated urinary tract infections due to *Escherichia coli* and *Proteus mirabilis*, Clin. Microbiol. Rev. 21 (2008) 26–59.

[12] K.K. Lai, S.A. Fontecchio, Use of silver-hydrogel urinary catheters on the incidence of catheter-associated urinary tract infections in hospitalized patients, Am. J. Infect. Control 30 (2002) 221–225.

[13] R.A. Weinstein, R.O. Darouiche, Device-associated infections: a macroproblem that starts with microadherence, Clin. Infect. Dis. 33 (2001) 1567–1572.

[14] G. Subbiahdoss, D.J. Silva, R. Kuijer, H. Mei, H. Busscher, Bridging the gap between in vitro and in vivo evaluation of biomaterial-associated infections, in: T.F. Moriarty, S.A.J. Zaat, H.J. Busscher (Eds.), Biomaterials Associated Infection, Springer, New York, 2013, p. 107e17.

[15] J.M. Schierholz, J. Beuth, Implant infections: a haven for opportunistic bacteria, J. Hosp. Infect. 49 (2001) 87–93.

[16] M.R. Sohail, D.Z. Uslan, A.H. Khan, P.A. Friedman, D.L. Hayes, W.R. Wilson, J.M. Steckelberg, S. Stoner, L.M. Baddour, Management and outcome of permanent pacemaker and implantable cardioverter-defibrillator infections, J. Am. Coll. Cardiol. 49 (2007) 1851–1859.

[17] K. Aljabri, A. Garlitski, J. Weinstock, C. Madias, Management of device infections, Card. Electrophysiol. Clin. 10 (2018) 153–162.

[18] D. Campoccia, L. Montanaro, C.R. Arciola, A review of the biomaterials technologies for infection-resistant surfaces, Biomaterials 34 (2013) 8533–8554.

[19] W. Lv, J. Luo, Y. Deng, Y. Sun, Biomaterials immobilized with chitosan for rechargeable antimicrobial drug delivery, J. Biomed. Mater. Res. A 101 (2013) 447–455.

[20] R. Foldbjerg, H. Autrup, Mechanisms of silver nanoparticle toxicity, Arch. Basic Appl. Med. 1 (2013) 5–15.

[21] J. Raphel, M. Holodniy, S.B. Goodman, S.C. Heilshorn, Multifunctional coatings to simultaneously promote osseointegration and prevent infection of orthopaedic implants, Biomaterials 84 (2016) 301–314.

[22] S. Kurtz, K. Ong, E. Lau, F. Mowat, M. Halpern, Projections of primary and revision hip and knee arthroplasty in the United States from 2005 to 2030, J. Bone Jt. Surg. Am. 89 (2007) 780–785.

[23] T.F. Moriarty, U. Schlegel, S. Perren, R.G. Richards, Infection in fracture fixation: can we influence infection rates through implant design? J. Mater. Sci. Mater. Med. 21 (2010) 1031–1035.

[24] R.O. Darouiche, Treatment of infections associated with surgical implants, N. Engl. J. Med. 350 (2004) 1422–1429.

[25] R.S. Namba, M.C. Inacio, E.W. Paxton, Risk factors associated with surgical site infection in 30,491 primary total hip replacements, J. Bone Jt. Surg. Br. 94 (2012) 1330–1338.

[26] N.J. Hickok, I.M. Shapiro, Immobilized antibiotics to prevent orthopaedic implant infections, Adv. Drug Deliv. Rev. 64 (2012) 1165–1176.

[27] S.B. Goodman, Z. Yao, M. Keeney, F. Yang, The future of biologic coatings for orthopaedic implants, Biomaterials 34 (2013) 3174–3183.

[28] A.G. Gristina, Biomaterial-centered infection: microbial adhesion versus tissue integration, Science 237 (1987) 1588–1595.

[29] J. Hasan, R.J. Crawford, E.P. Ivanova, Antibacterial surfaces: the quest for a new generation of biomaterials, Trends Biotechnol. 31 (2013) 295–304.

[30] Q. Xie, J. Xu, L. Feng, L. Jiang, W. Tang, X. Luo, C.C. Han, Facile creation of a super-amphiphobic coating surface with bionic microstructure, Adv. Mater. 16 (2004) 302–305.

[31] H.Y. Erbil, A.L. Demirel, Y. Avci, O. Mert, Transformation of a simple plastic into a superhydrophobic surface, Science 299 (2003) 1377–1380.

[32] N.M. Oliveira, A.I. Neto, W. Song, J.F. Mano, Two-dimensional open microfluidic devices by tuning the wettability on patterned superhydrophobic polymeric surface, Appl. Phys. Express 3 (2010) 085205.

[33] K. Tadanaga, J. Morinaga, A. Matsuda, T. Minami, Superhydrophobic superhydrophilic micropatterning on flowerlike alumina coating film by the sol-gel method, Chem. Mater. 12 (2000) 590–592.
[34] N.J. Shirtcliffe, G. Hale, M.I. Newton, C.C. Perry, Intrinsically superhydrophobic organosilica sol-gel foams, Langmuir 19 (2003) 5626–5631.
[35] A. Pozzato, S.D. Zilio, G. Fois, D. Vendramin, G. Mistura, M. Belotti, Y. Chen, M. Natali, Superhydrophobic surfaces fabricated by nanoimprint lithography, Microelectron. Eng. 83 (2006) 884–888.
[36] D.O.H. Teare, C.G. Spanos, P. Ridley, E.J. Kinmond, V. Roucoules, J.P.S. Badyal, S. A. Brewer, S. Coulson, C. Willis, Pulsed plasma deposition of superhydrophobic nanospheres, Chem. Mater. 14 (2002) 4566–4571.
[37] I. Woodward, W.C.E. Schofield, V. Roucoules, J.P.S. Badyal, Super-hydrophobic surfaces produced by plasma fluorination of polybutadiene films, Langmuir 19 (2003) 3432–3438.
[38] J.H. Park, J.K. Park, H.Y. Shin, The preparation of Ag/mesoporous silica by direct silver reduction and Ag/functionalized mesoporous silica by in situ formation of adsorbed silver, Mater. Lett. 61 (2007) 156–159.
[39] S.T. Dubas, P. Kumlangdudsana, P. Potiyaraj, Layer-by-layer deposition of antimicrobial silver nano-particles on textile fibers, Colloids Surf. A Physicochem. Eng. Asp. 289 (2006) 105–109.
[40] J. Ou, B. Pan, Y. Chen, C. Xie, M. Xue, F. Wang, W. Li, Substrate-independent sequential deposition process to obtain the lotus effect based on mussel-inspired polydopamine, Appl. Surf. Sci. 327 (2015) 149–153.
[41] J.T. Han, X.R. Xu, K.W. Cho, Diverse access to artificial superhydrophobic surfaces using block copolymers, Langmuir 21 (2005) 6662–6665.
[42] B. Wang, J. Feng, Y. Zhao, T. Yu, Fabrication of novel superhydrophobic surfaces and water droplet bouncing behavior – part 1: stable ZnO–PDMS superhydrophobic surface with low hysteresis constructed using ZnO nanoparticles, J. Adhes. Sci. Technol. 24 (2010) 2693–2705.
[43] T. Onda, S. Shibuichi, N. Satoh, K. Tsujii, Super-water-repellent fractal surfaces, Langmuir 12 (1996) 2125–2127.
[44] F. Shi, Z.Q. Wang, X. Zhang, Combining a layer-by-layer assembling technique with electrochemical deposition of gold aggregates to mimic the legs of water striders, Adv. Mater. 17 (2005) 1005–1009.
[45] S.T. Wang, L. Feng, L. Jiang, One-step solution-immersing process towards bionic superhydrophobic surfaces, Adv. Mater. 18 (2006) 767–770.
[46] Z. Wang, J. Oua, Y. Wang, M. Xue, F. Wang, B. Pan, C. Li, W. Li, Anti-bacterial superhydrophobic silver on diverse substrates based on the mussel-inspired polydopamine, Surf. Coat. Technol. 280 (2015) 378–383.
[47] E. Fadeeva, V.K. Truong, M. Stiesch, B.N. Chichkov, R.J. Crawford, J. Wang, E. P. Ivanova, Bacterial retention on superhydrophobic titanium surfaces fabricated by femtosecond laser ablation, Langmuir 27 (2011) 3012–3019.
[48] C. Sousa, D. Rodrigues, R. Oliveira, W. Song, J.F. Mano, J. Azeredo, Superhydrophobic poly(D-lactic acid) surface as potential bacterial colonization substrate, AMB Express 1 (2011) 1–9.
[49] W. Song, D.D. Veiga, C.A. Custódio, J.F. Mano, Bioinspired degradable substrates with extreme wettability properties, Adv. Mater. 21 (2009) 1830–1834.
[50] N.M. Alves, J. Shi, E. Oramas, J.L. Santos, H. Tomás, J.F. Mano, Bioinspired superhydrophobic poly (L-lactic acid) surfaces control bone marrow derived cells adhesion and proliferation, J. Biomed. Mater. Res. A 91A (2009) 480–488.
[51] A.R. Vancha, S. Govindaraju, K.V.L. Parsa, M. Jasti, M. González-García, R.P. Ballestero, Use of polyethyleneimine polymer in cell culture as attachment factor and lipofection enhancer, BMC Biotechnol. 23 (2004) 1–12.
[52] N.M. Milović, J. Wang, K. Lewis, A.M. Klibanov, Immobilized N-alkylated polyethylenimine avidly kills bacteria by rupturing cell membranes with no resistance developed, Biotechnol. Bioeng. 90 (6) (2005) 715–722.

[53] I. Yudovin-Farber, J. Golenser, N. Beyth, E.I. Weiss, A.J. Domb, Quaternary ammonium polyethy-leneimine: antibacterial activity, J. Nanomater. 2010 (2010) 1–11, https://doi.org/10.1155/2010/826343.

[54] T. He, V. Chan, Covalent layer-by-layer assembly of polyethyleneimine multilayer for antibacterial applications, J. Biomed. Mater. Res. A 95 (2010) 454–464.

[55] L. Shen, B. Wang, J. Wang, J. Fu, C. Picart, J. Ji, Asymmetric free-standing film with multifunctional anti-bacterial and self-cleaning properties, ACS Appl. Mater. Interfaces 4 (2012) 4476–4483.

[56] S. Houis, E.M. Engelhardt, F. Wurm, T. Gries, Application of Polyvinylidene Fluoride (PVDF) as a Biomaterial in Medical Textiles, Woodhead Publishing Limited, 2010, pp. 342–352.

[57] M. Spasova, N. Manolova, N. Markov, I. Rashkov, Superhydrophobic PVDF and PVDF-HFP nano-fibrous mats with antibacterial and anti-biofouling properties, Appl. Surf. Sci. 363 (2016) 363–371.

[58] A. Venault, Y. Chang, D.M. Wang, J.Y. Lai, Surface anti-biofouling control of PEGylated poly(vinylidene fluoride) membranes via vapor-induced phase separation processing, J. Membr. Sci. 423–424 (2012) 53–64.

[59] G. Kang, Y. Cao, Application and modification of poly(vinylidene fluoride) (PVDF) membranes – a review, J. Membr. Sci. 463 (2014) 145–165.

[60] J.D. Brassard, D.K. Sarkar, J. Perron, Fluorine based superhydrophobic coatings, Appl. Sci. 2 (2012) 453–464.

[61] J. Benjamin, J. Privett, J. Youn, S.A. Hong, J. Lee, J. Han, J.H. Shin, M.H. Schoenfisch, Antibacterial Fluorinated Silica Colloid Superhydrophobic Surfaces, Langmuir 27 (2011) 9597–9960.

[62] M.A. Hammami, J.G. Croissant, L. Francis, S.K. Alsaiari, D.H. Anjum, N. Ghaffour, N.M. Khash, Engineering hydrophobic organosilica nanoparticle-doped nanofibers for enhanced and fouling resistant membrane distillation, ACS Appl. Mater. Interfaces 9 (2017) 1737–1745.

[63] K. Ellinas, D. Kefallinou, K. Stamatakis, E. Gogolides, A. Tserepi, Is there a threshold in the antibac-terial action of Superhydrophobic surfaces? ACS Appl. Mater. Interfaces 9 (2017) 39781–39789.

[64] A. Vilcnik, I. Jerman, A. Surca Vuk, M. Kozelj, B. Orel, B. Tomsic, B. Simoncic, J. Kovac, Structural properties and antibacterial effects of hydrophobic and Oleophobic sol-gel coatings for cotton fabrics, Langmuir 25 (2009) 5869–5880.

[65] H. Yang, Y. Deng, Preparation and physical properties of superhydrophobic papers, J. Colloid Inter-face Sci. 325 (2008) 588–593.

[66] C. Jin, Y. Jiang, T. Niu, J. Huang, Cellulose-based material with amphiphobicity to inhibit bacterial adhesion by surface modification, J. Mater. Chem. 22 (2012) 12562–12567.

[67] A. Kottmann, E. Mejia, T. Hemery, J. Klein, U. Kragl, Recent developments in the preparation of silicones with antimicrobial properties, Chem. Asian J. 12 (2017) 1168–1179.

[68] Z. Wang, H. Zhang, A.J. Chu, J. Jackson, K. Lin, C.J. Lim, D. Lange, M. Chiao, Mechanically enhanced nested-network hydrogels as a coating material for biomedical devices, Acta Biomater. 70 (2018) 98–109.

[69] F. Siedenbiedel, J.C. Tiller, Antimicrobial polymers in solution and on surfaces: overview and func-tional principles, Polymers 4 (2012) 46–71.

[70] A. Schmidtchen, M. Pasupuleti, M. Malmsten, Effect of hydrophobic modifications in antimicrobial peptides, Adv. Colloid Interface Sci. 205 (2014) 265–274.

[71] C. Giles, S.J. Lamont-Friedrich, T.D. Michl, H.J. Griesser, B.R. Coad, The importance of fungal pathogens and antifungal coatings in medical device infections, Biotechnol. Adv. 36 (2018) 264–280.

[72] I. Francolini, C. Vuotto, A. Piozzi, G. Donelli, Antifouling and antimicrobial biomaterials: an over-view, APMIS 125 (2017) 392–417.

[73] S. Taheri, A. Cavallaro, S.N. Christo, L.E. Smith, P. Majewski, M. Barton, J.D. Hayball, K. Vasilev, Substrate independent silver nanoparticle based antibacterial coatings, Biomaterials 35 (2014) 4601–4609.

[74] H. Klasen, Historical review of the use of silver in the treatment of burns. I. Early uses, Burns 26 (2000) 117–130.

[75] P.L. Nadworny, J. Wang, E.E. Tredget, R.E. Burrell, Anti-inflammatory activity of nanocrystalline silver in a porcine contact dermatitis model, Nanomed. Nanotechnol. Biol. Med. 4 (2008) 241–251.

[76] L.J. Locht, K. Smidt, J. Rungby, M. Stoltenberg, A. Larsen, Uptake of silver from metallic silver surfaces induces cell death and a pro-inflammatory response in cultured J774 macrophages, Histol. Histopathol. 26 (2011) 689–697.

[77] B.J. Privett, A.D. Broadnax, S.J. Bauman, D.A. Riccio, M.H. Schoenfisch, Examination of bacterial resistance to exogenous nitric oxide, Nitric Oxide 26 (2012) 169–173.

[78] Y. Lu, D.L. Slomberg, M.H. Schoenfisch, Nitric oxide-releasing chitosan oligosaccharides as antibacterial agents, Biomaterials 35 (2014) 1716–1724.

[79] M.L. Jones, J.G. Ganopolsky, A. Labbé, C. Wahl, S. Prakash, Antimicrobial properties of nitric oxide and its application in antimicrobial formulations and medical devices, Appl. Microbiol. Biotechnol. 88 (2010) 401–407.

[80] L. Yang, X. Wang, D.J. Suchyta, M.H. Schoenfisch, Antibacterial activity of nitric oxide-releasing hyperbranched polyamidoamines, Bioconjug. Chem. 29 (2018) 35–43.

[81] S. Radin, P. Ducheyne, Controlled release of vancomycin from thin sol-gel films on titanium alloy fracture plate material, Biomaterials 28 (2007) 1721–1729.

[82] C.S. Adams, V. Antoci, G. Harrison, P. Patal, T.A. Freeman, I.M. Shapiro, J. Parvizi, N.J. Hickok, S. Radin, P. Ducheyne, Controlled release of vancomycin from thin sol-gel films on implant surfaces successfully controls osteomyelitis, J. Orthop. Res. 27 (2009) 701–709.

[83] A.A. Campbell, L. Song, X.S. Li, B.J. Nelson, C. Bottoni, D.E. Brooks, E.S. DeJong, Development, characterization, and anti-microbial efficacy of hydroxyapatite-chlorhexidine coatings produced by surface-induced mineralization, J. Biomed. Mater. Res. 53 (2000) 400–407.

[84] I. Francolini, P. Norris, A. Piozzi, G. Donelli, P. Stoodley, Usnic acid, a natural antimicrobial agent able to inhibit bacterial biofilm formation on polymer surfaces, Antimicrob. Agents Chemother. 48 (2004) 4360–4365.

[85] J. Odeberg, A. Wirsén, Å. Norberg, J. Frie, G. Printz, H. Lagercrantz, G. H. Gudmundsson, B. Agerberth, B. Jonsson, A novel cysteine-linked antibacterial surface coating significantly inhibits bacterial colonization of nasal silicone prongs in a phase one pre-clinical trial, Mater. Sci. Eng. C 93 (2018) 782–789.

[86] D. Yang, Q. Zhang, Q. Wang, L. Chen, Y. Liu, M. Cong, H. Wu, F. Li, C. Ji, J. Zhao, A defensin-like antimicrobial peptide from the manila clam Ruditapes philippinarum: investigation of the antibacterial activities and mode of action, Fish Shellfish Immunol. 80 (2018) 274–280.

[87] T. Ren, M. Yang, K. Wang, Y. Zhang, J. He, CuO nanoparticles-containing highly transparent and superhydrophobic coatings with extremely low bacterial adhesion and excellent bactericidal property, ACS Appl. Mater. Interfaces 10 (2018) 25717–25725.

[88] P. Majumdar, E. Lee, N. Patel, S.J. Stafslien, J. Daniels, B.J. Chisholm, Development of environmentally friendly, antifouling coatings based on tethered quaternary ammonium salts in a crosslinked polydimethylsiloxane matrix, J. Coat. Technol. Res. 5 (2008) 405–417.

[89] P. Majumdar, E. Crowley, M. Htet, S.J. Stafslien, J. Daniels, L. VanderWal, B.J. Chisholm, Combinatorial materials research applied to the development of new surface coatings XV: an investigation of polysiloxane anti-fouling/fouling-release coatings containing tethered quaternary ammonium salt groups, ACS Comb. Sci. 13 (2011) 298–309.

[90] N. MacCallum, C. Howell, P. Kim, D. Sun, R. Friedlander, J. Ranisau, O. Ahanotu, J. J. Lin, A. Vena, B. Hatton, T.S. Wong, J. Aizenberg, Liquid-infused silicone as a biofouling-free medical material, ACS Biomater. Sci. Eng. 1 (2015) 43–51.

[91] C. Pretti, M. Oliva, E. Mennillo, M. Barbaglia, M. Funel, B.R. Yasani, E. Martinelli, G. Galli, An ecotoxicological study on tin- and bismuth-catalysed PDMS based coatings containing a surface-active polymer, Ecotoxicol. Environ. Saf. 98 (2013) 250–256.

[92] S.A. Sommer, J.R. Byrom, H.D. Fischer, R.B. Bodkhe, S.J. Stafslien, J. Daniels, C. Yehle, D.C. Webster, Effects of pigmentation on siloxane–polyurethane coatings and their performance as fouling-release marine coatings, J. Coat. Technol. Res. 8 (2011) 661–670.

[93] A. Vaterrodt, B. Thallinger, K. Daumann, D. Koch, G.M. Guebitz, M. Ulbricht, Antifouling and antibacterial multifunctional polyzwitterion/enzyme coating on silicone catheter material prepared by electrostatic layer-by-layer assembly, Langmuir 32 (2016) 1347–1359.

[94] G. Huang, Y. Chen, J. Zhang, Nanocomposited coatings produced by laser-assisted process to prevent silicone hydogels from protein fouling and bacterial contamination, Appl. Surf. Sci. 360 (2016) 383–388.

[95] X. Sun, F. Zhang, Y. Chen, Z. Cheng, Y. Su, J. Hang, L. Jin, N. Li, D. Shang, L. Shi, Preparation and properties of crosslinked network coatings based on perfluoropolyether/poly(dimethyl siloxane)/acrylic polyols for marine fouling–release applications. J. Appl. Polym. Sci. (2015), https://doi.org/10.1002/APP.41860.

[96] G.C. Daniels, E.B. Iezzi, P.A. Fulmer, J.H. Wynne, Synergistic antimicrobial and surface free energy of sol–gel coatings containing fluorosilanes and quaternary ammonium salts, Prog. Org. Coat. 95 (2016) 91–99.

[97] Q. Xie, C. Ma, C. Liu, J. Ma, G. Zhang, Poly(dimethylsiloxane)-based polyurethane with chemically attached antifoulants for durable marine antibiofouling, ACS Appl. Mater. Interfaces 7 (2015) 21030–21037.

[98] A. Tiwari, L.H. Hihara, High performance reaction–induced quasi-ceramic silicone conversion coating for corrosion protection of aluminium alloys, Prog. Org. Coat. 69 (2010) 16–25.

[99] M.S. Selim, S.A. El-Safty, M.A. El-Sockary, A.I. Hashem, O.M.A. Elenien, A.M. EL-Saeed, N.A. Fatthallah, Smart photo-induced silicone/TiO$_2$ nanocomposites with dominant [110] exposed surfaces for self-cleaning foul-release coatings of ship hulls, Mater. Des. 101 (2016) 218–225.

[100] C. Sousa, D. Rodrigues, R. Oliveira, W. Song, J.F. Mano, J. Azeredo, Superhydrophobic poly(L-lactic acid) surface as potential bacterial colonization substrate, AMB Express 1 (2011) 1–9.

[101] Y. Liu, H. Cao, S. Chen, D. Wang, Ag nanoparticle-loaded hierarchical superamphiphobic surface on an Al substrate with enhanced anticorrosion and antibacterial properties, J. Phys. Chem. C 119 (2015) 25449–25456.

[102] J.A. Lichter, K.J.V. Vliet, M.F. Rubner, Design of antibacterial surfaces and interfaces: polyelectrolyte multilayers as a multifunctional platform, Macromolecules 42 (2009) 8573–8586.

[103] N.A. Smirnov, S.I. Kudryashov, A.A. Nastulyavichus, A.A. Rudenko, I.N. Saraeva, E.R. Tolordava, S.A. Gonchukov, Y.M. Romanova, A.A. Ionin, D.A. Zayarny, Antibacterial properties of silicon nanoparticles, Laser Phys. Lett. 15 (2018). 105602-1-1056024.

[104] Q.B. Xu, L.J. Xie, H. Diao, F. Li, Y.Y. Zhang, F.Y. Fu, X.D. Liu, Antibacterial cotton fabric with enhanced durability prepared using silver nanoparticles and carboxymethyl chitosan, Carbohydr. Polym. 177 (2017) 187–193.

[105] M.S. Khalil-Abad, M.E. Yazdanshenas, Superhydrophobic antibacterial cotton textiles, J. Colloid Interface Sci. 351 (2010) 293–298.

[106] P.S. Goh, W.J. Lau, M.H.D. Othman, A.F. Ismail, Membrane fouling in desalination and its mitigation strategies, Desalination 425 (2018) 130–155.

[107] A. Bogler, S. Lin, E. Bar-Zeev, Biofouling of membrane distillation, forward osmosis and pressure retarded osmosis: principles, impacts and future directions, J. Membr. Sci. 542 (2017) 378–398.

[108] P.S. Goh, A.F. Ismail, A review on inorganic membranes for desalination and wastewater treatment, Desalination 434 (2018) 60–80.

[109] S. Jiang, Y. Li, B.P. Ladewig, A review of reverse osmosis membrane fouling and control strategies, Sci. Total Environ. 595 (2017) 567–583.

[110] D. Saeki, T. Tanimoto, H. Matsuyama, Prevention of bacterial adhesion on polyamide reverse osmosis membranes via electrostatic interactions using a cationic phosphorylcholine polymer coating, Colloids Surf. A Physicochem. Eng. Asp. 443 (2014) 171–176.

[111] M. Ahonen, A. Kahru, A. Ivask, K. Kasemets, S. Kõljalg, P. Mantecca, I.V. Vrcek, M.M.K. Toivola, F. Crijns, Proactive approach for safe use of antimicrobial coatings in healthcare settings: opinion of the COST action network AMiCI, Int. J. Environ. Res. Public Health 14 (2017) 1–23.

[112] C. Adlhart, J. Verran, N.F. Azevedo, H. Olmez, M.M.K. Toivola, I. Gouveia, L.F. Melo, F. Crijns, Surface modifications for antimicrobial effects in the healthcare setting: a critical overview, J. Hosp. Infect. 99 (2018) 239–249.

[113] V. Marassi, L. Di Cristo, S.G.J. Smith, S. Ortelli, M. Blosi, A.L. Costa, P. Reschiglian, Y. Volkov, A. Prina-Mello, Silver nanoparticles as a medical device in healthcare settings: a five-step approach for candidate screening of coating agents, R. Soc. Open Sci. 5 (171113) (2018) 1–21.

[114] S. Castiglioni, A. Cazzaniga, L. Locatelli, J.A.M. Maier, Silver nanoparticles in orthopedic applications: new insights on their effects on osteogenic cells, Nano 7 (2017) 1–9.

[115] O. Bondarenko, K. Juganson, A. Ivask, K. Kasemets, M. Mortimer, A. Kahru, Toxicity of Ag, CuO and ZnO nanoparticles to selected environmentally relevant test organisms and mammalian cells in vitro: a critical review, Arch. Toxicol. 87 (2013) 1181–1200.

[116] M. Connolly, M. Fernandez-Cruz, A. Quesada-Garcia, L. Alte, H. Segner, J.M. Navas, Comparative cytotoxicity study of silver nanoparticles (AgNPs)in a variety of rainbow trout cell lines (RTL-W1, RTH-149, RTG-2) and primary hepatocytes, Int. J. Environ. Res. Public Health 12 (2015) 5386–5405.

[117] Y. Li, J.A. Bhalli, W. Ding, J. Yan, M.G. Pearce, R. Sadiq, C.K. Cunningham, M.Y. Jones, W. A. Monroe, P.C. Howard, T. Zhou, T. Chen, Cytotoxicity and genotoxicity assessment of silver nanoparticles in mouse, Nanotoxicology 8 (2014) 36–45.

[118] I.M.M. Paino, V. Zucolotto, Poly(vinyl alcohol)-coated silver nanoparticles: activation of neutrophils and nanotoxicology effects in human hepatocarcinoma and mononuclear cells, Environ. Toxicol. Pharmacol. 39 (2015) 614–621.

[119] G. Oberdörster, Safety assessment for nanotechnology and nanomedicine: concepts of nanotoxicology, J. Intern. Med. 267 (2010) 89–105.

[120] P.M. Hext, J.A. Tomenson, P. Thompson, Titanium dioxide: inhalation toxicology and epidemiology, Ann. Occup. Hyg. 49 (2005) 461–472.

[121] W. Lin, Y. Xu, C.C. Huang, Y. Ma, K.B. Shannon, D.R. Chen, W.H. Yue, Toxicity of nano- and micro-sized ZnO particles in human lung epithelial cells, J. Nanopart. Res. 11 (2008) 25–39.

[122] A.R. Ribeiro, P.E. Leite, P. Falagan-Lotsch, F. Benetti, C. Micheletti, H.C. Budtz, N.R. Jacobsen, P.N. Lisboa-Filho, L.A. Roch, D. Kühnel, D. Hristozov, J.M. Granjeiro, Challenges on the toxicological predictions of engineered nanoparticles, NanoImpact 8 (2017) 59–72.

CHAPTER 12

Superhydrophobic antireflective polymer coatings with improved solar cell efficiency

Swarnalata Sahoo, Sukanya Pradhan, Sonalee Das
SARP-Laboratory for Advanced Research in Polymeric Materials CIPET, Bhubaneswar, India

1. Introduction

Reflect, reuse, and refocus on superhydrophobic antireflective (AR) polymer coatings with improved solar cell efficiency provide many valuable properties in different surroundings. The most copious renewable energy source in the world is solar energy that converts solar energy or light energy to another form of usable energy [1–3]. The crucial factor of the solar cell is it does not emit any greenhouse gases in the process of energy generation production. However, as compared to other fuel sources, the cost of solar is high. Usually, two types of technologies such as solar photovoltaics (PV); where photo means light and voltaic means electricity and solar thermal that controls the solar energy. A PV cell, or solar cell, is an electrical tool that converts sun's heat into direct current electricity such as current, voltage, or resistance, etc. by using semiconductor such as silicon. Further, when the light rays strike cell, the semiconductor material absorbs a portion of light energy that transferred to the semiconductor thereby inducing loose electrons to flow freely in a certain direction. In this way, the flow of electron produces electrical energy from light energy. Whereas, solar thermal is an electrical device that utilizes light energy directly from the sun for electricity (electrical energy) production.

The electrical efficiency is a physical property which represents the amount of electrical energy produced by a cell for certain insolation. Further, the maximum efficiency can be given by the ratio between output powers of a cell to the incident solar power. Therefore, the conversion efficiency or electrical efficiency is a crucial factor in the PV system. However, it is the most expensive. Hence, the selection of the material is driven by choosing cost efficiency and other properties. In addition, the higher power conversion efficiency (PCE) is a crucial research area that leads to the development of PV solar devices. Moreover, higher power efficiency indicates the solar devices more cost competitive as compared with other traditional sources of energy. Several works of literature reported regarding the uses of conjugated polymer coatings in electronics and PV solar cell to enhance the efficiency of solar cell [3–8]. Polymer offers many prospective applications in solar cell technologies that can help to achieve the total cost efficiency by

optimizing three major parameters such as lower cost, durability, and greater design flexibility as compared with other materials in current use. Several reports have also been disused about the utilization of carbon nanotubes (CNTs), graphene, and semiconducting polymer which can be easily deposited on Si wafers in order to increase the percentage of solar efficiency. Hence, nowadays the polymer coating-based solar cell have gained maximum power efficiency conversion of 5% [8, 9]. The organic polymer coating deposition by several techniques such as screen printing, spray deposition, and inkjet printing are utilized to reduce the polymer coating based PV solar cell which can compete for the need of current grid electricity. In addition, all the technique permits devices to be successfully fabricated on plastic-based substrates for the development of flexible surfaces at lower temperature. Hence, qualities such as flexibility and lightweight are primarily the reason for the reduction of cost solar cell (PV). Moreover, various works of literature have also been developed the more efficient solar cells which produce the efficiency of more than 10%.

The design of solar cell (Fig. 1) is complex which consists of mainly three layers of many different materials such as topmost layer, middle layer, and bottom layer. The topmost layer of solar cell made up of glass material with an AR coat and metallic strips in which the glass protects the materials, while the AR coat helps to transmit more sunlight to reach the semiconductors. AR coating [5] on the top of glass cover in the topmost layer produces better transmission, lower reflection, and more efficiency that can be achieved by using silicon nitride or titanium dioxide coatings of nanometer scales. The middle layer of solar cell plays a vital role which created solar energy through PV effect. Primarily, the middle layer consists of two semiconductor layers in which the first layer is made up of n–type and the second layer is made up of p-type materials. The n–type layer is usually made
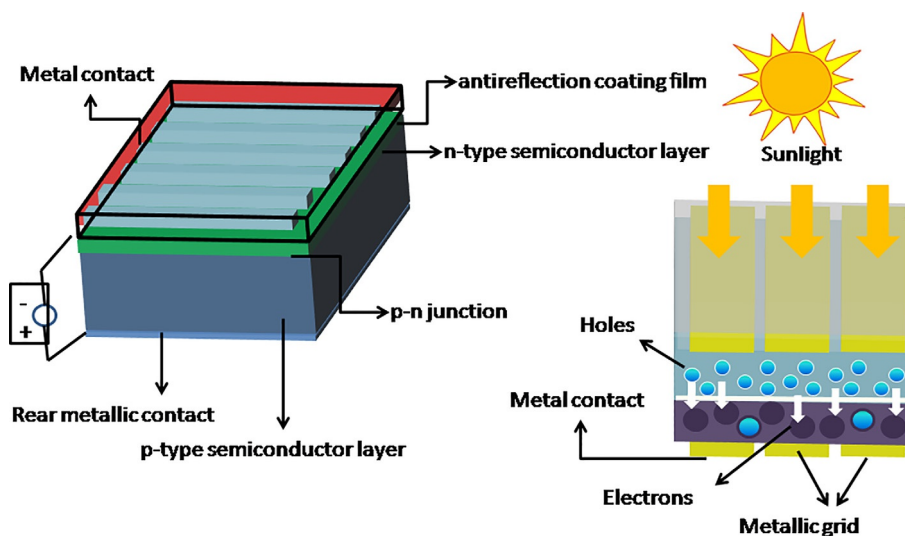
Fig. 1 Design of solar cell.

by silicon mixed with less amount of phosphorous which makes the silicon material negatively charged; whereas p–type layer made by silicon mixed with small amounts of boron which makes the silicon positive charged. Similarly, the bottom layer consists of a rear metallic electrode with the metallic grid present lower to the p–type semiconductor creates an electric current. Besides these three above layer, the final layer known as the reflective layer is present to reduce the loss of light energy in the solar cell system.

The percentage of efficiency is usually decreased by the reflection process and by dust. Hence, current interest in superhydrophobic characteristics of ARCs has been diverted owing to its potential utility in solving key technological issues. Superhydrophobic AR coating is the properties of the material which repels water, solid particles, and viscous liquids. Primarily, it acts as an antidust coating [6] and makes the surface highly water repellent (superhydrophobic) in which water contact angle (WCA) is greater than 150 degrees. In this case, if the water droplets fall on the AR-coated surface, it starts rolling down carrying dust particles. The superhydrophobic antireflective polymer (SHAP) coatings of the surface can be made using two pathways such as by making a rough surface with a low surface energy material and the chemical surface modification with a material having low surface energy. Similarly, the major parameter, that is, refractive index (RI) of the medium determines the amount of percentage of light transmission of the medium. Moreover, high transparency plays a vital role in improving the performance of solar devices and optical equipment such as solar panels, lenses, windows, etc. Generally, the SHAP coating is a type of coating which is used to reduce the reflection of light rays and to enhance the transmittance of incoming light as well as scattering [10]. Duparré et al. [11] investigated that can be a trade-off between both the features such as scatter loss and hydrophobicity. The SHAP coating by chemical vapor deposition method exhibits good trade between scatter loss and hydrophobicity [12].

In this chapter, recent developments in SHAP coatings for solar cell applications are described. Many approaches for SHAP have been discussed to achieve the ideal AR efficiency by paying particular focus to devise design and prospective improvements. The approaches such as layer-by-layer assembly, dip coating, sol–gel, vapor deposition, spin coating, spray coating, etching, lithography, nanoimprinting, vacuum sintering, and micro–replication have been discussed [7]. In addition, the fundamentals of antireflection and superhydrophobicity properties are also described in detail.

2. Theoretical aspect of antireflective coatings

To determine the superhydrophobicity and wettability properties of a solid surface, contact angle determination is mainly used. If the solid surface is smooth and homogeneous the contact angle of a liquid to the solid surface is determined by Young's equation (1) [13]:

$$\cos\theta = \frac{\gamma_{SV} - \gamma_{SL}}{\gamma_{LV}} \tag{1}$$

where γ_{SV}, γ_{LV}, and γ_{SL} are the interfacial tension values of solid–vapor, liquid–vapor, and solid–liquid interfaces, respectively. However, the theoretical model assumed by the scientist Wenzel and Cassie-Baxter was for chemical heterogeneous and rough solid surface.

Generally, the model developed by Wenzel reported that the liquid penetrates completely into the indentation in a solid surface, which is given as follows [14]:

$$\cos\theta_W = r\cos\theta \tag{2}$$

where θ_W indicates the contact angle of the rough surface, r is the roughness factor of the surface, and θ is the Young's contact angle on a symmetrical smooth surface.

From Eq. (2) it has been concluded that if θ is less than 90 degrees, the roughness of the surface increases with enhanced wetting properties of the surface. If θ is greater than 90 degrees, the roughness factor decreases with decreasing roughness factor.

Further, another model, Cassie–Baxter proposed that, when θ is greater than 90 degrees, the air bubbles are penetrated due to the roughness properties of the surface. In this case, the liquid creates two interfaces such as liquid-solid interface and liquid-vapor interface. Hence, the apparent contact angle is expressed as the following equation [15]:

$$\cos\theta_C = f_1\cos\theta_1 + f_2\cos\theta_2 \tag{3}$$

where θ_C is the apparent contact angle to the solid surface and f_1, f_2 are the apparent contact angle of liquid-solid and liquid-vapor interface, respectively. At the liquid–vapor phase, the interface is $(1-f)$, if the fraction of solid (f) phase is wetted by the liquid phase. For vapor, if $\theta = 180$ degrees, then the apparent contact angle can be calculated as the following equation:

$$\cos\theta_C = f\cos\theta + (1-f)\cos 180° = f\cos\theta + (1-f) \tag{4}$$

In this model, Cassie–Baxter assumed that the contact angle of the interface is assumed to be static or constant. Depending on the chemical heterogeneity, surface reorganization and surface roughness the contact values can vary with the probe liquid over the contact area (Fig. 2) [16].
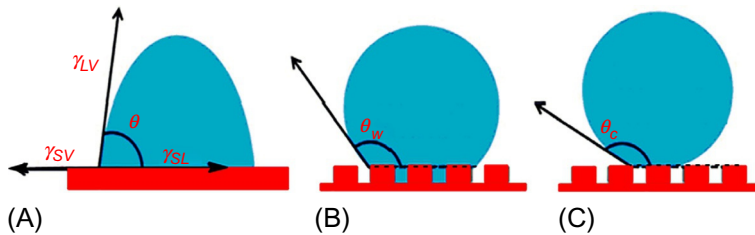
Fig. 2 Liquid droplet on solid surfaces. (A) Young's model, (B) Wenzel's model, (C) Cassie's model.

3. Types of antireflective coatings

3.1 Introduction

The concept of antireflective coatings (ARCs) had been first noticed in the 19th century by Lord Rayleigh when he observed the tarnishing on a glass increasing its transmittance instead of reducing it. This has led to the development of achieving anti reflection property by varying the RI. But, in 1817, the actual ARC was developed by Fraunhofer during an experiment which concluded the reduction in reflection as a result of etching a surface in sulfur and nitric acid vapor atmosphere. The prime requirement of optical and optoelectronic equipment is maximum efficiency in the light collection. In this regard, the topmost covering of the solar panels has served well for the purpose through its better transmission and glare reduction properties which are achieved by the coatings made up of silicon nitride or titanium dioxide coatings of nanometer range. It has been studied earlier that a normal solar panel absorbs only one-fourth of the incident solar radiation, thereby reflecting the remaining radiation which could contribute to the net efficiency. The emergence of antireflective coatings that has been commercially manufactured had solved these issues through various modifications.

3.2 Types of antireflective coatings

ARCs have been classified into following types on the basis of uniformity, layer composition, and surface topography:

3.2.1 Type I

This type of ARCs is divided into subtypes on the basis of its homogeneity represented in Fig. 3. They are:

Homogenous antireflective coatings

This type of coating consists of a single homogenous layer of RI "n" which is contributed to the restriction on the RI and the thickness of the coating. The RI (n) must be equal to
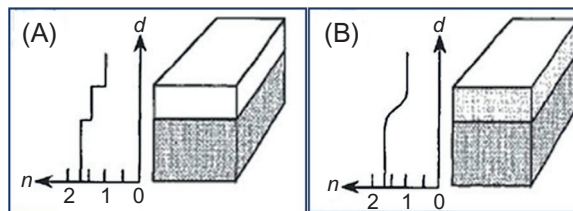
Fig. 3 (A) Homogenous (B) inhomogenous antireflective coating.

$\sqrt{n_{air}}$ $\sqrt{n_{substrate}}$ and thickness equal to one–fourth of the wavelength (λ). However, multiple layers in this type of coating help in achieving null reflectance at certain wavelength though the above rule is not obeyed [5].

Inhomogeneous antireflective coatings

The inhomogeneous type of ARC achieves its properties by following the RI gradient approach [17]. The reflectance from the abrupt interfaces is gradually reduced with the depth due to the changes in RI value of air to the substrate. This type of coating can be assumed to be consisting of a large number of sublayers if the RI between the adjacent sublayers is negligible [18].

3.2.2 Type II

This type of coating has been classified into the following types on the basis of its layer composition represented in Fig. 4.

Unit layer antireflection coatings

The selection criteria of the material for this type of coating is a tedious task as the RI of BK7 glass is 1.5151 at 633 nm and the calculation says that the RI must be approximately 1.22. These type of coatings are generally used for moderate suppression of reflectance to around 2.5% over a wide range of spectral range from 450 to 1100 nm at normal incidence. The unit layer antireflection coating from magnesium fluoride is the common coating of this type as it RI is around 1.38. Although the performance characteristics
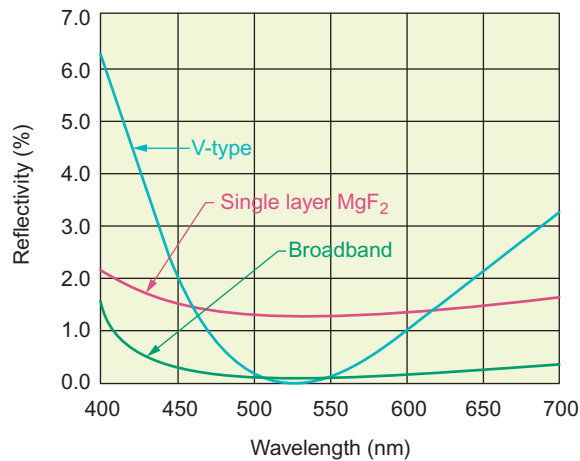
Fig. 4 Plot between reflectivity and wavelength showing the comparison of single-layer MgF_2, V, and broadband coatings.

of magnesium fluoride-based unit layer ARC are not unique, still its broad range of wavelength zone is its major advantage.

Double-layer antireflection coating

The double-layer antireflection coating has been employed in order to further reduce the reflectance. However, the prime and necessary condition for this type of coating with equal optical thickness $n_1 d_1 = n_2 d_2 = \lambda/4$) is to give zero reflectance is

$$n_1/n_2 = \sqrt{n_0/n_s}$$

This type of coatings is known as V-coatings due to its shape profile diagram and also as quarter–quarter coatings owing to their thickness relationship [19]. These double-layer coatings are specially used in laser applications where resistance to higher intensity laser radiation is extremely important [20].

Multilayer antireflection coatings

In this type of coating, multiple layers of alternating layers of low RI materials and high index materials are used to obtain reflectance as low as possible at a particular wavelength. According to the mathematical model for multilayer coatings, it has been concluded that by considering the RI and the thickness of the film, the net sum of all the reflected vectors must be minimized.

In a study [21] on multilayers of Si substrate, it has been reported that the incorporation of additional Si layer in between the greater index Ge and the lower index SiO_2 has resulted in maximum blue transitivity at 480 nm. Similarly, in many biological species such as Coleoptera, alternate high and low RI layers facilitate optical interference.

Gradient refractive index antireflection coatings

This type of coatings have different RI profile with different curves, viz., as linear, parabolic, cubic, quintic, exponential, exponential-sinusoid, etc. and comply with Rayleigh effect. Sheldon and Haggerty [22] have demonstrated the gradient RI profiles under transverse electric waves corresponding to linear, concave, and convex-parabolic and cubic curves. In a different study, Xi et al. [23] have also proposed the gradient RI profile of the structure derived from 450 SiO_2 nanorods which has resulted a net RI of 1.0526 which corresponds to a quintic profile. However, the disadvantages of this type of coating could be attributed to two major factors (a) the difference in RI between the upper surface of GRIN coating and ambient air (b) the existence of mismatch due to the complex and real RI obtained for the absorbing substrate and the transparent ARC. This shortcoming violates the Rayleigh effect and suggests that a multilayer ARC facilitates destructive interference.

3.2.3 Type III (based on the surface topography)

The requirement of the omnidirectional antireflection property has driven to the emergence of this type of coating based on surface topography.

Porous antireflection coating

These types of coatings are generally made up of porous silicon and find its major application in the field of solar energy harvesting [24, 25]. It consists of nanometer-sized voids with a large hydrogenated surface. But yet there is no perfect study [26] reported which states the relationship between RI and porosity. Studies on porous silicon have demonstrated the reflective properties on the outer region of p/n+ junction with regards to solar cells by etching the outermost region in the presence of HF/HNO_3.

Biomimetic photonic nanostructures ("moth's eye")

The optical systems have been fabricated by nature so well that it justifies scientific sense to reproduce them. For example, scallop eyes inspired chromatic aberration minimization, horsefly cornea inspired extreme UV-optics and human deformable eye lenses inspired liquid lenses, etc. The camouflaging strategy of some insects and the exceptional photon collection capability of nocturnal creatures have motivated scientists to analyze the eyes of such creatures, especially moths and butterflies and transparent wings of hawk moths. Studies demonstrated that these nanostructures have a gradient RI relationship between chitin and ambient of which makes it clear that antireflection property is chiefly due to exceptional transmission. Boden et al. [27] studied the antireflectivity which showed that moth's eye arrays of 250 nm exhibited similar performance as the double-layer antireflection which has been already discussed in the earlier section.

Textured surface antireflection coating

Surface texturing also provides the information about the substrate AR as explained by many scientific communities and the reason for antireflection is due to light trapping and multiple internal reflections phenomena. A new texturing geometry was explained to produce maximum efficacy solar cells with a null antireflection property that has three perpendicular planes that provide a platform for multiple internal reflections [28]. Surface texturing imparts a reduction of reflectance to the tune of approximately 10% in mono-crystal Si and reflection losses are reportedly minimized to nearly 1% in case of amorphous Si using surface texture.

Antireflection grating

The prime requirement for broadband antireflection over a large region gets fulfilled by the surface relief gratings. The grating structures are based on the similar principle of creating a continuous gradient of RI and their efficacy has been proved in the solar, microwave, and THz wavelength ranges. However, antireflection have been observed to be

less effective for solar cells because gratings that help to propagate the zeroth diffraction orders and do not provide to higher diffraction orders which apparently contribute to the total energy collected in the solar cell.

4. Recent progress toward the development of superhydrophobic antireflective polymer coatings with improved solar cell efficiency

Wang et al. [28] studied the synthesis and characterization of superhydrophobic ARC with high transmittance that can be used for solar cell applications. The authors prepared superhydrophobic sol–gels by hydrolyzing tetraethoxysilane (TES) and thereafter, reacting it with hexamethyldisilazane (HMDS). The prepared superhydrophobic sol–gels were aged for 48, 72, 96, or 168 h, respectively, to render it superhydrophobic. The antireflective glass coatings were fabricated through layer–by–layer (LBL) deposition technique using poly(allylamine hydrochloride)/poly(acrylic acid) (PAH/PAA) polyelectrolyte indicating a transmittance of 96%. Heat-treated ARCs up to 220°C rendered PAH/PAA multilayer to be hydrophobic with uniform distribution of pore size. This observation corroborated with the SEM micrographs confirming the presence of nanopores distributed uniformly throughout the surface. The authors observed that aging of the superhydrophobic sol–gels led to an increase in superhydrophobicity with an average WCA of 162.6, 164.4, and 163.5 degrees, respectively due to the NH_3 produced during the hydrolysis reaction of TEOS with HDMS. After spin coating, the superhydrophobic AR polymer coatings displayed high transmittance of 96.4%±0.2% with a WCA of 158.4 degrees and contact angle hysteresis (CAH) 1.8 degrees as compared to neat AR coatings. This was due to the large RI of superhydrophobic sol–gel. After calcination of superhydrophobic AR PAH/PAA Coatings with nanosilica, the WCA increased to 161 degrees with CAH of 5 degrees. The morphological studies of the superhydrophobic polymer AR Polymer Coatings using AFM (Fig. 8 reproduced from Ref. [28]) indicated submicrometer-sized structures which were composed of many nanometer-sized structures. This resulted in a structure similar to the lotus leaf with dual scale roughness property. Impact test of the coatings indicated high transmittance of 96% with an increase in CAH of 4.6±0.2 degrees. Advancing WCA of the coatings increased 7.2±5.0 degrees. The observed increase of CAH was due to the high speed of the plastic bullet during the impact test which led to the overall increase in the RMS roughness of the coatings. Thus, the authors concluded that the synthesized superhydrophobic AR coating based on (PAH/PAA) polyelectrolyte calcined with nanosilica obtained through LBL technique indicated high transmittance with improved WCA and good mechanical properties (Fig. 5).

Prado et al. [2] developed multifunctional sol–gel ARCs with improved superhydrophobic self-cleaning capacity for solar cell application. The AR coating was prepared based on tetraethyl orthosilicate (TEOS), Pluronic F127 using ethanol and distilled water. The
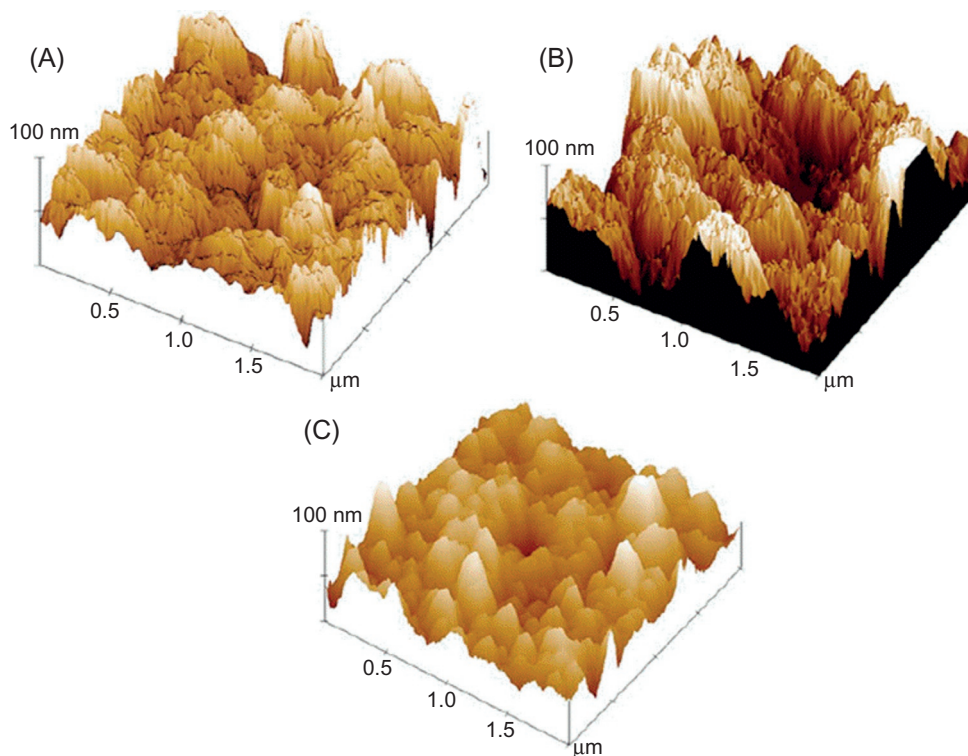
Fig. 5 AFM morphology of the AR polymer coating (A) before heat treatment, (B) after heat treatment, (C) after immersion in water for 1 week.

superhydrophobic films were synthesized using titanium *n*-butoxide (n–BuTi) and absolute ethanol. AR–coated glass was developed using mesoporous TiO_2/SiO_2 layers. The TiO_2 AR–coated glass presented a transmittance of 95.9% as compared to a neat glass with a transmittance of 91.2%. It was observed from methylene blue degradation tests that all the TiO_2 AR–coated glass is photoactive. The unique morphological arrangement of nano-structured inner SiO_2 and outer TiO_2 layers and the increase in the surface area has resulted in improved self–cleaning ability with high photocatalytic activity.

Choi and Huh [29] described the synthesis and characterization of one–step biomimetic antireflective, self–cleaning coating for light harvesting application in organic solar cells. The authors prepared the template by combining UV-assisted molding with subsequent hydrophobization of nanoparticles through one–step replication method. The prepared template was then subjected to further ultraviolet-ozone (UVO) treatment that resulted in the formation of dual nanometer-scale roughness with microstructured surface. The one–step replication method provides large surface area conducive for different applications. Polyurethane acrylate (PUA) functionalized prepolymer with a

perfluoropolyether (PFPE) backbone was considered to be the UV-curable precursor anchored with Al_2O_3 nanoparticles. The solar cell was fabricated using ITO-coated glass. The presence of fluorine groups led to both self-cleaning and development of AR properties due to its low surface energy and relatively low RI. The developed ITO-coated glass indicated superhydrophobicity with contact angle >156 degrees due to multiscale hierarchical surface morphology and low surface energy of fluorine. The AR properties of the ITO-coated glass were analyzed through UV-Vis spectroscopy. The ITO-deposited glass used as a substrate for solar cell devices indicated >8% reflectance over a visible region due to the high reflective power of ITO. The reflectance of ITO-coated glass was found to be higher by twofolds as compared to the optical bare glass. The UV-cured flat PFPE layer exhibited transmittance greater than the uncoated ITO glass. On the other hand, the cured dual rough PFPE layer on ITO glass indicated slightly lower reflection in comparison to uncoated ITO glass. This was due to the low RI (i.e., 1.37) of the transparent cured PFPE layer which gave rise to an increased transmission owing to the insertion of an intermediate RI layer in between air (i.e., 1.00) and the glass substrate (i.e., 1.52) which suppresses the interfacial Fresnel's reflection. The durability and stability of the coatings were investigated using QUV Accelerated Weathering Tester with UVA-340 lamp irradiated at 60°C. It was observed that the transmittance, AR and superhydrophobic properties of the coatings remained unaltered even after 200 h of UV exposure due to the higher bonding energy of C—F bonds, that is, 488 kJ mol^{-1}. This indicates that the coatings can be used as solar cells with higher withstanding efficiency toward long exposure to sunlight. Thus, the authors concluded that the methodology adopted for the fabrication of organic solar cells using one-step UV-assisted replica molding with acrylate-functionalized PFPE precursor on ITO glass can have practical applications in the field of solar cells due to its large surface area, dual scale roughness, low surface energy, and low RI.

Gan et al. [30] fabricated AR transparent polymer-coated graphene/silicon (G/Si) electrodes for application in Schottky junction PV solar cells. In comparison to the conventional monocrystalline Si solar cells, the assembly of G/Si only requires the transfer of graphene films onto silicon substrates at room temperature thereby avoiding high-temperature furnaces and vacuum systems. This assembly has also led to achieving the PCE of nearly 2% [31]. Apart from this method chemical doping, creation of micro-nanostructure on Si substrate and light trapping with antireflection coatings (ARC) can be other alternative strategies to increase antireflection properties and PCEs (10%). [32, 33]. Polymers are also novel candidates which can be applied in the field of ARC coatings as compared to inorganic materials owing to their lightweight, flexibility, stretching, and bending capabilities. The authors demonstrated the applicability of polymethylmethacrylate (PMMA) ARC coatings on G/Si substrates as transparent conductive electrodes with excellent light absorption for solar cell applications. The optical property of the PMMA ARC coatings on G/Si substrates was investigated using

transmission electron microscopy (TEM). It was observed that the transmittance of PMMA/G–Si ARC coatings (i.e., 97.4%) was slightly lower than the neat graphene coatings (i.e., 96%) in the region of 400–800 nm. However, the PV performance of the PMMA/G–Si ARC coatings was superior as compared to the uncoated ones with PCE of 6.55%. The observed phenomenon was due to the increase in short circuit current density (Jsc), which reduces the resistance of Schottky junctions thereby enhancing the light absorption ability. For further improvement in the PCE of the PMMA/G–Si ARC coatings, it was chemically doped via HNO_3 vapor treatment, which indicated an increase in PCE to about 13.34%. Thus the above methodology can be a cost-effective technique for the fabrication of solar cells with excellent light transmission ability (Fig. 9 reproduced from Ref. [30]) (Fig. 6).

Leem et al. [34] fabricated highly transparent antireflective moth-eye nanopatterned UV cured Norland Optical Adhesive (NOA) 63 coatings (ARC) on glass for application in solar PV systems. Glass has been a candid material for application in the field of optoelectronics due to its high optical transparency, low cost, and good thermal stability. They are basically used to safeguard the PV systems against UV radiation, external shock, and corrosive acidic environment. However, the optical reflection of glass degrades with time due to its high RI (nearly 1.5) which can reduce the PCE of solar cells. Hence, in order to overcome this disadvantage, we require ARCs that can reduce the optical losses caused by Fresnel surface reflection (FSR). The FSR phenomenon of glass can be decreased via the formation of biomimetic moth-eye structures on the surface of the glass, composed of tapered conical gratings having wavelengths smaller than the incident light [35–39]. In recent decades, soft imprint lithographic method has gained momentous attention in
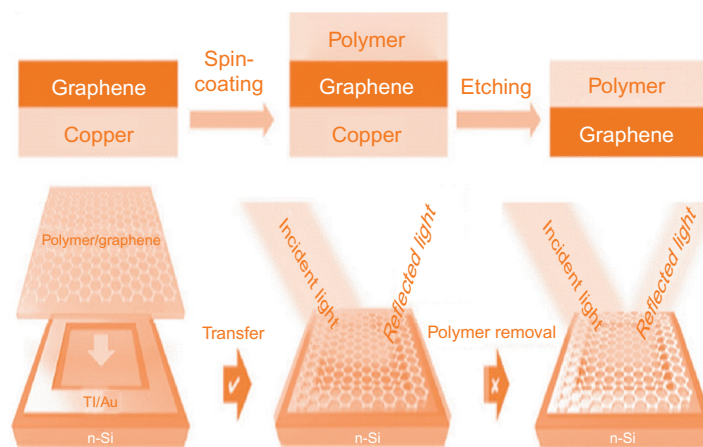
Fig. 6 Fabrication of polymer-coated G/Si solar cells.

comparison to other nanolithography techniques for fabricating micro- or nano-patterns onto UV-curable poly-dimethylsiloxane (PDMS) polymers. PDMS offers various advantages which include low free surface energy, flexibility, transparency, and hardness owing to its simplicity, low-cost, and tenability. In addition, the NOA63 polymers are quite beneficial as ARC owing to their similar RI of 1.56 with almost no absorption in the wavelength region between 350 and 1800 nm. The author observed that less work has been carried out regarding the performance improvement of III–V semiconductor-based multijunction PV module systems with conical nanogratings (NGs) patterned polymer films. Hence, the author investigated the effect of UV, thermal, and wetting behavior on the efficiency behavior of PDMS/NOA63 NG ARC coatings. The NOA63 NGs coatings exhibited a hydrophobic surface with a contact angle of 112 degrees and solar-weighted transmittance (T_{sw}) of 93.2%.

Superhydrophobic polymeric coating surface with CNT covering improves the solar cell by producing a large contact angle. Zhao et al. [40] has been successfully synthesized the silica-covered CNT by using sol-gel method and they described that the surface energy of the polymeric material was significantly reduced with static WCA of 156 degrees, thereby making the surface superhydrophobic. This also shows good acid, alkali, and aging resistance, which might be used as a good practical application in the future. Similarly, Jinguang and Qi [41] have been described the recent development in the fabrication and ARC surfaces based on nanostructure arrangement of silicon and nonsilicon materials. Moreover, Prado et al. [2] described the antireflective hydrophobic coatings based on porous silica and found the increase in transmission of light for wavelength range of 350–850 nm; which would be helpful for depositing a hydrophobic layer of thickness less than 3.5 nm without destroying any properties of ARC.

Hiralal et al. demonstrated the ZnO nanowire-based ARCs for organic PV solar cell and found that the coating produces the additional benefits to the solar cell such as it lowers the rate of degradation and also lowers the absorption of UV radiation. The presence of ZnO on AR coating is a photocatalytic semiconductor in nature which catalyzes redox reactions in the presence of water and oxygen thereby permitting the breakdown of organic molecules on its coating surface. This can be used as a self-cleaning agent for organic materials for reduction issues from soiling [42].

5. Fabrication of superhydrophobic coatings

Wetting behavior is generally classified into four different categories based on the WCA (θ), that is, 0 degrees $< \theta <$ 10 degrees (superhydrophilic), 10 degrees $< \theta <$ 90 degrees (hydrophilic), 90 degrees $< \theta <$ 150 degrees (hydrophobic), and 150 degrees $< \theta <$ 180 degrees (superhydrophobic). Recent decades have witnessed momentous attention toward the development of superhydrophobic surface. Polymers reinforced with nano-fillers with distinctive features like low cost, good processability, flexibility, good scratch,

and abrasion resistance have been used as candid materials for the fabrication of super-hydrophobic coatings [43]. The two important factors which are responsible for the fabrication of superhydrophobic coatings include roughening of the surface and chemical modification of coatings with low surface energy materials [44]. Different models such as Wenzel's and Cassie's are used for correlating and understanding the relation between superhydrophobicity phenomenon, surface roughness, and chemical modification [15, 45, 46].

6. Future prospect and challenges

From the above literature findings, it is imperative that the AR coating materials have shown rapid application with potential prospects in the field of lenses, lasers, solar cells, diodes, optical and optoelectronic devices, screens, sensors, antiglare glasses for automotive applications, and even military equipment. It is necessary to focus some parameters of investments such as efficiency, stability, energy yield, and span of life instead of focusing solely on initial capital investment because the capital cost of installation of the solar panel is too high. Hence, the future scope can be divided into two parts; wherein, the first part aims to the improvement of the materials performance by continuous optimizing process and the second part aims to build a request on manufacturing technology. The performance improvement includes many multifunctional activities such as self-cleaning, light-trapping, durability, and so on [12]. Moreover, ARCs should have significant properties such as thermal, mechanical, long term durability, etc. This is due to the high mechanical strength of the SHAP coating makes the material suitable for self-cleaning and AR. Hence, high power conversion and cost reduction are obtained. Hybrid ARCs with self-cleaning ability have found extensive application in low emission applications. The conventional single and bilayer ARCs are still used for laser applications owing to minimum reflectance at smaller wavelengths. However, in the present era, the single and bilayer coatings are replaced by advanced ARCs that is, moth-eye ARCs due to its economic feasibility. Bionic nanostructures based on moth eye have resolved the issues related with omnidirectional ARCs to be used for different optical equipment and solar cells with improved transmittance. The fabrication process is also cost-effective and feasible for stacking multilayer coatings. In recent decades, ARCs have found wide application in the field of PV cells; however, the coatings lack mechanical resilience and strong adhesion strength. In addition, ARCs used for outdoor application gets peeled off from the substrate due to poor adhesion strength. For instance, ARCs based on ceramic material show brittle fracture due to microcracks and voids. Thus, it is imperative that the mechanical strength, adhesion strength, and thermal stability of the ARCs need to be improved for finding applications in harsh

environmental conditions. The other factors which need prime attention are the compressive and tensile failure of ARCs. The prime focus should be toward the development of polymer ARCs reinforced with nanofillers, which exhibits ductile failure with improved mechanical stability. Another area which needs attention is the development of cost-effective single ARCs and hybrid multifunctional ARCs with improved mechanical strength, thermal stability, superamphiphobic property, scratch resistivity, and antiglare property for finding application in the field of solar cells. Hence, the developments of innovative materials for SHAP coating techniques are the most essential part to expand the range of applications which can lead to the large-scale production in the industry. In addition, it is also required to carry out accurate measurements and different models for better understanding of the fabrication of SHAP coatings and to overcome the above challenges.

The following are some of the main parts in which the research could be directed to resolve issues:

- Although ARCs have exemplified their application in the field of solar PV still it poses some challenges owing to their performance over time period.
- The biological aspect of antireflection remains unsought which could be explored by considering photonic nanostructures in butterflies, squids, etc.
- Novel developments in optical devices provide a platform containing the immense potential for customization of ARCs to meet the requirements of the cutting edge technology and product improvisation.

7. Conclusions

In the present chapter, the recent progress in SHAP coatings has been described in detail. But, there are still some issues for the fabrication process in the manufacture of SHAP coatings. Based on the findings polymeric ARCs can be used to increase the efficiency, antireflection or transmission, and self-cleaning performance which encourage the technology or industry to increase the mechanical strength of the developed products. ARCs have been used in a wide range of applications starting from optical and optoelectronic devices to automotive and aerospace applications. Further, in other fields such as electrochromism and green architectural strategies have also led to the integration of AR property and electrochromism into unity. The performance characteristics of the solar cell also get impaired by the accumulation of dust, microbes, and moisture. The development of hydrophobic, hydrophilic, and antimicrobial coatings is also achieving greater demand due to its hybrid characteristics. In conclusion, a simple, cost-effective with high-performance solar cell can be developed which might provide new ideas and new concept for the development of SHAP coating surfaces.

References

[1] A. Cannavale, F. Fiorito, M. Manca, G. Tortorici, R. Cingolani, G. Gigli, Multifunctional bioinspired sol–gel coatings for architectural glasses, Build. Environ. 45 (2010) 1233–1243.

[2] R. Prado, G. Beobide, A. Marcaide, J. Goikoetxea, A. Aranzabe, Development of multifunctional sol-–gel coatings: anti-reflection coatings with enhanced self-cleaning capacity, Sol. Energy Mater. Sol. Cells 94 (2010) 1081–1088.

[3] H. Hanaei, M.K. Assadi, R. Saidur, Highly efficient antireflective and self-cleaning coatings that incorporate carbon nanotubes (CNTs) into solar cells: a review, Renew. Sust. Energ. Rev. 59 (2016) 620–635.

[4] Z. Han, Z. Wang, X. Feng, B. Li, Z. Mu, J. Zhang, S. Niu, L. Ren, Antireflective surface inspired from biology: a review, Biosurf. Biotribol. (4) (2016) 137–150.

[5] H.K. Raut, V.A. Ganesh, A.S. Nair, S. Ramakrishna, Anti-reflective coatings: a critical, in-depth review, Energy Environ. Sci. 4 (2011) 3779–3804.

[6] A. Mishra, V. Rathi, G. Era, Super hydrophobic antireflective coating to enhance efficiency of solar PV cells, Int. J. Eng. Res. Electr. Electron. 3 (2017) 2395–2717.

[7] H. Hattori, Anti-reflection surface with particle coating deposited by electrostatic attraction, Adv. Mater. 13 (2001) 51–54.

[8] J. Han, Y. Dou, M. Wei, D.G. Evans, X. Duan, Antireflection/antifogging coatings based on nanoporous films derived from layered double hydroxide, Chem. Eng. J. 169 (2011) 371–378.

[9] C. Alex Mayer, S.R. Scully, B.E. Hardin, M.W. Rowell, M.D. McGehee, Polymer-based solar cells, Mater. Today 10 (2007) 28–33.

[10] U. Mehmood, F.A. Al-Sulaiman, B.S. Yilbas, B. Salhi, S.H.A. Ahmed, M.K. Hossain, Superhydrophobic surfaces with antireflection properties for solar applications: a critical review, Sol. Energy Mater. Sol. Cells 157 (2016) 604–623.

[11] A. Duparré, M. Flemming, J. Steinert, K. Reihs, Optical coatings with enhanced roughness for ultrahydrophobic, low-scatter applications, Appl. Opt. 41 (2002) 3294–3298.

[12] G.R.J. Artus, S. Jung, J. Zimmermann, H.-P. Gautschi, K. Marquardt, S. Seeger, Silicone nanofilaments and their application as superhydrophobic coatings, Adv. Mater. (20) (2006) 2758–2762.

[13] A. Nakajima, A. Fujishima, K. Hashimoto, T. Watanabe, Preparation of transparent superhydrophobic boehmite and silica films by sublimation of aluminum acetylacetonate, Adv. Mater. (16) (1999) 1365–1368.

[14] R.N. Wenzel, Resistance of solid surfaces to wetting by water, Ind. Eng. Chem. 28 (8) (1936) 988–994.

[15] A.B.D. Cassie, S. Baxter, Wettability of porous surfaces, Trans. Faraday Soc. 40 (1944) 546–551.

[16] M. Owen, A review of significant directions in fluorosiloxane coatings, Surf. Coat. Int. B Coat. Trans. 87 (2) (2004) 71–76.

[17] J.A. Dobrowolski, D. Poitras, P. Ma, H. Vakil, M. Acree, Toward perfect antireflection coatings: numerical investigation, Appl. Opt. 41 (2002) 3075–3083.

[18] K.Q. Salih, N.M. Ahmed, Multilayer antireflection coatings model for red emission of silicon for optoelectronic applications, Int. J. (2009).

[19] J.T. Cox, G. Hass, Antireflection coatings for optical and infrared materials, in: Physics of Thin Films, vol. 2, Academic Press, New York, NY, 1968, p. 239.

[20] C.G. Bernhard, Structural and functional adaptation in a visual system, Endeavour 26 (1967) 79–84.

[21] H.A. Macleod, H.A. Macleod, Thin-Film Optical Filters, CRC Press, 2010.

[22] B. Sheldon, J.S. Haggerty, A.G. Emslie, Exact computation of the reflectance of a surface layer of arbitrary refractive-index profile and an approximate solution of the inverse problem, JOSA 72 (8) (1982) 1049–1055.

[23] J.Q. Xi, M.F. Schubert, J.K. Kim, E.F. Schubert, M. Chen, S.Y. Lin, W. Liu, J.A. Smart, Optical thin-film materials with low refractive index for broadband elimination of Fresnel reflection, Nat. Photonics 1 (3) (2007) 176.

[24] L. Schirone, G. Sotgiu, F.P. Califano, Chemically etched porous silicon as an anti-reflection coating for high efficiency solar cells, Thin Solid Films 297 (1–2) (1997) 296–298.

[25] K. Grigoras, A. Krotus, V. Pacebutas, J. Kavaliauskas, I. Simkiene, EMRS Conf Proc., Strasbourg, 1995.

[26] V. Lehmann, U. Gösele, Porous silicon formation: a quantum wire effect, Appl. Phys. Lett. 58 (8) (1991) 856–858.

[27] S.A. Boden, D.M. Bagnall, Bio-mimetic subwavelength surfaces for near-zero reflection sunrise to sunset, in: Conference Record of the 2006 IEEE 4th World Conference on Photovoltaic Energy Conversion, vol. 2, IEEE, 2006, May, pp. 1358–1361.

[28] S.-D. Wang, Y.-Y. Shu, Superhydrophobic antireflective coating with high transmittance. J. Coat. Technol. Res. (2013), https://doi.org/10.1007/s11998-012-9468-9.

[29] S.-J. Choi, S.-Y. Huh, Direct structuring of a biomimetic anti-reflective, self-cleaning surface for light harvesting in organic solar cells, Macromol. Rapid Commun. 31 (2010) 539–544.

[30] X. Gan, Ruitao, H. Zhu, L.-P. Ma, X. Wang, Z. Zhang, Z.-H. Huang, H. Zhu, W. Ren, M. Terrones, F. Kang, Polymer-coated graphene films as anti-reflective transparent electrodes for Schottky junction solar cells. J. Mater. Chem. A (2016), https://doi.org/10.1039/C6TA06261J.

[31] X.M. Li, H.W. Zhu, K.L. Wang, A.Y. Cao, J.Q. Wei, C.Y. Li, Y. Jia, Z. Li, X. Li, D.H. Wu, Graphene-on-silicon Schottky junction solar cells, Adv. Mater. 22 (2010) 2743–2748.

[32] C. Xie, X. Zhang, Y. Wu, X. Zhang, X. Zhang, Y. Wang, W. Zhang, P. Gao, Y. Han, J. Jie, Surface passivation and band engineering: a way toward high efficiency graphene–planar Si solar cells, J. Mater. Chem. A 1 (2013) 8567–8574.

[33] X. Zhang, C. Xie, J. Jie, X. Zhang, Y. Wu, W. Zhang, High-efficiency graphene/Si nanoarray Schottky junction solar cells via surface modification and graphene doping, J. Mater. Chem. A 1 (2013) 6593–6601.

[34] J. Woo Leem, X.-Y. Guan, M. Choi, J. Su Yu, Broadband and omnidirectional highly-transparent coverglasses coated with biomimetic moth-eye nanopatterned polymer films for solar photovoltaic system applications, Sol. Energy Mater. Sol. Cells 134 (2015) 45–53.

[35] S. Ji, J. Park, H. Lim, Improved antireflection properties of moth eye mimicking nanopillars on transparent glass: flat antireflection and color tuning, Nanoscale 4 (2012) 4603–4610.

[36] W. Leem, J.S. Yu, J. Heo, W.K. Park, J.H. Park, W.J. Cho, D.E. Kim, Nanostructured encapsulation coverglasses with wide-angle broadband antireflection and self-cleaning properties for III–V multi-junction solar cell applications, Sol. Energy Mater. Sol. Cells 120 (2014) 555–560.

[37] Y.M. Song, Y. Jeong, C.I. Yeo, Y.T. Lee, Enhanced power generation in concentrated photovoltaics using broadband antireflective coverglasses with moth eye structures, Opt. Express 20 (2012) 916–923.

[38] J.W. Leem, Y. Yeh, J.S. Yu, Enhanced transmittance and hydrophilicity of nanostructured glass substrates with antireflective properties using disordered gold nanopatterns, Opt. Express 20 (2012) 4057–4066.

[39] Y.M. Song, H.J. Choi, J.S. Yu, Y.T. Lee, Design of highly transparent glasses with broadband antireflective sub wavelength structures, Opt. Express 18 (2010) 13063–13071.

[40] L. Zhao, W.H. Xu, J.Q. Liu, W.L. Liu, J.S. Yao, M. Li, X.Q. Wang, Y.Z. Wu, Superhydrophobic surface fabricated by modifying silica coated multiwalled carbon nanotubes composites, J. Sol-Gel Sci. Technol. 69 (2014) 107–113.

[41] C. Jinguang, L. Qi, Recent advances in antireflective surfaces based on nanostructure arrays, Mater. Horiz. 2 (1) (2015) 37–53.

[42] P. Hiralal, C. Chien, N.N. Lal, W. Abeygunasekara, A. Kumar, H. Butt, H. Zhou, H.E. Unalan, J.J. Baumberg, G.A. Amaratunga, Nanowire-based multifunctional antireflection coatings for solar cells, Nanoscale 6 (2014) 14555–14562.

[43] S. Das, S. Kumar, S.K. Samal, S. Mohanty, S.K. Nayak, A review on superhydrophobic polymer nano-coatings: recent development and applications, Ind. Eng. Chem. Res. 57 (2018) 2727–2745.

[44] Y. Feng, Z. Liu, W. Liu, The preparation and properties of Y_2O_3/AlN anti-reflection films on chemical vapor deposition diamond, Thin Solid Films 520 (2011) 734–738.

[45] R.N. Wenzel, Surface roughness and contact angle, J. Phys. Colloid Chem. 53 (1949) 1466–1467.

[46] C.-L. Lin, Z.-W. Yan, C.-H. Chen, Electrochromic and photoelectrochromic properties of sol–gel derived tungsten trioxide/titania composite thin films, Res. Chem. Intermed. 43 (2017) 3553–3562.

CHAPTER 13

Interfacial slip-and-drag reduction by superhydrophobic polymer coating

J. Bruce Ralphin Rose
Aeronautical Engineering, Anna University Regional Campus, Tirunelveli, India

1. Introduction

Superhydrophobic surfaces have excellent water–repellency and self–cleaning character-istics. Water repellency is an essential behavior to use the surfaces for many applications such as airplane and wind turbine antiicing, drag reduction at high speeds, oil–water sep-arations, and the preparation of surfaces with anticorrosion requirements [1] Conversely, self-cleaning characteristics facilitate the development of antibacterial surfaces, water purifications, optical devices, and state-of-the-art textile fabrics [2]. Drag reduction is a primary assignment for any aerodynamists who practices aerospace engineering related applications. Basically, the wettability of a solid surface is defined based on the water con-tact angle "θ" (WCA). If the WCA magnitude is $\theta \leq 90$ degrees, then the surface has significant wettability and hence it is known as hydrophilic surfaces. On the other hand, if $\theta > 90$ degrees, then the surface holds temperate wettability condition which is com-paratively greater than hydrophilic surface and consequently it is called as hydrophobic surface. Further, if the WCA $\theta \geq 150$ degrees, then the surface has excellent self-cleaning properties and this can be achieved only through the nonwetting smooth surfaces known as superhydrophobic in nature [1]. Superhydrophobic surfaces are available with micro and Nanometer length scales and WCA is the crucial parameter to confirm the surface characteristics from the angle at which liquid–vapor interface meets a solid surface.

The water penetration into the micro and nanopores depends on chemical hydropho-bicity and topology features of the material surfaces. Surface roughness and low surface energy are the primary constraints that decide the amount of water penetration into the gap exist across the protrusions. The low surface energy flocks the air layer on the material surface which in turn creates the air-liquid interface [3]. Hence, the air-liquid interface builds the contact angle, $\theta > 150$ degrees that is essential for preparing the superhydro-phobic surfaces. The angle between advancing angle and sliding angle is known as hys-teresis angle (β) that has a strong influence on the characteristics of wettability and it is maintained at less than 5 degrees because of the air-liquid interface. Few superhydropho-bic surfaces contain infused layer like rose petal effect which affects the contact area through the modified micro and nanostructures [3].

The interfacial slip-and-drag reduction is an essential requirement for the aviation industry since it has a straightforward relationship with the specific fuel consumption (SFC) of an airplane. Drag reduction of about 1% could save several gallons of fuel in the course of airplane operation within the safe life period. It is the crucial reason for the efforts taken by the aerodynamists across the globe toward the airplane drag reduction at various missions. The potential challenges associated with the establishment of large slip-and-drag reduction includes the droplet contact angle, Reynolds number (Re) of the flow, pressure-driven laminar or turbulent nature of the flows and the temperature. Airplane icing is a meteorological risk that influences the dynamic stability of the airplane as the supercooled water droplets (SWD) impinges on the aerodynamic surfaces. Earlier (from 1990 to 2010) in the Aviation industry, nearly 240 accidents have been reported because of the icing accretion problem on the nose, empennage, wings, and engine nacelle. The tiny portion of ice or supercooled liquid water content (LWC) exists in the clouds, which remains in the liquid state even below 0°C are the key sources of ice accretion in flight. Here, an instantaneous phase change process occurs in the solid–liquid interface based on the heat transfer performance of the aerodynamic surface. The phase diagram (pressure-temperature diagram) should be prepared in a log scale in order to evaluate the degree of solidification under various icing circumstances. However, the performance of airplane antiicing and de-icing systems also could influence the rate of ice accretion through the phase change heat transfer.

The assumption of no-slip boundary condition yields good accuracy for macroscopic flows because the slip length (b) is approximately neglected ($b \approx 0$). As the mean free path of fluid (λ) increases, the no-slip condition starts to become invalid especially in the micro and nanolevel fluid dynamics-based applications. The drag reduction in airplanes can be categorized as a microfluidic problem that contains the slip length in the order of micrometers. Numerous studies in recent years have been reported the influence of wettability and surface roughness in the slip length [4, 5]. Computational fluid dynamics (CFD)-based codes and icing simulation tools play a vital role in the prediction of WCA and icing effects. At the microscopic level, different types of ice accretion occur on the aerodynamic surfaces; namely, (a) Rime ice, (b) Glaze ice, (c) Horn ice, and (d) Runback ice. Measurement of the critical distance between icing clouds and airplanes is essential to predict the different icing patterns that are needed to analyze the basic data and modeling. Hence, the present chapter is devoted to analyzing the materials and methods available to minimize the aerodynamic drag through superhydrophobic polymer coatings especially at the icing conditions.

2. Interfacial slip

The composite interface (superhydrophobic surface and fluid) preparation for drag reduction is possible only by ensuring the higher contact angles. Hydrophobicity of a

surface produces high slip lengths because of the large shear stresses (τ) in the liquid–solid interface [6]. The polymer surfaces should be suitably modified to achieve minimum shear stresses that in turn reduce the resistance to droplet sliding [7]. Surface energy is directly proportional to the critical shear stress and the contact angle plays a vital role in the magnitude of critical stress. Moreover, slip length is influenced by the contact angles and atmospheric conditions especially on the superhydrophobic coatings. As the contact angle $\theta \leq 140$ degrees, the hydrophobicity of polymer surface decreases and the slip length will be in the order of few molecular diameters. Fig. 1 shows the slip at the liquid–solid interface and the no–slip condition in the macroscopic flows.

Flow visualization techniques and indirect flow measurements are widely used to measure the micro and nanoscale slip length. Hot film anemometry and micro particle image velocimetry (μPIV) are the two important techniques to measure the slip velocities within a few microns from the plate surfaces [8]. From the studies, it has been observed that the shear rate for slip length at different polymer surfaces can be optimized through superhydrophobic coatings. The solution for ice accretion problem on aerodynamic surfaces is a potential application corresponding to the interfacial slip velocities at different contact angles. The low Re flows exhibit several flow instabilities and the selection of an appropriate slip model is mandatory for the solution accuracy in the course of experimental or computational analysis [9]. Here, the dynamic slip model has been utilized because of the nonmonotonic characteristics of flow curve as the function of shear stress.

3. Drag reduction mechanisms by polymer coatings

Active drag reduction methods utilize viscoelastic polymeric additives at minuscule additive concentrations to improve the flow field characteristics. Low surface energy and surface roughness are the major parameters to be considered in the course of preparation of superhydrophobic surfaces. The rougher surfaces would attain higher slip because of the high shear stress which induces the microbubble cavitations. As the root mean square
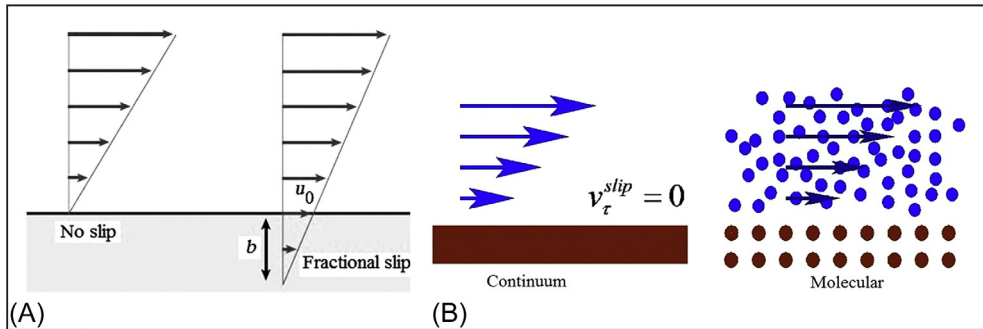
Fig. 1 Slip at the liquid-solid interface.

(RMS) roughness–scale decreases to nanoscale (about 1 nm), the surface energy decreases in the case of hydrophobic surfaces [10]. This air–liquid interface offers higher contact angle and small contact hysteresis (the difference between an advancing angle and receding angle) in superhydrophobic surfaces. In addition to diluted polymer solutions, surfactants, and suspended solid particles also can be used for developing competent drag plunging substances. The hydrodynamic coils exist in the polymer solutions influence the turbulent eddies through microbubble induced vortices. Hence, the degree of drag reduction depends on the ppm concentration of the polymer additives along with the anionic and cationic characteristics.

Passive drag reduction techniques were motivated by nature, such as the microstructures of shark skin, riblets, dimples, and wavy walls. In the boundary layer control mechanisms, the usage of riblet is one of the competent passive drag reduction techniques. The riblet surface delays the turbulence transition and affects the local flow field adjacent to the wall with minimal shear stress rate. A new passive–active interactive technique has been introduced in modern airplanes to overcome the limitations associated with active and passive drag reduction strategies.

3.1 Superhydrophobic coatings

The use of superhydrophobic coatings is primarily focused toward water repellency and low adhesion of liquid drops to such coatings. It helps to decrease the microscopic water droplet accumulation on any surface before the LWC freezes. Ice and fluid adhesion on a solid surface depends on the intermolecular forces that interact at the fluid–solid interface. A droplet impinging on a hydrophilic surface (see Fig. 2) spreads on the surface and does not recoil to avoid freezing. In this context, wettability and repellency are the two significant characteristics of solid surfaces in terms of theoretical and practical aspects. Superhydrophobic polymer coatings are water-repellent surfaces on which LWC adhesion is low as compared to the hydrophobic surfaces [11].
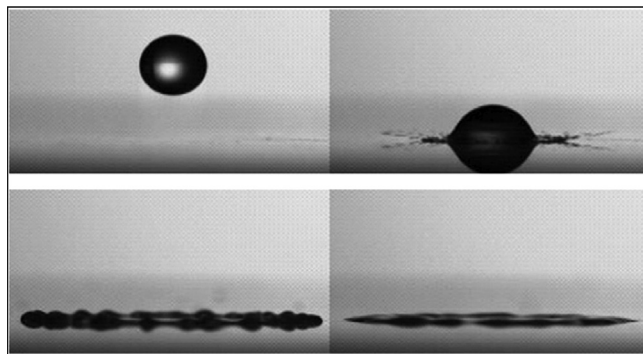
Fig. 2 Drop-by-drop impact and spreading on the ordinary surface.

The drop-by-drop impact on the surface with superhydrophobic coating is highlighted in Fig. 3. Here, the drop impinging on a superhydrophobic surface recoils and a partial or absolute drop rebound is noticed. If the drop totally rebounds after impact, then the free energy barrier (FEB) helps to detach the droplet from the surface with microtexture prior to freezing. Shedding of a drop by peripheral force input is also valuable for icing mitigation. The measurement of the contact angle at superhydrophobic layer can be done through Goniometer as indicated in Fig. 4.

4. Aircraft icing problem

Ice accretion on airplane wings creates adverse flight conditions that affect the entire aerodynamic characteristics in a specific mission segment [12]. According to the Federal Aviation Regulations (FAR) reports, icing is a serious issue at the flight altitudes between 7000 and 9000 ft above the mean sea level in the winter season. Except for winter, the icing problem occurs up to 20,000 ft because the supercooled LWC turns into ice on
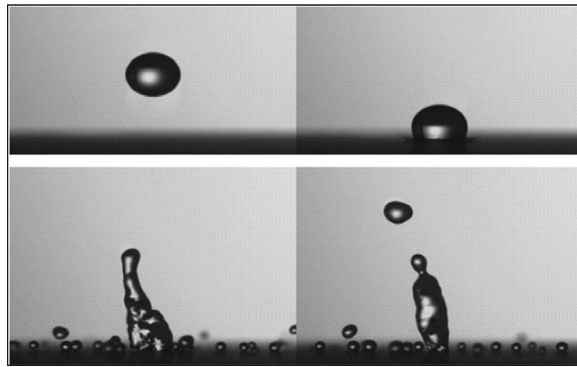
Fig. 3 Drop-by-drop impact on the surface with superhydrophobic coating.
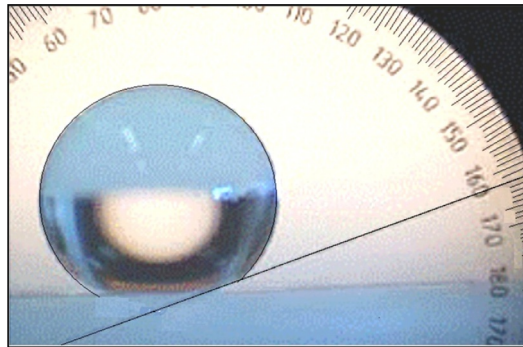
Fig. 4 Measurement of contact angle at superhydrophobic layer.

wings, airframes, engines, rotors, etc. It should be noted that icing occurs whenever there is an apparent humidity exists in the atmosphere and the local surface temperature drops less than the freezing point. The major parameters to be considered for optimizing the interfacial slip and contact angle are the LWC, droplet size, cruising Mach number (M), surface roughness and local temperature [13]. The icing system performance also varies based on the types of cloud environment and duration of flight through the icing clouds. For the certification process, the airplane manufacturer should demonstrate the airworthiness at specific icing conditions to ensure the air safety at different altitudes.

4.1 Icing mechanism on airplane wings

Firstly, the impinging water droplet on the airplane wing surface or leading edge (LE) freezes and then the ice accretion begins at different scales based on the prevailing conditions. This process may lead to the formation of different ice shapes such as rime ice, horn ice, etc. on the wing LE. Fig. 5 presents the transitional flow separation from the ice tip because of the high reverse pressure gradient. Subsequently, an unbalanced and unsteady separated shear layer is formed up to the mid-chord in the microscopic scale that leads to the induced vortex shedding [14]. In fact, the vortices first roll up on the shear layer and then circulation is created because of adverse pressure gradients. Although the use of antiicing systems would prevent the wing LE from freezing, a meager quantity of water may turn into ice at the downstream that frequently forms the runback ice on spanwise edges. Vargas and Kreeger developed the ice accretion models that can be employed through 3D ice accretion codes for computational simulation of icing problems [15]. A detailed understanding of ice accretion is essential for drag reduction especially at swept-back wings. Icing intensity and pilot action required at various levels of cloud LWC are summarized in Table 1.

4.2 Computational investigation of icing problem

In the computational investigation of the icing problem, the free energy (FE) formulation is used with microtextures. The microtextures are developed based on the FAR icing conditions with nonuniform rough surfaces. The FE landscape is an essential parameter to customize the boundary layer drag through superhydrophobic coatings. For the proposed application, a numerical analysis for an iced airfoil is studied prior to the
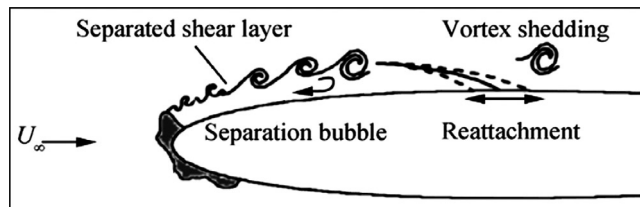
Fig. 5 Schematic diagram of flow separation on the iced airfoil.

Table 1 Icing intensity and pilot action summary

Intensity	Airframe accumulation	Pilot action	LWC (g/m³)
Trace	Ice becomes perceptible. Rate of accumulation of ice is slightly greater than the rate of loss due to sublimation.	Unless encountered for 1 h or more, de-icing/antiicing equipment and heading or altitude change not required.	<0.1
Light	The rate of accumulation may create a problem if flight in this environment continues for 1 h.	De-icing/antiicing is required occasionally to eradicate or avoid accumulation or altitude change required.	0.11–0.16
Moderate	The rate of accumulation is such that even short encounters become potentially hazardous.	De-icing/antiicing is required or heading or altitude change required.	0.61–1.2
Severe	The rate of accumulation is such that de-icing/antiicing equipment fails to reduce or control the hazard.	Immediate heading or altitude change required.	>1.2

superhydrophobic coating to compute the aerodynamic coefficients (C_L and C_D) around the airfoil [16]. A 2D airfoil is analyzed with step-by-step ice accretion at the wind speed of 175 m/s and the local temperature 243 K. Since the steady level flight assumption is valid at the icing conditions, the angle of attack (AoA) range was maintained from 0 degrees to 3 degrees for all the roughness textures.

The 2D airfoil is designed with NACA 6-series configuration through ANSYS Design Modeler (ADM) and meshed using ICEM CFD. The most significant hazard of structural icing is the disruption of airflow over aircraft surfaces. Hence, the wing surface is designed with 2D spike-valley like microtexture as stated in the FAR–25 (Appendix C) guidelines. The computational analysis using ANSYS fluent tool has been done to compute the disruption in airflow due to the slip in the heterogeneous surface. The surface roughness would reduce the lift coefficient (C_L) and increase the drag which causes the aircraft to stall at a lower AoA [17]. To preserve the cruising altitude and counteract the effects of drag during a flight in icing conditions, the AoA is increased and excess power mode is enabled for the engine(s).

4.3 Numerical simulation of ice profiles

The advent of supercomputers and parallel processing strategies help to solve the most complicated engineering problems in a short time period. The applications of numerical

simulations can be extended for a wide range of structural (creep, fatigue, fracture, vibration, and noise) and thermodynamic (heat and mass transfer and fluid flow) problems in engineering. Recent research findings promise various software programs and tools for creating passive icephobic surfaces with and without coatings. Although present icing systems used for ice removal are generally effective, they require the uninterrupted supply of hot air from the power plants or chemical treatment of aerodynamic surfaces at regular intervals. Polymer coatings on aerodynamic surfaces enhance the efficiency of standard anti-/de-icing systems or it can be replaced if the motion of droplets is adequate to eliminate the ice accretion. ANSYS has been evolved as a popular and complete package with its powerful capabilities to model and simulate the icing problems in the solid-liquid interface.

4.4 Meshing

The meshing or discretization process is done for the numerical analysis using software and the properties of mesh are given below. Hybrid mesh geometry parameters are assigned that includes the control volume size and number of nodes and elements. Mesh growth rate was maintained at 1.20 with a minimum edge length of 2.66×10^{-4}. The meshing of the iced airfoil is also done using ICEM CFD software with 577,300 nodes and 563,788 elements. The hybrid meshed control volume with the airfoil is presented in Fig. 6. Unstructured triangular meshes are used with fine meshes near the nonuniformly aligned pillars to obtain accurate results as shown in Fig. 7. The top surface of the airfoil is assumed with full ice accretion and it consists of 16 microscopic ice bubbles on the top surface and LE.
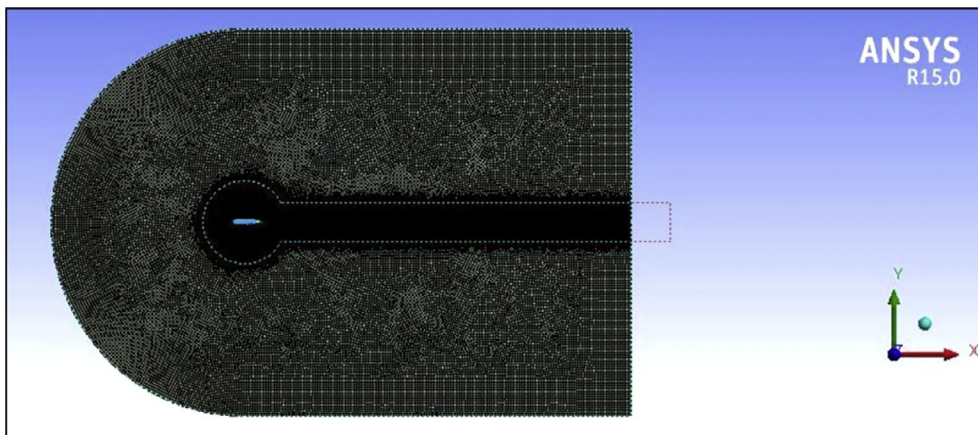
Fig. 6 2D airfoil and control volume with hybrid mesh.
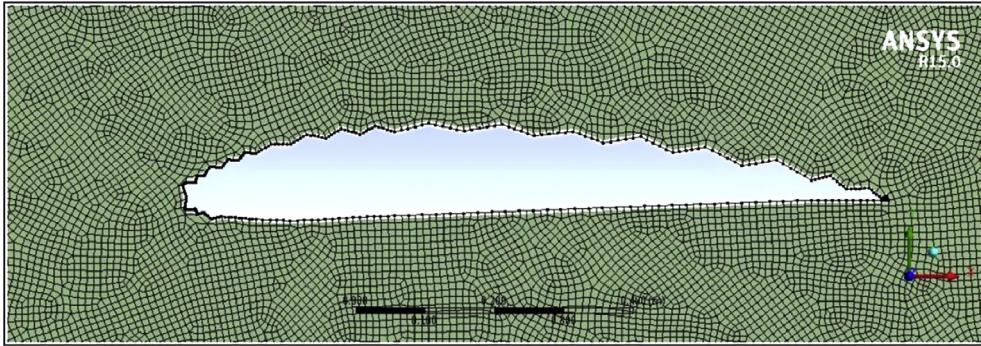
Fig. 7 Meshed airfoil with full ice bubbles on the top surface.

4.5 Velocity profiles—Computational analysis

The rate of freezing after the droplet impact depends on the temperature of the aircraft skin and the air temperature. Here, the sliding resistance is measured in terms of skin friction coefficient for with and without polymer coatings. Since the temperature inclusion induces the normalized FE, the local metastable state is assumed for the numerical simulation. Fig. 8A shows the velocity profile at 0 degrees AoA without any ice formation on the airfoil surface. Here, the cruising speed of an airplane is assumed as 175 m/s and the maximum velocity (about 264 m/s) occurs at the top of the airfoil near the quarter chord point. As the AoA increases to 3 degrees (Fig. 8B), the velocity increases further and satisfies the real condition.

The reference velocity and pressure profile data without ice accretion at 0 degrees AoA are captured from the CFX postprocessing module. Fig. 9A shows the velocity profile for 0 degrees AoA with rime ice accretion (two bubbles model) at LE. Here, the velocity magnitude decreases to 243 m/s from 264 m/s (reference value) as the ice profile
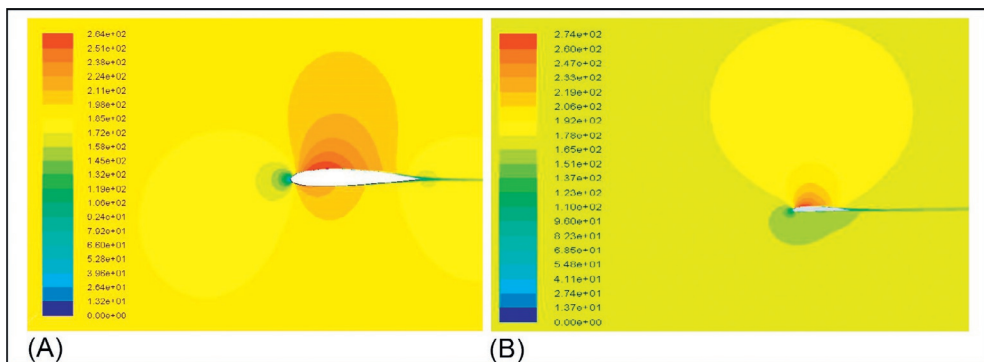
Fig. 8 Velocity profile without ice accretion over airfoil for (A) 0 degrees AoA and (B) 3 degrees AoA.
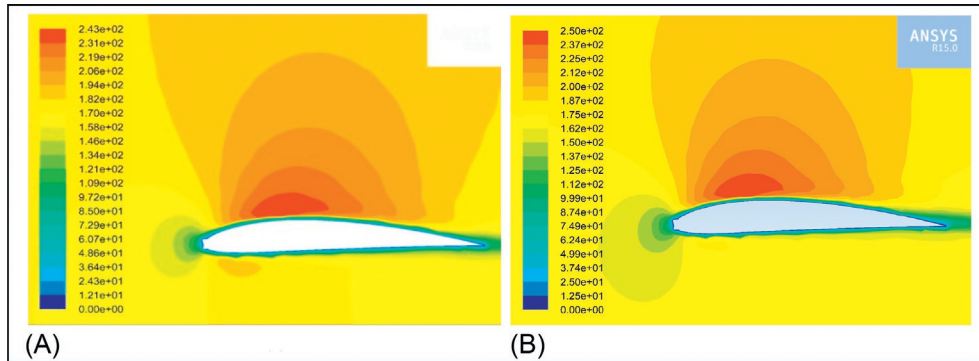
Fig. 9 Velocity profile with rime ice accretion at airfoil LE for (A) 0 degrees AoA and (B) 3 degrees AoA.

initiates the separation eddies from the LE of airfoil. The velocity gradient indicates the influence of ice accretion on the dynamic pressure that is obviously proportional to the aerodynamic coefficients (C_L and C_D). As the AoA increases, velocity magnitude is decreased to 249 m/s from 274 m/s as shown in Fig. 9B. The large water droplets exist in the cumuliform clouds produce clear, hard, and glossy ice profiles on the aerodynamic surfaces. The C_L and C_D distribution is fully modified as the AoA increases beyond 3 degrees and it causes the discomfort to the passengers by influencing the stability characteristics of airplanes.

The velocity profiles obtained for the airfoil with four ice bubbles model are highlighted in Fig. 10. It shows the influence of ice accretion at the quarter chord part of the airfoil on the velocity profile specifically in the LE region. The velocity magnitude decreases to 226 m/s from 243 m/s for 0 degrees AoA case as compared with Fig. 9. It clearly shows the influence of microscopic slip occurs due to the surface roughness at the liquid–solid interface. Here, the surface roughness is in the microscopic level (approximately 20 μm) which is accepted for many boundary layer flows at low Re [18].
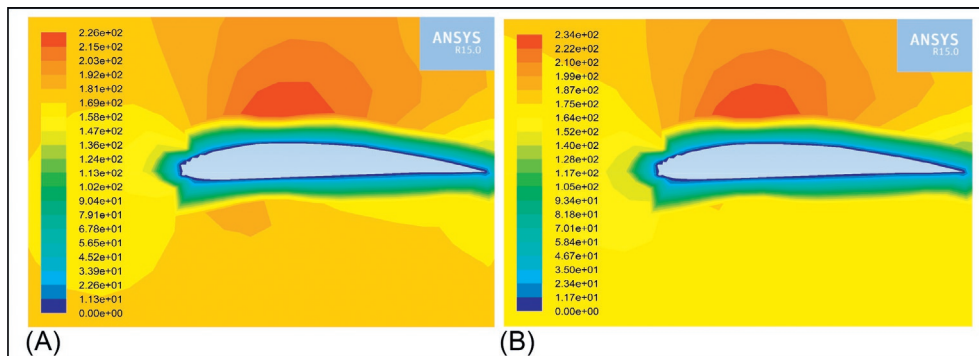
Fig. 10 Velocity profile with four ice bubbles model for (A) 0 degrees AoA and (B) 3 degrees AoA.

The growth of ice accretion reduces the velocity by 12% for this condition as shown in Fig. 10B. As the AoA and the ice bubbles added (in terms of supercooled droplets) increase, the dynamic pressure around the airfoil is fully modified and it increases the C_D value significantly. The CFD analysis is then further extended to investigate the drop–let sliding resistance on the airfoil surface during half iced condition at the top surface. The velocity profile shows the separation eddies due to ice formation as the flow mech–anism is open configuration and the advancing side of droplet desires to overcome the energy barriers (Fig. 11). The velocity decreases up to 40 m/s that affect the stall speed and stability configuration of airplanes according to the flight duration through icing clouds.

In the next case, the numerical analysis is done by assuming the fully developed ice on the top surface of the airfoil. Fig. 12 shows the velocity distribution around a fully iced airfoil and velocity decreased enormously from 264 to 217 m/s because of the separated flow after the mid-chord region. It shows the influence of droplet impingement on the C_D value and its severity toward airplane stability even at 0 degrees AoA (Fig. 12A).
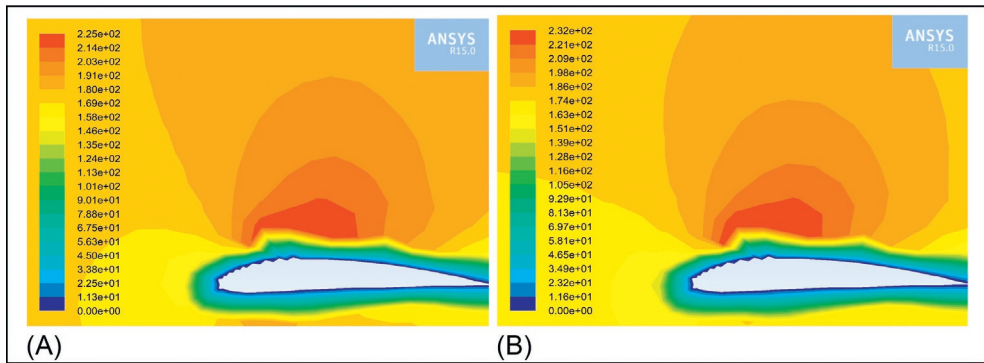
Fig. 11 Velocity profile with half iced airfoil at top surface for (A) 0 degrees AoA and (B) 3 degrees AoA.
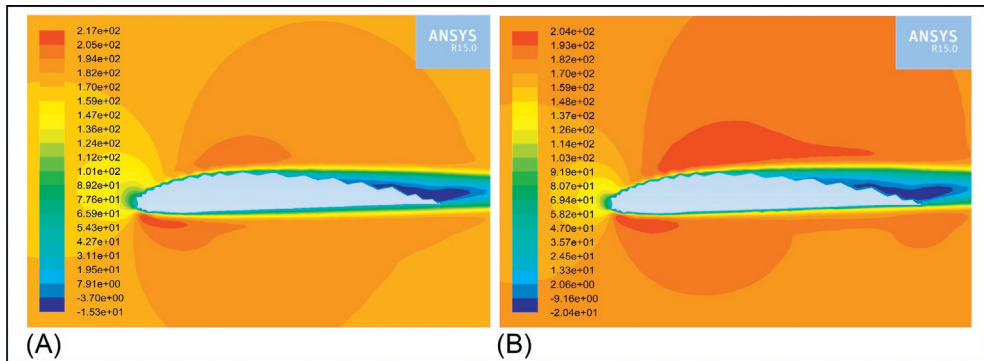
Fig. 12 Velocity profile with fully developed ice at top surface for (A) 0 degrees AoA and (B) 3 degrees AoA.

The precise geometry of the aerodynamic surface determines the pressure gradients in the boundary layer and slip length at various flow conditions. Since the SFC is a major concern, the functions of icing systems and their performance should be optimized by state-of-the-art methods like superhydrophobic polymer coatings [19]. The velocity distribution summary obtained for the CFD analysis is presented in Fig. 13. Here, the maximum and minimum velocity magnitudes are taken into consideration at different AoA with FAR 25 (Appendix C) guidelines. Subsequently, it is validated using wind tunnel experiments at the same *Re* and flow similarities.

5. FAR 25 (Appendix C) analysis

In order to obtain the airworthiness certifications for the ice protection systems, the specific airplane must be able to operate safely in the course of continuous maximum and intermittent maximum icing conditions mentioned in Appendix C of FAR requirements. Appendix C covers all the possible icing rates that are anticipated for a given airplane in flight. Few major conditions prescribed by FAR for the icing analysis are summarized below:

➢ Icing intensity can be related to Appendix C if icing rates are needed to be quantified.
➢ Icing effects influence each airplane differently based on their airspeed and wing thickness.
➢ Intense icing rates are not possible or applicable for a few airplane configurations.

The icing analysis is done according to the terms listed in FAR 25. The continuous air layer between the microtextures of the superhydrophobic coating is essential to minimize the skin friction drag [20]. The effective area is reduced in the solid–liquid boundary by the nanometer scale air pockets exist in the superhydrophobic coatings [21]. According to the FAR 25 regulations, the droplet size was maintained at 15 µm and layers of fluid and
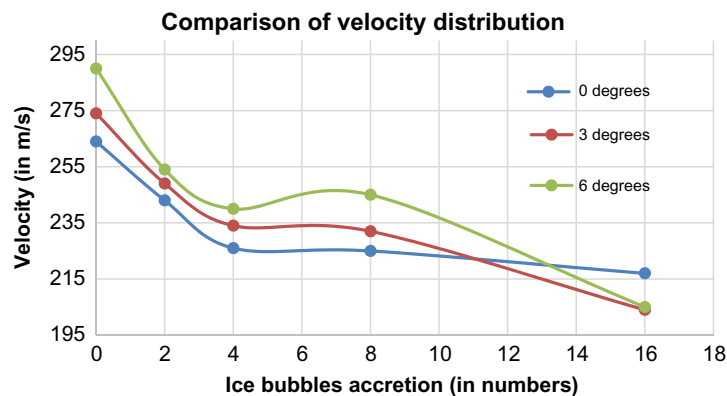
Fig. 13 Comparison of velocity distribution from CFD analysis.

solid surfaces were created for the numerical simulations. Fig. 14 shows the velocity contours with one and two supercooled droplet layers with droplets of size as mentioned by FAR 25. It is noticed that the velocity decreases as the bubble layers are added and the overall LE radius increases based on the icing intensity mentioned in Table 1. Here, the velocities over the one and two supercooled droplet layers are 94 and 36 m/s, respectively, with a reasonable interfacial slip length.

5.1 Droplet sliding on coated surfaces

The silicone–toluene mixture properties are assigned for applying the coating properties on the surface. The superhydrophobic film layer with contact angle >150 degrees helps to minimize the viscosity near the wall. Firstly, the skin friction coefficient is quantified through coating analysis with a meshed water droplet and plate interaction for the horizontal sliding case as shown in Fig. 15. Subsequently, the skin friction coefficient is compared with a superhydrophobic film coated and uncoated airfoils to compute the influence of air layers in the drag reduction.
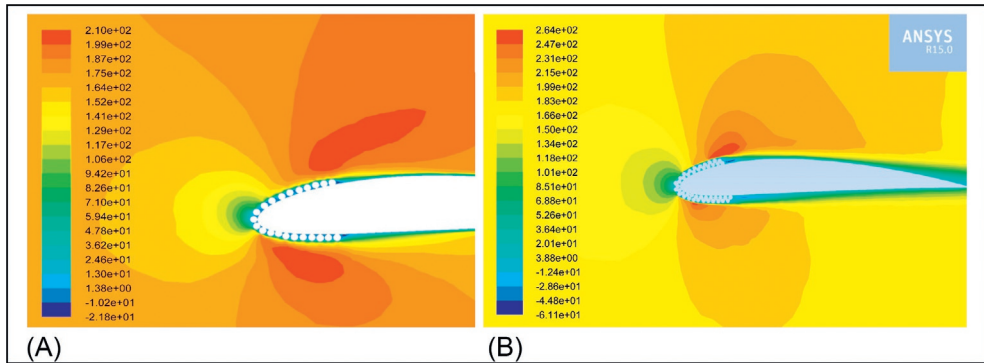
Fig. 14 Velocity contours obtained with supercooled droplet layers. (A) One layer and (B) two layers.
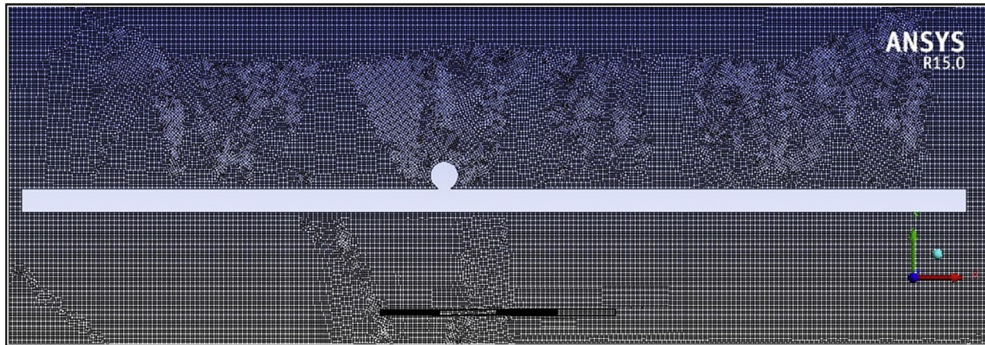
Fig. 15 Meshed water droplet and plate interaction for horizontal sliding.

5.2 Water droplet and plate interaction analysis

For the water droplet and plate interaction analysis, the fine hybrid mesh is developed to capture the skin friction accurately. Totally, 339,740 nodes and 337,900 elements were used for the analysis of skin friction coefficient. The boundary conditions and the operating condition are similar to the previous CFD analysis except for the wall slip boundary condition. Initially, the plate is analyzed without any surface coating for different droplet size and sliding speeds. The liquid intrusion problem exists in the porous substrates enhances the wettability and reduces the contact angles [22]. Hence, higher skin friction is observed for the uncoated surface and droplet interaction in Fig. 16A. For the superhydrophobic polymer-coated surface, the skin friction coefficient is nearly 18% less than the previous case as shown in Fig. 16B. Hence, the results are found to be within the limits and it has proven the feasibility of superhydrophobic coating for aerodynamic surfaces.

5.3 Water droplet and airfoil interaction analysis

The information obtained from water droplet and plate interaction analysis for horizontal sliding case is extended for the wing surface skin friction and wetting analysis with and without polymer coating. Initially, the wing is analyzed without any coating by setting the boundary conditions such as velocity, $V = 175$ m/s, temperature, $T = 243$ K, and other prevailing standard atmospheric conditions at the specific altitude. Fig. 17 shows the plot between the skin friction coefficient and the different chordwise positions of the wing. The skin friction coefficient is comparatively higher in the uncoated wing surface as expected (Fig. 17A). The coated surface properties are assumed as follows; Surface roughness—59 nm, S/A ratio—1.82, thickness about 200–300 nm and the diameter of water droplets are 15.5 μm. For the polymer-coated surface, the skin friction coefficient is decreased up to approximately 42% because of the microridge geometries. It is experimentally validated with aluminum plates with polymer coatings through contact angle measurements.

6. Experimental investigation

The wind tunnel experiments have been conducted at a low–speed, open–circuit suction–type subsonic wind tunnel facility shown in Fig. 18. The test section Re is customized to validate the computational analysis results with experiments. An experimental prototype has been prepared with polymer coating using silicone-toluene mixture and rime ice-shape profile inclusions. The test section size is about 300 mm × 300 mm and it is equipped with three-component force balance mechanism for drag-and-lift measurements. The pressure coefficient (C_p) distribution of the NACA 6-series airfoil at different AoA also computed for the ice bubbles accretion on clean wing configuration.
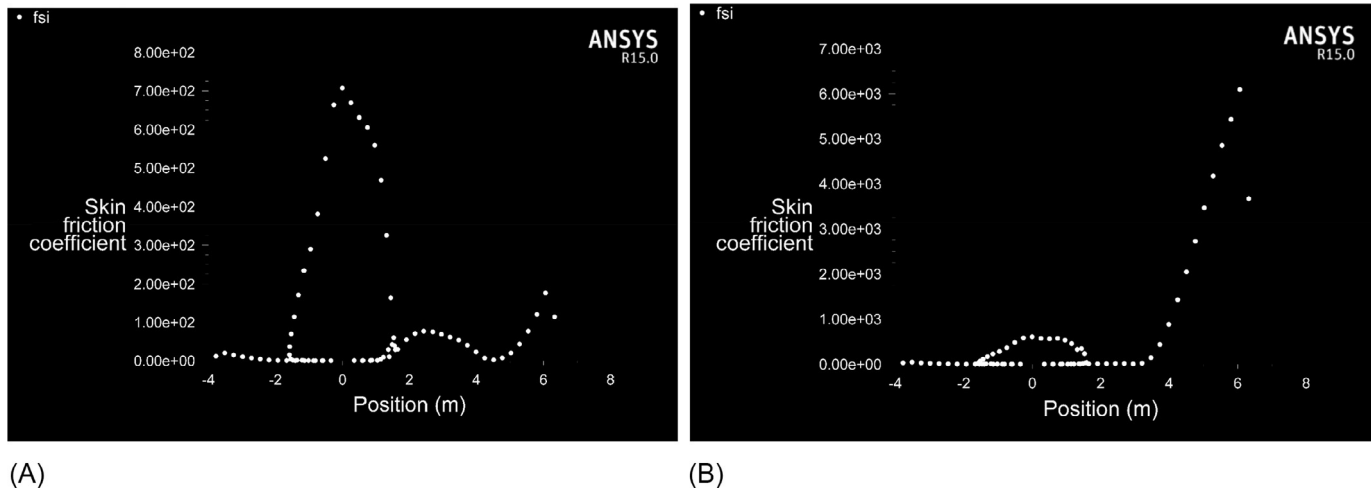
Fig. 16 Skin friction coefficient obtained at the plate surface (A) without coating and (B) with coating.
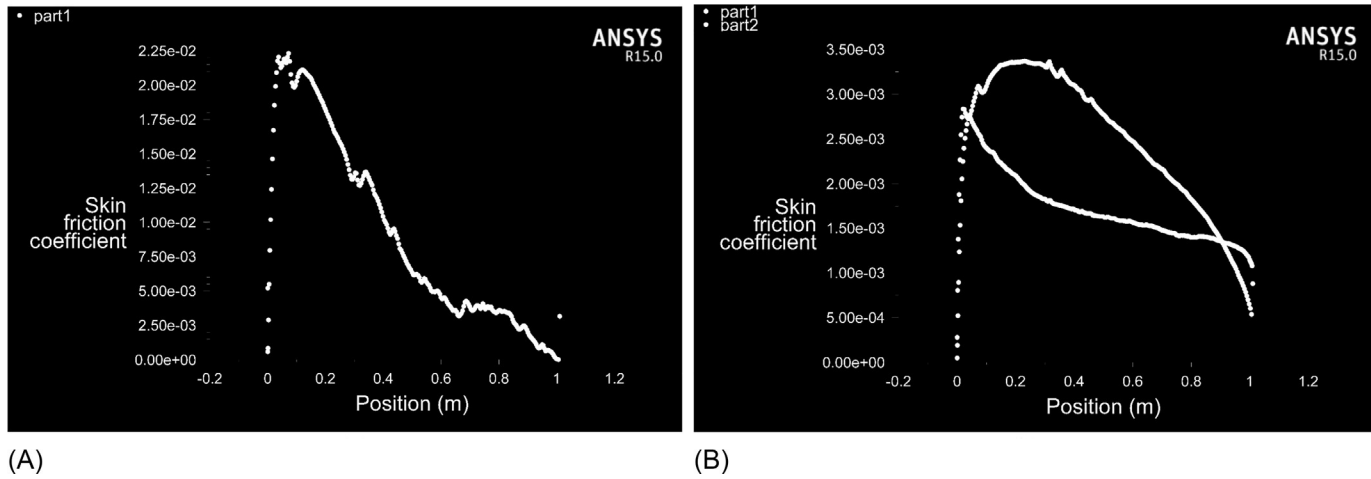
Fig. 17 Skin friction coefficients computed for (A) clean wing and (B) coated wing.

Fig. 18 Computerized low-speed subsonic wind tunnel facility.

The local pressure gradient of the laminar flow increases with superhydrophobic coatings that in turn reduce the slip length [23]. On the other hand, slip length drastically increases for high Re flows with significant air bubble–induced flow separation.

The experimental prototype wing model is prepared using Balsa wood material and the polymer coating has been applied to it. The geometric dimensions of the model are as follows; Wing Span = 247 mm, Chord = 100 mm, and maximum thickness = 16 mm. The droplet contact angles have been measured on the shear–free surface and coated surfaces as shown in Fig. 19. At the coated surface, the contact angle is comparatively higher (>170 degrees) and it reveals the fact that large interfacial slip is possible through polymer coating. The subsonic tunnel balance has three component electrical strain gauge balances to measure the lift, drag, and pitching moments separately. Hence, the percentage of

(A)   (B)
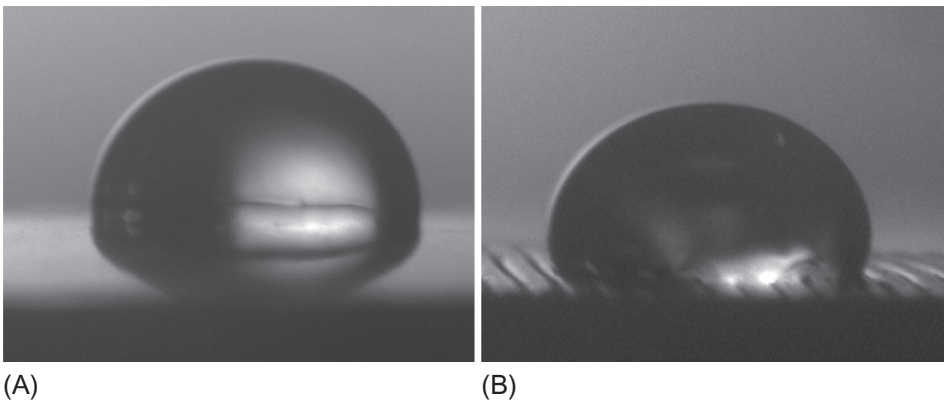
Fig. 19 Droplet geometry captured on (A) shear-free surface and (B) coated surface.

possible drag reduction can be measured directly for various ice shapes with maximum accuracy.

The presence of even a scarcely visible layer of ice can limit the functions of wings, propellers, windshields, antennas, and air intakes. For example, ice accumulated on the empennage reduces its ability to balance the airplane in the course of the nose to pitch downward and it leads to a catastrophic phenomenon called tail stall. Hence, three different ice models according to FAR 25 are prepared to compute the drag imposed by supercooled droplets upon impingement. The models are coated with a silicone-toluene mixture with the binding material. Horn ice, Rime ice, and mixed ice shapes are prepared using wax material with dimensional similarity as displayed in Fig. 20.

6.1 Computation of lift and drag coefficients

All antiicing systems must be turned on before the airplane entering through visible moisture at the ambient temperatures of 4°C or less. Hence, the supercooled liquid was injected over the wing model to observe the resistance to wettability at different airspeeds. The curves of lift-and-drag coefficients are prepared at various AoA using a three-component balance system. Fig. 21 shows the maximum C_L for the clean wing configuration at all AoA and the C_L vs α curve is validated with NACA airfoil data. On the other hand, the C_D magnitude is kept in minimum for the clean wing configuration over the range of AoA until the stall speed is reached (Fig. 22). After reaching the AoA about 15 degrees, the lift started to decrease for clean as well as iced wing configurations because of the stall phenomenon. However, the boundary layer separation

(A)   (B)

(C)   (D)
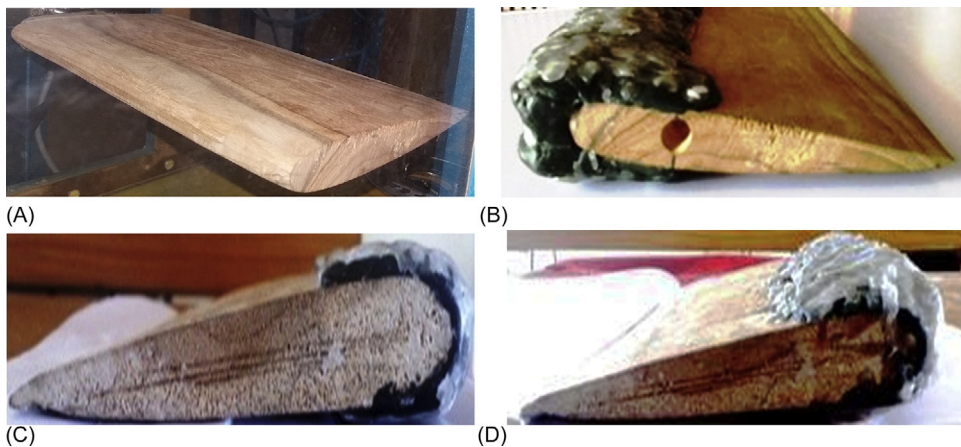
Fig. 20 Wooden models with ice profiles for wind tunnel testing. (A) Clean wing, (B) wing model with horn rice, (C) wing model with rime rice, (D) wing model with mixed rice.
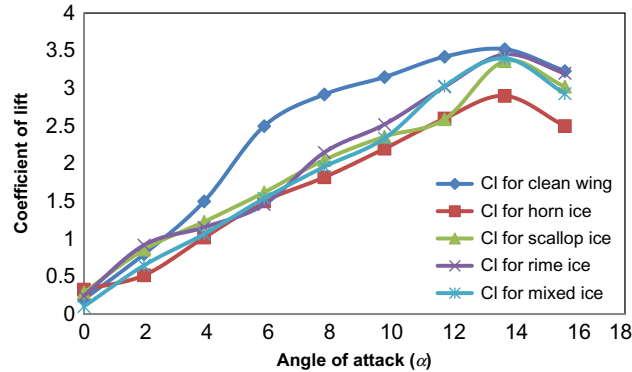
Fig. 21 C_L vs α comparison for different ice shapes at velocity 30 m/s.
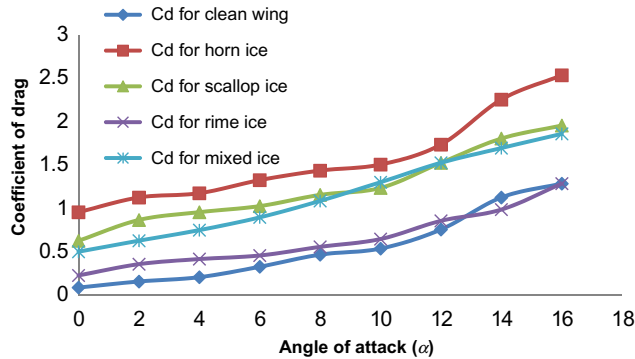
Fig. 22 C_D vs α comparison for different ice shapes at velocity 30 m/s.

occurs earlier for the iced wing configuration because of the air resistance offered by eddies and contact angle hysteresis.

The experimental results revealed several interesting facts toward the possible drag reduction by superhydrophobic coatings. Based on the amount of supercooled droplets accretion the pressure distribution profile over the wing body has been continuously modified and the air–entrapped layers increase the local thickness of the airfoil. The slip length is found to be independent of flow rate as long as the laminar flow prevails over the wing surface. Hence, according to the type of ice formation, slip length would be mod–ified and it begins to influence the aircraft performance.

7. Conclusions

The icing problem is quite common for all airplanes and suitable preventative measures should be taken to ensure the air safety at all levels. Drag reduction through

superhydrophobic polymer coating is a novel strategy to optimize the airplane performance as well as icing problems. However, the coating techniques should be cost effective and reliable for the safe life period of airplanes. Superhydrophobic surfaces are used to create drag reduction in both laminar and turbulent flows by establishing an apparent slip velocity along with an air-water interface trapped within the surface roughness. FAR 25 icing guidelines are followed here to emphasize the potential applications of superhydrophobic polymer coating toward antiicing and drag reduction applications. Since the icing problem cannot be avoided completely but the effects have to be minimized by optimizing the aerodynamic coefficients at various AoA. The computational results corresponding to C_L and C_D are validated with the wind tunnel experiments for various degrees of droplet accretions on the airfoil surface. Hence, it is concluded that the superhydrophobic coating is an effective mechanism to handle icing problems as well as the drag reductions significantly at various operating conditions.

References

[1] S.C. Camello, S. Lee, C. Lum, M.B. Bragg, Generation of full span leading-edge 3D ice shapes for swept-wing aerodynamic testing, in: 8th AIAA Atmospheric and Space Environments Conference, Washington, DC, 2016.

[2] E. Jiaqiang, Y. Jin, Y. Deng, W. Zuo, X. Zhao, D. Han, Q. Peng, Z. Zhang, Wetting models and working mechanism of typical surfaces existing in nature and their application of super hydrophobic, Adv. Mater. Interfaces (2017), https://doi.org/10.1002/admi.201701052.

[3] J.-H. Kim, Dynamic Wetting and Drag Reduction on Superhydrophobic and Liquid-Infused Surfaces, (Doctoral Dissertations) May 2014, http://scholarworks.umass.edu/dissertations2/724, 2016.

[4] E. Lauga, M.P. Brenner, H.A. Stone, Microfluidics: the no-slip boundary condition, in: J. Foss, C. Tropea, A.L. Yarin (Eds.), Handbook of Experimental Fluid Dynamics, Springer, New York, 2007, pp. 1219–1240.

[5] O.I. Vinogradova, Slippage of water over hydrophobic surfaces, Int. J. Miner. Process. 56 (1999) 31–60.

[6] P.A. Thompson, S.M. Troian, A general boundary condition for liquid flow at solid surfaces, Nature 389 (1997) 360–362.

[7] J. Kim, C.-J.".C.J.". Kim, Nanostructured surfaces for dramatic reduction of flow resistance in droplet-based microfluidics, in: Technical Digest. MEMS 2002 IEEE International Conference. Fifteenth IEEE International Conference on Micro Electro Mechanical Systems (Cat. No.02CH37266), IEEE, 2002, pp. 479–483.

[8] F.J. Lim, W.R. Schowalter, Wall slip of narrow molecular weight distribution polybutadienes, J. Rheol. 33 (8) (1989) 1359–1382.

[9] B.B. William, Wall Slip and Boundary Effects in Polymer Shear Flows, (Ph.D. dissertation), Dept. of Chemical Engineering, Univ. of Wisconsin, Madison, WI, May 2000.

[10] A.K. Balasubramanian, A.C. Miller, O.K. Rediniotis, Microstructured hydrophobic skin for hydrodynamic drag reduction, AIAA J. 42 (2) (2003), Technical notes.

[11] W.B. Roberts, Calculation of laminar separation bubbles and their effect on airfoil performance, AIAA J. 18 (1) (1980) 25–31.

[12] G.E. Fujiwara, M.B. Bragg, S. Camello, C. Lum, Computational and experimental ice accretions of large swept wings in the icing research tunnel, in: 8th AIAA Atmospheric and Space Environments Conference, AIAA AVIATION Forum, (AIAA 2016-3734), 2016.

[13] M.B. Bragg, A. Khodadoust, S.A. Spring, Measurements in a leading-edge separation due to simulated airfoil ice accretion, AIAA J. 30 (6) (1992) 1462–1467.

[14] M.G. Potapczuk, C.S. Bidwell, Swept wing ice accretion modelling, in: 28th Aerospace Sciences Meeting, NASA TM 103114, 1990.
[15] M. Vargas, R.E. Kreeger, Measurement of the critical distance parameter against icing conditions on a NACA 0012 swept wing tip, in: 1st AIAA Atmospheric and Space Environments Conference, NASA/TM—2011-216966, AIAA–2009–4123, 2011.
[16] J. Bruce Ralphin Rose, J.L. Joseph Antony, Hamilton, Experimental investigation on the alternate coating method for aircraft anti–icing applications, SAGE J. 231 (2017) 3.
[17] A.P. Broeren, M.G. Potapcuzck, J.T. Riley, P. Villedieu, F. Moens, M.B. Bragg, Swept-wing ice accretion characterization and aerodynamics, in: 5th AIAA Atmospheric and Space Environments Conference, AIAA Paper 2013-2824, 2013.
[18] A.P. Broeren, M.G. Potapczuk, A.M. Lee Malone, B.P. Paul, B.S. Woodard, Ice accretion test results for three large scale swept wing models in the NASA icing research tunnel, in: 8th AIAA Atmospheric and Space Environments Conference, Washington DC, 2016.
[19] J. Bruce Ralphin Rose, T. Satheesh, Computational investigation of icing conditions on the velocity profiles of a commercial aircraft, Int. J. Veh. Struct. Syst. 8 (4) (2017) 219–223.
[20] S.G. Pouryoussefi, M. Mirzaei, M.-M. Nazemi, M. Fouladi, A. Doostmahmoudi, Experimental Study of Ice Accretion Effects on Aerodynamic Performance of an NACA 23012 Airfoil, K.N. Toosi University of Technology, Tehran, 2015.
[21] W. Chen, A.Y. Fadeev, M.C. Hsieh, D. Oner, J. Youngblood, T.J. McCarthy, Ultrahydrophobic and ultralyophobic surfaces: some comments and examples, Langmuir 15 (1999) 3395–3399. American Chemical Society.
[22] G.E.C. Fujiwara, B.D. Wiberg, B.S. Woodard, A.J. Mortonson, M.B. Bragg, A hybrid airfoil design method for icing wind tunnel tests, in: 5th AIAA Atmospheric and Space Environments Conference, San Diego, CA, June 24–27, 2013.
[23] S.C. Camello, M.B. Bragg, A.P. Broeren, C.W. Lum, B.S. Woodard, S. Lee, Effect of ice shape fidelity on swept–wing aerodynamic performance, in: 9th AIAA Atmospheric and Space Environments Conference, Denver, Colorado, 2017.

Further reading

[24] J.-L. Barrat, L. Bocquet, Large slip effect at a nonwetting fluid-solid interface, Phys. Rev. Lett. 82 (1999) 4671–4674.
[25] G. Fang, W. Li, X. Wang, G. Qiao, Droplet motion on designed microtextured superhydrophobic surfaces with tunable wettability, Langmuir 24 (2008) 11651–11660. American Chemical Society.

CHAPTER 14

Superhydrophobic coatings for medical applications

Hossein Yahyaei, Hesam Makki, Mohsen Mohseni
Department of Polymer Engineering and Color Technology, Amirkabir University of Technology, Tehran, Iran

1. Biocompatibility

Biocompatibility is often considered as the compatibility between body elements and a foreign surface comes into contact with body [1, 2]. Adjustment of protein adsorption and cell adhesion on surfaces is a key aspect in the field of biomedicine and tissue engineering. Fundamental and practical interests to extend the investigation of the interaction between proteins or cells and surfaces can delight the requirement properties for biocompatibility of coatings. The interaction of cells and proteins with the surfaces is function of both surface properties and cell and protein behavior. The cells adhesion will be strongly impacted by the physiological activity of cells, such as the cell metabolic state, the charge on the cell surface, the hydrophobicity of the cell, and the contact time of the cells and materials. From the other side of view (material surface), it is well known that cell adhesion and protein adsorption onto a surface are highly impacted by distinct surface properties such as roughness, chemical composition, and surface energy.

From the point of view of cell biology, most known mammalian cells exhibit the instinct to adhere onto a surface in order to carry out normal metabolism, proliferation, and differentiation. At first, usually the foreign surface is confronted with blood and body fluids and it will be coated with proteins from blood and interstitial fluid. Therefore, cell adhesion behavior and the blood compatibility are the most relevant terms that can define the tolerance of the body in contact with a foreign interface [3]. If the newly formed interface triggers a negative response, for example, coagulation of blood proteins, making allergic reactions or alteration of plasma proteins, it means that there is low blood compatibility. Focal cell adhesions take place through the binding between the cluster integrin receptor (transmembrane receptors form clusters known as the integrins) and the ligand of the extracellular matrix (ECM). If the cells are not able to synthesize and deposit their own ECM molecules in a relatively short time, they will undergo apoptosis.

Since cell adhesion and viability and blood compatibility depend on protein adsorption, we will focus on the role of surface properties in interaction with proteins.

There is a common knowledge that inhibition of blood plasma protein absorption followed by platelet adhesion at the interface can substantially enhance the blood

compatibility of the foreign surface [3–5]. Small proteins in the blood usually absorbed first and this process is followed by replacement of larger proteins. Moreover, the composition of adsorbed proteins is not similar to blood plasma and the adsorbed proteins change the conformation on the surface. These might lead to a considerable change in biological properties of adsorbed material. On the other words, adsorption of small proteins at the initial stages might end to cell adhesion to the surface and deteriorate cell properties. Among plasma proteins, fibrinogen plays an important role in platelet adhesion to the surface. After platelet adhesion, activation of them occurs and leads to formation of thrombin and coagulation of platelet. Therefore, it is reasonable to stop this process in the very initial stages, that is, the protein adsorption to the synthetic surfaces [6, 7]. As a matter of fact, decreasing adhesion of proteins to the surface or degrading the adsorbed proteins are among the most common methods to enhance the biocompatibility of synthetic surfaces that will come into contact with body elements. Fig. 1 shows a scheme of sequences of thrombus formation on a synthetic surface.

In 1965, Lyman et al. [8] indicated a relationship between the interfacial parameters of polymeric material and their blood compatibility. Afterwards, a great deal of efforts has been devoted to establish a reasonable relationship between polymer interfacial properties and their biocompatibility [1–3, 8–11]. Based on these studies, surface modification of medical devices is the most common method used to enhance biocompatibility of such systems and many different parameters, for example, surface charge, chemistry of modified surface, surface topology, and surface energy of the implants, found to be influential in protein adsorption and platelet adhesion [12–16]. Although our focus, in this chapter, will be on the biocompatibility of superhydrophobic coatings, for a better understanding of the mechanisms by which different superhydrophobic systems exert biocompatible properties, a brief introduction to the most important influential parameters seems necessary. Therefore, first, the effect of surface charge, surface topology, surface functional groups, and surface energy of coatings on protein adhesion will be addressed and then, several cases in which superhydrophobic systems are employed to enhance biocompatibility in medical applications will be reviewed. It is worth noting that biosystems have often complicated chemical structures consisting of variety of chemical moieties, therefore, the interaction between them and the synthetic surface is also rather complicated. As
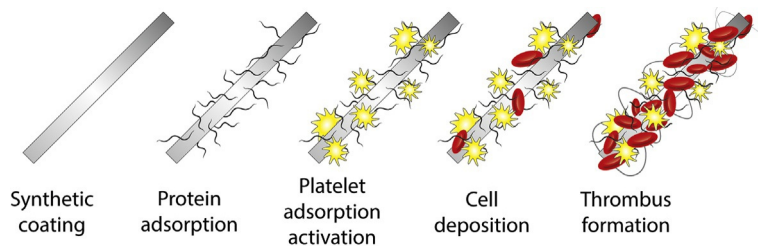
Fig. 1 Sequences of thrombus formation on a synthetic coating.
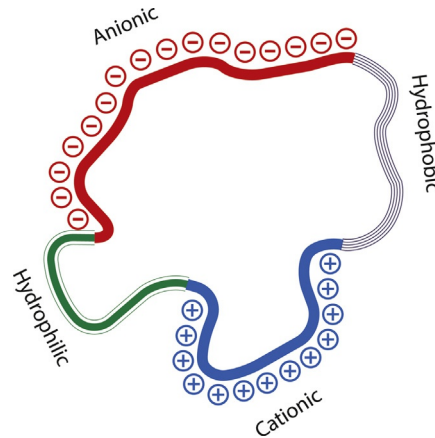
Fig. 2 Different patches of protein surface.

illustrated in Fig. 2, the surface of protein might have totally different chemical groups with different degree of hydrophilicity and hydrophobicity.

As already mentioned, since the biomaterial surface comes into contact with blood, it is of great importance to study the surface properties of such material. Since protein adsorption is a matter of formation of different interactions, that is, electrostatic, hydrogen bonding, Van der Waals, etc., between surface and protein, understanding the contribution of each interaction seems crucial. Therefore, in the following sections, first we review the effect of surface charge, then we address the most important findings about the effect of surface topology and surface chemistry. Then, after giving an overview on the effect of surface energy, we review the most relevant case studies in which superhydrophobic systems are being employed in medical and bio-applications.

2. Charge density of surface

There are several well-known models developed to study the interaction between a charged surface and a charge particle in an electrolyte, for example, Helmholtz, Gouy-Chapman, and Stern models. However, these models explain particle with uniform surface charge distribution and proteins usually have asymmetrical distribution of different functional groups at the surface leading to an asymmetrical surface charge distribution [17]. Moreover, the protein molecules have rather complex chemical structures and the molecular conformation can be influenced by several factors. For instant, different protein conformation might form at different pH, therefore, the protein conformation close to a charged surface, which has a rather different pH as compared to the bulk value, can be totally different from the normal conformation in the blood. Accordingly, the behavior of proteins at the charged surfaces cannot be accurately predicted. Despite the abovementioned complexities, a great deal of efforts has been devoted to this and it

emphasizes on the importance of such effect [17–20]. Having several researches reviewed, one cannot draw a specific conclusion on the effect of surface charge on biocompatibility of synthetic coatings such that, on the one hand, it has been shown that negatively charged surfaces usually trigger plasma coagulation and on the other hand, positively charged ones enhance the activation and adhesion of platelet.

3. Effect of surface topology

Second influential parameter that we review is the effect of surface topology on biocompatibility of synthetic coatings. This, of course, is of great importance in case of biocompatibility of superhydrophobic coatings since most of them benefit from controlled surface roughness. On the other word, one has to first address such effect in order to give a complete overview on biocompatibility of superhydrophobic coatings. There is a common knowledge that hydrophobic systems and rough surfaces are susceptible for protein adsorption [21]. However, roughness found to be supportive for endothelialization by decreasing the shear forces close to the surface. Note that healthy endothelium layer is one of the most blood compatible systems [21]. It is rational that the mechanical adhesion between protein and synthetic surface can increase by increasing the surface roughness due to the interlocking of protein segments into the pores on the surface. Therefore, one has to take this into account when protein adsorption of the surface is of crucial importance. This effect can be enhanced when other contributions of adhesion mechanisms come into play, such as reversible work of adhesion which is significantly importance when like-like interactions form between protein segments and the synthetic coating. On the other hand, as mentioned above, a rough surface can provide a suitable place for the formation of endothelium that is one of the most successful methods for producing biocompatible surfaces. It is also worth emphasizing that altering surface roughness can significantly change other surface properties such as wettability, surface energy, and surface residual stress, each can play an important role in biocompatibility [22].

4. Surface functional group

Surface chemistry not only dictates what type of interaction forms between surface and body elements by functionalization of the surface but also affects the surface charge, surface topology, and surface energy of the coatings as well. Thus, singling it out as a separate effect does not seem rational. However, in this chapter, we review the effect of surface functional groups such that the other properties are mostly preserved. On the other word, by the surface functional group, we mean the effect of changing surface functional groups in cases that the net surface charge, surface topology, and surface energy are not significantly changed.

During decades, scientists tried several methods in order to modify the surface of polymer coatings to gain high degree of biocompatibility, for example, chemical and

physical modification and radiation [23]. Among the chemical modifications, self-assembly of monolayers, grafting, and plasma modifications have been mostly used. Grafting is often used to form a permanent chemically modified surface, it consists of grafting a protein or other type of material to modify the surface chemistry. Grafting a specific protein to the surface can increase the biocompatibility of the surface to great extent, however, can also lead to conformational change in the protein structure. It is also worth noting that during grafting process, residues of toxic monomers can remain on the surface which results in lowering the biocompatibility of the system [23]. Physical modification of surface by proteins or synthetic polymers can also be employed which facilitates the process of surface modification, however, the drawback of such method is instability of the modified surface during service life. Self-assembled monolayers can significantly increase the control over functionalization of the surface [24]. It can also provide functional groups on the surface in order to initiate other surface modifications.

Based on the literature, surface repelling protein functional groups usually benefit from a hydrophilic nature, hydrogen bond acceptors, and lack of hydrogen bond donors and they also provide neutral charge to the surface [25]. For instance, adding hydroxyl groups to the surface can considerably decrease fibrinogen absorption to the surface by two mechanisms, namely, formation of a hydrated layer around the coating and also increasing selectivity of albumin absorption over fibrinogen [26, 27]. Amine and methyl functionalization were not successful in order to reduce the amount of fibrinogen adsorption, however, the effect of carboxylic groups proved to be positive in this respects [28, 29]. Therefore, as illustrated in this section, the effect of surface functional groups, regardless of their influence on the surface energy, topology, and charge, seems to be critical to obtain a high degree of biocompatibility.

5. Surface energy

So far, it is established that preventing of denaturation of adsorbed proteins from the surface can lead to biocompatibility, since protein adsorption and denaturation is mainly the initial stage of thrombosis for most cases. Several approaches to decrease protein adhesion are mentioned, namely, tuning surface charge, surface topology, and surface chemistry. The last and the most important approach that we discuss in this chapter is tuning surface energy, particularly by means of employing hydrophobic/hydrophilic segments in the coating, in order to obtain a biocompatible surface. Note that, superhydrophobic surfaces are being widely used in this respect and in the following section we will review biological and medical applications of such systems.

There is a common knowledge that the lowest amount of protein adsorption is obtained for surfaces with lowest free energy, which is the case for superhydrophilic and superhydrophobic surface. It is also well established that hydrophilic surfaces are suitable for biocompatible applications such that a layer of water forms on top of the surface

which decreases the interaction between surface and protein [30, 31]. It is worth noting that although using hydrophilic polymers most of the time reduces the protein adsorption, there are a few cases in which it does not lead to higher degree of biocompatibility due to other mechanisms. On the other hand, hydrophobic coatings increase the protein adsorption, however, it can lead to a higher degree of biocompatibility if a specific type of protein, for example, albumin instead of fibrinogen in most cases, is adsorbed and preserves its natural conformation. In conclusion, there is not an agreement in the literature whether hydrophilic systems are the most suitable candidates for medical applications or hydrophobic ones [32].

Due to the high degree of complexity of biocompatibility, one cannot give a unique solution by which a biocompatible surface is produced for all applications and under any conditions. It becomes more complex when it comes to the relation between biocompatibility and surface energy of the material. For instance, Baier et al. claims that surfaces with critical surface tension of 20–30 dyn/cm show biocompatibility [33]. Andrade et al. say that the lowest difference between surface energy of the coating and surface tension of blood results in the most biocompatibility [34]. Other scientists believed that the dispersive and polar contribution of surface tension of the coating is crucial for biocompatibility [9, 34, 35] and Bruck claims that surface energy-related properties cannot guarantee biocompatibility [10].

All in all, due to the high uncertainty about the exact effect of each parameter, in order to show a clear picture of bio and medical applications of superhydrophobic coatings, one needs to review various studies for different cases and under different conditions prior to draw a conclusion in this regard. Therefore, in the following section, we review the most important studies on this issue.

6. Case study

Luo et al. [36] have been counted some advantages of perfluoro polymers such as chemical and biological inert properties, strongly electronegativity, and ultralow surface energy. Therefore, they have considered these polymers as good candidates in electrical and biomedical applications. Electropolymerizing in ionic liquids has been used to prepare a controllable surface morphology from poly(3,4-ethylenedioxythiophene) (PEDOT). By changing the process of electropolymerization, smooth or superhydrophobic porous films were prepared. The results showed that smooth surface with water contact angle (CA) about 114 degrees and hydrophobic properties. By increasing the surface roughness, water CA increased to 124 degrees and porous surface showed superhydrophobic properties and water CA about 153 degrees. Trypan blue staining was used to assay cell viability. It was observed that superhydrophobic surfaces provided direct cell adhesion and cell growth.

Gristina et al. [37] deposited tetrafluoroethylene (C$_2$F$_4$)-fed plasmas to investigate the cell growth and adhesion. The reaction of different cell lines to various topographical features was studied. Also, it was compared with response of sell on flat samples with the same chemical composition. In atomic force microscopy (AFM) images, it was observed that decreasing the DC in deposition of coating increased surface roughness. They found that changing the time of coating deposition affected the water CA, so that increasing the deposition time increased water CA and deposition times longer than 90 min produced superhydrophobic surfaces with water CA of more than 150 degrees. Note that cytocompatibility has been studied with 3T3 cell. After 48 h, the area covered by cells on ribbon-like superhydrophobic surfaces was larger than that observed for fibroblasts grown on hydrophobic and flat fluorinated substrates. After 96 h of culture, the cells appeared almost confluent on the superhydrophobic roughest surfaces. 3-(4,5-Dimethylthiazol-2-yl)-2,5-diphenyltetrazolium bromide (MTT) assay was also used to study growth of MG63 osteoblasts on rough and smooth surface. After 96 h of culture, cells grown on structured surfaces exhibit a better activity than those grown on the flat surfaces. The area covered by cells was larger on superhydrophobic with respect to hydrophobic structured surfaces, and much larger than that on smooth fluorinated surfaces. Accurate scanning electron microscopy (SEM) analysis also showed that cells cultured on structured surfaces appear notably more spread than those grown on flat surfaces.

Mahadik et al. [38] applied a base catalyzed superhydrophobic sol–gel coating by using methyltriethoxysilane (MTES) and trimethoxymethylsilane (TMMS) on glass substrate by dip-coating method. The coatings were applied at different dipping times ranging from 5 to 20 h. The increase of dipping time simultaneously enhances the roughness of surface and the hydrophobicity properties of the coating surface. It was observed that increasing of dipping time increased surface roughness and water CA. Dipping period of 20 h created a surface with 717 nm surface roughness and water CA of about 168 degrees. Surface energy for superhydrophobic coating was reported about 10 mJ m^{-2}. Cell adhesion, growth, and morphology have been investigated and it was observed that bone marrow mesenchymal stem cell (BMMSC) was adhered to the material and flattened growth morphology with minor filopodia. The cells homogeneously grow on the material and partially contact with the superhydrophobic coating material. It has been concluded that the superhydrophobic materials hold a minimum adhesion to BMMSC and a capability to inhibit the introduction and growth of the attached platelets, which is whispered to be capable to effectively prevent thrombosis.

Senesi et al. [39] fed plasma enhanced-chemical vapor deposition (PE-CVD) with C$_2$F$_4$ and applied a nanostructured "Teflon-like" coating on polyethylene terephthalate (PET) substrates. The depositing time were chosen differently (20, 50, and 90 min) resulting in ribbon-like nanostructured CF$_x$ coatings with different roughness's. The authors reported that increasing depositing time increased water CA and long-time deposition prepared superhydrophobic coatings with water CA more than 150 degrees.

AFM images showed that for 90 min deposition time sample, the Teflon-like ribbon-structured appeared on the surface of coating. The superhydrophobic behavior of the surface has been explained by the possibility for a droplet to maintain an air layer below it. It was observed that the surface wettability can be easily switched from super-hydrophobic to hydrophobic only by reducing the deposition time. Adhesion, spread and growth of 3T3 fibroblasts cell on the different structured samples were estimated in comparison with cell behavior on a flat surface. The results showed the greatest pref-erence of cells for nanostructured samples with respect to the flat ones. On superhydro-phobic surfaces, cell culture time increased. The SEM images showed higher number of cell and better cell morphology on the surface of nanostructured coating with highest water CA.

Hejazi et al. [40] studied the role of micro/nanostructure on the surface of superhy-drophobic polypropylene (PP)/nano-silica coating on cell adhesion. Based on both qual-itative and quantitative evaluations, it was found that the superhydrophobic coatings with only nanoscale roughness strongly prevented adhesion and proliferation of 4T1 mouse mammary tumor cells as compared to the superhydrophobic surfaces with microscale structure.

In another work of this group [41], it was investigated that topography is more impor-tant or superhydrophobicity in cell adhesion. As a matter of fact, the effects of different topographies and wettability on cell adhesion behavior of polymeric surfaces were inves-tigated. PP surfaces with different wettability were obtained by controlling phase sepa-ration method. It was concluded that surface topography played a more significant role in cell adhesion behavior rather than superhydrophobicity, since the nanoscale topography highly inhibited the cell adhesion as compared to the microscale topography.

In another research work, Ranella et al. [42] prepared silicon surfaces with gradient of surface roughness and wettability and viability and adhesion of fibroblast cell was inves-tigated by authors. The results showed that optimal cell adhesion was obtained for small roughness ratios, independently of the surface wettability and chemistry, indicating a nonmonotonic dependence of fibroblast adhesion on surface energy. Finally, it was con-cluded that the dependency of fibroblast cell response on the artificial structures was sys-tematically investigated and demonstrated that a fundamental parameter that determined cell adhesion on three-dimensional (3D) substrates was not solely the degree of roughness or surface chemistry but the synergy of both, which determined the wettability or surface energy of the culture substrate.

Hsiao et al. [43] modified the surface of polyurethane (PU) with plasma polymer-ization of hexamethyldisiloxane (HMDSO) and tetrafluoromethane (CF_4) as precursors. Controlling the HMDSO/CF_4(fH) monomer flow ratio prepared a superhydrophobic coating with coexisting micro- and nanoscale morphology. SEM images showed that the hierarchical-scale surface roughness should be attributed to the superhydrophobicity. It was observed that by increasing the monomer flow rate the morphology of the films

increasingly appears a dendritic–like one, which led to an increase in the surface area in contact with air. The increasing of surface area could cause water contact with the surface reduced and the water droplets were not directly in contact with the films, indicating a larger water CA. The surface roughness of PU substrate has been reported 2.32 nm, whereas by feeding of monomer at flow rates of 30, 50, and 80 sccm, the coatings with surface roughness of 49.93, 69.26, and 75.93 nm were obtained, respectively. Attenuated total reflectance (ATR)-Fourier transform infrared (FTIR) and X-ray photoelectron spectroscopy (XPS) analysis confirmed the micron–scale 3D network film surface film of SiO_x, and also the CF functional group, CF_2 bonding. The synergistic effect of such low surface energy compounds on the surface and coexisting micro– and nanoscale surface morphology provided a superhydrophobic coating with water CA about 161 degrees. Myoblasts were incubated on the surface of PU substrate and PU coated. PU substrate showed biocompatibility, but viable cells on the coated PU were more. The adsorption of fibrinogen on the surface of PU and coated samples were studied by SEM images. It was observed that adsorbed filamentous fibrinogen covered the surface of the blank PU substrate, while coated specimens had no fibrinogen adsorption. In consequence, no platelet adhesion on the superhydrophobic surface was reported but the blank PU substrates had numerous platelet adhesions and multifocal platelet aggregations. According to the results, it has been concluded that the superhydrophobic coating containing SiO_x and CF functional group, CF_2 bonding increased cell viability and cell proliferation, reduced platelet adhesion and fibrinogen adsorption and due to the biocompatibility and blood compatibility it can robust and noncytotoxic and may prevent thrombosis when in directly contact with blood.

Hou et al. [44] prepared a superhydrophobic PP coating by dropping of PP solution (mixture of *p*-xylene and methyl ethyl ketone) on the glass substrate and evaporating the solvent at 25°C in a vacuum oven. SEM images showed the film held a porous structure. Water CA showed superhydrophobicity by indicating 158 ± 4 degrees. While water CA for smooth PP has been reported about 110 degrees. In blood compatibility antifouling surfaces that show low platelet adsorption is important in anticoagulation. The surfaces were in contact with platelet-rich plasma (PRP) and SEM images indicated the surface of PP was covered by platelet and most of the adhered platelets were distorted with pseudopodia. Numerous adherent blood cells and fibrin on the original PP film as some aggregates were observed when the surface was in contact with fresh human whole blood. However, on the surface of superhydrophobic PP had nearly no adhered platelets. It was also clearly observed that blood cells and fibrin adhesion was suppressed on the PP superhydrophobic surface. The reason has been explained that when immersing the whole patterned surface into the human PRP or whole blood solution, air layers on the superhydrophobic parts form "virtue walls" that prevent the direct contact of the surface and the platelets and cells.

There are several studies in the literature regarding incorporation of organic/inorganic hybrid systems designed for medical applications. For instance, Li et al. [45] synthesized a polyhedral oligomeric silsesquioxane (POSS)-acrylic copolymer (PAC) utilizing solution free radical polymerization. The 10 wt% solution of polymer in ethyl acetate solvent were deposited on the cupper net and after drying at ambient temperature transmission electron microscopy (TEM) characterized the morphology of PAC self-assembly aggregates. After evaporation of solvent, the polymer was prone to aggregation, forming many nanoscale spherical particles with diameters of 20–40 nm. The coating was applied on the glass substrate by two different methods: spraying (superhydrophobic POSS-acrylic copolymer [SPAC]) and spin coating (hydrophobic POSS-acrylic copolymer [HPAC]). SEM images showed the smooth surface for HPAC and rough surface with numerous nanoscale outshoots on the surface of each microscale spherical protrusion on SPAC. The water CA has been reported for HPAC about 106 degrees, whereas it has been about 158 degrees for SPAC. XPS analysis showed the existence of carbon, oxygen, and silicone atoms on the surface of SPAC. Since there was a higher silicone ratio than theoretical amount, it can confirm the migration of the POSS groups containing silicone to the coating surface. The authors have explained that the POSS functional groups can easily transfer to the air–copolymer solution interface (outside of the droplets) due to their self-aggregation behavior and surface mobility and prepared a superhydrophobic coating. The adsorption of bovine serum albumin (BSA) and bovine fibrinogen (BFG) from their respective PBS solutions on the surface of SPAC and HPAC were evaluated. The results showed lower adsorption of BSA and BFG on the surface superhydrophobic coating (SPAC) in comparison to hydrophobic coating (HPAC). The amount of adsorbed BFG decreased by 25 approximately 64%, which is deemed to be one of the major factors affecting platelet adhesion. The platelet adhesion experiments on the HPAC and SPAC surfaces was carried out as next blood compatibility experiment and polyvinyl chloride (PVC) was used as reference. Pseudopodia were clearly observed on the surface of PVC, implying that they have been extremely activated. However, for HPAC surface, the number of adhered platelets dramatically decreased (∼79%) as 40 compared with that on the PVC surface and their morphology was maintained with almost no pseudopodia More exhilaratingly, the adhering platelets nearly disappeared, and few pseudopodia as well as deformation were observed on the SPAC surface which could be a good clue to approve low protein adsorption and blood compatibility of superhydrophobic coating.

Sun et al. [46] coated a aligned carbon nanotube (ACNT) films by two fluorinated polycarbonate (PC) urethane with 30% and 50% fluorinated alkyl side chains (labeled: FPCU20 and FPCU50, respectively). After a typical dip-coating and subsequent drying process, the polymers formed a thin coating on the outer wall of the carbon nanotubes, and thus nanostructured polymer films may be made. Wettability of the surface of fluorinated polycarbonate urethanes (FPCUs) and nanostructured (ACNT coated specimens)

were invested by water CA. Both fluorinated PU were hydrophobic with water CA of 109 and 113 degrees. While, the nanostructured one coating showed superhydrophobicity with water CA about 163 and 168 degrees for FPCU20 and FPCU50, respectively. It has been explained by the cooperation between the relatively low surface free energy of the polymers and the surface roughness induced by the special nanostructure of the ACNTs. In order to evaluate blood compatibility, adhesion of platelet on the surfaces was studied by PRP method. The smooth FPCU20 and FPCU50 films showed significant platelet adhesion. The adhered platelet spread out, pseudopod, and activated. However, the situation on the surface of nanostructured superhydrophobic coatings was different.

A very small number of attached platelets in a circular plate-like shape with diameters of about 2–4 mm, platelet surface was quite smooth and free of pseudopods, implying that they had not been further activated. Immunofluorescence experiments and flow cytometer analysis were carried out to investigate the platelet activation by these materials. Statistical analysis indicated that not only the early activation of platelets but also the further activation of platelets were significantly reduced on the nanostructured superhydrophobic FPCU20 film, in comparison with the corresponding smooth film. Similar results have been reported for FPCU50. It has been concluded that because the surface chemical composition remains unchanged during the dip-coating process, it can be inferred that the special nanostructure and the superhydrophobicity derived from it play crucial roles in this blood compatibility effect.

Milionis et al. [47] prepared a superhydrophobic coating by adding dispersion of hydrophobized fumed silica (HFS) in acetone into acrylonitrile butadiene styrene (ABS) solution and spraying on aluminum substrates. Water, blood, and plasma CA were measured and aluminum alloy 6061, polystyrene (molecular weight of 500,000 g/mol) and commercial polytetrafluoroethylene (PTFE) were used as reference. Blood and plasma were found to have higher θ_{static} on the least hydrophobic surfaces compared to water and glycerine mixtures, possibly due to coagulation effects and interaction of solid components, present on these liquids, with the surface. A distortion on the receding contact line was observed on the superhydrophobic surface for blood (not for plasma). Among the surfaces tested, the ABS/HFS surface showed the lowest roll-off angles for blood and plasma (17 and 12 degrees, respectively) and exhibited no blood trail.

Huang et al. [48] coated 316L stainless steel (SS) by superhydrophilic and superhydrophobic TiO_2 nanotube (TNT) arrays to improve hemocompatibility and corrosion resistance. Electrochemical anodization of Ti films deposited on SS and vertically aligned superhydrophilic amorphous TNTs was fabricated. Superhydrophilic anatase crystal was induced by calcination. The superhydrophilic surface was converted to superhydrophobic by suing fluorosilanization. SEM image was used to investigate coating morphology. A dense array of vertically aligned nanotubes with diameter of $\sim$55 nm and wall thickness

of $\sim 5\,nm$ grew from SS–Ti. The annealing process thickened the nanotube wall ($\sim 10\,nm$) and decreased the tube diameter and silanization did not changed the morphology. In XPS analysis showed the well-known outermost of oxide film that was covered by hydroxyl group and water vapor adsorbed on the hydroxylated layer by forming hydrogen-bonded network on the surface after calcination. Also, the peaks of CF_2 and CF_3 were observed after silanization. After deposition of Ti, the water CA did not change, but by anodization, the CA decreased from 77.4 ± 8.4 to 3.8 ± 2.3 degrees. Silanization increased water CA significantly up to 152.2 ± 0.8 degrees. Abundant platelets adhered on SS surface, and the adherent platelets were mainly dendritic or spread dendritic. The adherent platelet number on superhydrophilic surface was significantly reduced and the platelet shape was primarily dendritic. It was remarkable that adherent platelets were barely found on modified superhydrophobic surfaces with highly suppressed round or dendritic shape. It should be mentioned that superhydrophilic surface activated the formation of fibrin network into which platelets became entrapped.

Ye et al. [49] prepared a durable and stable superhydrophobic coating with high biocompatibility and antibacterial properties. Styrene-*b*-(ethyleneco-butylene)-*b*-styrene elastomer (SEBS) was dissolved in mixture of *p*-xylene and decanol with the ratio of 4/2, 4/3, and 4/4, respectively. Decanol acted as both a polymer precipitator to induce phase separation and a "liquid template" to stabilize superhydrophobic structure. Many irregular micropores that composed of intermingled sticks and beads, appeared on the flat film containing 4/2 ratio of solvents which showed 110 degrees water CA. The porous structure expands to the whole surface with increasing decanol to $3\,mL$. Surface roughness increased and water CA was raised to 163 degrees. By using 4/4 ratio of solvent inhomogeneity and size of pores increased, surface roughness decreased and water CA has been reported 156 degrees. Biofouling (BFg) adsorption on the surface of coating was studied by XPS and it was reported that the coverage of BFg on casted films decreased substantially with increased hydrophobicity. The BFg adsorption on the surface of original SEBS was 3 times more than SEBS prepared with 4/4 solvent ration. *Escherichia coli* were selected to evaluate the bacterial adhesion on SEBS surfaces. In SEM images, many *E. coli* on the surface of original SEBS were observed. In contrast, no *E. coli* were observed on the superhydrophobic surface of SEBS coating with 4/4 solvent ratio, confirming the high antibacterial surface has been obtained. On the surface of flat SEBS were covered by large number of platelets which most of them were activated. While, no platelet covered surface of superhydrophobic SEBS coating. The time of clot formation of whole blood on the surface of superhydrophobic coatings were three or four times longer than smooth SEBS surface. Hemolysis ratio on the surfaces of superhydrophobic SEBS was about one-eighth of that on the surface of original SEBS.

Fu et al. [50] synthesized a cross-linked quaternary ammonium salts (QAS) functionalized fluorinated coating. In the first step, free radical solution polymerization was used to synthesis the QAS-functionalized fluorinated copolymer. In the second step,

fluorinated copolymer was dissolved in the mixture of acetonitrile and butyl acetate. Hexamethylene diisocyanate (HMDI) was added and ultrasounded for 10 min. Poly (urea–formaldehyde) nanoparticles (PUF NPs) containing active methylol groups were added and ultrasonicated for another 10 min. The final mixture was sprayed onto glass slide or other substrates. FTIR has been used to study functional group in the coating. The peak at 3300 cm^{-1} was assigned to the stretching vibration of the hydroxyl —OH in poly 2-hydroxyethyl methacrylate (PHEMA). The existence of the C-N$^+$ stretching vibration band was confirmed by the band at 1450 cm^{-1} in the spectrum of poly quaternary ammonium dimethylaminoethyl methacrylate (PQDEMA). The bands at 1140 and 1250 cm^{-1} were corresponding to the CF_2 and CF_3 groups, respectively. Both the FTIR and ^{1}H NMR results showed that the QAS-functionalized fluorinated copolymers were successfully synthesized by the free radical polymerization method. Furthermore, FTIR analysis confirmed reaction of isocyanate groups in HMDI with hydroxyls in the fluorinated resin. In SEM images, surface of CF_2 resin and nanocomposite coating PUF–FC2 was compared. FC2 had an intuitionistic smooth surface with no distinct apophyses, while with the addition of PUF NPs, micro/nanoscaled protuberances and cavities could be clearly seen from the surface of PUF–FC2. Actually, agglomeration of PUF NPs caused these protuberances and cavities. AFM images calculated surface roughness. It was reported that the surface roughness were 8.31 nm for pure copolymer coating and PUF NPs increased it up to 318.72 nm. Water CA for pure fluorinated copolymer was about 111 degrees and it has been reached to 162 degrees for PUF–FC coating. The authors have explained that the larger-sized cavities could trap more air in pockets on the liquid/solid interface. Therefore, the water droplet could not penetrate into the surface, resulting in high CA and low adhesion.

Gram-positive *Staphylococcus aureus* and Gram-negative *E. coli* were set as model bacteria to evaluate antibacterial properties of nanocomposite coatings. All the bacteria on the PUF–FC surface were killed with only 3 h contact and the composite coatings containing QAS groups were more effective toward *S. aureus* than *E. coli*. On the basis of these data, the PUF–FC nanocomposite coatings had excellent antibacterial performances, which could be applied to biomedical and related fields.

Loo et al. [51] changed the surface feature of PVC by using tetrahydrofuran (THF) as solvent and nonsolvents (i.e., ethanol and methanol). PVC was dissolved in THF at 60°C. After cooling, different concentration of ethanol was added into PVC–THF solution and poured as coating. The surface of original PVC was smooth and hydrophobic with water CA bout 80 degrees. Surface treatment by methanol increased hydrophilicity, whereas increasing ethanol concentration from 15 to 35 v/v increased water CA from 73 to 150 degrees. The colonization of *Pseudomonas aeruginosa* PAO1 onto unmodified PVC surface was rapid, and individual bacterial cells could be seen after 6 h incubation. On the surface of treated PVC, the secretion of ECM layers was evident at 18 h and *P. aeruginosa* PAO1 start to form microcolonies at 24 h of incubation. The initial

attachment of *P. aeruginosa* PAO1 was delayed to 18 and 24 h, respectively, in the PVCs treated with 25% (v/v) and 35% (v/v) ethanol.

Ozkan et al. [52] incorporated small-sized copper nanoparticles (Cu NPs) onto a curable silicone polymer by aerosol–assisted chemical vapor deposition (AACVD) method. Pure polydimethylsiloxane (PDMS) did not showed any absorbance in UV spectrum, but coating with Cu NPs a broad peak at 310 nm appeared. SEM images showed very rough surface consisting of interlocking particles with surface protrusions around 3–5 μm length and spherical Cu NPs were uniformly attached to the surface protrusions. The surface roughness (root mean square) was measured by AFM. Glass substrate surface roughness showed 0.132 nm and about PDMS it was 2.175 nm.

However, with Cu–incorporation, the roughness of the hybrid film has been reported 0.230 μm. Water CA of glass substrate was about 48 degrees and original PDMS was hydrophobic with water CA about 111 degrees. During the AACVD process, PDMS with low surface energy was cured resulting in a highly rough surface with water CA up to 155 degrees. The Gram–negative bacterium, *E. coli* and the Gram–positive bacterium, *S. aureus*; a glass sample (control), a bare polymer sample (PDMS), a CVD–treated polymer (S-PDMS), and a Cu–coated CVD–treated polymer sample (Cu-PDMS) were all which used to study antibacterial properties. The results showed that no difference in number of bacteria was observed between glass and PDMS surface after 15 min. However, significant bacterial kill was reported for all exposure times for copper-coated PDMS.

A 2.3-log reduction in bacterial numbers was achieved after 10 min of exposure to the sample coated with Cu NPs and >4 log reduction was achieved after 15 min with the materials containing Cu NPs. In the case of *S. aureus*, there was no detectable kill of *S. aureus* on the surface of either bare PDMS or CVD treated PDMS after 1 h. The superhydrophobic Cu NP coated demonstrated a 0.69 log reduction in viable bacteria after 15 min. Furthermore, the superhydrophobic coating greatly prevented the adhesion of both types of bacteria compared to glass and PDMS samples.

Ren et al. [53] synthesized sol of nano–silica with 20 nm particle size by using tetraethylorthosilicate (TEOS) in alkaline media. They synthesized hydrophobic sol of nano–silica with concentration of approximately 0.084 mol/L utilizing 1*H*,1*H*,2*H*,2*H*-perfluorooctyltriethoxysilane (POTS). Moreover, CuO NP was synthesized by employing copper acetate dehydrate. Glass slide was used as substrate, first both sides of substrate were coated with 20 nm nano–silica. After drying, the equal mixture of sol of hydrophobic nano–silica and CuO was sprayed on one side of substrate and dried at room temperature to obtain the F–SiO$_2$– and CuO–coated glass. Poly(methyl methacrylate) (PMMA), PC, and poly(ethylene terephthalate) (PET) were used as substrate, too. TEM showed CuO NPs were spherically shaped with a diameter of 3–5 nm, some of the CuO NPs were anchored on the F–SiO$_2$ NPs surface and some were found free in the suspension. To investigate the surface feature of coatings, SEM and AFM were used. The CuO coating showed a smooth

surface without any distinct protuberances. The F-SiO$_2$ coating and FSiO$_2$- andCuO-coating all showed hierarchically micro/nanoscale structures, which formed by the aggregation of silica NPs and CuO NPs. The lowest surface roughness has been reported 3.6 nm for CuO coating. The surface roughness for F-SiO$_2$-coated glass has been reported 32.6 nm and for F-SiO$_2$- and CuO-coated glass it was about 27 nm. The reduction of surface roughness by the presence of CuO has been explained by occupying the cavities by CuO NPs. The superhydrophobic coatings (F-SiO$_2$-coated glass and F-SiO$_2$- and CuO-coated glass) showed water CA 163 and 160 degrees, respectively. The superhydrophobic characteristics of coating showed, reduction in adhesion of bacteria (*E. coli*) by up to 3.2 log cells/cm^2 as compared to bare glass. In addition, thanks to CuO NPs, the F-SiO$_2$- and CuO-coated glass the live/dead staining test exhibited excellent bactericidal performance against *E. coli*.

Song et al. [54] used fluoropolymer as superhydrophobic coating in controlling drug delivery system. The fluoropolymer was formed a coating on drug-loaded electrospun fibrous mat by electrospray. The results indicated that the superhydrophobic coating could be simply fabricated on the drug-loaded electrospun mat by the electrospray approach, and the thickness of the superhydrophobic coating could be finely controlled by varying the deposition time. It was further revealed by drug-release profiles that compared with drug-loaded electrospun mats, drug released sustainably from the samples coated with superhydrophobic layer, and the drug-release rate could be controlled by the thickness of superhydrophobic layer.

Falde et al. [55] used layered superhydrophobic electrospun meshes composed of poly (ε-caprolactone) (PCL) and poly(glycerolmonostearate-*co*-ε-caprolactone) (PGC-C18) as a local source of chemotherapeutic delivery. The coating extended total drug-release time by layering drug within a central layer that provided a delay before initial drug release. It was demonstrated through imaging and release studies which the nonwetted Cassie-Baxter state persisted for a prolonged and tunable period of time, though not indefinitely under rigorous conditions, and that drug release closely followed wetting of drug-containing layers. It has been shown the tunability of drug-release kinetics from this system by varying polymer hydrophobicity, drug content, and thickness of each layer.

7. Conclusion

Medical application is crucial filed and always demand for new technologies and materials. Employing superhydrophobic coatings as a new trend in the field of coating can find a good area in medical application. Biocompatibility and interaction of cell is a crucial mater in designing of biomaterials. Superhydrophobic coatings are good candidates due to the special surface feature and surface chemistry. The cell viability on the superhydrophobic coatings could be controlled by tuning surface chemistry and pattern.

Moreover, blood compatibility is a critical matter in biomaterial. The clot formation on the surface of blood contacting biomaterials restricts them. Superhydrophobic coating showed very good hemocompatibility with low fibrinogen adsorption and platelet activation. These coatings were very successful in killing bacteria on the surface of clinical devices. Also, superhydrophobicity found to be a good parameter for controlling release in drug delivery systems.

References

[1] T.G. Vladkova, Surface Engineering of Polymeric Biomaterials, Smithers Rapra, 2013.
[2] C.P. Sharma, Possible contributions of surface energy and interfacial parameters of synthetic polymers to blood compatibility, Biomaterials 2 (1) (1981) 57–59.
[3] L.B. Koh, I. Rodriguez, S.S. Venkatraman, The effect of topography of polymer surfaces on platelet adhesion, Biomaterials 31 (7) (2010) 1533–1545.
[4] D.M. Wootton, D.N. Ku, Fluid mechanics of vascular systems, diseases, and thrombosis, Annu. Rev. Biomed. Eng. 1 (1999) 299–329.
[5] E.W. Davie, K. Fujikawa, Basic mechanisms in blood coagulation, Annu. Rev. Biochem. 44 (1) (1975) 799–829.
[6] B. Yin, T. Liu, Y. Yin, Prolonging the duration of preventing bacterial adhesion of nanosilver-containing polymer films through hydrophobicity, Langmuir 28 (49) (2012) 17019–17025.
[7] W.-H. Kuo, M.-J. Wang, C.-W. Chang, T.-C. Wei, J.-Y. Lai, W.-B. Tsai, C. Lee, Improvement of hemocompatibility on materials by photoimmobilization of poly (ethylene glycol), J. Mater. Chem. 22 (19) (2012) 9991–9999.
[8] D.J. Lyman, W.M. Muir, I.J. Lee, The effect of chemical structure and surface properties of polymers on the coagulation of blood. I. Surface free energy effects, Trans. Am. Soc. Artif. Intern. Organs 11 (1965) 301–306.
[9] D.H. Kaelble, J. Moacanin, A surface energy analysis of bioadhesion, Polymer 18 (5) (1977) 475–482.
[10] S.D. Bruck, Physicochemical aspects of the blood compatibility of polymeric surfaces, J. Polym. Sci. Polym. Symp. 66 (1) (1979) 283–312. New York: Wiley Subscription Services, Inc., A Wiley Company.
[11] E. Ruckenstein, S.V. Gourisankar, A surface energetic criterion of blood compatibility of foreign surfaces, J. Colloid Interface Sci. 101 (2) (1984) 436–451.
[12] M. Ahmed, B.F.L. Lai, J.N. Kizhakkedathu, R. Narain, Hyperbranched glycopolymers for blood biocompatibility, Bioconjug. Chem. 23 (5) (2012) 1050–1058.
[13] R.K. Kainthan, M. Gnanamani, M. Ganguli, T. Ghosh, D.E. Brooks, S. Maiti, J.N. Kizhakkedathu, Blood compatibility of novel water soluble hyperbranched polyglycerol-based multivalent cationic polymers and their interaction with DNA, Biomaterials 27 (31) (2006) 5377–5390.
[14] B.F.L. Lai, Y. Zou, X. Yang, X. Yu, J.N. Kizhakkedathu, Abnormal blood clot formation induced by temperature responsive polymers by altered fibrin polymerization and platelet binding, Biomaterials 35 (8) (2014) 2518–2528.
[15] R. Narain, Y. Wang, M. Ahmed, B.F. Lai, J.N.J.B. Kizhakkedathu, Blood components interactions to ionic and nonionic glyconanogels, Biomacromolecules 16 (2015) 2990–2997.
[16] S. Moradi, N. Hadjesfandiari, S.F. Toosi, J.N. Kizhakkedathu, S.G. Hatzikiriakos, Effect of extreme wettability on platelet adhesion on metallic implants: from superhydrophilicity to superhydrophobicity, ACS Appl. Mater. Interfaces 8 (27) (2016) 17631–17641.
[17] R.A. Hartvig, M. van de Weert, J. Østergaard, L. Jorgensen, H. Jensen, Protein adsorption at charged surfaces: the role of electrostatic interactions and interfacial charge regulation, Langmuir 27 (6) (2011) 2634–2643.
[18] M. Christelle, S. Devineau, J.-C. Aude, G. Lagniel, S. Chédin, V. Legros, M.-H. Mathon, Structural determinants for protein adsorption/non-adsorption to silica surface, PLoS One 8 (11) (2013) 81346.

Superhydrophobic coatings for medical applications

[19] S. Pasche, J. Vörös, H.J. Griesser, N.D. Spencer, M. Textor, Effects of ionic strength and surface charge on protein adsorption at PEGylated surfaces, J. Phys. Chem. B 109 (37) (2005) 17545–17552.

[20] N.L. Burns, K. Holmberg, C. Brink, Influence of surface charge on protein adsorption at an amphoteric surface: effects of varying acid to base ratio, J. Colloid Interface Sci. 178 (1996) 116–122.

[21] C. Werner, M.F. Maitz, C. Sperling, Current strategies towards hemocompatible coatings, J. Mater. Chem. 17 (32) (2007) 3376–3384.

[22] C. Wei, W.-J. Pan, M.-S. Hung, The effects of substrate roughness and associated surface properties on the biocompatibility of diamond-like carbon films, Surf. Coat. Technol. 224 (2013) 8–17.

[23] L. Tang, P. Thevenot, W. Hu, Surface chemistry influences implant biocompatibility, Curr. Top. Med. Chem. 8 (4) (2008) 270–280.

[24] E. Ruckenstein, Z.F. Li, Surface modification and functionalization through the self-assembled monolayer and graft polymerization, Adv. Colloid Interf. Sci. 113 (2005) 43–63.

[25] E. Ostuni, R.G. Chapman, R.E. Holmlin, S. Takayama, G.M. Whitesides, A survey of structure − property relationships of surfaces that resist the adsorption of protein, Langmuir 17 (18) (2001) 5605–5620.

[26] J. Benesch, S. Svedhem, S.C.T. Svensson, R.n. Valiokas, B. Liedberg, P. Tengvall, Protein adsorption to oligo (ethylene glycol) self-assembled monolayers: experiments with fibrinogen, heparinized plasma, and serum, J. Biomater. Sci. Polym. Ed. 12 (6) (2001) 581–597.

[27] M.C.L. Martins, B.D. Ratner, M.A. Barbosa, Protein adsorption on mixtures of hydroxyl- and methyl-terminated alkanethiols self-assembled monolayers, J. Biomed. Mater. Res. A: An Official Journal of The Society for Biomaterials, The Japanese Society for Biomaterials, and The Australian Society for Biomaterials and the Korean Society for Biomaterials 67 (2003) 158–171.

[28] V.A. Tegoulia, W. Rao, A.T. Kalambur, J.F. Rabolt, S.L. Cooper, Surface properties, fibrinogen adsorption, and cellular interactions of a novel phosphorylcholine-containing self-assembled monolayer on gold, Langmuir 17 (14) (2001) 4396–4404.

[29] M. Agashe, V. Raut, S.J. Stuart, R.A. Latour, Molecular simulation to characterize the adsorption behavior of a fibrinogen γ-chain fragment, Langmuir 21 (3) (2005) 1103–1117.

[30] B. Balakrishnan, D.S. Kumar, Y. Yoshida, A. Jayakrishnan, Chemical modification of poly (vinyl chloride) resin using poly (ethylene glycol) to improve blood compatibility, Biomaterials 26 (17) (2005) 3495–3502.

[31] M. Li, K. Gee Neoh, L.Q. Xu, R. Wang, E.-T. Kang, T. Lau, D.P. Olszyna, E. Chiong, Surface modification of silicone for biomedical applications requiring long-term antibacterial, antifouling, and hemocompatible properties, Langmuir 28 (47) (2012) 16408–16422.

[32] F. Puoci (Ed.), Advanced Polymers in Medicine, Springer, Berlin, 2015.

[33] R.E. Baier, V.L. Gott, A. Feruse, Surface chemical evaluation of thromboresistant materials before and after venous implantation, ASAIO J. 16 (1970) 50–57.

[34] E. Nyilas, W.A. Morton, R.D. Cumming, D.M. Lederman, T.-H. Chiu, R.E. Bailer, Effects of polymer surface molecular structure and force-field characteristics on blood interfacial phenomena. I, J. Biomed. Mater. Res. 11 (1977) 51–68.

[35] C.K. Akers, I. Dardik, H. Dardik, M. Wodka, Computational methods comparing the surface properties of the inner walls of isolated human veins and synthetic biomaterials, J. Colloid Interface Sci. 59 (3) (1977) 461–467.

[36] S.-C. Luo, S.S. Liour, H.-h. Yu, Perfluoro-functionalized PEDOT films with controlled morphology as superhydrophobic coatings and biointerfaces with enhanced cell adhesion, Chem. Commun. 46 (2010) 4731–4733.

[37] R. Gristina, E. D'Aloia, G.S. Senesi, A. Milella, M. Nardulli, E. Sardella, P. Favia, R. d'Agostino, Increasing cell adhesion on plasma deposited fluorocarbon coatings by changing the surface topography, J Biomed Mater Res B Appl Biomater 88 (2009) 139–149.

[38] S.A. Mahadik, F. Pedraza, S.S. Mahadik, B.P. Relekar, S.S. Thorat, Biocompatible superhydrophobic coating material for biomedical applications, J. Sol-Gel Sci. Technol. 81 (2017) 791–796.

[39] G.S. Senesi, E. D'Aloia, R. Gristina, P. Favia, R. d'Agostino, Surface characterization of plasma deposited nano-structured fluorocarbon coatings for promoting in vitro cell growth, Surf. Sci. 601 (2007) 1019–1025.

[40] I. Hejazi, J. Seyfi, E. Hejazi, G.M.M. Sadeghi, S.H. Jafari, H.A. Khonakdar, Investigating the role of surface micro/nano structure in cell adhesion behavior of superhydrophobic polypropylene/nanosilica surfaces, Colloids Surf. B: Biointerfaces 127 (2015) 233–240.

[41] S. Zangi, I. Hejazi, J. Seyfi, E. Hejazi, H.A. Khonakdar, S.M. Davachi, Tuning cell adhesion on polymeric and nanocomposite surfaces: role of topography versus superhydrophobicity, Mater. Sci. Eng. C 63 (2016) 609–615.

[42] A. Ranella, M. Barberoglou, S. Bakogianni, C. Fotakis, E. Stratakis, Tuning cell adhesion by controlling the roughness and wettability of 3D micro/nano silicon structures, Acta Biomater. 6 (2010) 2711–2720.

[43] C.-R. Hsiao, C.-W. Lin, C.-M. Chou, C.-J. Chung, J.-L. He, Surface modification of blood-contacting biomaterials by plasma-polymerized superhydrophobic films using hexamethyldisiloxane and tetrafluoromethane as precursors, Appl. Surf. Sci. 346 (2015) 50–56.

[44] X. Hou, X. Wang, Q. Zhu, J. Bao, C. Mao, L. Jiang, J. Shen, Preparation of polypropylene superhydrophobic surface and its blood compatibility, Colloids Surf. B: Biointerfaces 80 (2010) 247–250.

[45] H. Li, X. Zhao, G. Chu, S. Zhang, X. Yuan, One-step fabrication of superhydrophobic polymer surface from an acrylic copolymer containing POSS by spraying, RSC Adv. 4 (2014) 62694–66269.

[46] T. Sun, H. Tan, D. Han, Q. Fu, L. Jiang, No platelet can adhere—largely improved blood compatibility on nanostructured superhydrophobic surfaces, Small 1 (2005) 959–963.

[47] A. Milionis, K. Ghokulla Krishnan, E. Lot, M. Lawrence, Dynamic wetting of human blood and plasma on various surfaces, Colloids Surf. B: Biointerfaces 166 (2018) 218–223.

[48] Q. Huang, Y. Yang, R. Hu, C. Lin, L. Sun, E.A. Vogler, Reduced platelet adhesion and improved corrosion resistance of superhydrophobic TiO2-nanotube-coated 316L stainless steel, Colloids Surf. B: Biointerfaces 125 (2015) 134–141.

[49] W. Ye, Q. Shi, J. Hou, J. Jin, Q. Fan, S.-C. Wong, X. Xiaodong, i. Yin, Superhydrophobic coating of elastomer on different substrates with a liquid template to construct a biocompatible and antibacterial surface, J. Mater. Chem. B 2 (2014) 7186–7191.

[50] F. Yuchen, J. Jiang, Q. Zhan, X. Zhan, F. Chen, Robust liquid-repellent coatings based on polymer nanoparticles with excellent self-cleaning and antibacterial performances, J. Mater. Chem. A 5 (2017) 275–284.

[51] C.-Y. Loo, P.M. Young, W.-H. Lee, R. Cavaliere, C.B. Whitchurch, R. Rohanizadeh, Superhydrophobic, nanotextured polyvinyl chloride films for delaying *Pseudomonas aeruginosa* attachment to intubation tubes and medical plastics, Acta Biomater. 8 (2012) 1881–1890.

[52] E. Ozkan, C.C. Crick, A. Taylor, E. Allan, I.P. Parkin, Copper-based water repellent and antibacterial coatings by aerosol assisted chemical vapour deposition, Chem. Sci. 7 (2016) 5126–5131.

[53] T. Ren, M. Yang, K. Wang, Y. Zhang, J. He, CuO nanoparticles-containing highly transparent and superhydrophobic coatings with extremely low bacterial adhesion and excellent bactericidal property, ACS Appl. Mater. Interfaces 10 (30) (2018) 25717–25725.

[54] B. Song, S. Xu, S. Shi, P. Jia, Q. Xu, G. Hu, H. Zhang, C. Wang, Superhydrophobic coating to delay drug release from drug-loaded electrospun fibrous materials, Appl. Surf. Sci. 359 (2015) 245–251.

[55] E.J. Falde, J.D. Freedman, V.L.M. Herrera, S.T. Yohe, Y.L. Colson, M.W. Grinstaff, Layered superhydrophobic meshes for controlled drug release, J. Control. Release 214 (2015) 23–29.

Further reading

[56] J.D. Andrade, Interfacial phenomena and biomaterials, Med. Instrum. 7 (2) (1973) 110.

CHAPTER 15

Superhydrophobic surfaces for oil-water separation

Sanjay S. Latthe[a,b], Rajaram S. Sutar[b], A.K. Bhosale[b], Kishor Kumar Sadasivuni[c], Shanhu Liu[a]

[a]Henan Key Laboratory of Polyoxometalate Chemistry, Henan Joint International Research Laboratory of Environmental Pollution Control Materials, College of Chemistry and Chemical Engineering, Henan University, Kaifeng, People's Republic of China
[b]Self-cleaning Research Laboratory, Department of Physics, Raje Ramrao College (affiliated to Shivaji University, Kolhapur), Jath, India
[c]Center for Advanced Materials, Qatar University, Doha, Qatar

1. Introduction

Frequent oceanic oil spill accidents and most industries worldwide discharging immense level of oil in the surroundings is a serious threat to the environment. Effectual oil removal from affected water is the most essential exercise. Several traditional, expensive, and time-consuming physical, chemical, and biological methods are adopted for oil spill cleanup [1]. An oil-water separation process has become cheaper and environment-friendly by virtue of emergent smart materials like superhydrophobic surfaces. The superhydrophobic surface strongly repels water with contact angle (CA) higher than 150 degrees and mostly absorbs any kind of oil and organic pollutants with CA nearly equal to 0 degrees [2]. The use of superhydrophobic-superoleophilic meshes and/or sponges to conduct oil-water separation is growing, particularly to protect the environment and to recover precious oil [3]. To achieve efficient oil-water separation, the superhydrophobic-superoleophilic meshes/sponges must possess some unique properties. First, superhydrophobic meshes/sponges must show fine selectivity toward various oils and organic liquids for selective separation of oil from water. Second, along with fine selectivity, the superhydrophobic meshes/sponges should confirm high separation efficiency. Third, continuous oil-water separation is essential in most cases, so the repeatability in oil-water separation is required. Fourth, the oil-water separation efficiency should not be degraded for higher recycles; hence the reusability of the superhydrophobic meshes/sponges is of great importance. Finally, the superhydrophobic meshes/sponges must show mechanical, chemical, and thermal durability to avoid a reduction in oil-water separation efficiency [4].

Various chemical methods are adopted for the fabrication of the superhydrophobic-superoleophilic meshes/sponges for efficient oil-water separation. As the carbon nanotubes (CNTs) are hydrophobic in nature and show strong affinity toward oil, Lee et al. [5]

adopted chemical vapor deposition (CVD) technique to deposit vertically aligned CNT's (height > 5 µm) on stainless steel (SS) mesh. The as-prepared SS-CNT mesh effectively separates oil from water-in-oil emulsions with efficiency higher than 80%. Wang and Lin [6] also modified the polyurethane (PU) sponge from hydrophilic to superhydrophobic by dip coating it from the nanocomposite of CNT/poly-(dimethylsiloxane) (PDMS). The as-prepared superhydrophobic-superoleophilic sponge exhibited continuous removal of various oils (Soybean oil, motor oil, diesel, *n*-hexadecane, gasoline, and *n*-hexane) from the surface of the water with high separation efficiency. Gu et al. grafted polystyrene (PS) brushes onto the CNT's membrane by self-initiated photografting and photopolymerization (SIPGP) process [7]. The as-prepared free-standing and mechanically robust PS-g-CNTs membrane revealed excellent oil separation from water-in-oil emulsions with good repeatability and separation efficiency of more than 99%. Electrospinning technique can be effectively utilized to attain free-standing porous polymer membranes. Zhou and Wu [8] fabricated mechanically strong, flexible, and porous poly(vinylidene fluoride) (PVDF) membrane by electrospinning technique. The fibrous PVDF membrane with fiber diameter greater than 1 µm exhibited excellent superhydrophobicity and superoleophilicity. A diesel from water-in-diesel emulsion was separated efficiently by PVDF membrane with more than 99% separation efficiency. Lee et al. [9] also adopted an electrospinning method to attain highly porous PS nanofibers on a SS mesh. Several liters of gasoline, diesel, and mineral oil were effectively separated in a single step using the superhydrophobic-superoleophilic PS membrane. The electrospun polytetrafluoroethylene (PTFE) nanofibrous membranes also revealed good mechanical strength and corrosion-resistance with excellent gravity-driven oil-water separation [10]. Chang et al. [11] adopted low-cost and faster airbrush method over electrospinning to develop superhydrophobic-superoleophilic PS surface on SS mesh for oil (diesel)-water separation.

Several polymers, nanoparticles, and their nanocomposites are utilized to develop materials for oil-water separation. Yoon et al. [12] utilized slurry prepared from the nanocomposite of poly(diallyldimethylammonium chloride) (PDDA), sodium perfluorooctanoate (PFO), and silica nanoparticles to dip coat on SS mesh. The as-prepared SS mesh exhibited superhydrophilicity (water CA ~ 0 degrees) and oleophobicity (oil CA > 95 degrees). An efficient gravity-driven oil-water separation achieved and further methylene blue (MB) degradation achieved while separating an MB-oil mixture, by fitting graphene plug under modified SS mesh. Therefore, such smart meshes not only separate oil-water mixture but also purify water. Zhang et al. [13] adopted a simple solvothermal method to synthesize polydivinylbenzene (PDVB) polymer and deposited them on porous mesh and membranes during the polymerization process. A mixture of oil-seawater and stabilized emulsion separated with high repeatability, excellent reusability, and nearly 100% of separation efficiency. Li et al. [14] have grown 2-D hierarchical ZnO nanoflakes on Al-coated SS mesh through low-temperature hydrothermal process.

After stearic acid (SA) modification, the superhydrophobic SS mesh separates various kinds of oil from water. Zhang et al. [15] modified the hydrothermally synthesized ZnO nanoparticles using SA and the cotton textiles were drop coated using modified-ZnO/PS nanocomposite solution. The as-prepared superhydrophobic cotton textiles revealed good oil-water separation capability. The superhydrophobic-superoleophilic filter papers were also fabricated by colloidal deposition of PTFE nanoparticles and utilized for the potent separation of hexane, hexadecane, trichloromethane, silicone oil, and gasoline from water [16].

A new interesting trend in the development of superhydrophobic sponges or porous materials with magnetic properties is emerging [17–22]. These magnetic superhydrophobic materials shall be driven to the oily water area with the help of magnets and oil can be efficiently collected. Wu et al. [19] performed the hydrolysis and condensation of tetraethoxysilane (TEOS) and n-hexadecyltriethoxysilane (HDTES) in conjunction with Fe_3O_4 nanoparticles to achieve nanocomposite solution. A polyester material dip coated from this nanocomposite solution to attain durable, magnetic, and superhydrophobic surface that could efficiently separate petrol, diesel, and crude oil from water. Liu et al. [20] utilized dopamine self-polymerization method to anchor Fe_3O_4 nanoparticles on PU sponge to accord magnetic property and attain the superhydrophobicity through modification by long-chain heptadecafluoro-1,1,2,2-tetrahydrodecyltrimethoxysilane (FAS-17). The magnetic superhydrophobic PU sponge separated oils and heavy organic liquids from simulated seawater and revealed stable wetting properties under corrosive conditions. Besides, Zhang et al. [21] fabricated magnetically driven superhydrophobic meshes by surface modifying the ferrous meshes by long-chain FAS-17. The magnetic superhydrophobic meshes could act as floating micro-robot model to explore oil-contaminated wastewater in a closed system like pipelines. Tran and Lee [22] employed microwave method to grow ZnO flakes on PU sponge, incorporated Fe_3O_4 nanoparticles in the PU skeleton and subsequently modified it with SA to immobilize the Fe_3O_4 nanoparticles. The as-prepared durable, recyclable, reusable, magnetic, and superhydrophobic PU sponge revealed oil absorption capacity toward various oils such as hexane, toluene, dichloromethane, gasoline, soybean oil, diesel engine oil, vacuum pump oil and oil-in-water emulsion. Herein, we will mostly discuss on the simple, rapid, low-cost, and innovative methods for the fabrication of superhydrophobic-superoleophilic sponges/membranes for efficient oil-water separation application.

2. Superhydrophobic-superoleophilic surfaces for oil-water separation

2.1 Oil-water separation using Superhydrophobic-superoleophilic sponges

Mostly, the superhydrophobic modification of commercially available, low-cost, low-density, lightweight, three-dimensional, and highly porous PU or melamine sponges

developed to use it for efficient oil–water separation application. Abundant reports are available on a simple and single step superhydrophobic modification of sponges using low surface energy components like various alkylchlorosilanes [23, 24], FAS [25, 26], and thiols [27, 28]. Zhu et al. [23] modified the wettability of a PU sponge by simple immersion in methyltrichlorosilane (MTCS)/hexane solution to achieve superhydrophobicity. The hydrolysis of MTCS resulted in the highly porous polysiloxane coating on the skeleton of PU sponge. The superhydrophobic sponges revealed excellent oil-water separation ability and wetting stability against mechanical compression, all pH liquids and ultrasonication in an oil bath. Likewise, Zhang et al. [25] merely immersed a PU sponge in ethanol solution of fluoroalkylsilane (FAS) to achieve superhydrophobicity and modified sponge revealed oil separation efficiency greater than 96%. Ruan et al. [27] have simply utilized the mercapto-functionalized hydrophobic molecules (1H,1H,2H,2H-perfluorodecanethiol) for the superhydrophobic modification of the dopamine-modified melamine sponge. The as-prepared porous melamine sponges depicted excellent water repellency, oil absorbency, flame retardancy, and mechanical stability. This simplistic approach was utilized to prepare a large-area superhydrophobic sponge of size 120 cm × 70 cm × 5 cm. A very simple and innovative idea reported by Choi et al. [29] to develop polydimethylsiloxane (PDMS) sponge using sugar cube as a template. In this simple and quick preparation process of PDMS sponge, at first PDMS polymer solution was poured in a sugar cube template and after drying, it was simply immersed in water to dissolve sugar template (Fig. 1A and B). The optical and scanning electron microscope studies confirmed a highly porous skeleton of PDMS sponge necessary for effective
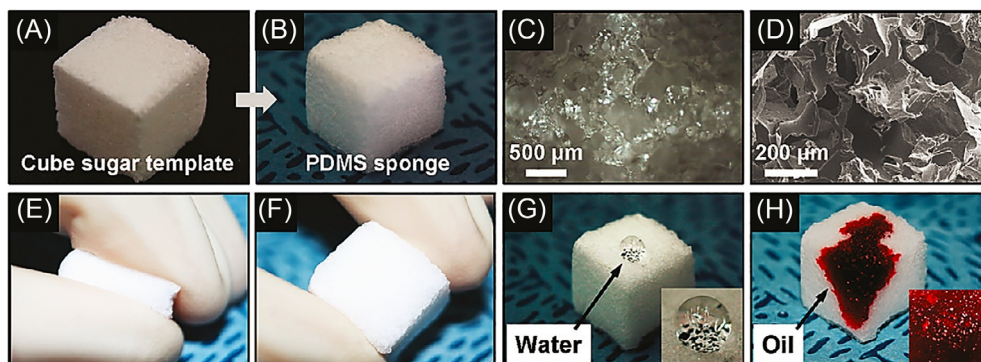
Fig. 1 Photograph of (A) sugar cube as a template and (B) as-replicated PDMS sponge, (C) optical microscope image of the PDMS sponge, (D) SEM image of the PDMS sponge, (E) mechanical compression and (F) recovery to the original shape, (G) strongly hydrophobic, and (H) superoleophilic wetting properties of PDMS sponge. (Insets: Magnified water and oil droplets). *(Reproduced with permission from S.-J. Choi, T.-H. Kwon, H. Im, D.-I. Moon, D.J. Baek, M.-L. Seol, J.P. Duarte, Y.-K. Choi, A polydimethylsiloxane (PDMS) sponge for the selective absorption of oil from water, ACS Appl. Mater. Interfaces 3 (12) (2011) 4552–4556. Copyright 2011, American Chemical Society.)*

oil–water separation (Fig. 1C and D). The as-prepared PDMS sponge revealed good elastic properties and recovered its original shape and size after volume compression of more than 50% (Fig. 1E and F). A water drop placed on PDMS sponge showed CA in the range of 120–130 degrees, whereas the oil drop gets completely absorbed (Fig. 1G and H). The PDMS sponge revealed quick removal of oil and organic liquids from water with excellent stability, reusability, and recyclability.

Recently, Wang and Chen [30] simply immersed the compressed melamine sponge into the hydrophobic polymer solution containing PDMS adhesive, curing agent, and ethyl acetate to render it superhydrophobically. A superhydrophobic melamine sponge exhibited excellent repellency toward the water, acidic, and basic corrosive liquids (Fig. 2A) due to uniform and dense hydrophobic polymer coating on the porous network structure of sponge (Fig. 2B and C). A superhydrophobic melamine sponge exhibited ultrafast separation of oils (n-hexane, n-octane, n-hexadecane, isooctane, and toluene) from the water-in-oil emulsions with separation efficiency greater than 99.98%. Yang et al. [31] utilized low-cost lignin as a natural phenolic polymer for hydrophobic
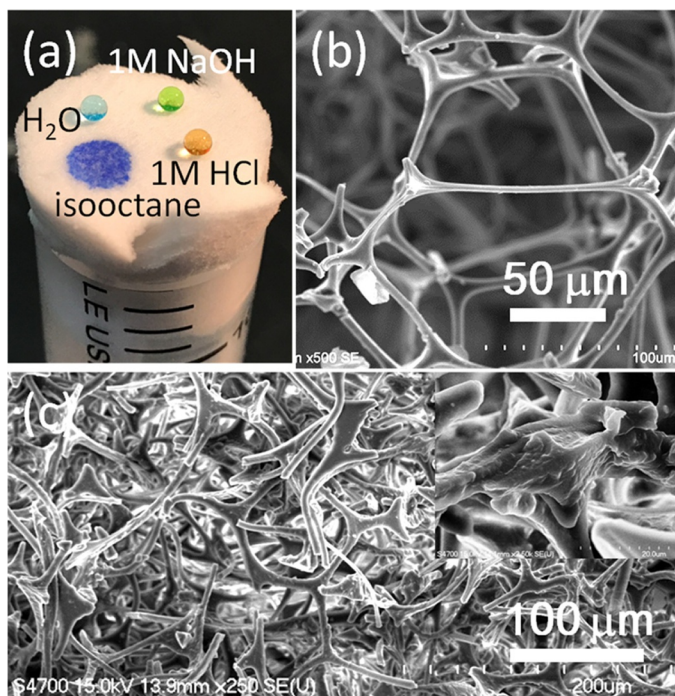
Fig. 2 (A) Photograph of water, sodium hydroxide, hydrochloric acid, and oil droplets on the superhydrophobic melamine sponge, SEM images of the (B) pure and (C) superhydrophobic melamine sponge. *(Reproduced with permission from C.-F. Wang, L.-T. Chen, Preparation of superwetting porous materials for ultrafast separation of water-in-oil emulsions, Langmuir 33 (8) (2017) 1969–1973. Copyright 2017, American Chemical Society.)*

modification of melamine sponge. The melamine sponge was immersed in alkaline solution of lignin (pH = 11) and pyrolyzed in nitrogen atmosphere at 400°C to form carbonized lignin with water CA greater than 140 degrees and oil CA equal to 0 degrees (Fig. 3A and B). The surface morphology confirmed uniform coating of lignin polymer on the porous network of the sponge (Fig. 3C). The modified melamine sponge revealed high selectivity toward various oils with fast separation efficiency of greater than 93%.

Hydrophobic carbon soot (CS) particles can be collected easily and cost effectively from the candle flame. Li et al. [32] obtained the hydrophobic CS by incomplete combustion of hydrocarbons from the mid-candle flame. The PU sponge immersed in the mixture of CS, hydrophobic silica nanoparticles, and PU resin to achieve stable superhydrophobicity. The CS–SiO$_2$–PU sponge showed excellent oil separation capacity from hot water and acidic, alkaline, and salt solutions. Beshkar et al. [33] prepared durable magnetic superhydrophobic PU sponge by immersing it in the colloidal solution of straw soot (carbon nanoparticles) and further modification was done by Fe$_2$O$_4$ nanoparticles and PDMS. The waste oil was easily collected from the surface of water through guiding the magnetic superhydrophobic PU sponge by a bar magnet. The wettability of sponge remained unchanged even after 30 absorption/desorption cycles. Gao et al. [34] obtained the CS particles from ethylene-oxygen combustion flame and dispersed it in 1,2-dichloroethane (DCE). The superhydrophobic-superoleophilic melamine sponge achieved by a uniform coating of as-grown CS particles onto the porous

(A)   (B)

(C)
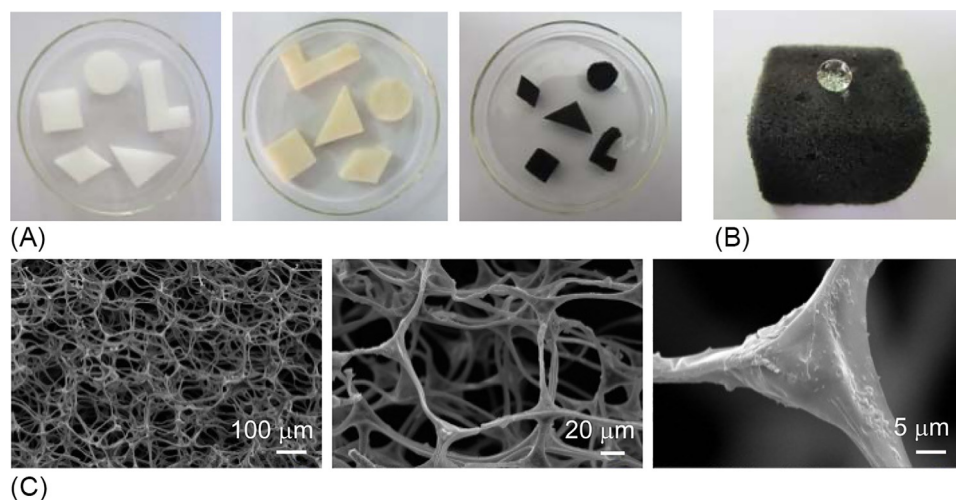
Fig. 3 (A) Fabrication process the hydrophobic tannin and melamine sponges through solution immersion, (B) photograph of water drop on the hydrophobic melamine sponge, and (C) SEM images of modified sponges at different magnifications. *(Reproduced with permission from Y. Yang, H. Yi, C. Wang, Oil absorbents based on melamine/lignin by a dip adsorbing method, ACS Sustain. Chem. Eng. 3 (12) (2015) 3012–3018. Copyright 2015, American Chemical Society.)*
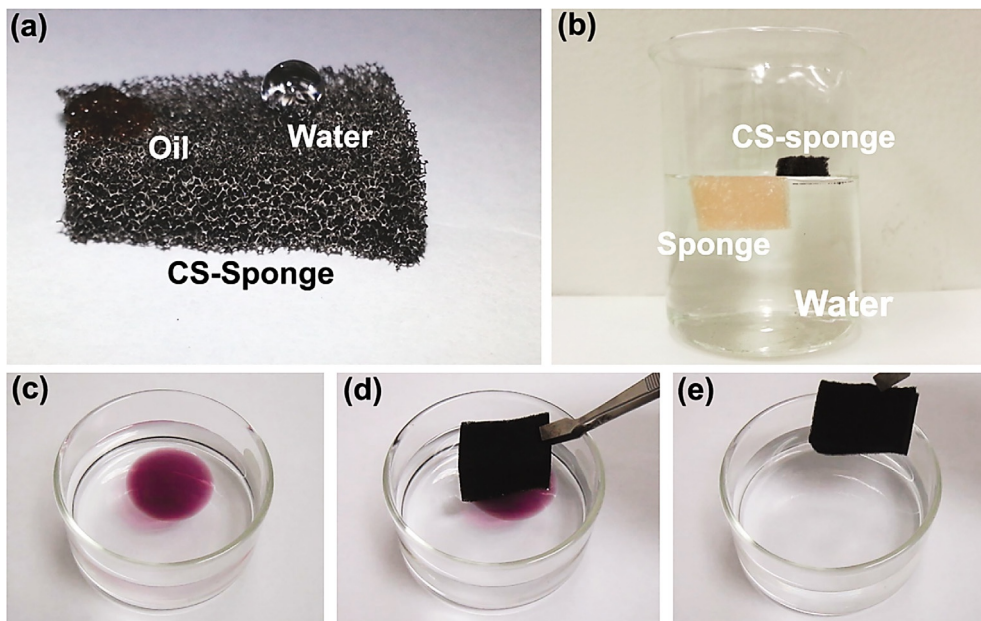
Fig. 4 Photographs of (A) oil and water droplets on the surface of CS-modified sponge; (B) pure and CS-modified sponge dropped on the water; (C–E) removal of engine oil from water surface using CS-modified sponge. *(Reproduced with permission from Y. Gao, Y.S. Zhou, W. Xiong, M. Wang, L. Fan, H. Rabiee-Golgir, L. Jiang, W. Hou, X. Huang, L. Jiang, J.-F. Silvain, Y.F. Lu, Highly efficient and recyclable carbon soot sponge for oil cleanup, ACS Appl. Mater. Interfaces 6 (8) (2014) 5924–5929. Copyright 2014, American Chemical Society.)*

skeleton through simple immersion in CS dispersion. The CS–modified sponge exhibited strong water repellency and oil absorbency without further chemical modification (Fig. 4A and B). An easy and fast recovery of engine oil floating on the water surface by CS-modified sponge confirms its high oil–water separation efficiency (Fig. 4C–E). The CS-modified sponge could absorb numerous oils and organic solvents with an absorption capacity of 25–80 times of its own weight. Oil can be recycled for more than 10 times with absolutely no change in an oil absorption capacity and wettability of the CS-modified sponge. Table 1 summarizes the comparison of the oil–water separation capability between the various superhydrophobic sponges.

2.2 Oil-water separation using superhydrophobic-superoleophilic meshes and membranes

Metallic meshes (SS mesh and copper mesh), woven, and nonwoven fabrics/textiles are generally used as potential substrates for oil–water separation. Parkin et al. [35] performed aerosol–assisted chemical vapor deposition (AACVD) of silicone elastomer on the copper mesh of various pore diameters. The rough, uniform, and adherently covered silicone

Table 1 Comparison of the oil-water separation capability of superhydrophobic sponges

Materials	Fabrication method	Types of absorbed oil/organic solvent	Separation efficiency (%)	Recycle ability (number)	Ref.
Methyltrichlorosilane (MTCS)/hexane	Solution immersion	Decane, dodecane, octane, crude oil, gasoline, bean oil, lubricating oil	~99.9	300	[23]
(1H,1H,2H,2H-perfluorodecanethiol)/ethanol	Solution immersion	Hexane, dimethylformamide, dimethylsulfoxide, toluene, ethanol, methanol, cyclohexane, chloroform, soybean oil, octadecene, pump oil, crude oil	~90	100	[27]
Polymerized octadecylsiloxane (PODS)	Solution immersion	Toluene, methylsilicone oil, 1,2-dichloroethane, light petroleum	~98	>50	[24]
CS/Fe$_2$O$_4$/PDMS	Solution immersion	Waste oil	~90	>30	[33]
Polydimethylsiloxane (PDMS) sponge	Template method	Chloroform, silicone oil, dichloromethane, motor oil, 1,2-dichlorobenzene, toluene, N,N-dimethylmethane, transformer oil, methanol, ethanol, acetone	~99	>20	[29]
Candle soot/hydrophobic silica	Solution immersion	Toluene, diesel, chloroform, hexane, tetrachloroethane, petroleum ether, kerosene, and heptane	>99	>15	[32]
CS	Solution immersion	4-Methyl-2-pentanone, cyclohexane, N-methyl-2-pyrollidinone, dimethylformamide, methanol, ethanol, acetone, hexane, tetrahydrofuran, benzene, dichloroethane, toluene, crude oil, soybean oil, used pump oil, engine oil, pump oil	~90	>10	[34]
Fluoroalkylsilane (FAS)/ethanol	Solution immersion	Gasoline, crude oil, hexane, petroleum ether	96–98	>10	[25]
PDMS adhesive (SE1700)	Solution immersion	Toluene, n-hexane, n-octane, n-hexadecane, and isooctane	>99.98	>05	[30]
Carbonized lignin	Dip adsorbing process	Hexane, gasoline, hexadecane, toluene, sunflower oil, gasoline, dichloromethane, styrene, chloroform, peanut oil, dodecane	>93	~05	[31]

elastomer on copper mesh revealed superhydrophobic-superoleophilic wettability with high oil-water separation efficiency and repeatability. Wang et al. [36] have employed a simple solution-immersion process to modify the nitric acid etched copper mesh by 1-hexadecanethiol (HDT). The as-prepared superhydrophobic copper mesh actively separated diesel from water and exhibited good stability in acidic, basic, and salt environment. Besides, the same strategy was adopted to modify the silver nitrate–etched copper mesh by 1-dodecanethiol to achieve superhydrophobic-superoleophilic porous surface [37]. Ren et al. [38] have grown $Cu(OH)_2$ nanoneedles (length > 2 μm and width ∼ 100–200 nm) on the copper mesh by simply immersing them in the aqueous solution of sodium hydroxide and ammonium persulfate. After SA modification, copper mesh exhibited excellent superoleophilicity and superhydrophobicity with water CA greater than 157 degrees and rolling angle less than 5 degrees (Fig. 5A–C). Besides, super-hydrophobic copper mesh revealed stable superhydrophobicity under harsh mechanical bending for any shape (Fig. 5D–F). It showed more than 99% of oil collection efficiency for hexadecane, gasoline, toluene, and mineral oil from water even after 25 cycles of repeated oil-water separation.

Wang et al. [39] fabricated superhydrophobic SS mesh using hydrophobically modified dual scale silica-coated PS particles (∼1 μm and 200 nm). At first, PS particles were coated with silica by Stober method using TEOS as a precursor. The obtained dual scaled silica-coated PS particles were modified with hexadecyltrimethoxysilane (HDTMS) and drop casted on SS mesh to attain rough hierarchical surface with good
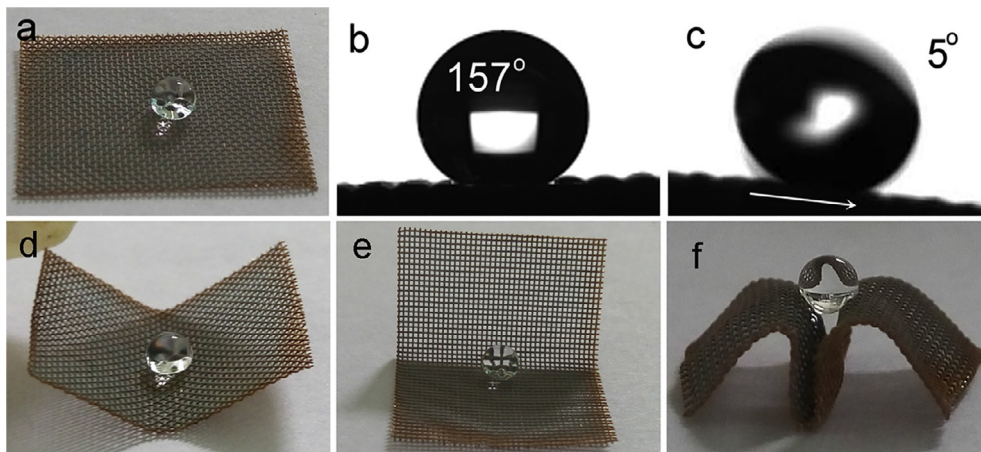
Fig. 5 Photographs of (A) spherical water drop, (B) contact angle, (C) rolling angle of water drop on the superhydrophobic copper mesh, (D–F) stable superhydrophobicity after mechanical bending in any shape. (*Reproduced with permission from G. Ren, Y. Song, X. Li, Y. Zhou, Z. Zhang, X. Zhu, A superhydrophobic copper mesh as an advanced platform for oil-water separation, Appl. Surf. Sci. 428 (2018) 520–525. Copyright 2017, Elsevier.*)

oil–water separation capability. Guo et al. [40] have fabricated mechanically stable superhydrophobic–superoleophilic SS mesh by simply spray coating the polyhedral oligomeric silsesquioxane (POSS) hybrid acrylic polymer synthesized through free radical solution polymerization. The as-prepared mesh composed of micro and nanospheres formed a hierarchical rough structure that strongly repels distilled water, milk, coffee, tea, green ink, red ink, and completely absorbs *n*-hexane, kerosene, isooctane, petroleum ether, and vegetable oil. Both wetting and oil–water separation properties remained the same after 20 sandpaper abrasion cycles. Geraldi et al. [41] merely spray coated a mixture of CS particles and PDMS on SS mesh that revealed a network of aggregated clusters forming porous morphology. The superhydrophobic–superoleophilic mesh depicted stability against the corrosive environments and achieved the oil–water separation efficiency of 96%. Yang et al. [42] used attapulgite fibrillate mineral (i.e., hydrated magnesium aluminum silicate) in conjunction with epoxy resin to spray coat the SS mesh for oil–water separation. The effect of various wt% of attapulgite into epoxy resin on wetting and morphological properties of the epoxy/attapulgite nanocomposite meshes were reported. A nanocomposite mesh prepared with 44.4 wt% of attapulgite into epoxy resin exhibited hierarchical rough surface morphology with water CA higher than 160 degrees (Fig. 6). The nanocomposite mesh demonstrated excellent oil–water separation efficiency (greater than 98%) for hexadecane, lubricating oil, and paroline (Fig. 7). The separation efficiency stayed intact even after 30 continuous separation cycles.
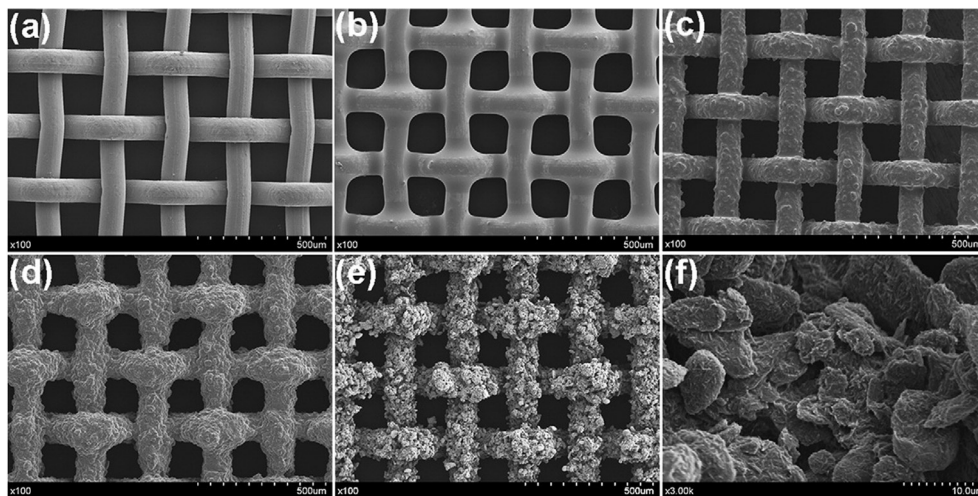
Fig. 6 SEM images of (A) pristine SS mesh (B) epoxy-coated SS mesh, and the epoxy/attapulgite nanocomposite meshes with (C) 16.7 wt%, (D) 28.6 wt%, and (E and F) 44.4 wt% of attapulgite. *(Reproduced with permission from J. Yang, Y. Tang, J. Xu, B. Chen, H. Tang, C. Li, Durable superhydrophobic/superoleophilic epoxy/attapulgite nanocomposite coatings for oil/water separation, Surf. Coat. Technol. 272 (2015) 285–290. Copyright 2015, Elsevier.)*
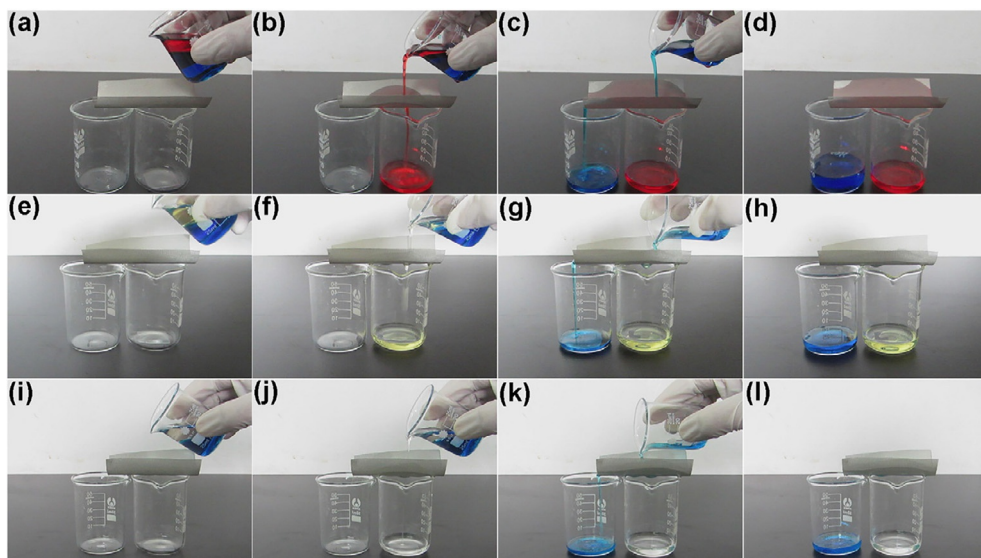
Fig. 7 An oil-water separation of a mixture of hexadecane/water (A–D), lubricating oil/water (E–H), and paroline/water (I–L) through the epoxy/attapulgite nanocomposite mesh. *(Reproduced with permission from J. Yang, Y. Tang, J. Xu, B. Chen, H. Tang, C. Li, Durable superhydrophobic/superoleophilic epoxy/ attapulgite nanocomposite coatings for oil/water separation, Surf. Coat. Technol. 272 (2015) 285–290. Copyright 2015, Elsevier.)*

Cortese et al. [43] attained superhydrophobic cotton textiles through etching oxygen plasma pretreatment and diamond-like carbon (DLC) coating using plasma–enhanced chemical vapor deposition (PECVD). The superhydrophobic DLC–coated cotton textiles efficiently absorbed and separated various oils such as DMSO, chlorobenzene, ethanol, acetone, hexane, dichloromethane, chloroform, gasoline, and olive oil with separation efficiency greater than 99%. The superhydrophobic wetting properties of DLC–coated cotton textiles found unaltered after long-time exposure to air (6 months), temperature $\sim 60^{\circ}$C (3 days), relative humidity $\sim 95\%$ (3 days), laundry washing cycles ($\sim$20), immersion in oil (1 month), acidic solution (pH $\sim$ 2 for 3 days) and alkaline solution (pH $\sim$ 12 for 3 days). Lei et al. [44] fabricated superhydrophobic cotton fabric by simply spray coating the PTFE nanoparticle dispersion. The chemically and mechanically durable PTFE-coated cotton fabric revealed stable oil–water separation efficiency of greater than 95% over 50 separation cycles. Recently, Gu et al. [45] performed superhydrophobic modification of biodegradable polylactic acid (PLA) polymer based nonwoven fabric for oil–water separation. Fig. 8 depicts a schematic explanation of fabrication of superhydrophobic PLA nonwoven fabric. At first, self-polymerized dopamine was utilized for the surface modification of PLA nonwoven fabric (Fig. 8A) to attain polydopamine (PDA)-modified PLA. The hydrophobic to hydrophilic wetting conversion confirms anchored hydroxyl and amino groups on PDA-modified PLA surface
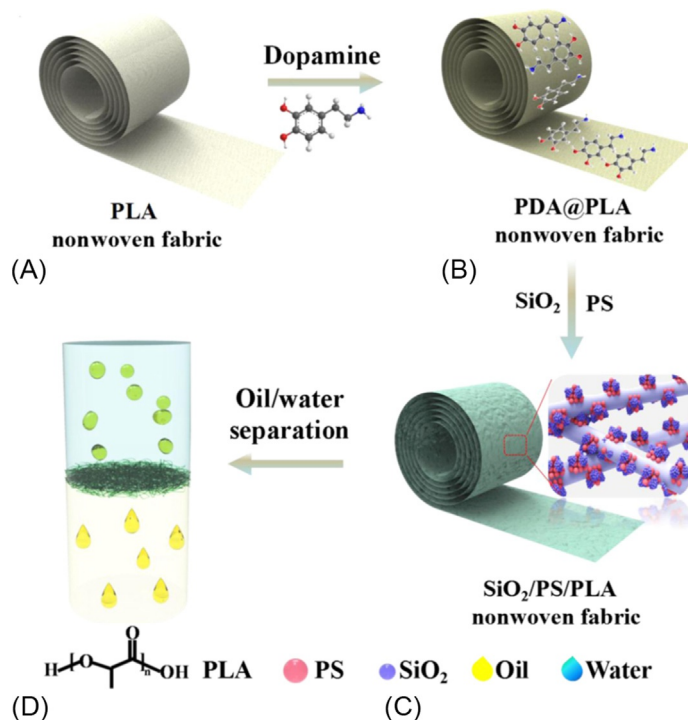
Fig. 8 A schematic explanation of the fabrication of superhydrophobic PLA nonwoven fabric for oil-water separation. (A) PLA nonwoven fabric, (B) PDA@PLA nonwoven fabric, (C) SiO$_2$/PS/PLA nonwoven fabric, and (D) oil-water separation. *(Reproduced with permission from J. Gu, P. Xiao, P. Chen, L. Zhang, H. Wang, L. Dai, L. Song, Y. Huang, J. Zhang, T. Chen, Functionalization of biodegradable PLA nonwoven fabric as superoleophilic and superhydrophobic material for efficient oil absorption and oil/water separation, ACS Appl. Mater. Interfaces 9 (7) (2017) 5968–5973. Copyright 2017, American Chemical Society.)*

(Fig. 8B). The hierarchical surface morphology responsible for superhydrophobicity and superoleophilicity attained by dense deposition of PS microspheres and SiO$_2$ nanoparticles on PDA-modified PLA surface (Fig. 8C). The as-prepared SiO$_2$/PS/PLA surface exhibited fine selectivity toward various oils and revealed excellent oil–water separation properties (Fig. 8D).

Li et al. [46] deposited hydrophobic CS particles on a SS mesh by holding it in the mid-flame of paraffin candle and then spray coated the hydrophobic silica nanoparticles (~50 nm) on it. The as-prepared CS/SiO$_2$ hybrid mesh revealed strong repellency toward pure water and droplets of pH ranging from 1 to 14, whereas the oil drops quickly spread on the surface. The hybrid mesh revealed strong ability to separate various oils and organic liquids mixed in pure water, hot water (~92°C), and strong corrosive solutions (1 M HCl, NaOH, and NaCl) with more than 98% of separation efficiency. Cao et al. [47] adopted the electrodeposition technique to attain roughness on copper meshes and then held it above candle flame to deposit CS nanoparticles. The agglomerated CS
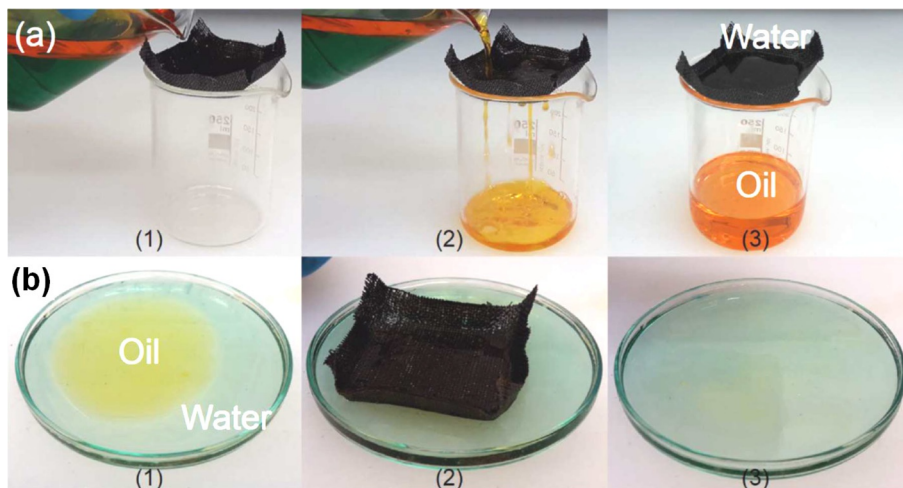
Fig. 9 A superhydrophobic SS mesh exhibiting (A) the separation and (B) collection of oil from oil/water mixture. *(Reproduced with permission from U. Zulfiqar, S.Z. Hussain, T. Subhani, I. Hussain, R. Habib ur, Mechanically robust superhydrophobic coating from sawdust particles and carbon soot for oil/water separation, Colloids Surf. A Physicochem. Eng. Asp. 539 (2018) 391–398. Copyright 2017, Elsevier.)*

nanoparticles formed a chain like rough hierarchical structure on which water drop achieved CA higher than 153 degrees and silicone oil spread completely. The CS deposited copper mesh quickly separated various oils (silicone oil, cyclohexane, *n*-hexane, *n*-heptane, petroleum ether, and liquid paraffin) from oil-water mixtures with oil separation efficiency greater than 90% even after 30 separation cycles. Recently, Zulfiqar et al. [48] deposited cheaply available sawdust (SD particles $\sim$37–74 μm) on polychloroprene adhesive-coated SS mesh with subsequent deposition of silicone polymer by dip coating. Thereafter, a thin layer of CS particles was applied on the as-prepared mesh by holding above a candle flame. The CS particles uniformly deposited on silicone covered SD exhibited highly rough and porous morphology required for superhydrophobicity and superoleophilicity. As depicted in Fig. 9, a superhydrophobic SS mesh easily and rapidly separated oil-water mixture. No trace of water was observed in separated oil confirming its potential in oil-water separation capability. Apart from excellent oil-water separation efficiency (>95%), the superhydrophobic SS mesh exhibited good recyclability, reusability, and mechanical stability. Table 2 summarizes the comparison of the oil-water separation capability between the various superhydrophobic meshes/membranes.

3. Summary and outlook

Oil expulsion in the environment is one of the key issues faced worldwide. This issue needs to be resolved urgently. In recent times, oil-water separation became a hot topic

Table 2 Comparison of the oil-water separation capability of superhydrophobic meshes/membranes

Materials	Fabrication process	Types of absorbed oil/organic solvent	Separation efficiency (%)	Recycle ability (number)	Ref.
CS/hydrophobic SiO_2	Spray coating	Kerosene, petroleum ether, toluene, chloroform, heptane	>98	>55	[46]
PTFE dispersion	Spray coating	Toluene, kerosene, gasoline, edible oil, trichloromethane	>95	>50	[44]
Epoxy/attapulgite nanocomposite	Spray coating	Hexadecane, lubricating oil, paroline	>98	>30	[42]
CS	Electrodeposition technique	Silicone oil, cyclohexane, liquid paraffin, n-hexane, n-heptane, petroleum ether	>90	>30	[47]
Polyhedral oligomeric silsesquioxane (POSS) hybrid acrylic polymer	Spray coating	n-Hexane, kerosene, isooctane, petroleum ether, and vegetable oil	~99	>25	[40]
$Cu(OH)_2$ nanoneedles	Solution immersion	Hexadecane, gasoline, toluene, mineral oil	>99	>25	[38]
Silicone elastomer (Sylgard 184)	Aerosol-assisted chemical vapor deposition	Hexane, petroleum ether, toluene	~99	>10 without drying	[35]
SiO_2/PS/PLA nonwoven fabric	Solution immersion	Hexane, toluene, silicone oil, pump oil, vegetable oil, soybean oil	~99	>10	[45]
PS—Silica particles coated with HDTMS	Drop casting	Chloroform	~96	>10	[39]
1–Dodecanethiol/ ethanol	Solution immersion	Chloroform	~94–97	>10	[37]
CS/PDMS	Spray coating	Silicone oil	~96	>05	[41]
SD/polychloroprene/ silicone polymer/ CS	Dip coating	Toluene, dichloromethane, n-hexane, chloroform	>95	>05	[48]
Diamond-like carbon (DLC)	PECVD	DMSO, chlorobenzene, ethanol, acetone, hexane, gasoline, chloroform, olive oil, dichloromethane	~99	>05	[38]
1-Hexadecanethiol (HDT)/ethanol	Solution immersion	Diesel	~98	Not reported	[36]

of discussion. Considering this cutting-edge problem, in the present article, we have specifically focused on summarizing the recent developments in the fabrication of superhydrophobic-superoleophilic materials for efficient oil–water separation application. Comparison between different types of separated oils, oil–water separation efficiency and recycle ability of various superhydrophobic materials have also been discussed. Since last two decades, tremendous development has been attained in the fabrication of superhydrophobic-superoleophilic sponges/meshes. In conjunction with costly, time-consuming and hectic procedures, few remarkable novel, simple, fast, cost-effective and robust methods have emerged. Polymer and CNT-based materials find potential application in constructing the superhydrophobic-superoleophilic sponges/meshes. The use of biodegradable materials is also emerging in this field. Recently, the cheaply available CS nanoparticles can be seen as a promising candidate in the development of oil–water separation materials. Generally, dip coating, spray coating, and solution immersion methods are found to be promising for uniform deposition of desired materials on sponges and meshes.

The superhydrophobic-superoleophilic sponge/mesh must exhibit high selectivity toward various oils and organic pollutants, efficient, and fast oil–water separation capability, good repeatability, and reusability, robust mechanical, chemical, and thermal stability. Regrettably, these properties of materials are limited to lab scale. The limitations are being faced in large-scale production of robust superhydrophobic-superoleophilic sponge/mesh as well as the rapid separation of oil from industrial oily wastewater, oil-in-water emulsions and oil–polluted seawater/rivers. Usually, the highly rough, porous hierarchical microstructure of superhydrophobic materials get damaged during repeated oil–water separation due to adverse mechanical and chemical effect, resulting in reduced oil separation efficiency. Therefore, it is an urgent requirement to develop large-scale and long-lasting specialized superhydrophobic materials through simple and inexpensive fabrication methods for efficient oil–water separation.

Acknowledgments

References

[1] R.K. Gupta, G.J. Dunderdale, M.W. England, A. Hozumi, Oil/water separation techniques: a review of recent progresses and future directions, J. Mater. Chem. A 5 (31) (2017) 16025–16058.

[2] S.S. Latthe, C. Terashima, K. Nakata, M. Sakai, A. Fujishima, Development of sol–gel processed semi-transparent and self-cleaning superhydrophobic coatings, J. Mater. Chem. A 2 (15) (2014) 5548–5553.

[3] B. Wang, W. Liang, Z. Guo, W. Liu, Biomimetic super-lyophobic and super-lyophilic materials applied for oil/water separation: a new strategy beyond nature, Chem. Soc. Rev. 44 (1) (2015) 336–361.

[4] L. Li, B. Li, J. Dong, J. Zhang, Roles of silanes and silicones in forming superhydrophobic and super-oleophobic materials, J. Mater. Chem. A 4 (36) (2016) 13677–13725.

[5] C.H. Lee, N. Johnson, J. Drelich, Y.K. Yap, The performance of superhydrophobic and superoleophilic carbon nanotube meshes in water–oil filtration, Carbon 49 (2) (2011) 669–676.

[6] C.-F. Wang, S.-J. Lin, Robust superhydrophobic/superoleophilic sponge for effective continuous absorption and expulsion of oil pollutants from water, ACS Appl. Mater. Interfaces 5 (18) (2013) 8861–8864.

[7] J. Gu, P. Xiao, J. Chen, F. Liu, Y. Huang, G. Li, J. Zhang, T. Chen, Robust preparation of superhydrophobic polymer/carbon nanotube hybrid membranes for highly effective removal of oils and separation of water-in-oil emulsions, J. Mater. Chem. A 2 (37) (2014) 15268–15272.

[8] Z. Zhou, X.-F. Wu, Electrospinning superhydrophobic–superoleophilic fibrous PVDF membranes for high-efficiency water–oil separation, Mater. Lett. 160 (2015) 423–427.

[9] M.W. Lee, S. An, S.S. Latthe, C. Lee, S. Hong, S.S. Yoon, Electrospun polystyrene nanofiber membrane with superhydrophobicity and superoleophilicity for selective separation of water and low viscous oil, ACS Appl. Mater. Interfaces 5 (21) (2013) 10597–10604.

[10] W. Qing, X. Shi, Y. Deng, W. Zhang, J. Wang, C.Y. Tang, Robust superhydrophobic-superoleophilic polytetrafluoroethylene nanofibrous membrane for oil/water separation, J. Membr. Sci. 540 (2017) 354–361.

[11] C.W. Tu, C.H. Tsai, C.F. Wang, S.W. Kuo, F.C. Chang, Fabrication of superhydrophobic and superoleophilic polystyrene surfaces by a facile one-step method, Macromol. Rapid Commun. 28 (23) (2007) 2262–2266.

[12] H. Yoon, S.-H. Na, J.-Y. Choi, S.S. Latthe, M.T. Swihart, S.S. Al-Deyab, S.S. Yoon, Gravity-driven hybrid membrane for oleophobic–superhydrophilic oil–water separation and water purification by graphene, Langmuir 30 (39) (2014) 11761–11769.

[13] W. Zhang, N. Liu, Y. Cao, Y. Chen, L. Xu, X. Lin, L. Feng, A solvothermal route decorated on different substrates: controllable separation of an oil/water mixture to a stabilized nanoscale emulsion, Adv. Mater. 27 (45) (2015) 7349–7355.

[14] H. Li, M. Zheng, L. Ma, C. Zhu, S. Lu, Two-dimensional ZnO nanoflakes coated mesh for the separation of water and oil, Mater. Res. Bull. 48 (1) (2013) 25–29.

[15] M. Zhang, C. Wang, S. Wang, J. Li, Fabrication of superhydrophobic cotton textiles for water–oil separation based on drop-coating route, Carbohydr. Polym. 97 (1) (2013) 59–64.

[16] C. Du, J. Wang, Z. Chen, D. Chen, Durable superhydrophobic and superoleophilic filter paper for oil–water separation prepared by a colloidal deposition method, Appl. Surf. Sci. 313 (2014) 304–310.

[17] C. Liu, J. Yang, Y. Tang, L. Yin, H. Tang, C. Li, Versatile fabrication of the magnetic polymer-based graphene foam and applications for oil–water separation, Colloids Surf. A Physicochem. Eng. Asp. 468 (2015) 10–16.

[18] P. Calcagnile, D. Fragouli, I.S. Bayer, G.C. Anyfantis, L. Martiradonna, P.D. Cozzoli, R. Cingolani, A. Athanassiou, Magnetically driven floating foams for the removal of oil contaminants from water, ACS Nano 6 (6) (2012) 5413–5419.

[19] L. Wu, J. Zhang, B. Li, A. Wang, Magnetically driven super durable superhydrophobic polyester materials for oil/water separation, Polym. Chem. 5 (7) (2014) 2382–2390.

[20] S. Liu, Q. Xu, S.S. Latthe, A.B. Gurav, R. Xing, Superhydrophobic/superoleophilic magnetic polyurethane sponge for oil/water separation, RSC Adv. 5 (84) (2015) 68293–68298.

[21] J. Zhang, H. Feng, W. Zao, Y. Zhao, H. Zhang, Y. Liu, Magnetically driven superhydrophobic meshes with the capacity of moving at air/water and oil/water interfaces, RSC Adv. 5 (59) (2015) 47892–47899.

[22] V.-H.T. Tran, B.-K. Lee, Novel fabrication of a robust superhydrophobic PU@ZnO@Fe3O4@SA sponge and its application in oil-water separations, Sci. Rep. 7 (1) (2017) 17520.

[23] Q. Zhu, Y. Chu, Z. Wang, N. Chen, L. Lin, F. Liu, Q. Pan, Robust superhydrophobic polyurethane sponge as a highly reusable oil-absorption material, J. Mater. Chem. A 1 (17) (2013) 5386–5393.

[24] Q. Ke, Y. Jin, P. Jiang, J. Yu, Oil/water separation performances of superhydrophobic and superoleophilic sponges, Langmuir 30 (44) (2014) 13137–13142.

[25] X. Zhang, Z. Li, K. Liu, L. Jiang, Bioinspired multifunctional foam with self-cleaning and oil/water separation, Adv. Funct. Mater. 23 (22) (2013) 2881–2886.

[26] G. Hayase, K. Kanamori, G. Hasegawa, A. Maeno, H. Kaji, K. Nakanishi, A superamphiphobic macroporous silicone monolith with marshmallow-like flexibility, Angew. Chem. Int. Ed. 52 (41) (2013) 10788–10791.

[27] C. Ruan, K. Ai, X. Li, L. Lu, A superhydrophobic sponge with excellent absorbency and flame retardancy, Angew. Chem. Int. Ed. 53 (22) (2014) 5556–5560.

[28] B. Wang, J. Li, G. Wang, W. Liang, Y. Zhang, L. Shi, Z. Guo, W. Liu, Methodology for robust superhydrophobic fabrics and sponges from in situ growth of transition metal/metal oxide nanocrystals with thiol modification and their applications in oil/water separation, ACS Appl. Mater. Interfaces 5 (5) (2013) 1827–1839.

[29] S.-J. Choi, T.-H. Kwon, H. Im, D.-I. Moon, D.J. Baek, M.-L. Seol, J.P. Duarte, Y.-K. Choi, A polydimethylsiloxane (PDMS) sponge for the selective absorption of oil from water, ACS Appl. Mater. Interfaces 3 (12) (2011) 4552–4556.

[30] C.-F. Wang, L.-T. Chen, Preparation of superwetting porous materials for ultrafast separation of water-in-oil emulsions, Langmuir 33 (8) (2017) 1969–1973.

[31] Y. Yang, H. Yi, C. Wang, Oil absorbents based on melamine/lignin by a dip adsorbing method, ACS Sustain. Chem. Eng. 3 (12) (2015) 3012–3018.

[32] J. Li, Z. Zhao, R. Kang, Y. Zhang, W. Lv, M. Li, R. Jia, L. Luo, Robust superhydrophobic candle soot and silica composite sponges for efficient oil/water separation in corrosive and hot water, J. Sol-Gel Sci. Technol. 82 (3) (2017) 817–826.

[33] F. Beshkar, H. Khojasteh, M. Salavati-Niasari, Recyclable magnetic superhydrophobic straw soot sponge for highly efficient oil/water separation, J. Colloid Interface Sci. 497 (2017) 57–65.

[34] Y. Gao, Y.S. Zhou, W. Xiong, M. Wang, L. Fan, H. Rabiee-Golgir, L. Jiang, W. Hou, X. Huang, L. Jiang, J.-F. Silvain, Y.F. Lu, Highly efficient and recyclable carbon soot sponge for oil cleanup, ACS Appl. Mater. Interfaces 6 (8) (2014) 5924–5929.

[35] C.R. Crick, J.A. Gibbins, I.P. Parkin, Superhydrophobic polymer-coated copper-mesh; membranes for highly efficient oil–water separation, J. Mater. Chem. A 1 (19) (2013) 5943–5948.

[36] C. Wang, T. Yao, J. Wu, C. Ma, Z. Fan, Z. Wang, Y. Cheng, Q. Lin, B. Yang, Facile approach in fabricating superhydrophobic and superoleophilic surface for water and oil mixture separation, ACS Appl. Mater. Interfaces 1 (11) (2009) 2613–2617.

[37] Y. Song, Y. Liu, B. Zhan, C. Kaya, T. Stegmaier, Z. Han, L. Ren, Fabrication of bioinspired structured superhydrophobic and superoleophilic copper mesh for efficient oil–water separation, J. Bionic Eng. 14 (3) (2017) 497–505.

[38] G. Ren, Y. Song, X. Li, Y. Zhou, Z. Zhang, X. Zhu, A superhydrophobic copper mesh as an advanced platform for oil–water separation, Appl. Surf. Sci. 428 (2018) 520–525.

[39] Q. Wang, M. Yu, G. Chen, Q. Chen, J. Tian, Robust fabrication of fluorine-free superhydrophobic steel mesh for efficient oil/water separation, J. Mater. Sci. 52 (5) (2017) 2549–2559.

[40] D. Guo, K. Hou, S. Xu, Y. Lin, L. Li, X. Wen, P. Pi, Superhydrophobic–superoleophilic stainless steel meshes by spray-coating of a POSS hybrid acrylic polymer for oil–water separation, J. Mater. Sci. 53 (9) (2018) 6403–6413.

[41] N.R. Geraldi, L.E. Dodd, B.B. Xu, D. Wood, G.G. Wells, G. McHale, M.I. Newton, Bioinspired nanoparticle spray-coating for superhydrophobic flexible materials with oil/water separation capabilities, Bioinspir. Biomim. 13 (2) (2018) 024001.

[42] J. Yang, Y. Tang, J. Xu, B. Chen, H. Tang, C. Li, Durable superhydrophobic/superoleophilic epoxy/attapulgite nanocomposite coatings for oil/water separation, Surf. Coat. Technol. 272 (2015) 285–290.

[43] B. Cortese, D. Caschera, F. Federici, G.M. Ingo, G. Gigli, Superhydrophobic fabrics for oil–water separation through a diamond like carbon (DLC) coating, J. Mater. Chem. A 2 (19) (2014) 6781–6789.

[44] S. Lei, Z. Shi, J. Ou, F. Wang, M. Xue, W. Li, G. Qiao, X. Guan, J. Zhang, Durable superhydrophobic cotton fabric for oil/water separation, Colloids Surf. A Physicochem. Eng. Asp. 533 (2017) 249–254.

[45] J. Gu, P. Xiao, P. Chen, L. Zhang, H. Wang, L. Dai, L. Song, Y. Huang, J. Zhang, T. Chen, Functionalization of biodegradable PLA nonwoven fabric as superoleophilic and superhydrophobic material for efficient oil absorption and oil/water separation, ACS Appl. Mater. Interfaces 9 (7) (2017) 5968–5973.

[46] J. Li, R. Kang, X. Tang, H. She, Y. Yang, F. Zha, Superhydrophobic meshes that can repel hot water and strong corrosive liquids used for efficient gravity-driven oil/water separation, Nanoscale 8 (14) (2016) 7638–7645.

[47] H. Cao, J. Fu, Y. Liu, S. Chen, Facile design of superhydrophobic and superoleophilic copper mesh assisted by candle soot for oil water separation, Colloids Surf. A Physicochem. Eng. Asp. 537 (2018) 294–302.

[48] U. Zulfiqar, S.Z. Hussain, T. Subhani, I. Hussain, R. Habib ur, Mechanically robust superhydrophobic coating from sawdust particles and carbon soot for oil/water separation, Colloids Surf. A Physicochem. Eng. Asp. 539 (2018) 391–398.

Index

Note: Page numbers followed by *f* indicate figures and *t* indicate tables.